"The Implications of Metamorphism and Weathering of the Lesser Himalayan Formation in Eastern Nepal for Climate Change"

Thesis

UNRESTRICTED

"The Implications of Metamorphism and Weathering of the Lesser Himalayan Formation in Eastern Nepal for Climate Change".

A thesis presented for the degree of Doctor of Philosophy

Lee Oliver

BSc (Hons) Keele

2002

Department of Earth Sciences, The Open University

Submission Date: 30 September 2002
Award date: 26 February 2003

ProQuest LLC.
789 East Eisenhower Parkway
P.O. Box 1346
Ann Arbor, MI 48106 – 1346

Abstract

This study evaluates the significance of Sr-isotopes as a silicate weathering proxy in the context of Himalayan river systems. The dissolved load of the Bhote Kosi (central Nepal) displays a rapid increase in $^{87}Sr/^{86}Sr$ ratio immediately downstream of the Main Central Thrust, a feature common to other Himalayan tributaries of the Ganges. The results of statistical and mass balance analyses identify the weathering of radiogenic ($^{87}Sr/^{86}Sr$ >0.8) calc-silicate lithologies from the Lesser Himalayan Formation as the predominant control upon the dissolved $^{87}Sr/^{86}Sr$ ratio.

In situ laser ablation analysis of dolomite in these calc-silicates yields radiogenic $^{87}Sr/^{86}Sr$, indistinguishable from bulk rock ratios, confirming the presence of a highly soluble source of radiogenic strontium. The distribution of Rb-Sr isotopes suggests homogenisation of Sr-isotopes between silicate and carbonate at both grain-size and bulk-rock scale. Similar lithologies can be traced across much of the southern Himalaya, and multiple regressions from Bhote Kosi data successfully predict dissolved $^{87}Sr/^{86}Sr$ ratios in other major Himalayan rivers, indicating that findings from the Bhote Kosi are applicable across eastern Nepal.

Flux calculations indicate that at least 50% of the impact of the Bhote Kosi river on the global marine $^{87}Sr/^{86}Sr$ ratio can be traced to weathering of Lesser Himalayan carbonates. Hence a significant proportion of the increase in marine $^{87}Sr/^{86}Sr$ ratio over the past 7-10 Ma is ascribed to the exposure of these lithologies. The widespread

assumption that dissolved $^{87}Sr/^{86}Sr$ ratios are a proxy for silicate weathering rates is therefore undermined where ancient metamorphosed calc-silicate rocks are exposed in river catchments. Although this conclusion casts doubt upon the use of the marine strontium isotope record to quantify carbon dioxide drawdown resultant from present-day Himalayan silicate weathering, evidence suggests that prior to uplift of the Lesser Himalaya, dissolved Sr-isotope ratios in Himalayan runoff did provide an indication of silicate weathering rates.

Acknowledgements

Firstly, a great deal of thanks is due to Nigel Harris, Nancy Dise and Mike Bickle for setting up this project and for providing four years of first-rate supervision. All three have proved attentive yet relaxed and patient. Extra thanks are due to Nigel for the mobile phone calls etc. that have helped hold things together during this last year, and also, together with his family, for making me feel most welcome at their home in Cambridge.

I will never forget my time in Nepal and owe a great deal of thanks to those who helped make my (somewhat extended) stay such an amazing experience. Helen Williams proved both an excellent field assistant and guide to the sights and watering holes of Thamel, and is doubly thanked for collecting samples and providing excellent field observations in the Tibetan part of the Bhote Kosi. A year later I could not have asked for two better (albeit somewhat different) and more entertaining travelling companions in Josh West and Tubbs Thornton.

Particularly at this time my thoughts are with the wonderful people I met in Nepal. Vehicles, guiding and portering services were provided by the excellent (and cheap!) Mt Manaslu Trekking (in the street behind the Garuda Hotel should you be requiring their services), run by the unforgettable Krishna and Cheban, with special thanks also owing to Mardan, Baburam, Korma, Janak, Kumar, Suresh, Sabarjit and "little" Krishna. Comfortable accommodation was found at the Garuda, Tashi Dhargi, Heera and Alice Hotels in Kathmandu, and at the aptly named Bhote Kosi Hotel in Barabise.

On a more official note, the help of the International Centre for Integratred Mountain Development (ICIMOD) was invaluable in ensuring fieldwork success in 1999, through the loan of equipment, provision of information and the recommendations that allowed the export of my samples. I particularly wish to thank Richard Allen and Gopal Nokarmi, without whom the dataset for this work would have been considerably smaller. At the Department of Mines and Geology in Kathmandu I'd like to thank Bharat M. Jnawali for providing access to geological mapping of the Bhote Kosi valley and to Nanda R. Sthapit for granting permission for my samples to leave Nepal.

Back at the rather less attractive surroundings of the OU I'd like to thanks Mabs Gilmour, Peter Van Calsteren, Louise Thomas and Jo Rhodes for their tireless (and often thankless) work ensuring the smooth running of the labs. Special thanks is owing to Nick Rogers for his tremendous patience and effort in pushing through my ICPMS work at a particularly difficult time. Top quality thin and thick sections were provided by Kay, Brian, Mike and the rest of the team, while Andy Lloyd and John Taylor are thanked for help producing my conference posters and slides and for assorted other graphics and cartography advice. Thanks also to Janet Dryden, Gill Foulkes and Anita Chhabra for ensuring the smooth running of the department.

At Cambridge I am extremely grateful for the time and effort afforded my work by Hazel Chapman and Judith Bunbury, while thanks are also due to Rob Hughes for letting me both share his office and kip on his floor. ICP-AES and some IC analyses were carried at IACR-Rothamstead where thanks are due to Adrian Crossland and Paul Hargreaves. Laser ablation work was carried out at NIGL under the expert eye of Matt Horstwood, and I'm grateful to Randy Parrish for taking an interest in my work and allowing use of the NIGL facilities at short notice.

The bulk of this thesis was done in the hallowed chamber known as Z209 and I feel I must thank my office-mates over the years; Glynn, Helen, Dawn, Jenny (four years, poor girl!), Jodie, Macca, James, Steve, Severine, Andy "platinum pants" Richards and Chris. Even braver are those who have lived with me during the last four years – Helen, Liz, Bruce C, Chuck, Quintin, Tubsie, Sev, Della and Jim. Others who have helped make the OU experience more pleasant include Tom, Parkie, Yvonne, Smudger, Dan C, Luke, Dan M, Bruce S, Basak, Vinny, Nathalie, Aaron, Jason, Mark, Ed and Steve, along with Lee, Giles, Sheridan, Manish, Becky and the rest of the PSSRI crew. Special mention is owing to Dr Gav "Bufty Boy" Foster for partaking in conference drinking and adventures both home and abroad as well as advice and discussions of both a geological and (more often) non-geological nature.

My family have been tremendously supportive throughout the last four years and so massive thanks to Mum, Dad, Martin, Rowan and Liz.

As he fits into most of the above categories I guess I have to give him a paragraph of his own ..... "Dr Tubbs" Thornton has been a top mate, housemate and source of entertainment, contributing an immense amount to this project in the form of help in the lab, in the field and as a source of interesting ideas and discussion, particularly so in the early stages when he was my unofficial 4th supervisor at a time when he was busy writing up his own thesis. Most of all though I'd like to thank the old man for letting me join him on his final pilgrimage to Everest Basecamp.

On a slenderer and infinitely more attractive note, I'd like to finish by giving a mention to my girlfriend Joe. My supervisors may indeed have had a hard job but this is nothing compared with the patience required to go out with me over the last four years. I shall resist the temptation to get too gushing (see Thornton, PhD thesis, 1999) at this point - just to say thanks and lots of love.

Table of Contents.

List of Figures.

List of Plates

Plate 9. Sampled catchments of the Langtang Khola – Trisuli basin.

Key for plate 9.

List of Tables

Chapter 1

Introduction

This chapter introduces the concepts and discoveries that led to the initiation of this project. The chapter begins by describing the geological setting of the Himalaya, with particular detail provided for the Lesser Himalayan units that are the focus of this work. Following this the Himalayan weathering environment is described, focussing on how weathering in the Himalaya could be responsible for Cenozoic global cooling through carbon dioxide drawdown on a million-year timescale. Finally, an assessment is carried out of the current evidence both for and against the hypothesis that the marine strontium-isotope record provides a proxy for silicate weathering in the Himalaya, thereby providing a means of quantifying CO_2 drawdown and the climatic impact of the orogeny.

1.1. The Geological Setting of the Himalaya.

The 2800 km southwardly convex Himalayan mountain arc, of which Nepal occupies the central (800 km) section, was formed by north-south shortening and crustal thickening during convergence between the Indian and Asian continental crustal plates after their collision at ~50 Ma (Gansser, 1964; Le Fort, 1975a; Dewey *et al.*, 1988; Beck *et al.*, 1995). Since collision these plates have converged at N10°E at a rate of roughly 5

cm annually (Upreti, 1999) as evidenced by the occurrence of frequent seismic events in the region (Seeber and Armbruster, 1981; Jackson and Bilham, 1994; Pandey *et al.*, 1995; Billham *et al.*, 1997).

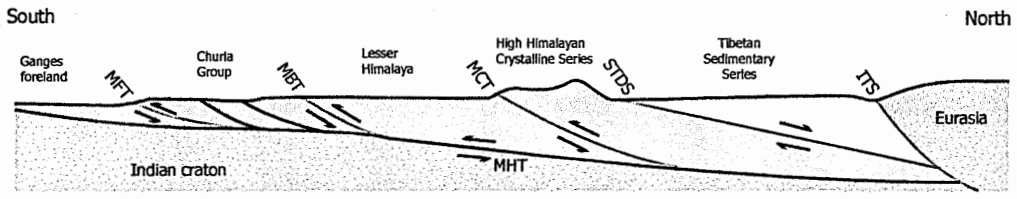

Fig. 1.1. Simplified structural cross-section of the central (Nepal) Himalaya.
Reproduced from Harris et al. (2001).

ITS; Indus Tsangpo Suture Zone. STDS; South Tibetan Detachment System. MCT; Main Central Thrust. MBT; Main Boundary Thrust. MFT; Main Frontal Thrust

The general structure of the central Himalaya is illustrated in fig. 1.1. The major tectonic elements of the orogen are bounded by north-dipping faults that generally strike parallel to the mountain range, each tectonic element forming an increasing high part of Himalaya toward the north (fig. 1.2). From north to south these zones are;

(i). **The Tibetan Sedimentary Series (TSS);** Weakly to unmetamorphosed marine sediments ranging in age from Cambro-Ordovician to Eocene and dominated by shelf carbonates. These rocks lie predominantly on the southern Tibetan Plateau, north of the main Himalayan range within its rain shadow, at an average altitude exceeding 5000 m. These rocks also form (together with the HHCS) some of the high Himalayan peaks including Mt. Everest, Manaslu, Annapurna and Dhaulagiri. The northern boundary of the TSS is the Indus-Tsangpo Suture (ITS).

Fig. 1.2. Simplified geology of the Himalaya.

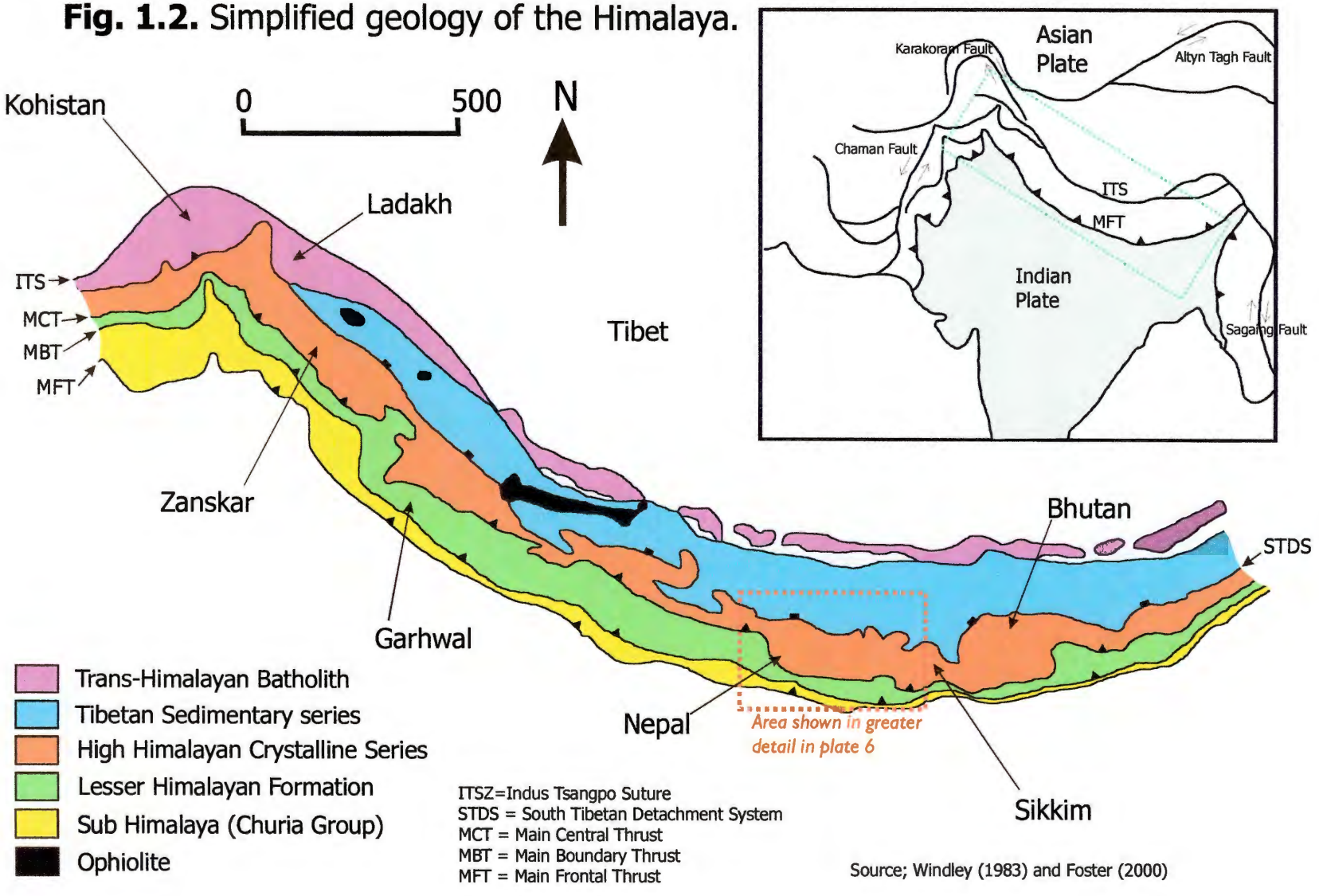

(ii). **The High Himalayan Crystalline Series (HHCS):** This unit includes high-grade (garnet – sillimanite) metamorphic basement rocks, Ordovician porphyritic biotite granites and Miocene muscovite leucogranites. Rocks of the HHCS reach altitudes in excess of 8000 m throughout the range, forming the bulk of the physiographical high Himalayan range. The HHCS is separated from the TSS by a north-dipping normal fault system, the South Tibetan Detachment System (STDS), and is emplaced over the Lesser Himalaya along the Main Central Thrust (MCT).

(iii). **The Lesser Himalayan Formation (LHF):** Reaching elevations up to 3000m, but mostly at elevations <1500m, these variably metamorphosed (up to garnet grade) sediments of Proterozoic to early Palaeozoic age are thrust over the Churia Group by the low-angle Main Boundary Thrust (MBT). The Outer Lesser Himalaya is a distinct external unit that does not outcrop in Nepal, and which possibly represents equivalents of the High Himalayan Crystalline Series that have escaped high-grade metamorphism (Bickle *et al.*, 2001).

(iv). **Churia (Siwalik) Group:** Folded and deformed Mid-Miocene to Pliocene river sediments of the Siwalik foredeep. This unit forms the low foothills of the "Subhimalaya". The Churia Group is separated from the modern foredeep by the active but discontinuous Main Frontal Thrust (MFT).

(v). **Recent alluvium:** Foreland alluvium of Pleistocene – Recent age.

1.2. Formation of the Himalaya.

Valdiya (1998) provides an excellent account of the geological history of the Himalaya, and the following is summarised from this work with additions where stated.

The history of the Himalaya essentially begins in the mid-Proterozoic when the northern margin of the Indian shield was flooded to form the Purāna Sea, which extended as far south as central India. Sediment supplied by the north-flowing rivers of peninsular India filled the basin, forming the units of the Lesser Himalaya Formation. This continued until the early Cambrian, when widespread crustal disturbance (the late Pan-African Orogeny, ~550-500 Ma), which was accompanied by granite emplacement, ended sedimentation in the "Lesser Himalayan Domain". Only in the far north of the Purāna Sea (the "Tethyan Domain") did sedimentation continue, interrupted by Pan-African tectonism. At around 300 Ma, another global tectonic upheaval (the Hercynian Orogeny) caused crustal rifting and a marine incursion along a rift valley, forming what is now the Outer Lesser Himalaya. In the Tethys domain (now the Tethys Ocean), sedimentation was interrupted, but soon continued again for the rest of the Phanerozoic.

The period between 130 and 50 Ma saw the subduction of the Tethys Ocean floor and the creation of a volcanic island arc in front of the Asian landmass. The exact timing of the collision of India, Asia and the island arc is debatable, but occurred sometime between 65 and 45 Ma, and possibly diachronously, with evidence suggesting that collision took place in the west at 65-55 Ma (Beck *et al.*, 1995), but later in the east,

between 50 and 45 Ma (Dewey *et al.*, 1988). The northern edge of the Indian Plate ridged up and the obduction of deep-sea sediments, basic and ultrabasic rock occurred. Many of the major Himalayan rivers of the modern day, including the Ganges and Brahmaputra, established their drainage during this time. The pressure of northward moving India caused sagging in belts to the north and south of the incipient Himalaya, with resultant marine incursion and sedimentation.

The period between 40 and 20 Ma saw thickening of the crust south of the suture line between the Asian and Indian plates (the Indus-Tsangpo Suture or ITS). Up until 25 Ma, much of the northward progression of India appears to have been accommodated through tectonic escape, with large portions of Southeast Asia moving along strike-slip faults (Taponnier *et al.*, 1986, 1990; Briais *et al.*, 1989, 1993; Schäerer *et al.*, 1990; Harrison *et al.*, 1992, 1994; Leloup *et al.*, 1993) such as the Altyn Tagh Fault (see fig. 1.2). It has been suggested that the importance of tectonic escape had waned by the late Oligocene, and became inconsequential by the mid Miocene (Copeland, 1997).

Dating of the Miocene leucogranites at the top of the HHCS suggests that movement on the MCT started in the latest Oligocene (Le Fort, 1981; Copeland *et al.*, 1988; Hodges *et al.*, 1992, 1996; Harrison *et al.*, 1995), continuing until 15 Ma (Copeland *et al.*, 1991; Harrison *et al.*, 1998) with the HHCS exposed by the Early Miocene (McFarlane, 1993; Hodges *et al.*, 1996). This thrust is regarded as the most significant thrust giving rise to the major geodynamic evolution of the Himalaya. It was originally assumed (Le Fort, 1975a; Molnar, 1984) that displacement on the MCT largely ceased when the MBT

became active, although recent work (Harrison *et al.*, 1998, 1999) suggests that it was reactivated at 6-8 Ma. At least 100 km of shortening has occurred along the MCT (Brunel, 1975; Arita, 1983; Pêcher, 1989; Schelling and Arita, 1991; Schelling, 1992), possibly 200 km or more (Gansser, 1964; Schelling, 1992; Srivastava and Mira, 1994; Parrish and Hodges, 1996; Harrison *et al.*, 1999), carrying a 20-30 km thickness of the HHCS over the Lesser Himalaya, and bringing together three units (the TSS, HHCS and LHF) that were originally deposited a large distance apart. The Siwalik foreland basin began to form at 25-20 Ma as a result of the erosion consequent from the thrusting.

Movement on the South Tibetan Detachment System, based on the dating of leucogranite bodies cut by the fault, took place between ~20 and 14 Ma (Copeland *et al.*, 1988; Hodges *et al.*, 1992, 1996; Harrison *et al.*, 1995), although Burchfiel *et al.* (1992) suggest a longer period of movement, from the Eocene to perhaps as recently as the Pliocene. Forming at a time of large-scale crustal thickening and subhorizontal shortening, the STDS has been interpreted as the result of the gravitational collapse of the thickened southern Tibetan crust. Displacement is likely to be in the order of tens of km (Burchfiel *et al.*, 1992), with at least 35 km of northward displacement demonstrable along a profile at on the north side of Mt. Everest. Individual segments of the STDS probably moved at different times although it is possible that movement began in all areas at the same time, but that movement in some areas outlasted that in others.

Burbank *et al.* (1996), studying changes in sediment accumulation rates, concluded that the MBT was first active at 11Ma, while DeCelles *et al.* (1998) observed that this thrust

carried rocks of ~15 Ma in age, cutting rocks as young as 2 Ma. The Lesser Himalaya is believed to have been first exposed at ~15 Ma, with extensive exposure by ~5 Ma, although this is still a matter of some debate (see section 1.7). Even more recently, in the last 2 Ma, a major deformation event is believed to have elevated the mountains to their greatest heights and displaced the Siwaliks along the MFT, arresting Siwalik deposition and leading to the formation of the Quaternary deposits of the Indus-Gangetic foreland basin (Schelling and Arita, 1991). The MFT is still active.

1.3. The Geology of Nepal and Southern Tibet.

1.3.1. The Tibetan Sedimentary Series.

Nomenclature for the TSS in Nepal is summarised from work by Bordet *et al.* (1975), Fuchs (1977), Bassoullet *et al.* (1977), Colchen *et al.* (1980) and Fuchs *et al.* (1988), whilst that for south-central Tibet is provided by Xianghui *et al.* (1996). Correlations of these units in the Indian Himalaya to the west and for the east of Nepal are given by Valdiya (1998), correlated units in other parts of Tibet can be found in Xianghui *et al.* (1996). Specific sections in southern Tibet are described by Burchfiel *et al.* (1992) and are discussed in the relevant parts of Chapter 2.

The TSS in Nepal and south-central Tibet to the north begins in the mid-Ordovician. Sandstones and conglomerates laid down during the Pan-African Orogeny are overlain by dolomitic limestones, limestones, dolomites and calcareous shale (the Nilgiri

Limestones of Nepal, Gyacun Group of southern Tibet) representing the return of marine conditions. The Silurian comprises a succession of shales and limestones known as the Dark Band Formation in Nepal and the Shiqipo and Pulu Formations in Tibet. The Devonian brought an increase in the prevalence of shallow water sandstones, interbedded with limestones, forming the Tilichi Pass Formation of Nepal, the Cool Spring Formation and Boqu Group of Tibet. The Carboniferous comprises limestones and dark shales formed in deeper waters as the shallow Indian shelf subsided (the Tilicho Lake Formation of Nepal, the Naxing Formation of Tibet) with sandstone deposits in the later Carboniferous (e.g. the Galong Formation in Tibet) related to the Hercynian Orogeny, which led to reduced or absent sedimentation in many parts of the Nepal Himalaya. Marine sediments return in the Permian, with shallow shelf limestones, dolomites, calcareous sandstones and carbonaceous shales observed in the Thini Chu Formation of Nepal and the Selung Formation in Tibet. Limestones and dolomites predominate in the Triassic and Jurassic together with interbedded shales deposited in a deeper water environment. The Triassic is known as the Thinigaon Formation in western Nepal, the Tsolhamo Formation in eastern Nepal and is composed of the Tulung Formation, Qulong Gongba Formation and Derirong Formation in Tibet. Nomenclature for the Jurassic units of Nepal varies, although it commonly comprises the Jomosom, Lamachelle and Saligram Formations, being know as the Caili Group and Menkadun Formation in Tibet. The Cretaceous units are the only part of the TSS not dominated by carbonate, comprising siliceous and calcareous sandstones, siltstones and siliceous shales formed by submarine slides and turbidity currents. Cretaceous units are absent from parts of Nepal, but where present are known as the Kagbeni Group in the west and

the Khampa Group in the east. The Gamba Group comprises the Cretaceous in south-central Tibet.

1.3.2. The High Himalayan Crystalline Series.

HHCS sediments are derived from a source with a depleted mantle Nd model age of 1800-2000 Ma (Bickle *et al.*, 2001). They were subsequently metamorphosed at ~500 Ma prior to Himalayan high-grade metamorphism (upper amphibolite to granulite facies; Pêcher *et al.*, 1989; Rai *et al.*, 1998) at ~35-20 Ma (Vance and Harris, 1999). The youngest garnet-grade rocks, exposed around the MCT, have peak-metamorphic ages as young as ~6 Ma (Harrison *et al.*, 1997).

The HHCS has been mapped throughout the entire Himalaya, although different names have been applied to its units in different areas, and the precise stratigraphic sequence, age and origin of the rocks remains unclear. The HHCS in Nepal has been studied in deep river gorges, the rest of the HHCS terrain being largely inaccessible. Perhaps the most extensive and best studied exposure is that of the Kali Gandaki section, described by Le Fort (1975a). The rocks here exhibit a homoclinal structure, dipping NE to NNE at angles of 30-75°, and are divided into three formations:

(i). Formation I is the lowest unit and consists of kyanite to silliminite-garnet two-mica banded gneisses of pelitic to arenaceous composition. The upper part of the formation is characterised by augen gneisses and migmatites with intercalations of calc-silicates and

quartzites. Formation I is 1400m thick in the Kali Gandaki, although increases in thickness eastwards (5000 m in the Marsyandi section; Upreti, 1999).

(ii). The top of Formation II consists of a coarse quartzite tens of metres thick, the remainder of the unit comprising alternations of pyroxene and amphibole bearing calc-gneisses and marbles. This unit is variable in thickness from 3500m in the Kali Gandaki to virtually zero in the Langtang section further east.

(iii). Formation III consists predominantly of rocks with a pelitic or greywacke composition. A 3000 m thick augen gneiss marks the top of the unit. Intruded into this upper part of the HHCS are young granites (24-19Ma; Guillot *et al.*, 1994).

Most recent workers (e.g. Stöcklin, 1980; Hodges *et al.*, 1988; Hubbard and Harrison, 1989; Copeland *et al.*, 1991) have placed the MCT above a thick ductile shear zone (the MCT zone) at the base of the HHCS. This thrust was first recognised by French researchers (e.g. Bordet *et al.*, 1972; Le Fort, 1975a; Pêcher, 1975) and corresponds to the MCT II of Hasimoto *et al.* (1973). Above the MCT zone is another thrust first identified by Heim and Gansser (1939) and termed the MCT I by Hashimoto *et al* (1973). The rocks of the MCT zone are believed to belong to the Lesser Himalaya, showing higher grade metamorphism than the rest of the LHF owing to their close proximity to the MCT, along which the HHCS hot slab was thrust over cold LHF.

Detail of the HHCS in sampled catchments, including revised terminology used by workers in the Langtang and Shisha Pangma regions, is provided in the relevant sections of Chapter 2, with correlations with the above outline provided where possible.

1.3.3. The Lesser Himalayan Formation.

In eastern Nepal, the HHCS thrust sheet reaches close to the MBT, although deep erosion reveals Lesser Himalayan units in large tectonic windows known as the Taplejung, Arun and Chautara-Okhaldhunga windows. West of Kathmandu a large tract of the Lesser Himalaya is exposed, although west of the Bheri River much of the LHF is again covered by crystalline nappes. In addition to numerous smaller folds the LHF is folded into an east-west trending mega-anticline (Upreti, 1999) known as the Trisuli-Gorkha-Pokhara anticline, the core of which exposes the oldest LHF rocks (the Kuncha Formation, no basement rocks are exposed). A corresponding syncline, the Mahabharat Syncline, occurs to the south.

Stöcklin and Bhattarai (1980) and Stöcklin (1980) first described the generally accepted nomenclature of the Lesser Himalayan Formation in Central Nepal. The same units are recognised in the more extensive geological mapping carried out by the Nepal Department of Mines and Geology (DMG) in the mid-1980s, although they are assigned different names, as shown in fig. 1.3, and there are some interpretative differences. The Malekhu Limestone and Dhading Dolomite of Stöcklin and Bhattarai are regarded as the same unit, separated in the Bhote Kosi section by the thrust-bound Galyang Formation

(Benighat Slates), which is interpreted as lying stratigraphically between the lower and upper part of the Dandogaon Phyllites of Stöcklin and Bhattarai. No other workers note the presence of thrust-delineated boundaries in the Nepal Lesser Himalaya. A more recent geological map produced by the Nepal DMG (Amatya *et al.*, 1994) uses the original nomenclature of Stöcklin and Bhattarai, but with different divisions (see fig. 1.3). The lowermost units of Stöcklin and Bhattarai's Lower Nawakot Group, the Kuncha Formation and Fagfog Quartzite, are named the Kuncha Group, while the remainder of Stöcklin and Bhattarai's Lower Nawakot Group, from the Dandagoan Phyllites upwards, together with the Upper Nawakot Group, are shown together simply as the Nawakot Group. This nomenclature is the one adopted in this work as it provides a way of conveniently discriminating between pure silicate units (the Kuncha Group) and calc-silicate units (the Nawakot Group). In addition, the division between these two units is easily observed in the field. The type descriptions of Stöcklin and Bhattarai (1980) and Stöcklin (1980), based largely on work carried out in the lower Trisuli area to the west of the Kathmandu Nappe, are described below. They correlate with units in western Nepal as show by Upreti (1999) and with rocks in other parts of the Himalaya (Valdiya, 1986; 1995). Additional detail relevant to the river basins sampled in this work is provided where appropriate in chapter 2.

Much of the Lesser Himalayan sequence has a ~2500 – 2900 Ma depleted-mantle model Nd age (Ahmad *et al.*, 2000). The units have been shown to range in age from Paleoproterozoic (~1800-2000 Ma) to uppermost Precambrian (~570 Ma) (Sakai, 1983,

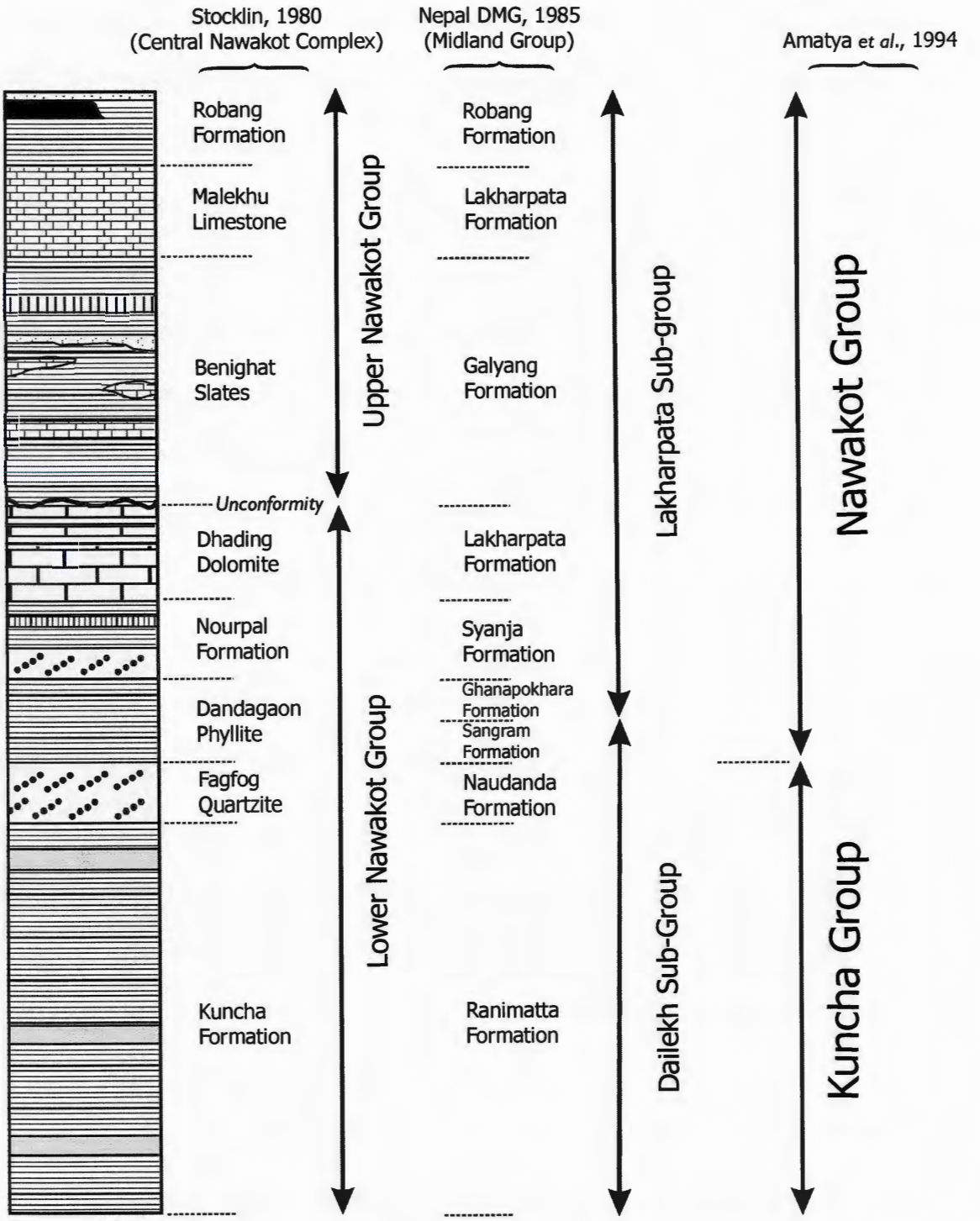

Fig. 1.3. Statigraphy of the Lesser Himalaya in Central Nepal.

1985; Valdiya, 1995, 1998; Parrish and Hodges, 1996). Minor exposures of continental Lesser Himalayan sediments deposited after the Pan-African Orogeny (e.g. the Tansen Group mapped by Amatya *et al.*, 1994) unconformably cap the units described below, but are not extensive and do not occur at all within the river basins sampled for this work. The Lesser Himalaya were metamorphosed at 1800Ma and possibly again at 500Ma (France-Lanord, 1993; Oliver *et al.*, 1995; Parish and Hodges, 1996; Ahmad *et al.*, 2000).

1.3.3.1. The Kuncha Group.

The oldest formation of the Lesser Himalaya in Nepal, possibly of the entire Lesser Himalaya, is the Kuncha Formation (Bordet, 1961), the base of which is nowhere exposed. The lower part of the formation consists of a monotonous sequence of flysch, with alternations of phyllites, phyllitic quartzites, phyllitic gritstones and fine quartz conglomerates. Basic volcanic material is locally interbedded. The rocks contain quartz, detrital feldspars, muscovite, tourmaline and opaques. Sericite and chlorite are present as the metamorphic minerals, although the metamorphic grade increases closer to the MCT, with tiny grains of garnet and biotite observed. These rocks are typically strongly foliated, displaying pronounced NNE mineral lineation, although this is missing in higher units, suggesting a phase of deformation prior to the deposition of the Fagfog Quartzite. Carbonates are believed to be absent except as cement material in some sandstones.

The Fagfog Quartzite (Arita *et al.*, 1973) rests over the Kuncha Formation with a sharp contact. This is a coarse to fine grained white orthoquartzite with phyllite intercalations. It displays frequently developed ripple marks and current bedding.

1.3.3.2. The Nawakot Group.

Overlying the Fagfog Quartzite is the Dandagaon Phyllite, distinctly darker than the Fagfog Quartzite and marking the first appearance of laminated calc-phyllites and thin dolomite bands. This unit passes up into the Nourpul Formation, which has a mixed lithology of slate and calcareous metasandstones with intercalated thicker quartzites. The overlying rock is the stromatolitic Dhading Dolomite, a massive to thick-bedded sequence of finely crystalline to micritic dolomite interbedded with black slates.

In the type locality the Benighat Slates overlies the Dhading Dolomite with a sharp contact which is possibly an erosional unconformity, although no angularity is seen in the contact at the outcrop scale (Stöcklin, 1980). The Benighat Slates consist of dark, soft slates and phyllites which contain a great deal of graphitic matter (up to 30-40%, Upreti and Rai, 2000). There are frequent intercalations of calc-phyllite, limestone and dolomite known as the Jhiku beds, which are difficult to distinguish in appearance from the rest of the unit. Conformably overlying the Benighat Slates is the Malekhu Limestone, the lower and upper parts of which comprise platy, yellow, dense, siliceous limestone beds with sericitic partings. The middle part of the unit is thicker, more thickly bedded and dolomitic. The overlying Robang Formation is predominantly

comprised of sericite-chlorite phyllites with prominent quartzites in the lower part. Chloritic and amphibolitic metadiabases showing synsedimentary relationships and intrusive gabbroic or dioritic bodies are present in this unit.

1.3.3.3. Lesser Himalayan Augen Gneisses.

First identified by Le Fort (1975a, b) and Pêcher and Le Fort (1977), these rocks are referred to in this work as the Lesser Himalayan Crystallines. They most commonly occur in the upper part of the Kuncha Formation (Stöcklin, 1980), although they are also noted within the units of the Nawakot Group (Amatya *et al.*, 1994; Rai, 1998; Upreti 1999). Rb-Sr isotopes suggest ages of ~1800 Ma (Trivedi *et al.*, 1983). Field evidence clearly indicates (Le Fort, 1975a, b; Stöcklin, 1980; Upreti, 1999) that the gneisses grade into and interlayer the low grade country rocks, precluding the possibility of the gneisses being thrust bound (e.g. Heim and Gansser, 1939; Gansser, 1964; Arita, 1983; Maruo and Kizaki, 1983). The gneisses are strongly foliated with a streaky appearance resulting from mineral lineation, a texture interpreted by Upreti (1999) as the result of strong deformation of the protolith, which probably consisted of either granite or siliceous volcanics, at a low temperature (300-350°C). It is believed that this temperature was no different from that pertaining during deformation of the surrounding metasedimentary country rocks, the differing physical properties of the metasediments and gneisses leading to the marked textural contrasts. The augen gneisses outcrop throughout Nepal but are most extensive in the tectonic windows of central and eastern Nepal (see plate 6), the largest exposures being in the Chautara-Ramechap-Okhadhunga tectonic window

where the gneisses are 2 km thick and extend for nearly 100 km (named the Melung-Salleri augen gneiss by Upreti, 1999).

1.3.4. Crystalline Nappes.

A large number of crystalline nappes and klippen are recognised throughout the Himalaya, five of which occur in Nepal (Upreti and Le Fort, 1999). Of these, the Karnali Nappe in the west consists of high grade gneisses (Hayashi *et al.*, 1984) and, as with the large thrust sheet that covers most of eastern Nepal, has a root zone clearly located within the HHCS. The other four nappes have a rather different geology, whilst their origin is debatable. Of these, the Kathmandu Nappe (see plate 6), first recognised by Hagen (1969) and mapped in detail by Stöcklin (1980) and Stöcklin and Bhattarai (1980), is of particular interest in this study, forming a component of the bedrock in some sampled catchments. The Mahabharat Thrust (MT) separates the crystalline rocks of the Kathmandu Nappe from the underlying metasediments of the Lesser Himalaya, and it is suggested that this fault is a direct continuation of the MCT (Stöcklin 1980; Pêcher and Le Fort, 1986; Pandey *et al.*, 1995), although this is debatable (Upreti and Le Fort, 1999; Upreti, 1999). The Kathmandu Nappe is preserved in the Mahabharat Range as an east-west synclinal structure (Mahabharat Syncline). The syncline is flanked by a series of folds both to the south and north of its axial trace, and it is these folds that give the nappe its oval shape in outcrop, with Kathmandu itself at the centre (Kumar, 1980). The geology of the nappe consists of the relatively high grade Bhimphedi Group, intruded by granites, and the unmetamorphosed to weakly metamorphosed Pulchowki

Group. Similar geology is noted in the remaining three Nepalese crystalline nappes; the Jajarkot Nappe, Parchauni Nappe and Dadeldhura Nappe (Fuchs and Frank, 1970; Stöcklin, 1980; Sharma *et al.*, 1984; Shrestha *et al.*, 1993; Upreti, 1996).

Three suggestions have been put forward to answer the question of the position of the root zones of the Kathmandu and other similar nappes. It was originally suggested (Hagen, 1969; Le Fort, 1975 a, b; Stöcklin, 1980) that the roots are located in the HHCS, the evidence for this being the crystalline nature of the Bhimphedi Group and the fact that no rocks comparable with those of the nappes are exposed between the nappe and the HHCS. In this interpretation, the rocks of the Pulchowki Group are regarded as belonging to the TSS. The main problem with this hypothesis is that the rocks of the HHCS were metamorphosed at temperatures and pressures greater than those of the Bhimphedi group (Rai *et al.*, 1998). A second suggestion is that the root zone lies in the MCT zone at the very top of the Lesser Himalaya (Fuchs and Frank, 1970; Arita *et al.*, 1974a, b), rocks of which are of the same metamorphic grade as those of the nappe. This second possibility seems unlikely as the rocks of the nappes have a lithology and stratigraphy very different from those of the MCT zone and do not display the same inverted metamorphic sequence, while the granites present in the nappe are not a feature of the MCT zone. More recent work (Upreti and Le Fort, 1999; Upreti, 1999) proposes that the rocks of the Kathmandu Nappe in particular actually belong to an intermediate zone of deposition between that of the Tibetan Sedimentary Series to the north and the Lesser Himalaya to the south, metamorphosed only to lower amphibolite facies in comparison with the upper amphibolite to granulite facies further north, owing to a

reduced overburden. The Mahabharat Thrust would then have carried the Bhimphedi Group rocks to their current position overlying the Lesser Himalaya. This interpretation requires splitting the original Kathmandu Nappe into two, the Kathmandu Nappe in the south and a separate Gosainkund Nappe to the north with its root in the HHCS. Isotopic analyses of rocks from the Kathmandu Nappe collected during this work might contribute some further evidence to this ongoing debate.

1.3.4.1. The Bhimphedi Group.

The lower Bhimphedi Group consists of about 10.5 km of Late Precambrian rock. The metasediments show a steady decrease in metamorphic grade from garnet amphibole grade to sericite-chlorite grade. The lowest formation is the Raduwa Formation, consisting of coarsely crystalline garnetiferous two-mica schists with quartzite intercalations. Chlorite schists are present close to the Mahabharat Thrust. A transitional contact is observed with the overlying 800m thick Bhainsedobhan Marble (Nagdir *et al.*, 1968-1973), a coarsely crystalline, well-bedded to massive white marble in which mica content increases towards the top and bottom of the unit (Kumar, 1980). There is a transitional contact with the 2000 m thick Kalitar Formation which lies above the marble. This is composed of biotite and biotite-muscovite schists, although garnet and amphibole are present in the lower part, with intercalations of quartzite and conglomerate. The overlying 400-500 m thick Chisapani Quartzite (Joshi, 1973) is a white, fine-grained orthoquartzite, noted as a good marker horizon (Upreti and Rai, 2000). There is a rapid transition to the Kulikhani Formation, comprising fine-grained

biotite schist and impure, strongly micaceous quartzite. The Markhu Formation (Joshi, 1973) is the youngest formation of the Bhimphedi Group, with a mixed lithology consisting of schists, quartzites and marbles, of which the latter predominate. Thickness is in the order of 1000 m but is greatly reduced in places.

1.3.4.2. The Pulchowki Group.

The Bhimphedi group passes into the 5-6 km thick Pulchowki Group without a significant sedimentation break, although there is a sharp metamorphic break across the contact (Kumar, 1980), and the presence of an unconformity is possible (Stöcklin, 1980). The lowermost unit is the Tistung Formation, a clastic sequence of metasandstones, siltstones and phyllites with occasional limestone intercalations. Metamorphic minerals are sericite and chlorite in the main part of the unit, although biotite is present in the lower part. The overlying Sopyang Formation comprises slates and subordinate argillaceous limestones, acting as a transitional zone into the Chandragiri Limestone (Auden, 1935), a 2000 m thickness of argillaceous limestone with a white, laminated quartzite interbedded in its upper third. The overlying Chitlang Formation (Hagen, 1969) consists predominantly of slate, with a white quartzite interbedded in its lower part and some argillaceous limestones appearing towards the top of the unit. The core of the Mahabharat Syncline is composed of the Top Limestone.

1.3.4.3. Granites of the Kathmandu Nappe.

A number of lensoid biotite-rich or tourmaline-rich granitic bodies are present in the Kathmandu Nappe and other crystalline nappes. These bodies intrude the Bhimphedi group and Titsung Formation of the Pulchowki group, but not the younger Pulchowki Formations. Contacts with the country rock are mostly discordant, cutting across bedding and schistosity planes, truncating folds and faults (Upreti and Rai, 2000). The age of the Palung-Simchar granite has been determined as 470 ±4 to 493 ±11 Ma (Schäerer and Allègre, 1983; Le Fort *et al.*, 1983). The granites have a similar mineral composition to associated gneisses with which they appear to be genetically related (Stöcklin, 1980). Since Cambro-Ordovician granite gneisses are characteristic of the HHCS these ages suggest correlation with the HHCS rather than the LHF where granite gneiss ages are ~1800 Ma.

In this study, only the rocks of Bhimphedi Group are exposed in sampled catchments, and even these are of minor importance in terms of catchment coverage. Owing to chemical similarities, these rocks are classified as part of the HHCS, and are shown as such on plates 2, 3, 6 and 7. The units of the Pulchowki Group, which do not share the chemical characteristics of the HHCS, are shown separately on plates 6 and 7.

1.3.5. The Churia (Siwalik) Group.

These Himalayan foreland basin fluvial sediments have been dated paleomagnetically at ~14 - <2 Ma (Tokuoka *et al.*, 1986; DeCelles *et al.*, 1998). They form the Churia Hills, the southernmost range of Nepal. The rocks of the Churia Group have a northward dip of varying angles with an overall E-W strike, and are divided into three parts;

(i). Lower Churia; Composed of alterations of mudstones, siltstones and shales with subordinate fine-grained sandstone.

(ii). Middle Churia; Marked by the appearance of thick (several to tens of metres) sandstones, alternating with subordinate mudstones. Biotite is abundant in the sands in addition to feldspar and quartz. Fining-up cycles are present from coarse sandstone to clay, with the clays preserving plants and, locally, freshwater molluscs.

(iii). Upper Churia; Characterised by coarse-grained units such as boulder conglomerates with minor mudstone intercalations.

In addition to the MBT and MFT, which form the boundaries of this tectonic unit, a number of E-W intra-Churia thrusts (Herail *et al.*, 1986; Tokuoka *et al.*, 1986; Mugnier *et al.*, 1999) are noted. These thrusts, which cause the Churia Units to repeat throughout the zone, are believed to be shallow, joining the Main Himalayan Thrust below the Himalaya (the Main Himalayan Thrust is an unexposed low-angle décollement which

the MCT also joins, see fig. 1.1). The Churia Group sediments rest on older rocks belonging to Peninsular India.

1.3.6. Recent (Terai) Alluvium.

In Nepal, the Terai Plain gradually rises from an altitude of about 100 m in the south to 200 m in the north. Representing the northern edge of the Indo-Gangetic alluvial basin, it comprises Pleistocene – Recent alluvium with an average thickness of ~1500 m. Coarser units forming large alluvial fans lie closer to the mountain front while finer sediments occur in the south. Blind thrusts and thrust-propagated folds beneath these sediments are the result of a significant proportion of current Himalayan stress accumulating in this region.

1.4. The Himalayan Weathering Environment.

The weathering of bedrock consists of two principal processes. Physical denudation is the physical breakdown of rock into smaller particles, providing the suspended and bedload of rivers. Chemical weathering is the dissolution of bedrock (or suspended and bedload) minerals by ground or river water. The weathering agent most often involved is carbonic acid, which is formed by the dissolution of atmospheric, soil or metamorphic CO_2 in water. Different rock types chemically weather at different rates. Meybeck (1987) devised a scale of relative chemical weathering on the continents, from 1 for the most resistant rocks (granite and gneiss) to 12 for limestones and 80 for evaporites.

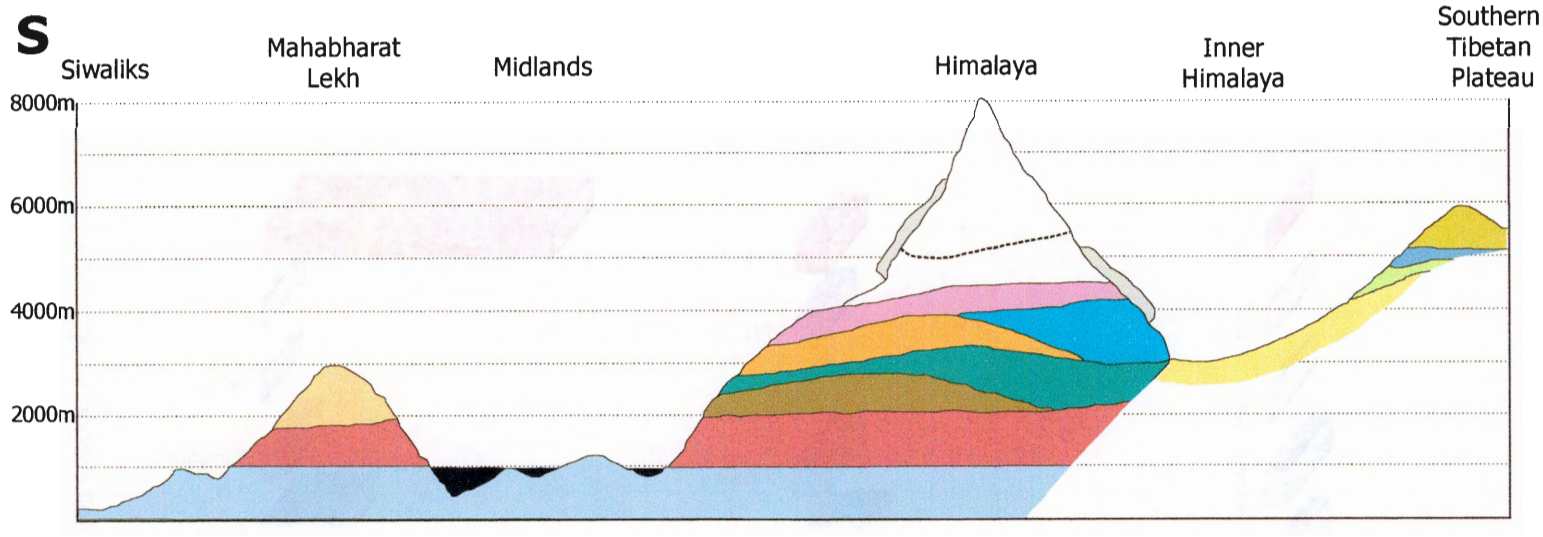

Fig. 1.4. Generalised altitudinal variation in the Himlayan region.

Source; Hagen, 1980

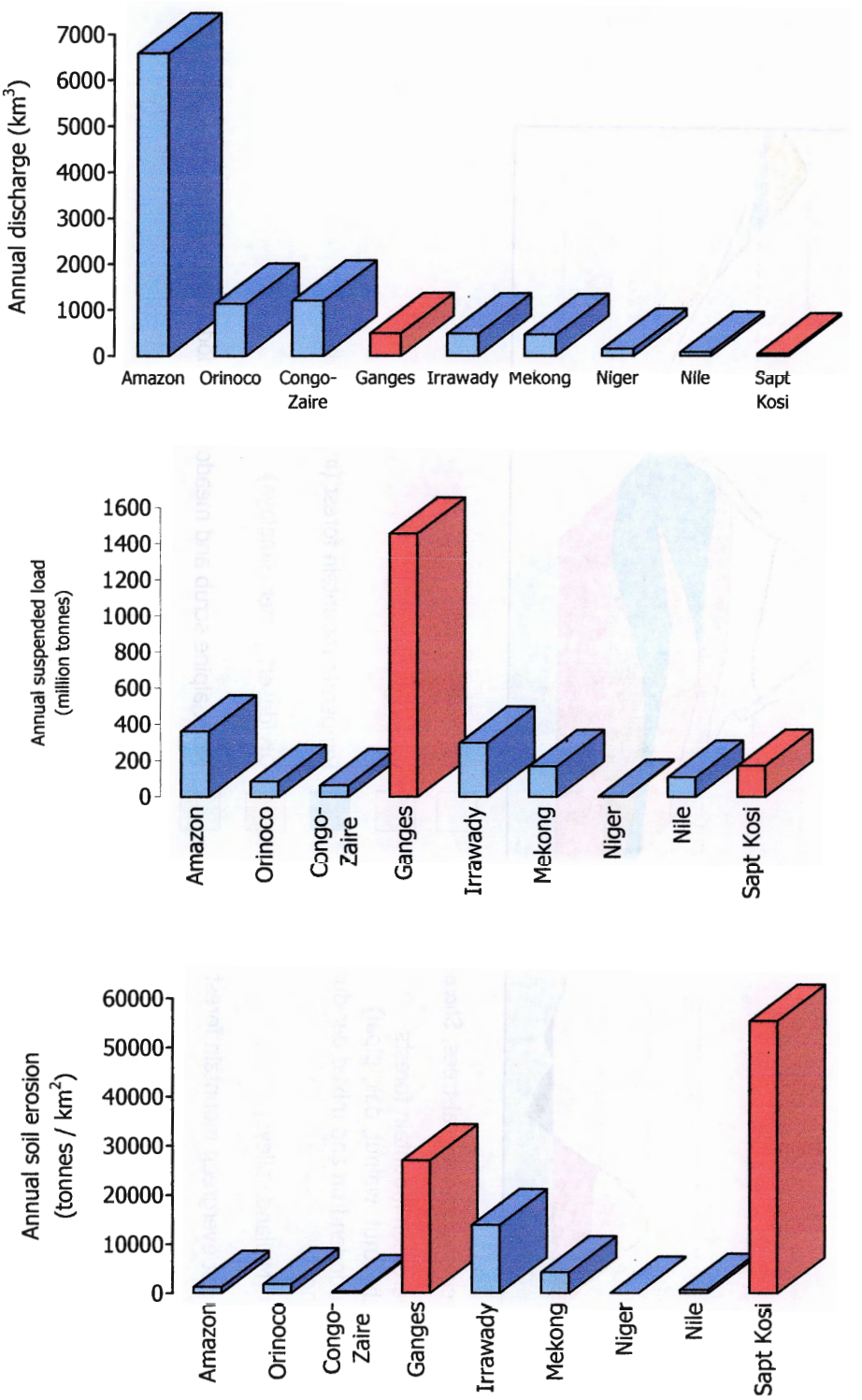

Fig. 1.5. Annual discharge, suspended load and soil erosion in eight major world rivers and a major Gangetic tributary.

Data sources; Alford, 1992; Pandey *et al*., 1994; Tejwani, 1996; Meybeck and Ragu, 1997

Carbonate and evaporite weathering is largely congruent (although incongruent carbonate weathering occurs in glacial terrains: Fairchild *et al.*, 1994; Fairchild and Killawee, 1995), and leaves little or no physical trace (Derry and France-Lanord, 1997), while silicate weathering is usually incongruent, with different minerals weathering at different rates.

Nd and Sr-isotope data from Bengal Fan sediments reveal that the suspended load of the Ganges-Brahmaputra, both today and in the past 20Ma, is dominated by material from the High Himalayan Crystalline Series (>80%, France-Lanord *et al.*, 1993, Galy *et al.*, 1996). This is because it is in the physiographic high Himalaya (occupied predominantly by rocks of the HHCS) that physical denudation is at its highest owing to steep relief, the presence of only sparse vegetation (fig. 1.4), the prominence of periglacial-glacial processes and heavy monsoon precipitation. Soils are thin, supporting only subalpine forests in the lower reaches of the zone (fig. 1.4), with the upper reaches a permanent Arctic desert, much of it above the permanent snowline. These conditions mean that new mineral surfaces are constantly being exposed, but the low residence time of the secondary products of weathering means that the chemical weathering of minerals is less intense. This is known as a weathering-limited regime.

The huge sediment load carried by Himalayan rivers, particularly the Ganges, reflects this dominance of physical erosion on the Himalayan scale. Fig. 1.5 shows discharge and sediment load plotted for eight of the world's largest rivers, including the Ganges,

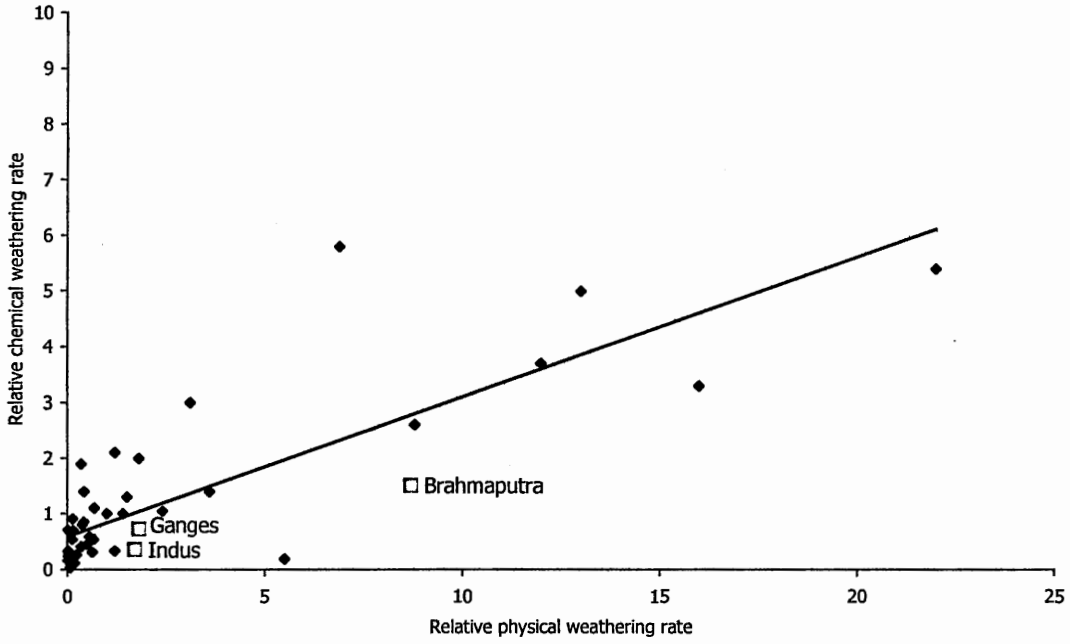

Fig. 1.6. Relative physical and chemical silicate weathering rates (normalised to the value for the Amazon) for 51 of the world's 60 largest rivers. Source; Gaillardet *et al.* (1999).

and also the Sapt Kosi, a major Himalayan tributary of the Ganges sampled during this study. The discharge of the Amazon is five times that of the Ganges, yet the Ganges carries four times more sediment annually to the Bay of Bengal that the Amazon does to the North Atlantic, more than any other river on the planet. Annual soil erosion per unit area (fig. 1.5) is an order of magnitude higher in the Ganges than in the Amazon, and twice that of the next highest river, the Irrawady. That this erosion is occurring in the Himalayan range, rather than the floodplain, is illustrated by the extremely high soil erosion rates in the Sapt Kosi. Fig. 1.6 shows relative chemical and physical silicate weathering rates for 51 of the 60 largest rivers in the world, calculated relative to the

Amazon by Gaillardet *et al.* (1999), again revealing the dominance of physical erosion in the Himalaya.

In the lower altitudes of the Ganges-Brahmaputra, mostly within the Lesser Himalaya, physical denudation is lower. The result of this is that excess soil formation is the factor acting to limit bedrock weathering (a transport-limited regime). Chemical weathering in this part of the basin is much higher, temperatures in the Lesser Himalaya being as much as 20°C higher than on the Tibetan Plateau and in the high Himalaya, a difference that can result in a sevenfold increase in dissolution rate (Lasaga *et al.*, 1994). Additionally, soil formation (Dhar *et al.*, 1988; Gardner and Walsh, 1996), aids chemical weathering, particularly through the presence of vegetation (temperate and tropical moist forests, see fig. 1.4), which increases (particularly silicate) weathering in the following ways;

(i). The secretion of organic acids and chelates by plants around their roots (in order to obtain nutrients from silicate minerals).

(ii). The production of an organic litter which decomposes producing organic acids and carbonic acid.

(iii). Plants anchor clay-rich soil against erosion, thereby allowing continued weathering of primary silicate minerals in-between rainfall episodes.

Berner (1995) shows that the presence of trees accelerates silicate erosion rates by 2-10 times. Galy and France-Lanord (1999) estimate the rate of chemical weathering on the southern Himalayan slopes to be 0.005 mm/yr for silicates and 0.06 mm/yr for carbonates. It is expected that rates will be higher than this average in the Lesser Himalaya, lower at higher altitudes in the High Himalayan Crystalline Series.

Rivers flowing from north of the Himalayan range, including the upper reaches of the Marsyandi, Bheri and Kali Gandaki (Galy and France-Lanord, 1999) and headwaters in the Garhwal Himalaya (Sarin *et al.*, 1992; Hasnain and Thayyen, 1996) are characterised by high SO_4^{2-} concentrations. This might result from either the dissolution of $CaSO_4$ minerals in evaporites or from the oxidation of sulphide minerals. High Cl^- concentrations (Galy *et al.*, 1999) and the presence of pyrite is TSS sediments (Bordet *et al.* 1971) suggests that both processes are potentially important, although there is no correlation between $[Cl^-]$ and $[SO_4^{2-}]$ (Galy *et al.*, 1999) suggesting that the latter is in fact the principal source of SO_4^{2-}. The formation of sulphuric acid in the process of sulphide oxidation can enhance rates of weathering to the north of the Himalaya where conditions are otherwise unfavourable for weathering owing to low precipitation levels, little soil development and low temperatures. This is reflected in the lack of vegetation, only alpine scrubland occurring between the desert climates of the "Inner Himalaya", immediately in the rainshadow of the main range, and the Tibetan Plateau (fig. 1.4). Estimated chemical erosion (Galy and France-Lanord, 1999) in the region is 0.02 – 0.05 mm/yr (Galy and France-Lanord 1999), still relatively low for carbonate rich basins. A significant role for sulphuric acid and for carbonic acid formed from metamorphic (rather than atmospheric) CO_2 might limit the long-term climatic impact of weathering in such basins (see section 1.5.2).

The Ganges-Brahmaputra floodplain consists of flat soils and alluvial material, through which groundwater circulates, and experiences heavy monsoon rainfall and high temperatures. Despite these favourable conditions, chemical weathering on the

floodplain is less than that in the Himalaya (Galy and France-Lanord, 1999), these authors estimating the silicate and carbonate chemical erosion rates for the flood plain at 0.001 and 0.004 mm/yr respectively, slightly higher for the Gomti River, which drains only the floodplain (0.003 and 0.009 mm/yr; Subramanian *et al.*, 1987; Sarin *et al.*, 1989). This may be the result of dry conditions prevailing outside of the peak monsoon months and the lack of carbonate material available for dissolution.

1.5. The Himalaya and Cenozoic Climate Change.

1.5.1. Temperature Change in the Cenozoic.

Oxygen isotope records of benthic foraminifera record ocean bottom water temperatures and ice volume, both of which reflect high-latitude surface temperatures. This record reveals that paleotemperatures were at their highest 55 million years ago, and have declined, albeit unevenly, 12 – 15 °C to the present (Miller *et al.* 1987; Zachos *et al.*, 1994), with the most rapid period of cooling occurring between 15 and 2 Ma. Atmospheric CO_2 content is the major factor determining the temperature of the atmosphere, and consequently that of the surface of the Earth and the oceans, and the Cenozoic is therefore likely to have been a period of declining atmospheric pCO_2. The relationship between paleotemperature and paleo-pCO_2 is poorly documented, although McCauley and DePaolo (1997) have attempted to interpret the $\delta^{18}O$ record as an estimate of the relative change in atmospheric CO_2 over time (fig. 1.7). This is done by using the exponential scaling function shown below (equation 1.1) assuming a 5°C

Fig. 1.7. Changes in marine $^{87}Sr/^{86}Sr$ ratios and atmospheric pCO_2 over the last 70 million years.

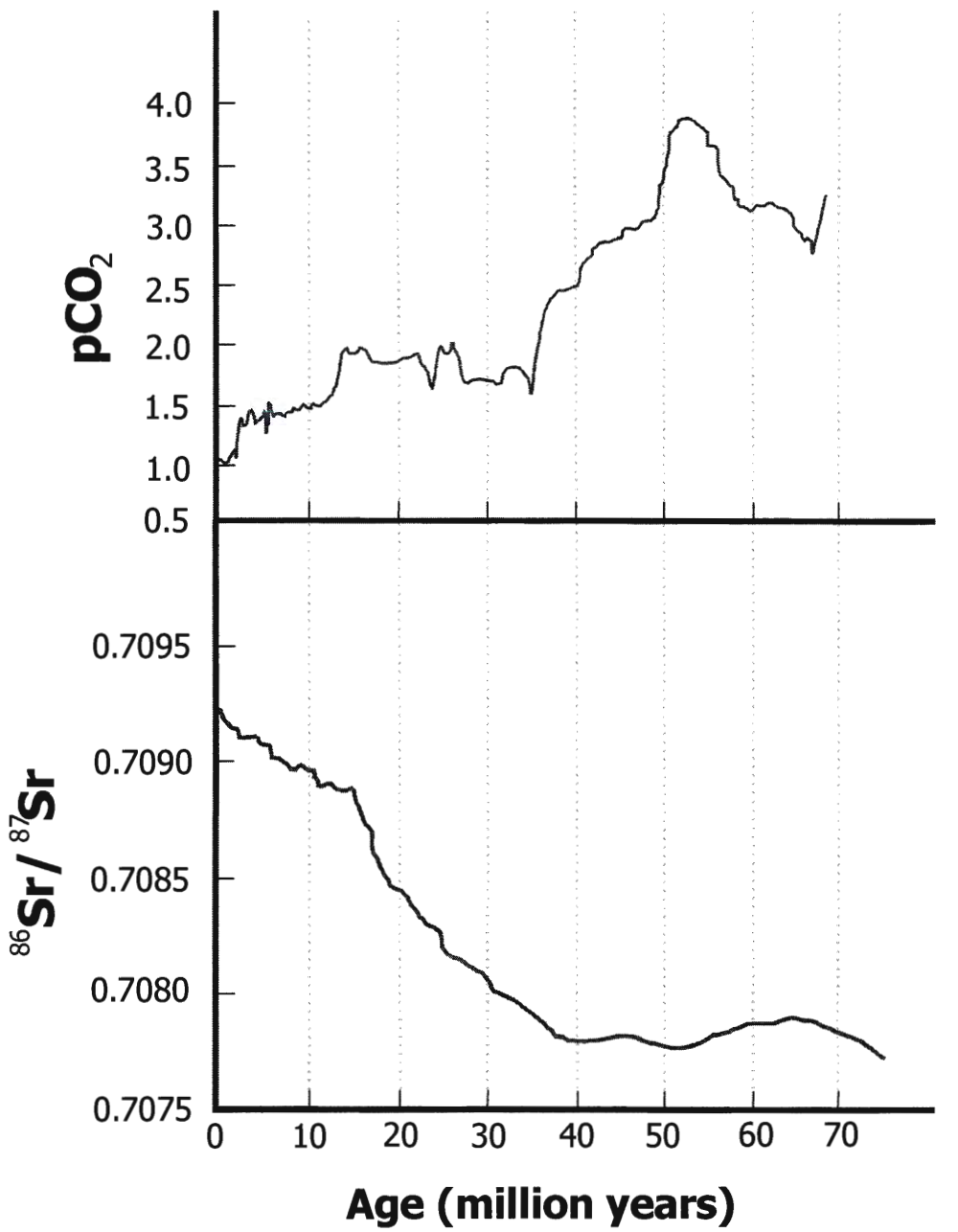

Data sources;
$^{87}Sr/^{86}Sr$: DePaolo (1985, 1986); Hess *et al.* (1986, 1991); Richter and DePaolo (1987, 1988); Farrell *et al.* (1995).
pCO2: Calculated by McCauley and DePaulo (1997) from the $\delta^{18}O$ record of Miller *et al.* (1987).

change in high-latitude temperature change per doubling of CO_2 to achieve a fourfold pCO_2 increase to account for the Paleocene temperature maximum when temperatures were at least 10°C warmer than present.

Equation 1.1.

$$R_{atm} = \frac{pCO_2(t)}{pCO_2(0)} = 1.4^{[\delta^{18}O(0) - \delta^{18}O(t)]}$$

1.5.2. The Effect of Himalayan Uplift on Atmospheric CO_2.

The Himalayan uplift has physically affected climate through the creation of a large elevated surface (the Tibetan Plateau) at upper atmospheric levels, which diverted and amplified jet stream meanders, while the presence of the high mountain range caused an intensification of the South Asian monsoon (Birchfield and Weertman, 1983; Ruddiman *et al.*, 1986; Ruddiman *et al.*, 1989; Kutzbach *et al.*, 1989; Ruddiman and Kutzbach, 1989). A potentially more extensive effect of the Himalayan Orogeny on climate is its impact on the carbon cycle.

Geological processes control the addition and removal of CO_2 from the atmosphere on a million-year timescale (Berner and Berner, 1997). CO_2 is added to the atmosphere through degassing by midocean ridge volcanism, plume volcanism, subduction zone volcanism, thermal metamorphism of carbonates, the diagenetic breakdown of organic

matter and $CaCO_3$ in the deep burial of sediments and the continental oxidative weathering of kerogen in shales. CO_2 is removed via the burial of organic matter in sediments, the weathering of Ca and Mg silicate minerals on the continents and possibly through the low-temperature alteration of submarine basalt. Work by France-Lanord and Derry (1997) demonstrates that Himalayan uplift may have had a significant effect upon CO_2 consequent from the net burial of organic carbon, but it is the effect of the orogeny on silicate weathering which is of interest in this study.

CO_2 from the atmosphere combines with groundwater supplied by rainfall to form carbonic acid (H_2CO_3) which attacks both silicate and carbonate rocks by hydrolysis.

Equation 1.1. Formation of carbonic acid;

$$CO_2 + H_2O \Leftrightarrow H_2CO_3$$

Silicate weathering at low temperatures involves the formation of clay minerals from primary silicate (equation 1.2). In this process, Ca^{2+} (or Mg^{2+}) and HCO_3^- are carried in solution by rivers to the ocean, where the ions are ultimately buried as Ca and Mg carbonate minerals (equation 1.3), returning 1 mol of CO_2 to the atmosphere. The net result of this process is the sequestration of 1 mol of CO_2 for every 2 mol of CO_2 consumed from the atmosphere.

Equation 1.2. Weathering of alkaline earth silicate minerals;

$$CaAl_2Si_2O_8 + 2CO_2 + 3H_2O \Rightarrow Al_2Si_2O_5(OH_4) + Ca^{2+} + 2HCO_3^-$$

Equation 1.3. Calcite precipitation in oceans;

$$Ca^{2+} + 2HCO_3^- \Rightarrow CaCO_3 + CO_2 + H_2O$$

Na^+ and K^+ silicate minerals undergo similar weathering reactions, as shown in equation 1.4. The overall effect on atmospheric CO_2 of the weathering of K^+ and Na^+ silicates is unclear, however, as alkalis are involved in "reverse weathering" reactions in the oceans, leading to the formation of Na and K silicates, converting HCO_3^- to CO_2 that returns to the atmosphere (Gaillardet, 1999).

Equation 1.4. Weathering of alkali silicate minerals;

$$2NaAlSi_3O_8 + 2CO_2 + 6H_2O \Rightarrow Al_2Si_4O_{10}(OH)_2 + 2Na^+ + 2HCO_3^- + 2H_4SiO_4$$

Carbonates do not affect CO_2 levels on a multimillion-year timescale as CO_2 consumed during carbonate weathering (equation 1.5) is returned through carbonate precipitation in the oceans (equation 1.3) (Berner, 1991).

Equation 1.5. Calcite dissolution on the continents;

$$H_2CO_3 + CaCO_3 \Rightarrow Ca^{2+} + 2HCO_3^-$$

As established in section 1.4, high runoff and vigorous physical erosion in the high Himalaya (as in any orogenic belt) generates a large volume of unweathered bedrock (Stallard and Edmond, 1983) in a highly pulverised form that promotes chemical weathering in the wet environment downstream (the Lesser Himalaya, floodplain and delta). Thus, the uplift of the Himalaya could potentially increase rates of removal of CO_2 from the atmosphere through the increased weathering of silicate minerals (Raymo *et al.*, 1988; Raymo and Ruddiman, 1992).

1.5.3. Theories to Explain Long-term Climate Change.

Until 1988 the leading theory to explain long-term climate change was the BLAG hypothesis (Berner *et al.*, 1983). The BLAG hypothesis assumes that mean global rates of seafloor spreading and subduction are the main controls on CO_2 delivery to the atmosphere (through metamorphism and volcanic degassing) and the primary driver of atmospheric CO_2 changes over time. In this hypothesis chemical weathering acts as a negative feedback to keep the climate in near-equilibrium. Thus, if faster spreading delivers increased CO_2, the earth is warmed, which speeds up chemical weathering through increased water vapour and vegetation levels. This in turn increases the rate of

global silicate chemical weathering (i.e. CO_2 drawdown), offsetting the increased spreading-generated CO_2 and maintaining a steady state.

When the CO_2 curves produced by the original BLAG model are compared with the benthic $\delta^{18}O$ record, both indeed show an overall trend towards cooler modern conditions. The BLAG model predicts a relatively cool episode in the early Eocene and a late Eocene peak in temperature, however, features which are not reflected in the oxygen isotope record. Major climate shifts in the 15-2 Ma period noted in the oxygen isotope record are also nowhere to be seen (McCauley and DePaulo, 1997) in BLAG predictions. A 1994 version of the BLAG model (GEOCARB II; Berner, 1994), using updated seafloor spreading rate data (Engebretson *et al.*, 1992) produces a far better fit, predicting the peak temperatures of the Eocene, cooling after 50 Ma, Oligocene moderation and cooling in the Miocene. This evidence suggests that changes in seafloor generation can account for some of the major changes in the Cenozoic climate record.

The Raymo-Ruddiman hypotheses (Raymo *et al.*, 1988; Raymo, 1991; Raymo and Ruddiman, 1992) elevates silicate weathering from a weak negative feedback to the major factor reducing long term CO_2 levels and thus controlling global climate, challenging the idea that climate is largely determined by the seafloor generation rate. This theory states that CO_2 levels in the atmosphere respond to the amount of chemical weathering taking place, which in turn can be stimulated by continental orogeny. Raymo and Ruddiman (1992) suggest that for the past 40 Ma both global CO_2 degassing and CO_2 consumption by mountain uplift have increased, the latter at a faster rate. Carbon

mass balance could be then achieved through a decrease in atmospheric CO_2 with its decelerating effect on weathering rates balancing the uplift effect. This allows for a higher weathering flux accompanied by a lowering of atmospheric CO_2. Less weight is given to temperature and pCO_2 as controls on the global silicate weathering rate. According to the Raymo-Ruddiman hypothesis, global cooling in the last 40 Ma is the result of the increased chemical weathering consequent from the uplift of the Himalaya

The main flaw in the Raymo-Ruddiman uplift-weathering hypothesis is a lack of natural feedback process to moderate a runaway situation in which all the CO_2 in the atmosphere is removed by silicate weathering, thus freezing the Earth. The hypothesis leaves volcanic input as the strongest source of CO_2, yet there is no mechanism by which volcanic input could respond to uplift-driven CO_2 changes, and thus act as a negative feedback to stabilise atmospheric CO_2 levels. The need for any such climate-weathering feedback is refuted by Edmund *et al.* (1995), who state that atmospheric CO_2 is not manintained at a stable state, except when sufficient mountain building brings about a fall in CO_2 levels. For the period of Cenozoic global cooling and Himalayan uplift, a number of suggestions have been put forward, however, to account for the CO_2 required to prevent the occurrence of a runaway effect;

(i). The slowing of chemical weathering rates (i.e. CO_2 extraction) in areas outside those actively uplifting (Sundquist, 1991).

(ii). Reduction in sedimentary carbon burial rates (Raymo and Ruddiman, 1992; Raymo, 1994). Carbon mass balance work carried out by Derry and France-Lanord (1996b),

concludes that the organic carbon reservoir *grew* in size during the Cenozoic, casting doubt on this theory.

(iii). CO_2 release from the metamorphism of Tethyan carbonates (Kerrick and Caldeira, 1993).

(iv). Weathering of uplifted Tethyan sediments rich in organic matter (Beck *et al.*, 1995).

(v). Decoupling of the deep ocean from surface pCO_2, due to decreased vertical mixing in warmer periods. Thus, large changes predicted for bulk ocean CO_2 by models could correspond to much smaller changes in atmospheric pCO_2 (McCauley and DePaolo, 1997).

(vi) The reconstitution of cation-rich solid phases (other than $CaCO_3$) in ocean sediments ("reverse weathering") (McCauley and DePaolo, 1997).

1.5.4. The CO_2 Drawdown Potential of the Ganges-Brahmaputra.

If we are to believe the Raymo-Ruddiman weathering-uplift hypothesis it is essential that Himalayan rivers inputs can account for the Cenozoic change in atmospheric CO_2. This and previous work has concentrated on the Ganges-Brahmaputra (G-B), the rivers (together with the Indus) that drain the Himalayan range itself. It should noted, however, that Tibetan uplift, closely linked with Himalayan tectonics, has impacted upon a number of other major world rivers sourced in Tibet including the Changjiang (Yangtze), Mekong, Irrawady and Salween. Therefore, the impact of the Himalayan

uplift on climate change is potentially even greater than outlined below for the Ganges-Brahmaputra.

It is the chemical weathering of silicates that is of importance in terms of impact upon atmospheric CO_2 levels. Fig. 1.8a shows the total cationic output from silicate weathering in 52 of the world's 60 largest rivers (data are unavailable for the others), while fig. 1.8b shows total annual output of Ca^{2+} and Mg^{2+} from silicate in the same rivers (both as calculated by Gaillardet, 1999). The importance of the Ganges is clear, falling behind only the Irrawady and Amazon in terms of cation output, matching the Amazon in output of crucial alkali earth metal ions. This latter fact is reflected in fig, 1.8c which shows CO_2 consumption in the same rivers, the Ganges again second in importance after the Irrawady. The Brahmaputra and Indus are of lesser importance in terms of cation output and consequently CO_2 consumption. Taken together, however, the Ganges-Brahmaputra system accounts for 4.9% (~5% also calculated by McCauley and DePaulo, 1997) of global silicate cationic output, 6.0% of silicate Ca^{2+} and Mg^{2+} output and 6.4% of global CO_2 consumption through silicate weathering, these values increasing to 5.7%, 6.7% and 7.0% respectively if the Indus is included. It is noted by Galy and France-Lanord (1999) that a significant fraction of the cationic charge in the Himalaya is balanced by SO_4^{2-} rather than HCO_3^- and therefore plays no role in long-term CO_2 drawdown. Accounting for this, the authors estimate that the G-B system accounts for only 1.3% of long term CO_2 uptake, although the importance of weathering by sulphuric acid also needs to be apportioned in estimates of the CO_2 drawdown of

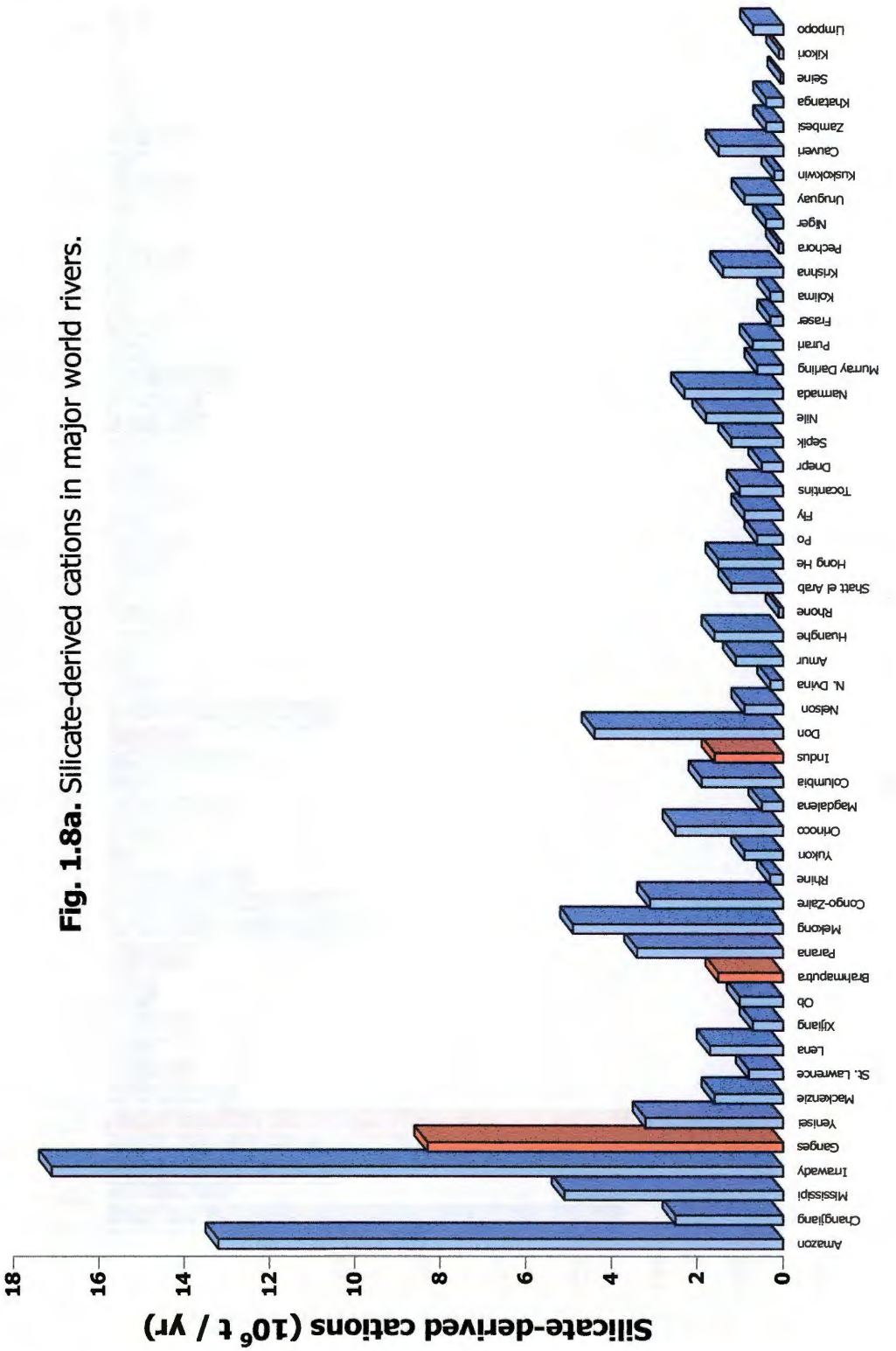

Fig. 1.8a. Silicate-derived cations in major world rivers.

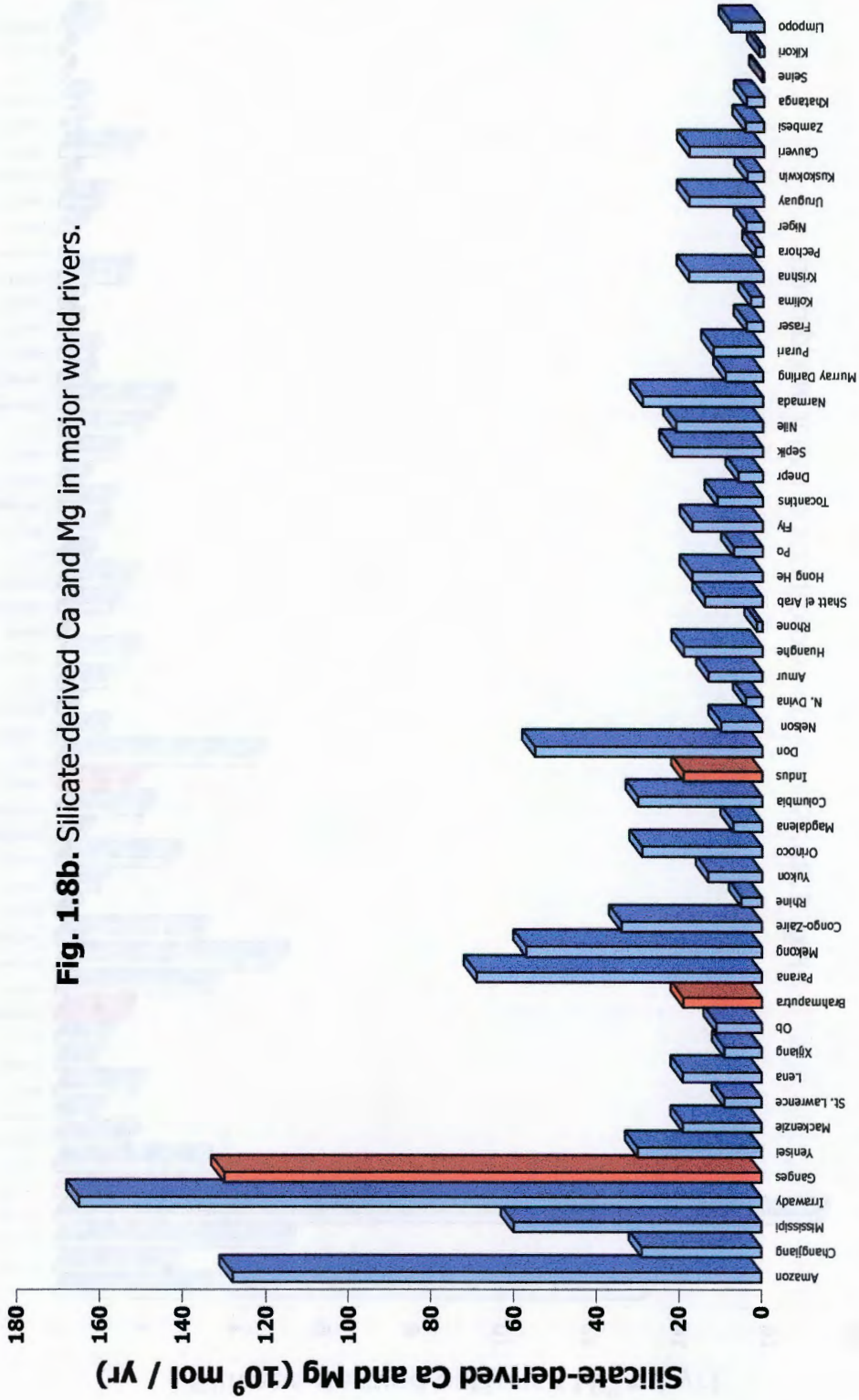

Fig. 1.8b. Silicate-derived Ca and Mg in major world rivers.

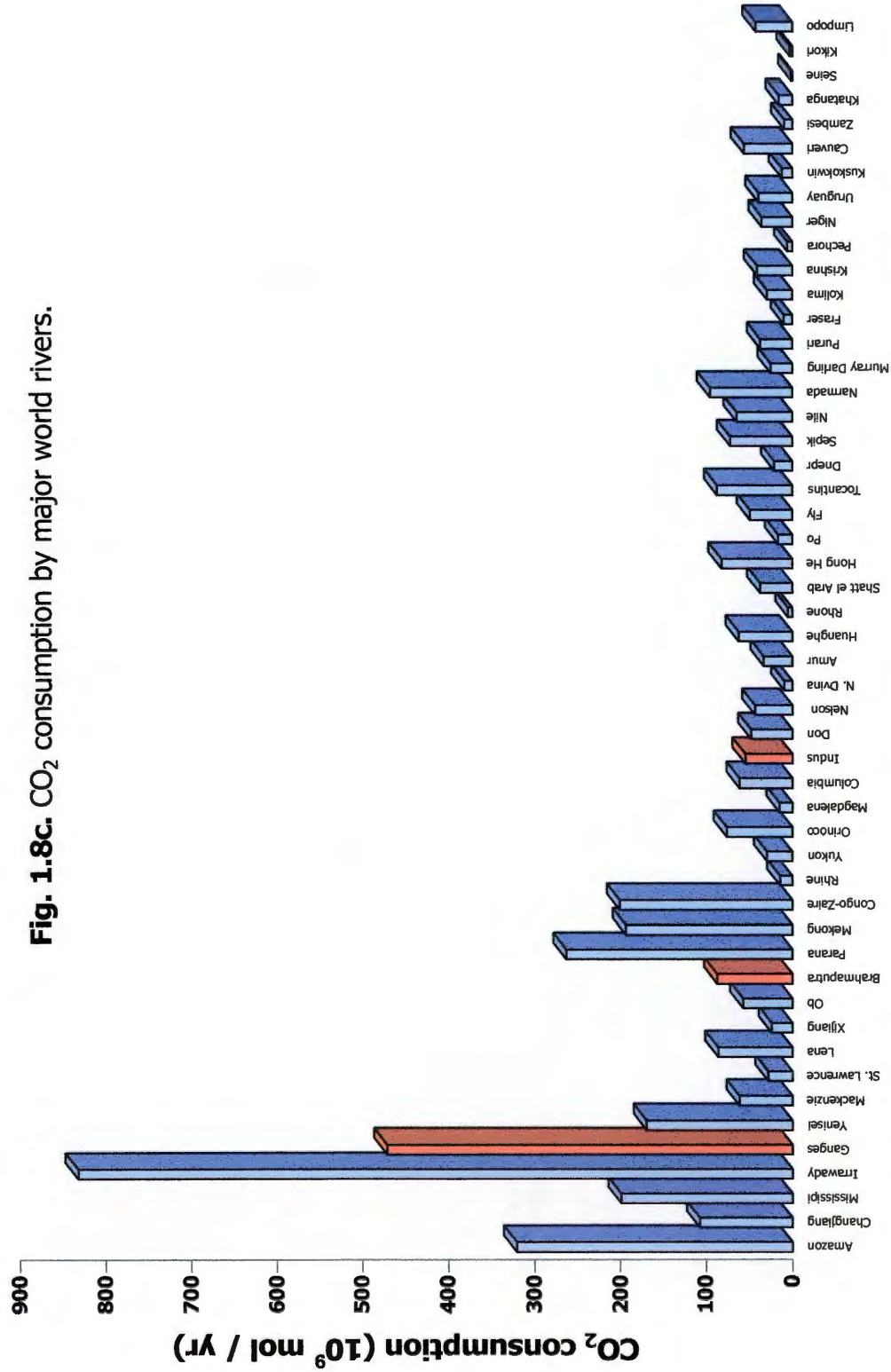

Fig. 1.8c. CO_2 consumption by major world rivers.

other major world rivers. Additionally, groundwater fluxes might increase the estimate for the Ganges-Brahmaputra considerably (Moore, 1997; Basu *et al.*, 2001).

McCauley and DePaolo (1997) construct a model to evaluate the impact of increased Cenozoic alkalinity fluxes from the Himalaya. The authors find that their reconstructed Eocene pCO_2, corresponding to the addition of 1.3×10^{19} Eq of alkalinity to the oceans in the past 40-50 Ma, is 40 times that of the modern pCO_2, and 10 times larger than their estimates of Eocene pCO_2 based on temperature changes indicated by the $\delta^{18}O$ record. In addition to the mechanisms described in section 1.5.3, which the authors believe could reduce this disparity by as much as an order of magnitude, the uncertainty associated with the calculated output of alkalinity from the G-B over the period of Himalayan uplift is considerable (~50%).

It is clear from the above summary that a great deal more work is required before we can assess the CO_2 drawdown potential of the Ganges-Brahmaputra (or any other major river) with great accuracy. It certainly seems that there are good reasons to account for the unrealistically high pCO_2 at 50 Ma required by the modelling of McCauley and DePaolo, and thus within the confines of our current knowledge (including the reduced CO_2 drawdown estimates of Galy and France-Lanord) the Raymo-Ruddiman hypothesis appears tenable.

1.6. The marine $^{87}Sr/^{86}Sr$ Record: A potential Himalayan Silicate Weathering Proxy?

When attempting to quantify the Raymo-Ruddiman hypothesis, a proxy for global silicate weathering is required. This is also required by the GEOCARB II model (Berner, 1994), which incorporates an uplift-induced silicate weathering expression. Raymo *et al.* (1988), Raymo and Ruddiman (1992) and Berner (1994) invoked the $^{87}Sr/^{86}Sr$ record in calcareous marine sediments as just such as proxy, particularly for the Cenozoic in which a steep increase in marine $^{87}Sr/^{86}Sr$ is observed (fig. 1.7). The marine Sr isotope record predominantly results from the balance of inputs to the oceans of hydrothermal fluids along midocean ridges ($^{87}Sr/^{86}Sr = 0.703$) and continental river input ($^{87}Sr/^{86}Sr = 0.71$; Palmer and Edmond, 1989). A third flux of strontium into the oceans, the redissolution of marine carbonate, is considered negligible (Richter *et al.*, 1992). Thus, an increase in marine $^{87}Sr/^{86}Sr$ will result from a decrease in the hydrothermal flux or an increased fluvial flux. Proponents of the Raymo-Ruddiman hypothesis attribute the rapid rise in marine Sr-isotope ratios in the Cenozoic to an increased fluvial flux resultant from Himalayan inputs. The rapid rise in marine Sr-isotope ratios in the Cenozoic is not a unique event, however, with several such increases noted in fig. 1.9 which cannot be linked to orogenic events, demonstrating that other controls are potentially important.

Fig. 1.9. The marine $^{87}Sr/^{86}Sr$ record over geological time.

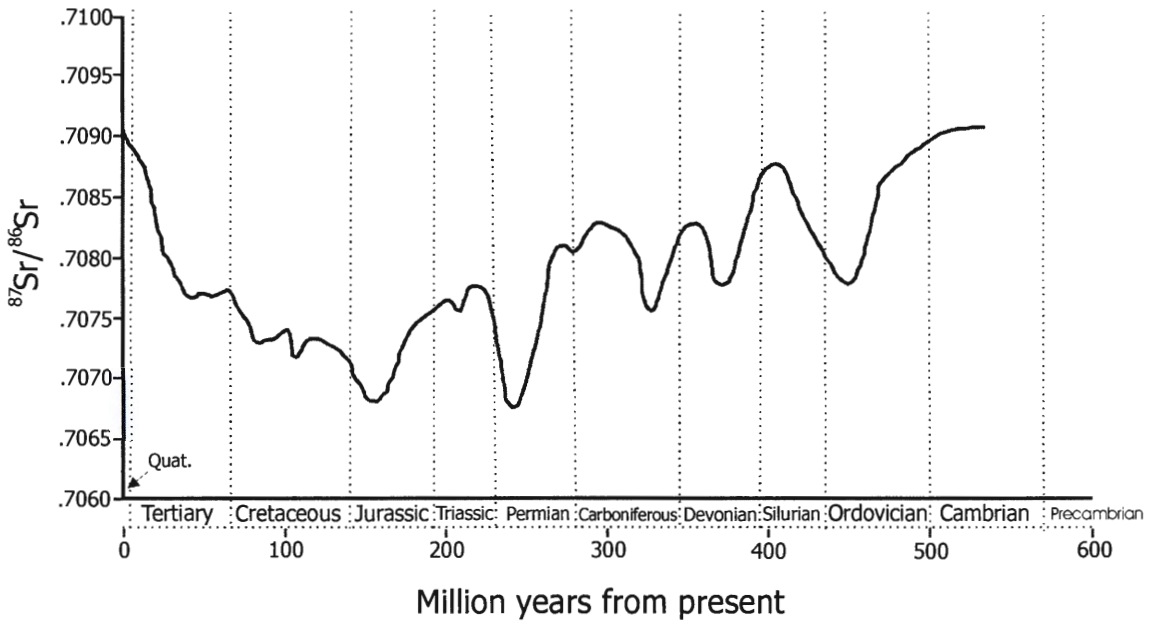

Source; DePaolo (1985, 1986); Hess *et al.* (1986, 1991); Richter and DePaolo (1987, 1988); Farrell *et al.* (1995)

Three conditions need to be met in order to demonstrate that Himalayan uplift can account for the Cenozoic changes in the marine $^{87}Sr/^{86}Sr$ curve (Richter *et al.*, 1992);

(i) The flux of Sr from the Himalaya needs to represent a significant portion of the total Sr carried to the oceans.

(ii) The timing of collision and the onset of the increase in the marine curve should be comparable.

(iii) The flux of radiogenic Sr eroded from the Himalaya must account for the increased Sr-isotope ratio required in the seawater curve.

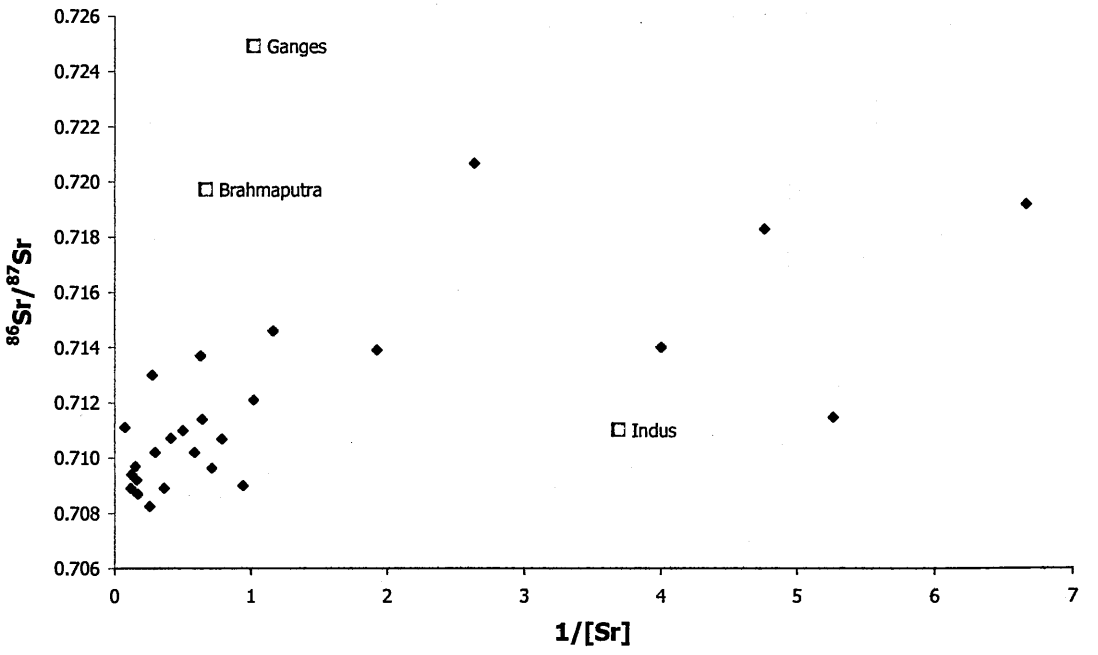

Fig. 1.10. Graph of $^{87}Sr/^{86}Sr$ vs $1/[Sr^{2+}]$ for 29 of the 60 largest rivers of the world (those for which data are available), illustrating the unique strontium chemistry of the Ganges-Brahmaputra. Sources; Stordal and Wasserburd, 1983; Wadleigh *et al.*, 1985; Palmer and Edmond, 1989; Krishnaswami *et al.*, 1992; Négrel *et al.*, 1993; Pande *et al.*, 1994; Hieronymus *et al.*, 1995; Cameron *et al.*, 1995; Douglas *et al.*, 1995; Yang *et al.*, 1996; Roy *et al.*, 1996; Gaillardet *et al.*, 1997.

Estimates of the global riverine Sr flux accounted for by the Ganges-Brahmaputra vary from 3.6% to 1.9% (Palmer and Edmond, 1989; Krishnaswami *et al.*, 1992; Galy *et al.* 1999; Basu *et al.*, 2001). Galy *et al.* (1999) demonstrate, that even with a strontium flux at the low end of this range, the Ganges-Brahmaputra has had a major control on the rate of change of the marine Sr isotope ratio in the last 50 Ma, and that the very high $^{87}Sr/^{86}Sr$ value of modern seawater is supported by the Himalayan strontium flux. This is

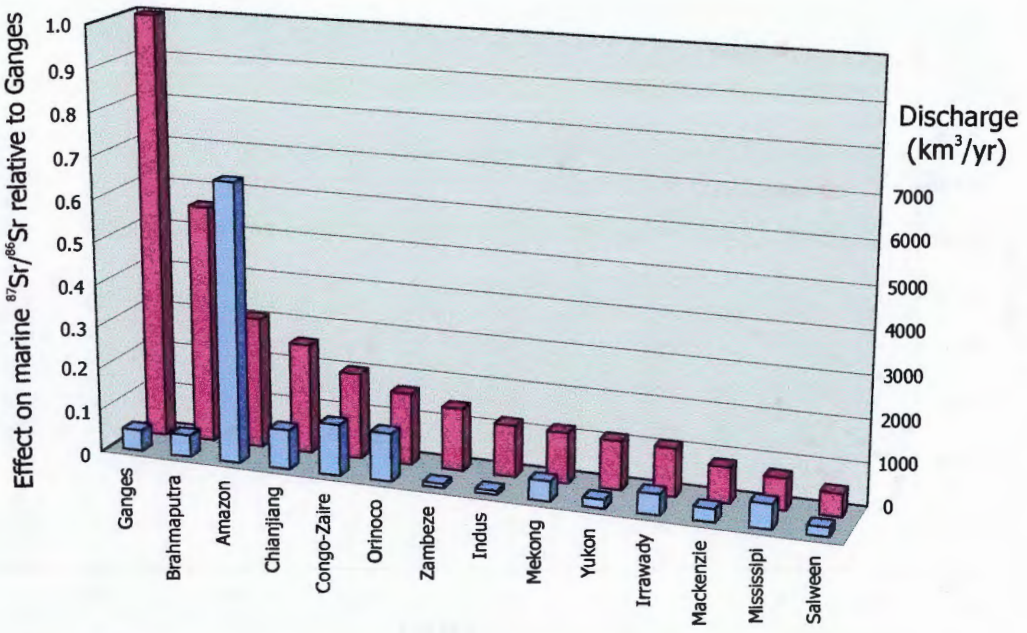

Fig. 1.11. The effect of major world rivers on marine $^{87}Sr/^{86}Sr$ (red) compared with total discharge (blue).
The effect of each river on seawater $^{87}Sr/^{86}Sr$, calculated from the Sr flux and isoptic ratio, is normalised to that of the Ganges (source; Harris, 2000). Discharge data are from Pande *et al.* (1994) and Meybeck and Ragu (1997)

because of the strontium chemistry of the Ganges-Brahmaputra (not the Indus, however), unique amongst major world rivers, with radiogenic Sr-isotope ratios combined with relatively high Sr^{2+} concentrations (fig. 1.10). Thus, the relative impact of the Ganges-Brahmaputra on marine Sr-isotope ratios is greater than their relative Sr flux (and indeed relative discharge, fig. 1.11). This is confirmed by the most recent work of Basu *et al.* (2001), which incorporates groundwater inputs, who calculate that the G-B system accounts for between 11% (0.7158) and 26% (0.7242) of the global Sr-isotope budget depending on the $^{87}Sr/^{86}Sr$ value assigned to this input.

The marine $^{87}Sr/^{86}Sr$ curve remains more or less constant at 0.7078 between 60 and 40 Ma prior to Himalayan uplift. It then displays an abrupt, rapid increase to ~0.7083 at 22

Ma, reaching 0.7089 by 10 Ma, with a subsequent more gentle increase to the present day value of 0.7092 (Burke *et al.*, 1982; DePaolo and Ingram, 1985; Koepnick *et al.*, 1985; DePaolo, 1986; Hess *et al.*, 1986) (fig. 1.7). Richter *et al.* (1992) model the hydrothermal, Himalayan river and remaining river fluxes to the oceans in the Cenozoic. This work shows that the hydrothermal Sr flux, if it has changed in proportion to the production of new ocean crust (using the data of Kominz, 1984), is both too small and does not have the right time evolution to account for changes in the marine Sr-isotope curve. Thus, the primary control on seawater $^{87}Sr/^{86}Sr$ was fluvial inputs, coincident with the timing of Himalayan uplift. These authors demonstrate that it is not possible to account for the observed variation in the seawater strontium by changing only in the $^{87}Sr/^{86}Sr$ of the Himalayan input. Therefore an increased Sr flux is required, its size depending in direct proportion to the Sr-isotope ratio, further work by Palmer and Edmond (1992) and Krishnaswami *et al.* (1992) affirming this conclusion. The marine carbonate sedimentation rate has increased in the last 40 Ma (Raymo *et al.*, 1988; Richter *et al.*, 1992) which would be predicted from an increased riverine Sr flux, the increased Sr delivery associated with increased Ca^{2+} and HCO_3^- leading to enhanced calcium carbonate formation.

Richter *et al.* (1992) estimate the Sr flux eroded from the Himalaya in the last 40 Ma at $1.5 \times 10^{17} - 2.4 \times 10^{17}$ moles (assuming an isotopic ratio of 0.7127), which is in good agreement with the estimated Sr flux of 2×10^{17} moles required in to satisfy the changes in the ocean Sr curve. Thus, the three requirements outlined above can potentially be satisfied and it is possible that the Himalayan uplift and resultant dissolved Sr inputs

from the Ganges-Brahmaputra could account for the Cenozoic changes in the marine Sr curve.

McCauley and DePaolo (1997) examine the relationship between the marine $^{87}Sr/^{86}Sr$ and benthic $\delta^{18}O$ records. By applying mass balance techniques, these authors constrain the hydrothermal, background continental and Himalayan Sr fluxes (assuming G-B $^{87}Sr/^{86}Sr$ of 0.742 for silicates and 0.7080-0.7092 for carbonate). A measure of the relative inputs of the riverine and hydrothermal CO_2 fluxes, determined from the marine $^{87}Sr/^{86}Sr$ record, is termed Qj by the authors. When Qj is high, it is expected that higher continental weathering rates drive the ocean and atmosphere towards higher pCO_2, low values should represent greater hydrothermal CO_2 release, driving the ocean and atmosphere to lower pCO_2. A comparison of Qj with the $\delta^{18}O$ record reveals good agreement throughout the Paleocene and Eocene (prior to the Himalayan collision) and captures much of the temperature decent during the Oligocene, before diverging in the late Eocene and Miocene. Whilst it is imperfect, the correlation observed between Qj and $\delta^{18}O$ demonstrates how the $^{87}Sr/^{86}Sr$ record can be interpreted to account for cooling in the Cenozoic.

Current knowledge therefore indicates that Himalayan uplift could account for observed changes in the marine Sr-isotope record and that these changes could reflect the falling pCO_2 of the Cenozoic atmosphere. For this to hold true, however, it is assumed that the radiogenic strontium flux from the Ganges-Brahmaputra is a reflection of an increased flux of alkali and, more importantly, alkaline earth cations from silicate weathering. A

great deal of research has been undertaken to prove this final link in the chain connecting Himalayan uplift and global cooling.

In theory proving this link should be a simple task. Silicate rocks, be they sedimentary, metamorphic or granitic, have high Rb/Sr ratios and therefore rapidly evolve high $^{87}Sr/^{86}Sr$, but have low total Sr. In contrast carbonates typically have little Rb but abundant Sr. Therefore, on the global scale, continental river chemistry is comprised of inputs from carbonate (with an average $^{87}Sr/^{86}Sr$ of <0.708) and those from silicates ($^{87}Sr/^{86}Sr = 0.72$) (Brass, 1976; Wadleigh *et al.*, 1985; Palmer and Edmond, 1989). The occurrence of such two-component mixing on the Himalayan scale needs to be established if we are to believe that Himalayan, and consequently marine, Sr-isotope ratios reflect increased silicate weathering and CO_2 drawdown from the Indo-Asian collision. An alternative hypothesis is that changes in $^{87}Sr/^{86}Sr$ might reflect changes in the Sr content or $^{87}Sr/^{86}Sr$ of the rocks being weathered. The exposure of previously buried extremely radiogenic rocks would weaken the correlation between $^{87}Sr/^{86}Sr$ and silicate weathering. If these radiogenic rocks were carbonates, a significant input from such units would very seriously undermine the use of marine $^{87}Sr/^{86}Sr$ as a meaningful measure of CO_2 drawdown rates in the Cenozoic.

1.7. Himalayan Strontium Chemistry and the Source of High $^{87}Sr/^{86}Sr$ in the Ganges-Brahmaputra.

Fig. 1.12a and b show a compilation of the range of strontium isotope and abundance data for the major Himalayan units. It can be seen that most of these units broadly conform to the requirements of the two component system. Silicate rocks from both the HHCS and LHF have low Sr concentrations and are radiogenic (with the vast majority of samples having $^{87}Sr/^{86}Sr$ >0.75). Carbonates from the TSS and HHCS display much higher Sr concentrations together with relatively low $^{87}Sr/^{86}Sr$ (except in occasional HHCS samples). Carbonates from the Lesser Himalaya are anomalous, containing little Sr and displaying a broad range of Sr-isotope ratios, from ratios comparable to carbonates of the TSS and HHCS, to extremely radiogenic ratios on a par with those of the most radiogenic silicates, although these are largely confined to dolomitic calc-silicate samples. If these radiogenic units make a significant contribution to dissolved Sr chemistry, then the use of dissolved $^{87}Sr/^{86}Sr$ as a silicate weathering proxy in Himalayan rivers is doubtful.

Studies of the dissolved Sr chemistry of Himalayan rivers, based mostly on Sr/Ca ratios, attribute a greatly variable proportion (8-89%) of dissolved Sr in Himalayan rivers to the weathering of silicate (Sarin *et al.*, 1990; Krishnaswami *et al.*, 1992; Singh *et al.*, 1998; Harris *et al.*, 1998; Galy *et al.*, 1999). Assuming that radiogenic Lesser Himalayan carbonates units are of minor importance, Krishnaswami *et al.* (1992) state that an average silicate contribution of ~30% (based on the findings of Sarin *et al.*, 1990) would

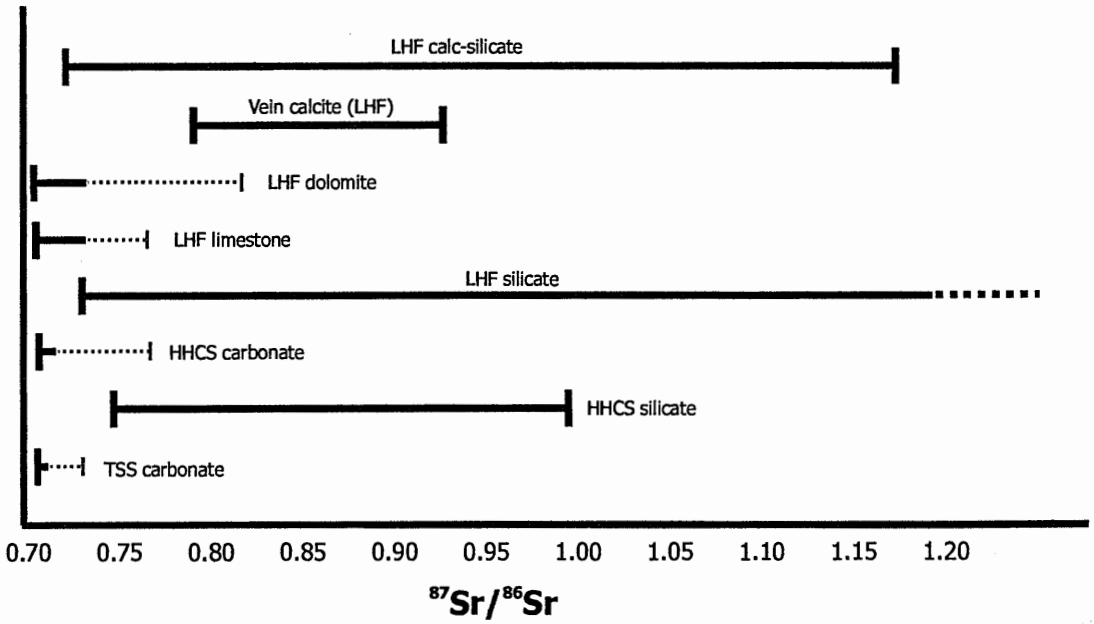

Fig. 1.12a. Sr-isotope values recorded for major Himalayan lithologies.
(Dotted red lines show less well documented extremes).
Compiled from Krishnaswami *et al.* (1992), Derry and France-Lanord (1996), Gardner and Walsh (1996), Quade *et al.*, (1997), Singh *et al.*, (1998), Harris *et al.* (1998), Blum *et al.* (1998), Galy *et al.* (1999), Jacobson and Blum (1999), English *et al.* (2000) and Bickle *et al.* (2001)

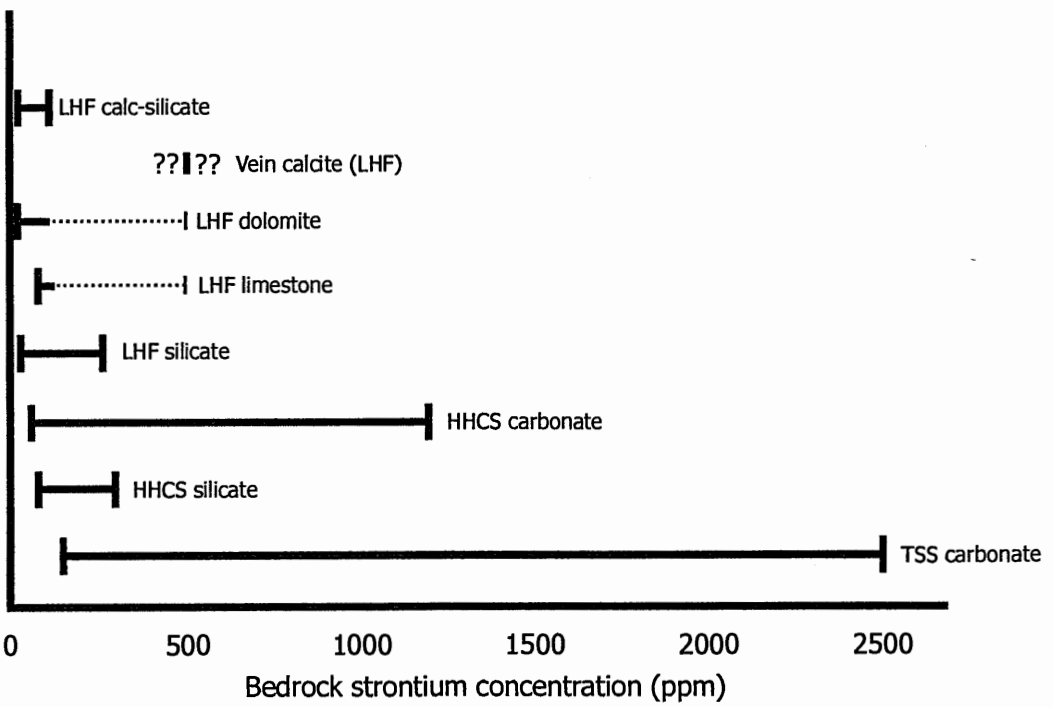

Fig. 1.12b. Sr concentrations recorded for major Himalayan lithologies.
(Dotted red lines show less well documented extremes).
Compiled from Krishnaswami *et al.* (1992), Derry and France-Lanord (1996), Gardner and Walsh (1996), Quade *et al.*, (1997), Singh *et al.*, (1998), Harris *et al.* (1998), Blum *et al.* (1998), Galy *et al.* (1999), Jacobson and Blum (1999), English *et al.* (2000) and Bickle *et al.* (2001)

be enough to account for the high Sr-isotope ratios in Himalayan rivers. Galy *et al.* (1999) arrive at the same conclusion based on an average 15-20% silicate contribution, both authors assuming that the weathering of Lesser Himalayan silicates yields $^{87}Sr/^{86}Sr$ comparable with bedrock ratios of 0.75->1.0 (Kai, 1981; Bhattacharya *et al.*, 1982; Trivedi *et al.*, 1984; Trivedi, 1990; Singh *et al.*, 1998; English *et al.*, 2000). A potential problem with such conclusions is that such rocks contain only minor amounts of easily releasable radiogenic Sr (Blum *et al.*, 1998, Shirey and Walker, 1998, Peucker-Ehrenbank and Blum, 1998; France-Lanord and Le Fort, 1988; Brantley *et al*, 1998). This problem might be mitigated by the preferential loss of ^{87}Sr from Rb sites in silicate minerals (Blum and Erel, 1995; Fairchild and Killawee, 1995), a significant role for easily exchangeable Sr present along grain boundaries and damaged mineral lattices (Bickle *et al.*, 2001) or the metamorphic exchange of radiogenic strontium from weathering-resistant radiogenic micas to more readily weathered feldspars (Edmond, 1992). Harris (1995), when suggesting that metasediments of the HHCS provided the major contribution of radiogenic Sr to Himalayan rivers, invoked the occurrence of such metamorphic exchange between silicate minerals, as do Galy *et al.* (1999) with regard to the Lesser Himalaya.

Pervasive metamorphism can also lead to the exchange of Sr between co-existing silicate and carbonate, as observed in high-grade metamorphic rocks outside of the Himalaya (Bickle *et al.*, 1995; 1997) and in the Lesser Himalaya (Bickle *et al.*, 2001). Palmer and Edmond (1992) suggested that such metamorphically altered carbonates might be largely responsible for the high $^{87}Sr/^{86}Sr$ of the Himalayan dissolved input into

the oceans. This suggestion was based on a two-component mixing diagram for the Ganges-Brahmaputra, which required the high [Sr], low $^{87}Sr/^{86}Sr$ component to be moderately radiogenic (0.7209). Later workers placed even greater significance on altered carbonates, providing evidence that they might constitute a significant proportion of the high $^{87}Sr/^{86}Sr$ endmember in the Himalayan system.

Several studies of the dissolved chemistry of Himalayan rivers have noted a conspicuous increase in $^{87}Sr/^{86}Sr$ crossing the MCT into the Lesser Himalaya, including France-Lanord and Derry (1996) in the Kali Gandaki river of central Nepal, Galy *et al.* (1999) in the Kali Gandaki, Trisuli and Bheri, English *et al.* (2000) in the Seti River of far western Nepal, and Bickle *et al.* (2001) in the Alaknanda River of the Garhwal Himalaya. Lesser Himalayan tributaries indeed record extremely high radiogenic Sr-isotope values (0.76-0.80, Galy *et al.*, 1999; 0.75-1.02, English *et al.*, 2000; 0.75-1.24, Bickle *et al.*, 2001). Harris *et al.* (1998) calculated that 63% of the dissolved load of the Bhote Kosi is acquired in the Lesser Himalaya, either directly or through further weathering of the suspended load (predominantly HHCS), while using both area-based and $\delta^{18}O$ based models, English *et al.* (2000) show that 40-53% of the Sr flux of the Seti River originates from the Lesser Himalaya. Bickle *et al.* (2002) calculate that 35% of the Sr flux of the Alaknanda is provided by the Lesser Himalaya, amounting to 56% of the seawater forcing flux owing to the extremely radiogenic nature of this input, while Galy *et al.* (1999) calculate an LHF contribution of up to ~35% in a number of rivers in the Nepalese Himalaya.

Such observations would initially appear to lend support to Krishnaswami *et al.* (1992) and Galy *et al.* (1999) and a prominent role for Lesser Himalayan silicates in determining dissolved Sr isotope values. However this conclusion is not consistent with the observed chemistry. As described in section 1.3.3.2 carbonates and calc-silicates (largely dolomitic) are prevalent in the upper part of the Lesser Himalaya. English *et al.* (2000) note that Lesser Himalayan tributaries are characterised by relatively high Sr, Ca and Mg concentrations, which would not be expected from silicate inputs, while a correlation between dissolved $^{87}Sr/^{86}Sr$ and $[Mg^{2+}]$ in this work suggests that dolomite weathering might be important. Blum *et al.* (1998), studying the Raikhot River of the Nanga Parbat region of northern Pakistan, which drains Lesser Himalayan gneisses (classified as part of the HHCS at the time of the original work, but shown to be part of the LHF by Whittington *et al.*, 1999), used mass balance to calculate that >82% of the alkalinity in this river was from carbonate weathering even though carbonate comprised a mere 1% of the bedrock. This carbonate material, including both carbonate in calc-gneisses and calcite veins and blebs in pure silicates, was found through leaching experiments to have $^{87}Sr/^{86}Sr$ ranging from 0.79 to 0.93 in the Raikhot watershed, but a more moderately radiogenic range of 0.72-0.77 in other parts of the Nanga Parbat region (Jacobson and Blum, 1999). The accuracy of leaching experiments involving such small amounts of carbonate material is doubtful, at least until the significance of easily-released silicate Sr along grain boundaries and within damaged crystal lattices has been quantified (Bickle *et al.*, 2001). Isotopic mass balance carried out by Harris *et al.* (1998) concludes that >90% of the dissolved strontium from the Lesser Himalaya is carbonate-derived. These authors overestimate the contribution from LHF carbonates by assuming

Sr/(Ca + Mg) ratios "typical" of Himalayan carbonates i.e. those of the TSS and HHCS. In fact carbonate material in the LHF is depleted in Sr giving lower Sr/(Ca + Mg) ratios (see chapters 5 and 7; also Singh *et al.*, 1998; Galy *et al.*, 1999; English *et al.*, 2000; Bickle *et al.*, 2001). Singh *et al.* (1998) and Galy *et al.* (1999) preclude the possibility of a major role for inputs from Lesser Himalayan carbonates on more than a local scale based on their low strontium abundance and a perceived sparsity of highly radiogenic samples. The principal aim of this study is to resolve this debate.

Work to reconstruct and interpret the dissolved $^{87}Sr/^{86}Sr$ record of the Ganges-Brahmaputra has been used as evidence both to support and refute a prominent role for radiogenic Lesser Himalayan carbonate. Fossil shells and paleosol carbonate record the $^{87}Sr/^{86}Sr$ ratio of lowland Himalayan river water in the Neogene (Quade *et al.*, 1997). This record shows that $^{87}Sr/^{86}Sr$ ratios increased in the late Miocene, which the authors suggest marks the exhumation of LHF metacarbonates with high $^{87}Sr/^{86}Sr$. This conclusion is inferred from the strong correlation between paleosol carbonate and detrital carbonate (from the past weathering of Himalayan carbonate) in both space and time, a correlation not noted between paleosol carbonate and detrital silicate, suggesting that past dissolved Sr-isotope ratios in the Himalayan rivers were controlled by carbonate, which became more radiogenic at 7 Ma (possibly consistent with extensive LHF exposure). This change is most marked in the Churia Group (Siwaliks) of Nepal, representing the ancestral Karnali, Narayani and Sapt Kosi (DeCelles *et al.*, 1998). Some Bengal Fan samples show lower ε_{Nd} values at ~7 Ma, indicative of an increased input from the LHF (rocks of which have considerably lower $^{\varepsilon}Nd$ compared with those of the

TSS or HHCS), although this is not the case in all samples and is not accompanied by an increase in LHF detrital sediment (Derry and France-Lanord, 1996a). The timing of exposure of the Lesser Himalaya is a matter of debate. Recent work, based on both Sr and Os-isotope studies of paleosols, suggests a change in source prior to 15 Ma (Chesley *et al.*, 2000), thus requiring an earlier exposure of the LHF. France-Lanord and Galy (2001) use Siwalik and Bengal Fan Nd and Os-isotope data to suggest the exposure of the LHF at 20 Ma, which would not correlate with increases in the $^{87}Sr/^{86}Sr$ of the Ganges-Brahmaputra noted by Derry and France-Lanord (1996a), Quade *et al.* (1997) or Chesley *et al.* (2000). Even assuming exposure of the Lesser Himalaya as early as 20 Ma an alternative source is required to explain the high $^{87}Sr/^{86}Sr$ of the Himalayan Sr flux between 40 Ma and 20 Ma, although modelling by English *et al.* (2000) suggests that the $^{87}Sr/^{86}Sr$ of the Ganges-Brahmaputra remained low (~0.715) prior to ~15 Ma.

Galy *et al.* (1999) interpret the high $^{87}Sr/^{86}Sr$ and low Sr flux (Derry and France-Lanord, 1996a) in the last 10 Ma as a result of an increased silicate:carbonate weathering ratio. These authors conclude, as mentioned above, that carbonate weathering (principally from the TSS with a high $[Sr^{2+}]$) acts to dilute radiogenic input principally derived from the Lesser Himalaya as a result of redistribution of ^{87}Sr from micas to easily weathered plagioclase (15-20% of total Sr). Derry and France-Lanord (1996a), France-Lanord and Derry (1997) and France-Lanord and Galy (2001) come to a slightly different conclusion; that there was a transition from physically dominated to chemically dominated weathering in the Himalayas in the late Neogene (with a return to the modern environment dominated by physical erosion at ~1 Ma). They suggest that the

consequence of such a transition was an increased weathering of radiogenic micas in proportion to carbonate, the weathering of which predominates in a system of physical erosion. Both the interpretations of Galy *et al.* (1999) and Derry and France-Lanord (1996a) would allow for changes in dissolved $^{87}Sr/^{86}Sr$ to correspond to changes in the proportion of silicate to carbonate weathering, although it is not entirely clear in such circumstances whether changes in Sr-isotope ratio in the Himalaya would reflect the Sr flux from silicate weathering.

The significance of a further source of Sr to Himalayan rivers, hot spring inputs, has been highlighted by Evans *et al.* (2001). Studying hot springs close to the STDS and MCT in the Marsyandi River, which rises from the Annapurna range in central Nepal, these authors conclude that small amounts of hydrothermal water (<1% of river discharge) account for large changes in dissolved mainstream $^{87}Sr/^{86}Sr$. This is owing to high Sr concentrations (15-115 μmol/l) coupled with high dissolved Sr-isotope ratios (~0.736-0.768) in the hot springs, far more concentrated and radiogenic than local tributary inputs. High Sr concentrations are also noted by Kortaba *et al.* (1982) in hot springs in the TSS (6-11 μmol/l), along the MCT (14-40 μmol/l) and in the LHF (18 μmol/l) in the Kali Gandaki basin. Evans *et al.* (2001) note that that both $[Sr^{2+}]$ and $^{87}Sr/^{86}Sr$ increase in the HHCS Formation I, where hot springs are concentrated in the Marsyandi, following a mixing line with hot spring compositions, suggesting that ~30% of the Sr flux at this point is hydrothermal. However, sampling was entirely during low river flow, perhaps exaggerating the impact of hot spring influx. The source of such hot spring strontium is debatable. High Na^+ and Cl^- concentrations suggest that buried

evaporites or basinal brines are potentially important sources. At least 40% of total hot spring alkalinity is believed by Evans *et al.* (2001) to be derived from silicate alteration, but mostly in the form of Na^+ (in excess of that from evaporite sources) and K^+. Sr sources are likely to be correlated with those of Mg^{2+} and Ca^{2+}, apportioned between evaporites, silicates (Mg^{2+} from biotite, Ca^{2+} from oligoclase alteration) and Lesser Himalayan carbonates, although it is not possible to accurately quantify the proportion of alkalinity (or strontium) attributable to each source. It should be noted that whilst hot springs are prevalent in the Kali Gandaki and Marsyandi, they are more scarce throughout most of the Himalaya.

High dissolved $^{87}Sr/^{86}Sr$ is acquired in the Himalaya, rivers entering the floodplain having Sr-isotope ratios of 0.725-0.768 with $[Sr^{2+}]$ of 0.3-1.8 μmol/l (France-Lanord and Derry, 1996). The surface water Sr budget of the Ganges-Brahmaputra is completed by floodplain inputs. These comprise rivers draining the Churia Group and Recent alluvium, the input from the in-situ weathering of the flood plain alluvium and rivers draining the Indian shield and Deccan Traps. The floodplain region clearly makes a significant contribution to the Ganges-Brahmaputra, lowering the extremely radiogenic Sr flux from the mountains to ~0.720 (France-Lanord and Derry, 1996), although its contribution is difficult to quantify owing to uncertainties in the hydrological budget and the fact that its strontium composition lies between that of the Lesser Himalaya and TSS (Galy *et al.*, 1999). Flood plain chemistry is dominated by silicate weathering (Derry and France-Lanord, 1996a; Galy *et al.*, 1999).

As exemplified by the above summary, study of the Himalayan dissolved strontium dynamics has focused on surface waters. It has long been suspected (e.g. Moore, 1997) that the groundwater strontium flux may be highly significant. Basu *et al.* (2001) have made the first attempts to quantify this flux for the Ganges-Brahmaputra, estimating it to be 1.4 times the river flux with an $^{87}Sr/^{86}Sr$ of 0.72-0.73, owing to Sr^{2+} concentrations ten times that of surface waters (4-6 μmol/l). Further study is certainly warranted in this field.

1.8. Strontium Chemistry of the Lesser Himalayan Carbonates.

Sr-isotope ratios in seawater in the early Proterozoic to late Precambrian, when the Lesser Himalaya were laid down, were between 0.705 and 0.707 (Veizer, 1989; Jacobson and Kaufman, 1999). The Rb/Sr ratios of Lesser Himalayan carbonates are typically too low to lead to a significant increase in $^{87}Sr/^{86}Sr$ between burial and exhumation (~0.02, Bickle *et al.*, 2001). Dolomitisation of diagenetic limestone is indicated by the low Sr concentration of LHF carbonates (fig. 1.12b) and is a common feature of limestones interbedded with clays (Yoo *et al*, 2000), prevalent in the Lesser Himalaya. Such dolomitisation can lead to $^{87}Sr/^{86}Sr$ ratios up to 0.708-0.716 (Banner, 1995).

To obtain even higher ratios the exchange of Sr between Rb-poor carbonate and Rb-rich silicate minerals is required (Palmer and Edmond, 1992). This could result from the multiple metamorphic events to which the Lesser Himalaya have been subjected.

Comparing $^{87}Sr/^{86}Sr$ and Rb/Sr ratios provides evidence for such exchange. Bickle *et al.* (2001), studying the Deoban Formation of the Garhwal Lesser Himalaya, note that the extreme Sr-isotope ratios noted in Lesser Himalayan calc-silicates (see fig. 1.12a) are "unsupported" i.e. their $^{87}Rb/^{86}Sr$ ratios are too low to produce plausible initial $^{87}Sr/^{86}Sr$ ratios, even when their age (possibly as old as 2500 Ma), and possible diagenetic effects, are considered. The authors conclude that isotopic exchange over 10-30 cm scales in the Deoban Formation could account for the observed Sr-isotope ratios in carbonate units. Massive dolomites in the same area display less radiogenic ratios (fig. 1.12a) and are often supported, while carbonates of the Outer Lesser Himalaya (Krol Formation) are also only moderately radiogenic (0.709-0.714) and generally supported for an initial $^{87}Sr/^{86}S$ of 0.710 and age of 2500 Ma.

1.9. Project Aims.

The first aim of this project is to better constrain the nature and source of strontium inputs from the weathering of the Lesser Himalaya through extensive sampling of LHF bedrock and tributaries draining the different LHF units in a "typical" Himalayan catchment. This is essential in achieving the principal aim of this work, to determine the influence of Lesser Himalayan carbonate units on dissolved $^{87}Sr/^{86}Sr$. This is done firstly through an established mass balance method and additionally through statistical analyses which do not require the use of often poorly constrained end-member chemistry, and have not as yet been applied to the problem of the source of the radiogenic Himalayan strontium flux. Through multiple regression analysis of the Bhote Kosi results it is

hoped that the strontium chemistry of other Himalayan rivers can be predicted, thus demonstrating the applicability of results to other parts of the Himalaya. The final aim of this work is to determine the contribution of Lesser Himalayan carbonate to the modern radiogenic strontium flux from the Himalaya and ascertain the implications of this input for the use of $^{87}Sr/^{86}Sr$ as a silicate weathering proxy, both in Himalayan rivers and in the marine record.

Plate 1. Satellite digital elevation image of the Nepal Himalaya and southern Tibetan Plateau showing sampled river catchments.

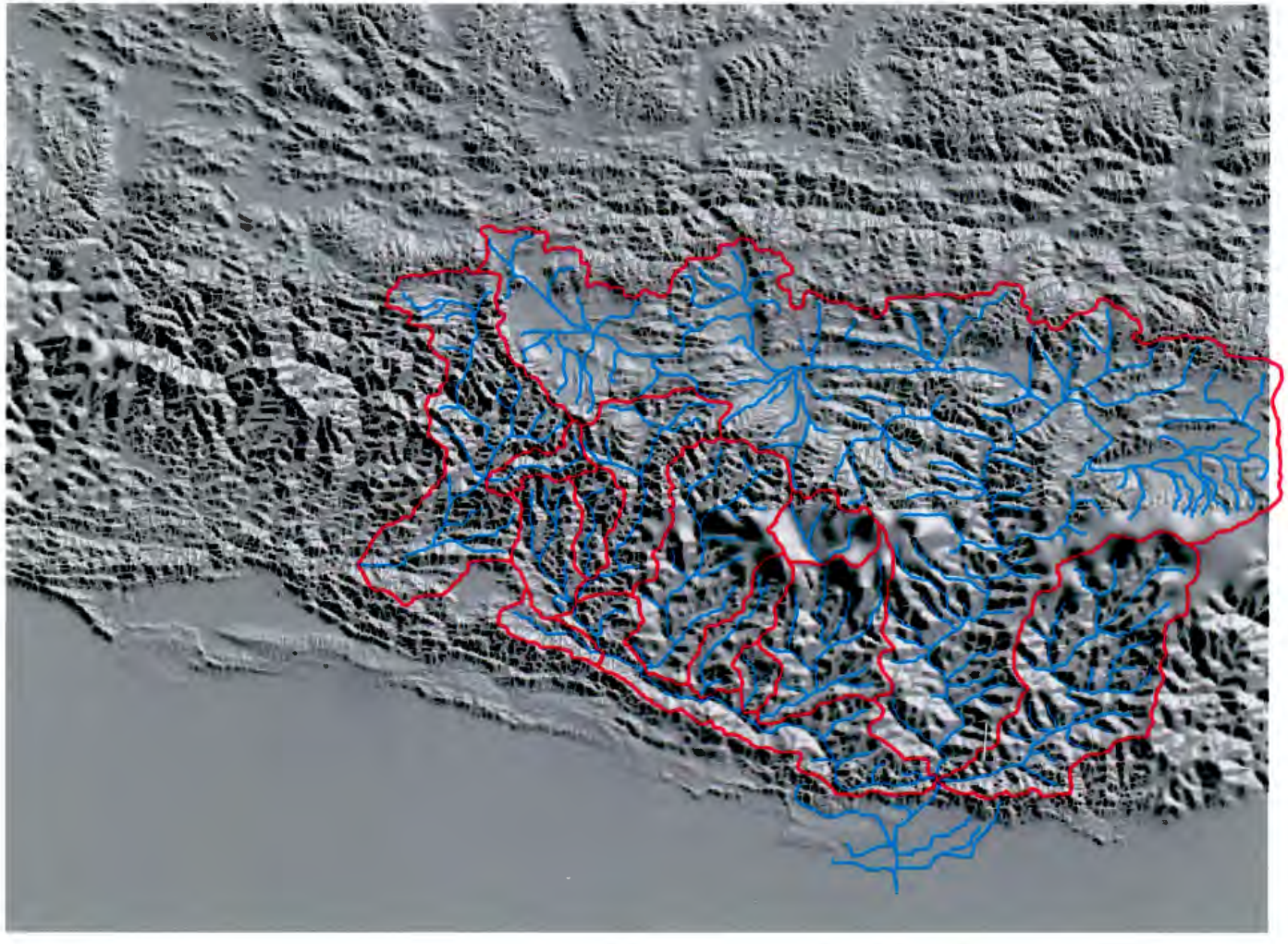

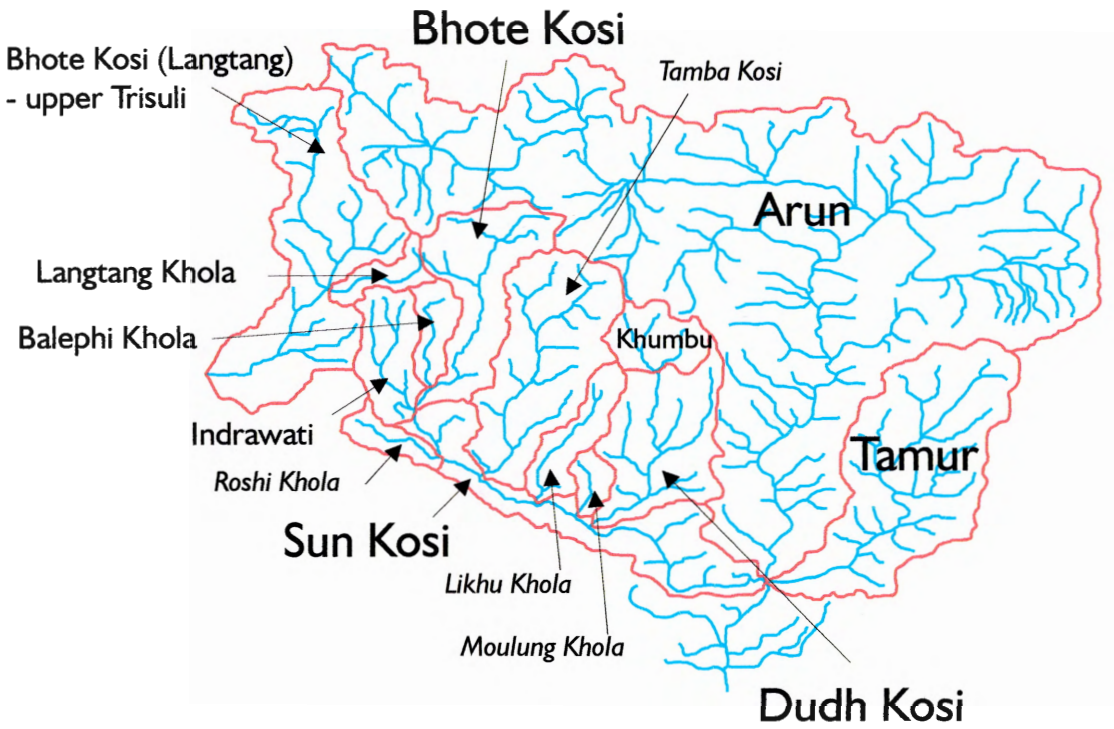

Key for plate 1.

Watersheds are marked in red, river courses in blue. Catchments not sampled in this study are shown in italics.

NB. River courses and catchments shown in plates 1, 6 and plate 7 were produced from satellite data using the computer programme TNT Lite™ and are therefore slightly different from those in plates 2, 3, 4, 5, 8 and 9 which were drawn from the relevant topographical maps.

Chapter 2

Field Localities: The Rivers of Nepal

This chapter introduces the river basins sampled in this study, providing geological, topographical, climatological and hydrological background data specific to these basins in order to help the reader interpret the chemical data in subsequent chapters. The rivers comprising the Sapt Kosi basin (see plate 7) are described first, beginning with the Bhote Kosi; the main river of interest in this study, followed by its major tributary, the Balephi Khola. Subsequent descriptions cover the Indrawati and Chak Khola, which join the Bhote Kosi to form the Sun Kosi, and a further major tributary of the Sun Kosi, the Dudh Kosi, which drains the Khumbu (Everest) region. Attention is then focussed on Sun Kosi itself, which was sampled in the far south-east of Nepal along with the Arun and Tamur rivers, which confluence to form the Sapt Kosi itself. The Langtang Khola - Trisuli is dealt with last as this river does not form part of the Sapt Kosi basin, instead draining into the Narayani. Detailed geological descriptions are provided for the Bhote Kosi, Dudh Kosi (Khumbu) and Langtang Khola - Trisuli basins.

Note on data used in this chapter.

The data used within this chapter are standard streamflow measurements made by the Department of Irrigation, Hydrology and Meteorology (DIHM) of His Majesty's

Government (HMG) Nepal and published by the International Centre for Integrated Mountain Development (ICIMOD) (Alford, 1992; Chalise *et al.*, 1996).

The collection of climate data in Nepal began in 1947, the collection of hydrological data in 1960. These records are the best available for Nepal, although records for not all stations go back the 30 years required by the World Meteorological Organisation (WMO) standard for producing a normal climatological map. Temperature records were produced by ICIMOD (Chalise *et al.*, 1996) using a model based on available temperature records, elevation, latitude and longitude. As temperature and precipitation values are taken from the extrapolated contour maps of Chalise *et al.*, the appropriate range of values is illustrated in the figures.

"Streamflow" refers to the volume of discharge per unit time (Qv, m^3/s) and is an index of the volume of surface water at a specific site and the energy available for sediment transport. "Specific runoff" is the depth of water produced per unit area (Q, mm/month) and is an index of the amount of water available at a specific point within a catchment basin (e.g. to cause erosion) (Alford, 1992).

2.1. Bhote Kosi ("River from Tibet").

The Bhote Kosi is the main focus of this study. The river was chosen because it provides a relatively easily accessible traverse of all the main Himalayan lithologies, and revealed interesting strontium chemistry in a pilot study (Harris *et al.*, 1998). Bhote Kosi is a

Plate 2. Geology of the Bhote Kosi basin.

Adapted from Nepal DMG map (Central Nepal), 1985; Burchfiel *et al.*, 1992; Searle *et al.*, 1997.

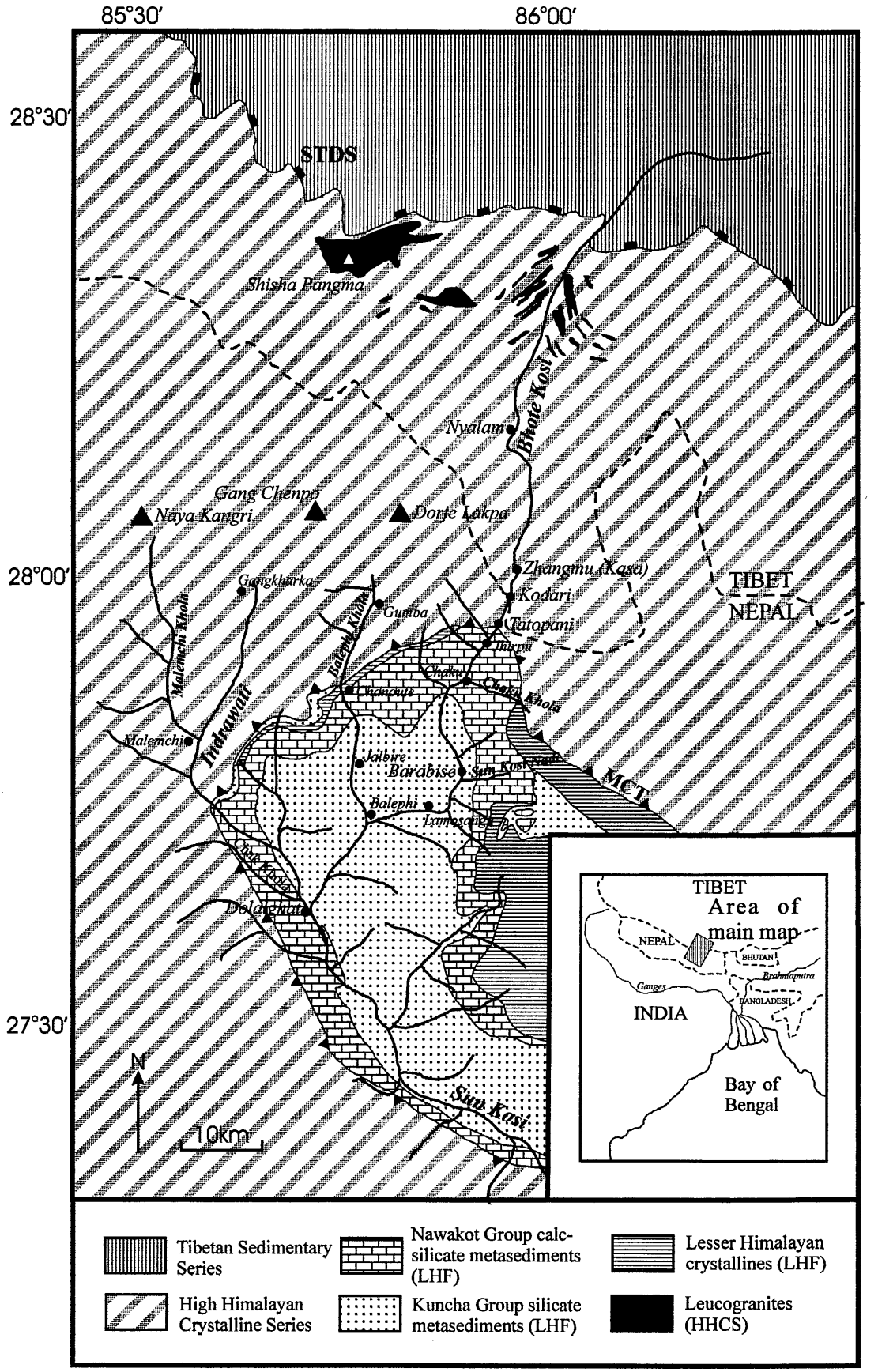

name affixed to numerous rivers in the Nepal, three of which were sampled during the course of this work. The river described in this section lies due north-east of Kathmandu, and is easily found on any map as its valley was chosen as the route for the Arniko (Friendship) Highway, linking Kathmandu and Lhasa. Technically, the Bhote Kosi ends at the town of Barabise (see plate 2) where it is joined by the Sun Kosi Nadi to become the upper Sun Kosi. In this work, however, the entire section as far downstream as Dolalghat (see plate 2) and the confluence with the Indrawati will be referred to as the Bhote Kosi.

2.1.1. Geology.

The geology of the Bhote Kosi basin is illustrated in plate 2. The TSS in the Bhote Kosi ranges from Ordovician to Jurassic. Burchfiel *et al.* (1992) describes the units up to the Carboniferous. Limestone is the dominant lithology in all units, interbedded with shales, siltstones and, in the Silurian-Carboniferous, sandstones. The units strike roughly east-west and dip moderately to gently northward, and all are heavily deformed.

The Nyalam Detachment is the name given by Burchfiel *et al.* to the South Tibetan Detachment System (STDS) in the Bhote Kosi (Nyalam) section. It consists of a zone of imbricate faults, fault breccia and fault gouge and varies in thickness from 20-100 mm. Lithologies within the fault zone are predominantly from the TSS. The structures of the Nyalam section indicate that the Nyalam Detachment formed as a north-dipping low angle normal fault with a northeasterly direction of movement. Both the HHCS and TSS

in the Bhote Kosi reveal structures related to the south-directed thrusting of the MCT, and younger extension-related structures from the STDS movement.

The footwall of the detachment consists of an "injection complex" of metasedimentary units, mostly quartz-biotite gneiss of upper amphibolite facies. These are intruded by leucogranite dykes, sills and larger bodies, including the Shisha Pangma pluton described below. Diopside-garnet (and possibly scapolite) marbles occur locally as interbeds up to 10 m thick. Quartzite beds 1 - 10 cm thick become increasingly abundant near the top of the sequence forming a 100m thick quartzite unit near the top. At the top of the quartzite thin beds of marble and calcareous schist are interbedded and become dominant before forming a transitional contact with a silty marble around 100m thick which is the uppermost unit of the HHCS in the Bhote Kosi section.

Located immediately below the STDS in the North-west of the catchment is the Shisha Pangma leucogranite intrusion. This large pluton is composed of multiple internal intrusions with many peripheral dykes and sills (Searle *et al.*, 1997). It is intruded into units of the "injection complex" described above, which is equivalent to the Langtang Lirung Unit described by Reddy *et al.* (1993) in the Langtang Khola valley (see section 2.10). Two types of granite are observed in the Shisha Pangma intrusion. Biotite leucogranites contain biotite ± muscovite ± tourmaline, tourmaline leucogranites (which form most of the high-level pluton, Searle *et al.*, 1997) contain tourmaline ± muscovite, with K feldspar, plagioclase and quartz present in both types.

The Lesser Himalayan Formation of the Bhote Kosi catchment forms part of the Ramechap tectonic window. The units of the upper valley form the northern limb of an N-S anticline, the core of which occurs a few km downstream of Barabise. The Main Central Thrust (MCT) is mapped at the village of Tatopani (Maruo *et al.*, 1973; Stöcklin and Bhattarai, 1980; Stöcklin, 1980; Upreti and Rai, 2000). Kyanite-bearing gneisses, which typically represent the base of the HHCS, were thought not to outcrop in the section, the basal rocks being essentially garnet-biotite bearing pelitic schists to psammitic schists with subordinate quartzites, although kyanite and staurolite have been recently reported in these rocks (Rolfo, pers. comm.), the presence of the former confirmed along strike (Upreti and Rai, 2000). Above this unit, in the area around Kodari, are amphibole-garnet-two mica-oligoclase gneisses with interlayers of garnet-two mica quartz-rich schist. Above these are fine-grained kyanite-garnet-two mica-oligoclase gneisses interlayered again with garnet-two mica quartz-rich schists. These rocks probably represent rocks of the MCT zone, not the hanging wall (Upreti and Rai, 2000), suggesting that the MCT might be placed further north beyond the Nepal-China border, although this is unconfirmed by other workers who have studied this section (e.g. Maruo, 1973; Stöcklin and Bhattarai, 1980; Stöcklin, 1980).

At Tatopani a coarse quartz-epidote-two mica-K feldpar-oligoclase augen orthogneiss with a thickness of 80-100m thick outcrops (Upreti and Rai, 2000, Rolfo; unpublished cross section), and was observed and sampled in this study, although it is too thin to be shown on plate 2. This unit belongs to the Lesser Himalaya Formation. Thicker sequences of crystalline rocks from the Lesser Himalaya occur immediately south of the

MCT on both the eastern and western sides of the valley, and are most extensive in the north-east portion of the drainage basin of the Sun Kosi Nadi tributary.

South of the Tatopani and the augen gneiss, the Bhote Kosi makes a complete traverse of the Lesser Himalaya as mapped by Stöcklin and Bhattarai (1980) and Stöcklin (1980). The more extensive Nepal Department of Mines and Geology (DMG) map ("Central Nepal", 1985) uses a different nomenclature, one published nowhere else. The correlations between the units described by Stöcklin and those described by the Nepal DMG are given in fig. 1.3. The rocks of the Chaku-Tatopani section are difficult to differentiate into their respective formations (Upreti and Rai, 2000). Some detail is provided from a recent traverse made by Rolfo *et al.* (unpublished cross section). These workers identify a ~500m zone of mylonitic epidote-oligoclase-two mica quartz-rich schists below the Tatopani augen gneiss (the Robang Formation of Stöcklin and Bhattarai), below which is an approximately equal thickness of calcite and dolomite marble with interlayered phyllites and quartzites (the Malekhu Limestone). Of approximately equal thickness again is a unit consisting of slate and oligoclase-two mica phyllites with carbonate interlayers, below which outcrop several kilometres of calcschist and epidote-two mica-oligoclase quartz-rich schists. These two units correlate with the Benighat Slates of Stöcklin and Bhattarai (1980) and appear to be calcareous throughout, carbonate lamillae as well as thicker dolomitic beds noted by the Nepal DMG (1985). The Dhading Dolomite forms the distinctive cliffs in the Bhote Kosi and Chaku Khola in the vicinity of the village of Chaku, but even this unit displays a much reduced thickness compared with the type section (Upreti and Rai, 2000). South of

Chaku, the Nourpal Formation and Dandagoan Phyllites are also difficult to distinguish, and are described by Rolfo *et al.* as phyllites and chloritoid-chlorite-garnet-oligoclase-two mica schists. No mention of carbonate material is mentioned by these authors, although dolomite, limestone and calc-silicates are described in the type sections of Stöcklin and Bhattarai and the Nepal DMG. The presence of carbonate material is confirmed in samples collected from this part of the section during this work. North of the town of Barabise (~10km) it becomes clear that the transition to the Kuncha Group silicates has occurred. Rolfo *et al.* note K-feldpar, garnet, albite and two micas in the quartz-rich schists and phyllites of this unit, which are interlayered with mica bearing quartzites.

2.1.2. Altitude.

The headwaters of the river rise on the Tibetan Plateau at an altitude of >5000m (fig. 2.1). The steepest section of the river is the gorge section in the High Himalayan Crystalline Series that occurs between Nyalam (close to the STDS) and Kodari (close to the MCT), and is known as the "Gates of Hell" by local Tibetans. Surrounding peaks form the highest points of the Bhote Kosi drainage basin, the largest of which is Shisha Pangma (8013 m). The section of the river occupied by the Nawakot Group calc-silicates, while much less steep than the HHCS section, still maintains an average gradient of around 5%, reaching as much as 10% as it drops in altitude from 1650 m at Kodari to <1000 m at the geological boundary between the Nawakot Group and the Kuncha Group (Knowles & Allardice, 1992). As far downstream as Barabise the river

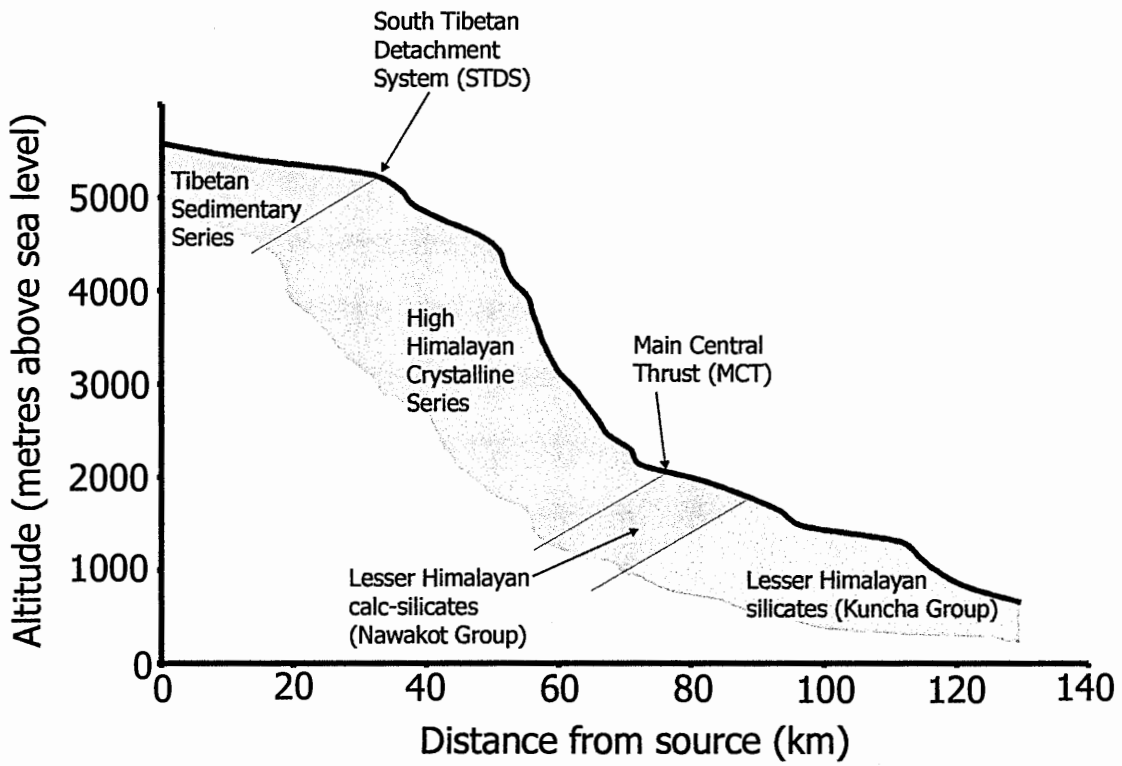

Fig. 2.1. Altitude and geology changes in the Bhote Kosi

occupies a steep, narrow valley including a number of sheer-sided gorges, a 3 km stretch downstream of Chaku being of particular note. Beyond Barabise the river takes on a gentler aspect, with an average gradient of <1%, meeting the Indrawati and Chak Khola at the town of Dolalghat (altitude ~ 650m), a total descent from source of around 5 km. Downstream of this tri-confluence the river is referred to as the Sun Kosi. The Bhote Kosi is likely to display area-altitude distributions broadly similar to those seen in the Dudh Kosi and Tamur (fig. 2.19), although almost certainly with a greater proportion of surface area at altitudes exceeding 5000m, reflecting the portion of the catchment that extends onto the Tibetan Plateau. Indeed, data available for the catchment of the Nepal

Department of Hydrology and Meteorology (DHM) hydrological station at Barabise show that 55% of this catchment area lies at altitudes in excess of 5000m.

2.1.3. Climate.

Fig. 2.2 illustrates the average monthly temperature and rainfall at Kodari (the most upstream point in the Bhote Kosi in Nepal), Barabise and Dolalghat (the lowest point of the basin). Altitude differences are reflected in the contrasting temperatures of these sites, with Kodari being approximately 5°C colder than Dolalghat throughout the year. Rainfall is highest at Kodari, with >1000 mm per month falling at the height of the monsoon; marginally less at Barabise. Rainfall at Dolalghat is much less, reaching a peak of just over 300 mm/month in the monsoon. This is illustrated in the annual rainfall contour map (fig. 2.3) for the Bhote Kosi basin, which clearly illustrates that the section between Kodari and Barabise receives the greatest rainfall. The amount of rain received decreases concentrically from this zone both northwards and southwards, with the very lowest rainfall received in the part of the basin north of the STDS in the Himalayan rain shadow. This pattern is repeated in the rainfall contour maps for September (fig. 2.4) and October (fig. 2.5), although by November (fig. 2.6) precipitation is low throughout the entire basin, with barely any rainfall at all in December (Chalise *et al.*, 1996).

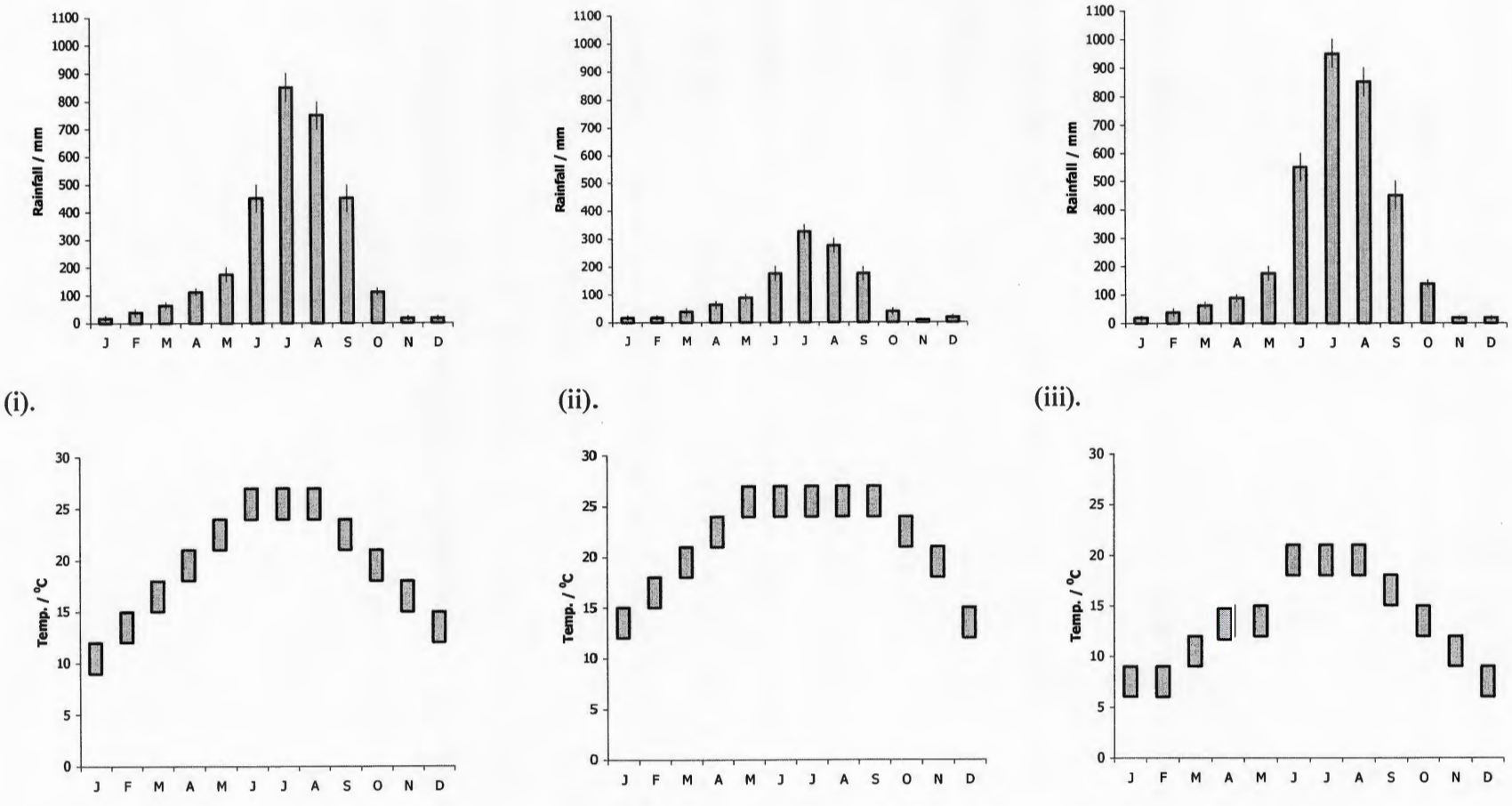

Fig. 2.2. Monthly variations in average rainfall and temperature in the Bhote Kosi.
(i). Barabise. (ii). Dolalghat. (iii). Kodari.

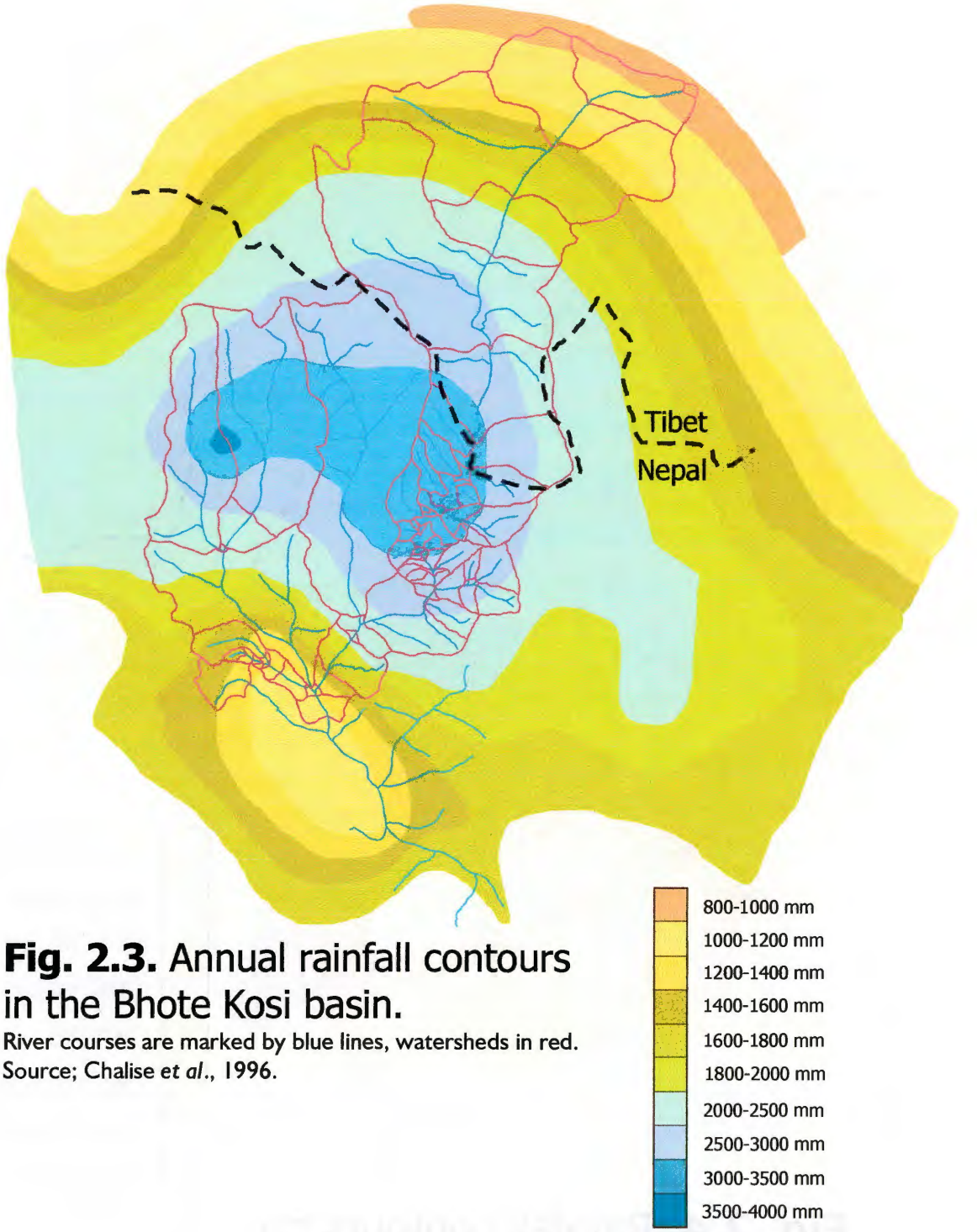

Fig. 2.3. Annual rainfall contours in the Bhote Kosi basin.
River courses are marked by blue lines, watersheds in red.
Source; Chalise *et al.*, 1996.

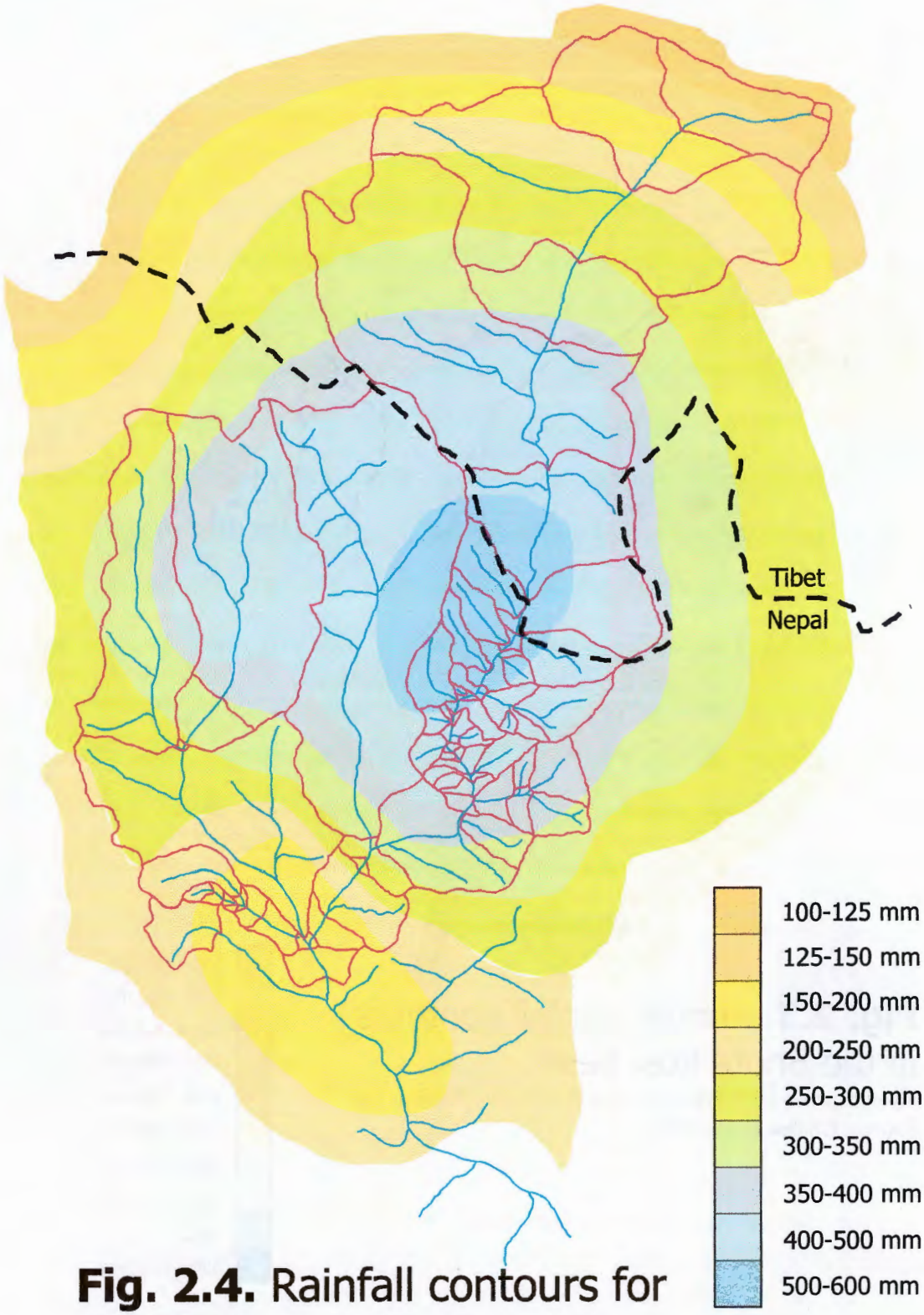

Fig. 2.4. Rainfall contours for the Bhote Kosi in September.

River courses are marked by blue lines, watersheds are shown in red.
Source: Chalise *et al.*, 1996.

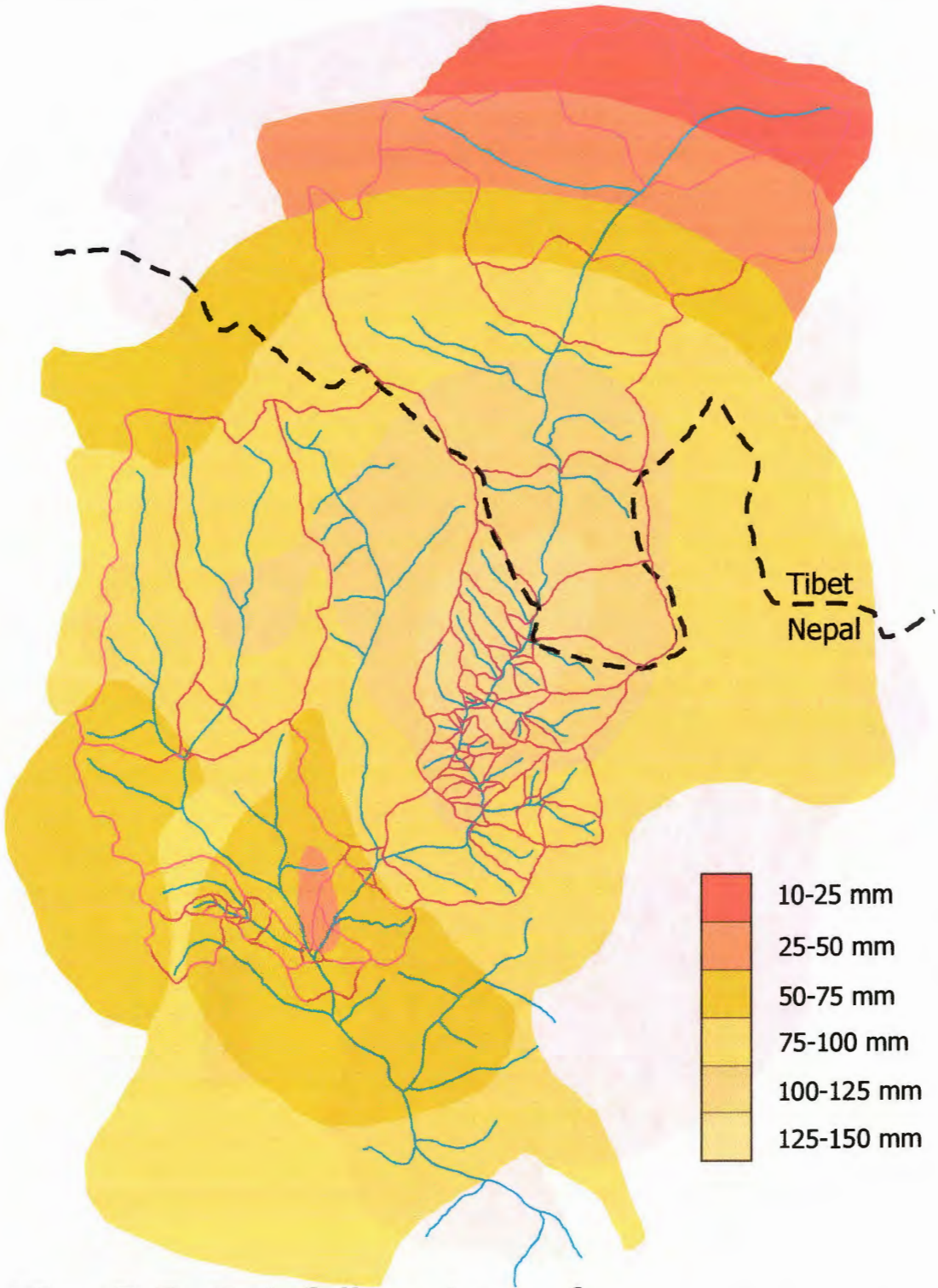

Fig. 2.5. Rainfall contours for the Bhote Kosi In October.

River courses are marked by blue lines, watersheds are shown in red.
Source: Chalise *et al.*, 1996.

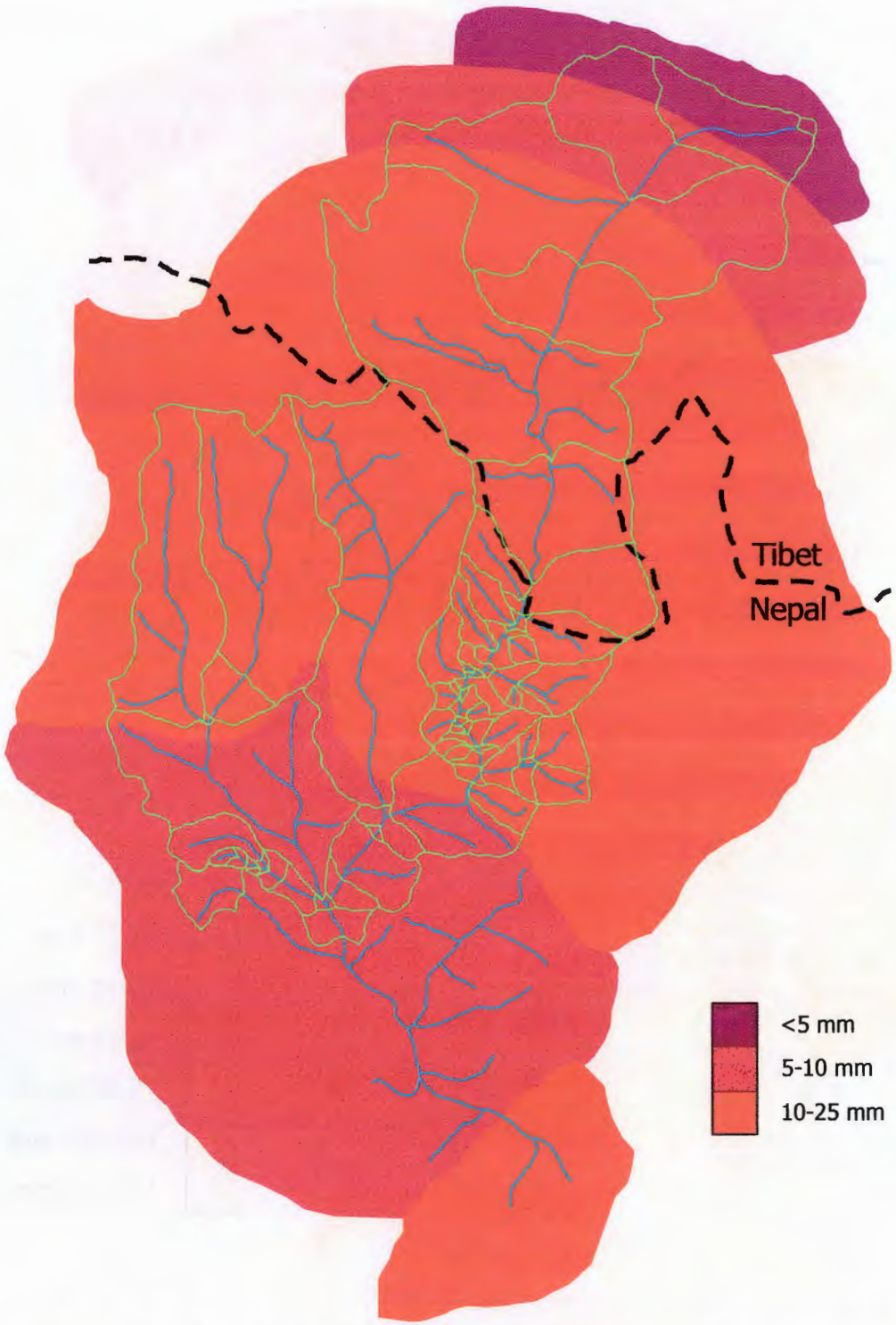

Fig. 2.6. Rainfall contours for the Bhote Kosi in November.

River courses are marked by blue lines, watersheds are shown in green.
Source: Chalise *et al.*, 1996.

2.1.4. Flow Characteristics.

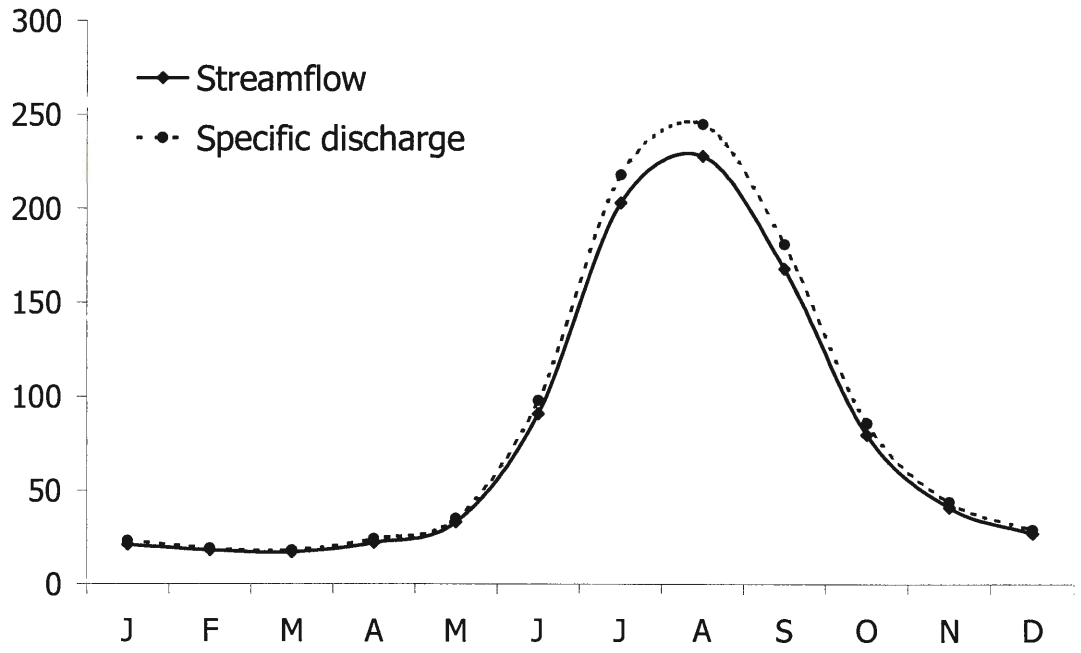

Fig. 2.7. Monthly variations in streamflow (m^3/s) and specific discharge (mm/month) in the Bhote Kosi at Barabise.

Fig. 2.7 shows the monthly changes in streamflow and specific discharge at Barabise. The river displays a typical monsoonal pattern, with a steeply rising limb from May through to the peak rainfall months of July and August, followed by a steeply descending limb from September onwards, with baseflow* reached by December. Flow begins to increase again in April and May reflecting snow and icemelt. Increases in discharge would not be expected in lower altitude basins until the onset of the monsoon in June. High altitude basins such as the Bhote Kosi also show a slower diminution of streamflow and specific discharge at the end of the monsoon when compared with lower altitude rivers (Alford, 1992).

*Baseflow is streamflow solely composed of groundwater flow, moving through soil to the river course, with no surface runoff input (i.e. flow in periods of little or no precipitation).

2.1.5. Land Use.

The landuse of the Bhote Kosi basin is not documented. Vegetation shows the typical Himalayan transition with altitude (see fig. 1.4), from the arid climate and largely bare rock of the Tibetan Plateau, through the snow-covered high Himalayan peaks to the alpine and then temperate forests of the gorge between Nyalam and Tatopani. The lower valley is occupied by semi-tropical vegetation. Agriculture is virtually non-existent on the Tibetan side of the border owing to the harsh climate and steep topography, but becomes increasingly evident downstream of Kodari where topography allows terrace construction.

The valley floor itself is occupied by the Arniko Highway, along which have grown small towns such as Nyalam, Zhangmu (Khasa), Kodari, Barabise and Dolalghat, along with numerous other smaller settlements. The surrounding countryside on the Nepalese side of the border is dotted with numerous small settlements, although land above 2000 meters is largely uninhabited. The closure of a cement factory at Lomosangu means that the only heavy industry evident in the Bhote Kosi basin is the production of hydroelectricity. At the time of sampling the only working project was a small dam and hydroelectricity plant at Lomosangu. This takes water out of the Bhote Kosi for a few

kilometres, but with a barely perceptible effect upon streamflow. The far larger Bhotekoshi Hydropower Project was being constructed at the time of sampling. This $95 million, 36 MW US-Nepalese joint venture involved the construction of a 60m long, 15m high dam just downstream of Tatopani with a power house built at Jhirpu (www.nepalnews.com.np). The workings present at the time of sampling had a negligible effect on water chemistry (see section 4.2.1.8). The Bhote Kosi was selected for the project because of its high gradient and the low population and relatively low amount of agriculture present in the valley (www.dams.org). The 120 MW Middle Bhote Koshi Project is currently being studied and has the potential for a far greater impact upon the river (www.ledco-nepal.com).

2.1.6. Sampling Strategy.

Plate 3 shows the catchments for all the Bhote Kosi samples collected in this study. Sampling of the river in Tibet was restricted to a brief trip in September 1998. Access to the river is difficult between Nyalam and Kodari, if not impossible. The river is far more accessible on the Nepali side of the border, and extensive sampling was undertaken in November - December 1998, September 1999 and late October - November 1999, in an attempt to build a complete picture of inputs into the main river and the resultant changes in mainstream chemistry. All major tributaries were sampled between Tatopani and Barabise, the focus of this study owing to the rapid increase in dissolved $^{87}Sr/^{86}Sr$ in this section observed by Harris *et al.* (1998). Where possible samples were collected in the main river both upstream and downstream of each tributary. Tributaries draining

only the Kuncha Group were sampled in the vicinity of Barabise to assess the dissolved chemistry arising from the weathering of this unit. Additional samples were take immediately upstream and downstream of both the dam and power house works of the dam project construction site and the Tatopani hot spring to determine the possible influences of these. Sampling of the mainstream continued at regular intervals all the way downstream to Dolalghat, where the Bhote Kosi, Chak Khola and Indrawati tri-confluence was sampled.

Repeat samples were collected to allow comparisons between 1998 and 1999 data, and in order to contrast data collected in September with the dry season data. Fig. 2.7 shows that in September river flow is still high, while those samples collected in late October - December largely reflect baseflow conditions.

2.2. Balephi Khola.

The Balephi Khola is the largest tributary of the Bhote Kosi (see plate 3), a typical fast-flowing Himalayan river that runs to the east of the Helambu region.

2.2.1. Geology.

The geology of the Balephi Khola is illustrated in the geological map of the Bhote Kosi basin (plate 2). The river rises in the High Himalayan Crystalline Series, which it drains in a steep sided valley for ~40 km before crossing the MCT into a narrow zone of Lesser

Plate 3. Sampled catchments in the Bhote Kosi (watersheds shown in red).

Adapted from Nepal DMG map (Central Nepal), 1985; Burchfiel *et al.*, 1992; Searle *et al.*, 1997.

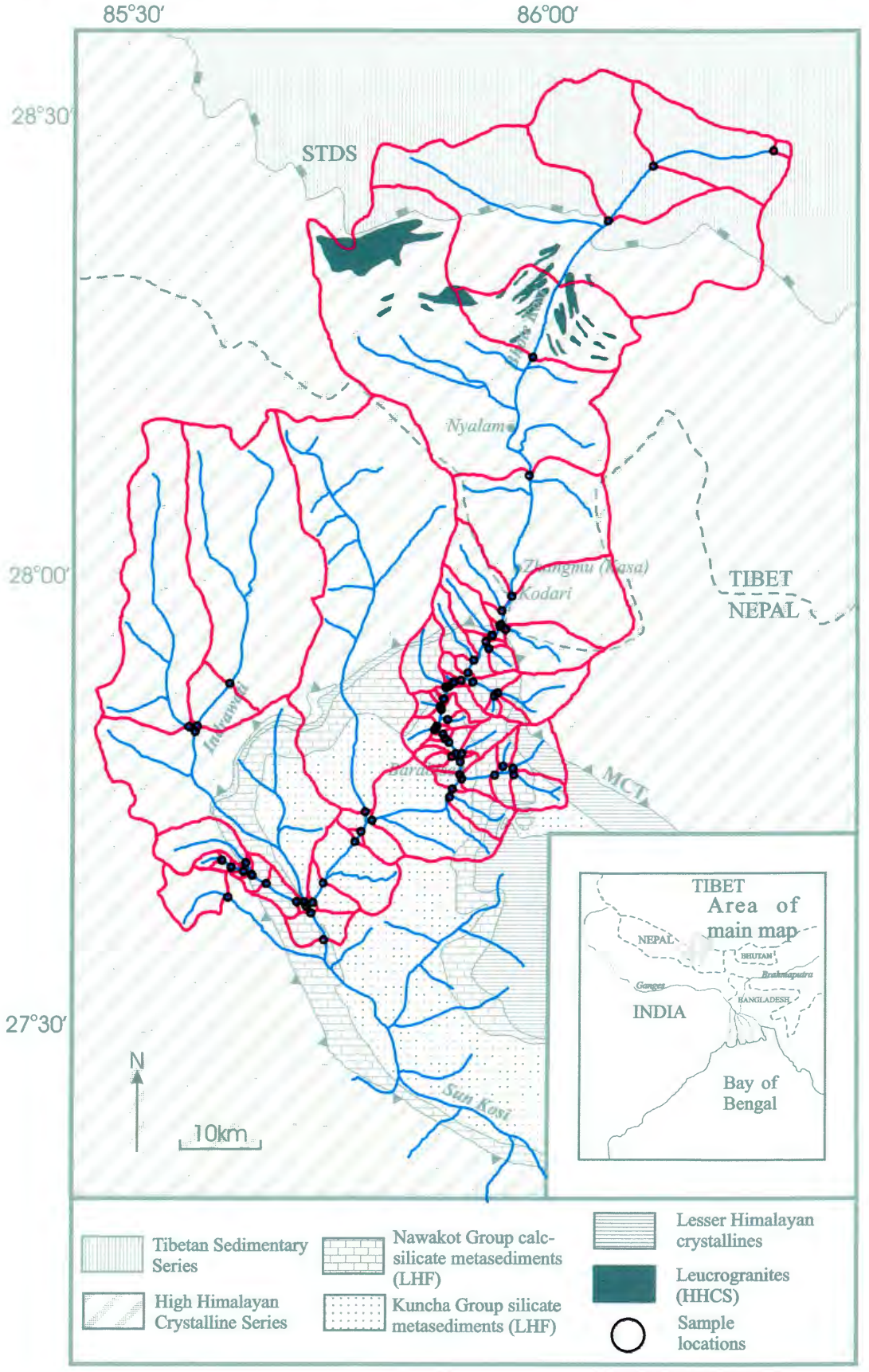

Key showing sample locality labels for plate 3.

NB. All labels have the prefix "BK" throughout this work.

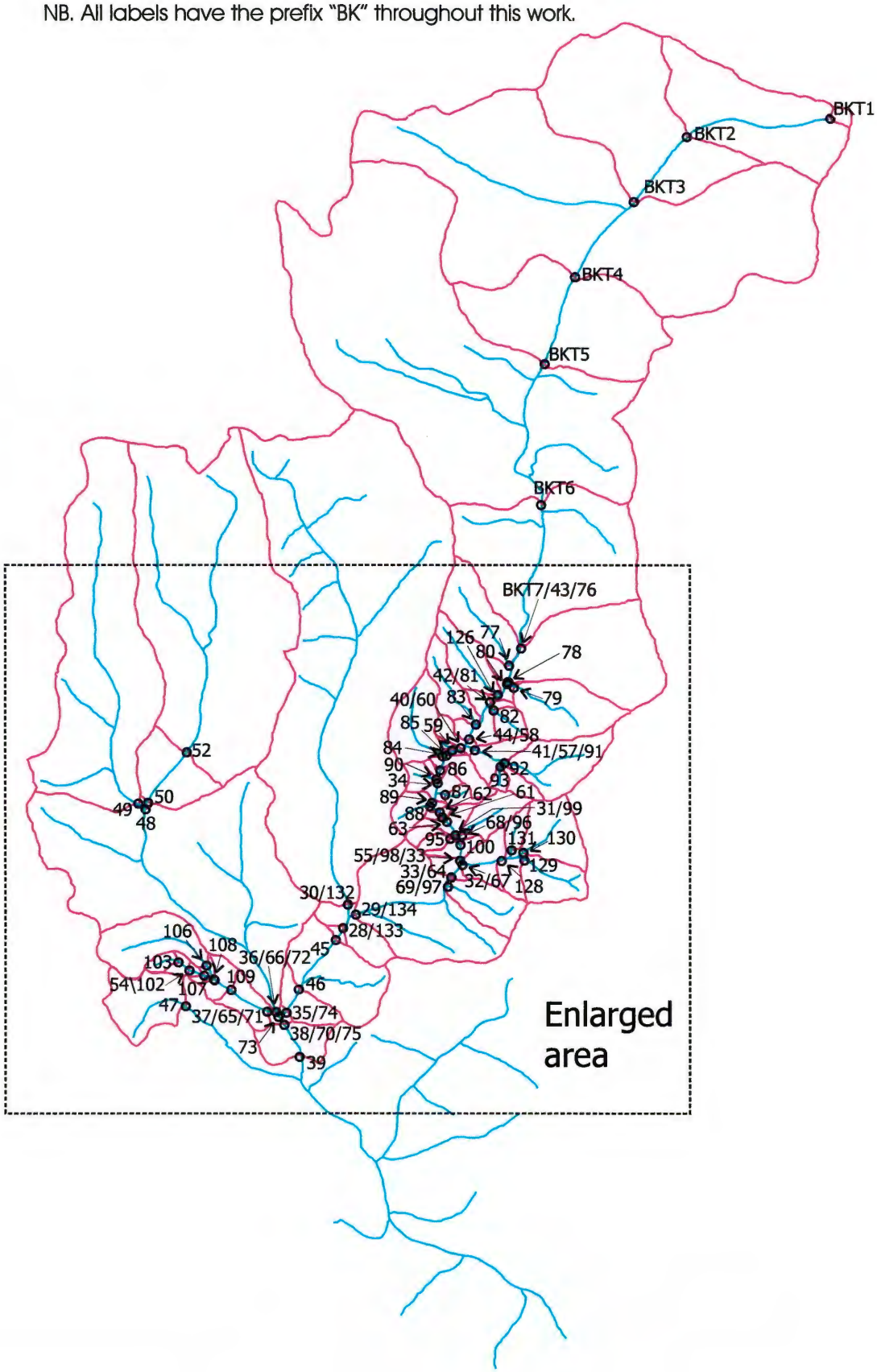

Key showing sample locality labels for plate 3 (enlarged area).

NB. All labels have the prefix "BK" throughout this work.

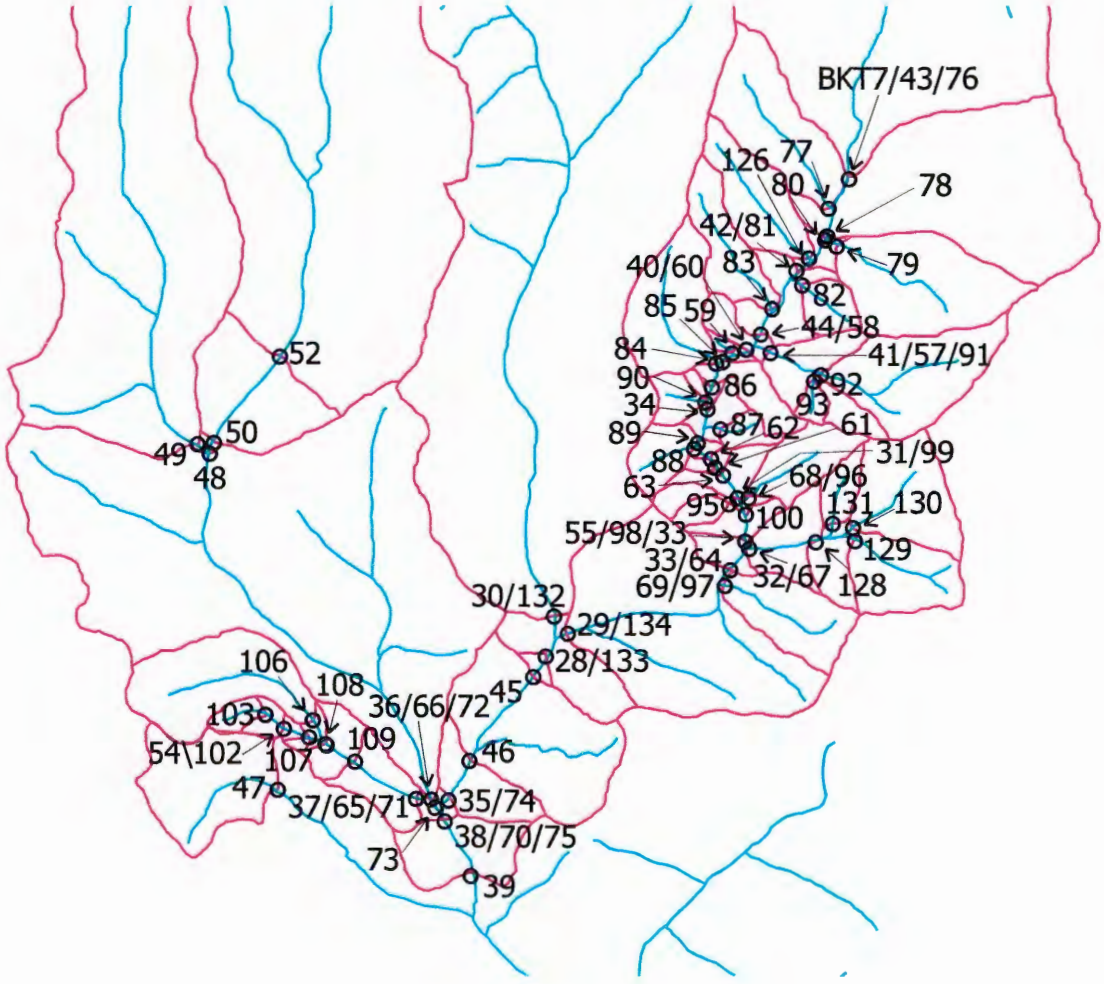

Himalayan crystalline gneisses, followed further downstream by thicker sequences of the Nawakot Group and the Kuncha Group. Only attenuated exposures of the Dandagoan Phyllites are present in the Balephi Khola catchment, while the Nourpal Formation is absent in the East side of the valley, with no units above the Dhading Dolomite exposed in the west (Nepal DMG, 1985).

2.2.2. Altitude.

The Balephi Khola rises on the southern slopes of Dorje Lakpa (6990m) and the other glaciated peaks of the Lingshing Himal. Between Gumba and Chanoute the average river gradient is 8%, although it rapidly flattens out, the average gradient between Chanoute and Jalbire being 2.5%, and only 1% downstream of Jailbre to the confluence with the Bhote Kosi at Balephi (Knowles & Allardice, 1992). Area-altitude relationship data are not available for the entire Balephi Khola, but have been calculated for the catchment of the DHM hydrological station at Jalbire (Alford, 1992). In this basin, >50% of the surface area lies above 3000m, similar to that calculated for other larger rivers originating in the HHCS (e.g. the Dudh Kosi and Tamur, see fig. 2.19).

2.2.3. Climate.

The Balephi Khola drainage occupies the part of the Bhote Kosi basin with the highest rainfall, with more 2000 mm of rain falling on most parts of the Balephi Khola catchment during the year (fig. 2.3). Fig. 2.8 shows the monthly rainfall at Jailbre in the

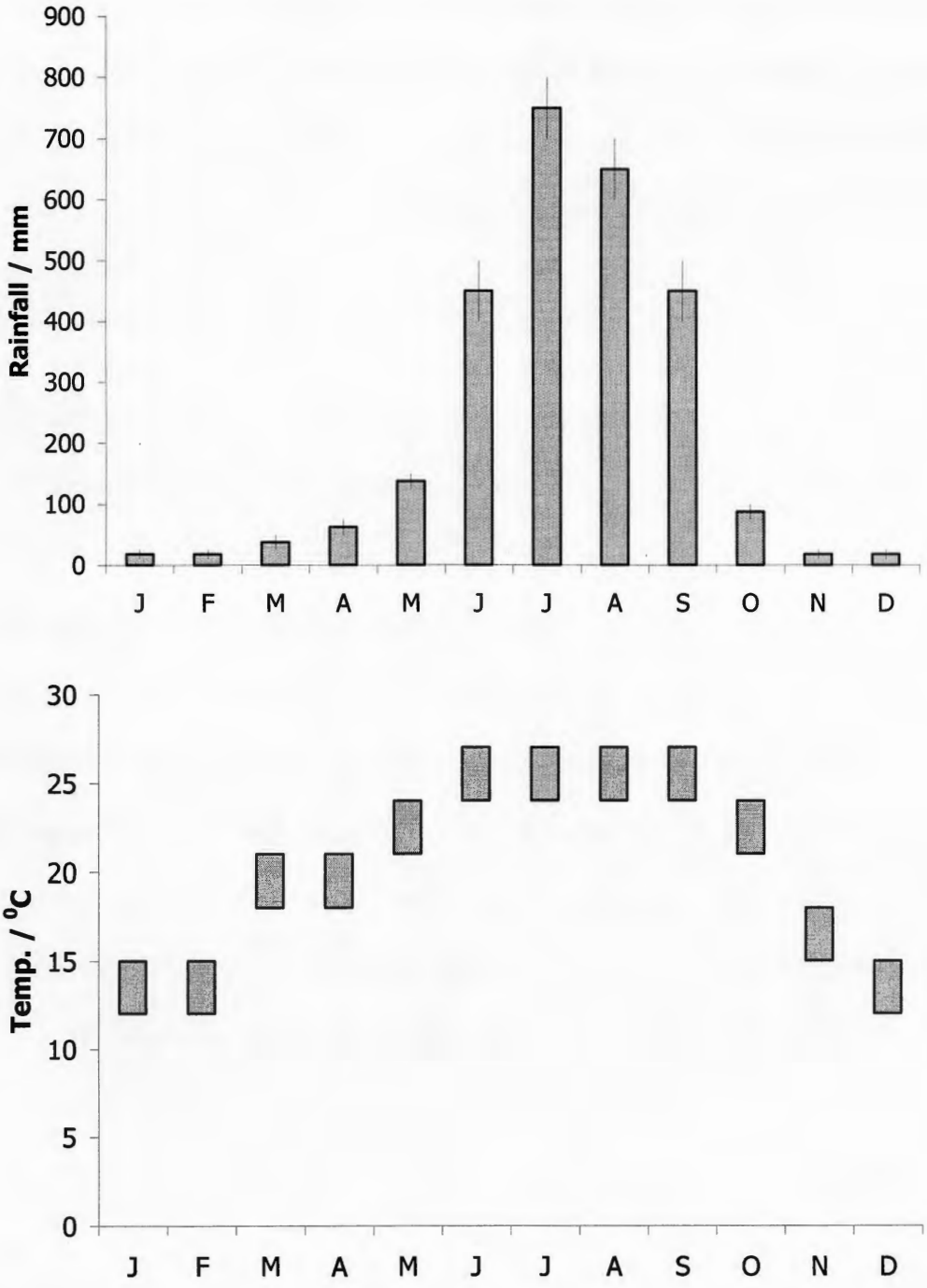

Fig. 2.8. Monthly variations in average rainfall and teperature in the in the Balephi Khola at Jalbire.

lower part of the river, which is similar to that at Barabise with rainfall in excess of 800m in the monsoon months, but with less than 20 mm of rain falling in the dry season. Average temperatures are in excess of 25°C, and even winter average temperatures never fall below 13°C.

2.2.4. Flow Characteristics.

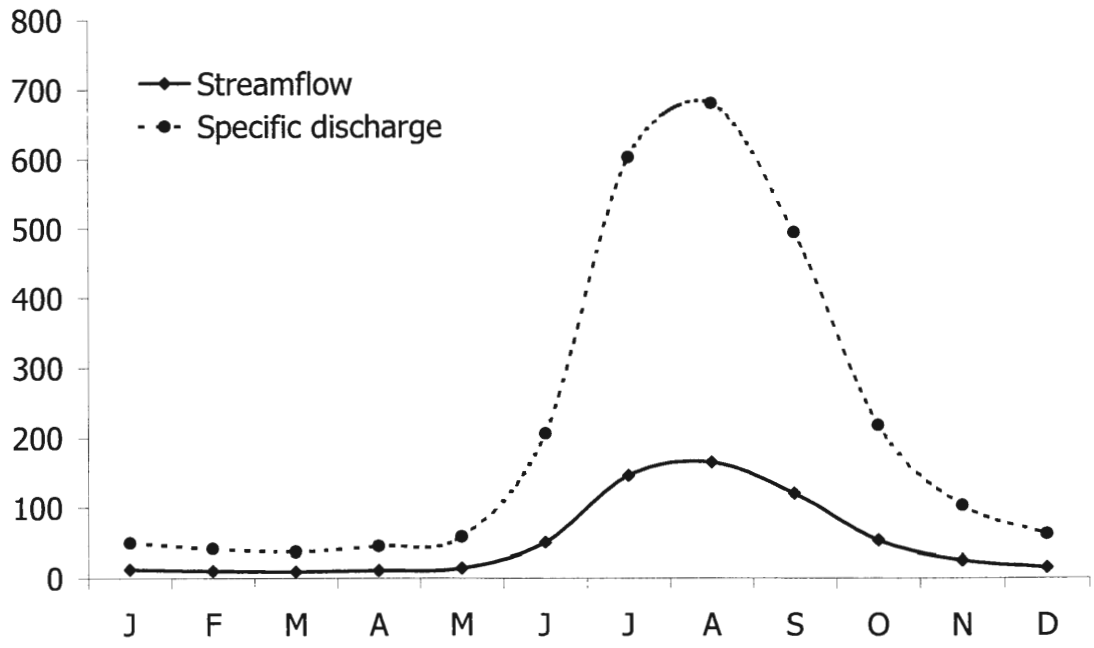

Fig. 2.9. Monthly variations in streamflow (m^3/s) and specific discharge (mm/month) for the Balephi Khola at Jailbre.

Fig. 2.9 is very different from fig. 2.7 (streamflow and specific discharge of the Bhote Kosi). Although the Balephi Khola has a relatively low streamflow, it has a very high specific discharge for the size of its catchment. Alford (1992) cites the cause of this as

the humid environment (throughout the catchment) creating a greater potential for land use hydrological interactions.

2.2.5. Land Use.

The catchment of the Balephi Khola is sparsely populated, although numerous small villages are situated on terraced hillsides below 2000 m. At higher altitudes dense mixed and pine forests predominate, some of which are protected within the Langtang National Park.

2.2.6. Sampling Strategy.

The Balephi Khola was sampled just upstream of the confluence of the river with the Bhote Kosi, in both the 1998 and 1999 dry seasons. In the Bhote Kosi samples were collected upstream and downstream of the confluence.

2.3. The Indrawati.

Draining the Helambu region to the North-east of Kathmandu, this river joins the Bhote Kosi at Dolalghat (plate 3).

2.3.1. Geology.

The geology of the Indrawati is shown on Plate 2. The upper portion of the river entirely drains rocks of the High Himalayan Crystalline Series, passing into the Lesser Himalayan Formation approximately 10 km downstream of the major settlement of Malemchi. The Indrawati drains an attenuated Nawakot Group sequence consisting only of the Benighat Slates and associated Jhiku Beds (Stöcklin and Bhattarai, 1980; Nepal DMG, 1985). These units form a contact with the Kuncha Group owing to the presence of the high-angle Kosi Fault (Upreti and Rai, 2000).

2.3.2. Altitude.

The Indrawati rises on the southern flanks of the Chimisegang Lekh and Kanjala Himal ranges, whose northern slopes drain into the Langtang Khola valley (see section 2.10). In its upper reaches the river has a steep gradient but below the confluence with the Malemchi Khola at Malemchi the river meanders through a gravel bed within a broad valley. The gradient downstream of Malemchi is roughly constant and never exceeds 1% (Knowles and Allardice, 1992).

2.3.3. Climate.

The upper reaches of the Indrawati receive the high levels of rainfall noted for the Balephi Khola, as shown in fig. 2.3 – 2.6. Annual rainfall in this region exceeds 2500

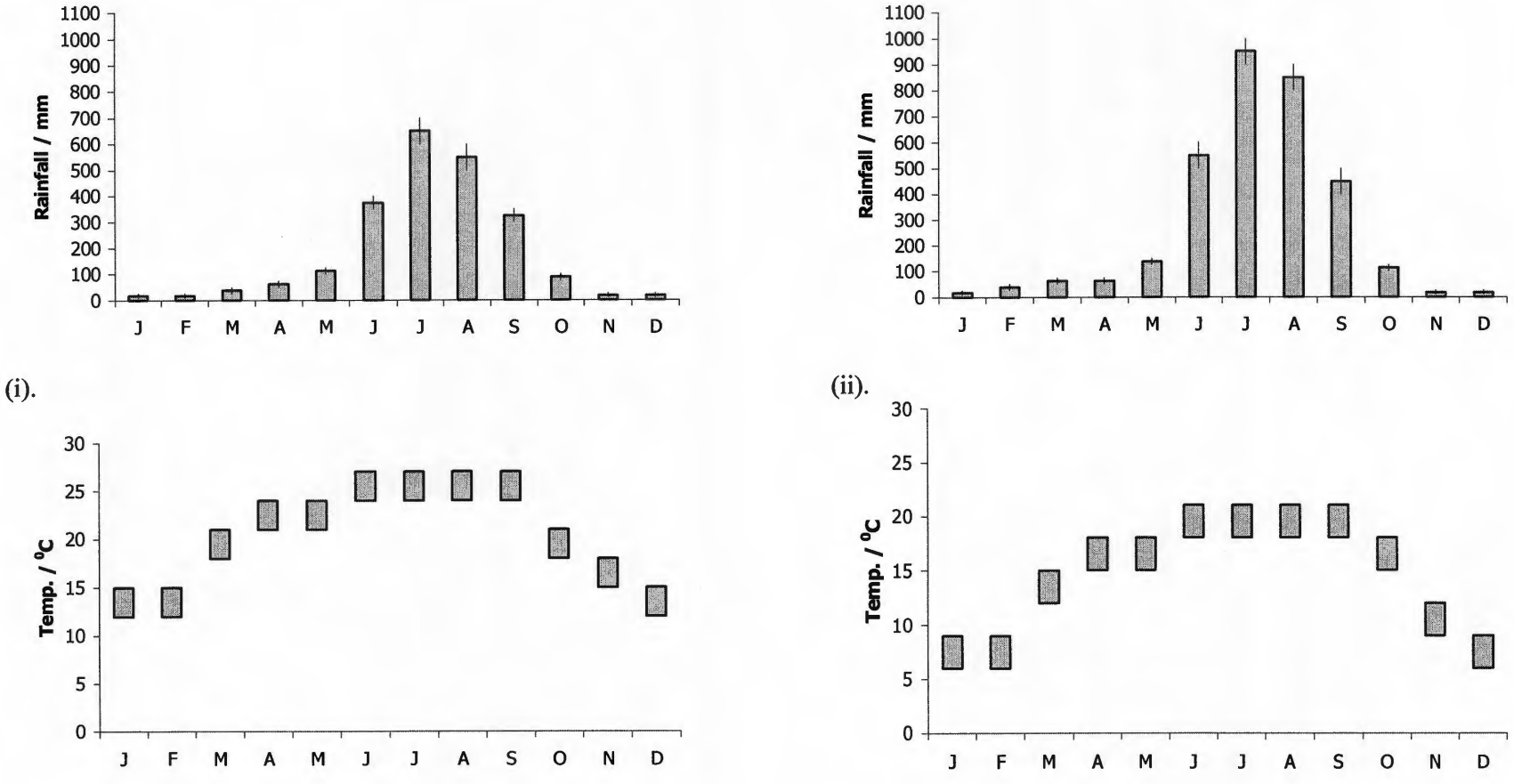

Fig. 2.10. Monthly variations in average rainfall and temperature in the Indrawati.
(i). Malemchi. (ii). Gangkharka.

mm and is greater than 3500 mm in some parts of the basin. Rainfall in the village of Gangkharka in this part of the basin exceeds >1000 mm in the peak monsoon months (fig. 2.10). Rainfall in the lower part of the basin is less, and is lowest at Dolalghat (fig. 2.2), which receives less than half the annual rainfall of the upper reaches of the basin. Average temperatures (fig. 2.10) are consistently lower at higher altitudes in the basin,an approximate difference of 5°C noted between Gangkharka (in the headwaters of the river) and Malemchi, which has a climate similar to that of Dolalghat.

2.3.4. Flow Characteristics.

Flow data are unavailable for the Indrawati. In its upper reaches the Indrawati is a typical fast mountain river, although its flow has waned considerably by the time it reaches Melamchi. Shallow braids and ledges have been created for fishing in the lower river, and it can be crossed by foot during periods of baseflow.

2.3.5. Land Use.

Like the upper reaches of the Balephi Khola, the upper part of the Indrawati basin consists of largely uninhabited dense forests below glaciated peaks. The lower part of the valley contains small settlements with terraces of various crops. A small (5 MW) hydroelectric project is planned for 2004 (www.ledco-nepal.com) although no work was evident during sample collection and there is not as yet no record of the project having begun.

2.3.6. Sampling Strategy.

The confluence of the Indrawati with the Malemchi Khola was sampled, while a further sample was collected in the Indrawati upstream of the confluence, just below a noted exposure of High Himalayan Crystalline Series marbles (Jnawali, unpublished geological map). The only further samples taken were at Dolalghat, just upstream of inputs from the Chak Khola, in November 1998 and September 1999.

2.4. The Chak Khola.

This relatively small, low altitude river joins the Indrawati a few hundred metres upstream of the outflow of the Bhote Kosi. Its western tributaries drain the carbonates and silicates of the Bhimphedi Group of the Kathmandu Nappe (see section 1.3.4.1), while the eastern side of the river basin drains the Benighat Slates of the LHF. The nature of the terrain means that the Chak Khola, like the adjoining Kathmandu Valley, is relatively heavily populated. Industry in the area includes the Everest Marble Quarry, from which several samples of the Bhainsedodhan Marble were collected (see table C4).

2.5. The Dudh Kosi (Khumbu Region).

2.5.1. Geology.

The Khumbu region lies in the western limb of the Arun Trans-anticline (Bordet, 1961). Plate 4 illustrates the simplified geology of the area. Unlike in the Bhote Kosi, where the units of the Tibetan Sedimentary Series occur on the Tibetan Plateau, the TSS units drained by the rivers of the Khumbu form the summits of the some of the basin's (indeed, the world's) major peaks, including Mt. Everest itself (8850 m), with the part of the mountain above 8,660m being composed of Ordovician limestone (Wang and Zhen, 1975), known as the Mt. Jolmo Lungma Formation. The overlying Permo-Carboniferous is only present north of Mt. Everest, and thus doesn't form part of the Dudh Kosi catchment (instead forming part of the Arun basin). Below the Mt Jolmo Lungma Formation is the North Col Formation (Yin and Kuo, 1978), the contact between the two being concordant in Everest itself, but faulted further north (Burg *et al.*, 1984). In the Everest Massif, this unit consists of a thick (1.3 - 1.5 km) sequence of chlorite-biotite phyllite, biotite-calcite metasandstone and impure quartzite. Crystalline limestone layers form the famous "yellow band" of the mountain. Further east in Nuptse (7879 m) and Lhotse (8501 m), the North Col Formation comprises biotite-epidote hornfels and calc-silicates. A low-angle north-dipping normal fault marks the STDS (Burchfiel *et al.*, 1992) in the Khumbu region

The remainder of the catchment consists entirely of units of the High Himalayan Crystalline Series. The uppermost part of the HHCS in this region comprises biotite muscovite gneiss (the Rongbuk Formation, Yin and Kuo, 1978), below which is a sequence of biotite-sillimanite paragneiss and micaschist (the Black Gneiss of Bordet, 1961). These rocks host networks of dykes and lens-shaped, sub-concordant bodies of tourmaline leucogranite. A sequence of biotite schists and biotite-muscovite-staurolite-garnet schists (the Lhotse Schists, Colombo *et al.*, 1995) is exposed in the south face of Lhotse, although northwards these wedge out completely.

The middle part of the HHCS in the Khumbu region is made up of sillimanite-cordierite orthogneiss (the Namche Migmatite Orthogneiss, Bordet, 1961), derived from Early Palaeozoic granitoids (Kai, 1981; Ferrara *et al.*, 1983; Tonarini *et al.*, 1994). The lower part of the HHCS in the Khumbu region comprises upper amphibolite to granulite facies migmatised orthogneiss of pelitic composition (Barun Gneiss; Bordet, 1961). This unit is characterised by garnet, biotite, sillimanite partly replacing kyanite, cordierite and spinel (Brunel and Kienast, 1986; Pognante and Benna, 1993; Borghi and Lombardo, 1995), and is cut by leucogranite veins and dykes (Visona and Lombardo, 2002).

Sampling of the Dudh Kosi was undertaken as far downstream as Phakding (see plate 5). The MCT occurs in the vicinity of the settlement of Jubing (altitude ~1500 m), approximately 20 km downstream of the lowest sample site. Here, garnet-biotite-sillimanite gneisses of the HHCS are separated by a thrust sheet of metasediments from

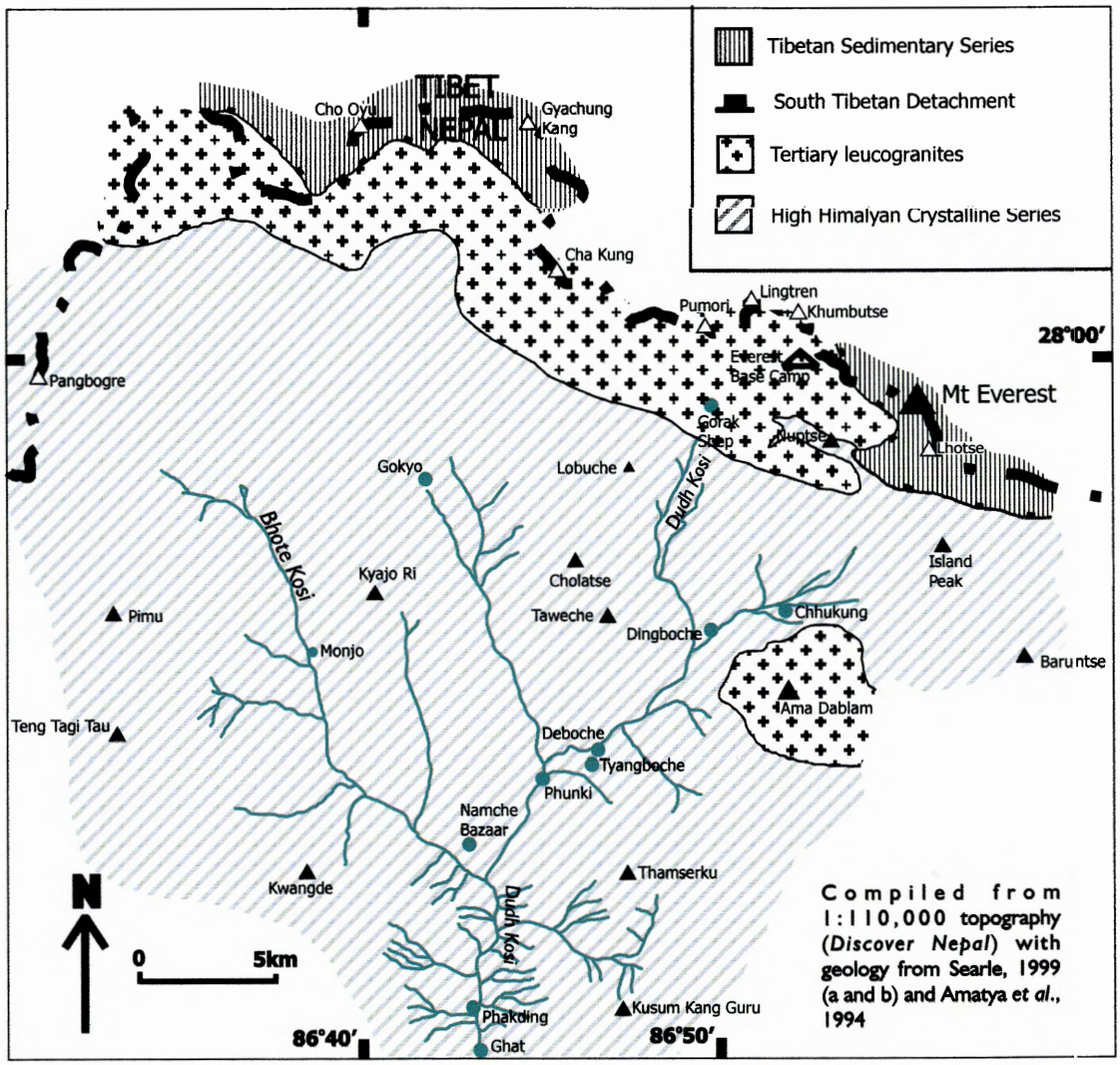

Plate 4. Geology of the Khumbu region.

Lesser Himalayan augen gneisses (the Phaplu Orthogneiss; Brunel, 1983), equivalent to the augen gneiss observed in the Bhote Kosi valley (Upreti, 1999).

Miocene leucogranite plutons and dyke or sill networks are emplaced in the upper part of the HHCS, close to the STDS. The Nuptse pluton is the largest (thickness 1-2 km) and most prominent in the catchment (Searle, 1999a and b). It is a nearly cylindrical laccolith with a gently north-plunging long axis which still retains a connection to its root zone (Carosi, 1999). The tabular Makalu pluton occurs in the extreme east of the Dudh Kosi catchment, although most of its drainage is into the Arun. Both bodies are fine to medium grained mica-tourmaline leucogranites. The time for generation and cooling of the Sagarmatha-Makalu granites falls between 24 and 12 Ma (Wager, 1965; Schäerer, 1984; Hubbard and Harrison, 1989; Villa, 1990; Hodges, 1993; 1996; Villa *et al.*, 1998).

2.5.2. Altitude.

The Dudh Kosi basin incorporates the highest peaks on the planet, although the source of the river itself are the numerous glaciers on the southern slopes of these mountains at altitudes of 5000 – 6000m. These form three main groups; the Khumbu Glacier group and Lhotse Glacier group are the source of the Dudh Kosi itself, while the even larger Ngozumpa Glacier group forms the Bhote Kosi (Khumbu)*, which joins the Dudh Kosi south of Namche Bazaar. The upper section of the river is unsurprisingly steep, with an average gradient of 8% and sections up to 12% (Knowles and Allardice, 1992). This

includes large gorge sections such as the one between the confluence of the Dudh Kosi and Imja Khola at Phunki, and the confluence of the Dudh Kosi and Bhote Kosi (Khumbu) south of Namche. Between Namche and Ghat the gradient eases a little (to an average 4%) before steepening again south of Ghat. South of the MCT the gradient of the river is considerably less (an average of 2.6%, Knowles and Allardice, 1992). Fig. 2.19 shows the area-altitude relationships in the entire Dudh Kosi basin.

*Referred to as the "Bhote Kosi (Khumbu)" to avoid confusion with the Bhote Kosi of section 2.1.

2.5.3. Climate.

Fig. 2.11 shows climatological data for Namche Bazaar (3400 m) and Tyangboche (3900 m) in the Khumbu. As in the other basins, a monsoonal climate is observed, although rainfall is generally less here than in the Bhote Kosi (south of the main Himalaya at least), Balephi Khola and Indrawati, never exceeding 350 mm even at the peak of the monsoon. Significant rainfall is still recorded in both September and October when sampling of this basin was undertaken, and was observed during our time in Khumbu. Average temperatures during the monsoon months rarely exceed 15°C at Namche 10°C at Tyangboche, while during the winter average temperatures of less than 5°C at Namche, and below freezing at Tyangboche, are normal.

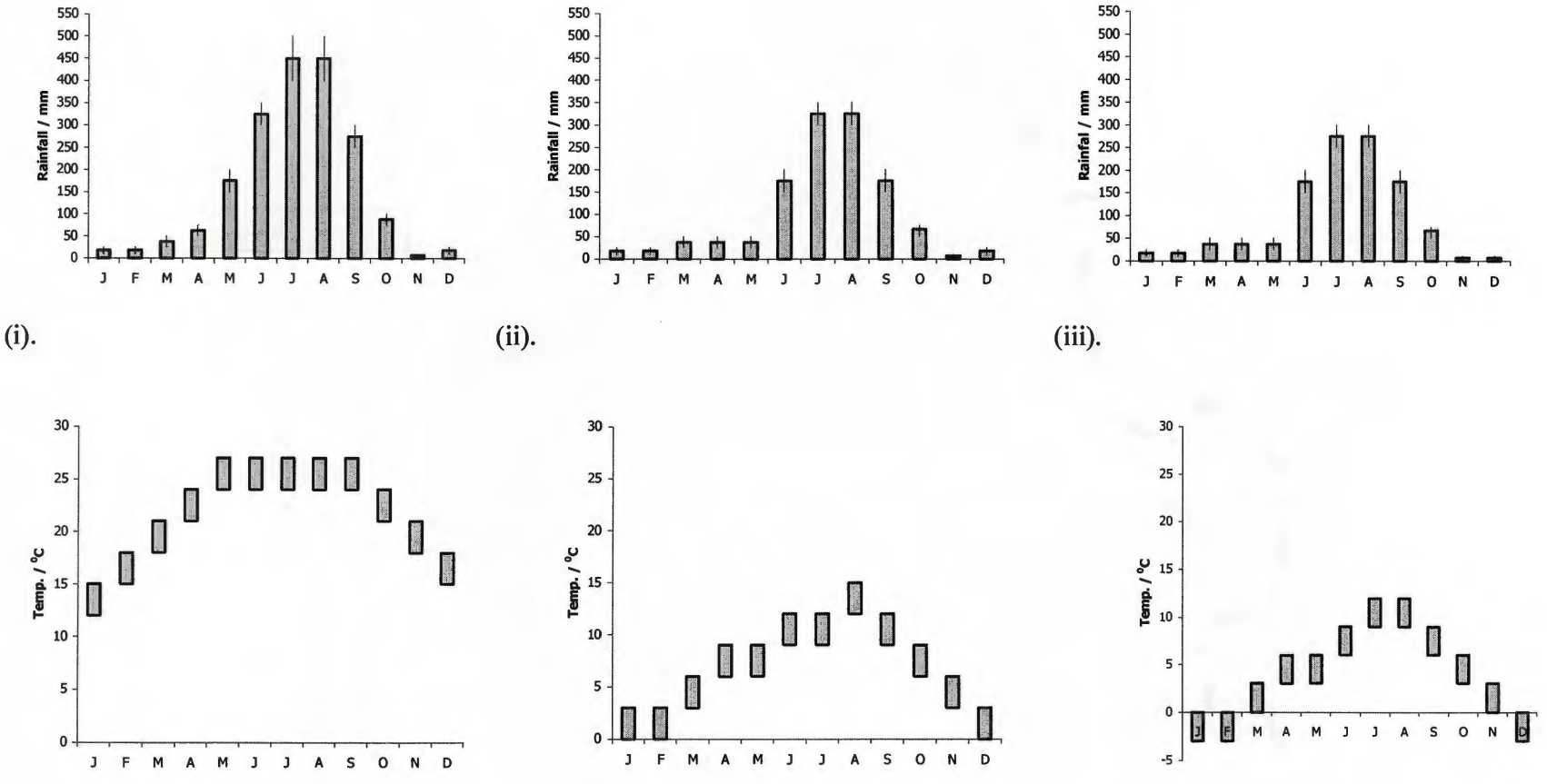

Fig. 2.11. Monthly variations in average rainfall and temperature in the Dudh Kosi.
(i). Lamidanda. (ii). Namche Bazaar. (iii). Tyangboche.

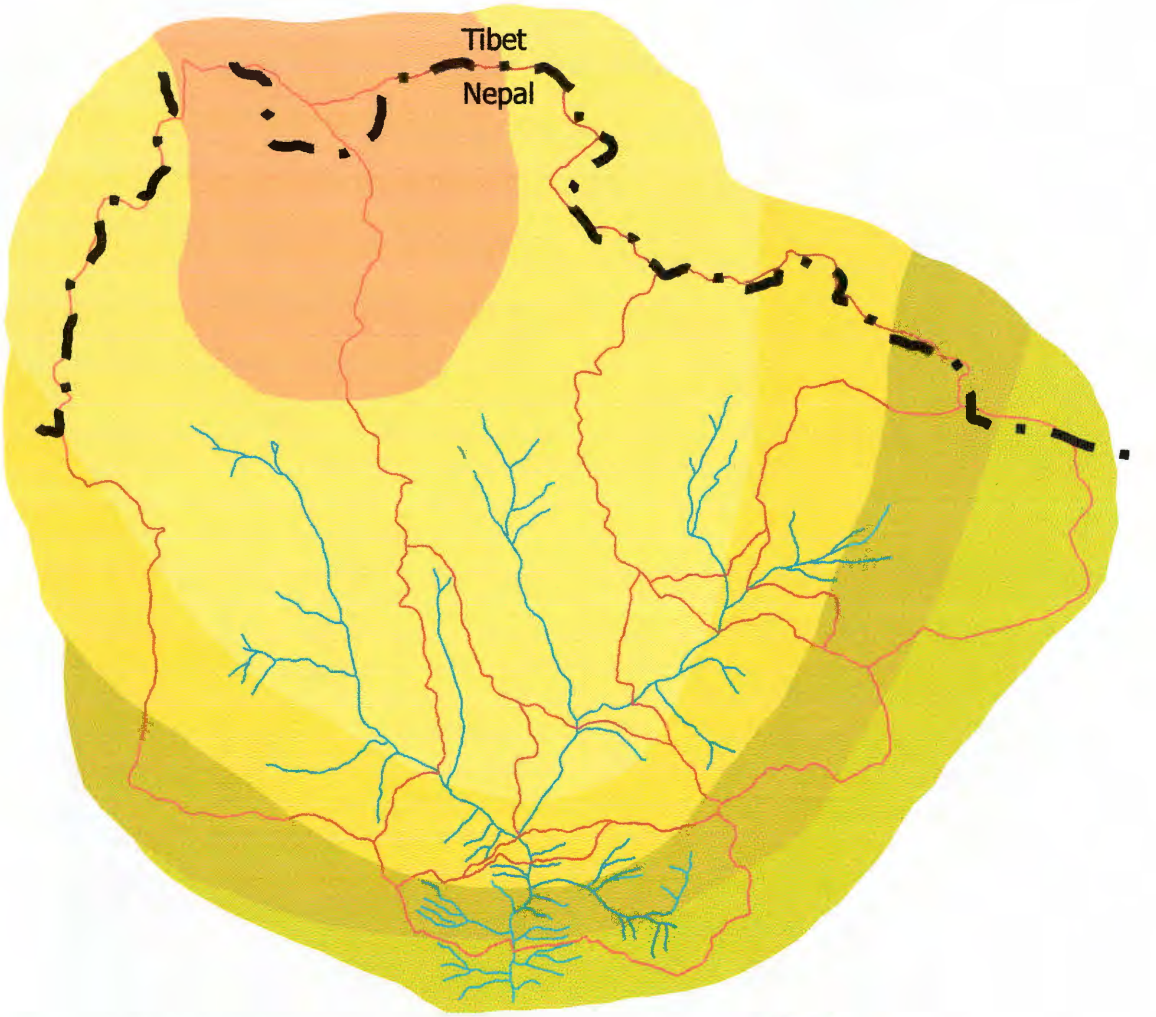

Fig. 2.12. Annual rainfall contours in the Khumbu region.
River courses are marked by blue lines, watersheds are shown in red.
Source: Chalise et *al.*, 1996.

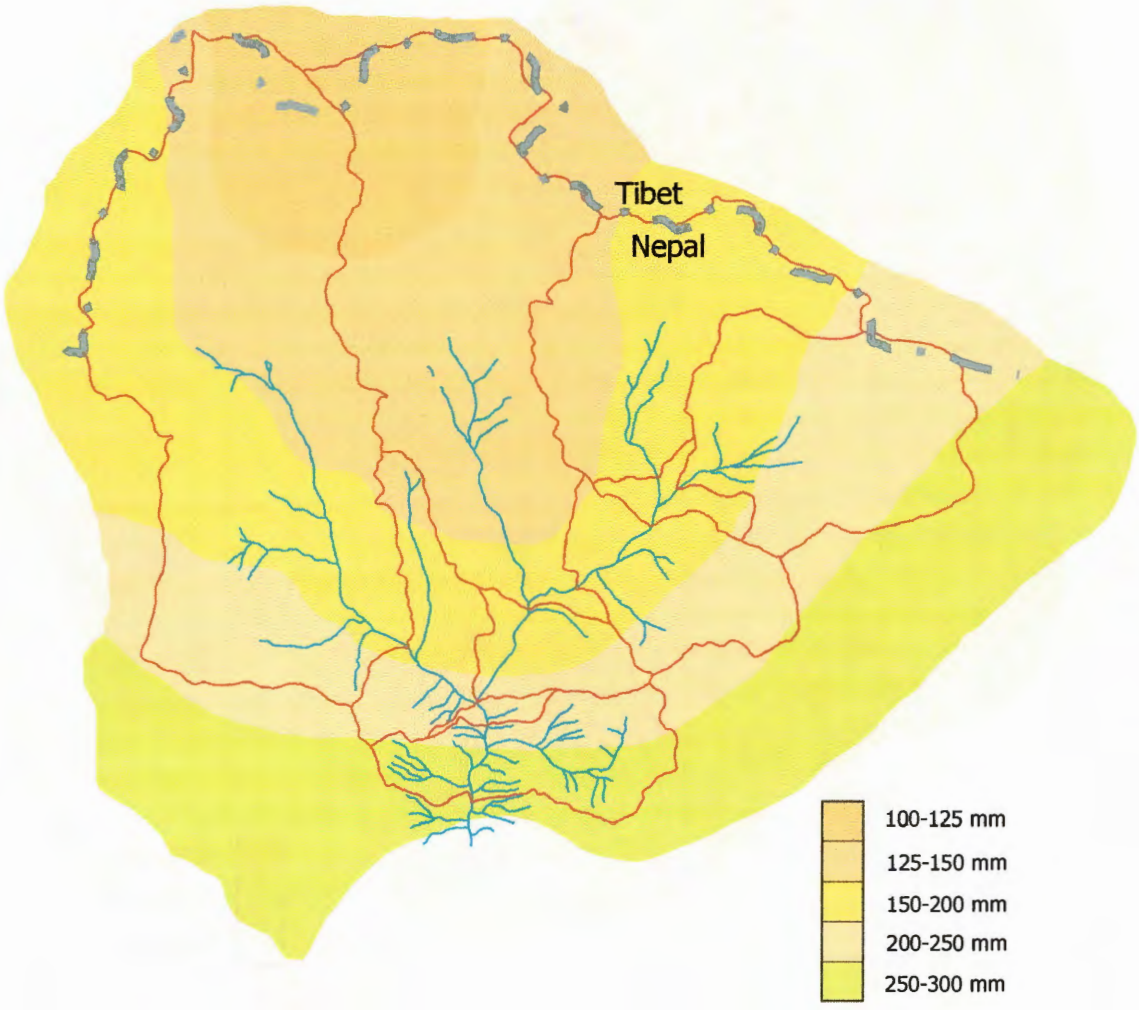

Fig. 2.13. Rainfall contours for the Khumbu region in September.

River courses are marked by blue lines, watersheds are shown in red.
Source: Chalise *et al.*, 1996.

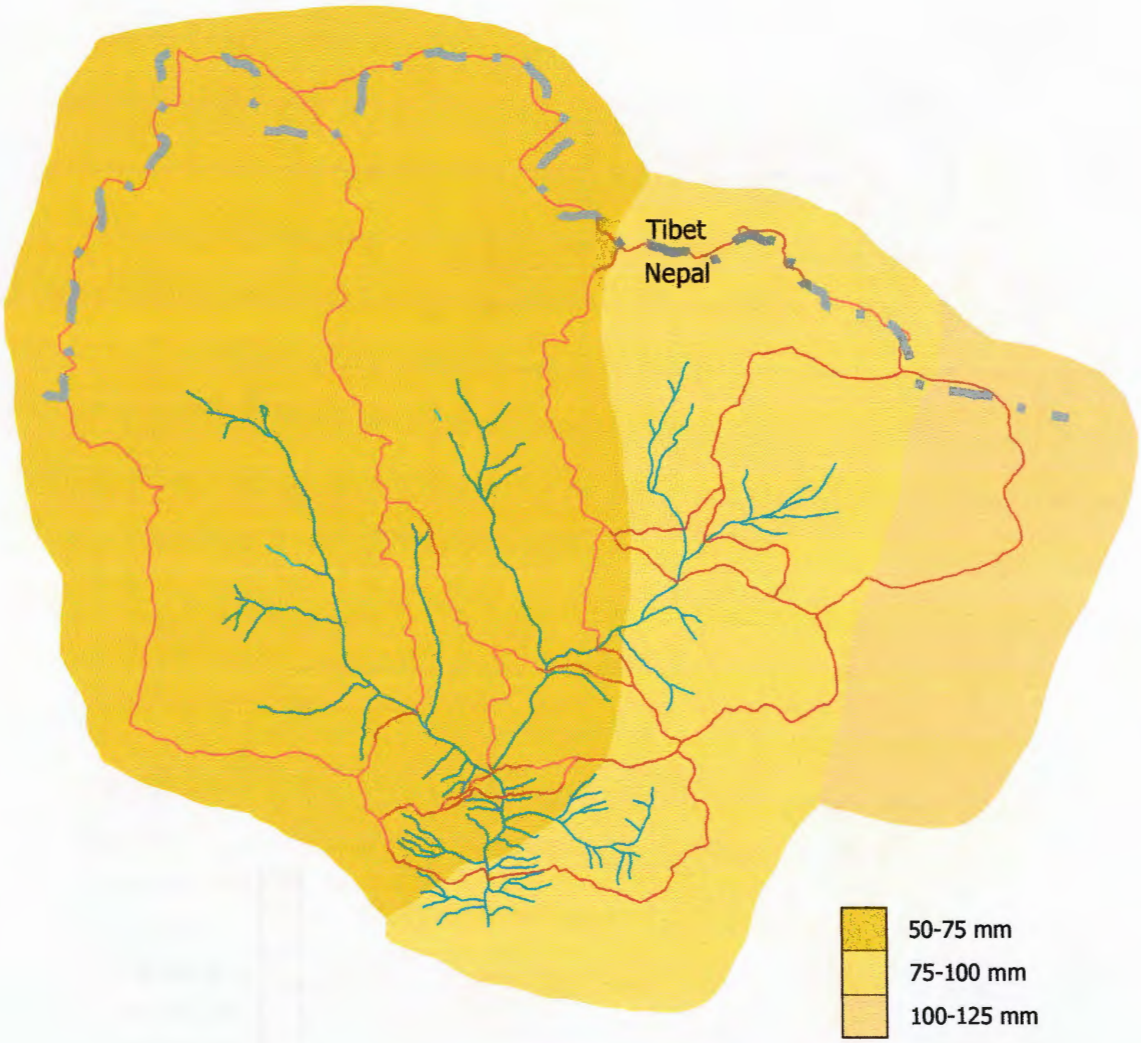

Fig. 2.14. Rainfall contours for the Khumbu region in October.
River courses marked by blue lines, watersheds in red.
Source: Chalise *et al.*, 1996.

Fig. 2.12 shows the average annual precipitation in the Khumbu region, which in this basin appears to decrease both with altitude and moving northwards. Rainfall is highest (1600 – 1800 mm) in the lowest part of the sampled catchment, in the region of Ghat. In contrast, the most northerly part of the catchment, around the Cho Oyu Massif, receives nearly half this amount of rain (snow). A similar pattern is seen in average rainfall for September (fig. 2.13). In October, rainfall is considerably lower (less than 125 mm in all areas), and a decreasing east to west pattern is noted (fig. 2.14).

Fig. 2.11 additionally shows climatological data for Lamidanda, south of the sample region shown in plate 5, firmly within the Lesser Himalaya in the slow flowing, heavily vegetated portion of the river leading up to the confluence with the Sun Kosi (see plate7). Monsoonal rainfall is slightly higher in this portion of the river, while average temperatures are much higher, never falling below 12°C, and exceeding 25°C in the summer.

2.5.4. Flow Characteristics.

Fig. 2.15 shows the monthly variation in streamflow and specific discharge at Lamidanda in the Lesser Himalayan Formation, the only site for which data are available. These data are not representative of the river at the sample sites used in this study. In the rivers of the Khumbu it would be expected the monsoon pattern less well defined, as very high altitude basins such as this are dominated by a cycle of snow

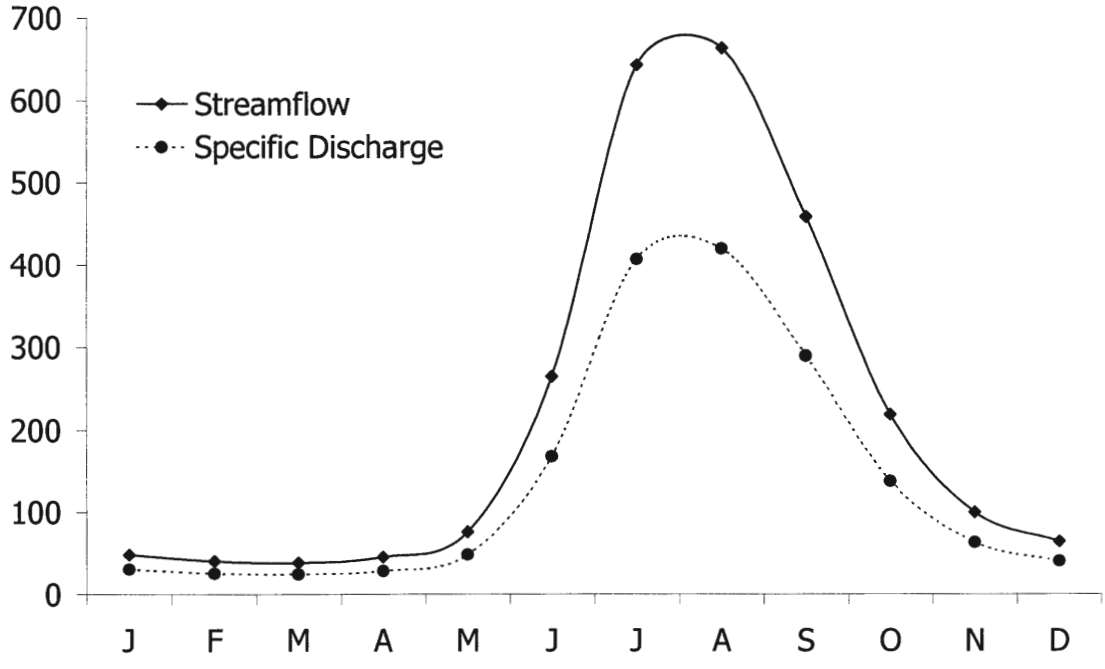

Fig. 2.15. Monthly variations in streamflow (m^3/s) and specific discharge (mm/month) in the Dudh Kosi at Lamidanda.

accumulation and melt (Alford, 1992). The Dudh Kosi is a major tributary of the Sun Kosi, contributing a considerably greater volume of water then the Bhote Kosi (the Dudh Kosi has a monsoonal flow of ~700 m^3/s while the peak flow of the Bhote Kosi is <250 m^3/s). The specific discharge is still less than that of the Balephi Khola (fig. 2.9), demonstrating the erosive power of the latter.

2.5.5. Land Use.

The upper parts of the Khumbu basin are areas of perpetual snow and ice, with exposed rock at altitudes below this. As altitude decreases, alpine vegetation is observed, with a

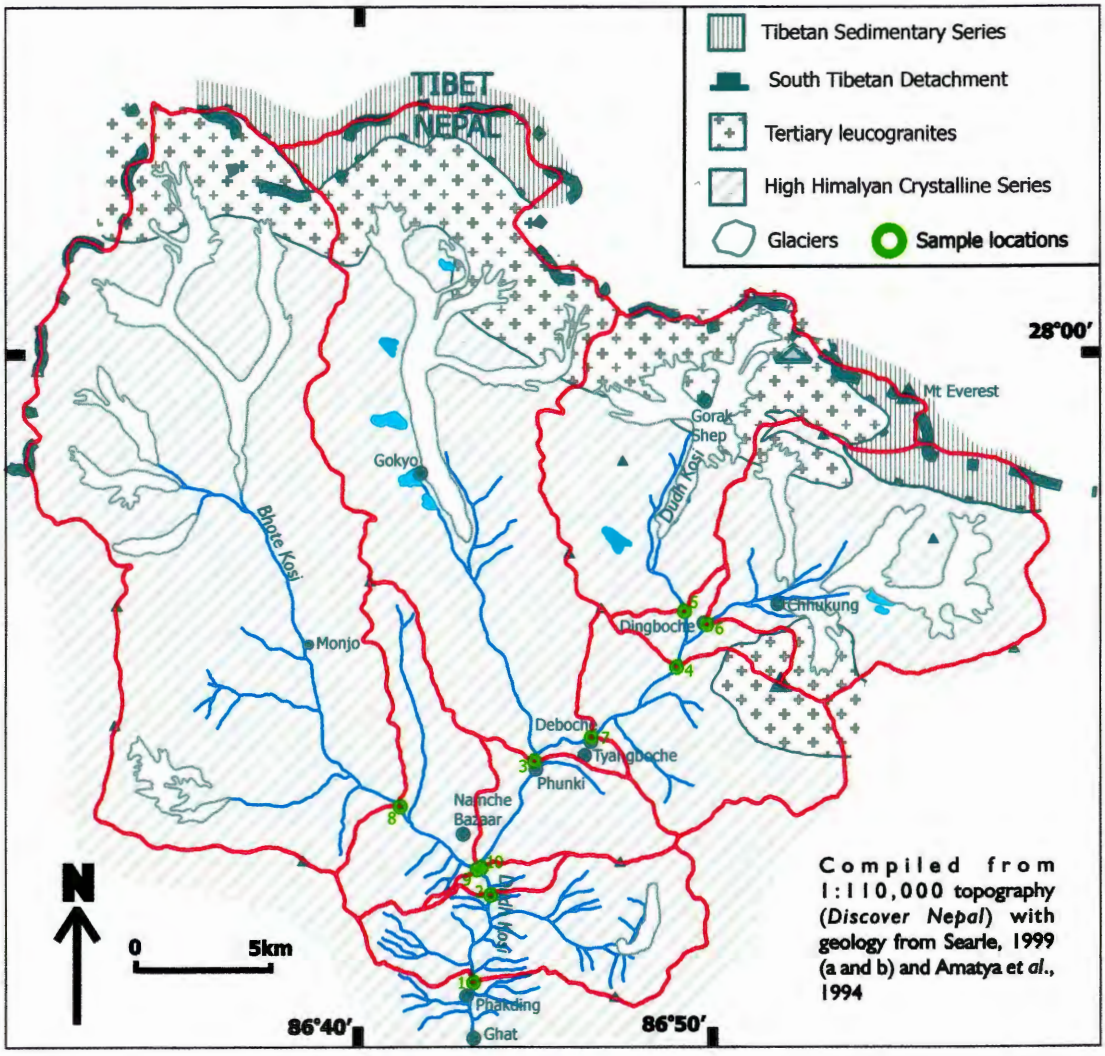

Plate 5. Sampled catchments in the Khumbu region.
Watersheds are marked in red.

more mixed fauna further down. Agriculture is limited, although some terracing is noted around Namche Bazaar and in the region downstream of the confluence of the Dudh Kosi and the Bhote Kosi (Khumbu).

2.5.6. Sampling Strategy.

Plate 5 shows the catchments of the samples collected in the Khumbu region. This was a reconnaissance study, with sampling only of the major confluences that build up the Dudh Kosi from the Khumbu Glacier downstream to the confluence with the Bhote Kosi (Khumbu) at Phakding.

2.6. Sun Kosi ("River of Gold").

The Sun Kosi flows eastwards through the great valley between the Mahabharat Lekh range and the Himalaya forming the watershed for most of eastern Nepal. The aforementioned Bhote Kosi, Balephi Khola, Indrawati and Dudh Kosi are all part of the Sun Kosi system. The name of the river refers to the abundance of reflective mica flakes in its waters.

2.6.1.Geology.

The geology of the Sun Kosi is illustrated in plate 6. The only significant portion of the Sun Kosi catchment draining the TSS is the upper part of the Bhote Kosi, the Tamba

Kosi also draining a very small section of TSS (see plate 7 for catchments). The other tributaries of this river; the Indrawati, Likhu Khola and Dudh Kosi, originate in the HHCS. All of these rivers cross the MCT and drain extensive sections of the Lesser Himalaya, including Nawakot Group calc-silicates, Kuncha Group silicate metasediments and crystalline silicates, exposures of the latter being particularly prevalent in the Tamba Kosi. The Chak Khola and Rosi Khola in the far West of the catchment drain the Kathmandu Nappe. The Sun Kosi itself, between the confluence of the Bhote Kosi and Indrawati to the confluence with the Dudh Kosi, runs along a relatively narrow exposure of Nawakot Group rocks. It subsequently cuts into the HHCS as it moves south towards its confluence with the Arun and Tamur near Chatra, where further Lesser Himalayan rocks are exposed north of the MBT.

2.6.2. Altitude.

The south-flowing tributaries of the Sun Kosi drain some of the most elevated terrain in the world (see descriptions of the Bhote Kosi, Indrawati and Dudh Kosi). The Sun Kosi itself originates innocuously as the Sun Kosi Nadi to join the Bhote Kosi at Barabise. In this work, however, the only the main section of the river from Dolalghat is referred to as the Sun Kosi. The main river is characterised by a shallow gradient, with an average of 0.2% (maximum of 0.6%) between Dolalghat (625 m) and Chatra (115 m) (Knowles & Allardice, 1992).

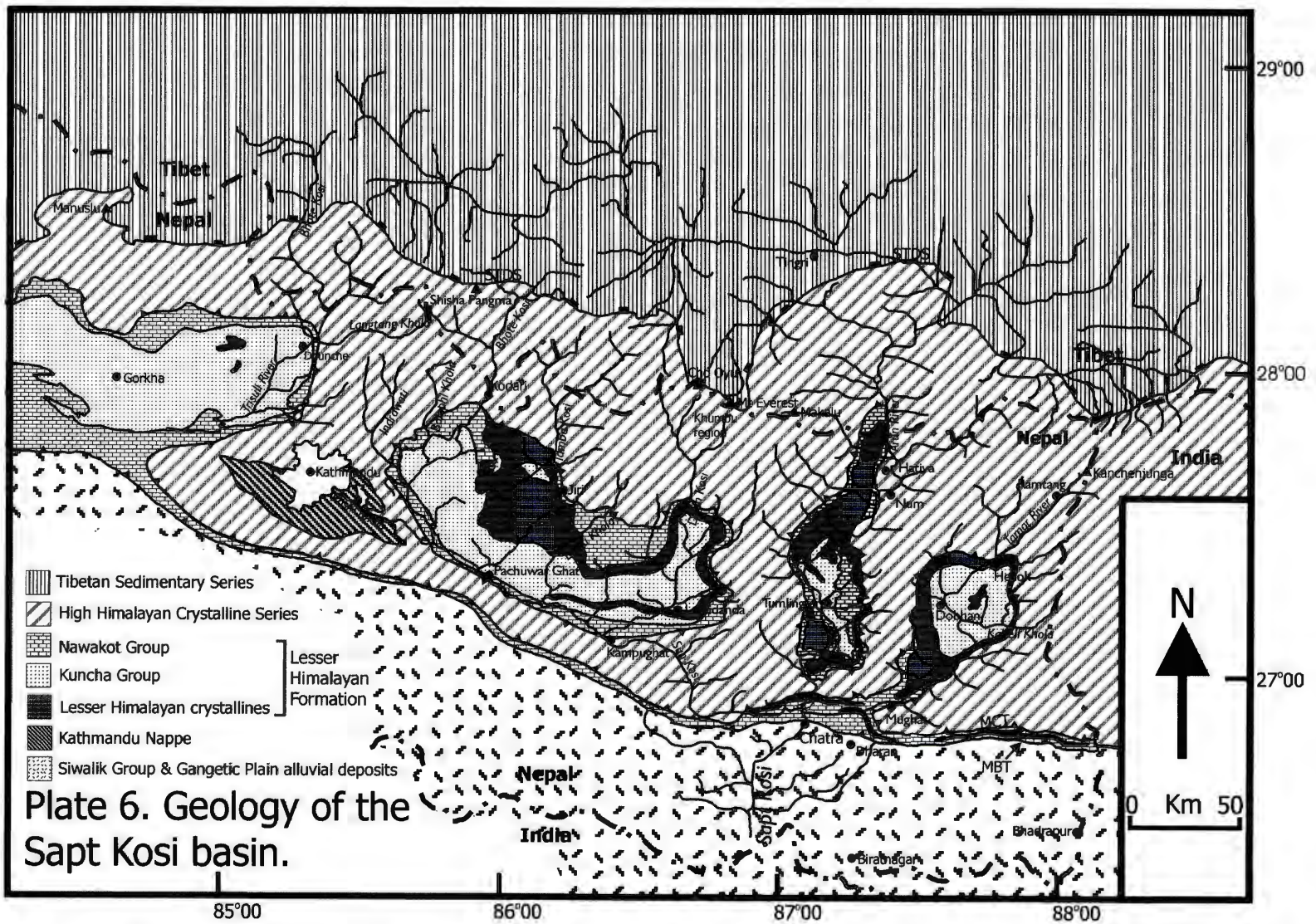

Plate 6. Geology of the Sapt Kosi basin.

Data sources; Nepal DMG 1:250,000 & 1:1,000,00 geological maps; Burchfiel *et al.* (1992); Amataya *et al.*, 1994; Searle *et al.*, 1997; Searle, 1999a and b

2.6.3. Climate.

The Sun Kosi basin experiences the full range of Himalayan climatic zones as described in chapter 1, with the exception that the catchment of this river never really reaches up onto the Tibetan Plateau.

Fig. 2.16 illustrates mean rainfall in November (when sampling of the Sun Kosi, Arun and Tamur at their confluence was carried out) in the Sapt Kosi basin, which includes the Sun Kosi catchment. Broadly speaking, rainfall is highest immediately south of main Himalayan range, and decreases southwards, although regions of very high altitude (e.g. Khumbu) receive less rainfall. Similar patterns are observed in average annual rainfall (Chalise *et al.*, 1996). The Sun Kosi valley receives more rainfall than does the Mahabharat Lekh to the north. Fig. 2.17 illustrates the climatic conditions of the Sun Kosi valley and monsoonal conditions are again observed. Peak summer rainfall, which is 200 - 300mm in Pachuwar Ghat, 300 - 400mm in Kampughat, is less than half that observed in the Bhote Kosi and Balephi Khola immediately south of the Himalaya. Average temperatures are typical of the lower altitudes of central Nepal, never lower than 10°C and exceeding 25°C in the summer at Pachuwar Ghat. At the lower altitudes of Kampughat, temperatures are approximately 5°C higher throughout the year.

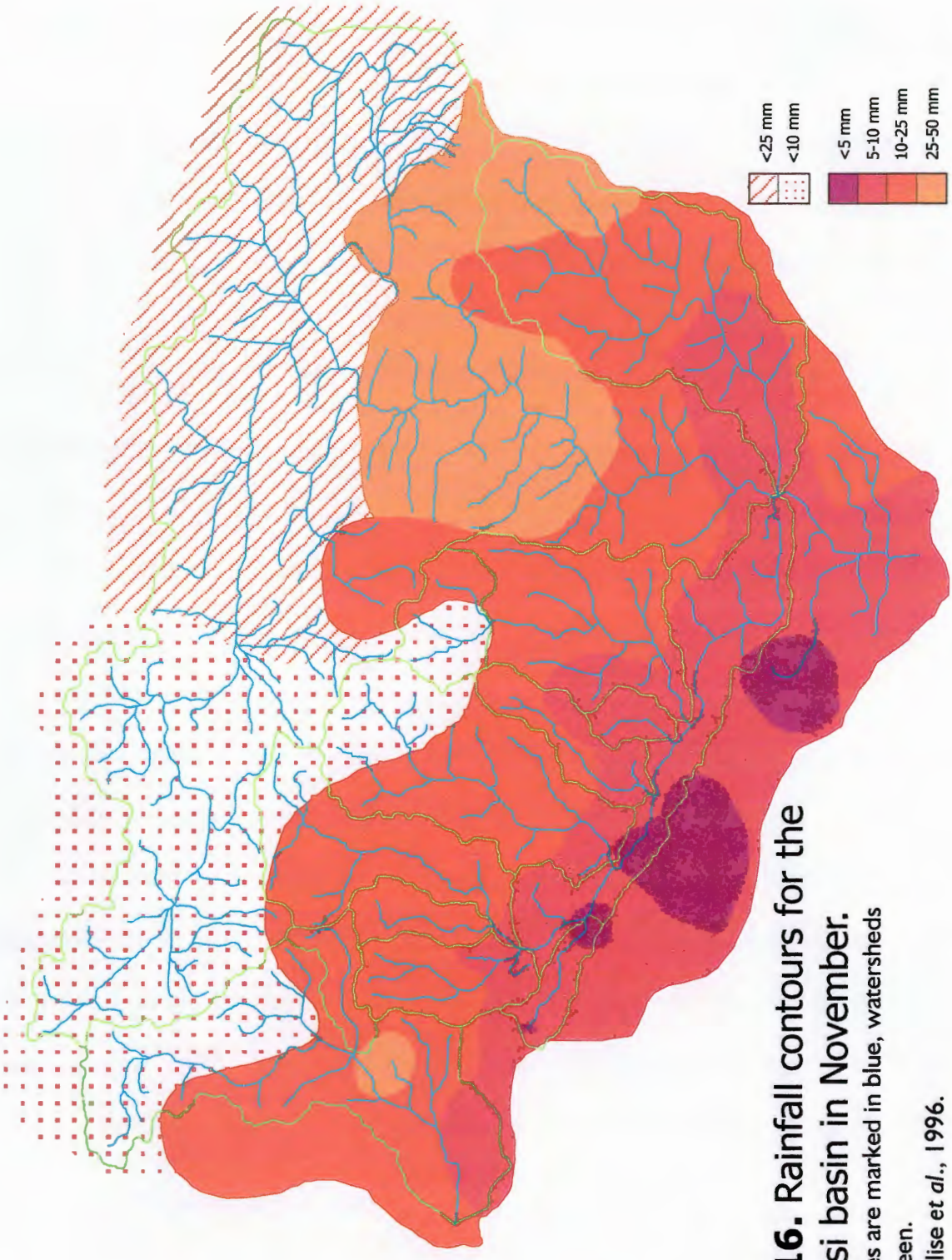

Fig. 2.16. Rainfall contours for the Sapt Kosi basin in November.
River courses are marked in blue, watersheds shown in green.
Source: Chalise *et al.*, 1996.

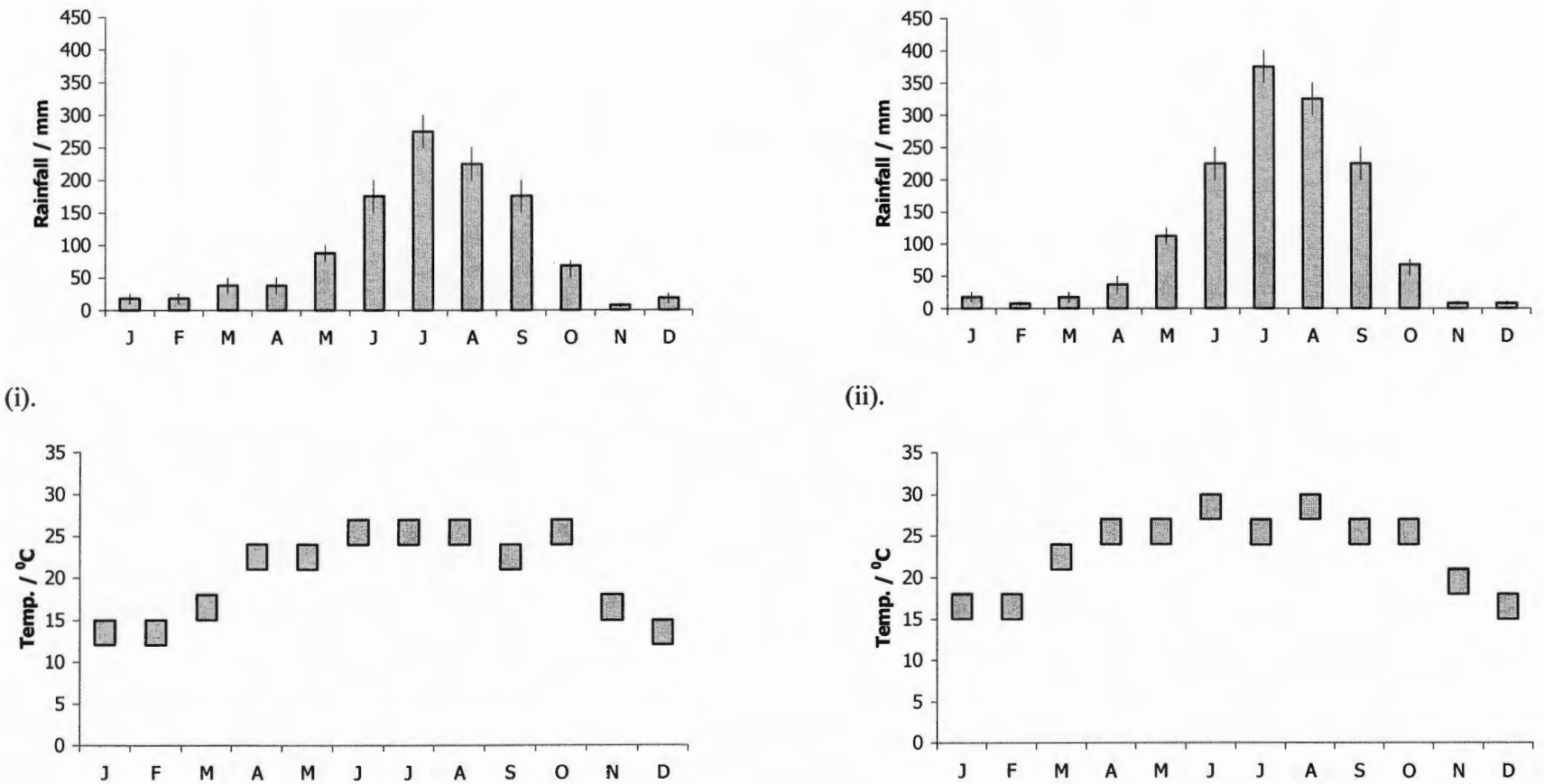

Fig. 2.17. Monthly variations in average rainfall and temperature in the Sun Kosi.
(i). Pachuwar Ghat. (ii). Kampughat.

2.6.4. Flow Characteristics.

Fig. 2.18 illustrates the monthly changes in streamflow and specific discharge in the Sun Kosi downstream of the Tamba Kosi (Pachuwar Ghat) and downstream of the Dudh Kosi (Kampughat). The huge increase in the volume of the river through the addition of the major south-flowing tributaries is clear both when comparing these two charts, and when comparing both with those for the Bhote Kosi and Indrawati. Alford (1992) notes anomalously low specific runoff in the lower section of the Sun Kosi, although it is unclear whether this is due to climate or consumptive water uses such as irrigation. This anomaly is not apparent in fig. 2.18, as tributary inputs mask the low streamflow and specific discharge of the Sun Kosi itself.

2.6.5. Land Use.

There are obviously a multitude of land uses in a basin as large as that of the Sun Kosi. Previous sections on the Bhote Kosi, Indrawati and Dudh Kosi give a idea of landuse in the major south-flowing tributaries. The Sun Kosi river itself occupies a valley of tropical vegetation, sometimes forming steep gorge sections, in other places meandering through a 2 km wide valley floor of gravel and rock. The lower altitudes of the basin are heavily cultivated, although there are no major towns downstream of Dolalghat. The hydropower potential of the Sun Kosi has yet to be harnessed although this may not be for long as a number of proposals have been outlined for the river (www.panasia.org.sg).

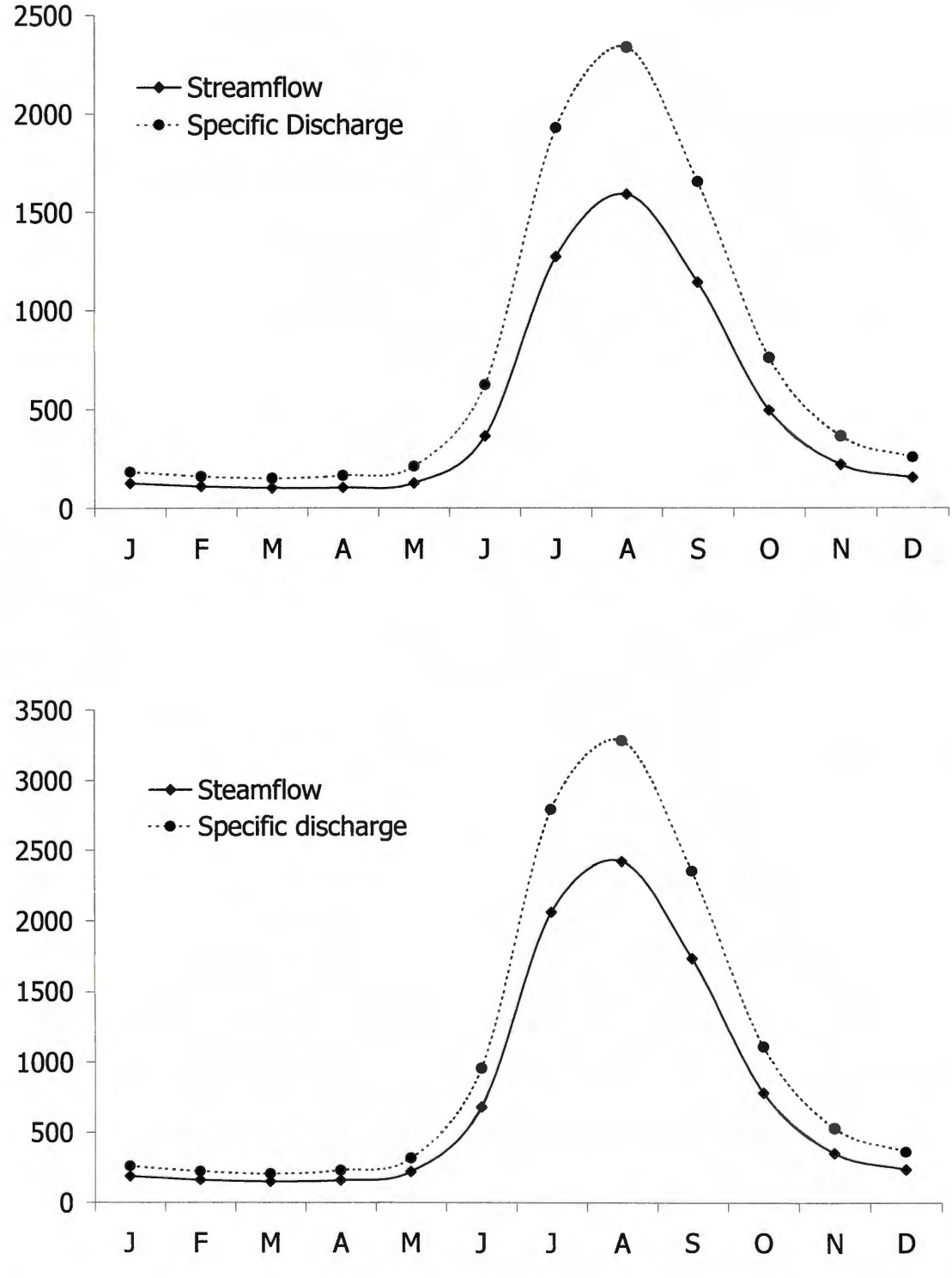

Fig. 2.18. Monthly variations in streamflow (m^3/s) and specific discharge (mm/month) at Pachuwar Ghat (above) and Kampughat (below) in the Sun Kosi.

2.6.6. Sampling Strategy.

The Sun Kosi was not itself a focus for intensive study. Samples were taken downstream of Dolalghat to assess the effects of the mixing of the Bhote Kosi, Chak Khola and Indrawati. Additionally, a single sample was taken at the very end of the river upstream of its confluence with the Arun.

2.7. The Arun River.

The Arun is one of the great rivers of the Himalaya, cutting both the Tibetan Marginal Range and the Himalaya itself.

2.7.1. Geology.

The Arun is important to this work as it provides a excellent example of a Himalayan river with the bulk of its catchment draining the Tibetan Sedimentary Series (plate 6 and plate 7). The river crosses a 6-7 km thickness of the HHCS inbetween the Everest and Kanchenjunga massifs, the geology being similar to that described for the Khumbu region. It then meanders southwards, cutting the MCT several times and draining Lesser Himalayan units of the Nawakot Group, Kuncha Group (although relatively little of these) and granitic orthogneiss (the Num Orthogneiss, Brunel, 1983; Lombardo *et al.*, 1993) in the Arun Valley tectonic window.

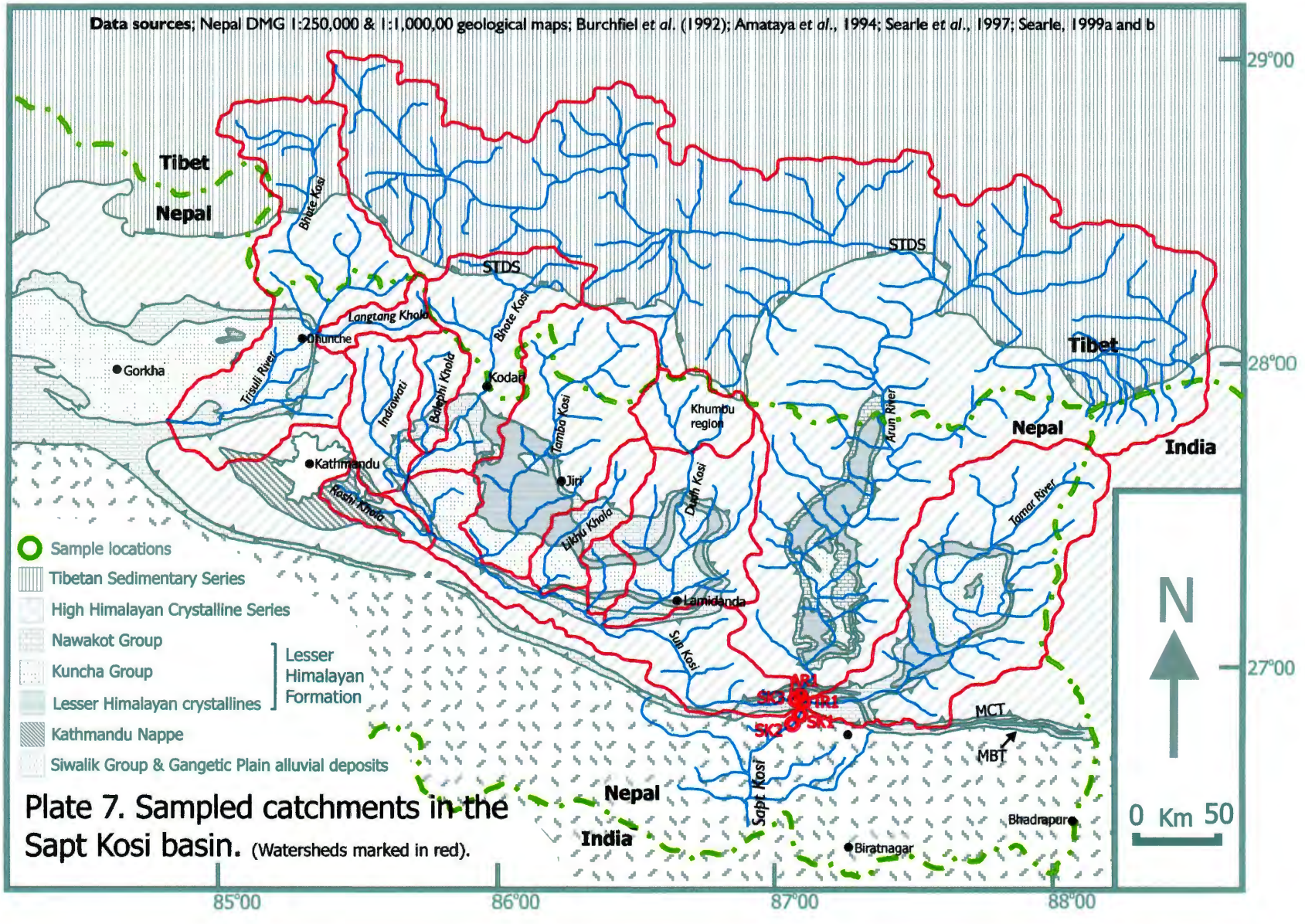

Plate 7. Sampled catchments in the Sapt Kosi basin. (Watersheds marked in red).

2.7.2. Altitude.

Sourced from the Peiku Tso Lake, the bulk of the huge Arun catchment (30,000 km^2, Hagen *et al.*, 1963) lies on the Tibetan Plateau, as shown by fig. 2.19. >80% of the surface area of the basin lies above 5500 m, 30% at 6500m or above. The river originates to the north-west of the Shisha Pangma Massif, where the western margins of its catchment abut the Bhote Kosi basin. The river flows in an easterly arc for 200km, first south-eastwards across the southern edge of the plateau at altitudes of over 5000m, with a gentle gradient, draining the northern slopes of the Himalaya, including Makalu (8463 m) and Mt Everest. It then turns sharply, heading southwards in a similar fashion to the larger Tsangpo-Brahmaputra (which lies to the north and east), cutting some of the steepest relief in the world (Alford, 1992). The Arun crosses the STDS at ~3000 m and the MCT (for the first time) at ~1500m. The gradient of the river eases south of the MCT and its lower section, between Tumlingtar (290 m) and Chatra (115 m), it has an average gradient of just 0.25% (maximum 0.4%) (Knowles & Allardice, 1992).

2.7.3. Climate.

Fig. 2.20 shows average temperatures and rainfall at Tumlingtar, in the lower reaches of the river (altitude ~ 400 m), and at the most northerly Nepali settlement on the river, Hatiya (~1250 m), approximately 30 km south of the MCT. At Tumlingtar, lowest average winter temperatures are 12°C, while average August temperatures reach 30°C. Hatiya is predictably cooler, with average temperatures ranging between 5°C in

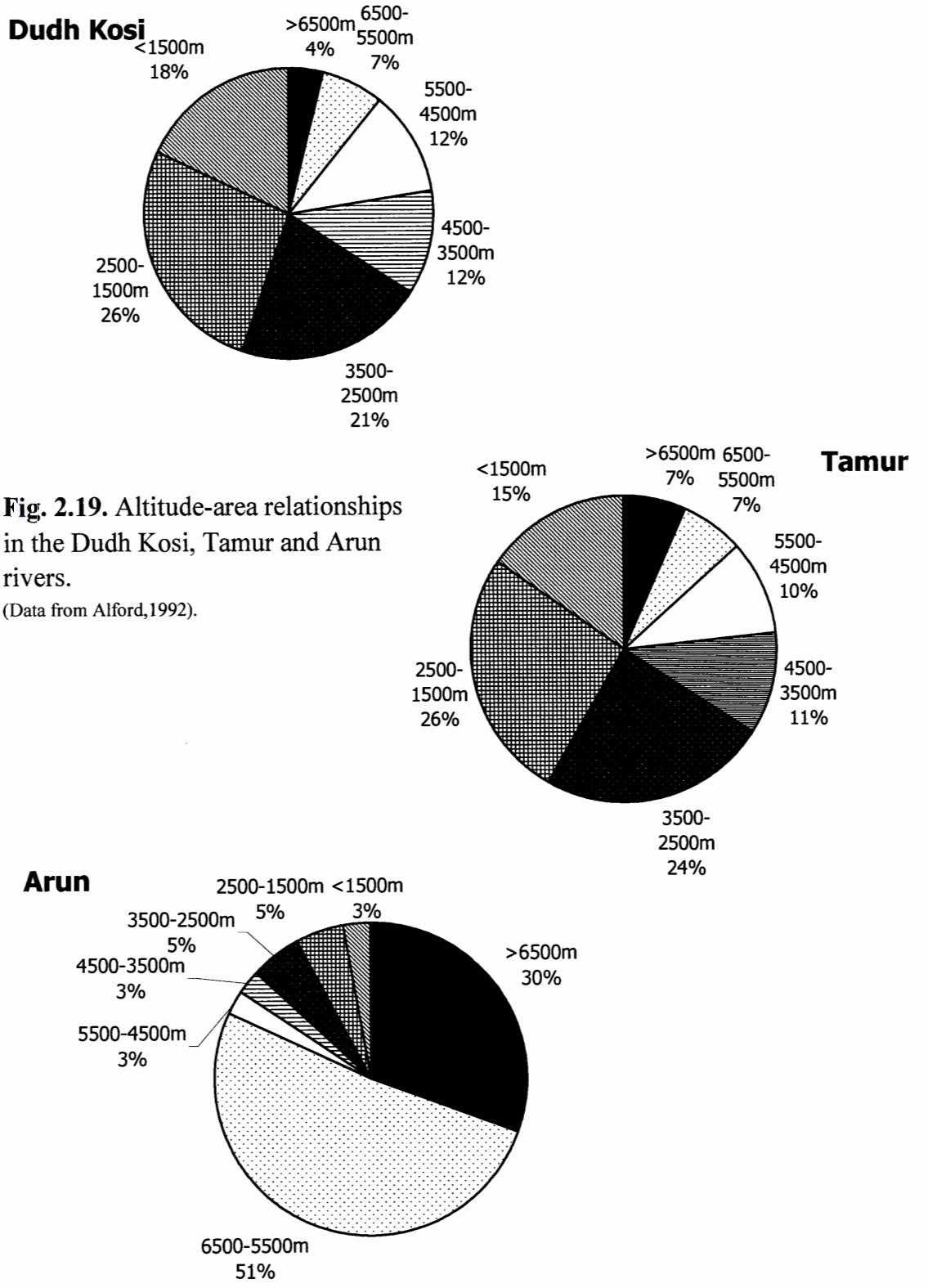

Fig. 2.19. Altitude-area relationships in the Dudh Kosi, Tamur and Arun rivers.
(Data from Alford,1992).

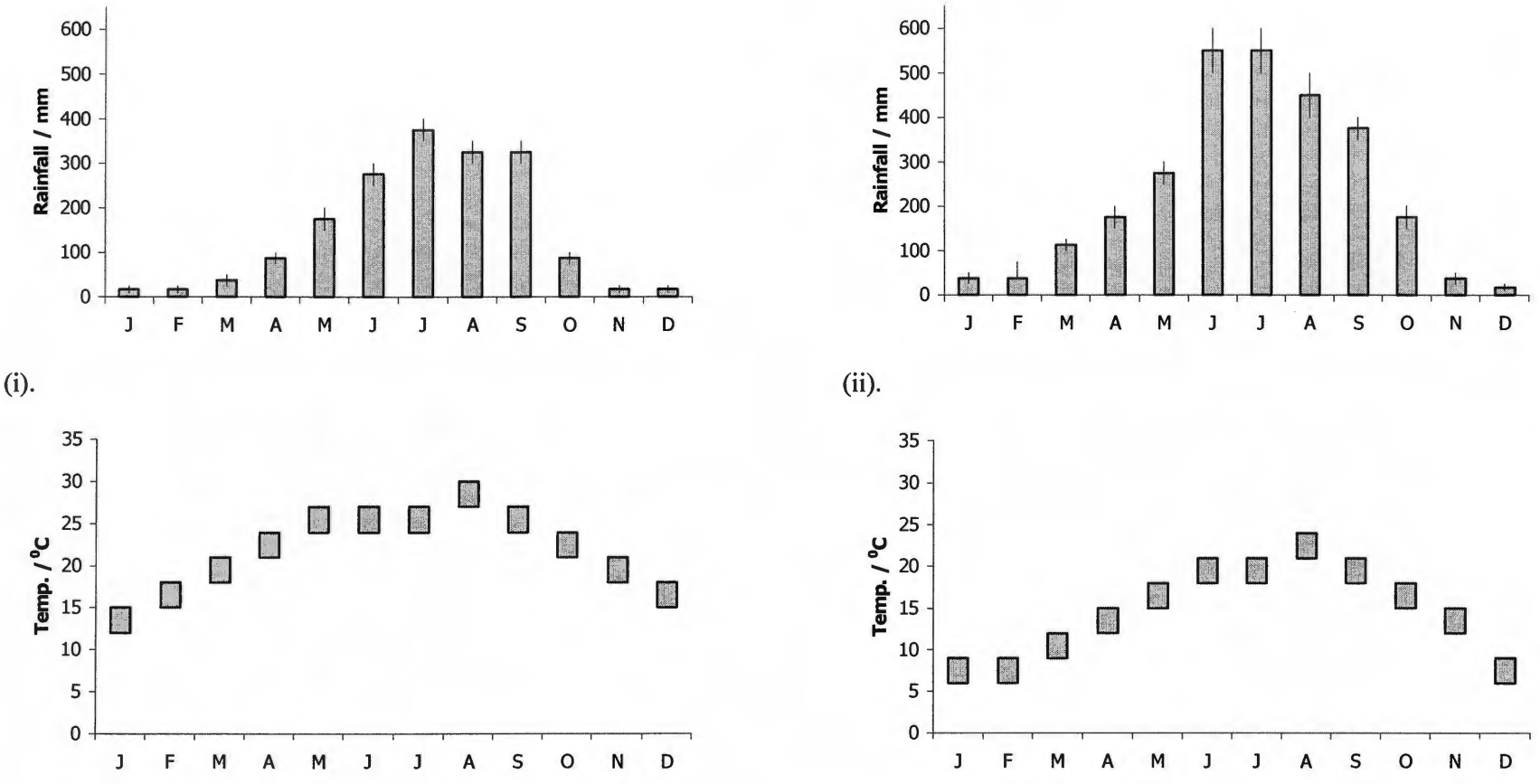

Fig. 2.20. Monthly variations in average rainfall and temperature in the Arun.
(i). Tumlingtar. (ii). Hatiya.

December and >20°C in the summer. The Arun valley receives some of the highest rainfall in Nepal, with monsoon monthly averages reaching in excess of 600 mm at Hatiya, less (~400 mm) at Tumlingtar. Only the Bhote Kosi, Indrawati and Kali Gandaki valleys receive more (Chalise *et al.*, 1996). Fig. 2.16 shows rainfall contours for the Sapt Kosi basin in November and it can be seen that at the time of sampling the average rainfall for the Arun valley is greater than anywhere else, although it is still minimal in this dry month..

2.7.4. Flow Characteristics.

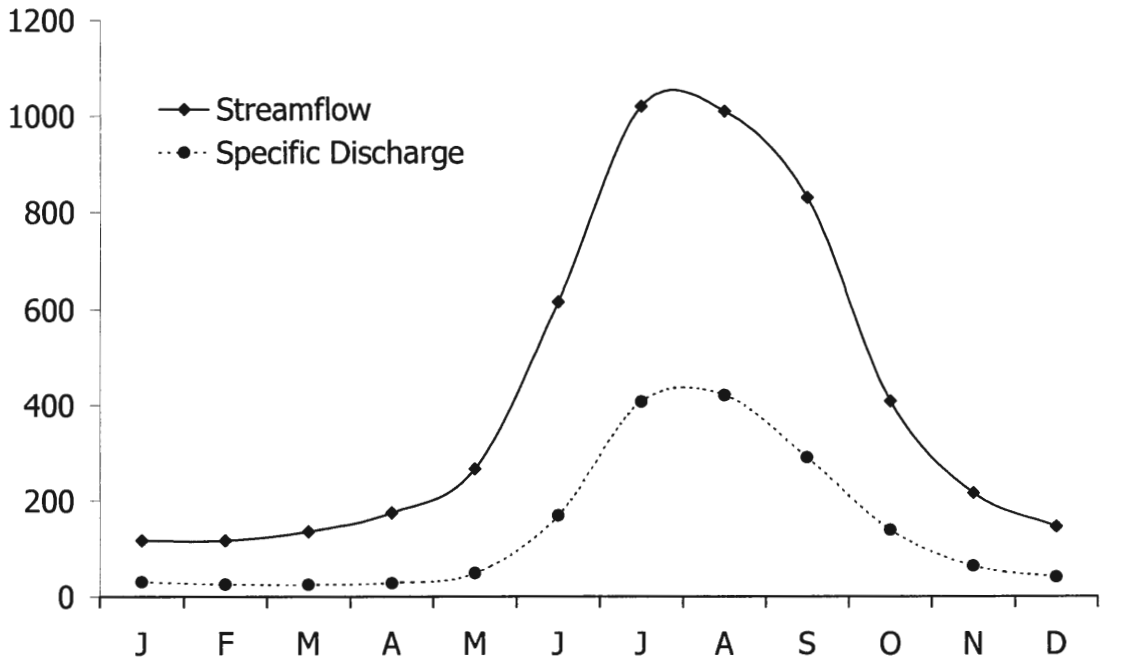

Fig. 2.21. Monthly variations in streamflow (m^3/s) and specific discharge (mm/month) in the Arun river at Tumlingtar.

Fig. 2.21 illustrates streamflow and specific discharge at Tumlingtar (below which little streamflow is added, Knowles and Allardice, 1992), in the lower reaches of the Arun. The monsoon pattern is slightly less stark in comparison with hydrographs for the other rivers sampled in this work, probably due to more constant inputs (snow and icemelt) from the Tibetan Plateau. Despite its large catchment area, the streamflow of the Arun is less than half that of the Sun Kosi throughout most of the year, while specific discharge is low relative to streamflow, perhaps reflecting the contrasting rainfall on either side of the Himalaya. The data plotted on fig. 2.21 reflect the nature of the river at Tumlingtar, where it occupies a broad lowland valley with a shallow gradient, and not the nature of the river in the steep gorges upstream of the MCT. Indeed, it is estimated that half of the rivers volume is added between Num (~750 m), ~50 km downstream of the MCT, and Tumlingtar (~350 m), a section in which the main river is joined by several major tributaries draining the eastern slopes of Makalu and Chamlang (7319 m).

2.7.5. Land Use.

The contrasts in vegetation and associated landuse within the Arun basin are wide ranging, and little can be added beyond the general Himalayan model (chapter 1). The section of the river on the Tibetan Plateau is characterised by the bare rock of the Gangdese Shan range, with limited cultivation and sheep and yak grazing in the poor soils of the river valley itself. The Friendship Highway crosses the watershed between the Bhote Kosi and Arun catchments to join another major Chinese highway linking

Lhasa with western Tibet, which runs along the Arun valley. Numerous small settlements have been established along the road (river), the largest of these being Tingri and Shegar. As the river turns to the south it enters thickly forested gorges in which human land use is largely negligible, with only a few villages north of Tumlingtar. Further downstream is the semi-tropical "jungle" of the Nepalese lowlands, with widespread villages and associated terraced agriculture downstream of Tumlingtar which has replaced forested land in the last 50 years.

The Arun has long been a focal point for supporters of exploiting Nepal's hydroelectric potential, although the controversial $923 million 402 MW Arun III hydroelectric project, involving the construction of a dam and 10 km tunnel near Num (www.ledco-nepal.com), has been shelved after the World Bank withdrew funding.

2.7.6. Sampling Strategy.

Only a single sample was taken from the Arun, at its most downstream point immediately prior to its confluence with the Sun Kosi and Tamur.

2.8. Tamur River.

The Tamur drains the far east of Nepal and provides an excellent example of a major Himalayan river (the sixth largest in Nepal) unaffected by inputs from the Tibetan Plateau.

2.8.1. Geology.

The Tamur provides a major contrast with the Arun, its catchment being encompassed by the Kanchenjunga Massif and other high mountains, so that the river catchment contains no Tibetan Sedimentary Series lithologies. The river rises within the High Himalayan Crystalline Series and associated Tertiary leucogranites, and drains the HHCS for some ~75 km of its length before crossing the MCT and draining the Lesser Himalayan augen gneisses and metasediments of the Kuncha Group (the Taplejung tectonic window) (plate 6 and plate 7). Only in its lowest reaches does the Tamur drain the Nawakot Group calc-silicates.

2.8.2. Altitude.

The Tamur basin lies to the east of the Arun catchment. Its north-eastern margins are defined by the arc of high peaks which also mark the north-eastern border of Nepal with Sikkim and the Tista river valley, the highest point in the catchment being Kanchenjunga itself (8598 m). The sources of the river are the glaciers of the lower slopes (>5000 m) of these mountains. The river descends rapidly through the HHCS, with an average gradient well in excess of 5%, crossing the MCT close to the settlement of Hellok (1430 m). Between Hellok and Dobhan (630 m), the average gradient is 4%, after which the river levels off somewhat before steepening again in its last 40 km (in the Nawakot Group) up to the confluence with the Sun Kosi and Arun. Between Dobhan and Chatra (115 m) the average gradient is 0.4%, with a maximum of 1% (Knowles &

Allardice, 1992). Fig. 2.19 shows the area-altitude relationships in the Tamur basin. It can be seen that 31% of the basin lies above 4500 m, although only 7% of the surface area constitutes the high peaks above 6500 m, with a fairly even distribution in the lower altitude zones (21% of surface area between 3500 and 1500 m, 26% between 2500 and 1500 m and 18% below 1500 m). This distribution is almost identical to that seen in the Dudh Kosi basin, and thus appears to be typical of large river originating in the HHCS.

2.8.3. Climate.

Fig. 2.22 demonstrates the climatic variation experienced in the Tamur basin, showing average temperatures and rainfall at Ramtang (~5000 m) at the snout of the Kanchenjunga Glacier, and at Mughat (~400 m) in the Nawakot Group units 30 km upstream of the confluence with the Sun Kosi and Arun. At Ramtang, only in the monsoon months does the average daily temperature exceed freezing, while at Mughat average temperatures exceed 10°C throughout the year, reaching ~30°C in August. Rainfall in the Tamur basin initially increases to the south-west from the high peaks, being highest in the vicinity of the MCT, after which it decreases downstream until the very lowest reaches of the river, where rainfall is again higher (Chalise *et al.*, 1996). Fig. 2.22 reflects these patterns, with monsoonal rainfall higher in the lowlands of Mughat, reaching a monthly average of ~375 mm in the monsoon months compared with ~275 mm on the higher ground of Ramtang. Fig. 2.16 shows rainfall in the Tamur catchment in November, which decreases uniformly south-west from Kanchenjunga, although in no part of the catchment does it exceed 50 mm. In the dry season, fig. 2.22

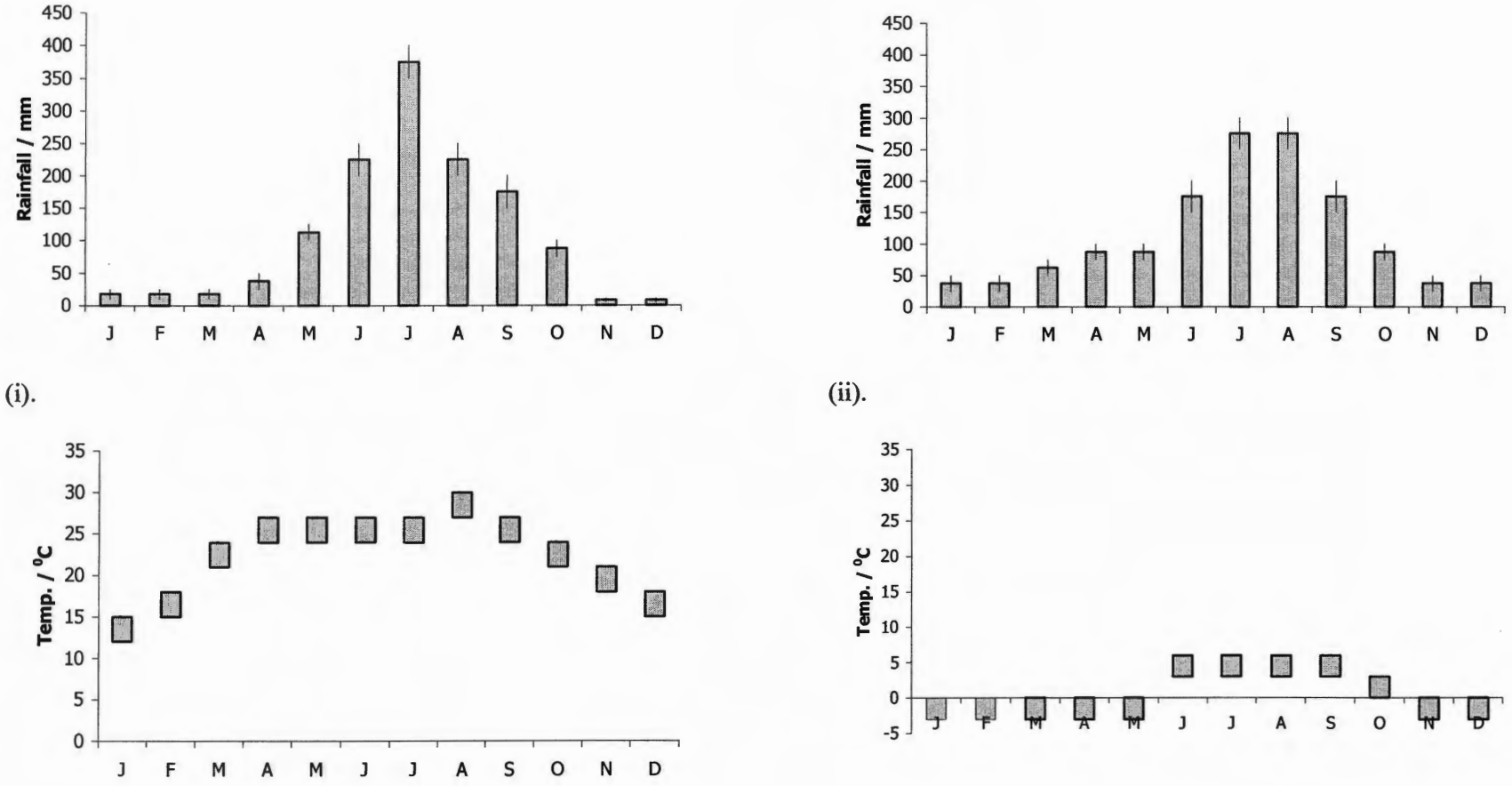

Fig. 2.22. Monthly variations in average rainfall and temperature in the Tamur.
(i). Mulghat. (ii). Ramtang.

shows that Ramtang receives more rainfall (November average of 37.5 mm) than Mughat (7.5 mm).

2.8.4. Flow Characteristics.

Fig. 2.23 illustrates streamflow and specific discharge for the Tamur at Mughat. The river has a considerably smaller volume than the Sun Kosi, being of a similar size to the Arun despite the large contrast in the size of the catchment areas of the two rivers. The

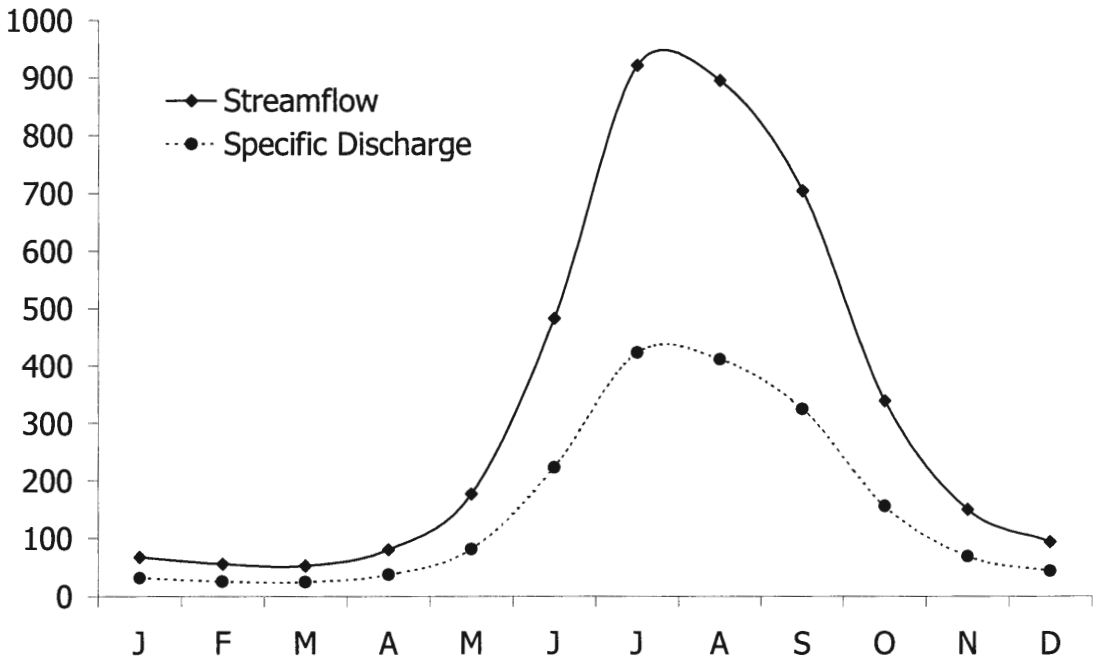

Fig. 2.23. Streamflow (m^3/s) and specific discharge (mm/month) for the Tamur at Mughat.

Kabeli Khola, which joins the Tamur mainstream approximately 10 km downstream of the MCT, adds about a quarter of the volume of the Tamur (Alford, 1992). As with the Arun, specific discharge is relatively low for the recorded streamflow of this river, although as with the Arun this reflects the low gradient and broad valley of the lower Tamur.

2.8.5. Land Use.

The upper reaches of the Tamur basin are protected within the Kanchenjunga Conservation Area, with the previously described gradation from perpetual snow and ice and bare rock, through alpine and sub-alpine to temperate and tropical forests (fig. 1.4). The lower reaches of the catchment, largely south of the MCT, see the appearance of greater population levels and associated terraced agriculture, which accounts for >75% of surface area in some parts (source; ICIMOD / MENRIS land use map), the result of considerable forest degradation in the area. The Tamur is as yet unaffected by the demands of hydropower although the 696 MW Tamur-1 project has been proposed (www.panasia.org.sg).

2.8.6. Sampling Strategy.

Only one sample was collected at the very bottom of the Tamur just before the confluence of the river with the Sun Kosi and Arun, in order to contrast the chemistry of the Tamur with the Sun Kosi and Arun basins.

2.9. Sapt Kosi ("Seven Rivers").

The Sapt Kosi represents the confluence of seven major Himalayan rivers (the Indrawati, Bhote Kosi, Tamba Kosi, Likhu Khola, Dudh Kosi, Arun and Tamur; see plate 7) and is one of the most significant tributaries of the Ganges.

2.9.1.Geology.

The Sapt Kosi drains the full Himalayan sequence, with more detail given above in the sections describing the Bhote Kosi, Indrawati, Dudh Kosi, Sun Kosi, Arun and Tamur. Downstream of Chatra the river crosses the MBT into the Siwaliks.

2.9.2. Altitude.

The huge Sapt Kosi catchment encompasses all of the extremes of the Himalaya, described in chapter 1 and in the aforementioned descriptions of the river's major tributaries above. The Sapt Kosi itself begins at the confluence between the Sun Kosi, Arun and Tamur just upstream of Chatra (115 m) (see plate 7). Downstream of Chatra the river disgorges onto the flat plains of the Terai and northern India, depositing large quantities of largely infertile micaceous sands (bihar.8m.com), a process accelerated by the presence of the Kosi Barrage 40 km downstream of Chatra.

2.9.3. Climate.

The climate of the different sections of the Sapt Kosi basin is described in previous sections of this chapter. Average monthly precipitation and temperatures at Chatra are shown in fig. 2.24. The far south of Nepal is the warmest part of Nepal, while rainfall is relatively high, although not comparable to that of the Bhote Kosi valley.

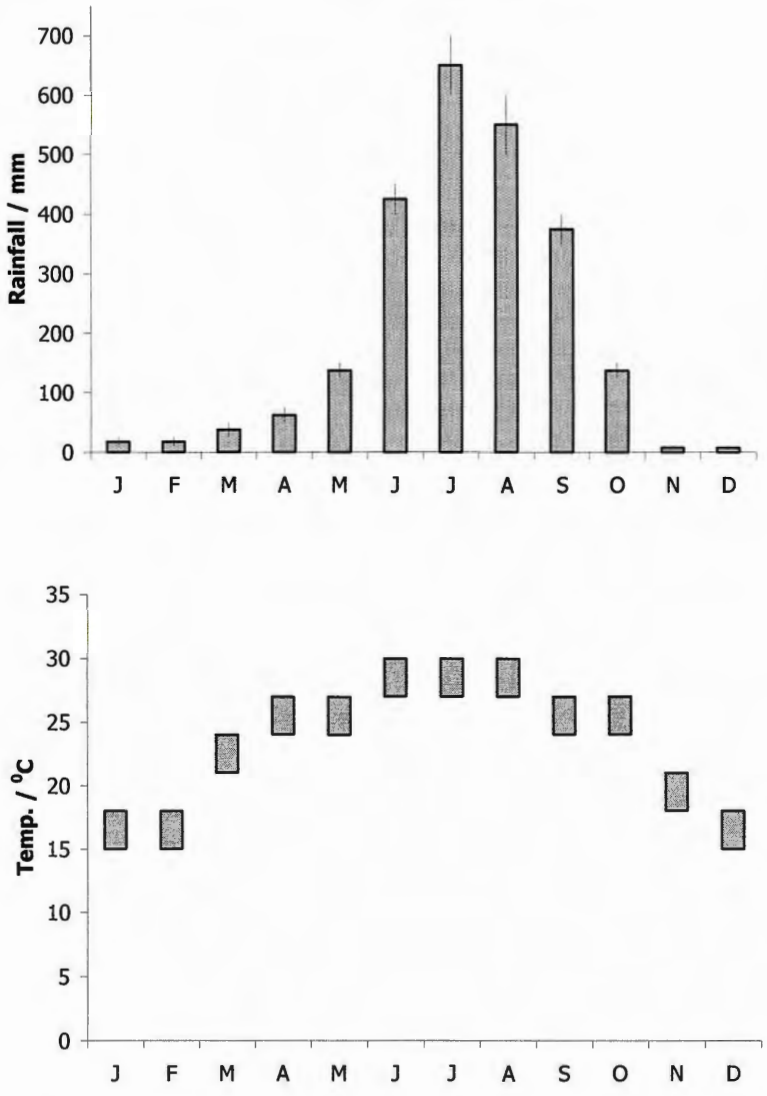

Fig. 2.24. Monthly variations in average rainfall and teperature in the Sapt Kosi at Chatra.

2.9.4. Flow Characteristics.

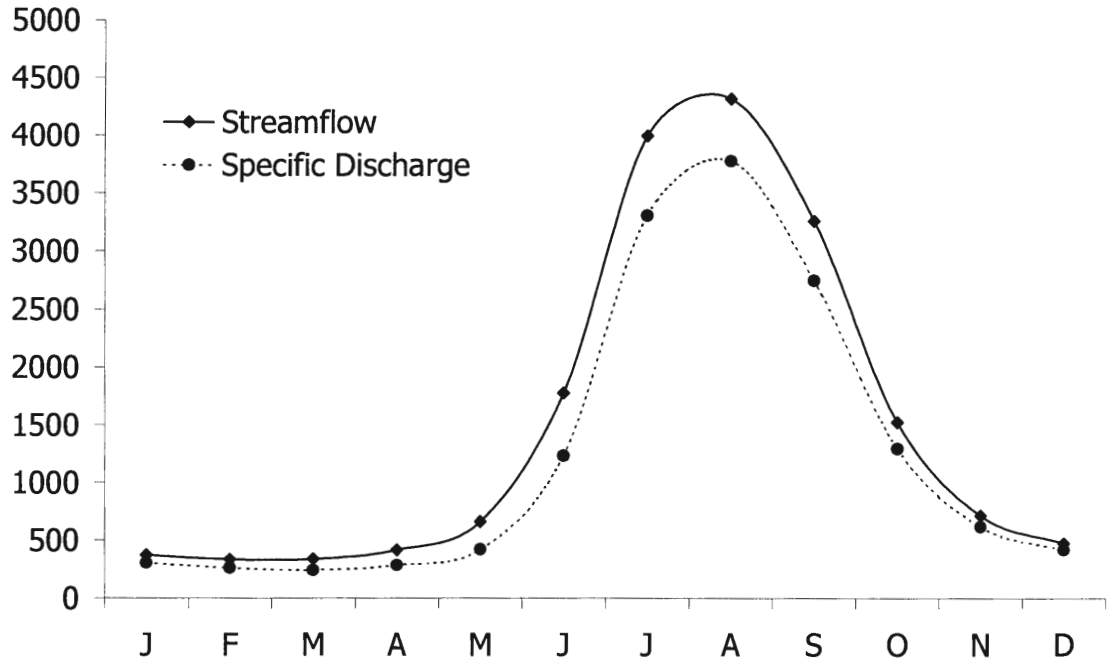

Fig. 2.25. Monthly variations in streamflow (m^3/s) and specific discharge (mm/month) in the Sapt Kosi at Chatra.

The Sapt Kosi is a truly massive river, with streamflow exceeding 4000 m^3/s at the height of the monsoon, and specific discharge greater than 3700 mm. When measured in November the river is only marginally above baseflow, however, with streamflow at ~700 m^3/s and specific discharge at ~300 mm. As in the lower Sun Kosi, the upper Sapt Kosi itself has anomalously low streamflow and specific discharge, the reason for this being unclear (Alford, 1992).

The Sapt Kosi has an average annual suspended load of 172 million tons (Alford, 1992; Tejwani, 1996), ~10 % of that of the Ganges and in excess of the total sediment load of the Mekong, Nile or Congo. When catchment size is taken into account, the Sapt Kosi's suspended load of 2,774 tons / km^2 is twice that of the Ganges itself and an order of magnitude greater than the Amazon (Tejwani, 1986) while estimated annual soil erosion (Tejwani, 1986) for the river is 55,480 tons / km^2, nearly twice that of the Ganges and more than forty times that of the Amazon. This is largely owing to the massive erosion taking place in the Himalayn rivers (such as those discussed above) that drain into the Sapt Kosi, as demonstrated by the 30 million tons of sediment provided by the Tamur (18% of total sediment at Chatra) at an incredible denudation rate of 5,147 tons/km^2/yr (Alford, 1992). Indeed, the Tamur has a sediment yield over twice that of the Sun Kosi and five times that of the Arun (Tejwani, 1986). The importance of the Sapt Kosi and its sediment load on a global scale is clear.

2.9.5. Land Use.

The variety of vegetation types and land uses in such large Himalayan basins are described in chapter 1 and in the above sections on the smaller rivers that form the Sapt Kosi. The high sediment load of the Sapt Kosi (see above) is commonly believed be a feature of land degradation in the Arun and Tamur, although the dynamic nature of the Sapt Kosi alluvial fan over the past 250 years, incorporating a 100 km westward shift suggests that the river has been depositing vast amounts of sediment for a long period before human watershed intervention began in the 1950s. The Kosi Barrage currently

restricts flow 40 km downstream of Chatra, although the project is viewed as a disaster by both Nepal and India (Rowe, 2001). The river is currently the subject of a feasibility study for the proposed 3,000 MW Sapta Koshi High Dam Multipurpose Project (www.doi.gov.np), which would necessitate the flooding of nearly 20,000 hectares (www.panasia.org.sg).

2.9.6. Sampling Strategy.

Two samples were taken below the major confluence (Tribeni Ghat) upstream of Chatra to determine the effect of the mixing of the three major rivers and the resulting chemical nature of this major component of the Ganges.

2.10. Langtang Khola / Trisuli ("Three Springs").

The Langtang Khola, sharing a watershed with the Bhote Kosi and Indrawati to the east, runs through the popular Langtang trekking area, and provides the opportunity to study a catchment within the High Himalayan Crystalline Series. The Langtang Khola is in fact a major tributary of the Bhote Kosi (Langtang)*, which is referred to as the Trisuli downstream of the confluence with the Langtang Khola at Syabrubensi. The Trisuli is one of the major rivers forming the Narayani, like the Sapt Kosi one of the most important tributaries of the Ganges itself. The Langtang Khola - Trisuli system upstream of Trisuli Bazaar provides an excellent contrast to the Bhote Kosi, draining similar

Plate 8. Geology of the Langtang Khola - Trisuli basin.

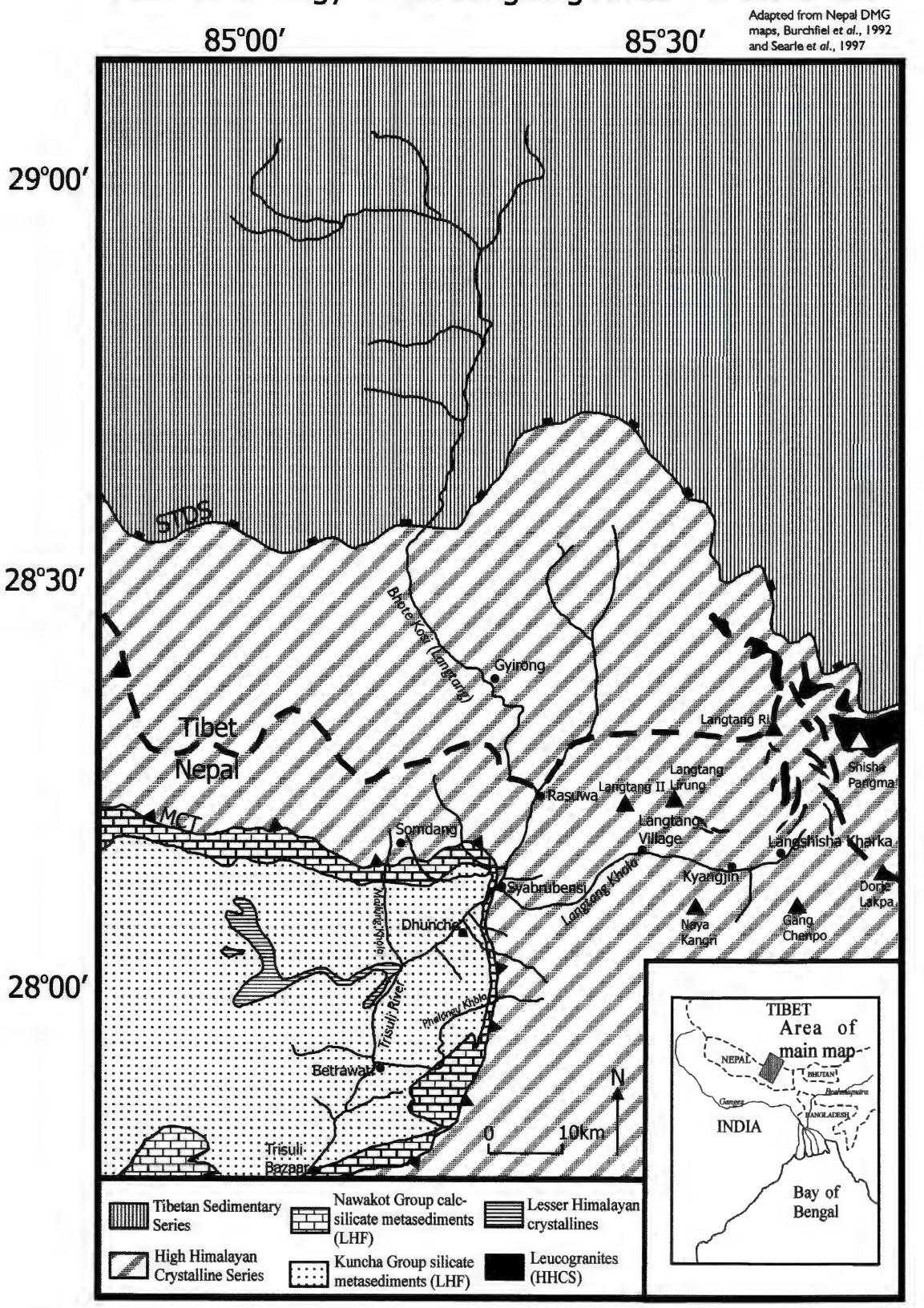

terrain and geology, but being relatively lacking in exposure of the Nawakot Group calc-silicates.

*The Bhote Kosi river in the Langtang region is referred to as "Bhote Kosi (Langtang)" to avoid confusion with the Bhote Kosi to the east which is the centre of this study, and the Bhote Kosi (Khumbu), which drains into the Dudh Kosi.

2.10.1. Geology.

The geology of the Langtang Khola - Trisuli area is illustrated in plate 8 while sample catchments are show in plate 9. The nature of the TSS units in the Bhote Kosi (Langtang) section is described by Burchfiel *et al.* (1992), where it is referred to as the "Gyirong section" after the town of Gyirong on the Tibetan side of the border. An Ordovician – Jurassic section is reported, with the rocks at the top of the Silurian and base of the Devonian missing due to faulting. Units above the Jurassic are not present owing to erosion. The Ordovician and base of the Silurian consists entirely of limestone. These are overlain by Devonian and Carboniferous sandstones and siltstones, in turn overlain by thick Permian limestones that persist all the way up to the Jurassic. Siliclastic Neogene units (the Gyirong Basin) unconformably overlie the Jurassic at the top of the N-S section studied by Burchfiel *et al.*, although the headwaters of the river to the north-west drain the Jurassic limestones.

The STDS in the Gyirong section is named by Burchfiel *et al.* (1992) as the Bhote Kosi Detachment (to add further confusion in this study). The faulting has a shallow

northwards dip placing Ordovician hanging wall units onto the leucogranite and "injection complex" of the HHCS footwall. Structures indicate south-verging deformation of probable Tertiary age with later multiple episodes of north-vergent deformation. The Bhote Kosi detachment must be younger than the leucogranite it truncates, which is probably upper Miocene in age, similar to other well-dated leucogranites in the HHCS (e.g. Schäerer *et al.*, 1986). North-south extension in this area continued into Pliocene-Quaternary time. The aforementioned "injection complex" is referred to as the Kyanjin Unit by Reddy *et al.* (1993) and Massey (1994).

The Langtang Khola catchment lies entirely within the High Himalayan Crystalline Series. The geology of the Langtang valley has been described by Reddy et al. (1993) and Massey (1994), with the following account summarised largely from this work using the nomenclature established by these authors.

The lowermost rocks of the HHCS of the Langtang Khola are known as the Lower Syabru unit (the MCT zone), and consist almost entirely of coarse-grained metapelites with occasional granitic gneiss (Inger 1991). The mineral assemblage of these units comprises muscovite + quartz + biotite + garnet + garnet + plagioclase ± kyanite ± tourmaline. Above the Lower Syabru Unit the appearance of K-feldspar and sillimanite marks the metamorphic transition into the Upper Syabru Unit, again dominantly pelitic but more quartz-rich than the Lower Syabru Unit. These rocks have a mineral assemblage consisting of quartz + biotite ± garnet + plagioclase + K-feldspar ± sillimanite, and become increasingly migmatitic at higher structural levels. Metre-sized

granitic bodies are present, including dykes that were intruded later than the melting that produced the migmatites. The Lower and Upper Syabru Units occupy the Langtang Khola valley upstream of the MCT at Syabrubensi eastwards to Kyanjin.

At Kyanjin the dominant lithology becomes augen gneiss, although a sharply defined boundary is not mappable (Massey, 1994). The mineralogy of the Kyanjin Unit comprises K-feldspar + quartz + plagioclase + biotite ± muscovite ± silliminite ± (rare) garnet. Reddy *et al.* (1993) recognised a division in this unit between lower structural levels where the augen are 2-3 cm in diameter, and upper structural levels east of Kyanjin, where augen up to 20 cm in diameter are noted. These latter rocks show affinity with Formation III identified by Le Fort *et al.* (1983), an augen gneiss recorded in the Annapurna and Manaslu regions, which is thought to be a deformed granitoid intruded at ~517 Ma. The Kyanjin Unit is locally migmatitic throughout and is intruded by garnet and tourmaline-bearing leucogranite dykes and sills. A narrow (1-2 km) exposure of this unit occurs in the Langtang valley upstream of Kyanjin for ~10 km eastwards, while Massey (1994) reports exposure in the higher ground on the northern side of the valley, occurring as a narrow zone for ~5km east and at least 5km west of Langtang village. Searle *et al.* (1997) also report exposure of the Kyanjin Unit in the east of the catchment around the northern flank of Shisha Pangma

The overlying Langsisa Unit is marked by a dramatic textural and mineralogical change. The rocks of this unit are fine-grained (< 0.2 mm) biotite gneisses with a mineral assemblage of quartz + K-feldspar + plagioclase + biotite. It was proposed that the

Langsisa unit was in fact the lowermost part of the TSS (Inger and Harris, 1992), but the local presence of sillimanite and evidence of partial melting confirm these rocks as part of the HHCS, possibly equivalent to the "Black Gneisses" noted by Bordet (1961) and Pognante and Benna (1993) in the Everest region. Rare calc-silicates are noted in the Langshisha Unit, although these are only a few metres thick. Pyroxene and plagioclase are noted in these rocks, quartz and garnet also being present in some samples. A broad exposure of the Langsisa Unit is mapped by Massey (1994), mantling the Kyanjin unit and occupying the mid-altitude ground eastwards of Kyanjin, in addition to a narrow zone north of the Kyanjin Unit exposures on the north side of the Langtang Valley.

The overlying Langtang Lirung Unit was defined by Reddy *et al.* (1993) on the basis of a sharp increase in the percentage of interlayered granitic material, from ~10% in the Langshisha Unit to ~50%. The rocks of this unit are only exposed in the inaccessible high peaks of the valley, float material suggesting that the metamorphic lithology of this unit is identical to that of the Langsisa Unit (Massey, 1994).

Numerous interlayered granitic bodies are present in the Langsisa and Langtang Lirung Units. They occur as foliation-parallel sheets between 3 and 50 cm in thickness, although larger bodies tens of metres thick are observed in inaccessible cliff sections, while granitic veins, pegmatites and dykes also occur (Massey, 1994). The same author also reports that in the foliation-parallel granites biotite is a modally major phase, in contrast to other Miocene Himalayan leucogranites in which muscovite is the most significant hydrous phase. Many of these granite sheets are closely related to the

surrounding country rock and have diffuse margins, suggesting either an in-situ origin or some melting of the country rock. The crosscutting granitic bodies have sharp boundaries and are undeformed except by late shear zones (Massey 1994), indicating late-stage intrusion. These tourmaline granite bodies only rarely contain biotite.

A large part of the upper Langtang valley was affected by a giant landslide which occurred around 25,000 years ago (Heuberger, 1984) and displaced approximately 10 km^3 of debris through a vertical distance of 2,000 m, generating fused rock (termed hyaloclastite or frictionite).

South of the confluence of the Langtang Khola and the Bhote Kosi (Langtang), the upper Trisuli crosses a thin (<1 km) section of Nawakot Group rock comprising only the Dandagoan Phyllites (Nepal DMG, 1985) before passing into the Kuncha Group. The river continues to drain the Kuncha Group and the outlying Nawakot Group units, the main river passing back into the Nawakot Group south of Trisuli Bazaar.

2.10.2. Altitude.

The Bhote Kosi (Langtang) is sourced on the Tibetan Plateau at an altitude of ~5400 m (see fig. 2.26), with the watershed to the east marking the western extent of the Arun catchment, that to the north being shared with the Tsangpo. The river crosses the STDS at ~4000 m before entering its steepest section, descending 3000 m in the HHCS before reaching the MCT at Syabrubensi (~1000 m). The highest parts of the catchment form

the watershed of this section, with the Ganesh Himal (7406 m) to the west and Langtang II (6581 m) to the east. The gradient of the river lessens considerably, with a relatively flat section between Syabrubensi and Dhunche, the gradient increasing again in the gorge section between Dhunche and Trisuli Bazaar, before the average gradient eases again, never exceeding 0.3% between Trisuli Bazaar and the confluence of the river with the Narayani (Knowles and Allardice, 1992). Area-altitude distribution data are available for the catchment of the Nepal DIHM hydrological station at Betrawati, revealing that more than 50% of the Langtang Khola-Trisuli catchment lies at altitudes greater than 5000 m, while <25% of the surface area of the catchment lies below 3000 m. This reflects the large portion of the Bhote Kosi (Langtang) catchment on the Tibetan Plateau. It is expected that the area-altitude distribution of the Langtang Khola alone is similar to that of other rivers originating from the glaciers of the HHCS (e.g. the Dudh Kosi and Tamur, see fig. 2.19).

The Langtang Khola is sourced at the Langtang Glacier, which stretches some 20 km north of the Langtang valley itself, abutting the lower flanks of the Shisha Pangma Massif (8013 m) to the east, Langtang Ri (7205 m) marking the most northerly point of the catchment. The river rapidly descends away from the glacier (~5800 m), the gradient easing for a few km north of Kyanjin before entering another steep descent, followed again by a shallower gradient for around 10 km upstream of Langtang village (see fig. 2.26). The river then enters its most rapid descent, from ~3500 m to ~1000 m south of Langtang village in a heavily forested gorge section. The river gradient lessens just

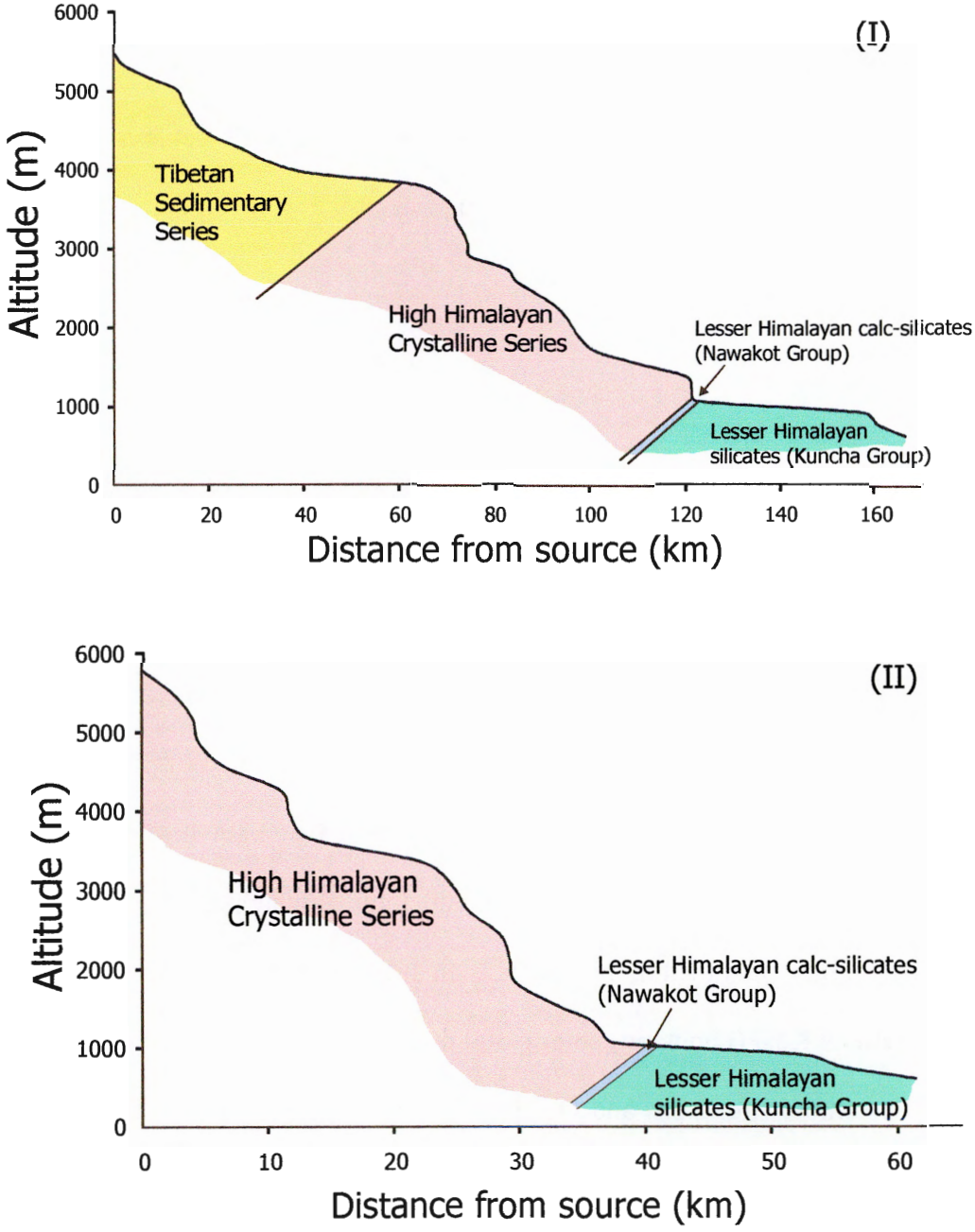

Fig. 2.26. Altitude and lithology changes in the Trisuli river system.
(i). Changes in the Bhote Kosi (Langtang) - upper Trisuli measured from the source of the Bhote Kosi (Langtang) on the Tibetan Plateau.
(ii). Changes in the Langtang Khola - upper Trisuli measured from the source of the Langtang Khola, the Langtang Glacier.

upstream of the MCT and the confluence with the Bhote Kosi (Langtang). The Langtang Khola valley incorporates numerous high peaks, with Langtang Lirung (7246 m)dominating the valley to the north, Naya Kangri (5846 m) and Gang Chenpo (6388 m) demarcating the watershed between the Langtang Khola and the Indrawati and Balephi Khola to the south. Dorje Lakpa (6966 m) protects the valley in the east.

2.10.3. Climate.

The Langtang valley is one of the wetter parts of Nepal, although greater rainfall is recorded to the south-east in the Indrawati, Balephi Khola and Bhote Khosi (Chalise *et al.*, 1996). Fig. 2.27 shows mean annual rainfall in the basin, which is highest in the far south of the sampled catchment, between Dhunche and Trisuli Bazaar, and in the far east of the catchment. This can be seen in the higher monthly rainfall noted in Betrawati and Kyanjin compared to Dhunche in the monsoon months in fig. 2.30. In these regions, average annual rainfall is between 2000 and 3000 mm, although rainfall decresases northwards, first rapidly and then more slowly, with average annual rainfall in the upper reaches of the Bhote Kosi (Langtang) being <500 mm. Almost identical rainfall patterns are noted in September (fig. 2.28) and October (fig. 2.29) when sampling of this river system was undertaken. In the dry season, however, rainfall is less at Betrawati and Kyanjin, although monthly averages don't exceed 75 mm at any station between November and March.

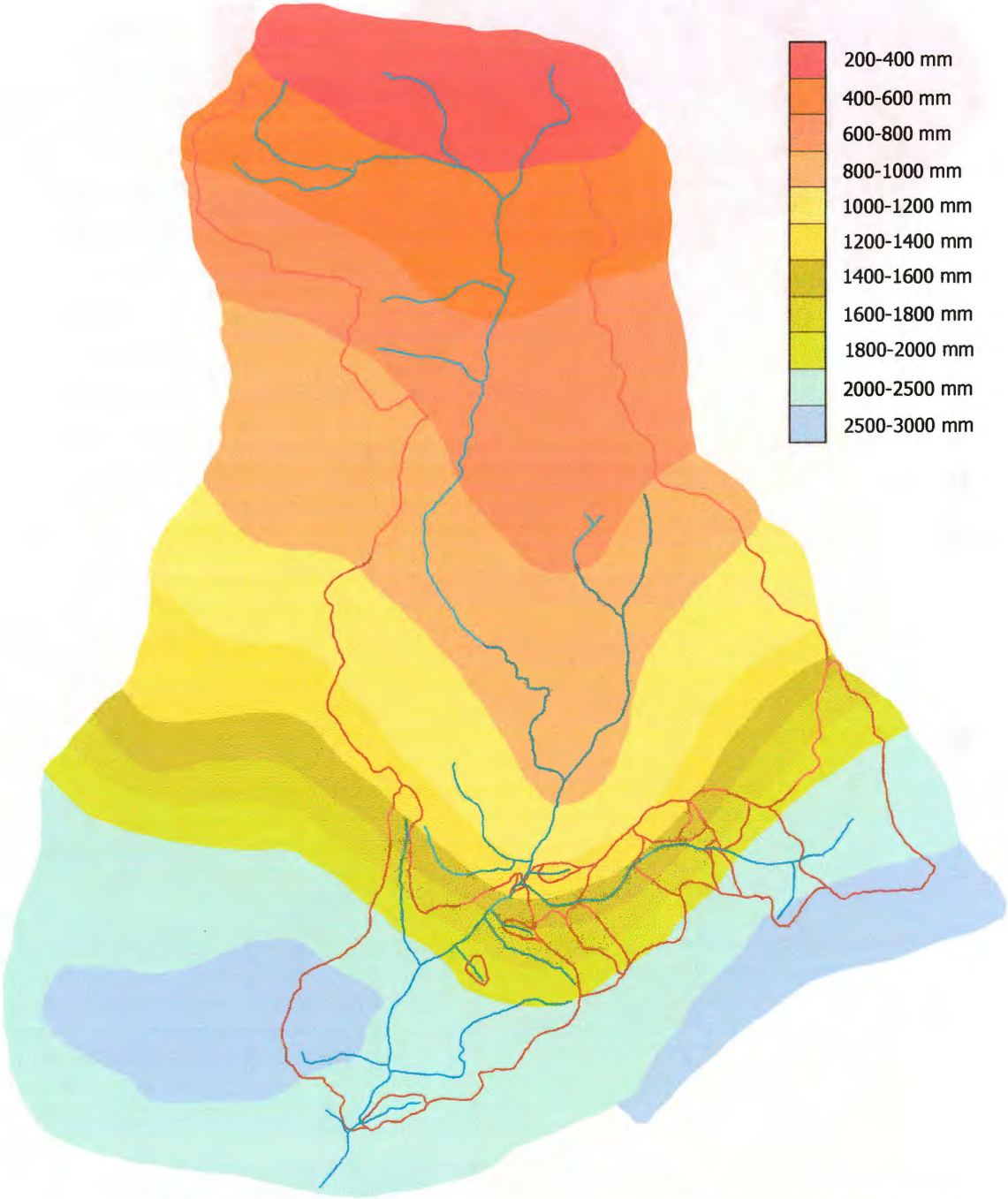

Fig. 2.27. Annual rainfall contours for the Langtang Khola - Trisuli.
River courses are marked by blue lines, watersheds are shown in red.
Source: Chalise *et al.*, 1996.

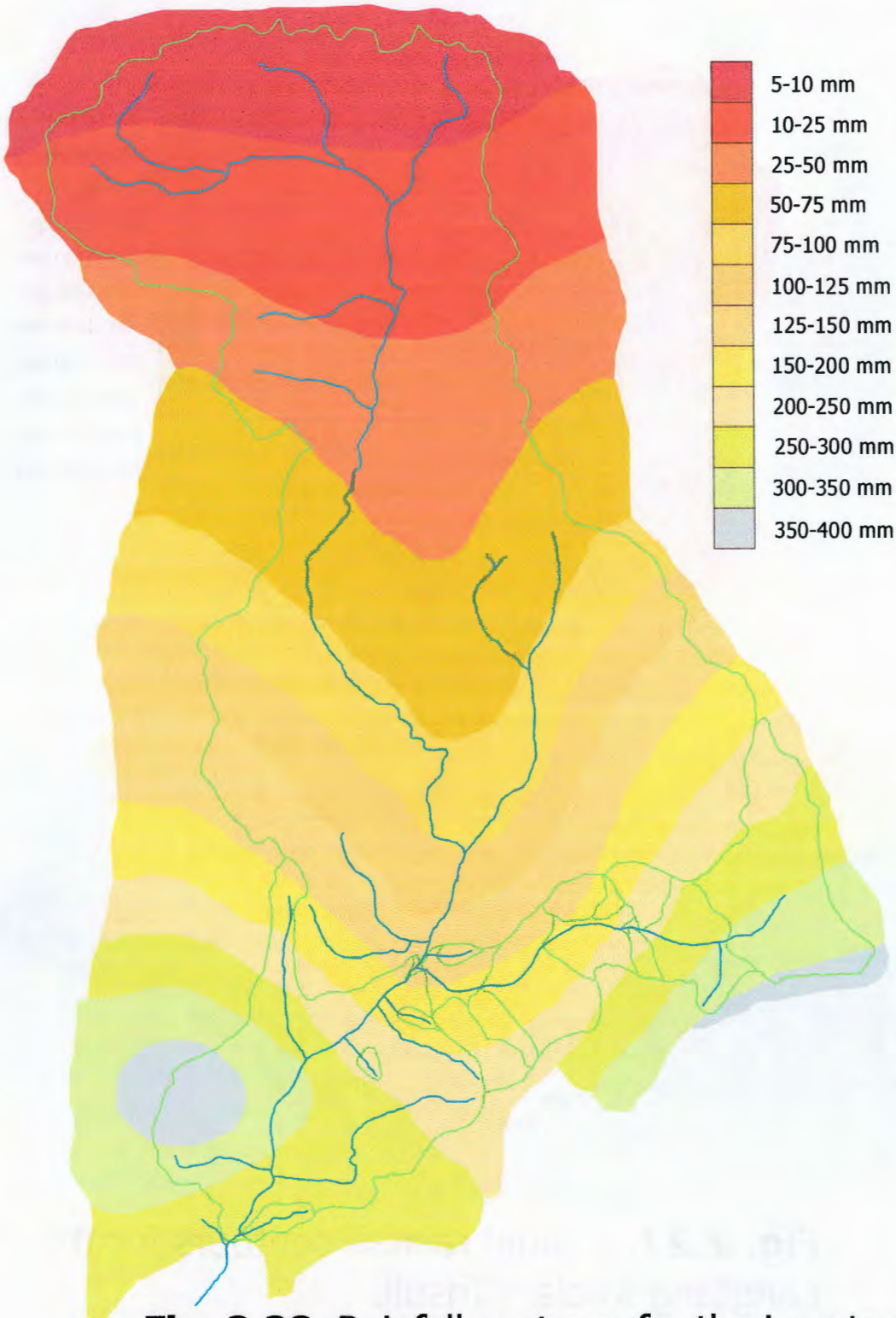

Fig. 2.28. Rainfall contours for the Langtang Khola - Trisuli in September.

River courses are marked by blue lines, watersheds in green.
Source: Chalise *et al.*, 1996

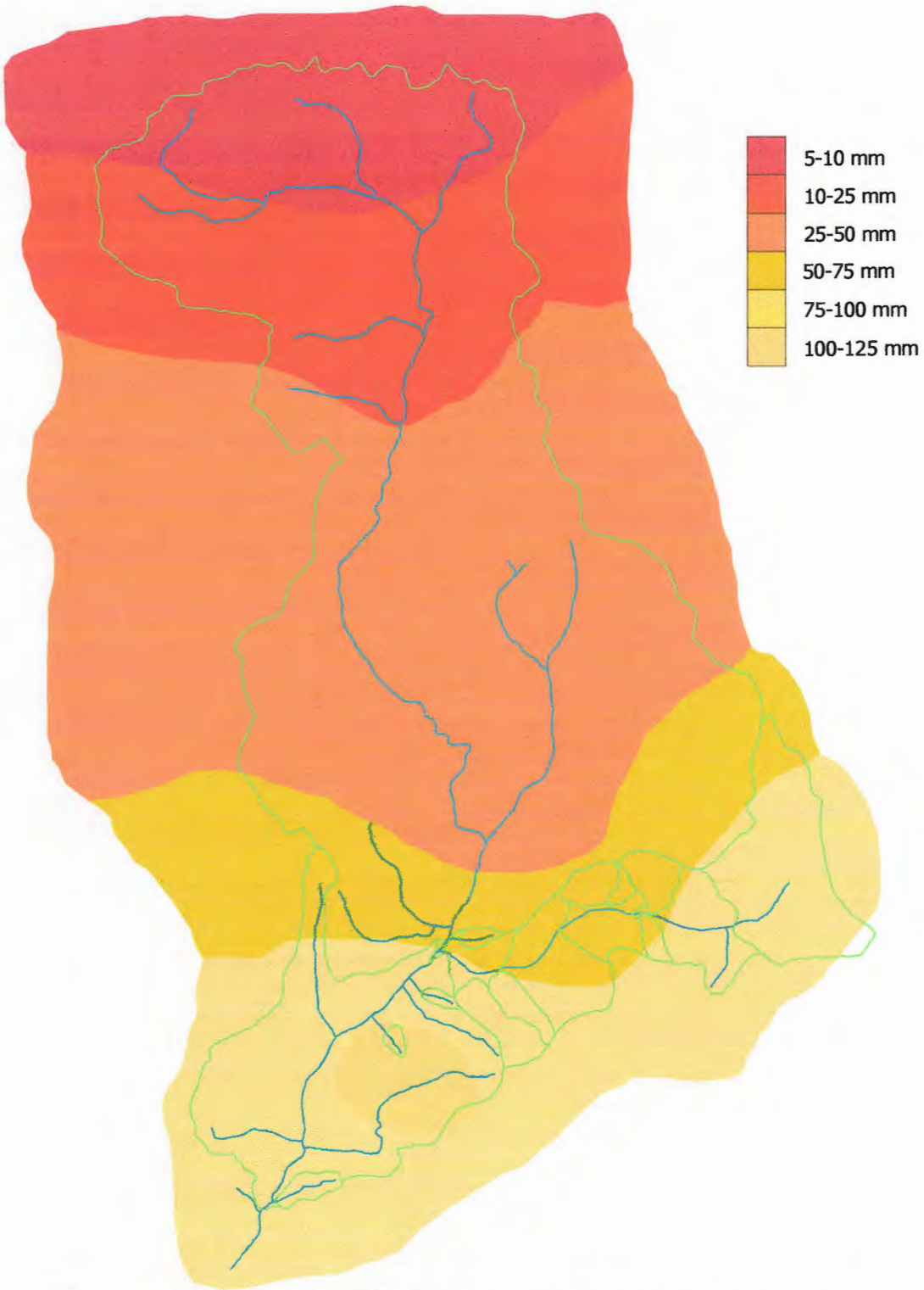

Fig. 2.29. Rainfall contours for the Langtang Khola - Trisuli in October.

River courses are marked by blue lines, watersheds are shown in green.
Source: Chalise *et al.*, 1996

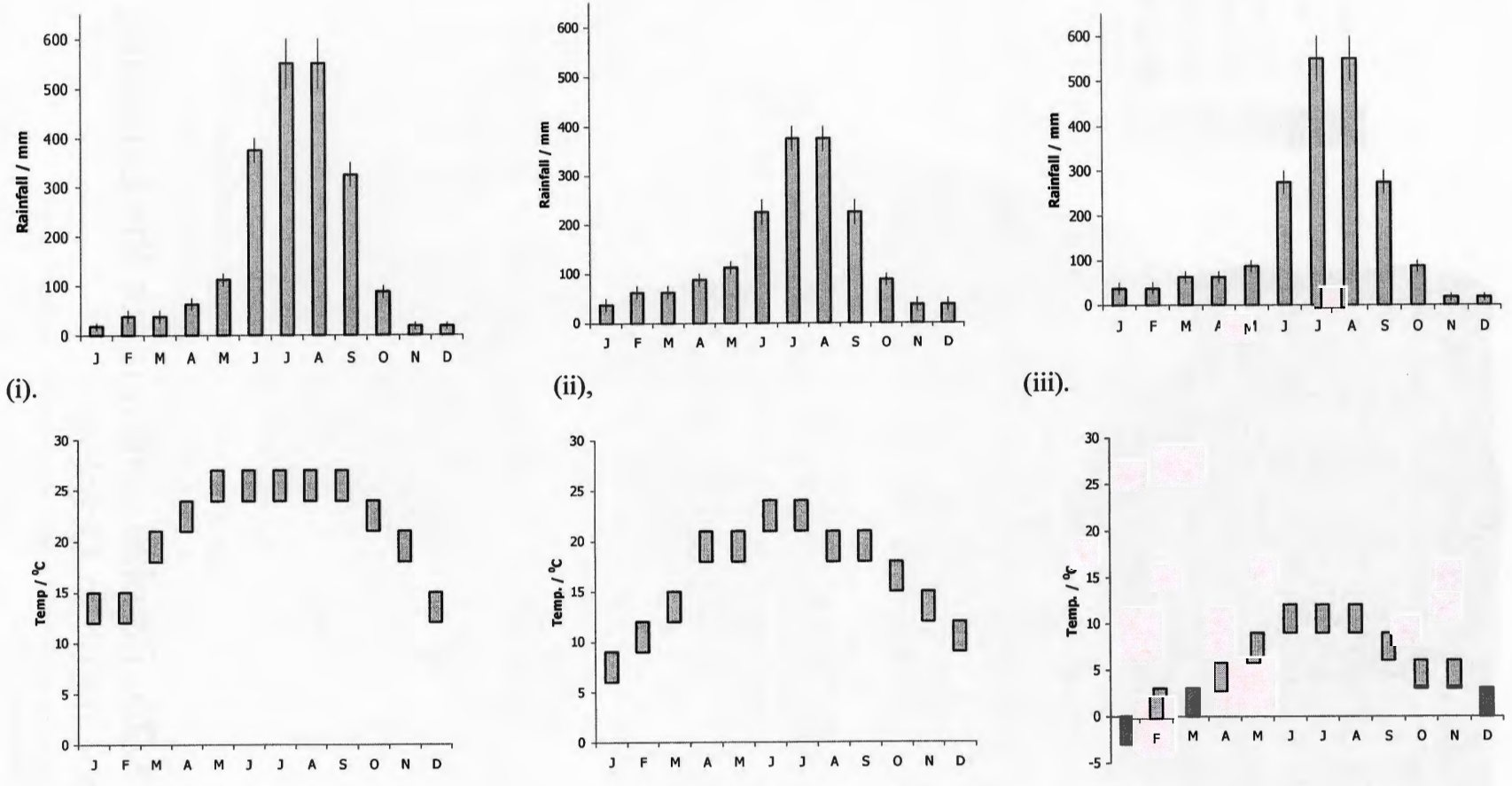

Fig. 2.30. Monthly variations in average rainfall and temperature in the Langtang Khola - Trisuli.
(i). Betrawati. (ii). Dhunche. (iii). Kyanjin.

Fig. 2.30 also demonstrates the contrasting climate of the subtropical Trisuli valley at Betrawati and the alpine conditions at Kyanjin. At Betrawati, average temperatures only fall below 20°C between December and February, although monsoon temperatures are not as high as those recorded at lower altitudes further south (e.g. in Chatra). Tempertaures at Dhunche tend to be a few degrees lower than those at Betrawati at any time during the year. At Kyanjing, average temperatures only exceed 10°C at the height of the monsoon season, while the winter months leave the settlement near or below freezing. Temperatures farther up the Langtang valley or at hgher altitudes in the Bhote Kosi (Langtang) will be even lower.

2.10.4. Flow Characteristics.

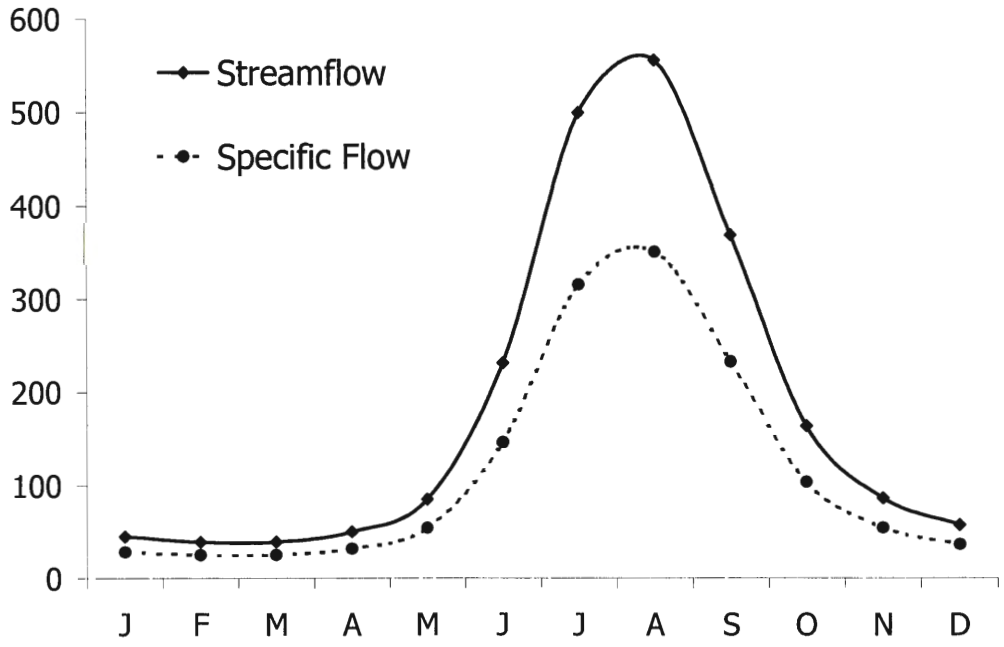

Fig. 2.31. Monthly variations in streamflow (m^3/s) and specific discharge (mm/month) for the Trisuli river at Betrawati.

Nepal DIHM sampling of the Langtang Khola – Trisuli is limited to one station at Betrawati, just upstream of the sample L21 (fig. 2.31). Even at this point (the river still has approximately 100 km to run before its confluence with Marsyandi) the Trisuli is of a size comparable with the Dudh Kosi at Lamidanda.

2.10.5. Land Use.

For the Langtang Khola portion of this basin, a land use map has been produced (fig. 2.32) by R. Collins of the Institute of Hydrology (UK) from digital data collected by the Mountain Environmental and Natural Resources Information System (MENRIS) at ICIMOD. Fig. 2.32 shows that the upper reaches of the Langtang Khola catchment are unvegetated ice and rock, with areas of (yak) grazing land noted in the flatter land close to the river between Langshisha Kharka and Kyanjin. Downstream of Langtang village the catchment is dominated by forest, with isolated areas of level and sloping terracing in the lowlands around Syabrubensi. Downstream of Syabrubensi, areas of fragile forest, shrub and level terracing are noted close to the river, while the upper parts of the valley remain more heavily forested. Further downstream, south of Betrawati, intensive agriculture becomes apparent. The land usage in the lower Bhote Kosi (Langtang) is similar to that of the Langtang Khola, with forested areas interspersed with grazing land and small areas of both level and sloping terracing. Such land usage probably continues uninterrupted north of the Nepalese border until the climate becomes too dry and the altitude too great to support forest and agriculture.

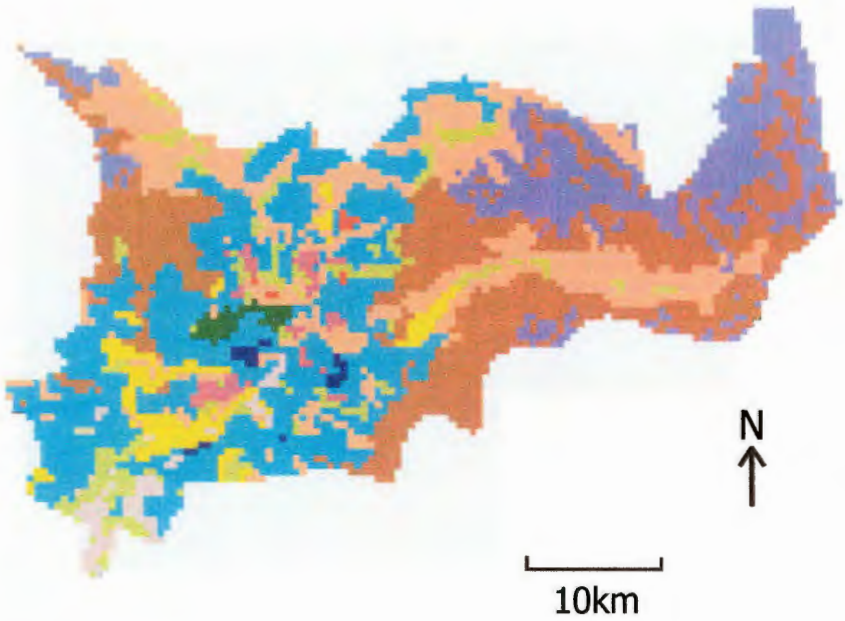

Grazing
Ice
Rock
Level terrace (intense)
Level terrace (medium)
Level terrace (light)
Sloping terrace (intense)
Sloping terrace (medium)
Sloping terrace (light)
Forest
Shrub
Fragile forest

Fig. 2.32. Land use in the Langtang region
(including the Langtang Khola, lower Bhote Kosi (Langtang) and upper Trisuli

Produced by R. Collins of the Institute of Hydrology (UK) from digital data obtained by the Mountain Environment and Natural Resources' Information Service.

Non-agricultural human land use in both the Bhote Kosi (Langtang) and Langtang Khola valleys is limited as both are sparsely populated. An exception is the gold mining operation located at Somdang in the far West of the Bhote Kosi (Langtang) catchment. At Betrawati a dam diverts around half the flow of the river to the hydroelectric power station at Trisuli Bazaar, one of Nepal's first hydroelectric schemes although now largely superseded by a second station 4 km downstream, the outflow from which can double the river flow in the driest months. Further projects on the Trisuli are under consideration (www.ledco-nepal.com) and damming of the Langtang Khola has also been proposed (www.panasia.org.sg).

2.10.6. Sampling Strategy.

A full reconnaissance of the Langtang Khola was undertaken to determine some of the variations in waters draining different units of the HHCS. The confluence between the Langtang Khola and the Bhote Kosi (Langtang) was also monitored, and the hot spring at Syabrubensi additionally sampled. The chemistry of the upper Trisuli (at Betrawati) was also of great interest as the river at this point has a geologically very similar drainage to the Bhote Kosi of section 2.1, with the important distinction that it lacks significant exposure of the Upper Nawakot Group of the Lesser Himalaya.

The majority of sampling was undertaken during the recession phase of the hydrograph (fig. 2.31) although before the baseflow conditions of November. Repeat samples were taken to allow comparison of October 1998 and September 1999 sampling.

Plate 9. Sampled catchments of the Langtang Khola - Trisuli basin.

Watersheds shown in red.

Adapted from Nepal DMG maps, Burchfiel *et al.*, 1992 and Searle *et al.*, 1997

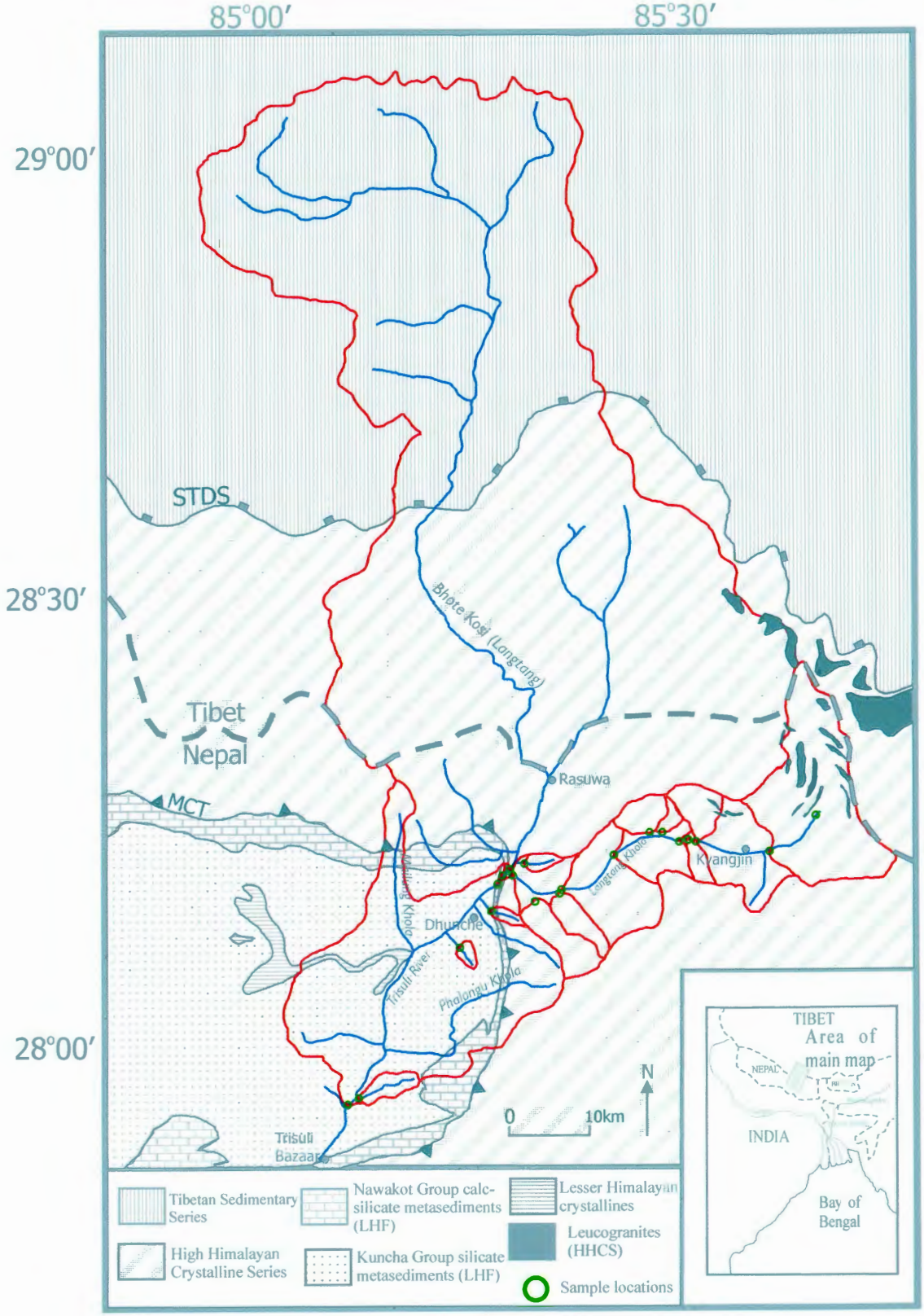

Key showing sample locality labels for plate 9.

NB. All labels have the prefix "L" throughout this work.

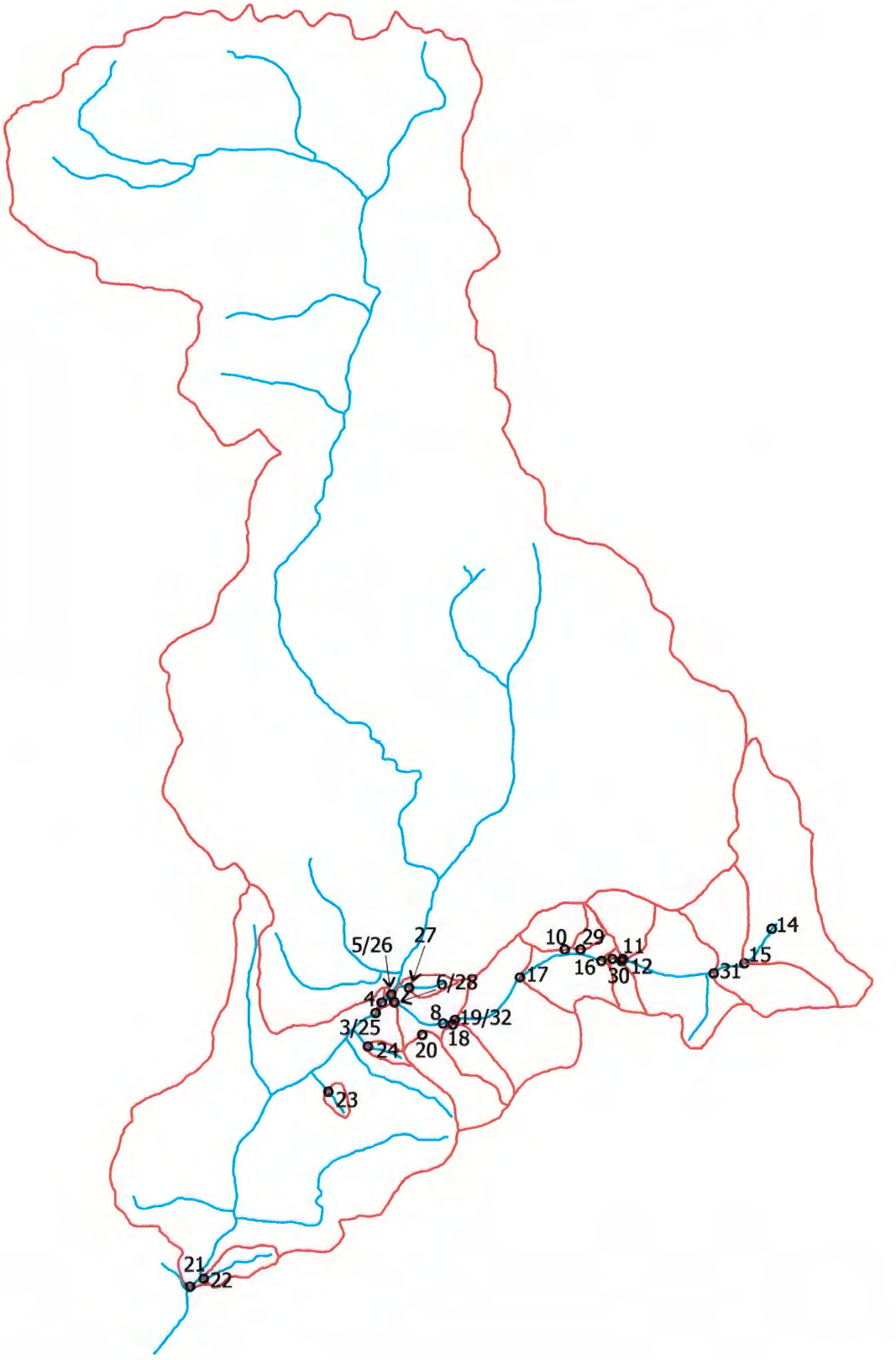

2.11. Summary of Overall Sampling Strategy.

The most detailed sampling for this study was undertaken within the basin of the Bhote Kosi, regarded as a good approximation of a "typical" central Himalayan river in terms of geology, land use, flow characteristics and climate. Sampling was focused upon tributaries of the main river draining the different parts of the Lesser Himalayan Formation (Nawakot Group, Kuncha Group and Lesser Himalayan crystalline gneisses), allowing the weathering inputs of these units on the main river to be assessed. Less detailed information was collected from the HHCS and TSS sections of the Bhote Kosi owing to the problems of sampling in Tibet. The sampling of the Langtang Khola and rivers of the Khumbu (Everest) region provides further detail of weathering in the HHCS. Isolating TSS-draining catchments in Nepal is difficult but data is provided by the chemistry of the upper Bhote Kosi and Bhote Kosi (Langtang). Sampling of the Langtang Khola – Trisuli system also provides a useful counterpoint to the Bhote Kosi as this river basin is similar to the Bhote Kosi in most respects, but with a much attenuated surface exposure of the Nawakot Group calc-silicates, the impact of which is the focus of this work.

It is vital, in order to draw conclusions in terms of the impact of Himalayan weathering upon the marine strontium record and atmospheric CO_2 drawdown, that results from the Bhote Kosi are demonstrated to be applicable on a larger scale. In attempt to achieve this, sampling of the Sun Kosi, Arun and Tamur was undertaken. These rivers join to

form the Sapt Kosi (also sampled), a major tributary of the Ganges and a river large enough to be important in terms of impact upon the marine $^{87}Sr/^{86}Sr$ record. The Sun Kosi, Arun and Tamur also provide some interesting contrasts in terms of catchment geology, topography and climate. The majority of the catchment of the Arun lies on the high-altitude (>5000 m) Tibetan Plateau within the TSS and the Himalayan rain shadow. By contrast, the much smaller Tamur basin is located solely south of the main Himalayan range, an area of much higher rainfall and greater erosion. The catchment of the Tamur is dominated by rocks of the HHCS and LHF, while rocks of the TSS are absent. The Sun Kosi catchment comprises a relatively large proportion of LHF bedrock, and is formed by a number of south-flowing tributaries (principally the Bhote Kosi, Tamba Kosi, Likhu Khola and Dudh Kosi; see plate 1) with catchments broadly similar in terms of geology, land use, vegetation and altitudinal variation. The Sun Kosi differs from the Tamur in that these tributaries progressively join the main river, which flows eastwards through the LHF units of semi-tropical southern plains.

Chapter 3

Methodology

3.1. Sample Collection Protocol.

The sampling strategy adopted for each river is described under the relevant sections of chapter 2. The majority of sampling was done between October and December. Himalayan rivers are in a pure recession phase dominated by baseflow at this time of year and streamflow is least variable both diurnally and annually (Alford, 1992). Three water samples were collected at each sample site. Two of these were filtered on-site through 0.1 μm cellulose nitrate filters and transferred to Nalgene™ bottles. One of these samples (for isotope analysis) was acidified using 200μl of Teflon distilled (TD) 6M HNO_3 or HCl. All samples were refrigerated in Kathmandu and on return to the UK.

The pH and temperature of the river water at each sample site were measured using a Hanna Instruments HI 9024 combined pH / temperature meter. The third water sample collected at each sample site was for alkalinity measurement. These samples were stored in glass bottles filled to the top to ensure minimal CO_2 degassing. A two-point Gran titration was carried out using sulphuric acid (H_2SO_4) on the day of collection. Bedload

samples were collected from the riverbed or sandbars. Representative bedrock was collected throughout the Bhote Kosi section along the Arnako Highway.

3.2. Analytical Techniques.

3.2.1. Ion Chromatography (IC).

Water samples were analysed for chloride (Cl^-), nitrate (NO_3^-) and sulphate (SO_4^{2-}) concentrations using a Dionex DX100 ion chromatograph at the Open University. 5 ml sample vials were rinsed three times with sample to prevent contamination (e.g. from airborne dust). Internal standards were made up by dilution of certified BDH™ standards on the day of analysis and used to calibrate the ion chromatograph. In addition, standards were run as samples throughout analysis runs to check reproducibility and accuracy (see table G1a and b). Samples of deionised water were also run to ensure adequate flushing between sample runs.

NB. A number of unacidified samples from the 1998 sample set, all from the Bhote Kosi, were unfortunately lost, and thus anion measurements were not possible (see appendix A).

3.2.2. Inductively Coupled Plasma Atomic Emission Spectroscopy (ICP-AES).

Water samples from 1998 were analysed by ICP-AES at the Institute of Arable Crops Research (IACR) – Rothamstead. The laboratory's own standards were used to monitor accuracy and reproducibility.

3.2.3. Inductively Coupled Plasma Mass Spectrometry (ICP-MS).

Water samples were analysed for Ca^{2+}, K^{+}, Mg^{2+}, Na^{+}, Sr^{2+} and Rb^{+} concentrations by ICP-MS using an Agilent 7500a at the Open University. All samples were transferred to test-tubes triple washed in sample solution prior to being acidified to 2% using Analar concentrated HNO_3. Drift was monitored using an internal standard of Be, In, Tm and Re while Fisher™ ICP standards were used to calibrate the machine. Reproducibility was assessed from repeat analyses of samples, calibration standards and the universal standards NIST 1640 and SLRS-4 (table G2). For 1998 samples, reproducibility between ICP-MS results and results of the earlier analysis by ICP-AES was within 5%, and thus any changes in chemical composition over time were deemed negligible. NIST 1640 and SLRS-4 were additionally used to assess accuracy (table G3), which was less than expected for Na^{+}, Mg^{2+}, Ca^{2+}, Si and K^{+}. Charge balance, the accuracy of repeats of calibration standards and good reproducibility between ICP-MS and ICP-AES repeats indicated that normalisation to standard values was unwarranted.

3.2.4. X-Ray Fluorescence (XRF) Analysis.

All rock and bedload samples for chemical analysis were crushed to a fine powder using a pre-contaminated agate ball mill. Prior to this, any weathered material was removed from bedrock samples and they were broken down into millimetre-sized fragments using stainless steel jaw crushers.

XRF analyses were carried out using standard procedures at the Open University (Potts *et al.*, 1984). All samples were dried overnight at ~100°C. For major element analysis rock powder was mixed with lithium metaborate/tetraborate flux (Johnson Matthey Spectroflux 100B™) and fused at 1100°C in a muffle furnace before being compressed in a brass mould to form a glass disc. For trace element analysis, sample powder was mixed with polyvinylpyrollidone (PVP) binder, emptied into a hardened steel mould and formed into a compressed powdered pellet using a hydraulic press. The pellet was dried overnight at ~100°C prior to analysis.

All analyses were undertaken on an ARL 8420+ dual ganiometer wavelength dispersive XRF spectrometer. Elemental intensities were corrected for background and peak overlap interferences. A drift normalisation monitor is built into the machine's software and corrects medium-term instrumental drift. Matrix corrections for major elements use the Traill-Lachance procedure, while trace element matrix corrections were made by normalising with the Compton scattered tube lines, or through a Lucas-Tooth correction using iron and Compton scatter peak intensities in the case of elements with atomic

number <27. Monitor samples (table G4) were included in all sample runs to check for any problems with sample preparation and analysis. Reproducibility and accuracy of major element analyses was better than 2%, and better than 3% for Rb and Sr analyses where abundance was greater than 10 ppm.

3.2.5. Sr and Nd Isotopic Analysis.

Sr isotopic analyses on water samples and Sr and Nd isotopic analyses on whole rock and bedload were carried out by Thermal Ionisation Mass Spectrometry (TIMS) using a Vacuum Generators Sector 54 machine at Cambridge University and Finnigan MAT 261 and 262 machines at the Open University, and by Multi Collector Inductively Coupled Plasma Mass spectrometry (MC-ICP-MS) using the Nu Instruments machine at the Open University.

3.2.5.1. Sample Preparation for Isotopic Analysis.

Bedrock and bedload powders were dissolved using a combination of 15M TD HNO_3, TD HF (48%), TD 6M HCl and quartz distilled (QD) 2.5M HCl. Water samples were dried down and redissolved in QD 2.5M HCl.

Sr and REE (where appropriate) fractions were separated using preconditioned cationic ion-exchange columns. Where Nd isotope analyses were required the REE fraction was

passed through a further set of columns, this time consisting of hydrogen-diethyl-hexyl-phosphate (HDEHP).

3.2.5.2. Sample Analysis Using TIMS.

For Sr analysis, samples were loaded onto single Ta filaments using TD H_2O and 10% phosphoric acid (H_3PO_4). For Nd analysis, samples were loaded onto a Ta (double) filament dissolved in TD H_20. A Re filament was used to promote ionisation of the sample.

Sr isotope analyses were typically run for 200 ratios with an ^{87}Sr beam >1pA. Mass fractionation correction was made to $^{86}Sr/^{88}Sr = 0.1194$. Nd isotope analyses required the collection of 200 ratios with ^{143}Nd and ^{144}Nd beams >2 pA and a mass fractionation correction of $^{144}Nd/^{146}Nd = 0.7219$. Total procedural blanks run regularly during all analysis runs were typically <1 ng Sr and <200 pg Nd. Reproducibility and accuracy were monitored by regular analysis of NBS 987 (table G5a) and a 1:10 dilution of the Johnson and Matthey Nd standard (table G5b), with sample values normalised to the accepted value of NBS 987 and the Open University running mean for TIMS analysis of the J and M standard. Repeat analyses of samples were also undertaken (see tables G6 and G7), with reproducibility for $^{87}Sr/^{86}Sr$ typically better than 4×10^{-5}.

3.2.5.3. Sample Analysis Using MC-ICP-MS.

Sr and Nd fractions for MC-ICP-MS analysis were evaporated and redissolved in 2% HNO_3 to give a solution with an Sr or Nd concentration of ~1.0 ppm. Sample solutions were nebulised using a Cetac Aridus™ desolvating nebuliser before being introduced into the Nu Instruments MC-ICP-MS. All analyses were carried out in static multi-collector mode. 200 ratios were collected for both Sr and Nd analyses.

Reproducibility and accuracy were monitored using the NBS 987 Sr standard and Johnson and Matthey Nd standard. As with the TIMS data, Sr-isotope data were normalised to the accepted value of NBS 987, Nd-isotope data were normalised to the Open University TIMS running mean of the J and M standard. This ensures an accurate comparison of TIMS and ICP-MS data. In addition, repeat sample analyses were carried out (see tables G6 and G7) to assess reproducibility, including repeats of samples originally analysed by TIMS at Cambridge. Reproducibility for $^{87}Sr/^{86}Sr$ was typically better than 5×10^{-5} including those samples run by both TIMS and MC-ICP-MS. Reproducibility for $^{143}Nd/^{144}Nd$ was typically better than 3×10^{-5}.

3.2.6. Laser Ablation Multi Collector Inductively Coupled Plasma Mass Spectrometry (LA-MC-ICP-MS).

For laser ablation analysis, 100 micron thick sections were cut and mounted in epoxy resin. Samples were run at the NERC Isotope Geoscience Laboratories (NIGL) on a VG

Elemental P54 multi collector inductively coupled plasma mass spectrometer connected to a 266 nm Nd:YAG laser ablation system. Samples were exposed to a 5 – 20 Hz laser beam with a spot size of 40μm. Data were normalised to an NBS 987 solution standard run with and without Rb to demonstrate the effectiveness of the within-run Rb correction. A 10 ppb Y solution was simultaneously aspirated during ablation using a Cetac Technologies MCN-6000 desolvating nebulisert, to allow for accurate focusing and centering of the instrument. Sample error was propagated according to reproducibility of an ablation standard (modern coral). Standard data is reproduced in table G8a and b. Sample analyses with an Rb/Sr ratio of >0.2 were rejected, as the Rb correction of the analysis software is known to be ineffective at such high levels of Rb. Also rejected were analyses in which the Sr beam size was $<10^{-11}$A.

3.3. Statistical Analysis.

3.3.1. Principal Components Analysis (PCA).

From a combination of X variables, principal components analysis selects a new set of hypothetical axes (the principal components) for the data. The first principal component (axis 1) represents the greatest amount of variance within the dataset, while the second principal component (axis 2) accounts for the most variability after the effect of the first principal component has been removed, the third principal component the greatest variance within the dataset after the effect of the first and second components has been

removed, and so on. This technique assumes normality, but little else needs to be adhered to during analysis.

The determination of principal components uses the eigenvalues of a correlation matrix. These eigenvalues, mathematical objects with origins in the algebra of linear transformations, were calculated using the computer software package ExcelStat™. The vector of the correlation coefficients gives the degree of correlation each variable has with a specific component, using the following formula;

$$V_c = \frac{\sqrt{\lambda}\, e}{|e|}$$

Where: Vc = the vector of correlation coefficients.

λ = the eigenvalue.

e = the eigenvector.

|e| = the square root of the sum of the square of e's co-ordinates.

3.3.2. Multiple Regression Analysis.

A simple linear regression examines the relationship between a single X (predictive, independent) and single Y (response, dependent) variable, where Y is a function of X ± statistical error. Experimental error is assumed to be in the Y measurements, with X

values being exact. Plotting X against Y, a simple linear regression produces a line through the scattered datapoints using the following equation:

$$Y = \alpha + \beta X + \varepsilon$$

Where: Y = the response or dependent variable.

α = the intercept of the line with the y axis.

β = the slope of the line.

X = the predictive or independent variable.

ε = the error term.

α and β are estimated using the method of least squares, calculating a value for the model where the sum of all squared errors is as small as possible.

In a multiple linear regression, the Y variable is predicted by the values of two or more X variables using the following equation:

$$Y = \alpha + \beta_1 X_1 + \beta_2 X_2 + \beta_3 X_3 \ldots\ldots\ldots\ldots\ldots \beta_n X_n + \varepsilon$$

Where: Y = the response or dependent variable.

α = the intercept of the line with the y axis.

$\beta_1 - \beta_n$ = the slopes of the line.

$X_1 - X_n$ = the predictive or independent variables.

ε = the error term.

In this way the coefficient of all the X variables is found with the minimal sum of squares error. The regression model implies that X_1 to X_n predict Y to some extent, the accuracy of this prediction reflected in the r^2, which is the proportion of the variation in Y explained by the X variables.

The multiple regression analyses in this work use the stepwise method. The software package ExcelStat™ is used to build the regression in stages, adding and taking out X variables one at a time until all possible X variable combinations have been tested. The computer then produces a model explaining the highest proportion of the variation in Y using only statistically significant X variables. The user sets the level of statistical significance, in the case of the analyses in this work a value of $p \leq 0.05$ was used i.e. it is 95% certain that differences between two groups are not due to chance. The stepwise method gives the best-fitting model, and this may be at the expense of a more practical model (i.e. easier to measure, more clearly ascribed to controlling processes) that might have an r^2 nearly as good.

Multiple regression analysis requires that X variables are not significantly inter-correlated (exhibiting multicollinearity), that data should be normally distributed and there is no pattern between the residuals and the Y estimates or X values. Violating these assumptions does not directly affect the fitting of the model, but does limit the scope of

statistical inference that can be made from the data. The computer programme eliminates any variables with high multicolinearity, while residual plots (see appendix H) show a random distribution of variance, which also shows that the data are normally distributed.

In the case of certain regression equations, it was found that better correlations were achieved by removing certain samples. The rationale behind these exclusions is explained in appendix H.

Chapter 4

Results: Water Chemistry

This chapter describes the downstream changes in the dissolved chemistry of the two main subareas sampled in this work, the Bhote Kosi and the Langtang Khola-Trisuli. Following this are descriptions of the chemistry of the rivers sampled in the Khumbu region (upper Dudh Kosi) and the large rivers sampled in southern Nepal.

4.1. Atmospheric Inputs.

All data are adjusted for rainfall inputs by subtracting values from the compilation of rainfall data in Galy and France-Lanord (1999), which draws on the work of Wake *et al.* (1990), Wake *et al.* (1993), Collins and Jenkins (1996), Handa (1969) and Sequira and Kelkar (1978). The values used are as follows;

$[Na^+]$ = 10 μmol/l

$[Ca^{2+}]$ = 22 μmol/l

$[Mg^{2+}]$ = 6.1 μmol/l

$[K^+]$ = 2.2 μmol/l

[Si] = 0.8 μmol/l

$[HCO_3^-]$ = 68 µmol/l

$[NO_3^-]$ = 3.9 µmol/l

These are values adjusted to account for an estimated evapotranspiration rate of 25% in the Nepalese Himalaya (Alford, 1992). The best estimate of $[Sr^{2+}]$ and $^{87}Sr/^{86}Sr$ in rainwater is provided by Galy *et al.* (1999), based on regular sampling of Kathmandu rainfall during the monsoon season, with values of 21 nmol/l and an $^{87}Sr/^{86}Sr$ ratio of ~0.714 (again after adjustment for 25% evapotranspiration). Values adjusted for atmospheric input are used when quoting downstream changes in chemistry in this chapter and throughout the statistical analysis and mass balance in chapter 5.

In the Bhote Kosi mainstream, below the MCT, atmospheric inputs typically account for <2% of dissolved Si, 3-6% of dissolved Mg^{2+}, 5-10% of dissolved Ca^{2+}, K^+, Sr^{2+}, HCO_3^- and SO_4^{2-} and 10-20% of dissolved Na^+. Contributions are typically at the upper end of these ranges in September samples, the atmospheric contribution to dissolved sulphate being particularly high at this time, reaching >25% in the lowest reaches of the river. Upstream of the MCT in the Bhote Kosi, calculated atmospheric contributions are lower than those given above, except in the cases of potassium and silica. Rainfall is calculated to supply typically >45% of the chloride in the Bhote Kosi and >15% of dissolved nitrate, and as much as 100% in certain samples. In tributaries draining the Lesser Himalayan Formation, atmospheric inputs are calculated to account for up to 40% of dissolved Na^+ and Sr^{2+} (although 10-20% is more typical) and up to 25% of dissolved

Ca^{2+}, while contributions to dissolved Mg^{2+}, K^+ and in certain cases Cl^-, are typically lower than the minimum values give above.

Atmospheric contributions to the dissolved load of the Langtang Khola and rivers of the Khumbu region are mostly the same as those given above for the Bhote Kosi downstream of the MCT, although greater contributions are observed to total dissolved Ca^{2+} (typically 5-20%, higher in some HHCS-draining tributaries), Mg^{2+} (up to 25% in the Langtang Khola, typically 30-60% in the Khumbu), K^+ (up to 20%) and HCO_3^- (up to 20% in the Langtang Khola, between 25 and 60% in the Khumbu and >50% in some HHCS-draining tributaries of the Langtang Khola). In the larger rivers sampled in southern Nepal atmospheric contributions are again broadly similar to those noted above for the Bhote Kosi downstream of the MCT, although contributions to dissolved Na^+ (5-10%) and Cl^- (20-45%) are notably lower.

4.2. Downstream Changes in Water Chemistry.

Variations in water chemistry with distance from river source are plotted in fig. 4.1 to 4.12 from data given in table A1 to A6 in appendix A.

4.2.1. The Bhote Kosi.

Downstream changes in the water chemistry of the Bhote Kosi are illustrated in fig. 4.1 through to fig. 4.6

4.2.1.1. The Tibetan Sedimentary Series (TSS).

The Bhote Kosi has a spring source with high concentrations (relative to those downstream in the Bhote Kosi and in other Himalayan rivers) of Ca^{2+} (~1500 µmol/l), Mg^{2+} (~500 µmol/l), HCO_3^- (>2500 µmol/l) and SO_4^{2-} (~1300 µmol/l) but more moderate amounts of K^+ (~35 µmol/l), Na^+ (~130 µmol/l), Si (~120 µmol/l), Cl^- and NO_3^- (<10 µmol/l). $[Sr^{2+}]$ is high (~3.5 µmol/l) in contrast with $[Rb^+]$ (~0.02 µmol/l) and $^{87}Sr/^{86}Sr$ (~0.711).

Chemistry in the TSS section of the Bhote Kosi shows a distinctive pattern consisting of a rapid increase in the concentration of cations and anions between the river's source and BKT2 (see plate 3 for sample locations), followed by an equally rapid decrease between BKT2 and BKT3 (on the STDS). This general pattern is most marked in the change in Mg^{2+}, Na^+ and SO_4^{2-}, while exceptions to this pattern are seen in values of K^+, HCO_3^-, Cl^- and Rb^+ concentrations. These show a consistent decline within the TSS. $^{87}Sr/^{86}Sr$ rises to ~0.72 between the source and BKT2 with little change occurring downstrem to BKT3.

4.2.1.2. The High Himalayan Crystalline Series (HHCS).

The progress of the Bhote Kosi through this lithology is also marked by a consistent pattern of change in the different cation and anion concentrations. Between the STDS

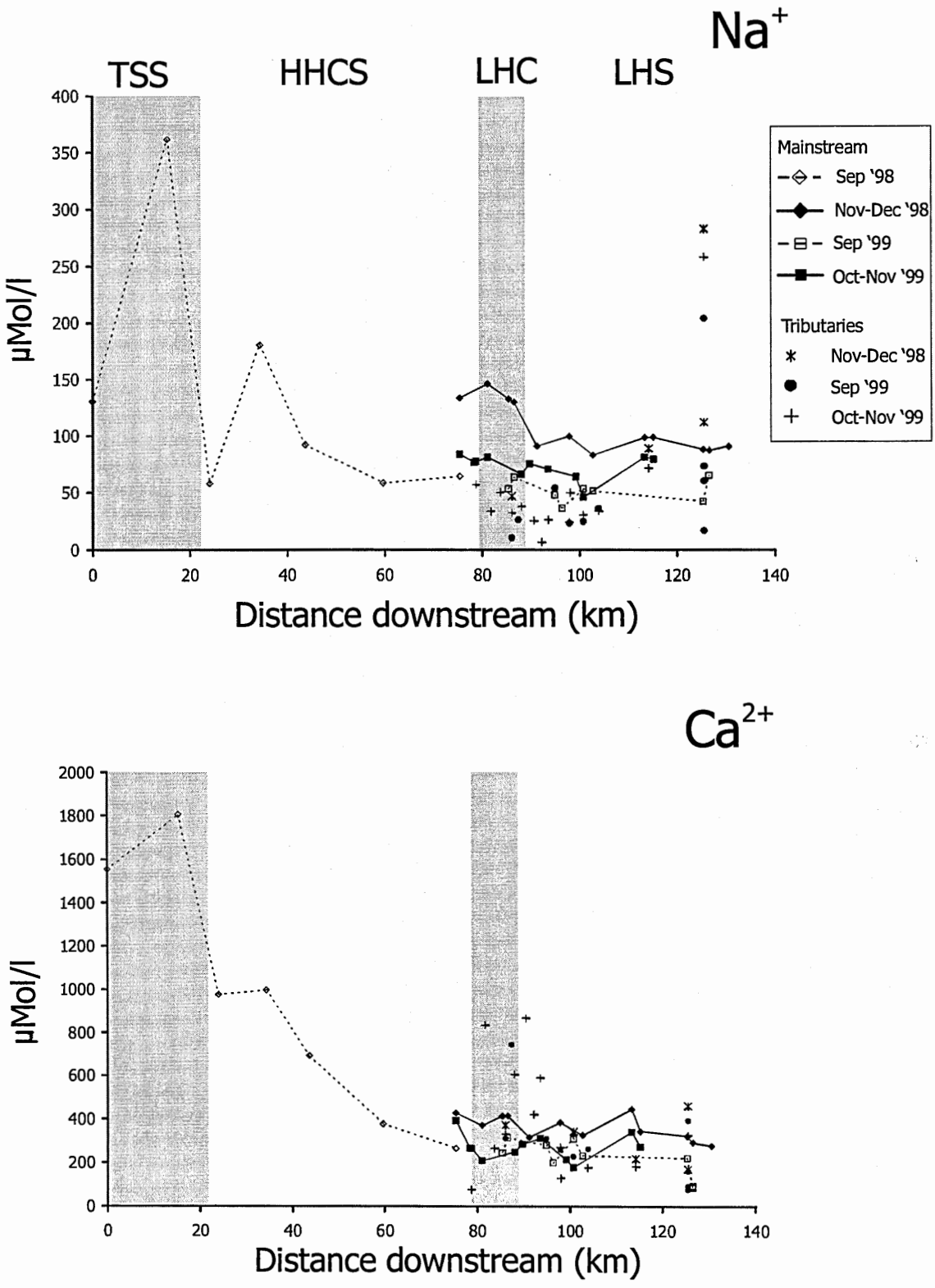

Fig. 4.1. Downstream changes in the concentration of dissolved sodium and calcium in the Bhote Kosi.

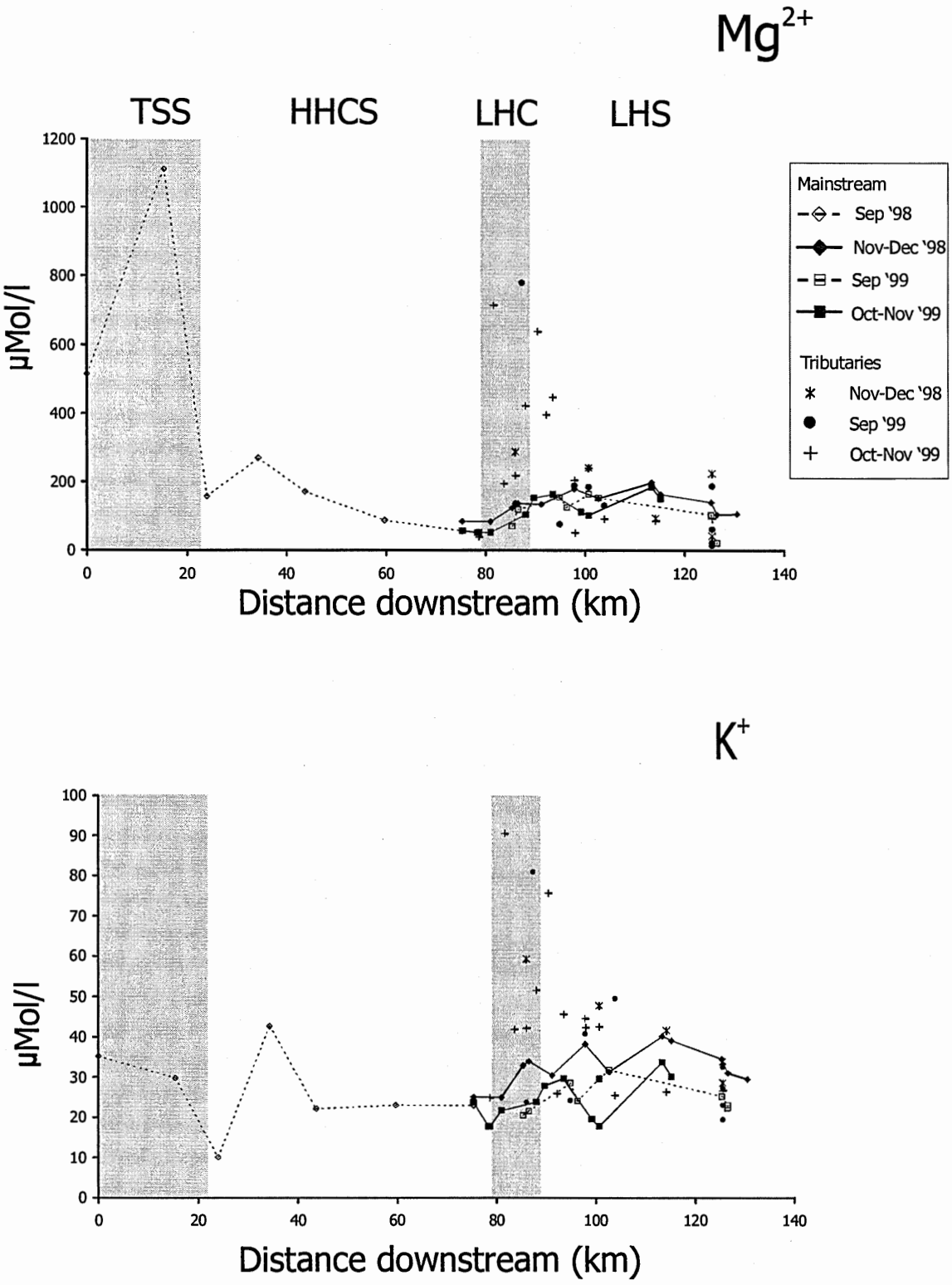

Fig. 4.2. Downstream changes in the concentration of dissolved magnesium and potassium in the Bhote Kosi.

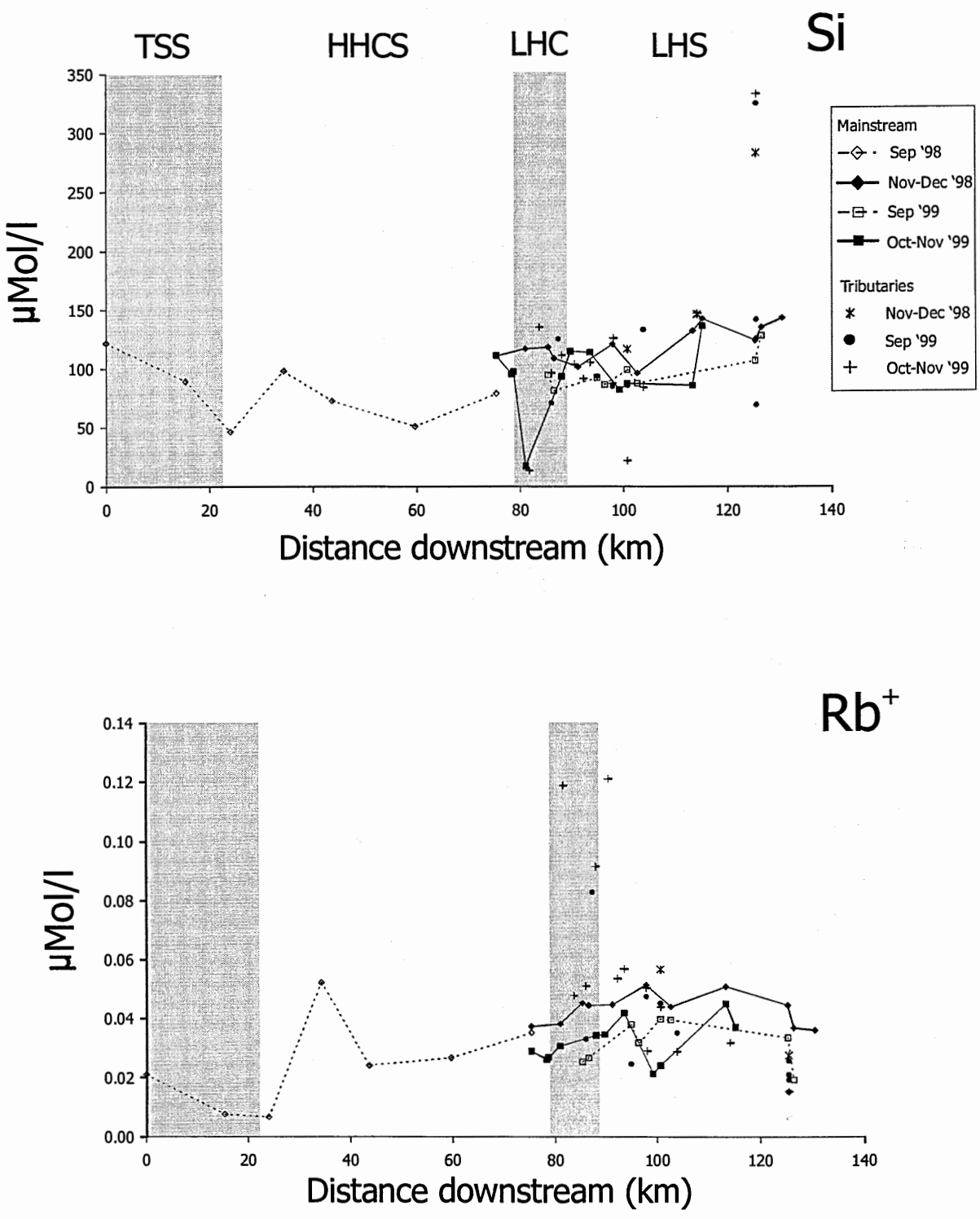

Fig. 4.3. Downstream changes in the concentration of dissolved silica and rubidium in the Bhote Kosi.

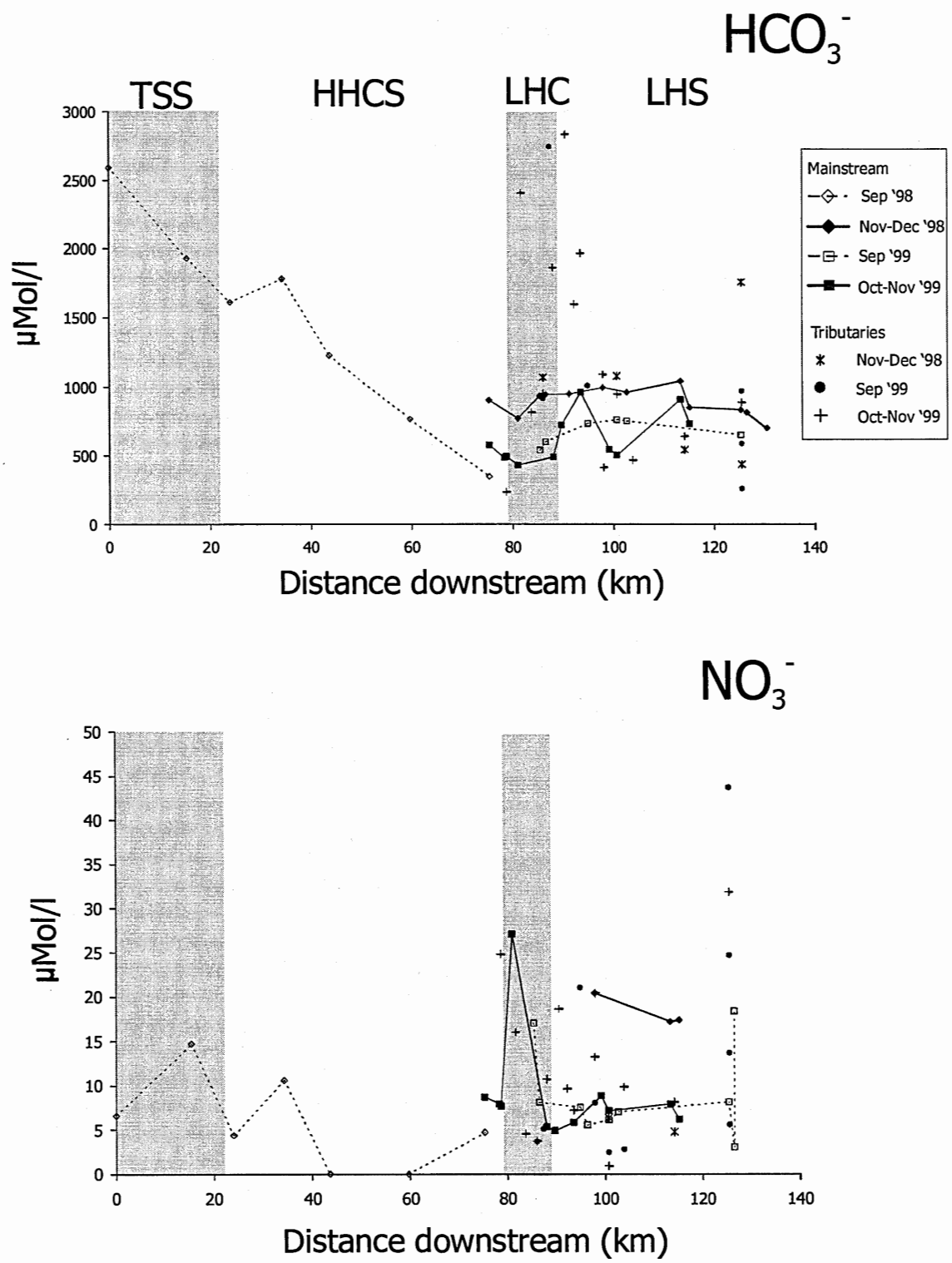

Fig. 4.4. Downstream changes in alkalinity and the concentration of dissolved nitrate in the Bhote Kosi.

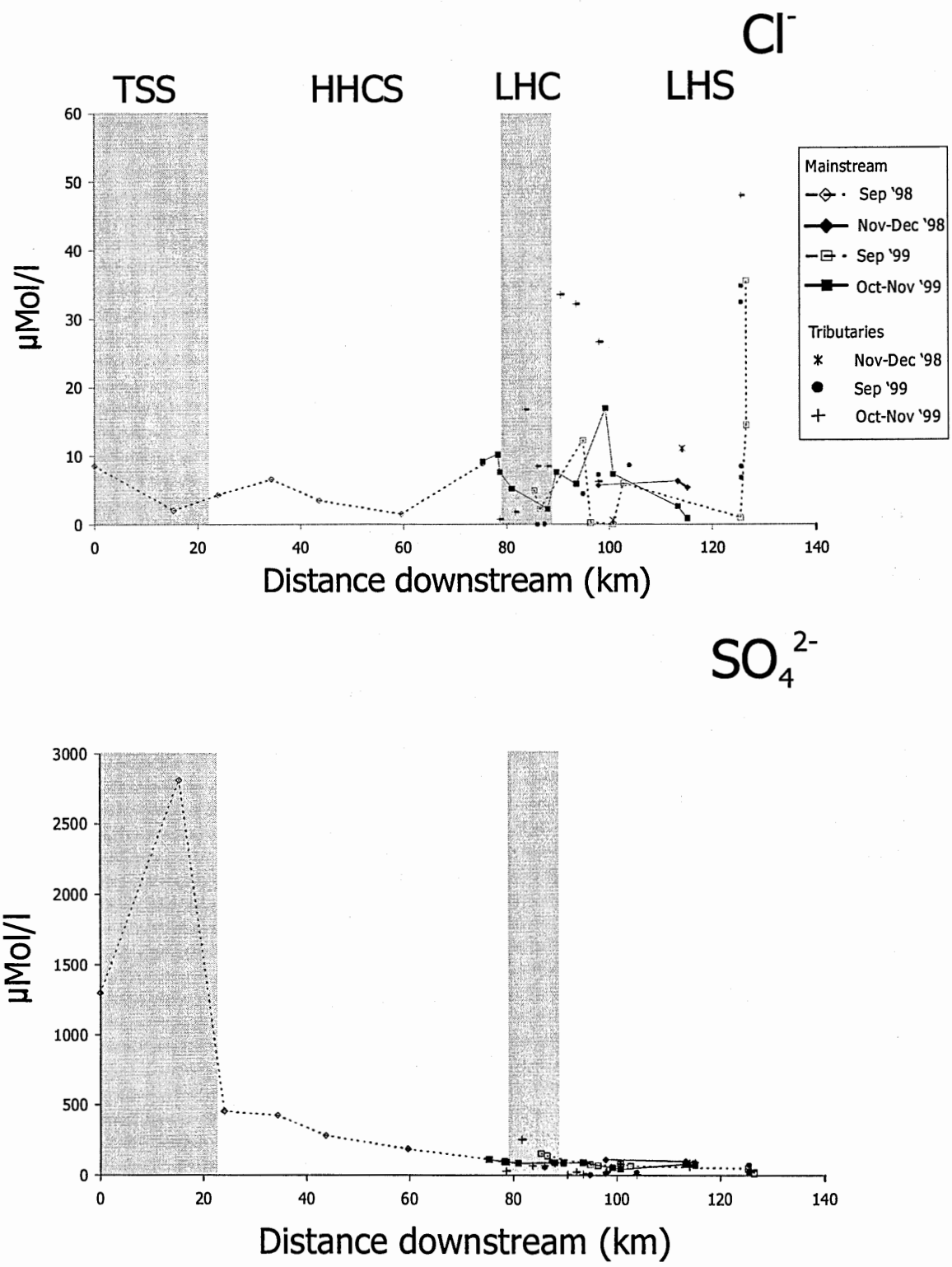

Fig. 4.5. Downstream changes in the concentration of dissolved chloride and sulphate in the Bhote Kosi.

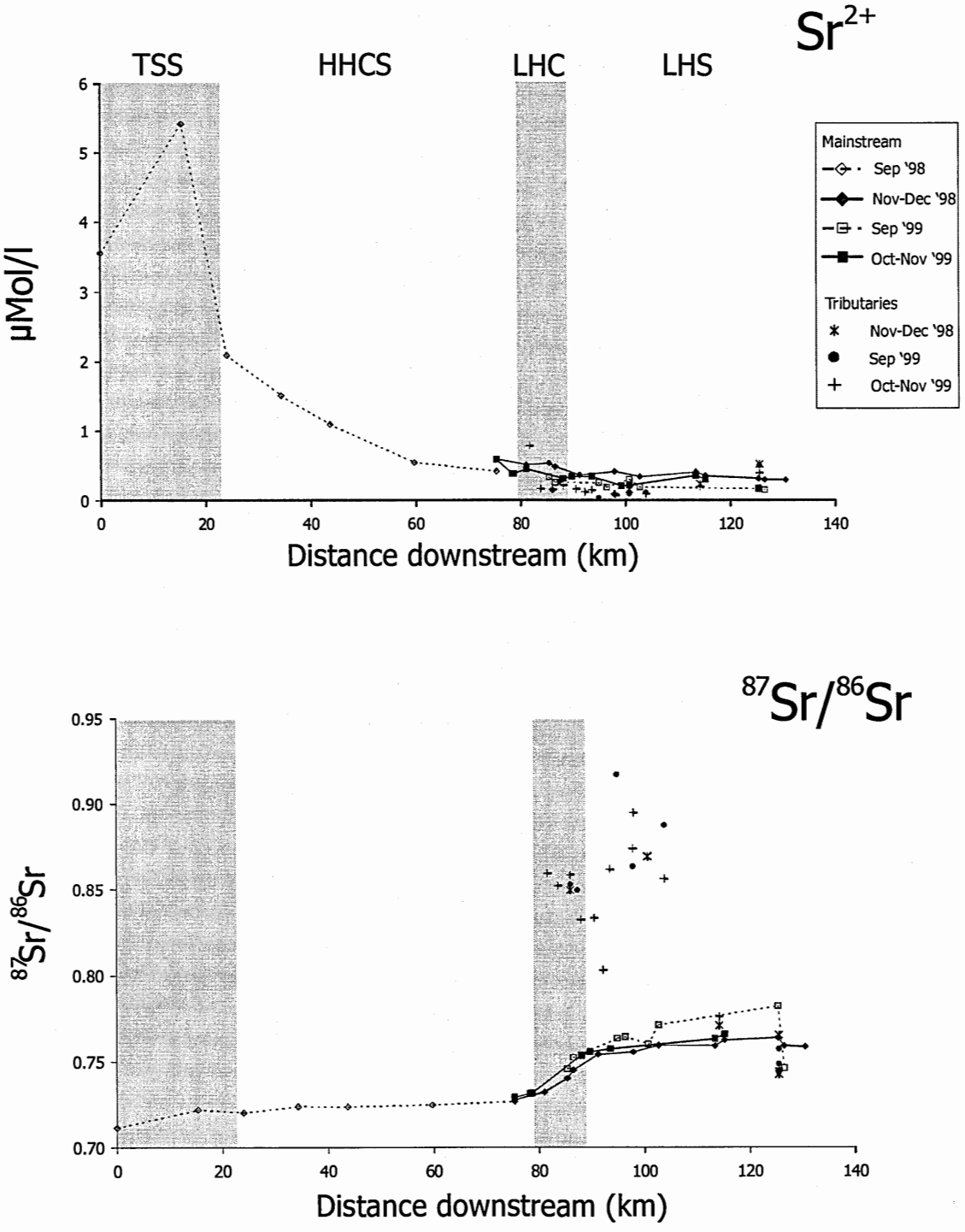

Fig. 4.6. Downstream changes in dissolved strontium concentration and $^{87}Sr/^{86}Sr$ in the Bhote Kosi.

and sample site BKT4 (33 km downstream from source) there is an increase in theconcentration of all measured cations and anions. This pattern is least marked in changes in Ca^{2+} and HCO_3^-, while $Sr^{2+}$and SO_4^{2-} concentrations are the only exception, displaying a remarkably consistent dilution throughout the HHCS. Downstream of BKT4 there is a consistent dilution of major cations and anions, a trend most marked in $[Ca^{2+}]$ (which falls from ~1000 µmol/l at BKT4 to ~300 µmol/l at the MCT) and HCO_3^- (which falls from ~1800 µmol/l to ~300 µmol/l). Both K^+ and Rb^+ concentrations, however, show no further decrease after BKT5 (44 km downstream from source) and, together with $[NO_3^-]$ and $[Cl^-]$ increase as the river passes across the latter part of the HHCS. $^{87}Sr/^{86}Sr$ increases in the HHCS, although by relatively little, from ~0.720 at the STDS to ~0.727 at the MCT.

4.2.1.3. The Lesser Himalayan Calc-Silicates of the Nawakot Group (LHC).

This is the most significant section of the river in terms of variation in $^{87}Sr/^{86}Sr$ ratio, a 10 km stretch in which $^{87}Sr/^{86}Sr$ rises from ~0.727 at the MCT to ~0.755. Most of this increase occurs in the downstream 5 km of this section, marked by the input of numerous tributaries (described in section. 4.2.1.6) draining predominantly Lesser Himalayan calc-silicates (see plate 3). The mainstream increase in $^{87}Sr/^{86}Sr$ is accompanied by similarly marked increases in K^+, Mg^{2+} and Rb^+ concentrations, together with a less substantial rise in Ca^{2+} and HCO_3^-. The concentration of Sr^{2+} continues to decline in this section, as do concentrations of Na^+, SO_4^{2-} and Cl^- (Cl^- changing particularly rapidly). Trends in Si and NO_3^- are confused in this section by the

presence of sample BK81 which has both anomalously high NO_3^- coupled with atypically low [Si]. This is perhaps resulting from a localised anthropogenic influence. Certainly fertiliser inputs could explain the NO_3^- peak although this explanation doesn't appear valid in explaining the low Si values.

4.2.1.4. The Lesser Himalayan Silicates of the Kuncha Group (LHS).

The chemistry of the dissolved load throughout the section of Lesser Himalayan silicates shows a further, more modest increase in $^{87}Sr/^{86}Sr$ from ~0.755 to ~0.76-0.77 (seasonal variations are significant in this part of the river, see section 3.2.1.9). $[Sr^{2+}]$ remains relatively constant at ~0.3 μmol/l. This section also sees a general increase in concentrations of Mg^{2+}, K^+, Si, Rb^+ and NO_3^-, but only minor changes in Na^+, Ca^{2+}, HCO_3^- and SO_4^{2-} concentrations. Some of the tributaries feeding into this segment of the river are of considerable size (e.g. the Balephi Khola) with consequent major impacts upon the water chemistry of the main river. It is possible that some of the mainstream samples from this section represent the incomplete mixing of these tributaries with the main river body, making it more difficult to pick out the broad trends in the LHF silicate section, although the effect on Sr chemistry is the most clear.

4.2.1.5. Mixing with the Indrawati and Chak Khola.

Inputs from the Indrawati and the Chak Khola at Dolalghat have a major influence on the Bhote Kosi as it becomes the Sun Kosi. Both rivers have lower $^{87}Sr/^{86}Sr$ than the

Bhote Kosi and thus reduce the $^{87}Sr/^{86}Sr$ ratio from that recorded at its outflow, also having the same effect on Rb^+ and K^+ concentrations. The effect on Ca^{2+}, Na^+, Mg^{2+} and HCO_3^- concentrations is less marked owing to an approximate balance between inputs from the Chak Khola (higher values than in the Bhote Kosi) and the Indrawati (lower values). All three rivers have relatively low $[Sr^{2+}]$ and $[SO_4^{2-}]$ concentrations. The Chak Khola has unusually high NO_3^- and Cl^- concentrations which have a major impact in determining values for the upper Sun Kosi, elevating $[Cl^-]$ and $[NO_3^-]$ from <1 μmol/l and ~10 μmol/l respectively at the outflow of the Bhote Kosi to values of >30 μmol/l Cl^- and ~20 μmol/l NO_3^- downstream of the tri-confluence.

4.2.1.6. Tributary Chemistry.

One tributary draining the High Himalayan Crystalline Series (the Jum Khola, BK79) is shown on fig. 4.1 – 4.6 (others were sampled but are not included owing to poor charge balance, see page A2). This river joins the Bhote Kosi in the LHF section of the mainstream but drains the HHCS almost exclusively (see plate 3). The Jum Khola displays a relatively (but not extremely) high $^{87}Sr/^{86}Sr$ ratio (0.75) coupled with relatively low major cation and anion concentrations (consistent with trends noted in the HHCS section of the main river). The exception to this is $[NO_3^-]$, which is markedly high in this tributary (~25 μmol/l) and seems to be responsible for the sharp NO_3^- peak in the early part of the LHF calc-silicate section of the main river. The prominence of this peak in the main river may be related to incomplete mixing between the Jum Khola

and the main river at this sample site owing to the necessity of sampling this confluence upstream of the Tatopani hot spring.

Numerous tributaries with catchments that are dominated by the Lesser Himalaya enter the Bhote Kosi in the lower (5 km) portion of the LHF calc-silicate zone and first few km of the LHF silicate section. These tributaries display very distinctive chemical characteristics, most prominent of which are their high Sr-isotope ratios, all in excess of 0.8. These tributaries are also characterised by low [Sr^{2+}] (<0.2 μmol/l) with the exception of the Kukundal Khola (BK82), which has a relatively high concentration of ~0.8 μmol/l), and low Na^+ (<50 μmol/l). In contrast, high concentrations are noted for Rb^+ (0.04-0.12 μmol/l), K^+ (generally >40 μmol/l) and Mg^{2+} (~200-~800 μmol/l). Values for Ca^{2+} and HCO_3^- are generally, but not consistently, higher than the Bhote Kosi mainstream. There seems to be little to chemically distinguish tributaries dominated by Lesser Himalayan calc-silicates from those dominated by purer silicates, although those dominated by silicate have lower Rb^+ (<0.06 μmol/l) and K^+ concentrations (<50 μmol/l).

The Balephi Khola joins the Bhote Kosi midway through the zone of LHF silicates. It appears to have little influence on the Sr chemistry of the Bhote Kosi, the $^{87}Sr/^{86}Sr$ and [Sr^{2+}] of the Balephi Khola being similar to that of the Bhote Kosi at the confluence. The major cation and HCO_3^- concentrations of the Balephi Khola (the catchment of which doesn't stretch as far North as the TSS) are lower than those of the Bhote Kosi, and the influence of this can be seen in falls in Bhote Kosi mainstream concentrations.

4.2.1.7. Hot Spring Chemistry.

One major hot spring is known in the Bhote Kosi basin, occurring at Tatopani and feeding directly into the main river (see plate 2 for location). The spring is characterised by extremely high concentrations of all measured species (with the exception of NO_3^-) and has a radiogenic Sr-isotope signature (~0.79). The Bhote Kosi was sampled upstream (BK78) and downstream (BK80) of the Tatopani hot spring. There is no discernable change in main river chemistry between these two sites and [Cl^-] (a good marker of hot spring inputs) actually falls downstream of the hot spring inputs.

4.2.1.8. The Bhote Kosi Dam Project.

Sample point BK80 also lies immediately upstream of the main construction site (now completed) of the Bhote Kosi dam. A sample (BK81) was also taken downstream of the dam site and there are no major changes in any of the measured chemical species between the two sites.

4.2.1.9. Seasonal and Annual Fluctuations.

In the Lesser Himalayan section of the Bhote Kosi, samples were collected during three periods (November-December 1998, September 1999 and late October-November 1999). This allows a comparison between data collected in different years and between

data collected in September 1999 (when monsoon rainfall was still occurring) and the true dry season (late October-December).

In terms of Sr chemistry there is little difference between 1998 and 1999 dry season data. September 1999 data, however, display higher $^{87}Sr/^{86}Sr$ values coupled with slightly lower $[Sr^{2+}]$ in the LHF silicate portion of the river. In terms of the other major chemical species it is difficult to identify consistent differences in values from the different sampling periods other than the fact that 1998 data displays consistently higher values of Na^+, Ca^{2+}, K^+, Rb^+ and HCO_3^-.

4.2.2. The Langtang Khola-Trisuli.

The changes recorded in this river are illustrated in fig. 4.7 through to fig. 4.12, measured from the source of the Langtang Khola (the Langtang Glacier). The true source of the Trisuli is that of the Bhote Kosi (Langtang) in Tibet. Unfortunately, sampling was impossible north of the Nepalese border.

4.2.2.1. The High Himalayan Crystalline Series.

Output from the Langtang Glacier (L14, see plate 9 for location of samples) is characterised by relatively high concentrations of Ca^{2+} (~350 μmol/l), Mg^{2+} (~100 μmol/l), K^+ (~50 μmol/l), Sr^{2+} (>0.7 μmol/l), Rb^+ (>0.07 μmol/l), HCO_3^- (~550 μmol/l), Cl^- (~25 μmol/l), NO_3^- (~40 μmol/l) and SO_4^{2-} (~170 μmol/l), with an $^{87}Sr/^{86}Sr$ of 0.738.

The 4 km between the snout of the glacier and the next downstream sample site (L15) sees a significant dilution of these species, with particularly sharp drops in K^+ (to ~25 µmol/l), Sr^{2+} (to ~0.4 µmol/l), Rb^+ (to <0.02 µmol/l), Cl^- (to ~1.5 µmol/l) and NO_3^- (to ~2 µmol/l). There is no significant change in $^{87}Sr/^{86}Sr$ between L14 and L15, however, and throughout the HHCS section of this river system (the Langtang Khola) $^{87}Sr/^{86}Sr$ remains at ~0.74 (± 0.003). Cation and anion concentrations are less constant, with the progress of the Langtang Khola broadly characterised by increasing concentrations of Na^+, K^+, Si, Rb^+ and Cl^-, mirrored by decreasing Ca^{2+}, Mg^{2+}, Sr^{2+}, HCO_3^- and SO_4^{2-}, while NO_3^- concentrations are erratic. These trends can be linked to tributary inputs throughout this section. The tributaries measured in the forested low altitude part of this section (L18 and L20) display slightly higher $^{87}Sr/^{86}Sr$ ratios and [Si] coupled with low concentrations of Sr^{2+}, Ca^{2+}, HCO_3^- and SO_4^{2-}.Those in the upper section of the river (L10, L11 and L29) are characterised by higher concentrations of Sr^{2+}, Ca^{2+}, HCO_3^- and SO_4^{2-} (see fig. 4.6 to fig. 4.12).

4.2.2.2. Input from the Bhote Kosi (Langtang).

The Bhote Kosi (Langtang), with a catchment incorporating significant TSS bedrock in addition to HHCS units (see plates 8 and 9), is marked by lower $^{87}Sr/^{86}Sr$ (~0.72) coupled with high concentrations of Ca^{2+}, Mg^{2+}, Sr^{2+}, HCO_3^- and SO_4^{2-}. Downstream of the confluence between the Langtang Khola and Bhote Kosi (Langtang) at Syabrubensi, the upper Trisuli takes on the characteristics of the former. This is particularly significant with regard to Sr chemistry, the $^{87}Sr/^{86}Sr$ of the upper Trisuli downstream of

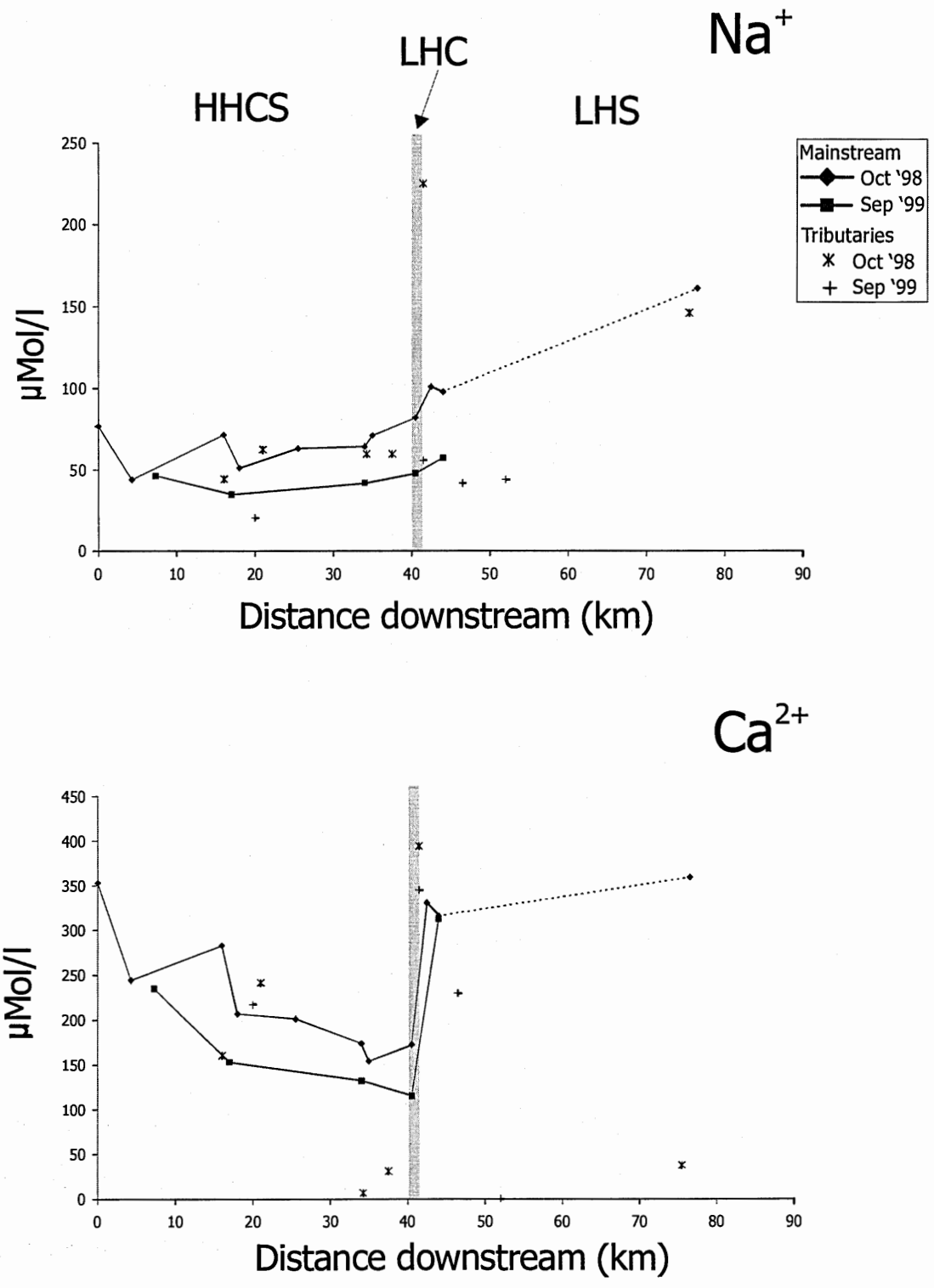

Fig. 4.7. Downstream changes in dissolved sodium and calcium concentrations in the Langtang Khola - Trisuli.

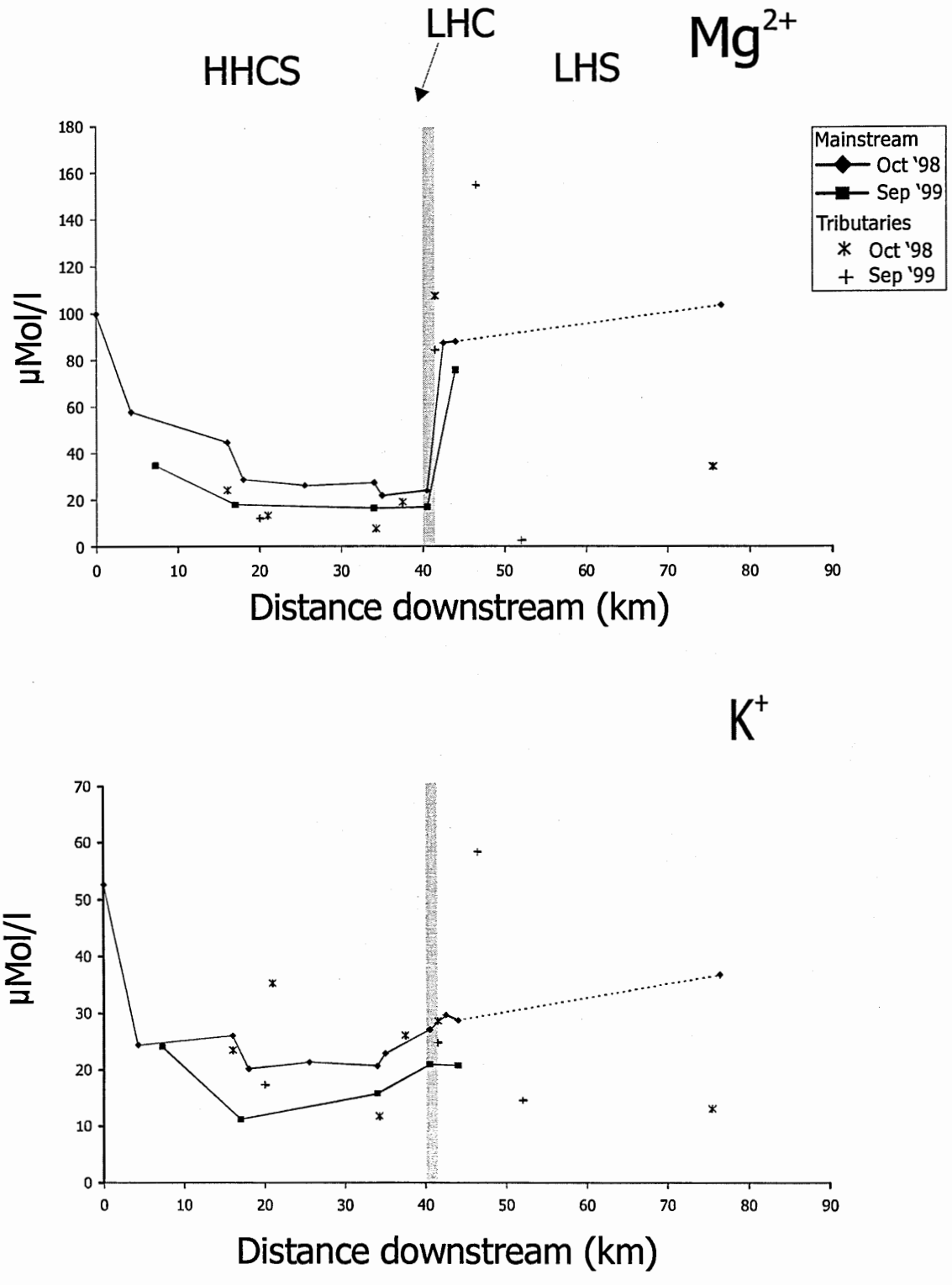

Fig. 4.8. Downstream changes in dissolved magnesium and potassium concentrations in the Langtang Khola - Trisuli.

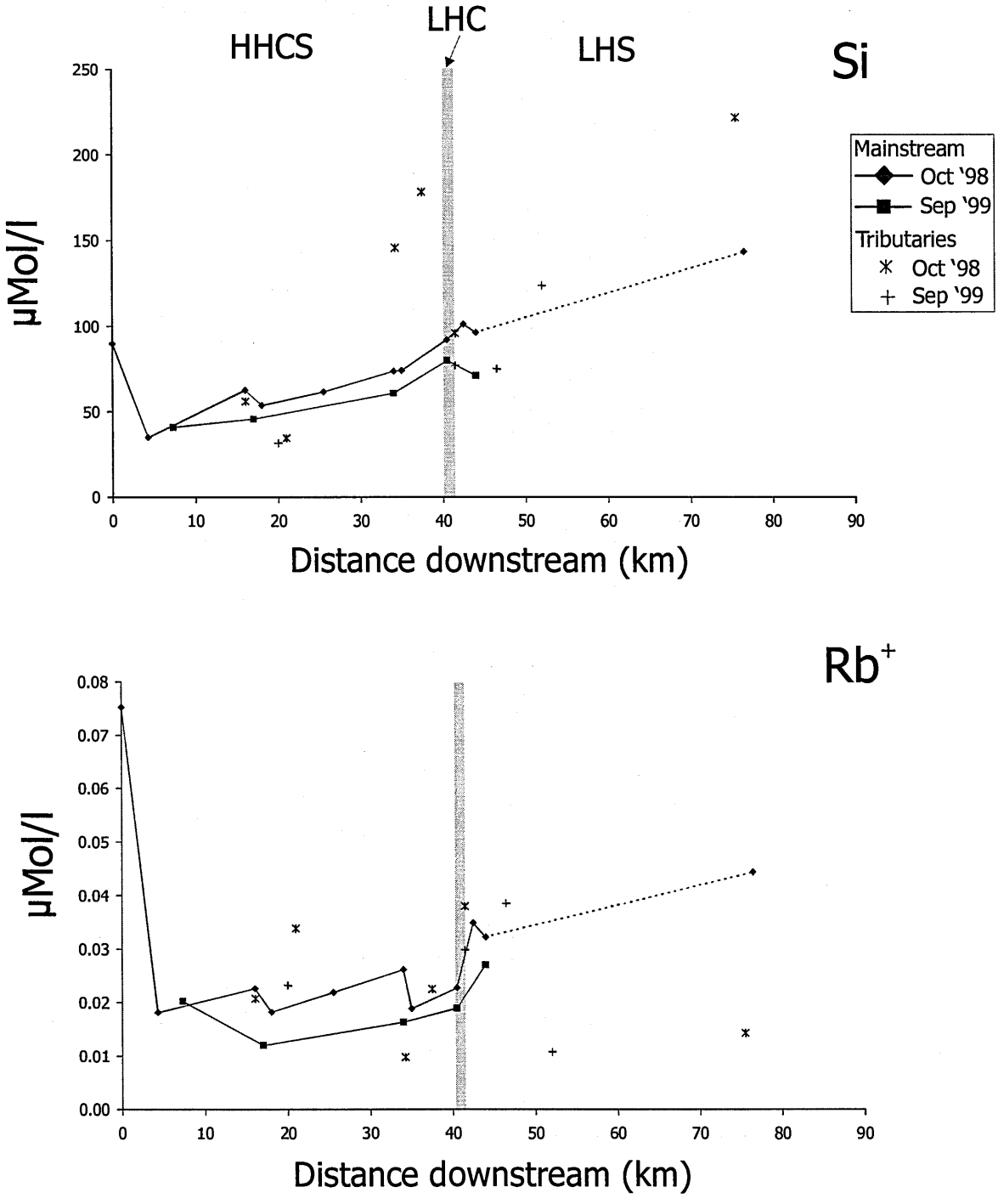

Fig. 4.9. Downstream changes in dissolved silica and rubidium concentrations in the Langtang Khola - Trisuli.

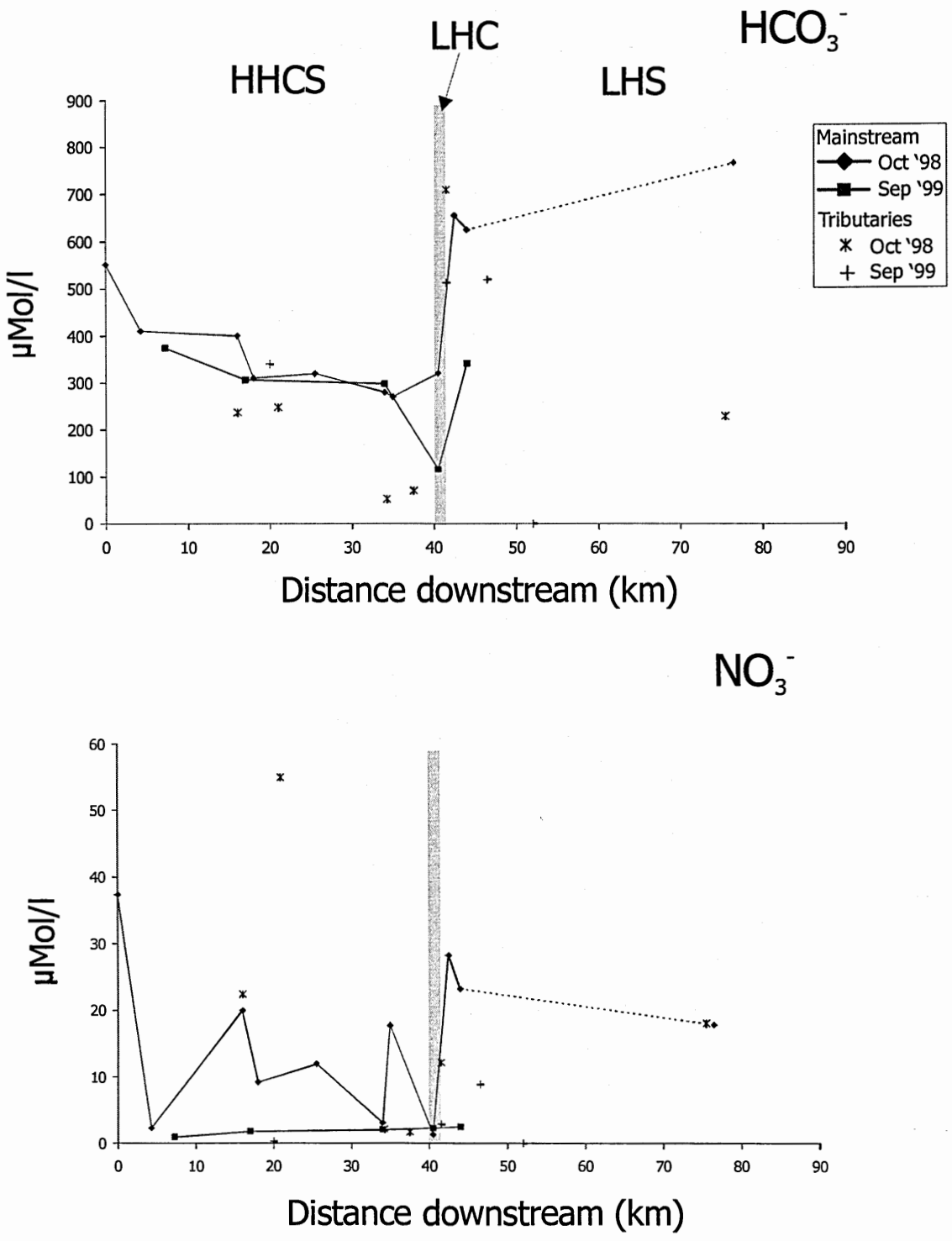

Fig.4.10. Downstream changes in alkalinity and dissolved nitrate concentrations in the Langtang Khola-Trisuli.

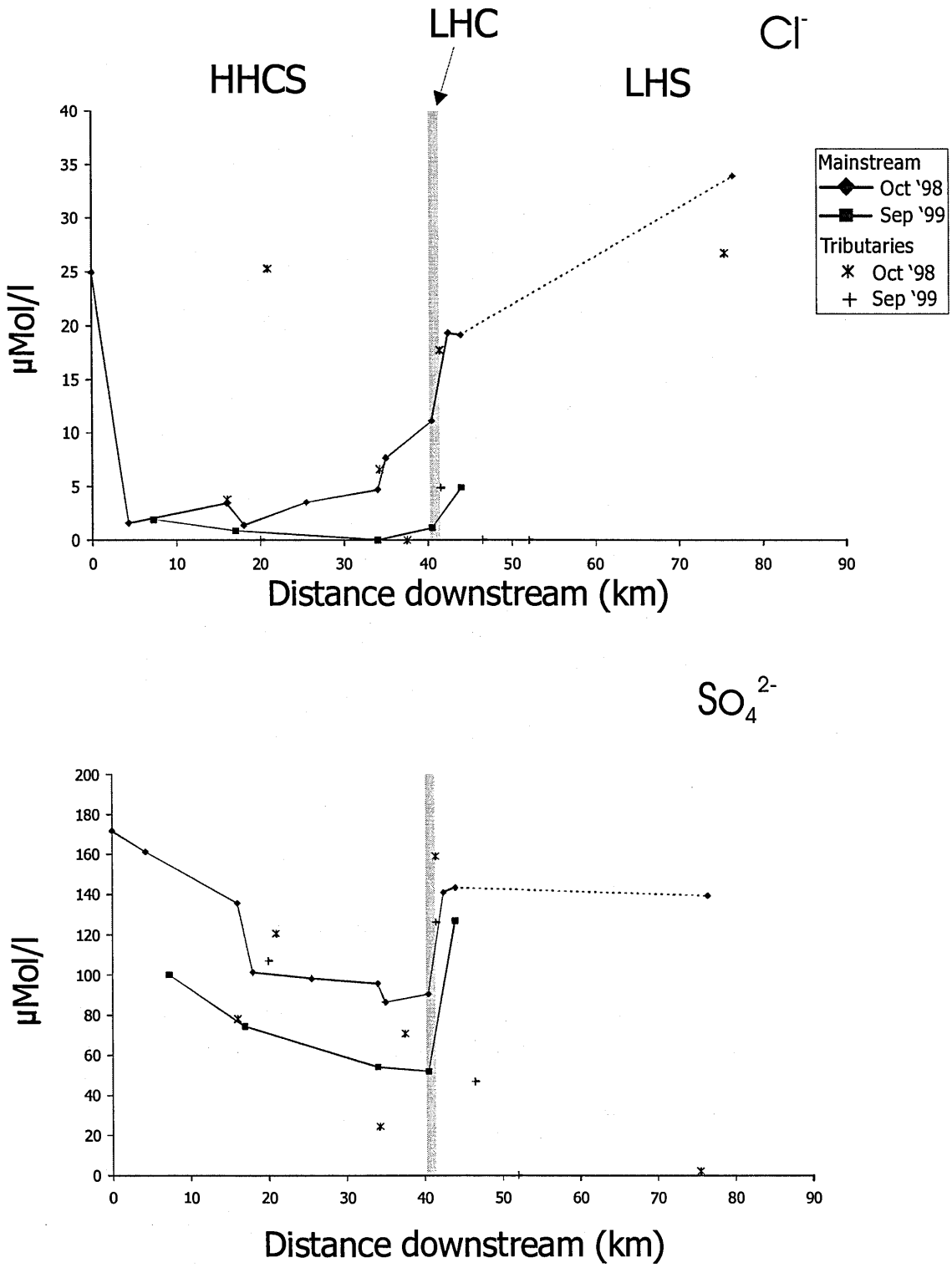

Fig.4.11. Downstream changes in dissolved chloride and sulphate concentrations in the Langtang Khola-Trisuli.

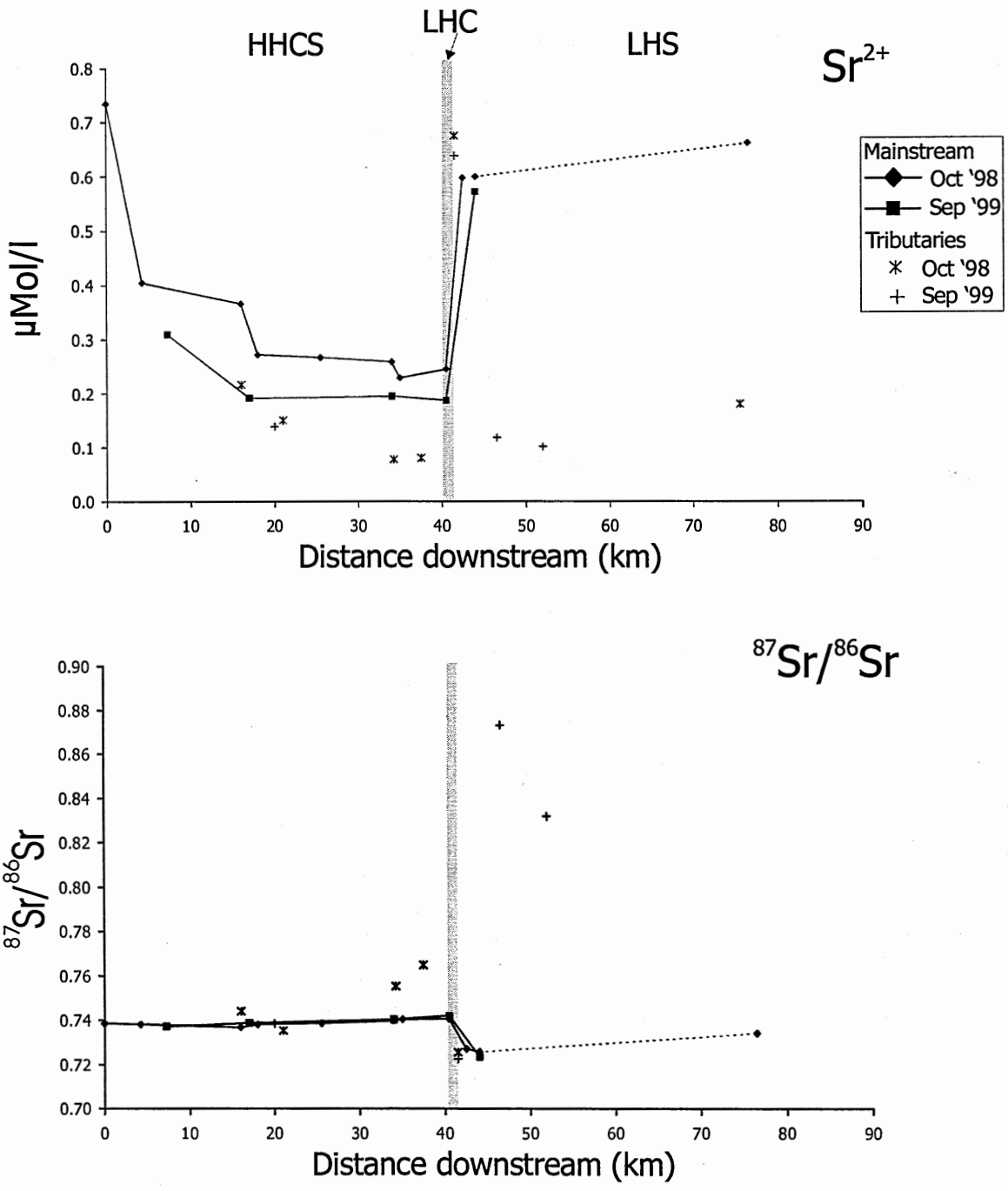

Fig. 4.12. Downstream changes in dissolved strontium concentrations and $^{87}Sr/^{86}Sr$ ratios in the Langtang Khola - Trisuli.

the Bhote Kosi (Langtang)/ Langtang Khola confluence being almost indistinguishable from that of the Bhote Kosi (Langtang) (0.726 and 0.725 in 1998, 0.723 and 0.722 in 1999).

4.2.2.3. The Lesser Himalaya.

The chemical changes at the Langtang Khola / Bhote Kosi (Langtang) confluence described above mask the effects of the attenuated exposure of the Lesser Himalayan calc-silicates in this section (plate 8). Lesser Himalayan tributaries are characterised by high $^{87}Sr/^{86}Sr$ (>0.80) and low $[Sr^{2+}]$ (<0.2 μmol/l), as already noted in the Bhote Kosi (section 4.2.1.6), while cation and anion concentrations are variable. The LHF section of the Trisuli is marked by increases in $^{87}Sr/^{86}Sr$ and concentrations of all measured cations, HCO_3^- and Cl^-. It should be noted, however, that the final downstream sample (L21) was collected in December 1998 (nearly two months later than other samples) and that this gap in sampling times may be an important factor explaining the recorded changes in this portion of the river.

4.2.2.4. Hot Spring Chemistry.

The hot spring at Syabrubensi was sampled both in 1998 and 1999 (see plate 8 for location). Like the Tatopani hot spring it is characterised by high values of all measured species (excluding NO_3^-) although there are some major chemical differences between the two springs. The Syabrubensi spring displays markedly lower Na^+, Rb^+ and Cl^-

concentrations, but higher [Mg^{2+}]. The impact of the Syabrubensi hot spring cannot be determined easily as it occurs close to the MCT, immediately downstream of the Bhote Kosi / Langtang Khola confluence. It is likely to be negligible, however, due to its very low flow.

4.2.2.5. Seasonal Variations.

Sr-isotope values are remarkably consistent when comparing 1998 and 1999 samples. All cation and anion values are consistently lower in samples obtained in 1999, possibly reflecting rainfall dilution as a result of the earlier time of collection (the September monsoon as opposed to October).

4.2.3. The Khumbu Region.

No significant downstream trends in water chemistry are noted in the Khumbu region, a fact partly due to the sparsity of samples collected, but more importantly owing to the fact that the Khumbu rivers all predominantly drain only the units of the HHCS (see map, plate 4). All samples collected from the region reveal a similar chemistry characterised by the following values.

[Na^{+}] = 33-56 μmol/l

[Mg^{2+}] = 4-12 μmol/l

[Si] = 43-86 μmol/l

$[K^+]$ =11-22 µmol/l

$[Ca^{2+}]$ = 80-137 µmol/l

$[Rb^+]$ = 0.017-0.037 µmol/l

$[Sr^{2+}]$ = 0.07-0.19 µmol/l

$[HCO_3^-]$ = 116-179 µmol/l

$[Cl^-]$ = 0-31 µmol/l

$[NO_3^-]$ = <3 µmol/l

$[SO_4^{2-}]$ = 46-87 µmol/l

$^{87}Sr/^{86}Sr$ = 0.743-0.755

Variations in geology do not provide an obvious explanation for the minor variations noted above, and they are possibly related to factors not measured in this study e.g. biological factors, soil variation.

4.2.4. Large Rivers of Southern Nepal.

The Arun River, with its vast drainage on the Tibetan Plateau (plate 7), is marked by prominently higher concentrations of Na^+, Sr^{2+}, Cl^- and SO_4^{2-} than other rivers described in this work. The mixed lithology drainage basin of the Sun Kosi is characterised by the highest Mg^{2+}, K^+, and to a lesser extent, Si, Ca^{2+} and Rb^+ concentrations of the major rivers. Dissolved Sr in the Sun Kosi is considerably more radiogenic ($^{87}Sr/^{86}Sr \sim 0.78$) than that in the Arun ($^{87}Sr/^{86}Sr \sim 0.73$) but neither are as radiogenic as the Tamur (~0.79), a smaller river lacking TSS bedrock in its drainage. This river is also

characterised by considerably lower Mg^{2+}, Ca^{2+}, Sr^{2+} and HCO_3^- concentrations. The dissolved chemistry of the Sapt Kosi samples results from the confluence of these three rivers, the $^{87}Sr/^{86}Sr$ of ~0.755 reflective of the larger amounts of Sr coming from the Arun.

Chapter 5

Interpretation of Water Chemistry

This chapter uses the data described in chapter 4 to determine the inputs typical of the main Himalayan lithologies, in order to subsequently determine the importance of each of these in determining the Sr chemistry of Himalayan rivers. A twofold approach is employed. Statistical analysis, in the form of principal components analyses, is used to pinpoint the most significant correlations in the Bhote Kosi, Langtang Khola-Trisuli, Khumbu and overall datasets, with emphasis on relationships involving dissolved $^{87}Sr/^{86}Sr$ ratios and Sr^{2+} concentrations. Multiple regression equations are then created using these datasets to independently predict Sr chemistry in the rivers sampled in southern Nepal (see plate 7 for locations), in order to test the relevance of these relationships to the Himalaya as a whole. The second technique employed is mass balance analysis, in the first section of the chapter to interpret downstream chemistry changes in terms of inputs from the weathering of different minerals, and in the final portion of the chapter, to estimate the relative contributions of different lithologies to the Sr chemistry of the rivers sampled in this study.

5.1. Downstream Changes in Mineral Contributions to Dissolved River Chemistry.

Amongst published mass balance calculations for Himalayan rivers, that of Blum *et al.*, (1998) is unique in that it enables an estimate to be made of the contribution from the weathering of major rock forming minerals to the dissolved alkalinity budget of a river at a particular sample site. This methodology is applied below in the case of Bhote Kosi (fig. 5.1 to 5.3 and table A1) and Langtang Khola-Trisuli (fig. 5.4 to 5.5 and table A2) in order to understand changes in the relative weathering rates of minerals and observe whether these coincide with changes in dissolved strontium chemistry.

5.1.1. Mass Balance Methodology.

(i). All data are corrected for atmospheric inputs using the dataset compiled by Galy *et al.* (1999) as described in section 4.1.

(ii). All remaining Na^+ in river waters is attributed to the weathering of albite to kaolinite. When this reaction is balanced, 2 mol of Si and 1 mol of HCO_3^- are subtracted for each mol of Na^+.

(iii). Remaining Ca^{2+} is attributed, in proportion to the Ca^{2+}/Na^+ ratio of plagioclase, to the weathering of anorthite to kaolinite. According to this reaction 2 mol of HCO_3^- are subtracted for each mol of Ca^{2+}. A Ca^{2+}/Na^+ ratio of 0.38 is used, based on the ratio of the silicate portion of bedload from the Raikot watershed in northern Pakistan, which is dominated by plagioclase (Blum *et al.*, 1998).

(iv). Remaining Si is attributed to the weathering of orthoclase to kaolinite, a reaction in which 0.5 mol of K^+ and 0.5 mol of HCO_3^- are subtracted for each mol of Si.

(v). Remaining K^+ is attributed to the weathering of biotite to vermiculite. In this reaction 1 mol of HCO_3^- is subtracted for every mol of K^+.

(vi). Excess Ca^{2+} and Mg^{2+} is attributed to carbonate weathering, with 2 mol of HCO_3^- subtracted for each mol of Ca^{2+} or Mg^{2+}.

Once these calculations have been completed the % of riverine HCO_3^- flux attributable to albite, anorthite, orthoclase, biotite and carbonate can be calculated.

5.1.2. Downstream Changes in Mineral Contributions to the Bhote Kosi.

Using the mass balance methodology described above, it is calculated that the TSS section of the Bhote Kosi is dominated by carbonate inputs (≥90%), with the remaining alkalinity flux largely derived from the weathering of albite and anorthite (see fig. 5.1 through to fig. 5.3). The calculated contribution from biotite is <1% with no contribution from orthoclase. The carbonate contribution decreases between source and sample site BKT2 (see plate 3 for sample localities), but increases in the latter portion of the TSS (up to BKT3), a reverse of the general trends seen in the majority of cation and anion concentrations.

In the HHCS section of the river there is an increase in the importance of silicate weathering, although carbonate is still calculated to dominate the river alkalinity budget (~80%). The estimated increase in the biotite contribution is the most rapid, but this still

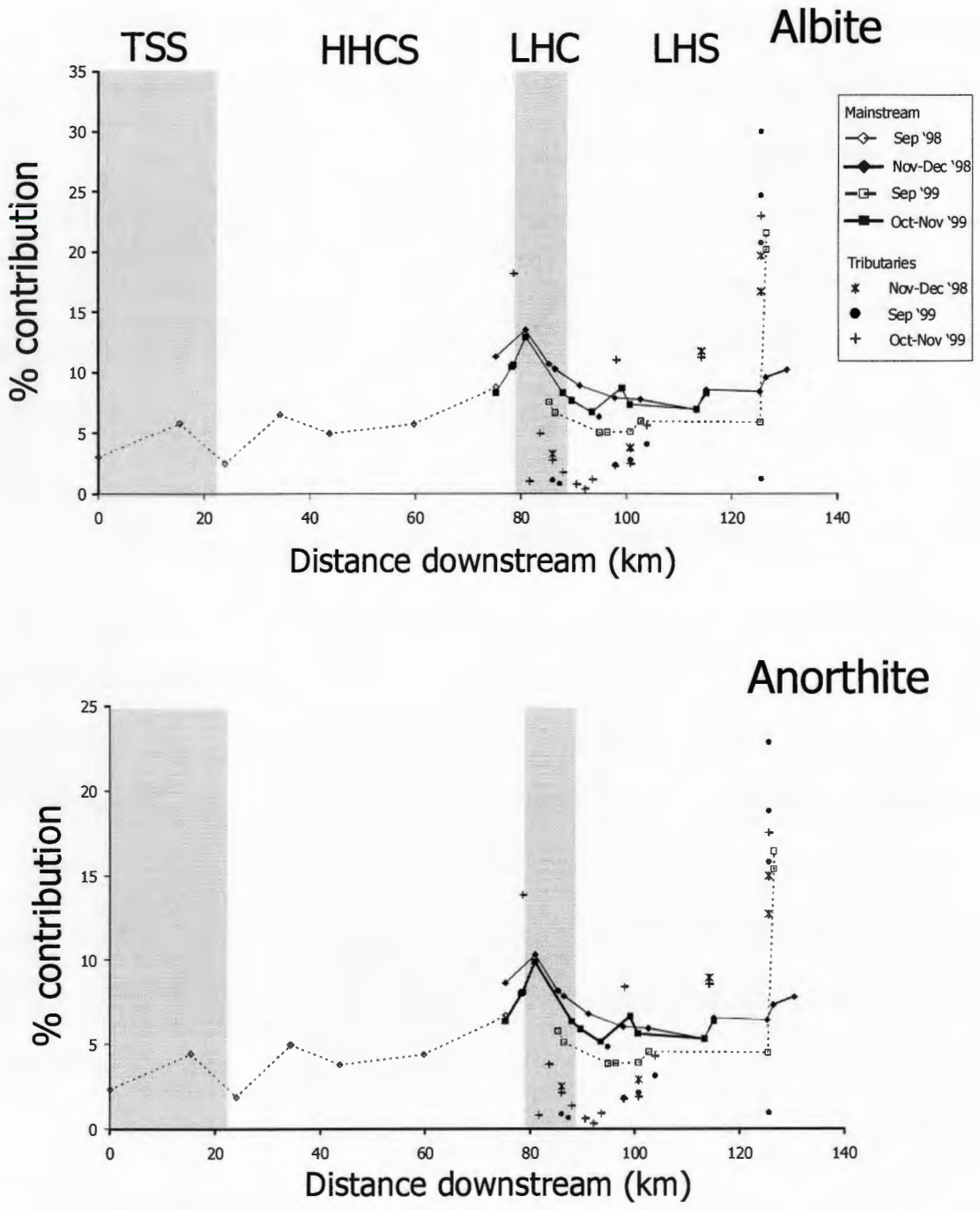

Fig. 5.1. Downstream changes in the calculated contribution of albite and anorthite to total alkalinity in the Bhote Kosi.

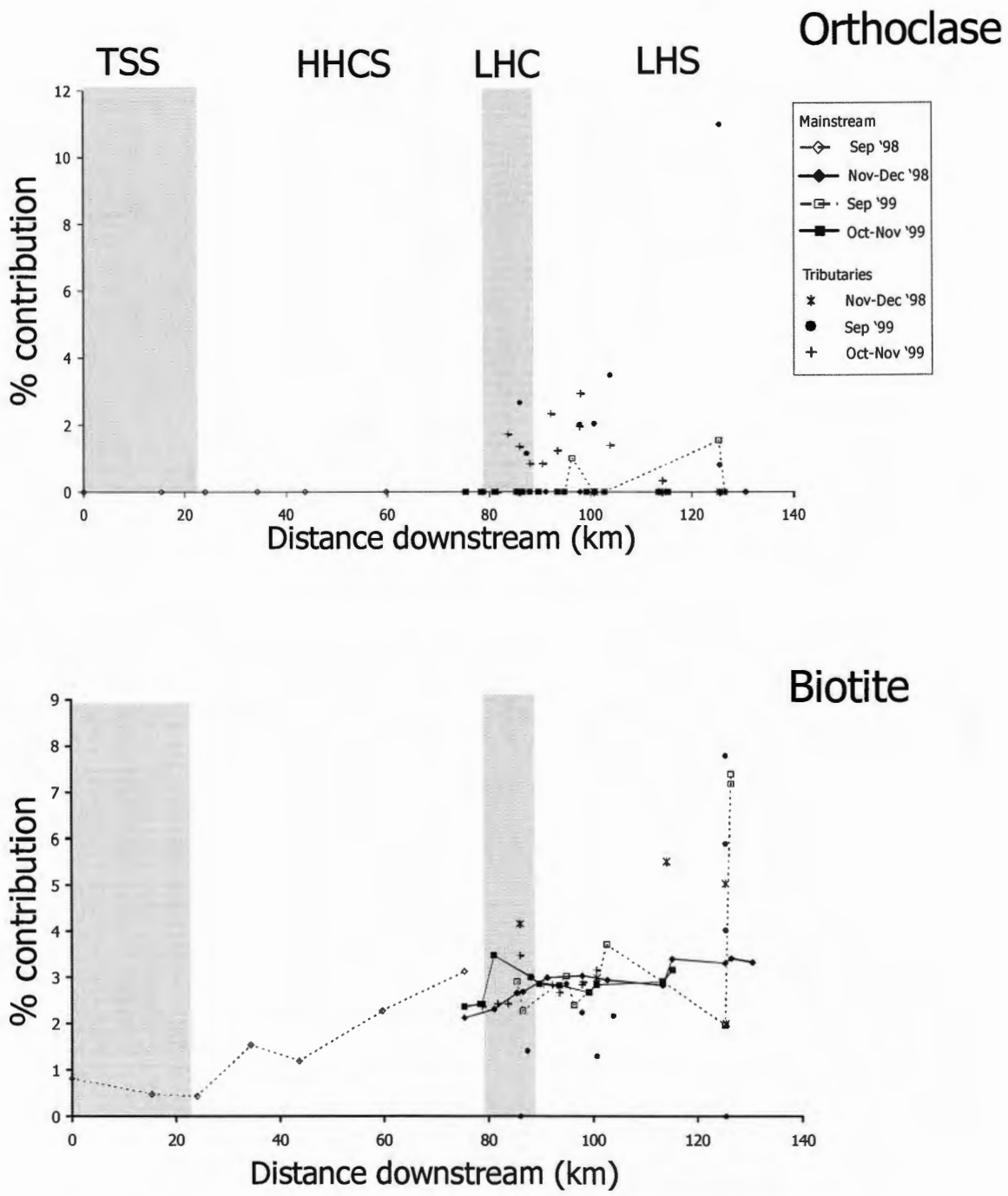

Fig. 5.2. Downstream changes in the calculated contribution of orthoclase and biotite to total alkalinity in the Bhote Kosi.

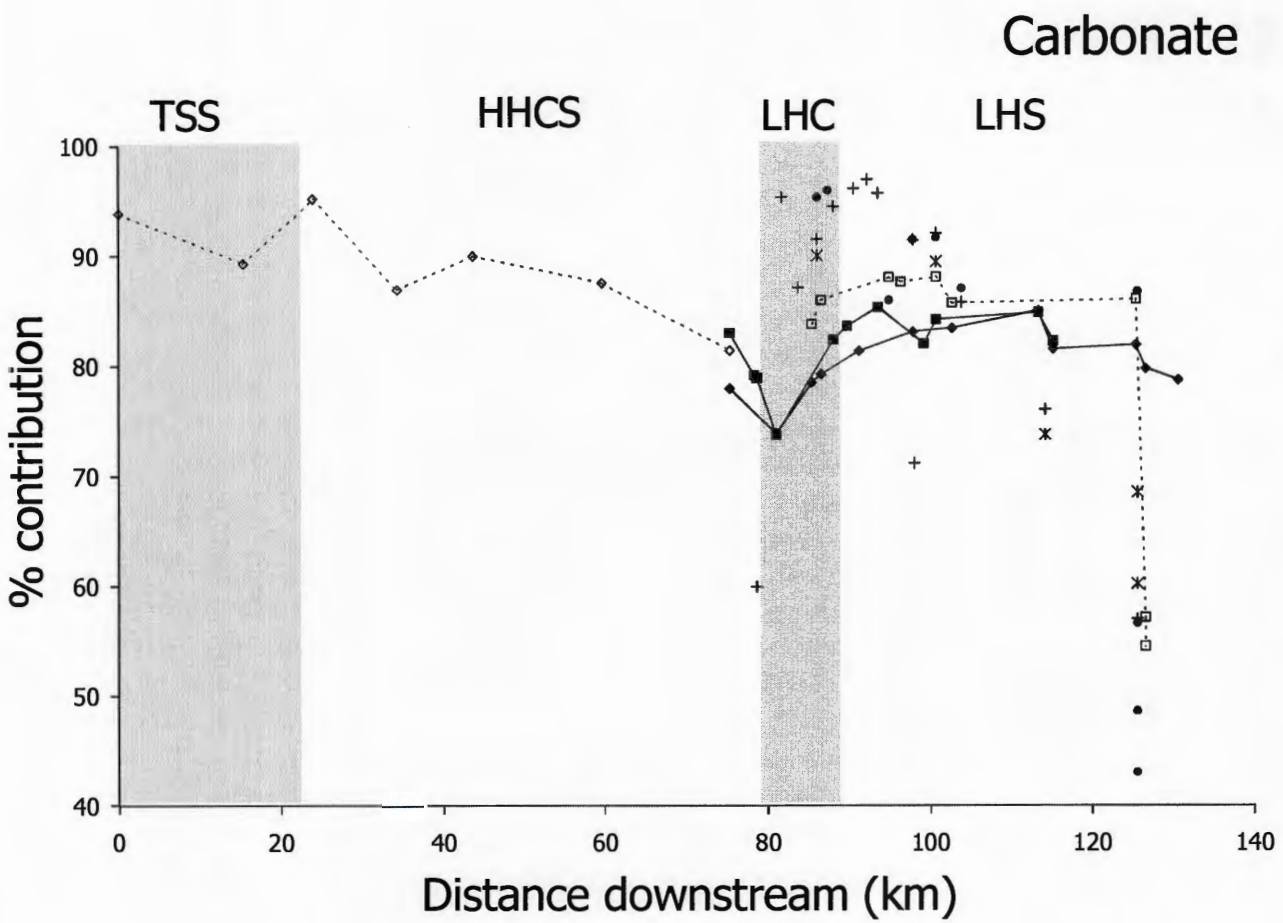

Fig. 5.3. Downstream change in the calculated carbonate contribution to total alkalinity in the Bhote Kosi.

only totals ~3% of alkalinity at the MCT. The Jum Khola tributary (draining only the HHCS) is characterised by a relatively low estimated contribution from carbonate (~60%), with the bulk of remaining alkalinity sourced from albite or anorthite. Biotite contributes ~2% with no contribution from orthoclase.

The trends observed in the crucial section of Lesser Himalayan calc-silicates (LHC) are initially continuous from those observed in the HHCS, with further increases in the calculated silicate contribution. The input of the largely calc-silicate draining tributaries is the cause of a major change, as already noted for cation, anion and Sr-isotope values (section 4.2.1.3). These tributaries are marked by high calculated carbonate contributions (≥90%) combined with relatively low inputs from albite and anorthite. The contribution from biotite is similar to that of the main river, while orthoclase inputs also become important (up to ~4%). In the Bhote Kosi mainstream, the input of these tributaries results in a rapid increase in the estimated carbonate contribution to alkalinity coupled with rapid decreases in the importance of albite and anorthite.

The above trends continue as the main river moves into the Lesser Himalayan silicate Kuncha Group (LHS) before values plateau out. The influx of the Balephi Khola, with a lower carbonate contribution in comparison with the Bhote Kosi, causes the carbonate estimate in the mainstream to drop, with corresponding slight increases in the importance of albite, anorthite and biotite (the latter is particularly important in the Balephi Khola at >5%). It is also noteworthy that carbonate contributions to total

alkalinity are slightly higher in this section of the river in the September dataset, with inputs from albite and anorthite correspondingly less important.

In the Indrawati and Chak Khola the proportion of alkalinity attributable to carbonate is typically less than that estimated for the Bhote Kosi. In the Indrawati, the dry season (1998) carbonate contribution is 60% (BK36), a value which falls to 48% when the river was sampled in September after rainfall (BK72), although it remains at a similar 56% when sampled in September, but not after rainfall (BK66). The chemistry of the Chak Khola is even more unpredictable. When measured in the dry season, the carbonate contribution is 57-68%, in September this is increased to 86% (BK65), although when measured in September after major rainfall (BK71) only 43% of alkalinity can be attributed to carbonate weathering. In both of these rivers calculated inputs from albite are in excess of 15%, considerably more in September, while contributions from anorthite exceed 10% (>15% in September). Biotite weathering input is prominent in the Indrawati (>5%), less so in the Chak Khola (<5%). In the dry season, the influence of these rivers upon the Bhote Kosi is minor. In September, however, the confluence of the Indrawati and Chak Khola with the Bhote Kosi results in a sharp decease in the calculated carbonate contribution to alkalinity from ~85% in the most downstream part of the Bhote Kosi to ~55%. Conversely, increases are noted in estimated contributions from albite (~5% to ~20%), anorthite (~4% to ~15%) and biotite (~2% to ~7%), but not orthoclase.

5.1.3. Downstream Changes in Mineral Contributions to the Langtang Khola-Trisuli.

The downstream progress of the Langtang Khola is defined by a consistent decline in the calculated contribution of carbonate to total alkalinity, mirrored by increasing contributions from albite, anorthite and biotite (see fig. 5.4 and fig. 5.5). These trends become more pronounced in the lower section of the river (towards Syabrubensi). Two tributaries (L18 and L20) sampled in this portion of the river are silicate dominated, carbonate contributions to alkalinity being ~30% and 0%. This pattern is observed in both sample sets, although carbonate contributions in October 1998 are marginally less in the lower part of the river than in September 1999.

As previously noted in section 4.2.2.2, changes occurring at the MCT are difficult to interpret. At this juncture, a rapid increase in the importance of carbonate is observed. In the September 1999 sample set the reason for this is clear, as the Bhote Kosi (Langtang) (with carbonate-derived alkalinity estimated at 86%) appears to all but overprint the chemical signature of the Langtang Khola. This makes the influence of the short section of LHF calc-silicates impossible to distinguish. The same rapid increase in carbonate contribution is observed in the October 1998 data, but it appears that the input of the Bhote Kosi (Langtang) cannot be responsible for this as the proportion of alkalinity (66%) derived from carbonate in this river at this time is identical to that of the Langtang Khola just above the MCT. A possible explanation for this observation is that the calc-silicates of the Lesser Himalaya are responsible for the increased carbonate

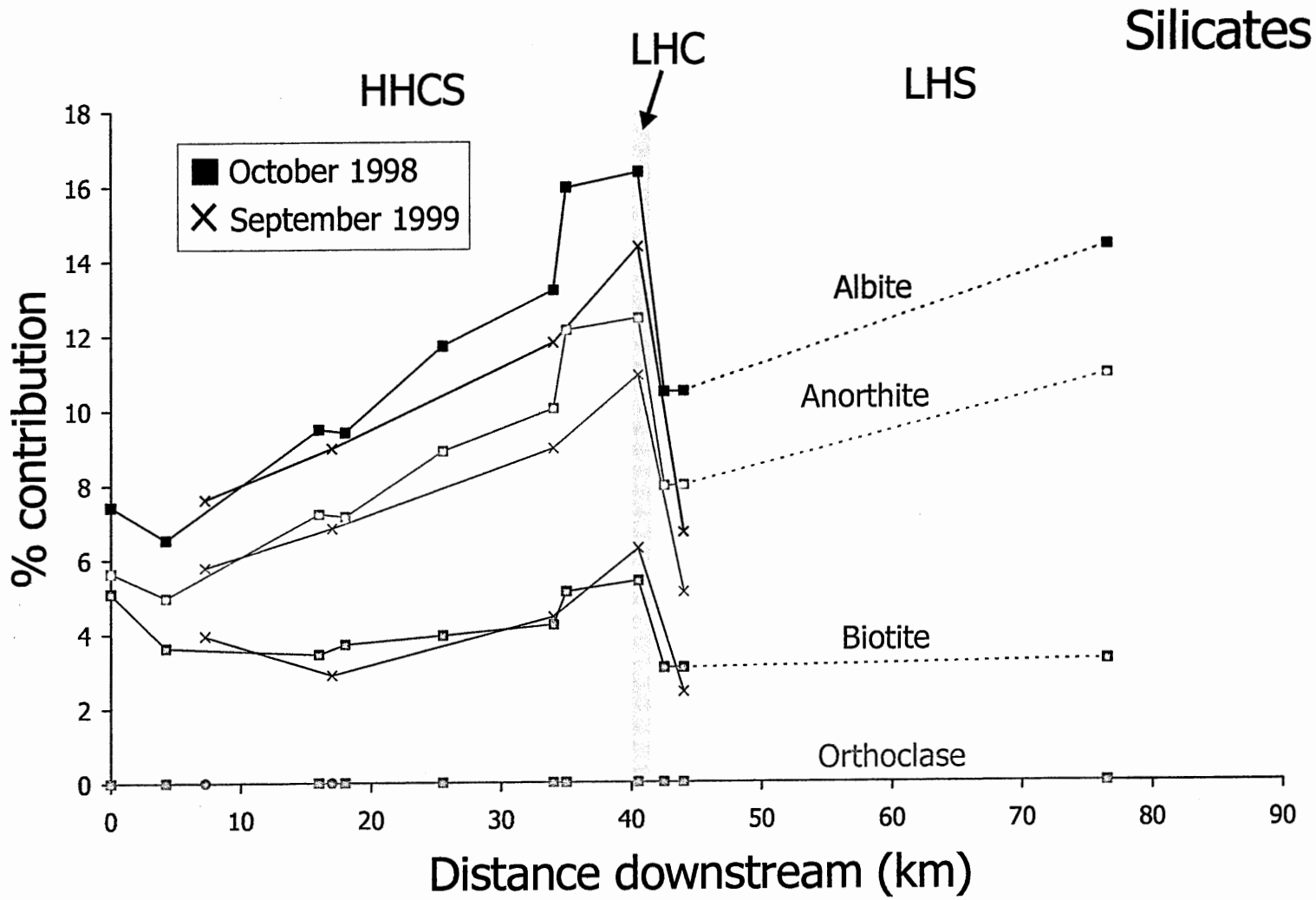

Fig. 5.4. Downstream changes in the calculated contribution of silicate minerals to total alkalinity in the Langtang Khola - Trisuli.

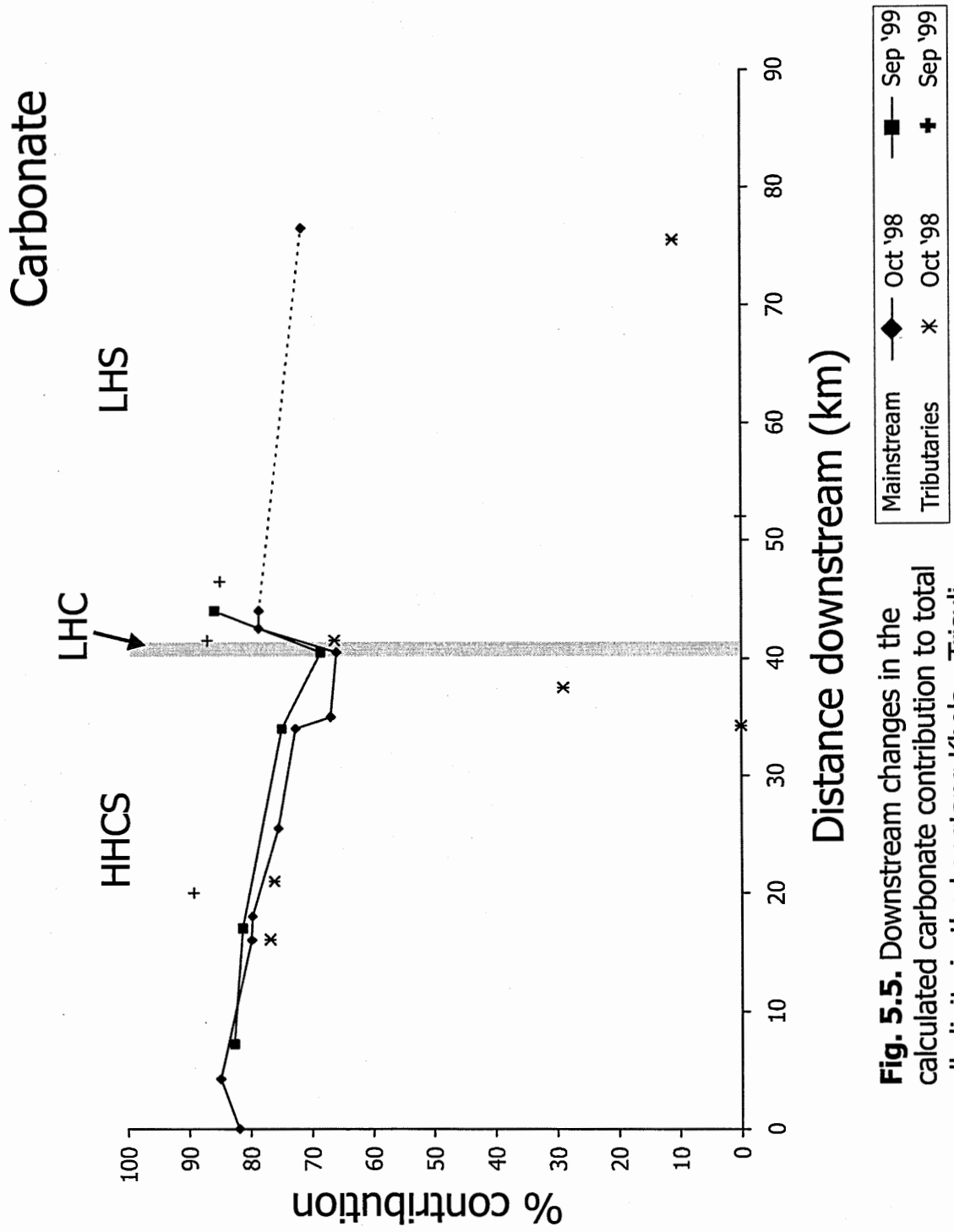

Fig. 5.5. Downstream changes in the calculated carbonate contribution to total alkalinity in the Langtang Khola - Trisuli.

contribution to alkalinity, although this seems highly unlikely considering that the influence of this thin unit could not be differentiated on any of the downstream cation or anion plots (fig. 4.7 – fig. 4.12). In 1998 the Bhote Kosi (Langtang) (sample L5, taken just above the confluence at Syabrubensi) appears to have anomalously high Na^+. If this is owing to a factor other than greatly increased silicate weathering (e.g. anthropogenic or hot spring input) then the mass balance will overestimate the proportion of albite and anorthite-derived alkalinity, and consequently underestimate the proportion of alkalinity derived from carbonate in this sample.

In the Lesser Himalayan silicates, a slight decline in the carbonate contribution to alkalinity is observed. As previously (section 4.2.2.3), it is unclear whether this is a factor of the later sampling of this downstream site, although a tributary sampled close to Trisuli Bazaar (L22) is indeed silicate dominated (>90%).

5.2. Weathering Regimes in the Bhote Kosi and Langtang Khola-Trisuli.

Downstream changes in $K^+/(Na^+ + K^+)$ and $Si/(Na^+ + K^+)$ ratios in the Bhote Kosi are shown in fig. 4.6. $K^+/(Na^+ + K^+)$ ratios increase consistently throughout the HHCS section of the river. This increase continues in the section of LHF calc-silicates, only more rapidly, reflecting high ratios in the tributaries entering the Bhote Kosi in this section of the river. This rise in $K^+/(Na^+/K^+)$ ratios in the Bhote Kosi is also noted by Harris *et al.* (1998) and interpreted as representing the change from a weathering-limited to a transport-limited weathering regime. Such a change might be expected due to the

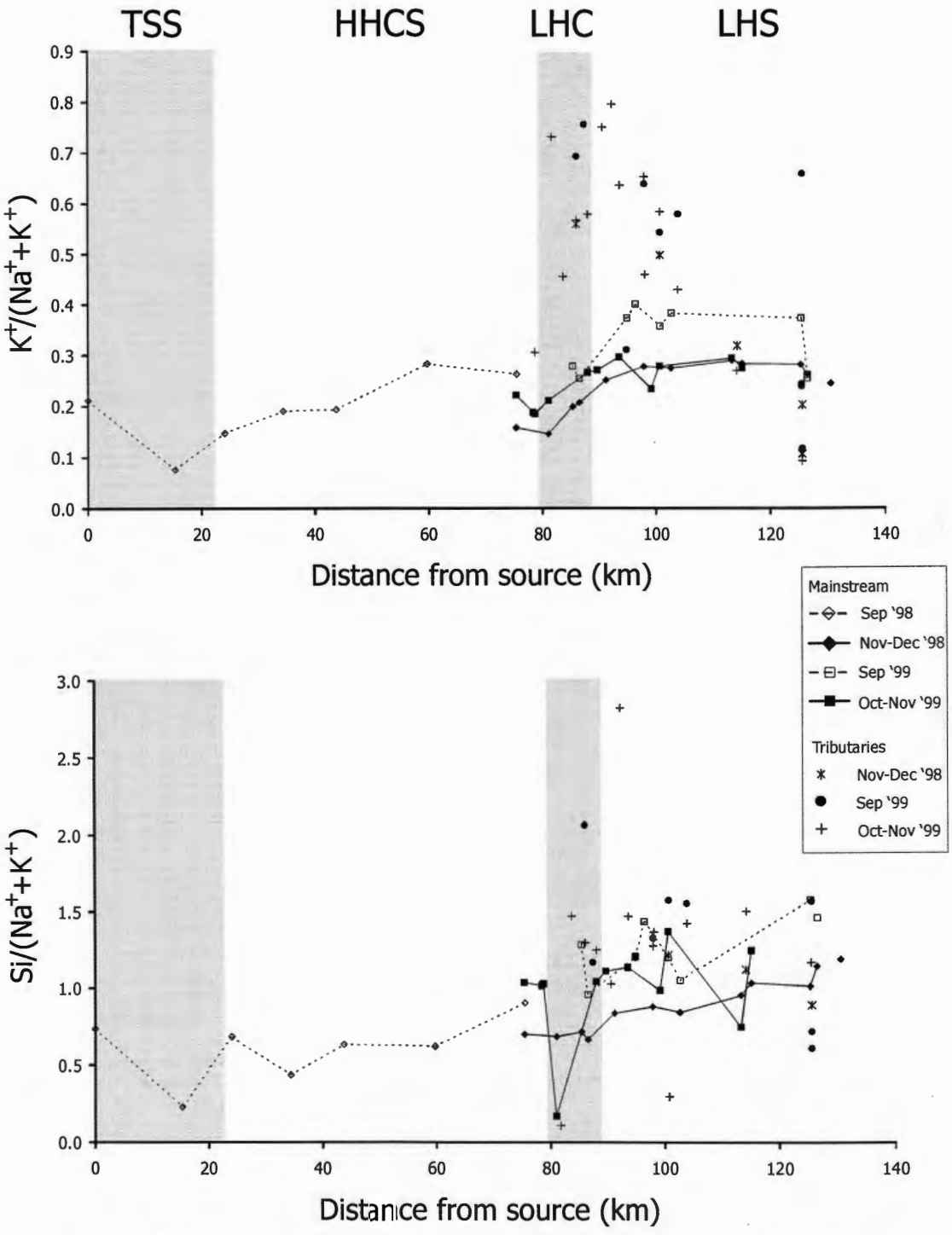

Fig. 5.6. Downstream changes in $K^+/(Na^+ + K^+)$ and $Si/(Na^+ + K^+)$ in the Bhote Kosi.

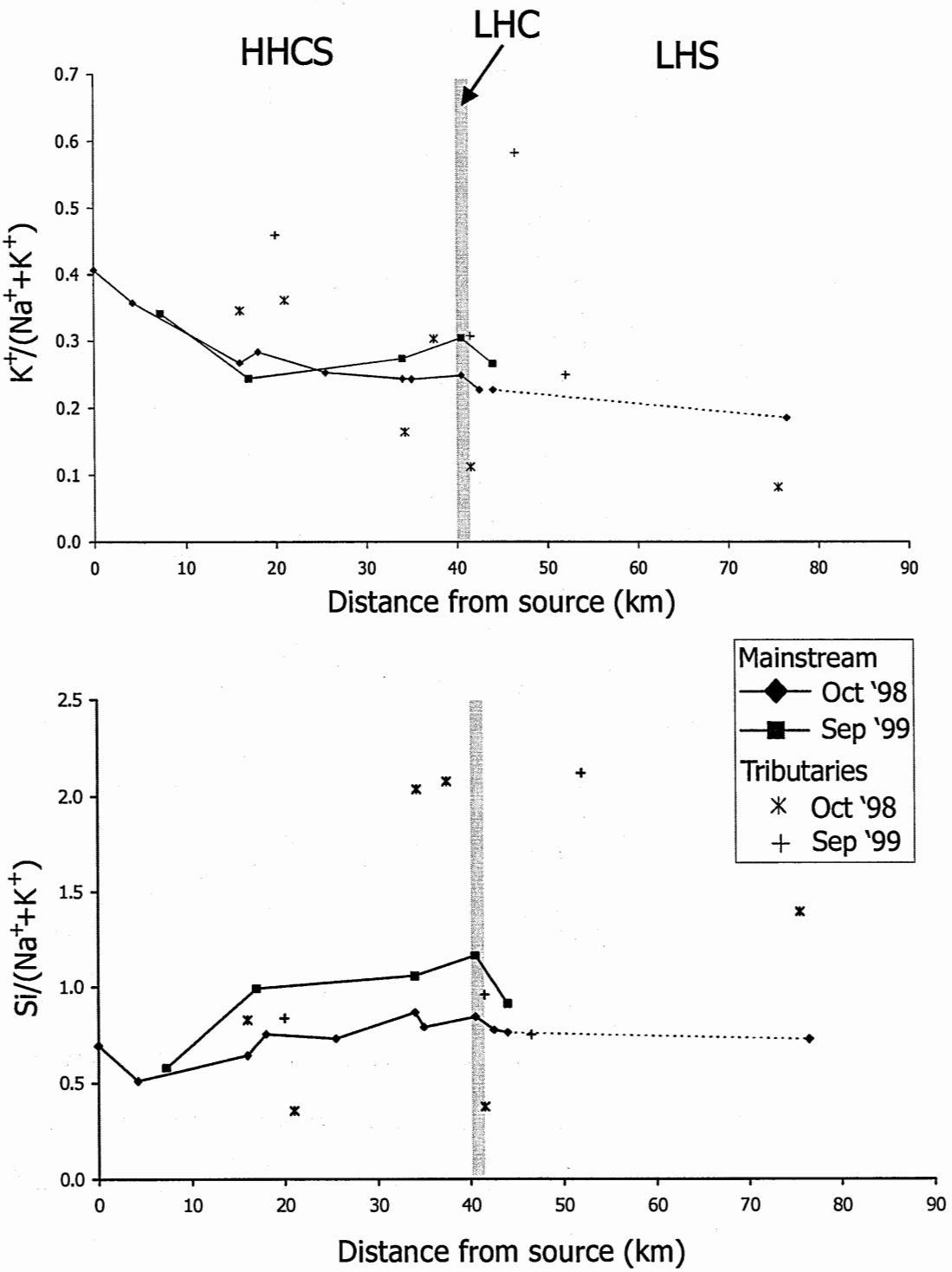

Fig. 5.7. Downstream changes in $K^+/(Na^+ + K^+)$ and $Si/(Na^+ + K^+)$ in the Langtang Khola-Trisuli.

transition from the cold, arid climate of the Tibetan plateau to the subtropical conditions of the lower Bhote Kosi valley. The high ratios in the LHF calc-silicate draining tributaries might result from the rapid exposure of silicate material owing to the rapid weathering of surrounding carbonate. The consistency of values in the LHF silicate section of the Bhote Kosi, and lower ratios in LHF silicate draining tributaries (e.g. BK61, BK95), in comparison with those dominated by the calc-silicates, perhaps suggests weathering in this part of the river is more weathering limited.

In mixed or silicate-dominated terrains, $Si/(Na^+ + K^+)$ ratios are regarded as indicative of the intensity of silicate chemical weathering in a river (Stallard and Edmond, 1983). In the Bhote Kosi, this ratio increases consistently downstream from source, although trends are slightly confused due to anomalous Si concentrations in some samples in the lower portion of the river. Such an increase in silicate chemical weathering intensity might well be expected as a result of the climate changes described above. The radiogenic tributaries draining LHF calc-silicates in some cases show elevated $Si/(Na^+ + K^+)$ ratios, although not in every case, and with only two tributaries showing a high degree of elevation. This perhaps indicates that the chemical weathering intensity of silicate is not especially high in these rivers.

The Langtang Khola displays a general downstream trend of decreasing $K^+/(Na^+ + K^+)$ coupled with increasing $Si/(Na^+ + K^+)$. This suggests that while chemical weathering increases downstream within the HHCS, again as might be expected owing to the change from a high altitude climate lacking in vegetative cover to a subtropical forest,

the weathering regime changes from transport to weathering-limited. Silicate dominated tributaries (L18 and L20) in the lower part of the Langtang Khola have much higher $Si/(Na^+ + K^+)$ ratios than the those of the mainstream, perhaps again providing evidence of more intense chemical weathering in the forested section of the river.

The $K^+/(Na^+ + K^+)$ and $Si/(Na^+ + K^+)$ ratios of the Bhote Kosi (Langtang) (except for the 1999 $K^+/(Na^+ + K^+)$ ratio) are lower than those of the Langtang Khola, and this is reflected in lower ratios in the upper Trisuli downstream of Syabrubensi. Both ratios continue to decline in the LHF section of the river. Tributaries in the upper Trisuli (L22 and L23), draining only the Kuncha Group silicates, are characterised by $K^+/(Na^+ + K^+)$ ratios similar to or lower than the mainstream, but $Si/(K^+ + Na^+)$ ratios higher than mainstream. Sample L24, draining both Nawakot Group calc-silicates and Kuncha Group silicates, by contrast has a $K^+/(Na^+ + K^+)$ ratio substantially elevated above mainstream, but a $Si(K^+ + Na^+)$ ratio close to that of the mainstream.

5.3. Statistical Analysis of River Chemistry by Principal Components Analysis.

Data for the Bhote Kosi (table A1 and table A2) and the Langtang Khola-Trisuli (table A3 and table A4) are used to perform principal components analyses as described in appendix G. The variables selected for use in the analyses are as follows:

(i). The concentrations of dissolved Na^+, Ca^{2+}, K^+, Mg^{2+}, Sr^{2+}, and Rb^+.

(ii). The concentrations of dissolved HCO_3^-, Cl^-, NO_3^- and SO_4^{2-} (except where noted).

(iii). Dissolved $^{87}Sr/^{86}Sr$ ratios.

(iv). The pH and temperature of river waters as measured in the field.

(v). The percentage of catchment area underlain by the four main lithological units outlined in chapter 1, namely the Tibetan Sedimentary Series (%TSS), the High Himalayan Crystalline Series (%HHCS), the Lesser Himalayan calc-silicate units of the Nawakot Group (%LHC) and the purer silicates of the Kuncha Group metasediments and Lesser Himalayan gneisses (%LHS). The variable %LHtotal refers to the total coverage of a catchment by the Lesser Himalaya (i.e. %LHC + %LHS).

Note: Although causality cannot be inferred from the statistical analyses described below, is important to note that the % catchment geologies are completely independent of the other variables (i.e. they can't possibly be influenced by the other factors incorporated into the analyses).

5.3.1. Analysis of Bhote Kosi Data.

Fig. 5.8 (see also table D1) shows that $^{87}Sr/^{86}Sr$ ratios in the Bhote Kosi are closely related to the proportion of Lesser Himalayan bedrock exposed in catchments. This can be seen by the clustering of the %LHtotal, %LHC and %LHS variables around $^{87}Sr/^{86}Sr$. %LHtotal provides the best correlation with $^{87}Sr/^{86}Sr$ ($r^2 = 0.57$), although the Nawakot Group calc-silicates ($r^2 = 0.47$) are predominant compared to the purer Kuncha Group silicates ($r^2 = 0.14$). The correlation between $^{87}Sr/^{86}Sr$ ratios and % LHF calc-silicate is shown in fig. 5.9. It is suggested that the correlation is weakened by three separate influences:

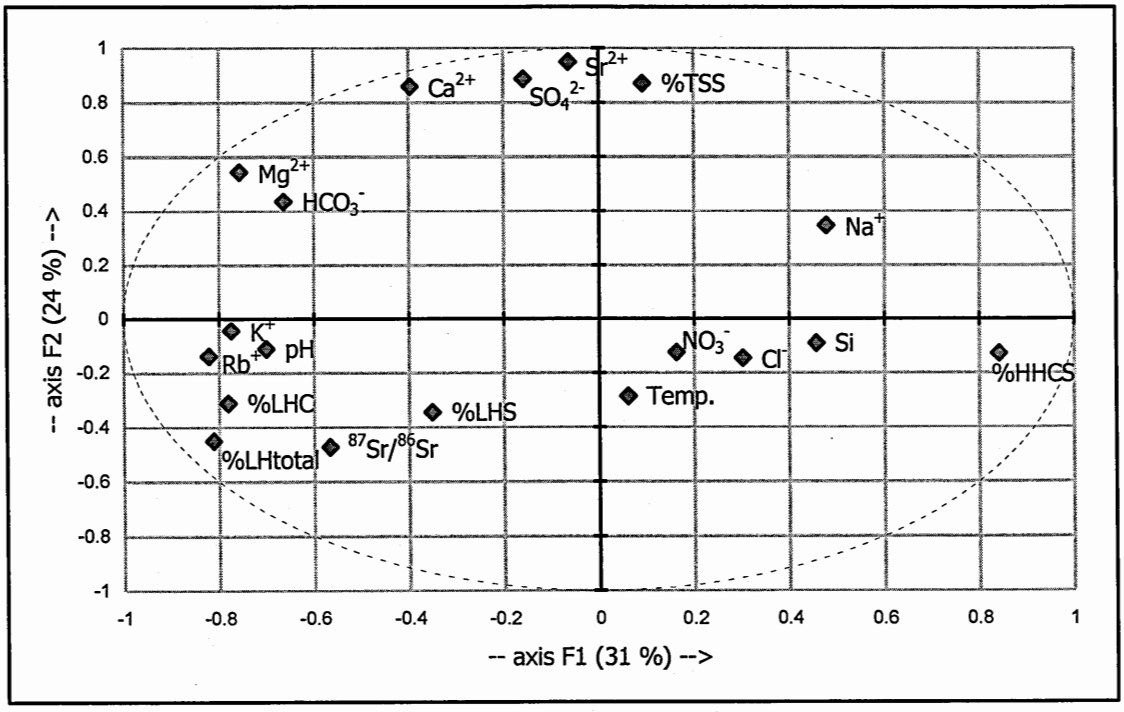

Fig. 5.8. Principal components analysis of all data from the Bhote Kosi basin (58 samples).

(i). Radiogenic inputs from Lesser Himalayan silicates.

(ii). Relatively low $^{87}Sr/^{86}Sr$ ratios in the Chak Khola river and its tributaries which drain a substantial outcrop of LHF calc-silicate. This may be due to the calc-silicates of the Chak Khola catchments having atypical chemistry, a suggestion not supported by rock samples collected from the area (see chapter 6 and appendix C). Alternatively, inputs from the Kathmandu Nappe (an important part of the Chak Khola catchment) might have higher $[Sr^{2+}]$ or lower $^{87}Sr/^{86}Sr$ than the HHCS units of the main Bhote Kosi section. A comparison with the Jum Khola and upper Indrawati catchments, which drain only the HHCS, reveals the Chak Khola indeed has substantially lower Sr^{2+}

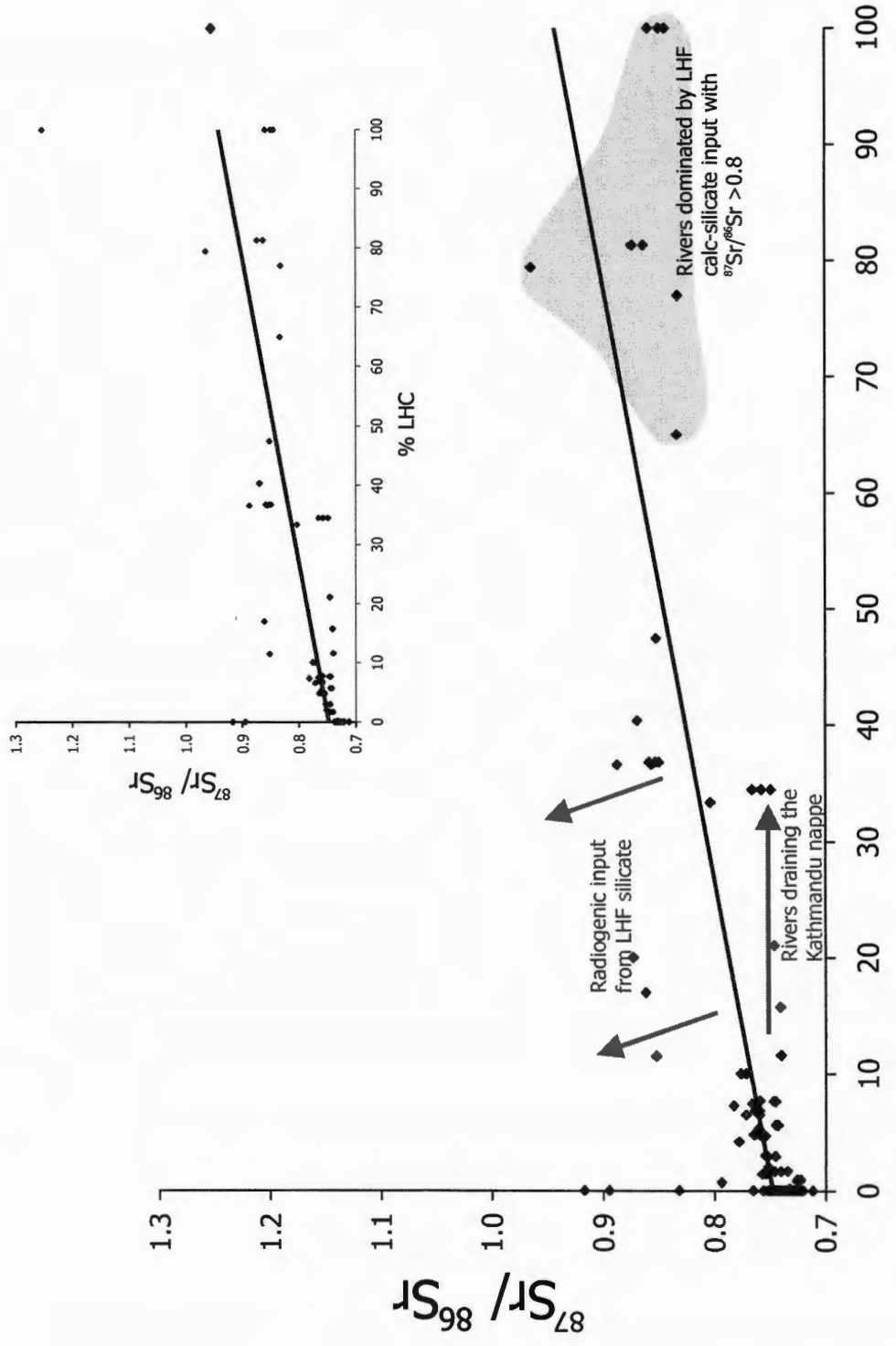

Fig. 5.9. Correlation between dissolved $^{87}Sr/^{86}Sr$ and % of Nawakot Group calc-silicates (%LHC) in the full dataset (main diagram) and in the Bhote Kosi only (inset).

concentrations, as does one of its tributaries draining substantial marble outcrops of the Kathmandu Nappe.

(iii). Isotopic variation within the Lesser Himalayan calc-silicate units, which is substantial (see chapter 7 and table C3).

Also clustering around the $^{87}Sr/^{86}Sr$ and %LH variables in fig. 5.8 are pH (likely reflecting the high pH of the LHF tributaries) in addition to $[Rb^+]$ and $[K^+]$, thus establishing a potential link between the weathering of Rb^+, K^+ and ^{87}Sr, which are likely to occur in the same sites within minerals (micas). In a separate cluster of points on fig. 5.8, $[Sr^{2+}]$ is closely linked with $[SO_4^{2-}]$ ($r^2 = 0.92$), $[Ca^{2+}]$ ($r^2 = 0.70$) and %TSS ($r^2 = 0.63$). This suggests that the Tibetan Sedimentary Series might act as a controlling influence on Ca^{2+}, Sr^{2+} and SO_4^{2-}, the correlations with $[Sr^{2+}]$ and $[Ca^{2+}]$ being the result of the high concentrations of these elements within the limestones that are the dominant lithology of the TSS. The correlation with $[SO_4^{2-}]$ might be the result of an important role in the TSS for weathering by sulphuric acid produced by sulphide oxidation (Galy and France-Lanord, 1999). Significant negative correlations are observed when comparing %LHF (calc-silicate, silicate and total) and $[Sr^{2+}]$, and when comparing %TSS and $^{87}Sr/^{86}Sr$. $[Mg^{2+}]$ and $[HCO_3^-]$ lie between the %LHF and %TSS variables on fig. 5.8, reflecting the high values of both of these species observed in the TSS section of the Bhote Kosi and the LHF-draining tributaries. The %HHCS variable sits largely isolated on fig. 5.8, suggesting that the HHCS exerts little control over the Sr chemistry of the Bhote Kosi. %HHCS has a weak negative relationship with $^{87}Sr/^{86}Sr$ ($r^2 = 0.31$), but has no significant relationship with $[Sr^{2+}]$. %HHCS shows negative or no significant relationships with all dissolved species with the exception of $[Na^+]$ and [Si]. Fig. 5.8

suggets that [NO_3^-], [Cl^-] and temperature are largely independent of geological influence, but closely related to each other, possibly reflecting anthropogenic inputs in the warmer lowlands of the river section.

5.3.2. Analysis of Bhote Kosi Mainstream Data.

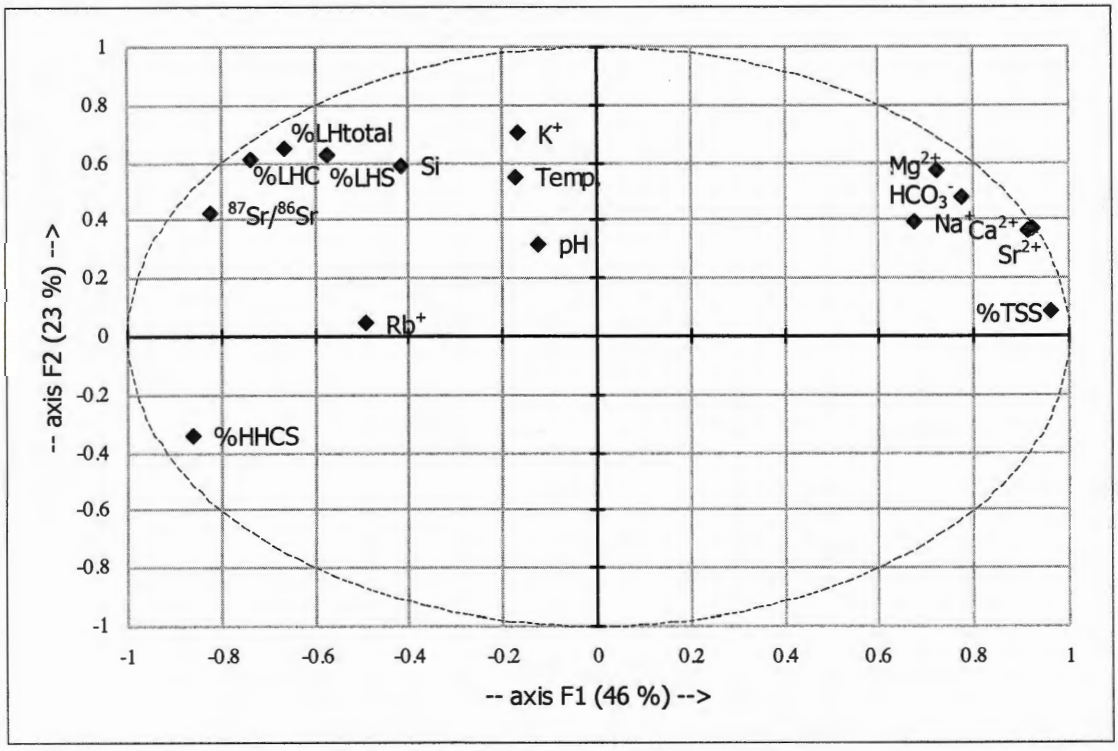

Fig. 5.10. Principal components analysis of Bhote Kosi mainstream data (33 samples).

There is a possibility of sample bias in the Bhote Kosi dataset resulting from the focus on sampling tributaries draining the Lesser Himalayan calc-silicate units. By selecting only the Bhote Kosi mainstream samples, this potential bias is removed. It also removes the influence of any peculiarities present in smaller tributaries (e.g. caused by

anthropogenic influences or atypical geology). Cl^-, NO_3^- and SO_4^{2-} concentrations are removed from this particular analysis as the measurement of these was not possible for a number of 1998 mainstream samples (see appendix G). Fig. 5.10 (see also table D2) reveals the relationships between $^{87}Sr/^{86}Sr$ and the Lesser Himalaya to be even stronger than described in section 5.3.1. There is an extremely good correlation between %LHC and $^{87}Sr/^{86}Sr$ ($r^2 = 0.86$), as shown in fig. 5.11. The main reasons for the improvement in this correlation (compared with the full Bhote Kosi dataset) is likely to be the exclusion of the Chak Khola and its tributaries and the natural averaging of LHF calc-silicate inputs in the main river. The correlation between $^{87}Sr/^{86}Sr$ and %LHS is considerably weaker ($r^2 = 0.47$) than that with the LHF calc-silicates.

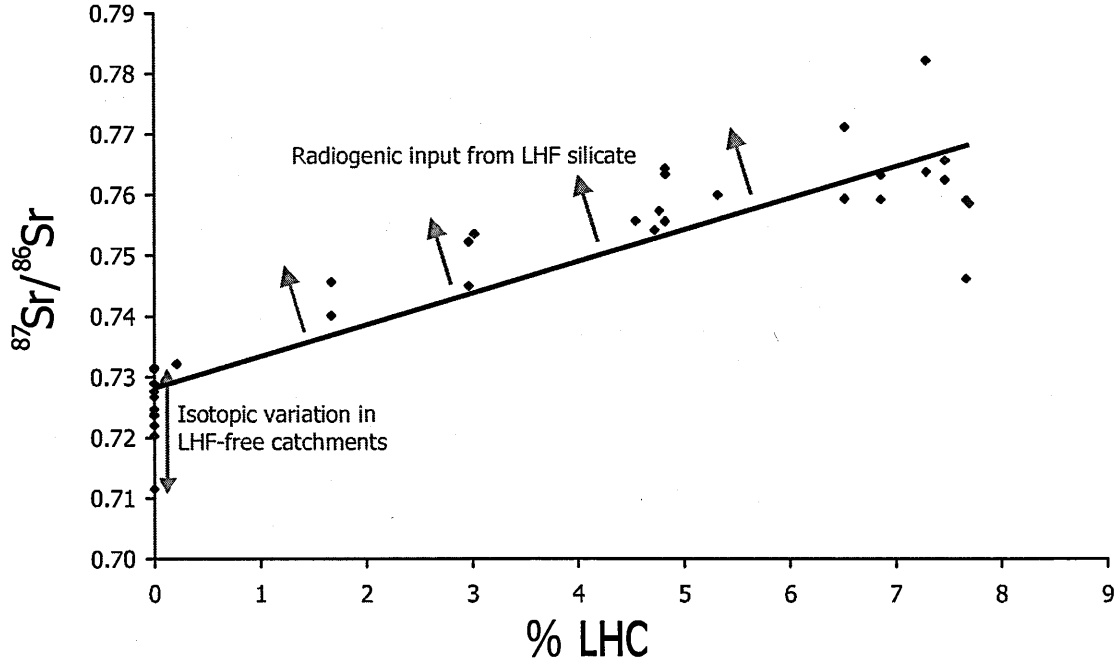

Fig. 5.11. Relationship between dissolved $^{87}Sr/^{86}Sr$ ratios and the % of Nawakot Group calc-silicate outcroppng in Bhote Kosi mainstream catchments.

Fig. 5.10 also shows a relationship between $^{87}Sr/^{86}Sr$ and [Si]. The correlations between the presence of Lesser Himalayan bedrock and $[K^+]$ and $[Rb^+]$ are weakened in the mainstream, possibly reflecting the absence of the high $[K^+]$ and $[Rb^+]$ LHF draining tributaries. The TSS appears to exert an even more dominant control on many aspects of Bhote Kosi mainstream chemistry than that observed in the full Bhote Kosi dataset, as evidenced by the tight cluster of $[Na^+]$, $[Mg^{2+}]$, $[HCO_3^-]$, $[Ca^{2+}]$ and $[Sr^{2+}]$ close to the %TSS variable. The correlations between %TSS and concentrations of Sr^{2+} and Ca^{2+} are particularly strong (r^2 = 0.80 and 0.86 respectively) reflecting the similar behavior of these two elements and the large amounts of both weathering from the TSS (fig. 4.1 and fig. 4.6). The %HHCS variable is even more isolated on fig. 5.10 than fig. 5.8. There are significant negative relationships between %HHCS and major species such as $[Ca^{2+}]$ (r^2 = 0.87), $[Sr^{2+}]$ (r^2 = 0.80), HCO_3^- (r^2 = 0.79) and $[Mg^{2+}]$ (r^2 = 0.54). There are relatively weak positive correlations between %HHCS and both $[Rb^+]$ and $^{87}Sr/^{86}Sr$ (r^2 = 0.24 and 0.29 respectively). This might indicate that while the HHCS contributes relatively little to the river chemistry of the Bhote Kosi, what it does contribute is relatively radiogenic compared to inputs from the TSS (as also suggested by the downstream changes in section 4.2.1.2).

5.3.3. Analysis of Bhote Kosi Catchments Draining Only the Lesser Himalaya.

Having identified in the previous two sections that the Lesser Himalaya appear to be the major source of radiogenic $^{87}Sr/^{86}Sr$ in the Bhote Kosi, catchments in this basin draining only the Lesser Himalaya are further examined in an attempt to define the source of this strontium more precisely (fig. 5.12, see also table D3). These tributaries incorporate a wide range of combinations of lithology from a drainage comprising 100% Nawakot Group calc-silicate to 100% Kuncha Group silicate, and also including catchments

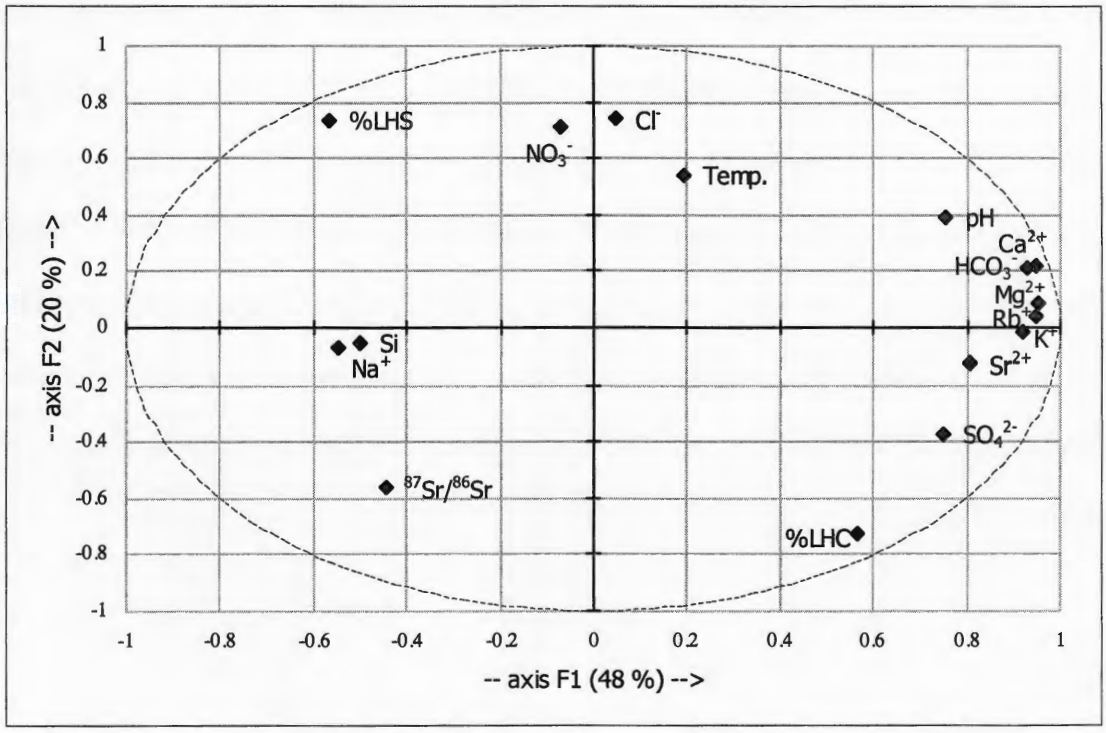

Fig. 5.12. Principal components analysis of Bhote Kosi catchments draining only the Lesser Himalaya (17 samples).

draining significant amounts of the Lesser Himalayan crystalline gneisses (incorporated with the Kuncha Group as the %LHS variable in these statistical analyses). Table D4 reveals no significant correlation between $^{87}Sr/^{86}Sr$ (see fig. 5.12 and 5.13) and any of the other variables incorporated into the PCA. This suggests that both the Nawakot Group and Kuncha Group are contributing significant radiogenic Sr. $[Sr^{2+}]$ shows significant positive correlations with $[Mg^{2+}]$, $[Ca^{2+}]$, $[SO_4^{2-}]$ and $[HCO_3^-]$, but displays stronger correlations with $[K^+]$ and $[Rb^+]$, which would not be expected in the case of typical two-component carbonate-silicate strontium mixing. Fig. 5.12 suggests that %LHC may have some control on $[HCO_3^-]$, $[Ca^{2+}]$, $[Mg^{2+}]$, $[Rb^+]$, $[K^+]$, $[Sr^{2+}]$ and $[SO_4^{2-}]$, while [Si] and $[Na^+]$ appear largely independent of geological control as with $^{87}Sr/^{86}Sr$.

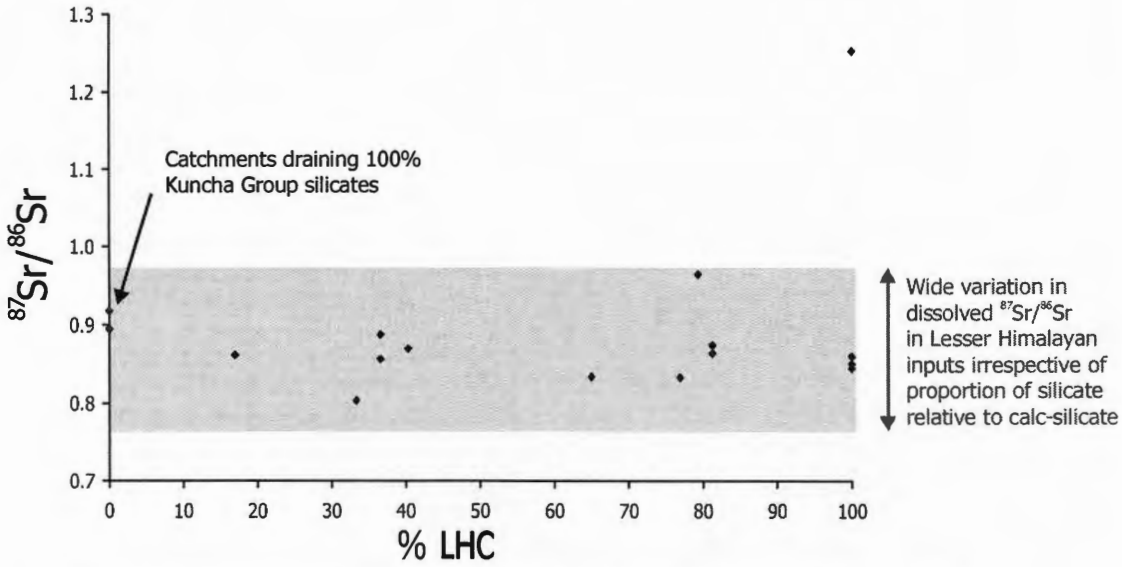

Fig. 5.13. Relationship between dissolved $^{87}Sr/^{86}Sr$ ratios and the % of Nawakot Group calc-silicate outcropping in catchments in the Bhote Kosi draining only the Lesser Himalaya.

5.3.4. Analysis of Bhote Kosi Catchments Upstream of the MCT.

The purpose of carrying out a principal components analysis on data from upstream of the MCT is to provide an indication of the controls on Sr chemistry for a river in the absence of exposures of the Lesser Himalayan Formation. Fig. 5.14 (see also table D4) reveals signs of classic two-component (silicate and carbonate) Sr mixing. $^{87}Sr/^{86}Sr$ values are positively correlated with %HHCS in catchments ($r^2 = 0.86$) while $[Sr^{2+}]$ again shows a positive correlation with %TSS ($r^2 = 0.66$). %TSS also shows correlations with $[Ca^{2+}]$, $[HCO_3^-]$, $[SO_4^{2-}]$ and $[Mg^{2+}]$.

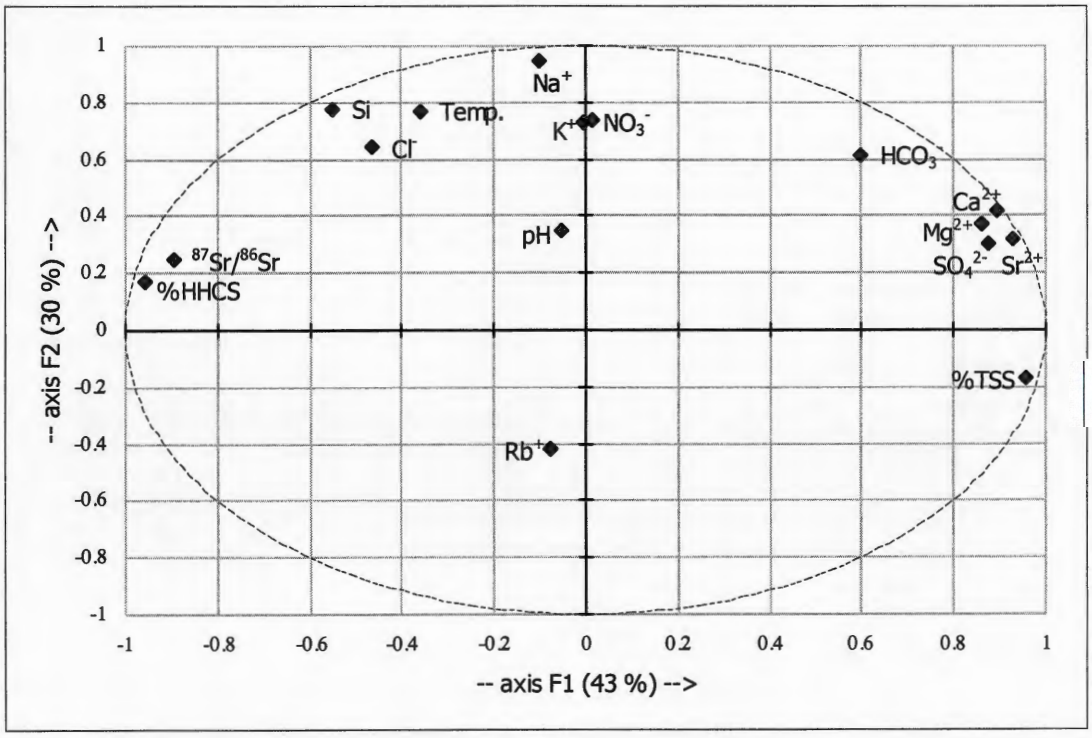

Fig. 5.14. Principal components analysis of Bhote Kosi catchments upstream of the MCT (20 samples).

5.3.5. Analysis of Bhote Kosi Samples Collected During September.

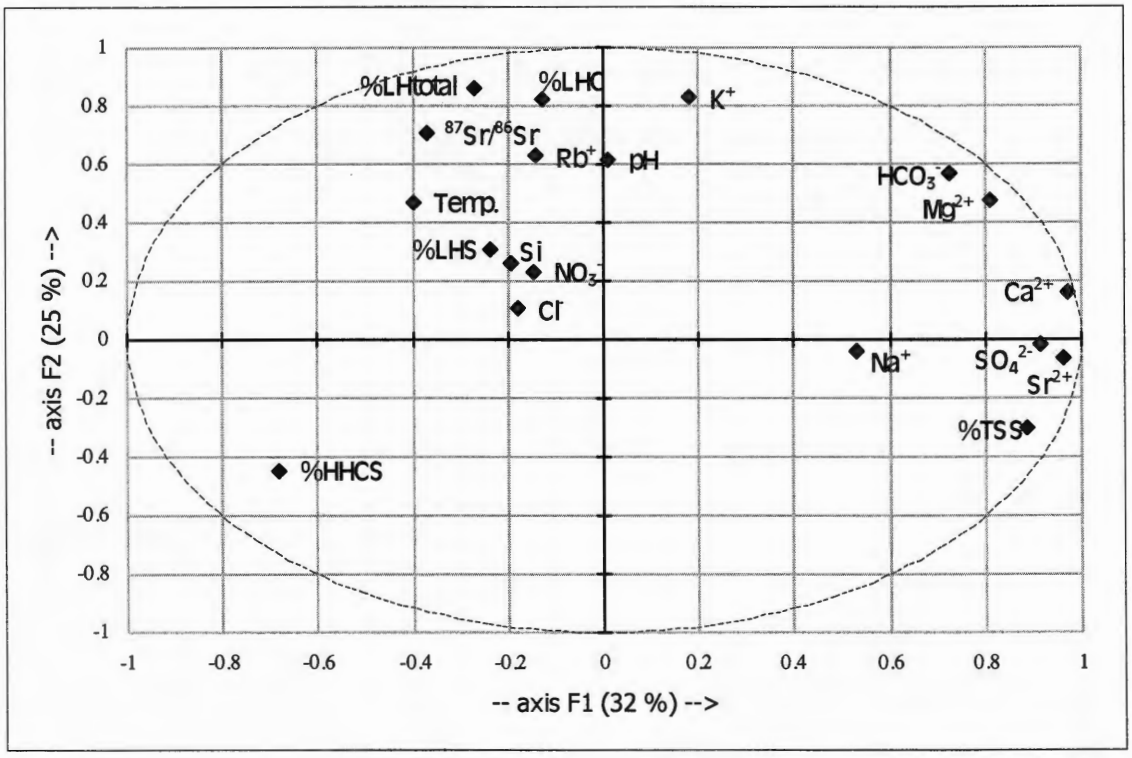

Fig. 5.15. Principal components analysis of data from Bhote Kosi samples collected in September (29 samples).

September sampling was carried out to provide an indication of the monsoon chemistry of the Bhote Kosi (the dry season proper starting in October, compare the difference between September and October rainfall in fig. 2.2). Rainstorms were still occurring during the September 1999 sampling season. Fig. 5.15 (see also table D5) is broadly similar to fig. 5.8 (total Bhote Kosi data). Table D5 reveals a notable difference. This is the increased importance of the relationship between Kuncha Group silicates (%LHS) and $^{87}Sr/^{86}Sr$ relative to that with Nawakot Group calc-silicates (%LHC). The r^2 for the

correlation between $^{87}Sr/^{86}Sr$ and %LHS is 0.14 when all Bhote Kosi data are considered, increasing to 0.52 using only September data. The r^2 with %LHC, conversely, is 0.47 for all Bhote Kosi samples, falling to 0.24 when only September data are considered. The correlation between dissolved $^{87}Sr/^{86}Sr$ ratios and %LHC in September is shown in fig. 5.16.

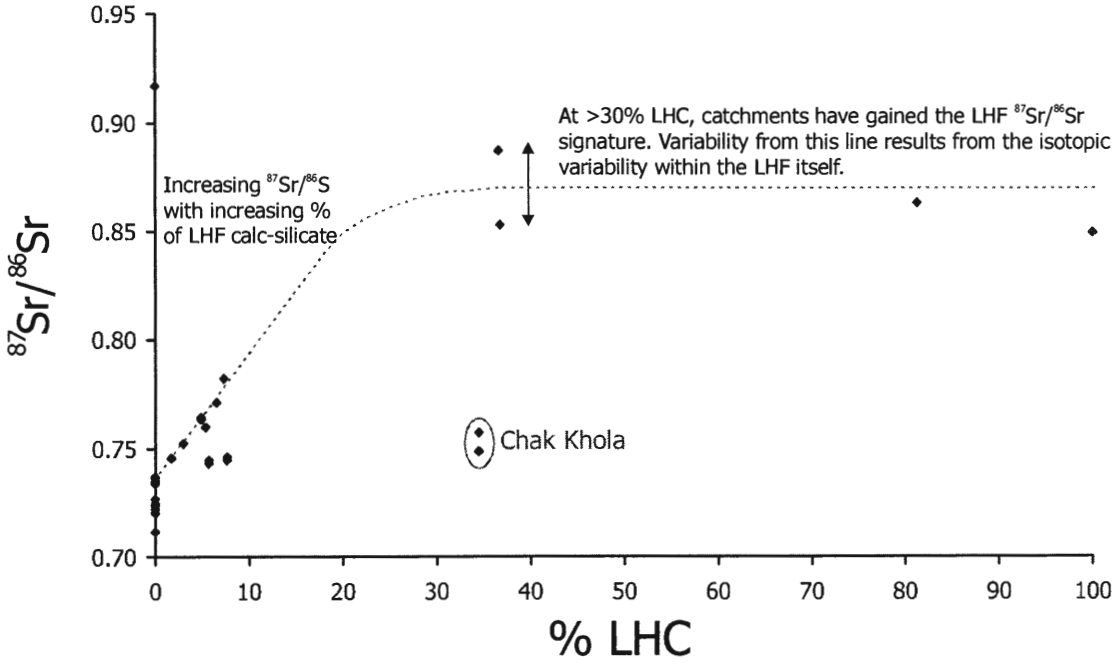

Fig. 5.16. Correlation between dissolved $^{87}Sr/^{86}Sr$ ratios and the proportion of Nawakot Group calc-silcate (%LHC) in Bhote Kosi catchments sampled in September.

5.3.6. Analysis of Bhote Kosi Samples Collected in the Dry Season (October-December).

Fig. 5.17 (see also table D6) incorporates Bhote Kosi samples collected in the November-December 1998 and late October-November 1999 sampling seasons. No rainstorms were noted in the Bhote Kosi valley during these periods of collection. While not shown by fig. 5.17, table D6 shows that in the dry season the Lesser Himalayan calc-silicates appear to become more important in controlling $^{87}Sr/^{86}Sr$ (r^2 = 0.52 compared with 0.24 in the September dataset) relative to the LHF silicates (r^2 = 0.09 compared

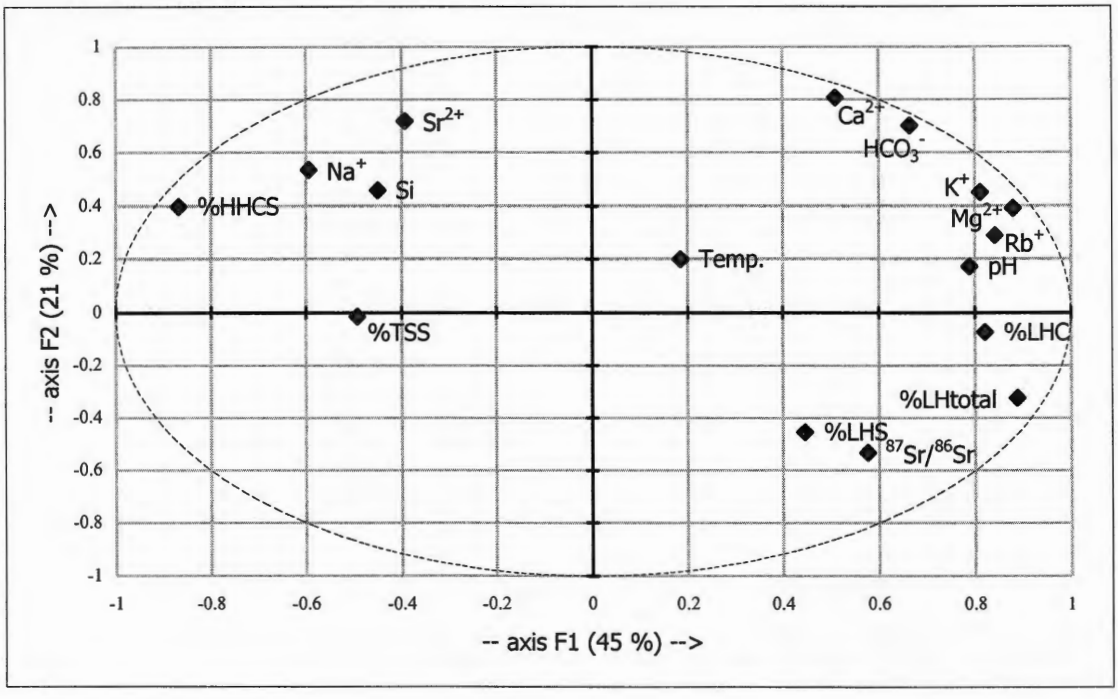

Fig. 5.17. Principal components analysis of Bhote Kosi samples collected in late October – December (44 samples).

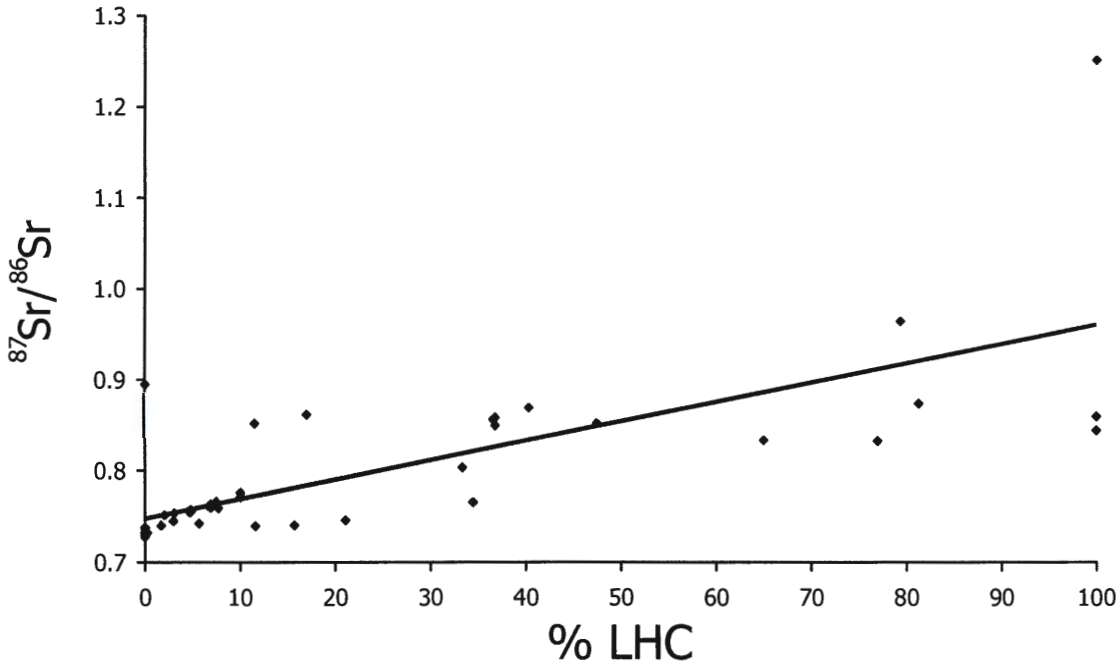

Fig. 5.18. Correlation between dissolved $^{87}Sr/^{86}Sr$ ratios and the proportion of Nawakot Group calc-silicates in Bhote Kosi catchments sampled in the dry season (late October - December).

with 0.52 in September). Fig. 5.18 illustrates the correlation between $^{87}Sr/^{86}Sr$ and %LHC) for dry season samples. It should be noted that the removal of September samples removes all samples from upstream of the MCT, and thus fig 5.16 provides an improved picture of chemistry changes in response to variations in the relative amounts of HHCS and LHF in catchments. The negative correlation between %HHCS and $^{87}Sr/^{86}Sr$ is more significant in the dry season (r^2 = 0.46 compared with 0.31 for all Bhote Kosi samples and with no significant relationship for September data). There is also a positive correlation between %HHCS and $[Sr^{2+}]$ (r^2 = 0.29), while there is no significant correlation when all Bhote Kosi data are incorporated, and a negative correlation noted when using September data (r^2 = 0.36). This possibly reflects higher

concentrations of Sr^{2+} coming from the HHCS in comparison with the LHF, a situation not repeated for any of the other cations, hinting that LHF units may be extremely depleted in Sr. In fig. 5.17 the previously noted close relationship between Sr^{2+} and Ca^{2+} is no longer seen. [Sr^{2+}] clusters with [Na^{+}] and [Si], plotting close to %TSS and %HHCS. [Ca^{2+}] and [HCO_3^{-}] plot close together but separately from [K^{+}], [Mg^{2+}], [Rb^{+}] and pH, which themselves are clustered close to %LHC.

5.3.7. Analysis of Langtang Khola-Trisuli samples.

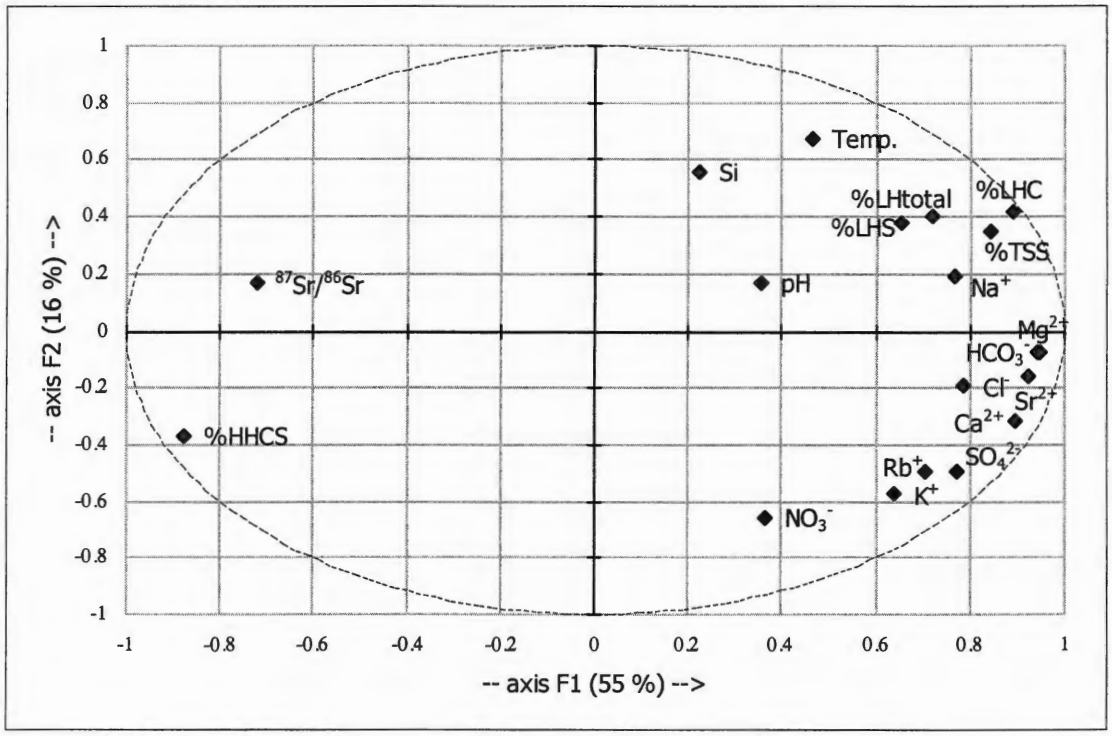

Fig. 5.19 Principal components analysis incorporating data from the Langtang Khola – Trisuli basin (21 samples).

The Lesser Himalaya are not truly represented in this analysis (fig. 5.19, see also table D7). Some small LHF-draining catchments (see appendix G) are omitted due to poor charge balance (see appendix G), while the confluence of the Bhote Kosi (Langtang) with the Langtang Khola at the MCT masks the influence of the LHF in the Upper Trisuli. Negative correlations are observed between $^{87}Sr/^{86}Sr$ and the amount LHF present in catchments, but these correlations merely reflect the less radiogenic nature of the Bhote Kosi (Langtang). The $^{87}Sr/^{86}Sr$ of samples L22-24 reveals that the Lesser Himalaya in the Langtang Khola-Trisuli basin are just as radiogenic as the LHF units of the Bhote Kosi. The Sr chemistry in the upper Trisuli system appears to be controlled by a balance between inputs from the TSS, which has a negative correlation with $^{87}Sr/^{86}Sr$ ($r^2 = 0.49$) but a positive one with $[Sr^{2+}]$ ($r^2 = 0.58$), and HHCS inputs which clearly have higher $^{87}Sr/^{86}Sr$ (%HHCS has a positive correlation with $^{87}Sr/^{86}Sr$ with an r^2 of 0.46) but lower $[Sr^{2+}]$ (negative relationship with an r^2 of 0.59). Such two-component mixing would also explain the negative correlations between $^{87}Sr/^{86}Sr$ and most cation and anion concentrations, as emphasised by fig. 5.19. in which %TSS plots at one end of axis F1 (which explains 55% of the variability in the dataset) together with most of the chemical species, while %HHCS is located at the opposite end of the axis with only $^{87}Sr/^{86}Sr$ in close proximity.

5.3.8. Analysis of Khumbu Region Samples.

For Khumbu samples granite was regarded as a separate geological unit (its catchment coverage referred to as % granite) and not merely incorporated as part of the HHCS (as in the Bhote Kosi and Langtang Khola analyses). Fig. 5.20 (see also table D8) suggests

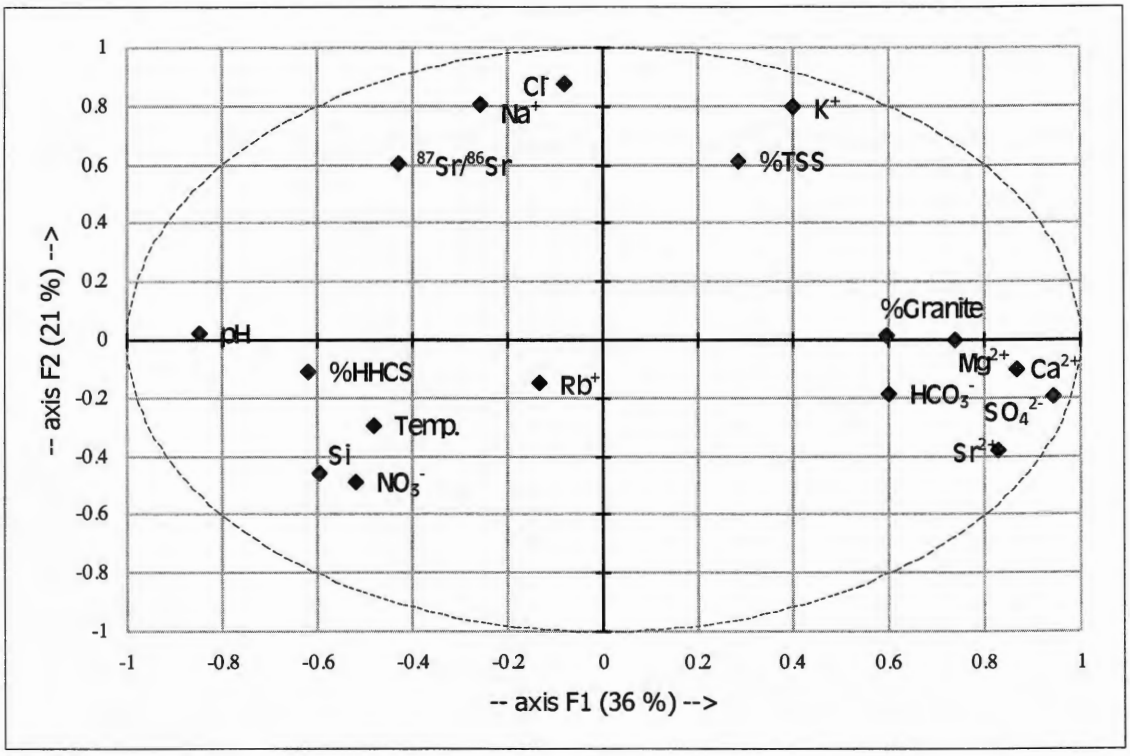

Fig. 5.20. Principal components analysis incorporating data from the Khumbu region (9 samples).

that the Khumbu area has the most uniform geology in terms of Sr-isotope ratios. There are no significant correlations between dissolved $^{87}Sr/^{86}Sr$ and any of the other variables incorporated into the PCA. The amount of TSS present in catchments apparently has very little bearing on the chemistry of Khumbu catchments (with the exception of a positive correlation with $[K^+]$) in contrast to findings from the Bhote Kosi and Langtang Khola-Trisuli basins. This may be a consequence of the fact that TSS rocks in this region outcrop only at very high altitudes (forming the summits of both Mt Everest and Cho Oyu). The overall chemical composition of the Khumbu rivers is largely

independent of variability in bedrock coverage (table D8), suggesting that factors not measured in this study (e.g. detailed geological variations, land use and vegetation coverage and type) may have a greater bearing on dissolved Sr chemistry in this basin.

5.3.9. Analysis of All Sampled Catchments.

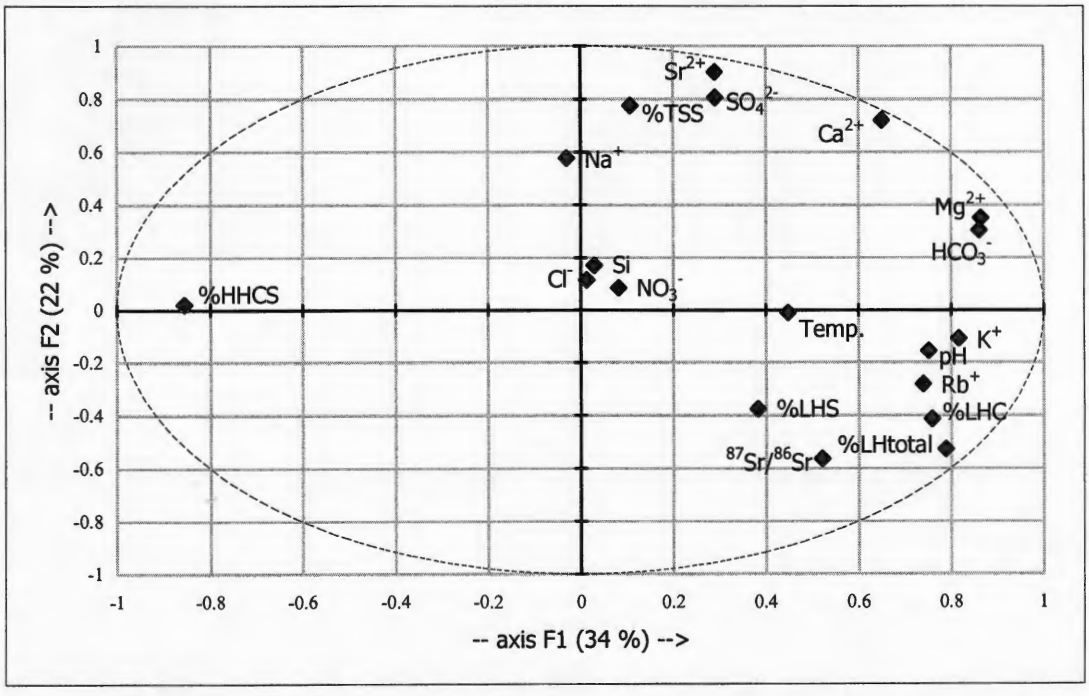

Fig. 5.21. Principal components analysis incorporating all data from this study (92 samples).

Combining data from the Bhote Kosi, Langtang Khola-Trisuli and Khumbu catchments with results from the large rivers measured in southern Nepal gives the most complete picture of Himalayan river chemistry available from the sampling done for this study (fig. 5.21, see also table D9). $^{87}Sr/^{86}Sr$ is portrayed in fig. 5.21 (as in fig. 5.8) as a

balance between radiogenic inputs from the LHF ($r^2 = 0.60$) and less radiogenic inputs from the TSS and the HHCS. Table D9 suggests that inputs from calc-silicates (%LHC, $r^2 = 0.51$) are of apparently greater importance than those from purer Kuncha Group silicate units (%LHS, $r^2 = 0.18$). In table D9 $^{87}Sr/^{86}Sr$ ratios are positively correlated with K^+ and Rb^+ concentrations but negatively correlated with Sr^{2+} and Na^+ concentratons. $[Sr^{2+}]$ and $[Ca^{2+}]$ appear to be controlled by the balance between TSS inputs and HHCS inputs, with little apparent influence from the LHF. The TSS and HHCS have the same influence on Mg^{2+} and HCO_3^-, although concentrations of these also appear to be strongly influenced by inputs from LHF calc-silicates. Si and NO_3^- concentrations both show correlations with $[Cl^-]$, although the reason for this is unclear.

5.3.10. Summary of Principal Component Analyses.

The principal components analyses described above reveal strong statistical links between high dissolved $^{87}Sr/^{86}Sr$ values, high K^+ and Rb^+ concentrations, and the amount of Lesser Himalayan bedrock present in a catchment. These correlations exist when both the Nawakot calc-silicate units and the Kuncha silicate units of the Lesser Himalaya are considered, although correlations are notably stronger with the former (with the exception of the September dataset). Sr^{2+} concentrations show strong correlations with SO_4^{2-} and Ca^{2+} concentrations, all of these species displaying strong positive correlations with the amount of Tibetan Sedimentary Series bedrock present in catchments. Thus, the picture that emerges from the principal components analyses is of Sr chemistry being largely controlled by the mixing of high $^{87}Sr/^{86}Sr$ and low $[Sr^{2+}]$ inputs from the LHF with low (relatively) $^{87}Sr/^{86}Sr$ and high $[Sr^{2+}]$ inputs from the TSS.

Within the Lesser Himalaya (fig. 5.11) it is difficult to distinguish between inputs from Nawakot Group calc-silicates and the silicates of the Kuncha Group and Lesser Himalayan gneisses, suggesting that the carbonate material within the LHF is quite likely to be highly radiogenic, but depleted in [Sr^{2+}], in sharp contrast to "typical" carbonate. The association between $^{87}Sr/^{86}Sr$ and [K^+] and [Rb^+] suggests that the weathering of micas (containing abundant K^+ and Rb^+, both easily removed from mica interlayer sites, Taylor *et al.*, 2000) might be important in producing the high $^{87}Sr/^{86}Sr$ ratios recorded in the dissolved input from both the LHF calc-silicates and silicates.

The High Himalayan Crystalline Series appears to have little role in determining dissolved Sr chemistry in Himalayan rivers judging from the principal components analyses. %HHCS shows negative correlations with both $^{87}Sr/^{86}Sr$ and Sr^{2+} concentration in both the Bhote Kosi and the full datasets (fig 5.8 and 5.21, see also table D1 and table D9). Above the MCT, however, in both the Bhote Kosi and in the Langtang Khola-Trisuli, HHCS inputs appear to become important in determining dissolved chemistry, and there are indications that dissolved $^{87}Sr/^{86}Sr$ might be a proxy for silicate weathering. These datasets are marked by the strong positive correlations between dissolved $^{87}Sr/^{86}Sr$ and %HHCS and between Sr^{2+} concentrations and %TSS, with equally strong opposing negative correlations between $^{87}Sr/^{86}Sr$ and %TSS and Sr^{2+} concentrations and %HHCS. In the case of the Bhote Kosi these relationships start to break down as soon as the river crosses the MCT into the Nawakot Group calc-silicates.

5.4. Predicting $^{87}Sr/^{86}Sr$ in Nepalese Rivers Using Regression Analysis.

The principal components analyses of the previous section provide a good overview of the chemical relationships in the Bhote Kosi, Langtang Khola-Trisuli and Khumbu catchments, identifying potential controls on Sr chemistry. Such information is of little use in ascertaining the connection between $^{87}Sr/^{86}Sr$, silicate weathering rates and climate change unless it can be shown to be applicable to the Himalaya as a whole, or at least a significant portion of the range. In order to test the validity of the data collected in this study as representative of the central Himalaya, multiple regression analyses were carried out using all or part of the data from the Bhote Kosi, Langtang Khola-Trisuli and Khumbu basins, and used to independently predict $^{87}Sr/^{86}Sr$ in the Sapt Kosi, Sun Kosi, Arun and Tamur rivers.

5.4.1. Analysis Using the Full Data Set.

Incorporating all Bhote Kosi, Langtang Khola-Trisuli and Khumbu data the following multiple regression equation results:

Equation 5.1.

$$^{87}Sr/^{86}Sr = 0.758681 + 2.291093\ E^{-3}\ \%LHC + 1.309310\ E^{-3}\ \%LHS - 3.495273\ E^{-5}\ [HCO_3^-]$$

$r^2 = 0.70$

$r^2 = 0.62$ (incorporating only %LHC and %LHS variables)
$r^2 = 0.51$ (incorporating only the %LHC variable)

This equation once again demonstrates the importance of the Lesser Himalaya in determining dissolved $^{87}Sr/^{86}Sr$ in the sampled catchments, as a consequence of its extremely radiogenic input. In addition, it reaffirms the greater prominence of the Nawakot Group calc-silicate units relative to the purer silicates. The negative influence of HCO_3^- concentrations is less easily understood, but is most likely a proxy for inputs from the much less radiogenic carbonates of the TSS, characterised by high $[HCO_3^-]$.

Equation 5.1 produces excellent predictions (see table 5.1 and fig. 5.22) for the dissolved $^{87}Sr/^{86}Sr$ ratios of the large rivers sampled in southern Nepal. Predictions for the Sapt Kosi, Sun Kosi, Arun and Tamur rivers are all within 0.01 of observed values (better than 0.0025 in the case of the Sapt Kosi and Sun Kosi). Considering equation 1 is based purely on the amount of measured Lesser Himalayan coverage in the catchments concerned, taking no account of detailed geological variations within the Lesser Himalaya (aside from the broad division into calc-silicates and silicates), let alone numerous other factors likely to influence Himalayan river chemistry (e.g. land use, vegetation, altitude), such accuracy is perhaps surprising, but demonstrates the overwhelming influence of geology upon dissolved $^{87}Sr/^{86}Sr$ in the rivers of the Nepal Himalaya. Data from September through to December are incorporated in this multiple regression suggesting the implications of this work are perhaps valid for the entire sampling period (late monsoon / dry season).

Sample	River	**Actual $^{87}Sr/^{86}Sr$***	Full data	Bhote Kosi	Bhote Kosi (dry season)		Difference predicted / actual values		
							Full data	Bhote Kosi	Bhote Kosi (dry season)
SK1	Sapt Kosi	**0.756521**	0.757308	0.763004	0.762476		0.000787	0.006483	0.005955
SK2	Sapt Kosi	**0.753414**	0.755671	0.761134	0.759485		0.002257	0.007720	0.006071
SK3	Sun Kosi	**0.777701**	0.776614	0.780559	0.773902		-0.001087	0.002858	-0.003799
AN1	Arun	**0.728828**	0.738503	0.744751	0.745483		0.009675	0.015923	0.016655
TN1	Tamur	**0.793565**	0.783858	0.789864	0.791287		-0.009707	-0.003701	-0.002278
L21	Trisuli	**0.734071**	0.749412	0.755502	0.757440		0.015341	0.021431	0.023369
						Mean (excl. L21)	**0.004702**	**0.009686**	**0.009688**
						Mean (incl. L21)		**0.007337**	**0.006952**

* $^{87}Sr/^{86}Sr$ values adjusted for rainfall input

Table* 5.1. Comparison between measured $^{87}Sr/^{86}Sr$ ratios and those predicted by multiple regression using the full and Bhote Kosi datasets.

Equation 5.1 implies that for a river catchment in which no LHF bedrock is present, $^{87}Sr/^{86}Sr$ is largely determined by $[HCO_3^-]$. This is likely to be broadly true since rivers draining the TSS have high $[HCO_3^-]$ but low dissolved $^{87}Sr/^{86}Sr$ in comparison to those draining the HHCS. It is not expected, however, that a multiple regression based on data from the Bhote Kosi could predict dissolved $^{87}Sr/^{86}Sr$ ratios in rivers with dissimilar geology (such as those with no Lesser Himalayan bedrock).

5.4.2. Analysis Using Bhote Kosi Data.

The following equation results from a multiple regression analysis of samples from the Bhote Kosi catchment only.

Equation 5.2.

$$^{87}Sr/^{86}Sr = 0.769347 + 2.250902\ E^{-3}\ \%LHC + 1.240804\ E^{-3}\ \%LHS - 3.990264\ E^{-5}\ [HCO_3^-]$$

$r^2 = 0.68$
$r^2 = 0.59$ (incorporating only %LHC and %LHS variables)
$r^2 = 0.47$ (incorporating only the %LHC variable)

Again, this equation produces excellent predictions of dissolved $^{87}Sr/^{86}Sr$ in the major rivers sampled in southern Nepal. In the Sapt Kosi, Sun Kosi and Tamur, the difference

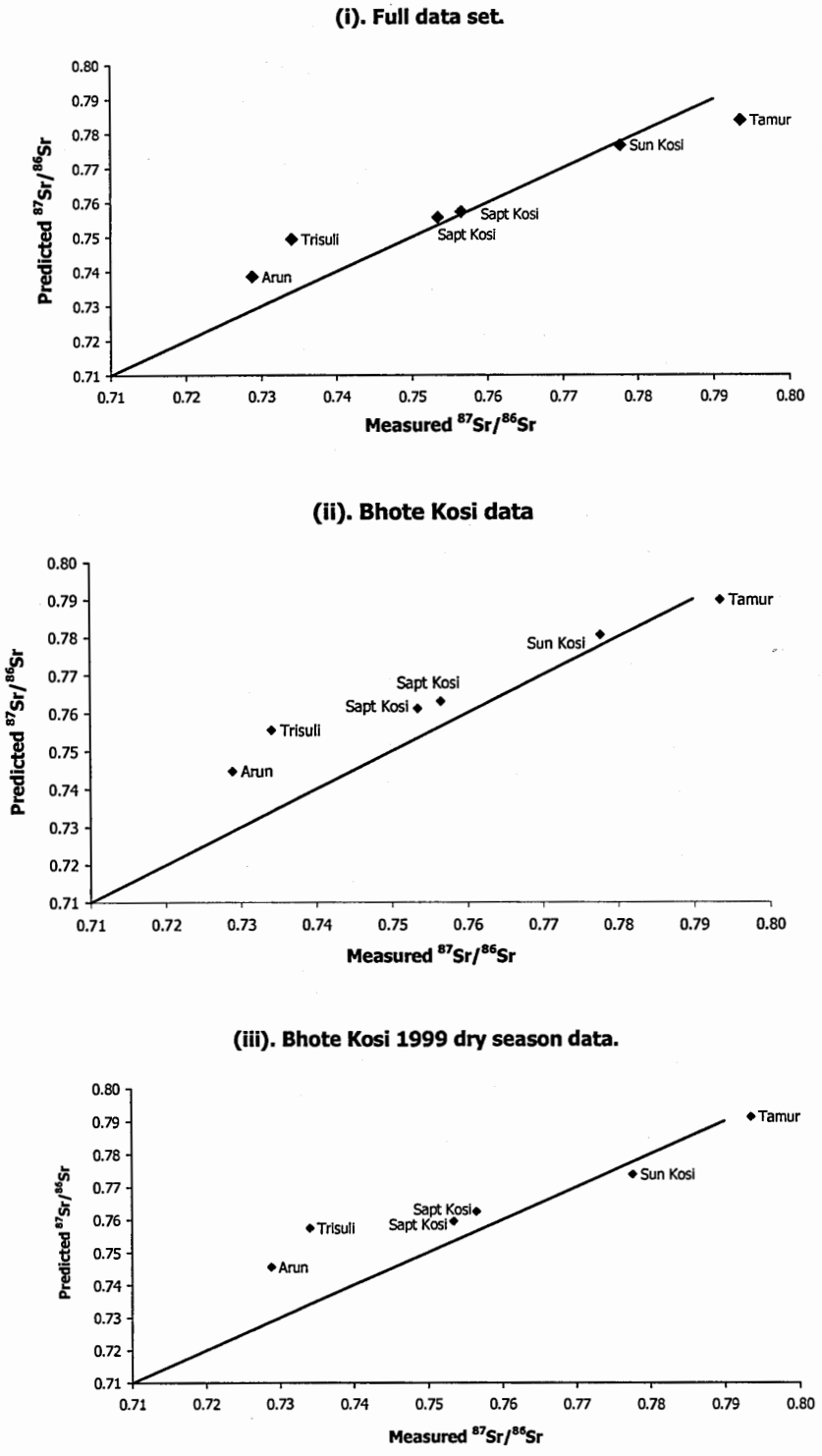

Fig. 5.22. Comparison of measured $^{87}Sr/^{86}Sr$ ratios with those predicted by multiple regression.

between measured and predicted results is <0.01. Using equation 5.2, the predicted value for the Arun is not as good as with equation 1, (~0.016 higher than the measured value). The influence of the Lesser Himalaya appears to be less important in the Arun than in the Bhote Kosi, possibly because the Lesser Himalayan rocks in this catchment are less radiogenic than those of the Bhote Kosi. Another possibility is that the $[HCO_3^-]$ correction is not enough to account for TSS inputs into the Arun, which include substantial amounts of Quaternary sediment. Using this equation to predict the $^{87}Sr/^{86}Sr$ of the Trisuli at also gives a fairly substantial overestimate. This is perhaps due to the small amount of Lesser Himalayan calc-silicate in this catchment being less radiogenic than in the Bhote Kosi, where a more complete LHF sequence is exposed.

5.4.3. Analysis Using Dry Season Bhote Kosi Data.

The rivers which confluence in the Chatra region were sampled in mid November, during the driest part of the year in Nepal. Excluding the September samples from the Bhote Kosi dataset produces a multiple regression equation with a different form.

Equation 5.3.

$$^{87}Sr/^{86}Sr = 0.791076 + 2.610779\ E^{-3}\ \%LHtotal - 6.383368\ E^{-5}\ [HCO_3^-] - 1.643003\ E^{-3}\ \%LHS$$

$r^2 = 0.72$

$r^2 = 0.62$ (incorporating only %LHtotal and $[HCO_3^-]$ variables)

$r^2 = 0.52$ (incorporating only the %LHtotal variable)

As before, the equation reveals that the % of Lesser Himalayan bedrock in a catchment can be used to make reasonably good predictions (see table 5.1 and fig. 5.22) of dissolved $^{87}Sr/^{86}Sr$, and again that calc-silicate units are more crucial in determining high $^{87}Sr/^{86}Sr$, with lower $^{87}Sr/^{86}Sr$ being predicted by this equation for catchments in which a greater proportion of LHF bedrock is comprised of LHF silicate (Kuncha Group and LHF gneisses). Again, an adjustment is made based on $[HCO_3^-]$. Using this equation improves predictions for the Tamur, but overall predictions are better using equation 5.1.

5.5. Predicting Strontium Concentrations in Nepalese Rivers Using Regression Analysis.

5.5.1. Analysis Using the Full Dataset.

A multiple regression analysis of all data collected in this study (incorporating Bhote Kosi, Langtang Khola-Trisuli and Khumbu samples) to predict Sr^{2+} concentrations in the large rivers sampled in southern Nepal, produces the following equation:

Equation 5.4.

$$[Sr^{2+}] = -0.174785 + 3.885699\ E^{-3}\ [SO_4^{2-}] + 1.383661\ [Si]$$

$r^2 = 0.86$

$r^2 = 0.66$ (incorporating only the $[SO_4^{2-}]$ variable)

Sample	River	$[Sr]^{2+}$ µmol/l*	Full data	Full data (geology only)	Bhote Kosi	Bhote Kosi (geology only)	Dry season 1999		Difference predicted / actual values				
									Full data	Full data (geology only)	Bhote Kosi	Bhote Kosi (geology only)	Dry season 1999
SK1	Sapt Kosi	**0.4267**	N/A	0.5203	N/A	0.7623	N/A		N/A	0.0936	N/A	0.3356	N/A
SK2	Sapt Kosi	**0.4437**	0.4568	0.5203	0.4876	0.7623	0.4389		0.0131	0.0766	0.0439	0.3186	-0.0048
SK3	Sun Kosi	**0.3720**	0.4076	-0.0212	0.4056	0.1330	0.3750		0.0356	-0.3932	0.0336	-0.2390	0.0030
AN1	Arun	**0.6708**	0.5271	0.9452	0.6196	1.2581	0.5369		-0.1437	0.2744	-0.0512	0.5873	-0.1339
TN1	Tamur	**0.2330**	0.4296	-0.0765	0.4369	0.0604	0.3889		0.1967	-0.3094	0.2039	-0.1726	0.1559
L21	Trisuli	**0.6611**	0.5652	0.5016	0.6507	0.6117	0.5540		-0.0958	-0.1594	-0.0103	-0.0493	-0.1070
								Mean (excl. L21)	**0.0973**	**0.2295**	**0.0832**	**0.3306**	**0.0744**
								Mean (incl. L21)			**0.0686**	**0.2837**	**0.0810**

*$[Sr]^{2+}$ adjusted for rainfall input

Table 5.2. Comparison between measured strontium concentrations and those predicted by multiple regression using the full and Bhote Kosi datasets.

This states that the best predictions of Sr^{2+} concentrations are produced based largely on the relationship between $[Sr^{2+}]$ and $[SO_4^{2-}]$ (as shown in fig. 5.21). Predictions using this equation are reasonable (see table 5.2), the mean difference between measured and predicted values being 0.1, with a difference between measured and predicted values of between 3% and 21% in the different rivers. This indicates that the relationship between $[Sr^{2+}]$ and $[SO_4^{2-}]$ is perhaps one likely to be observed throughout the Himalaya. The regression underestimates $[Sr^{2+}]$ in the TSS-dominated Arun catchment, but overestimates are calculated for the Sun Kosi and the Tamur, which have little or no TSS drainage. Equation 5.4 thus works best for those rivers with similar geology to the Bhote Kosi i.e. the Sapt Kosi and to a lesser extent the Sun Kosi.

In contrast with $^{87}Sr/^{86}Sr$ ratios, geological coverages does not provide the best set of variables for predicting Sr^{2+} concentrations. A multiple regression based only on % geology produces the following equation:

Equation 5.5.

$$[Sr^{2+}] = -7.645502\ E^{-2} + 1.782032\ E^{-2}\ \%TSS$$

$r^2 = 0.84$

Predictions based on equation 5.5 (see table 5.2) are extremely poor, the mean difference between measured and predicted strontium concentrations often greater than 100%. This is despite an excellent r^2, demonstrating that while the relationship between %TSS and

dissolved $^{87}Sr/^{86}Sr$ is good for the Bhote Kosi, this is unlikely to be true for all other Himalayan rivers. The Tibetan Sedimentary Series is quite possibly the predominant source of Sr^{2+} in the Himalaya, but riverine concentrations are likely determined, unlike $^{87}Sr/^{86}Sr$ ratios, by the interaction of a combination of factors (altitude, temperature, vegetative cover and land use likely among them.

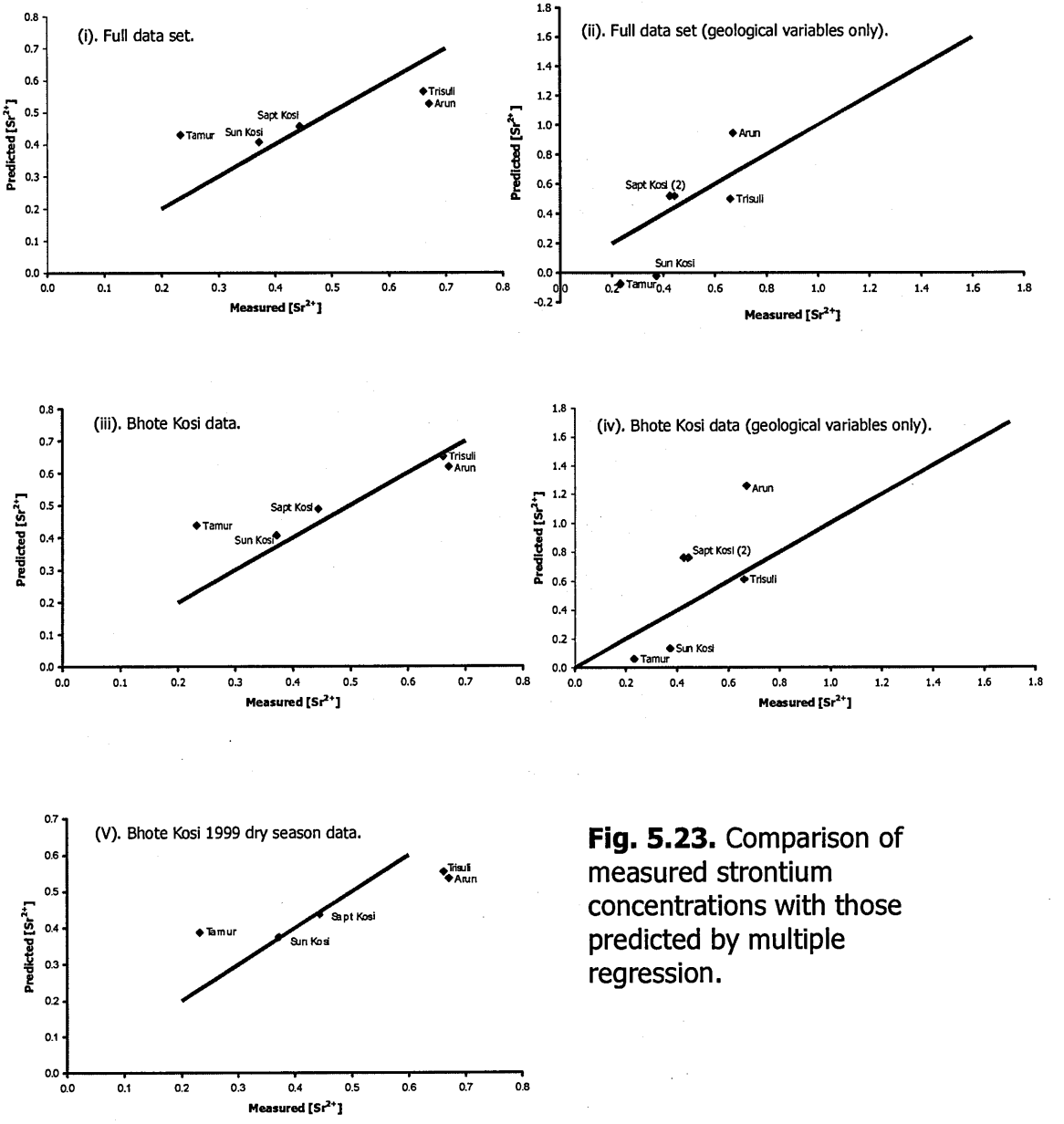

Fig. 5.23. Comparison of measured strontium concentrations with those predicted by multiple regression.

5.5.2. Analysis Using the Bhote Kosi Data Set.

Using only data from the Bhote Kosi produces a regression very similar to equation 5.4:

Equation 5.6.

$$[Sr^{2+}] = -6.231318\ E^{-2} + 3.434186\ E^{-3}\ [SO_4^{2-}] + 1.457083\ E^{-3}\ [Na^{+}]$$

$r^2 = 0.86$

$r^2 = 0.69$ incorporating only the $[SO_4^{2-}]$ variable.

Again, sulphate concentrations explain the greatest amount of variability in $[Sr^{2+}]$ within the dataset. High sodium concentrations are observed in the TSS, while a positive correlation between $[Na^{+}]$ and %HHCS is noted in table D6. Predictions using equation 5.6 are slightly improved in comparison with those using equation 5.4.

Using only variations in geological coverage (equation 5.7, below) affords no improvement from equation 5.5.

Equation 5.7.

$$[Sr^{2+}] = -0.533555 + 2.922723\ E^{-2}\ \%TSS + 1.893975\ E^{-2}\ \%LHS$$

$r^2 = 0.95$

$r^2 = 0.90$ (incorporating only %TSS).

Again, it is the proportion of TSS bedrock present in catchments that has by far the predominant influence (%LHS makes little difference as shown by the partial r^2).

5.5.3. Analysis Using Bhote Kosi Data for the 1999 Dry Season.

Strontium concentrations are likely to be affected far more by seasonal or yearly differences in compared with $^{87}Sr/^{86}Sr$, as evidenced by comparing September and dry season data for the Bhote Kosi. A further multiple regression analysis (equation 5.8) was carried out for $[Sr^{2+}]$ using only Bhote Kosi dry season 1999 data (1998 dry season data were excluded as anion data are lacking for most of these samples).

Equation 5.8.

$$[Sr^{2+}] = 0.376109 - 0.402119\ ^{87}Sr/^{86}Sr + 2.200954\ E^{-3}\ [SO_4^{2-}] + 1.033650\ E^{-3}\ [Na^{+}]$$

$r^2 = 0.81$

$r^2 = 0.53$ (incorporating only $^{87}Sr/^{86}Sr$ and $[SO_4^{2-}]$)

$r^2 = 0.33$ (incorporating only $^{87}Sr/^{8S}r$)

This regression highlights the negative relationship between $^{87}Sr/^{86}Sr$ and $[Sr^{2+}]$ previously noted in the principal components analyses (fig. 5.17), and incorporates the previously established correlation between $[Sr^{2+}]$ and $[SO_4^{2-}]$. In addition, an adjustment is made based on Na^+ concentrations, as seen in equation 5.6. Predictions of Sr^{2+}

concentrations using equation 5.8 are on average better than those using equation 5.4 (the full dataset) and equation 5.6 (Bhote Kosi data) (see table 5.2 and fig. 5.23), and are again particularly good for the Sapt Kosi and Sun Kosi, with a difference between actual and predicted values of <0.005 μmol/l). Again, equation 5.8 considerably underestimates the [Sr^{2+}] ofthe Arun and Langtang Khola-Trisuli, draining substantial TSS bedrock, and overestimates that of the Tamur, with no TSS bedrock.

5.5.4. Summary of Findings from Multiple Regressions.

The preceding attempts to predict dissolved $^{87}Sr/^{86}Sr$ ratios were more successful than those trying to predict Sr^{2+} concentrations. The most likely reason for this is that dissolved isotope ratios are much less sensitive to hydrological influence. Equations 5.1 - 5.3 suggest that Sr-isotope values in the Himalaya are largely determined by geology, with high $^{87}Sr/^{86}Sr$ inputs from the Lesser Himalaya balanced against the less radiogenic inputs of the TSS and HHCS, as previously shown by the principal components analyses. Inputs from the Nawakot Group calc-silicates are clearly more important than those from silicates. The statistical importance of HCO_3^- in these equations is undoubted although its chemical significance is difficult to determine. The most likely explanation is that it represents a correction based on the high HCO_3^- concentrations of the TSS. The success of the regression predictions for $^{87}Sr/^{86}Sr$ suggests that findings in the Bhote Kosi (in terms of $^{87}Sr/^{86}Sr$ ratios) can be applied on a Himalayan scale.

The relatively poor predictions of [Sr^{2+}] produced by the multiple regression equations 5.4 – 5.8 indicate that the factors determining Sr^{2+} concentrations might be more numerous and complex and that [Sr^{2+}] is more sensitive to seasonal and annual differences. Relative values (i.e. high Sr^{2+} concentrations in the TSS, low in the HHCS and LHF) are likely to be applicable across the chain, and similar relationships have been are observed in other studies (e.g. Galy *et al.*, 1999; English *et al.*, 2000).

5.6. Determining the Source of Strontium in the Himalaya: A Mass Balance Approach.

In this section, the strontium budget of monolithologic tributaries and river sections is apportioned to four contributing sources; atmospheric inputs and evaporite, carbonate and silicate weathering. Additionally, the measured [Sr^{2+}] and $^{87}Sr/^{86}Sr$ of the monolithologic catchments are used to define Sr endpoints for the TSS, HHCS and LHF. Combining these two approaches, an estimate of the contribution of evaporites, carbonates and silicates from each major lithology to the total strontium budget of the Bhote Kosi and sampled major Himalayan rivers can be made.

5.6.1. Sources of Sr in the TSS, HHCS and LHF.

According to equation 5.9 (below), riverine strontium is assumed to originate from the four sources listed above. After correction for atmospheric inputs, all chloride is assumed to originate from the dissolution of evaporites and thus the [Sr^{2+}] from

evaporites is calculated from the best estimate of the $[Sr^{2+}]/[Cl^-]$ ratio of evaporite input into Himalayan rivers. Again after atmospheric correction, and following an adjustment based on $[Cl^-]$ for Na^+ originating from evaporites, remaining Na^+ is assumed to have originated from silicate weathering. Sr^{2+} from silicates is thus calculated based on the best estimate of the $[Sr^{2+}]/[Na^+]$ ratio of silicate inputs into Himalayan rivers. Carbonate contributions to total $[Sr^{2+}]$ are based on the best estimate of the $[Sr^{2+}]/[Ca^{2+}]$ ratio of carbonate inputs into Himalayan rivers, assuming that all Ca^{2+} originates from carbonate, subsequent to a correction for Ca^{2+} originating from silicate which is based on $[Na^+]$.

Equation 5.9 (from Galy *et al.*, 1999).

(i).

$$[Sr^{2+}]_{Riv} = [Sr^{2+}]_{Atm} + [Sr^{2+}]_{Ev} + [Sr^{2+}]_{Sil} + [Sr^{2+}]_{Car}$$

(ii).

$$[Sr^{2+}]_{Ev} = [Cl^-]^*_{Riv} ([Sr^{2+}]/[Cl^-])_{Ev}$$

(iii).

$$[Sr^{2+}]_{Sil} = ([Na^+]^*_{Riv} - [Cl^-]^*_{Riv}) ([Sr^{2+}] / [Na^+])_{Sil}$$

(iv).

$$[Sr^{2+}]_{Car} = ([Ca^{2+}]^*_{Riv} - 0.2 ([Na^+]^*_{Riv} - [Cl^-]^*_{Riv})) ([Sr^{2+}]/[Ca^{2+}])_{Car}$$

Where;

Riv = river.

Atm = atmosphere.

Ev = evaporite.

Sil = silicate.

Car = carbonate.

*Corrected for atmospheric input.

It is assumed that contributions, from basinal brines and the alteration of buried evaporites, silicates and carbonates, entering rivers from hot springs are incorporated within the sources described above for surface weathering. The low concentration of cations and anions in Bhote Kosi surface waters relative to the Tatopani hot spring (see section 4.2.1.7) and other Himalayan hot springs (Kortaba *et al.*, 1981; Galy *et al.*, 1999; Evans *et al.*, 2001) strongly suggest that hot spring contributions are minimal. The atmospheric contribution is taken from data compiled by Galy and France-Lanord (1999), except for $[Sr^{2+}]$ and $^{87}Sr/^{86}Sr$, which are from Galy *et al.* (1999), and contributions from this source are discussed in section 4.1.

5.6.2. The Evaporite Contribution to Strontium Budgets.

Evaporite units are not described in geological accounts of the Bhote Kosi section (e.g. Maruo *et al.*, 1973; Stöcklin, 1980; Stöcklin and Bhattarai, 1980; Burchfiel *et al.*, 1992; Upreti, 1999; Upreti and Rai, 2000) although the presence of undocumented (even trace)

amounts could have a major impact on Sr chemistry. Deeply buried evaporite formations could also affect surface chemistry through dissolution by circulating thermal springs (Galy *et al.*, 1999). The $[Cl^-]/[Sr^{2+}]$ ratio of evaporites in the TSS and HHCS is estimated to be 650 by Galy *et al.* (1999) based on the dissolved chemistry resulting from the dissolution of evaporites in the Mustang Graben, and a thermal spring in the same region in which NaCl represents 70 Eq%. A ratio of 1750 is used in the Lesser Himalayan tributaries based on thermal springs in this zone (Kortarba *et al.*, 1981).

5.6.3. The Silicate Contribution to Strontium Budgets.

Since oligoclase alteration is the main silicate alteration reaction in Himalayan catchments (Galy and France-Lanord, in press), silicate Sr can be determined by $[Na^+]/[Sr^{2+}]$ ratios. Based on catchments draining only silicate units with $X_{Ca} \sim 0.3$ ($X_{Ca} = [Ca^{2+}]/\Sigma cations$), Galy *et al.* (1999) assign the silicate endmember a $[Na^+]/[Sr^{2+}]$ ratio of 700-1000. Low X_{Ca} values result in rivers draining silicate rocks which contain minimal vein calcite, and these rivers therefore best represent carbonate-free chemistry. Of the sampled catchments in this study draining silicate rocks (table E4) only three (L18, L20 and L22 from the Langtang Khola catchment, see plate 9 for locations) had an $X_{Ca} < 0.3$. The $[Na^+]/[Sr^{2+}]$ of these samples (average ~775) fell within the range defined by Galy *et al.*, and the lower value (700) adopted by these authors is the one used in this study and provides an estimate of the maximum silicate strontium input.

An alternative calculation of silicate Sr in catchments draining the Lesser Himalaya (silicate* in table E1) is made to account for the strontium depletion of the LHF. A comparison of the mean Na/Sr ratios for TSS, HHCS and LHF bedrock collected from the Bhote Kosi (table 6.1) shows that LHF units have Na/Sr ratios ~1.6 times lower than rocks of the TSS and HHCS. Thus, a Na/Sr ratio of 1200 is used to calculate the revised silicate contribution, giving a more realistic assessment of the silicate Sr contribution in LHF-draining rivers.

5.6.4. The Carbonate Contribution to Strontium Budgets.

Galy *et al.* (1999) state that TSS and HHCS carbonates have $[Ca^{2+}]/[Sr^{2+}]$ ratios between 1000 and 2000. In this study a value of 1500 is used based both on these data and on the $[Ca^{2+}]/[Sr^{2+}]$ ratios of limestones collected from the TSS of the Bhote Kosi section (samples T17 and T18, see table C1) and a selection of marbles collected from the Kathmandu Nappe in the Chak Khola catchment (BK53, BK104 and BK105, see table C4). The chemistry of carbonate of the Lesser Himalaya is very different and a $[Ca^{2+}]/[Sr^{2+}]$ of 4000 is applied to LHF catchments to account for the strontium depletion of the LHF. This is based on the mean $[Ca^{2+}]/[Sr^{2+}]$ of the purest dolomites collected from the Bhote Kosi section (see table E5) as identified from fig. 7.2. The purest carbonates, which are all limestones, show even higher Ca/Sr ratios but a higher ratio is not used in the mass balance as dolomites are by far the most prevalent carbonates of the LHF in the Bhote Kosi.

5.6.5. Sources of Strontium in the Tibetan Sedimentary Series.

Based on the four source model outlined above, Sr^{2+} concentrations are calculated for monolithologic catchments in each of the three lithologic successions of the Himalaya. Sr budget predictions for TSS catchments (BKT2 and BKT3) produce serious underestimates, predicting <35% of the total Sr of both catchments. This phenomenon was also observed by Galy *et al.* (1999) who attributed the excess Sr to the recrystallisation of low-Sr calcite from surface waters, observing that carbonate easily precipitates in the arid climate of the Tibetan Plateau. Enrichment of surface waters in Sr due to this process has been reported in glaciated carbonate catchments (Fairchild *et al.*, 1994; Webster *et al.*, 1994) while Sr enrichment of supersaturated groundwaters resultant from carbonate precipitation is observed by Reeve and Perry (1994). A similar effect would result from the secondary precipitation of gypsum (Galy *et al.*, 1999). Hot springs are unlikely to provide such a large amount of Sr^{2+}, most inputs from this source being accounted for in the calculated evaporite contribution, although $[Cl^-]/[Sr^{2+}]$ ratios of less than 650 have been noted in hot springs (Evans *et al.*, 2001). Owing to the apparent paucity of hot springs in the Bhote Kosi, low-Sr carbonate and evaporite reprecipitation is the most likely cause of the underestimates of total dissolved strontium resulting from the mass balance.

The reprecipitation described above would result in a serious underestimate of the carbonate contribution to total Sr in the Bhote Kosi upstream of the STDS. Despite this the mass balance for BKT2 and BKT3 still shows that carbonate dominates the Sr

budget of the TSS. Evaporite contributions account for <1% of total [Sr^{2+}] while silicates contribute 30% at sample site BKT2, only 10% further downstream at BKT3. If the Sr excess noted above is assumed to be the result of the reprecipitation of low-Sr carbonate (carbonate** in table E1) then this silicate contribution would fall to <10% and <4% respectively. Atmospheric contributions are <1%. The carbonate domination of TSS inputs revealed in the upper Bhote Kosi agrees with the findings of Galy *et al.* (1999) for the Kali, Marpha and Marsyandi rivers and English *et al.* (2000) for the Seti.

5.6.6. Sources of Strontium in the High Himalayan Crystalline Series.

Incorporating a larger number of smaller catchments, the calculated contributions of the four sources to the total [Sr^{2+}] of HHCS catchments are more variable. Estimates of total Sr^{2+} using the mass balance are much more convincing for the HHCS, ranging from 49% to 222%, although in the majority of cases predicted and actual Sr^{2+} concentrations agree to within 25%-50%. The mass balance underestimates Sr^{2+} concentrations in the highest parts of the Langtang Khola, the most likely explanation again being the reprecipitation of low-Sr carbonate in this glaciated terrain. Serious overestimates occur in catchments draining the Kathmandu Nappe, which is regarded as part of the High Himalayan Crystalline Series in this study as silicate rocks collected from the nappe have chemical compositions similar to those from the main HHCS. The Jhiku Khola and Chak Khola, which drain the Kathmandu Nappe, are characterised by very high concentrations of Na^+ (260-390 μmol/l). This suggests that a large proportion of the Na^+ in these rivers might not originate from silicate, and consequently an overestimate of the Sr originating from

silicates in these catchments is likely, consequently leading to the overestimtes of the overall strontium concentration of these rivers.

Atmospheric strontium contributions in HHCS catchments vary from 3 to 22% and are highest in the dilute, pure silicate catchments of the lower Langtang Khola and the Khumbu region. These rivers also show the highest silicate contributions (up to 70%) and correspondingly low carbonate Sr inputs (as low as 0%). In the upper reaches of the Langtang Khola and Indrawati, the lowest silicate contributions (as low as 18%) and highest carbonate inputs (up to 72%) are observed.

5.6.7. Sources of Strontium in the Lesser Himalaya.

Predictions of the proportion of Sr^{2+} derived from the four different sources in the LHF (see table E1) are characterised by an even greater level of variation than for the HHCS. The mass balance approach, especially when using the revised Na/Sr of 1200 for silicate (silicate*) provides mostly reasonable estimates of total dissolved strontium, the exceptions being samples BK93 (238%) and BK61 (369%). The source of the overprediction in these cases is unclear, but both of these samples were collected from relatively small, dilute rivers. In contrast, the [Sr^{2+}] predicted for samples BK82 (32%) and BK129 (56%) is much less than that measured. Both of these catchments drain the Malekhu Limestone unit suggesting that this unit might have the chemical composition of a "typical" Himalayan limestone, rather than that of an LHF dolomite. Reasonable

estimates of $[Sr^{2+}]$ can be obtained if a $[Ca^{2+}]/[Sr^{2+}]$ of 1500 is used in the mass balance calculation for these samples.

Atmospheric contributions range from 3-36% and are highest in catchments dominated by the Kuncha Group silicates. In most cases evaporite contributions are low (<5%) although three catchments, BK90 (7%), BK88 (10%) and BK95 (18%) appear to derive a markedly higher amount of Sr^{2+} from this source. As all three catchments are located in close proximity there may be a source of high $[Cl^-]$ to explain these three results (e.g. undocumented hot springs). Two of these catchments have a zero contribution from silicate, strongly suggesting an overestimate of the evaporite contribution. Excluding these catchments, maximum silicate contributions to Sr^{2+} in the Lesser Himalaya range between 7% and 62% (ranging between 4% and 55% using the revised Na/Sr), carbonate contributions between 12% and 82% (minimum estimates, using the revised Na/Sr for the silicate contribution increases this range to 18-86%). A similarly wide-ranging variability in silicate and carbonate contributions is noted in Lesser Himalayan catchments by English *et al.* (2000). Tributaries draining predominantly or entirely the calc-silicate units tend to have a greater carbonate contribution although this is not strictly the case, silicate-draining tributaries also showing high carbonate contributions (e.g. BK87 = 81%). This is indicative of an important role for trace carbonate in some rivers draining the Kuncha Group and Lesser Himalayan gneisses (as previously demonstrated by Blum *et al.*, 1998).

5.6.8. Calculating the Source of Strontium in the Bhote Kosi and Other Major Himalayan Rivers.

Using the $^{87}Sr/^{86}Sr$ and $[Sr^{2+}]$ of the monolithologic catchments, endpoints representing a "typical" composition for the TSS, HHCS and LHF can be established, both for the Bhote Kosi catchment and regionally for the Nepal Himalaya. Equation 5.9 is then used to determine the average contributions from the atmosphere, evaporites, silicates and carbonates from these units. As the dissolved chemistry remains reasonably constant during the dry season, rivers are used as a natural averaging tool to help define the endpoints for the TSS and HHCS sections. In the case of the TSS sample BKT3 (from the STDS) is taken to be representative of the TSS input into the Bhote Kosi (table E1). For the HHCS endpoint, Bhote Kosi mainstream data is precluded owing to upstream inputs from the TSS. Thus, an average is taken from two large HHCS-draining basins (see table E1); the Langtang Khola (sample site L6 just upstream of the MCT, see plate 9, the repeat sample, L28 is not used owing to a poor charge balance) and the Indrawati north of Malemchi (i.e. north of the MCT; sample BK48, see plate 3), both of which have catchments adjoining that of the Bhote Kosi. The Bhote Kosi in the Khumbu region (sample Ev9, the only sample from Khumbu with a TSS-free catchment, see plate 5) provides a further large HHCS-draining basin, but mass balance for this sample (see table E3) produced a serious overestimate of $[Sr^{2+}]$, indicating that the mass balance was not providing accurate estimates of the Sr contributions from the different sources in this case. The mean silicate (49%) and carbonate (37%) contributions calculated from the two catchments show roughly reversed proportions to those calculated by Galy *et al.*

(1999) (carbonate 60%, silicate 40%). This might reflect small variations in the amount of carbonate present in the HHCS in the different sampling areas, a factor likely to have a major effect on estimates of relative carbonate and silicate contributions. This is because HHCS carbonates are characterised by high Sr^{2+} concentrations (up to ~1000 ppm, see table C2 and table C4).

For the LHF endpoint it was not possible to use large catchments as a natural averaging tool. Thus, mean values for smaller LHF-draining catchments were used (see table E1), excluding the two catchments which produced very large overestimates of Sr in the mass balance. The calculated carbonate Sr contribution for this study of ~70% is higher than that (40%) of Galy *et al.* (1999), although the calculations in this previous study, with one exception, were based on LHF catchments solely draining the Kuncha Formation silicates.

Using the above methodology, the following endpoint values for the Bhote Kosi are obtained.

TSS; $^{87}Sr/^{86}Sr = 0.7202$

$1/[Sr^{2+}] = 0.477$

NB. The $^{87}Sr/^{86}Sr$ ratio above is almost identical to the ratio of 0.7209 identified by Palmer and Edmond (1992) for their "high strontium concentration endmember" in the Ganges basin.

Contributions to [Sr^{2+}] (for use with data adjusted for atmospheric input, therefore this contribution is excluded);

Evaporite = 0.3%

Silicate = 3.8%

Carbonate** = 95.9%

** Carbonate is calculated including excess [Sr^{2+}] after calculating other contributions based on the assumption that the Sr excess noted in TSS rivers results from the reprecipitation of low-Sr carbonate.

HHCS; $^{87}Sr/^{86}Sr = 0.7379$

$1/[Sr^{2+}] = 4.648$

Contributions to [Sr^{2+}] (again for use with data adjusted for atmospheric input);

Evaporite = 5.6%

Silicate = 53.9%

Carbonate = 40.5%

LHF (September); $^{87}Sr/^{86}Sr = 0.8793$

$1/[Sr^{2+}] = 12.608$

Contributions to $[Sr^{2+}]$ (for samples adjusted for atmospheric input);

Evaporite = 2.9%

Silicate = 25.8%

Carbonate = 71.3%

LHF (dry season); $^{87}Sr/^{86}Sr = 0.8656$

$1/[Sr^{2+}] = 8.321$

Contributions to $[Sr^{2+}]$ (for samples adjusted for atmospheric input);

Evaporite = 4.2%

Silicate = 26.1%

Carbonate = 69.7%

Two endpoints were calculated for the LHF to reflect the difference between samples collected in the September 1999 late monsoon and those collected in the main dry season (late October – December). The silicate contribution is the maximum calculated (i.e. not silicate* in table E1).

To calculate the contributions of different lithologies to the Sr chemistry of the large rivers sampled in southern Nepal, further data from Galy *et al.* (1999) and English *et al.* (2000) were incorporated with that from this study to generate a different set of endpoints better reflecting the Central Himalaya as a whole (see table E2). For the TSS

and HHCS, data from large catchments was used as for the Bhote Kosi. As with the Bhote Kosi endpoints, atmospheric contributions are not included as data adjusted for rainfall inputs are used in the subsequent calculations in this chapter.

TSS; $^{87}Sr/^{86}Sr = 0.7185$

$1/[Sr^{2+}] = 0.328$

Contributions to $[Sr^{2+}]$;

Evaporite = 6.7%

Silicate = 3.1%

Carbonate** = 90.2%

**Again, calculated carbonate input includes excess $[Sr^{2+}]$ after calculating other contributions.

HHCS; $^{87}Sr/^{86}Sr = 0.7435$

$1/[Sr^{2+}] = 6.185$

Contributions to $[Sr^{2+}]$;

Evaporite = 6.5%

Silicate = 66.4%

Carbonate = 27.1%

LHF; $^{87}Sr/^{86}Sr$ 0.8471

$1/[Sr^{2+}] = 5.777$

Contributions to $[Sr^{2+}]$;

Evaporite = 6.2%

Silicate = 31.9%

Carbonate = 61.9%

As for the Bhote Kosi, the silicate contribution is the maximum value calculated (table E2).

The TSS, HHCS and LHF endpoints are used to define triangular regions in $^{87}Sr/^{86}Sr$ vs $1/[Sr^{2+}]$ space plots for the Bhote Kosi (fig. 5.24 and fig. 5.25) and the Central Himalaya (fig. 5.26). Fig. 5.24 illustrates the downstream changes in the relative contributions of the TSS, HHCS and LHF in the Bhote Kosi mainstream. Although individual samples are not labeled, the figure is easily understood as, with rare exceptions, dissolved $^{87}Sr/^{86}Sr$ continuously increases downstream. Samples taken from the river above the MCT (BKT1-7, BK43, BK76) plot along the TSS-HHCS mixing line, contributions from the HHCS increasing downstream of the STDS, reaching ~40-50% at the MCT. Downstream of the MCT, the rapidly and then steadily increasing contribution of the Lesser Himalaya is observed. The September 1999 samples are marked by relatively higher contributions from the HHCS and LHF, particularly those samples collected after rainfall. The final downstream chemistry of the Bhote Kosi at Dolalghat can be

calculated for the dry season using fig. 5.24 (sample BK35) and for the September data using fig. 5.25 (sample BK74), which utilises the September endpoint for the LHF and provides a better fit for the September Bhote Kosi data. Fig. 5.26 is used to calculate contributions of each lithology in the Sapt Kosi, Sun Kosi, and Arun at their downstream points in the Chatra region and in the Trisuli at Trisuli Bazaar. Using fig. 5.24 – fig. 5.26 and the results of the mass balance presented above, the evaporite, silicate and carbonate inputs from the TSS, HHCS and LHF can be calculated for the major rivers in this study, as sumarised in table 5.3 and fig. 5.27. The Tamur is excluded as it does not drain the TSS and this does not conform with the three-source mixing of fig. 5.26.

	Bhote Kosi (September)	Bhote Kosi (Dry season)	Langtang K - Trisuli	Arun	Sun Kosi	Sapt Kosi	Sapt Kosi (rpt)
Atmospheric	**11.1**	**6.3**	**3.1**	**3.0**	**5.3**	**4.7**	**4.5**
TSS	**38.2**	**58.1**	**75.6**	**77.6**	**53.0**	**62.9**	**61.1**
Evaporite	0.1	0.2	5.1	5.2	3.6	4.2	4.1
Silicate	1.5	2.2	2.3	2.4	1.6	1.9	1.9
Carbonate	36.6	55.7	68.2	70.0	47.8	56.7	55.1
HHCS	**17.8**	**9.4**	**8.7**	**14.6**	**0.0**	**8.6**	**7.6**
Evaporite	1.0	0.5	0.6	0.9	0.0	0.6	0.5
Silicate	9.6	5.1	5.8	9.7	0.0	5.7	5.0
Carbonate	7.2	3.8	2.4	4.0	0.0	2.3	2.1
LHF	**32.9**	**26.2**	**12.6**	**4.9**	**41.7**	**23.8**	**26.7**
Evaporite	1.0	1.1	0.8	0.3	2.6	1.5	1.7
Silicate	8.5	6.8	4.0	1.6	13.3	7.6	8.5
Carbonate	23.5	18.3	7.8	3.0	25.8	14.7	16.5

Table 5.3. Contributions of the major Himalayan lithologies to the Sr budget of the Bhote Kosi and other major Himalayan rivers.

Fig. 5.24. Strontium mixing diagram for the Bhote Kosi.

- September samples are shown by closed symbols, dry season samples by open symbols.

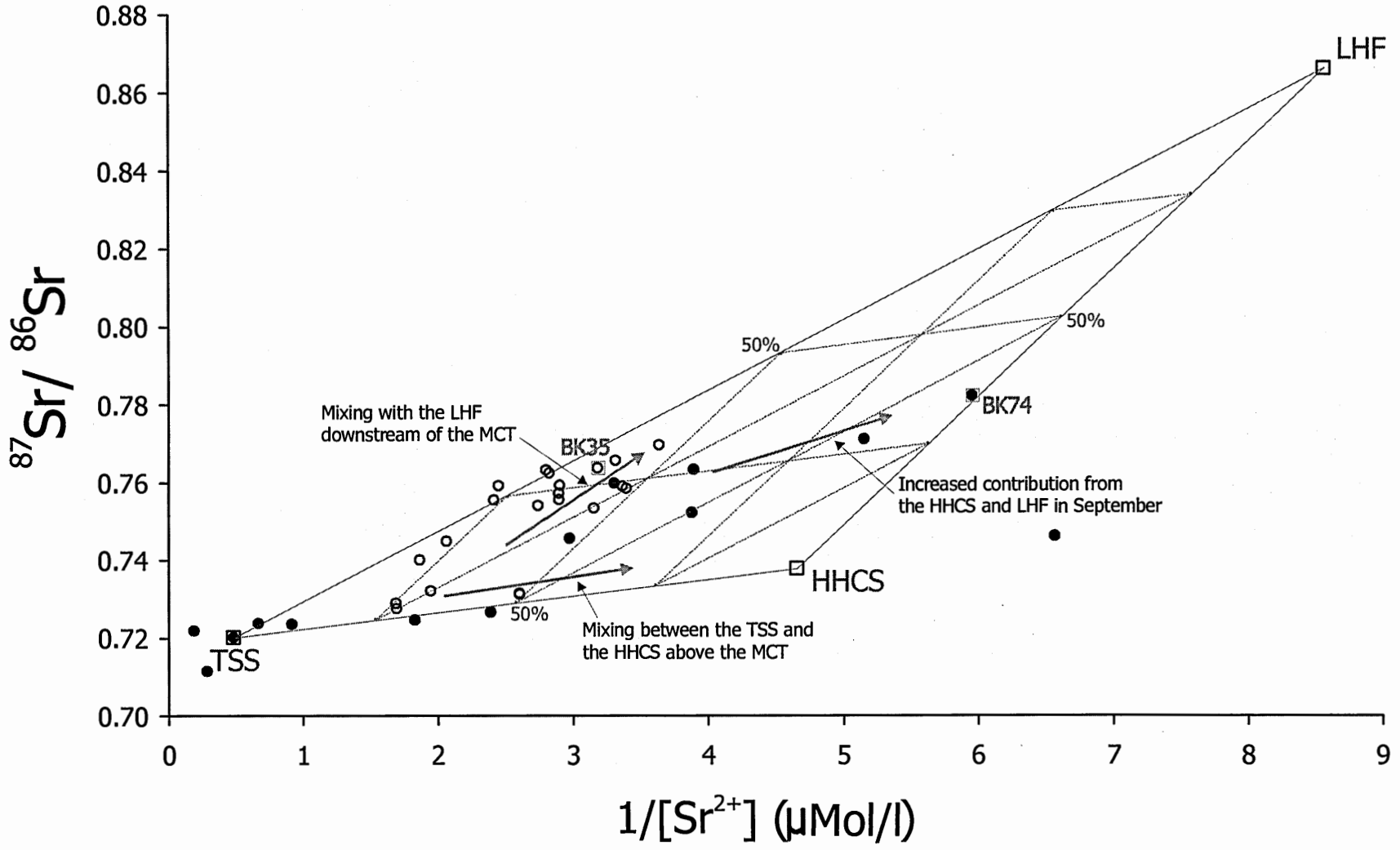

Fig. 5.25. Strontium mixing diagram for the Bhote Kosi using only September data.

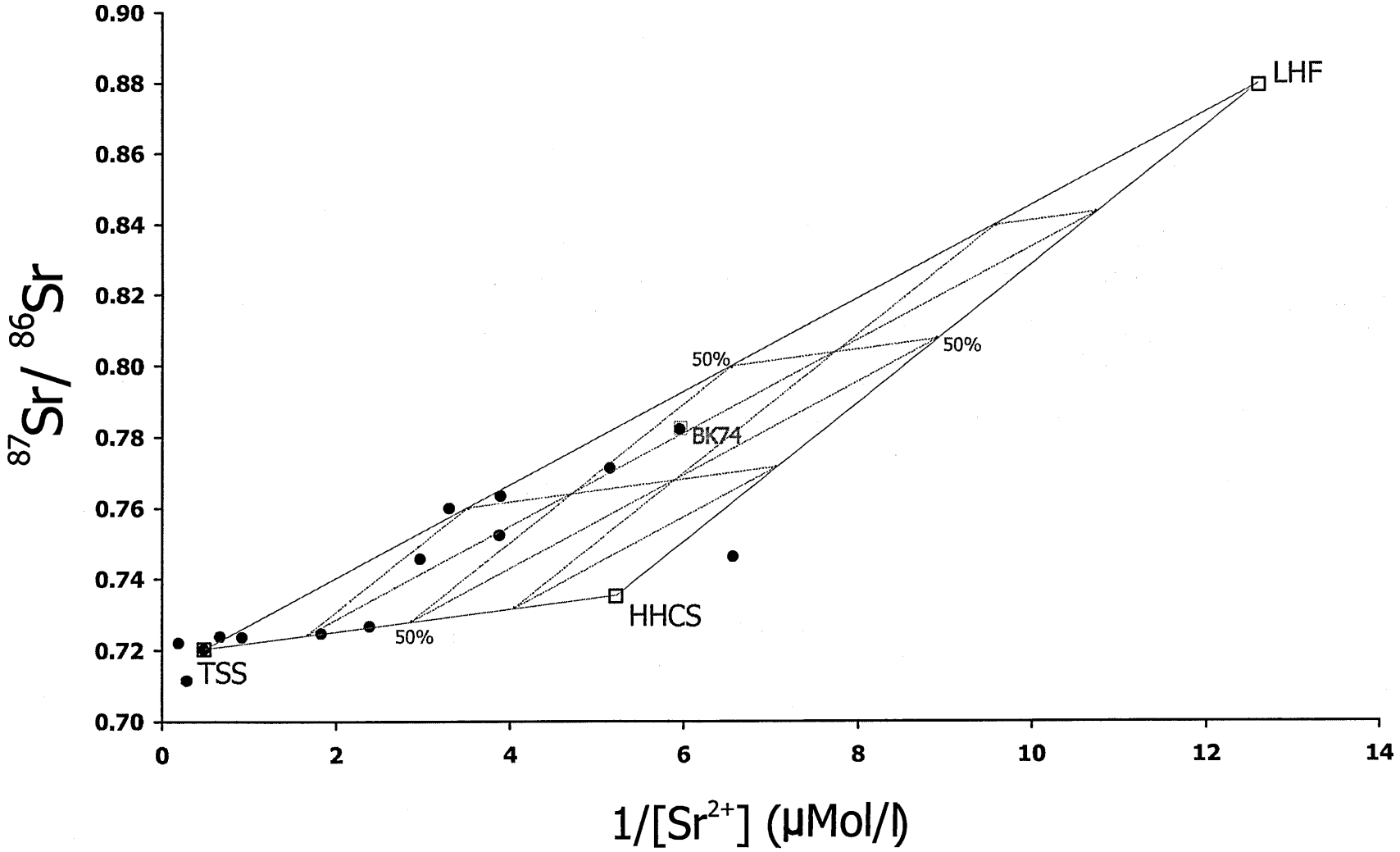

Fig. 5.26. Strontium mixing diagram for the Nepal Himalaya.

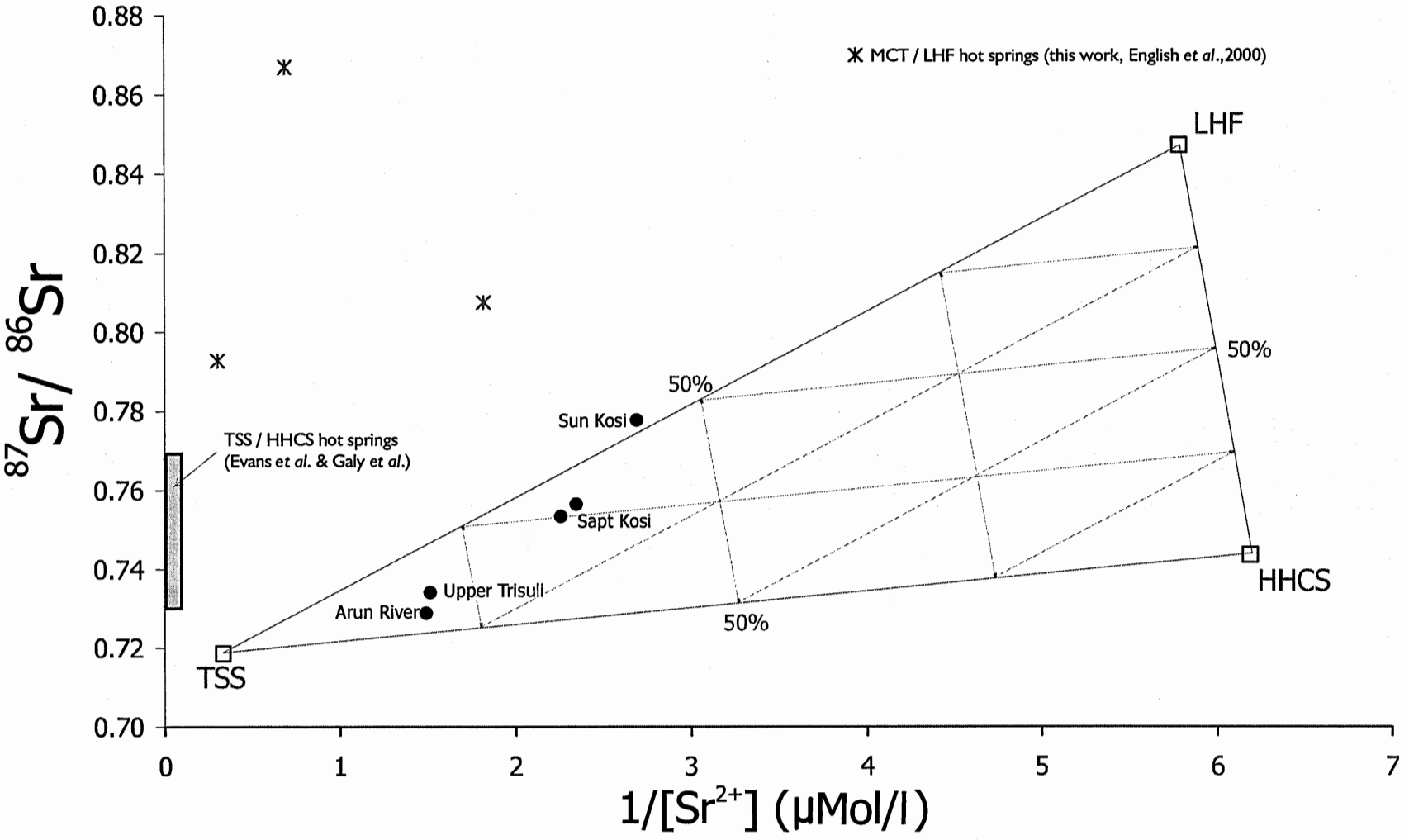

Table 5.3 and fig. 5.27 show that the Sr chemistry of the Bhote Kosi in the dry season is dominated by inputs from two major sources; carbonate from the Tibetan Sedimentary Series, characterised by high [Sr^{2+}] and relatively low $^{87}Sr/^{86}Sr$ ratios, and carbonate from the Lesser Himalaya, characterised by low [Sr^{2+}] and high $^{87}Sr/^{86}Sr$. Silicate weathering has a definite, but accessory, role in determining the Sr characteristics of the river at this time, with Lesser Himalayan silicate input (which is highly radiogenic) contributing more than silicate from the HHCS (moderately radiogenic) and TSS. A marked change is observed in the same river when sampled during September, as although carbonates for the TSS and LHF are still the largest contributors of Sr^{2+}, the proportion derived from the TSS is much lower (37% as compared wth 56%), while that from the LHF is slightly increased (23% compared to 18%). The HHCS influence is stronger, and silicate weathering has a greater role to play as a result. Total silicate contributions amount to 24% as opposed to 18% in the dry season, the bulk of this increase attributed to a greater contribution from HHCS silicate (10% up from 5%). It is possible that inputs from the TSS, which largely outcrops in the Himalayan rain shadow, remain roughly constant while the input of Sr weathered from the HHCS and LHF increases during September owing to increased erosion of these units as a result of monsoon rainfall. This is likely to be especially true of the HHCS, where rainfall is at its highest in the Himalayan range.

Both the Upper Trisuli and Arun river systems (even more so than the Bhote Kosi) are dominated by inputs from the carbonate of the TSS. As in the Bhote Kosi, the main source of radiogenic strontium is input from carbonate of the LHF, with a lesser role for

silicate, both from the LHF and HHCS. The lower $^{87}Sr/^{86}Sr$ and higher $[Sr^{2+}]$ of these rivers is clearly a function of greater input of Sr from TSS carbonate relative to these. The Sapt Kosi samples reveal a similar picture to the Bhote Kosi in the dry season (when the Sapt Kosi was sampled), although the presence of a greater extent of TSS outcrop in the catchment of this river is apparent. LHF carbonate inputs are once again the most important source of radiogenic Sr.

Results from the Sun Kosi reveal some of the problems associated with the mass balance approach. The Sun Kosi does not plot within the confines of the mixing triangle (fig. 5.26), resulting in a calculated zero contribution from the HHCS. This seems highly unlikely in a river with a catchment which is 60% underlain by HHCS bedrock. Uncertainties associated with endpoint determination might explain this, as a wide range of dissolved strontium concentrations were recorded in rivers draining both the HHCS and LHF (see table E1-E3). It is also possible that another source of Sr to Himalayan rivers has an impact. This source would need to contribute high Sr^{2+} concentrations at high $^{87}Sr/^{86}Sr$ ratios. Values for hot springs from the TSS and HHCS (Evans *et al.*, 2001; Galy *et al*, 1999) and from the LHF (this study; English *et al.*, 2000) are marked on fig. 5.26. Thermal springs are shown to be a major source of radiogenic Sr to the Marsyandi River in the Annapurna region of Nepal (Evans *et al.*, 2001). This river is known to be fed by abundant hot springs and there is at present no evidence for a significant input into other major Himalayan river systems.

Fig. 5.27. Bar chart showing the contributions, calculated by mass balance, of the major Himalayan lithologies to the strontium budget of major Nepalese rivers sampled in this study.

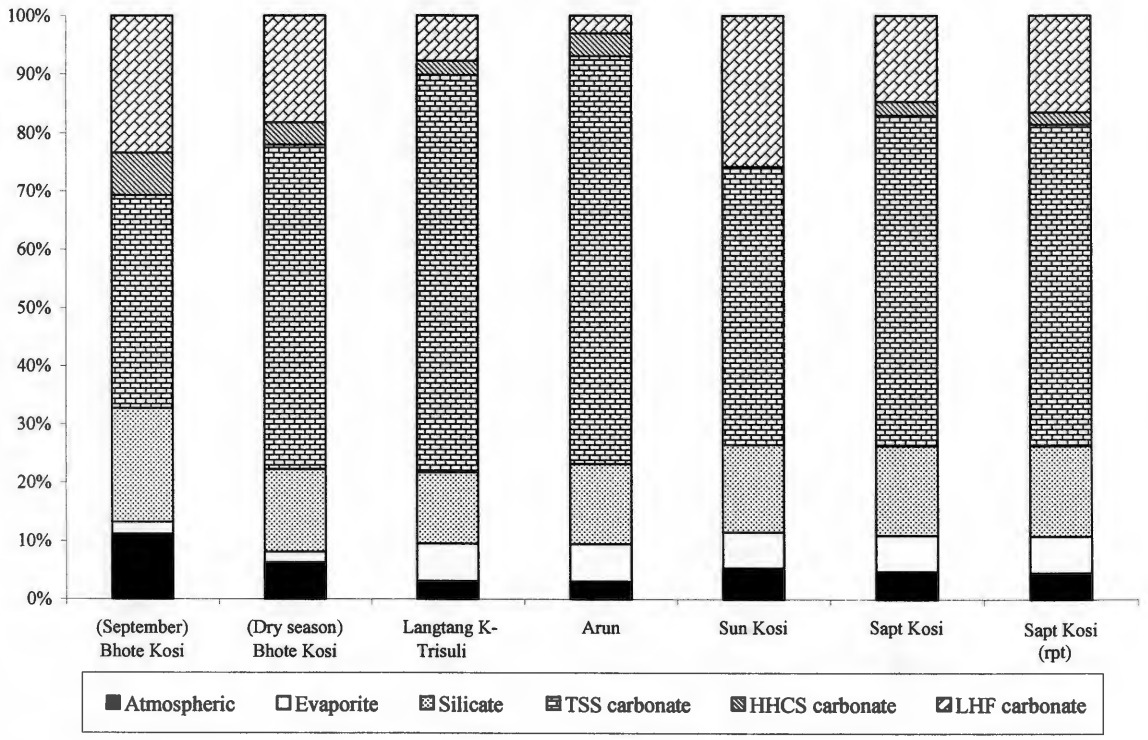

The dominance of Sr river chemistry by TSS carbonate inputs is also noted by *Galy et al.* (1999) for the Narayani, Kali and Trisuli basins, with overall carbonate contributions to $[Sr^{2+}]$ totalling 67-78%, a range encompassing the results from this work. Silicate Sr equals 12-19% in both this study and in the work of Galy *et al.* (1999). Galy *et al.* (1999) found that the predominant source of silicate Sr was the Lesser Himalaya. The results presented above demonstrate that such a finding is true for the Sapt Kosi, Sun Kosi and the Bhote Kosi in the dry season, while the High Himalayan Crystallines are shown to be the predominant source of silicate Sr in the Arun, Langtang Khola-Trisuli and the Bhote Kosi in September. The role of Lesser Himalayan carbonates is largely

dismissed by Galy *et al.* (1999) owing to their low [Sr^{2+}], and indeed these units make a relatively small contribution (<15%) to the Kali, Trisuli and Narayani. Such a conclusion is only valid, however, if LHF carbonate inputs are assumed to be significantly less radiogenic than those from LHF silicate. Assuming that LHF carbonates are radiogenic, the contribution to the rivers such as the Bhote Kosi, Sun Kosi and Sapt Kosi in this study is important. The contribution of carbonate to Lesser Himalayan inputs (62-71%) is likely to be more accurate in this work owing to the greater number of monolithologic tributaries included. Only one catchment draining the Nawakot Group calc-silicates was used to define the LHF endpoint of Galy *et al.* (1999).

5.7. Interpretative Summary.

The information in this chapter provides a complete picture of the inputs from the major Himalayan lithologies into the dissolved load of the sampled rivers, and by implication from the multiple regression analyses, other Himalayan rivers.

Input from the Tibetan Sedimentary Series, exemplified by the headwaters of the Bhote Kosi, is characterised by high cation, HCO_3^- and SO_4^{2-} concentrations, as evidenced by the principal components analysis correlations between concentrations of these species and the amount of TSS bedrock outcropping in catchments. Mass balance estimates reveal that, for rivers draining all of the Himalayan lithologies, the majority of Sr^{2+} results from the weathering of TSS carbonates with an $^{87}Sr/^{86}Sr$ of ~0.72. The TSS

appears to be the low $^{87}Sr/^{86}Sr$, high $[Sr^{2+}]$ endmember identified by Palmer and Edmond (1992).

Despite being characterised by low Sr^{2+} concentrations, Lesser Himalayan inputs are extremely important in the Himalayan system owing to extremely radiogenic, although highly variable, $^{87}Sr/^{86}Sr$ ratios (0.80 – 1.25). The vital influence of LHF inputs is demonstrated by the rapid elevation of dissolved $^{87}Sr/^{86}Sr$ ratios downstream of the MCT in the Bhote Kosi and the strong correlations between % LHC, %LHS and %LHtotal and $^{87}Sr/^{86}Sr$ in the principal components analyses. The multiple regression analyses for the Bhote Kosi demonstrate that the amount of Lesser Himalayan bedrock present in catchments can be used to predict dissolved $^{87}Sr/^{86}Sr$ in other Himalayan rivers.

The role of the HHCS is less clear. Characterised by low Sr^{2+} concentrations relative to the TSS and low $^{87}Sr/^{86}Sr$ ratios relative to the Lesser Himalaya, correlations between the amount of HHCS bedrock present in catchments and either $[Sr^{2+}]$ or $^{87}Sr/^{86}Sr$ are generally low or non-existent. Despite being the most prevalent bedrock lithology in terms of surface area, and occupying the most actively eroded part of the Himalayan range, the Sr contribution to major rivers from the HHCS demonstrated by mass balance is surprisingly little. These units are the major source of silicate Sr, however, in certain large rivers. In addition, data from samples in the Bhote Kosi catchment collected in September suggest a greater role for the HHCS in the monsoon.

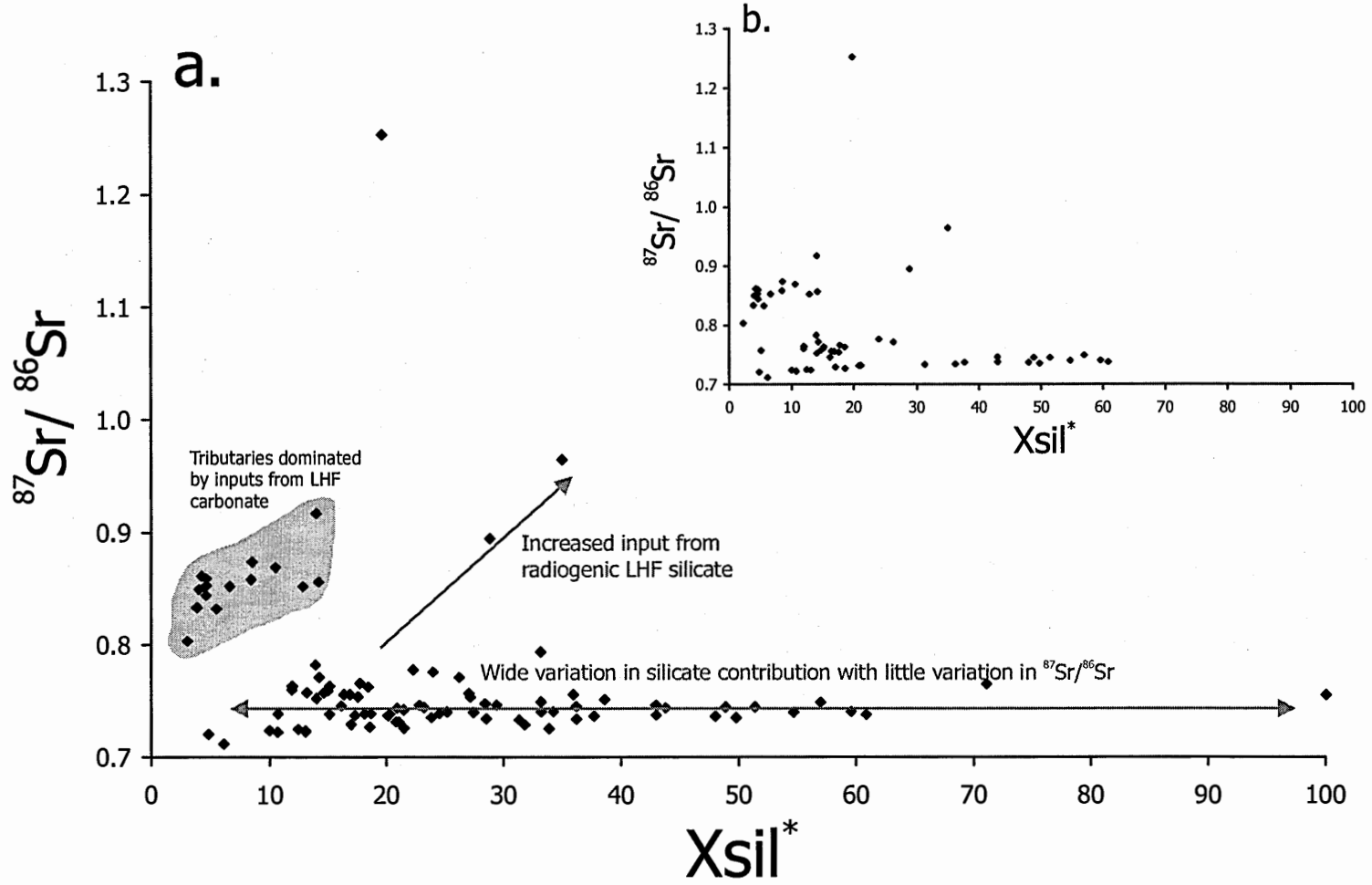

Fig. 5.28. Plots of $^{87}Sr/^{86}Sr$ vs Xsil for the complete dataset (a) and data from the Bhote Kosi only (b).

* Xsil is defined as the silicate contribution (%) to total alkalinity as defined by Blum *et al.* (1998) i.e. sum of albite, anorthite orthoclase and biotite contributions.

a.

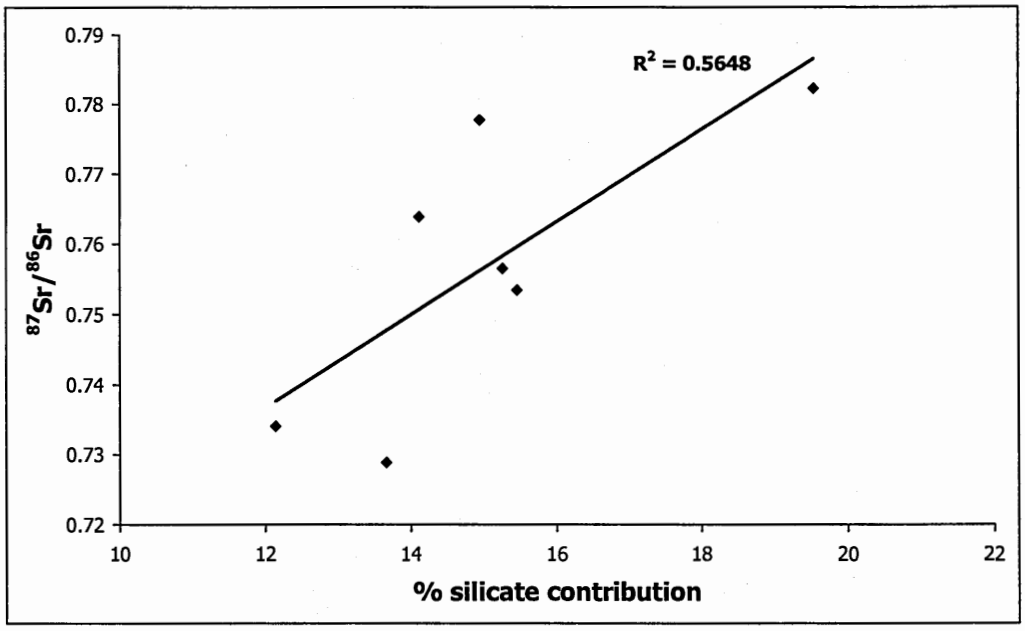

b.

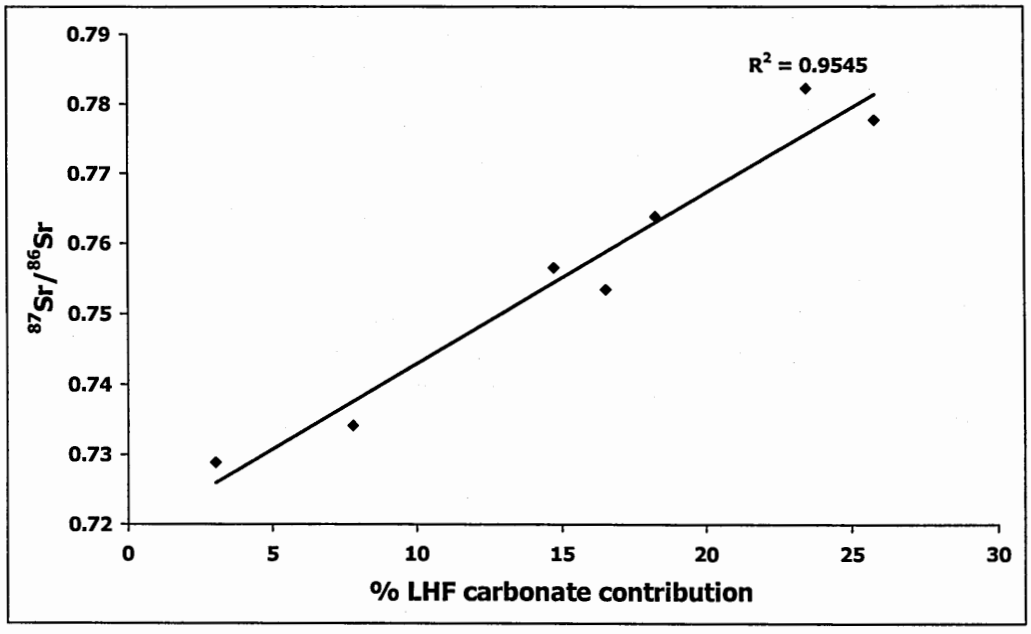

5.29. Correlation between dissolved $^{87}Sr/^{86}Sr$ ratios and % silicate (TSS, HHCS and LHF combined) (a) and % LHF carbonate (b) contributions calculated from mass balance (see section 4.6).

A minimal role for the silicate-dominated HHCS and the importance of the Lesser Himalayan carbonate inputs suggests that dissolved $^{87}Sr/^{86}Sr$ ratios in the Himalaya may in fact be a poor proxy for silicate weathering. Fig. 5.28 shows dissolved $^{87}Sr/^{86}Sr$ plotted against the silicate contribution to alkalinity (calculated as described in section 5.1.1 and referred to as Xsil on the figure). No correlation is revealed by this diagram; high $^{87}Sr/^{86}Sr$ ratios are related to the presence of Lesser Himalayan rock, regardless of it being carbonate or silicate, in catchments. The extremely radiogenic catchments draining only or predominantly the Lesser Himalaya are outlined on the diagram, while the remaining catchments include a full range of silicate contributions, from <5% to 100%, but with no correlation with $^{87}Sr/^{86}Sr$. Fig. 5.29 shows the correlation between dissolved $^{87}Sr/^{86}Sr$ ratios and the % silicate contribution to the total Sr budget as calculated for major river basins in section 5.6.8 and given in table 5.3. A positive correlation can indeed by seen ($r^2 = 0.56$) although any hope that indeed $^{87}Sr/^{86}Sr$ ratios are a silicate weathering proxy is dispelled by the far superior correlation ($r^2 = 0.95$) between $^{87}Sr/^{86}Sr$ and the % contribution from Lesser Himalayan carbonate. Fig. 5.30 shows $^{87}Sr/^{86}Sr$ ratios plotted against Xsil for catchments draining only the TSS and HHCS. A broad correlation can be seen in this case, reflecting the higher $^{87}Sr/^{86}Sr$ (0.73-0.74) of the silicate-dominated HHCS in relation to the TSS. The correlation is stronger in the Bhote Kosi dataset. Variations from this correlation possibly reflect the isotopic variability of silicate inputs, both in terms of contrasts between the TSS and HHCS silicates, and variability within the TSS and particularly the HHCS (which incorporates both substantial granite bodies and the Kathmandu Nappe in this work).

Fig. 5.30. Plots of $^{87}Sr/^{86}Sr$ vs Xsil for catchments draining only the TSS and HHCS, using the complete dataset (a) and samples from theBhote Kosi only (b).

* Xsil is defined as the silicate contribution (%) to total alkalinity as defined by Blum *et al.* (1998) i.e. sum of albite, anorthite orthoclase and biotite contributions.

From the data presented in this and the previous chapter it is apparent that there are two major factors that result in dissolved $^{87}Sr/^{86}Sr$ ratios being a poor proxy for silicate weathering:

(i). Large changes in inputs from the weathering of HHCS silicate might not be reflected in the $^{87}Sr/^{86}Sr$ record, which is largely controlled by the balance between inputs from the TSS and LHF.

(ii). According to the mass balance, approximately two-thirds of the crucial input from the Lesser Himalaya is from carbonate.

The significance of this second statement is dependent upon a crucial assumption made in the mass balance calculations of section 5.6; that the carbonate of the Lesser Himalayan calc-silicates is radiogenic. An alternative hypothesis to explain the high $^{87}Sr/^{86}Sr$ of inputs from the LHF calc-silicates is that rapid weathering of less radiogenic carbonate material results in the rapid exposure of fresh, highly radiogenic silicate material (particularly micas) to weathering. The correlations noted between $^{87}Sr/^{86}Sr$ and K^+ and Rb^+ concentrations, in addition to the high $K^+/(Na^+ + K^+)$ ratios of the LHF calc-silicate tributaries, argue in favour of this scenario. It is assumed that the carbonate material of the LHF calc-silicates must be radiogenic to some extent, as if it were not so, unrealistically high $^{87}Sr/^{86}Sr$ values would be required from the silicate portion of the calc-silicates to explain the highly radiogenic values noted in the LHF calc-silicate draining tributaries of the Bhote Kosi and Langtang Khola-Trisuli. The extent of $^{87}Sr/^{86}Sr$ enrichment in the carbonate of these rocks is unclear, and needs to be ascertained in order to validate the interpretations made in this chapter.

Chapter 6

Bedload Chemistry.

This chapter provides an overview of the downstream changes in strontium, rubidium and neodymium chemistry in bedload samples collected from the Bhote Kosi and Langtang Khola – Trisuli. Bedload chemistry reveals the nature of the material that is not entering the dissolved phase, and therefore a comparison of bedload and bedrock chemistry will provide further information of what is entering the dissolved load in different river sections. Additionally, the Nd-isotopic composition of bedload can be examined to reveal inputs from the Lesser Himalaya, which has a ε_{Nd} (typically less than –20) distinct from that of the Tibetan Sedimentary Series and High Himalayan Crystalline Series (typically between –15 and – 20, see fig. 6.1). Priority in this study was given to analysis of water and bedrock samples, and thus the bedload dataset is comparatively sparse, comprising full elemental and isotopic analyses only for samples collected in 1998, supplemented by a selection of major and trace element XRF analyses from 1999 (see appendix B). Examination of bedload data still reveals some interesting trends, particularly when used in conjunction with the dataset for the Bhote Kosi of Harris *et al.* (1998), collected in October 1995. This earlier study provides details for the upper reaches of the river, whereas the sampling and analysis of bedload in this chapter

focuses downstream of the Main Central Thrust, where the crucial changes in dissolved strontium chemistry take place.

6.1. Changes in the Bedload Chemistry of the Bhote Kosi.

This section describes the downstream changes in the Bhote Kosi in 1998, incorporating data from samples collected between September and November. Some final comments are made with regard to possible seasonal variability using the limited analyses of September and dry season 1999 samples.

6.1.1. Changes Upstream of the Main Central Thrust.

Based on the data of Harris *et al.* (1998), bedload $^{87}Sr/^{86}Sr$ in the TSS section of the river varies from 0.720 to 0.733 (fig. 6.1), broadly maintaining a proportional relationship with Rb concentrations which vary between 98 and 128 ppm, and an inversely proportional relationship with Sr concentrations, which range between 122 to 184 ppm. Leachate analyses reveal carbonate bedload material to be less radiogenic than average ($^{87}Sr/^{86}Sr$ = 0.712-0.717), comparable with TSS carbonate and calc-silicate whole rock (see table C1 and fig. 1.12a).

Downstream of the South Tibetan Detachment System a marked increase in $^{87}Sr/^{86}Sr$ was observed by Harris *et al.* (1998), from 0.733 to 0.755 at the MCT, with no clear trend in Rb or Sr concentrations. Leachate $^{87}Sr/^{86}Sr$ remains relatively unradiogenic

(~0.725), although a ratio of 0.762 is recorded immediately upstream of the MCT. This suggests the presence of radiogenic carbonate in the HHCS of the Bhote Kosi, although none was found in this study (table C2). The only bedload sample obtained for this study from upstream of the MCT in the Bhote Kosi (BKT4), collected 10 km downstream of the STDS in 1998, is reasonably consistent with the findings of Harris *et al.* (1998), with a Sr-isotope ratio of 0.725 coupled with relatively high concentrations of both Sr (214 ppm) and Rb (174 ppm). Nd-isotope data from Harris *et al.* (1998) shows an increase in ε_{Nd} between the STDS (-16.8) and the MCT (-15) (fig. 6.1). Sample BKT4 records a ε_{Nd} value of –18.6, incongruous with findings of this previous study, although more consistent with observed Nd-isotope values for the HHCS bedrock (~ -18 to –22 in the Bhote Kosi, see fig. 7.1).

6.1.2. Changes in the Lesser Himalayan Formation.

Assuming a Sr-isotope ratio of 0.755 at the MCT (i.e. that of Harris *et al.*, 1998), the Bhote Kosi bedload undergoes an increase in $^{87}Sr/^{86}Sr$ within the Lesser Himalayan calc-silicates of an even greater magnitude than that seen in the dissolved load (fig. 6.1), reaching 0.828 at the boundary between the Nawakot Group and the Kuncha Group. Assuming Sr and Rb concentrations of 118 and 97 ppm respectively at the MCT (again from Harris *et al.*, 1998), this section of the river is also marked by a decrease in Sr concentration (to 64 ppm) and an increase in Rb (to 115 ppm) (fig. 6.1 and fig. 6.2). Changes in Nd-isotope ratios are equally as marked, with a substantial decrease to a ε_{Nd}

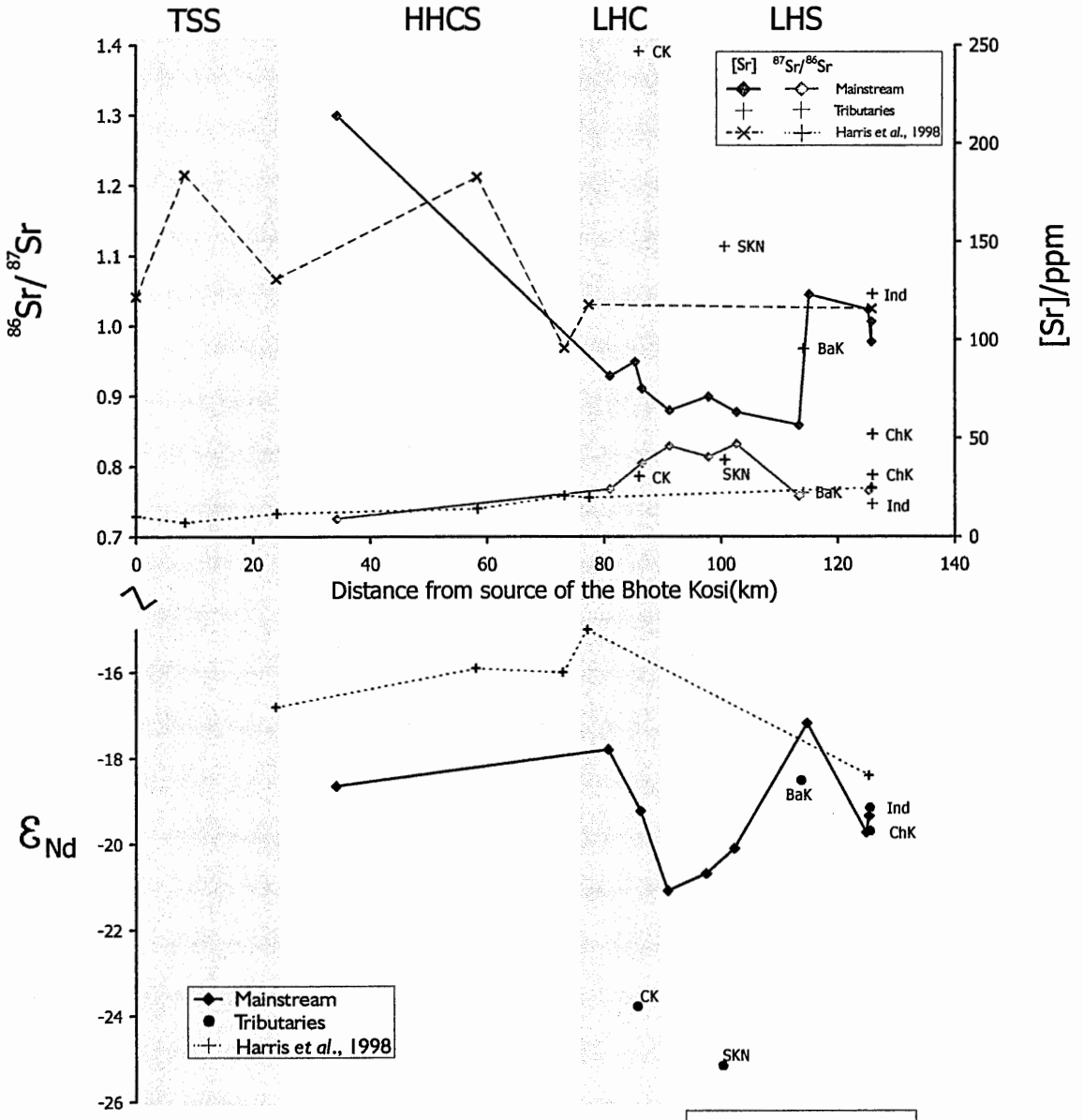

Fig. 6.1. Downstream variation in the $^{87}Sr/^{86}Sr$, strontium concentration and ε_{Nd} in the Bhote Kosi.
Tributaries are shown at the point of entry into the mainstream.

Tributaries;
Chaku Khola (CK)
Sun Kosi Nadi (SKN)
Balephi Khola (BaK)
Indrawati (Ind)
Chak Khola (ChK)

of –21.1 at the point where the main river leaves the Nawakot Group calc-silicates. This confirms the high level of Lesser Himalayan input to this section of the river.

The impact of the Lesser Himalayan Kuncha Group silicates is less easy to decipher owing to significant changes that result from the input of the Balephi Khola. In the section of the Bhote Kosi between the boundary of the Nawakot Group and Kuncha Group, and the confluence of the Bhote Kosi and Balephi Khola, little change in bedload Sr chemistry is observed. $^{87}Sr/^{86}Sr$ remains at ~0.8 with an Sr concentration of ~60 ppm. ε_{Nd} increases slightly, with a value of –20.1 observed immediately upstream of the Balephi Khola confluence.

Bedload inputs from the Lesser Himalaya can be gauged from analysis of bedload from the Sun Kosi Nadi, a tributary catchment of which comprises >90% LHF. The bedload of the Sun Kosi Nadi is extremely radiogenic ($^{87}Sr/^{86}Sr$ = 1.11) and has a low Sr concentration (39 ppm). A ε_{Nd} value of –25.2 is consistent with Lesser Himalayan bedrock (fig. 7.1). The Chaku Khola was also found to have a low Nd-isotope ratio ($^{\varepsilon}Nd$ = -23.8) suggesting that the bedload of this river is also dominated by the Lesser Himalaya (although the LHF comprises only 43% of catchment bedrock). The Chaku Khola has a similar bedload strontium chemistry to the Sun Kosi Nadi (30 ppm of Sr with $^{87}Sr/^{86}Sr$ = 1.39).

6.1.3. Input from the Balephi Khola.

The Balephi Khola, the largest tributary of the Bhote Kosi, has a far more profound effect on bedload strontium chemistry than it does upon dissolved Sr, possibly indicative of a high physical chemical weathering ratio, as might be expected from a river which has a very high specific discharge relative to streamflow (fig. 2.9). Downstream of the confluence between the two rivers bedload $^{87}Sr/^{86}Sr$ drops to 0.757 while the Sr concentration increases to 123 ppm (both values comparable to those recorded by Harris *et al.*, 1998 at the MCT). A drop in ε_{Nd} (to –17.2) confirms that these changes are the result of inputs from the HHCS, the predominant lithology of the Balephi Khola. It is noted, however, that the HHCS signature (both in terms of $^{87}Sr/^{86}Sr$ and ε_{Nd}) of the Bhote Kosi downstream of the confluence with the Balephi Khola is more pronounced than that of the Balephi Khola itself. This is most likely a result of incomplete bedload mixing, a potential problem when collecting material without the use of sediment traps.

Further downstream in the Bhote Kosi, towards Dolalghat, the Sr-isotope ratio of the bedload increases again, accompanied by a decrease in ε_{Nd}, reflecting further input from the Lesser Himalaya. A bedload sample collected immediately upstream of the confluence of the Bhote Kosi with the Indrawati has 115 ppm of Sr with an $^{87}Sr/^{86}Sr$ of 0.765, a Rb concentration of 109 ppm and a ε_{Nd} of –19.7. These values are almost identical to those of Harris *et al.* (1998), collected from a similar location in October 1995 (with the exception of a lower ε_{Nd} of –18.4 in this earlier study).

6.1.4. Inputs from the Indrawati and Chak Khola.

The Chak Khola and Indrawati, like the Balephi Khola and Bhote Kosi, have a bedload strontium chemistry that reflects the amount of Lesser Himalayan bedrock in their respective catchments. The Chak Khola, draining a greater proportion of LHF bedrock (35% compared with 16% in the Indrawati), has a bedload that is both more radiogenic ($^{87}Sr/^{86}Sr$ = 0.787) but with less total Sr (52 ppm) when compared with the Indrawati (123 ppm, $^{87}Sr/^{86}Sr$ = 0.747). Rb concentrations are approximately equal (~140 ppm) in both rivers. Despite being a considerably smaller river, the Chak Khola appears to have the dominant effect on the bedload of the Bhote Kosi. The bedload of the Sun Kosi downstream of the confluence between the Bhote Kosi, Chak Khola and Indrawati contains less strontium (109 ppm) than that of the Bhote Kosi or Indrawati, with a more radiogenic isotope ratio (0.768). ε_{Nd} increases slightly, from –19.7 to –19.3, between the downstream site of the Bhote Kosi (BK35) and the upper Sun Kosi sample (BK39).

6.1.5. Seasonal Variations in Bedload Chemistry.

In the Lesser Himalaya, the pattern of decreasing Sr concentration is common to both 1998 and 1999, and September and dry season, data, with low Sr concentrations marking tributaries draining the LHF units regardless of the time of collection (fig. 6.2). In the absence of isotopic data for 1999, it can only be assumed that the $^{87}Sr/^{86}Sr$ of these tributaries would be consistently high. The impact of the Balephi Khola is far more pronounced in the dry season, perhaps merely reflecting poor sediment mixing as cited

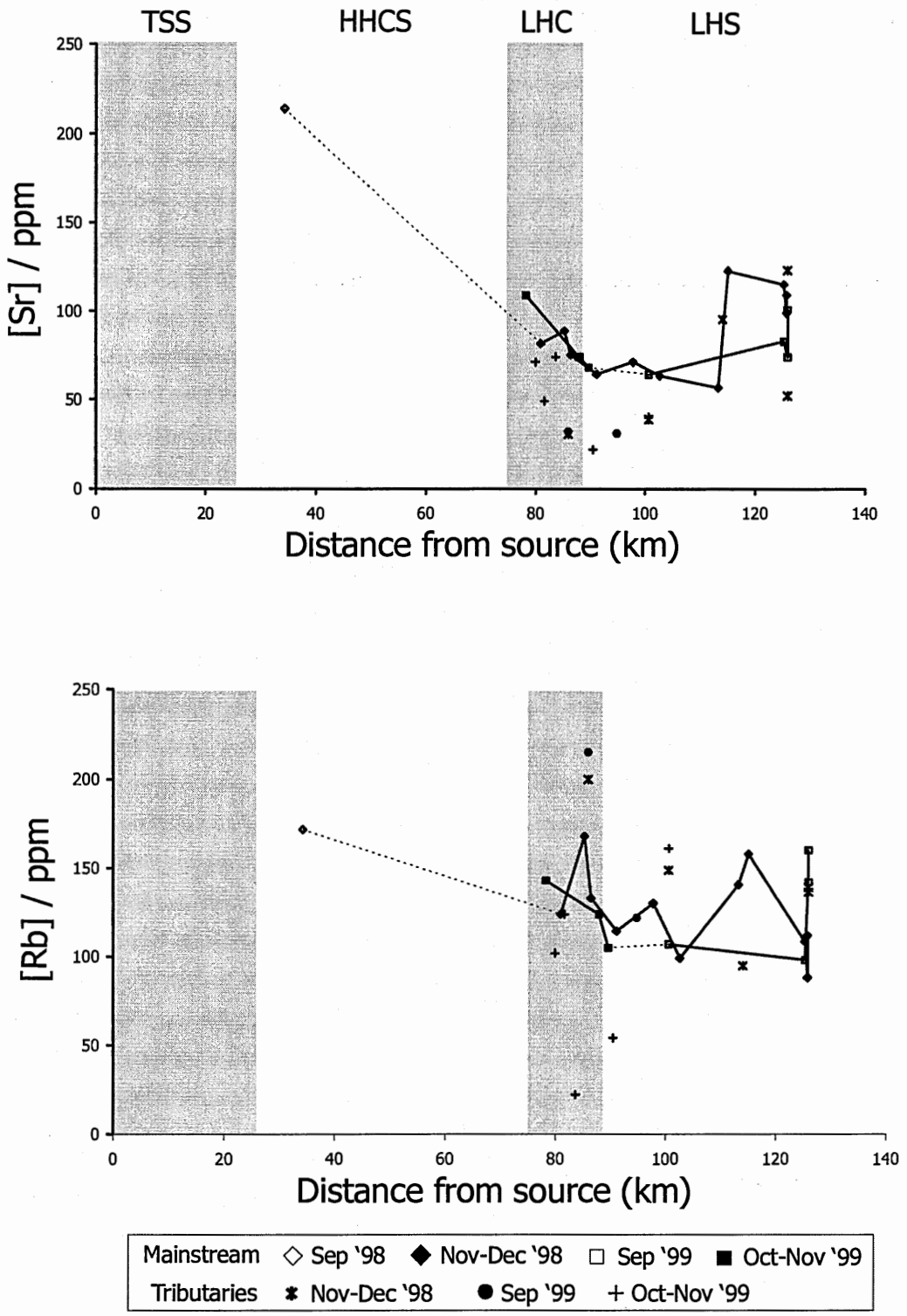

Fig. 6.2. Downstream variations in strontium and rubidium concentration in the bedload of the Bhote Kosi.

above, while the impact of the Indrawati and Chak Khola noted above for the dry season (1998) is apparently reversed in the September 1999 dataset. Increased concentrations of both Sr and Rb downstream of the tri-confluence possibly reflect a greater input from the Indrawati in September.

6.2. Bedload Chemistry of the Langtang Khola – Trisuli.

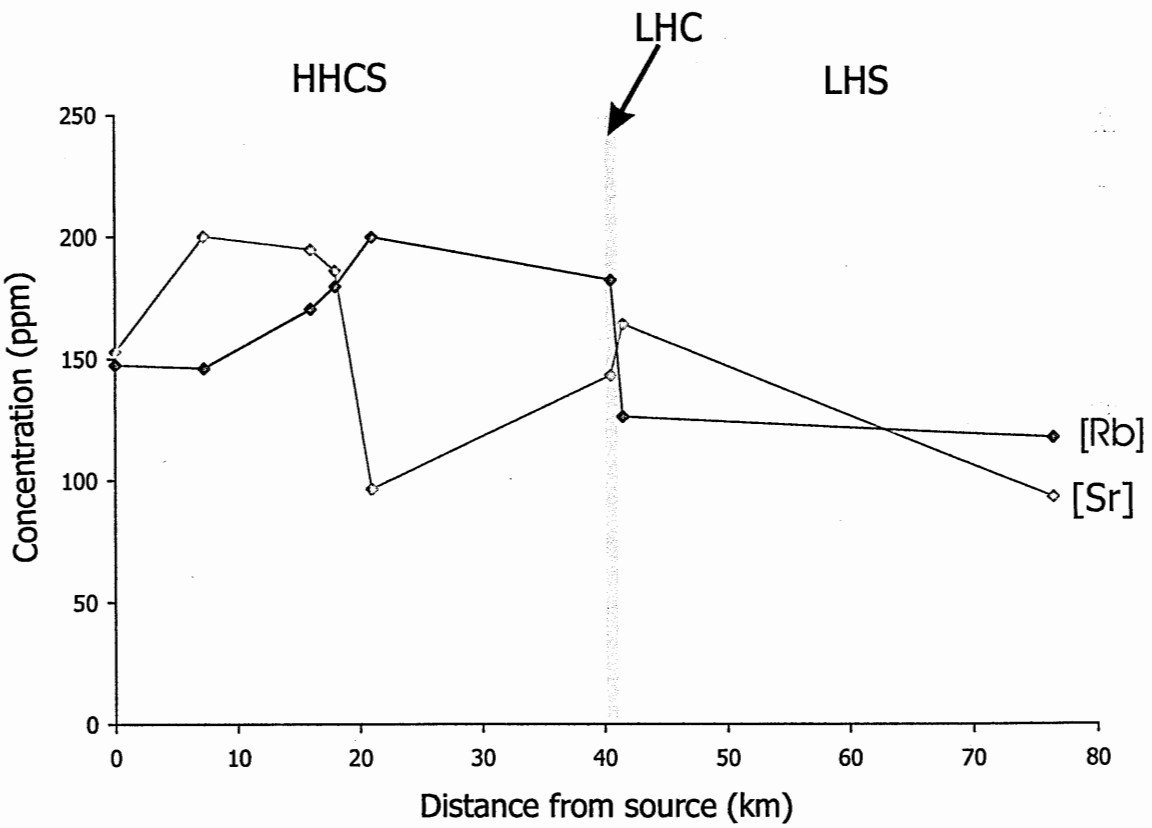

Fig. 6.3. Downstream changes in strontium and rubidium concentrations in the Langtang Khola - Trisuli.

Lacking isotopic data, the Langtang Khola – Trisuli dataset reveals only limited information (fig. 6.3). Patterns previously noted in the Sr and Rb concentrations of the

dissolved load of this river are reproduced in the bedload. The river section from the Langtang Glacier downstream to the MCT is marked by increasing Rb (from ~150 ppm to ~200 ppm), coupled with decreasing Sr (~250 ppm to ~150 ppm in 1999, as low as ~100 ppm in 1998). Input from the Bhote Kosi (Langtang) causes an increase in Sr and a slight decrease in Rb, while in the Lesser Himalaya Sr concentrations decline (to 93 ppm) with little change in Rb noted.

6.3. Interpretation of Bedload Data.

Bedload is dominated almost entirely by silicate material as shown in fig. 6.4, appreciable carbonate material being present only in samples BKT4 (10 km downstream of the STDS) and samples BK82 and BK90 (tributaries draining the Nawakot Group calc-silicates). In terms of strontium chemistry, this silicate material follows similar trends to those noted for the dissolved load (see fig. 5.6).

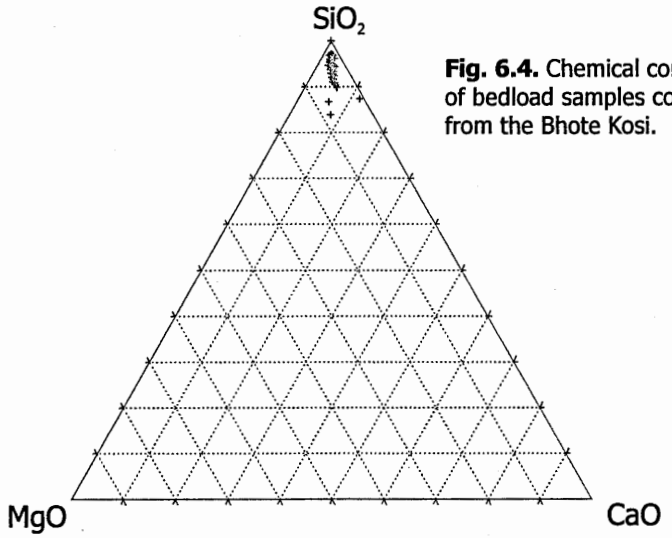

Fig. 6.4. Chemical composition of bedload samples collected from the Bhote Kosi.

In the HHCS $^{87}Sr/^{86}Sr$ increases downstream, although the increase of this ratio in the bedload is of a greater magnitude than in the dissolved load. This reflects the radiogenic nature of the HHCS silicate material ($^{87}Sr/^{86}Sr$ of HHCS silicate bedrock can be > 1, see fig. 1.12a). The lower impact of the HHCS on the dissolved load is likely to be due to the fact that much of this material is highly resistant to chemical weathering. Indeed, material from the HHCS predominates in the suspended load of Himalayan rivers (Derry and France-Lanord, 1996a). Additionally, the isotopic impact of the HHCS on the dissolved load of the Bhote Kosi is likely to be moderated by the rapid dissolution of relatively unradiogneic, Sr-rich carbonates, the presence of which is confirmed in this and other studies (see sections 6.1 and 6.2, table C2 and fig. 1.12a) and which are known to make a significant contribution to the HHCS dissolved input (see section 5.6.8). The impact of the HHCS upon bedload chemistry is further demonstrated by the major impact of the Balephi Khola on the bedload of the Bhote Kosi, although the effect in this case is to cause a fall in the Sr-isotope ratio.

The Bhote Kosi bedload data of this study has been of great use in filling the gap left by the previous work of Harris *et al.* (1998). These authors sampled up to the MCT and then subsequently at Dolalghat, recording only a modest increase in bedload $^{87}Sr/^{86}Sr$, and thus assuming that the most significant changes in bedload strontium chemistry occurred in the HHCS. With an expanded dataset it can now be seen that bedload $^{87}Sr/^{86}Sr$ increases with equal rapidity in the upper part of the Lesser Himalaya, and Nd-isotope analyses reveal that this is principally the result of input from the LHF rather than continued weathering of HHCS bedload. An increase in $^{87}Sr/^{86}Sr$ is also observed

(from 0.717 to 0.753) in the bedload of the Seti Khola as it crosses the Lesser Himalaya (English *et al.*, 2001). The radiogenic nature of Lesser Himalayan input to bedload is affirmed by samples collected from the Chaku Khola and Sun Kosi Nadi, which have very low ε_{Nd} coupled with extremely high $^{87}Sr/^{86}Sr$. The rapidity of the increase in the Bhote Kosi indicates that levels of physical erosion remain high in the upper part of the Lesser Himalaya section of the river, as indicated by the nature of the river at this point; deep and relatively narrow flowing through steep gorges. Much less so than the dissolved load, the bedload Sr-isotope ratio of the Bhote Kosi is strongly influenced by inputs (largely HHCS) from the Balephi Khola, causing a decease in $^{87}Sr/^{86}Sr$ and increase in ε_{Nd}, accounting for the moderate rise in $^{87}Sr/^{86}Sr$ described by Harris *et al.* (1998) between the MCT and Dolalghat.

With a larger dataset, it might be possible to determine endpoints for the TSS, HHCS and LHF in $^{87}Sr/^{86}Sr$ vs ε_{Nd} space. With the limited data available in this study, and the wide range of both Sr and Nd-isotope values of all three of the major Himalayan lithologies (fig. 6.5), this is a difficult proposition. An approximation of the contribution of the LHF to bedload can be made, however, assuming that the combined bedload input of the TSS and HHCS into the Bhote Kosi has an ε_{Nd} of –15 and $^{87}Sr/^{86}Sr$ of 0.755 (the MCT sample of Harris *et al.*, 1998 and close to the values of 0.75 and –16 used by Derry and France-Lanord, 1996a for their study of the sediments of the Bengal Fan), and that input from the LHF has an ε_{Nd} of –25 and $^{87}Sr/^{86}Sr$ of 1.11 (the sample from the Sun Kosi Nadi; again similar to values are used by Derry and France-Lanord, 1996a). A simple mixing calculation shows an increasing contribution from the LHF throughout

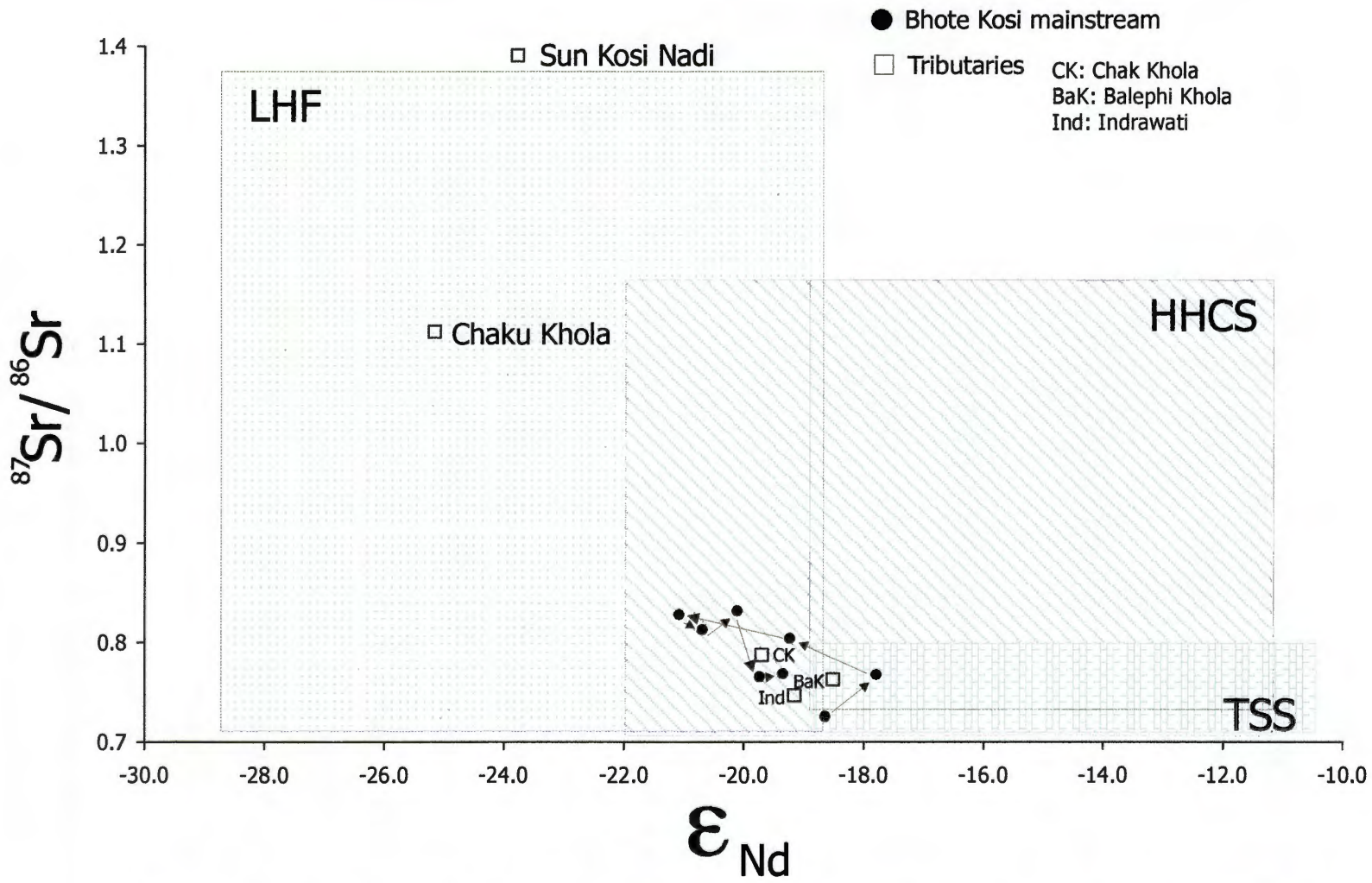

Fig. 6.5. $^{87}Sr/^{86}Sr$ vs ε_{Nd} for bedload samples analysed from the Bhote Kosi.
TSS, HHCS and LHF ranges are defined by the data of Deniel *et al.*, 1987; Ayres, 1997; France-Lanord *et al.*, 1993; Inger and Harris, 1993; Massey, 1994; Parrish and Hodges, 1996; Harris et al., 1998; Prince, 1999; Ahmad *et al.*, 2000; Miller *et al.*, 2001 and White *et al.*, 2002.

the Nawakot Group section of the Bhote Kosi, with the LHF accounting for 61% of Nd (ε_{Nd} = -21.1) and 21% of Sr ($^{87}Sr/^{86}Sr$ = 0.828) at the boundary between the Nawakot Group and Kuncha Group. At Dolalghat, the LHF accounts for 47% of Nd ($^{\varepsilon}Nd$ = -19.7) but a mere 3% of Sr ($^{87}Sr/^{86}Sr$ = 0.765).

From this brief study of bedload in the Bhote Kosi the following can be concluded;

(i). Downstream of the MCT, bedload samples comprise almost exclusively silicate material, suggesting that all carbonate has entered the dissolved load.

(ii). The High Himalayan Crystalline Series contributes a far greater proportion of the material comprising the bedload phase in comparison with the dissolved phase. This reflects not only the high mechanical erosion within the HHCS, but also the status of the HHCS as the predominant silicate lithology (in terms of catchment coverage) in the Bhote Kosi, a situation analogous to that of the entire Himalaya (Derry and France-Lanord, 1996a).

(iii). Strontium chemistry in the bedload of the Bhote Kosi, on crossing the Lesser Himalayan calc-silicates, shows a pattern similar to that for the dissolved load; i.e. it is marked by increasing $^{87}Sr/^{86}Sr$ coupled with decreasing Sr concentrations. Nd-isotope analysis confirms that this change is due to Lesser Himalayan rather than to dissolution of bedload material originating upstream.

(iv). Bedload in tributaries draining the Nawakot Group consists of extremely radiogenic ($^{87}Sr/^{86}Sr$ >1.1) silicate material providing an upper limit for the Sr-isotopic ratio of the silicate component of the Lesser Himalayan calc-silicates.

Chapter 7

Bedrock Chemistry.

This chapter presents an analysis of the mineralogy and chemical composition of bedrock samples collected from the Bhote Kosi valley. Carbonates, silicates and calc-silicates are described in turn. The primary focus of the chapter is on the contrasts between the rocks of the Lesser Himalaya and those of the Tibetan Sedimentary Series and High Himalayan Crystalline Series, and how these differences might explain the observed impact of the Lesser Himalaya upon the dissolved strontium chemistry of the Bhote Kosi.

Several traverses were obtained from various parts of the Nawakot Group, and although these proved to be of less use than was initially hoped, owing largely to the difficulty of identifying calc-silicates in the field, the results of analysis of two of these are described. In the final part of the chapter, we present the first laser ablation MC-ICP-MS analyses of carbonate material from Himalayan (LHF and HHCS) calc-silicates.

Fig. 7.1. shows a εNd vs $^{87}Sr/^{86}Sr$ plot for samples collected for this study from the Bhote Kosi catchment (Nd isotopic analysis was not undertaken for all samples described in this chapter). In most cases the Bhote Kosi samples fall within the zones

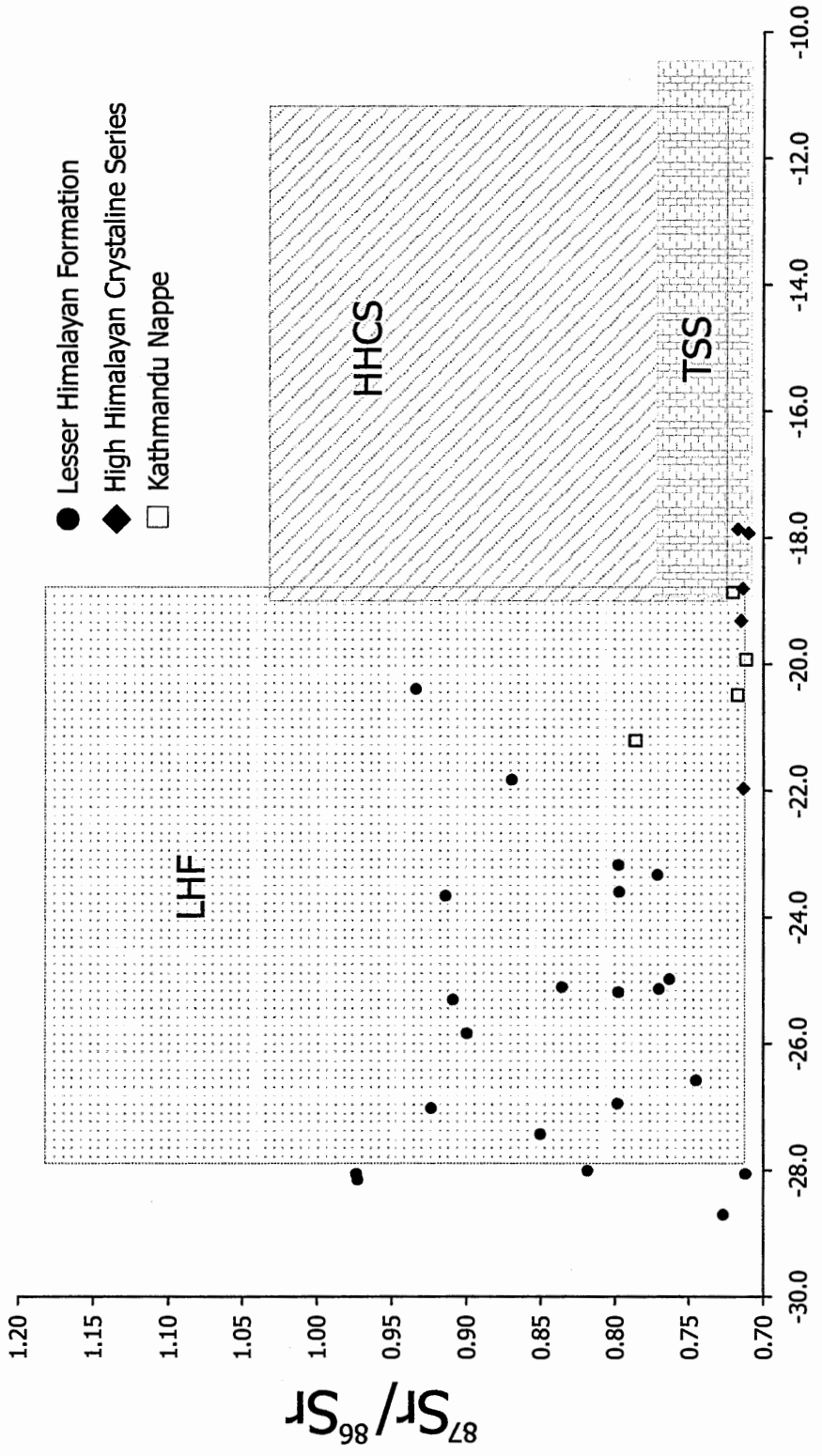

Fig. 7.1. $^{87}Sr/^{86}Sr$ vs ε_{Nd} for bedrock samples analysed from the Bhote Kosi.
TSS, HHCS and LHF ranges are defined by the data of Deniel *et al.*, 1987; Ayres, 1997; France-Lanord *et al.*, 1993; Inger and Harris, 1993; Massey, 1994; Parrish and Hodges, 1996; Harris *et al.*, 1998; Prince, 1999; Ahmad *et al.*, 2000; Miller *et al.*, 2001 and White *et al.*, 2002.

defined by previous Himalayan bedrock studies, although in both the HHCS and Lesser Himalaya certain samples have ε_{Nd} values lower than those previously recorded (as low as –22 in the HHCS, -29 in the LHF). This may be because some of the samples analysed were calc-silicates, in which secondary processes might have altered isotopic compositions. There is little doubt that we have placed the samples into the right geological groupings, however, as the STDS and MCT are reasonably well defined and mapped in the Bhote Kosi valley. Rocks from the Kathmandu Nappe have $^{\varepsilon}$Nd values (-19 to –22) that fall between those of the TSS / HHCS and LHF. This supports the hypothesis of Upreti and Le Fort (1999) that the Kathmandu Nappe represents an intermediate zone of deposition between the TSS and LHF, although again a number of calc-silicates are included.

7.1. Carbonates.

Two samples from the Tibetan Sedimentary series were clearly identifiable (>95% CaO) as pure carbonates on a SiO_2-MgO-CaO plot (fig. 6.2). Sample T17 is a micritic limestone (see table C1) with extensive sparry calcite veining, while sample T18 is a coarse (~1 mm) poorly sorted biosparite (incorporating largely bivalve and gastropod fragments). Both samples have what might be described as a "typical" carbonate composition, comprising >98% calcite with abundant strontium (~250 ppm, although this is relatively low for carbonate of the TSS, see fig. 1.12b) and very little Rb (<4 ppm). Sample T17 was selected for isotopic analysis and was found to have an $^{87}Sr/^{86}Sr$ of 0.708, a typical value for TSS carbonate (fig. 1.12a), also giving an expectedly low $^{87}Rb/^{86}Sr$ of 0.048.

A selection of marbles were collected from sample site T29 in Formation II of the High Himalayan Crystalline Series. Of these, only one sample (T29c) was considered to have sufficient purity (plotting separately from the calc-silicates in fig. 7.2) to be considered a reasonable approximation of carbonate composition in the HHCS. This sample is a coarse-grained (1-2 mm) marble comprising >90% calcite in thin section. Dispersed evenly amongst the calcite crystals are fine (0.02 - 0.5 mm) crystals of rounded quartz, pyroxene, biotite, plagioclase and opaque iron oxides. Sample T29c contains the highest concentrations of Sr of any sample analysed for this study (>1000 ppm) although substantial Rb is also present (56 ppm) owing most likely to the presence of the occasional biotites. Isotopic analysis of the sample yields an $^{87}Sr/^{86}Sr$ of 0.710, in agreement with previous work (fig. 1.12a), and an $^{87}Rb/^{86}Sr$ of 0.151 is calculated.

Carbonates collected from the Lesser Himalaya are limestones and form a distinct group from the more numerous calc-silicate lithologies (carbonates have <25% SiO_2, calc-silciates >25% in fig. 7.2). Sample BK13a and samples BK127c-f are from the same location within the schist, phyllite, quartzite and carbonate intercalations of the Dandgaon Phyllites and Nourpul Formation (the two units are indistinguishable in the field). The samples are all extremely fine grained and concentric layering is observed in both hand specimen and thin section, giving the samples the appearance of stromatolites (the presence of stromatolitic limestone in the Nawakot Group is noted by Stöcklin, 1980). Carbonaceous material is also present. XRF analysis (table C3) suggests that impurities within these samples are minimal e.g. low Rb values of 1-9 ppm. As has been demonstrated elsewhere in the Himalaya (fig. 1.12a and b), these limestones are characterised by relatively low levels of strontium (37-49 ppm),

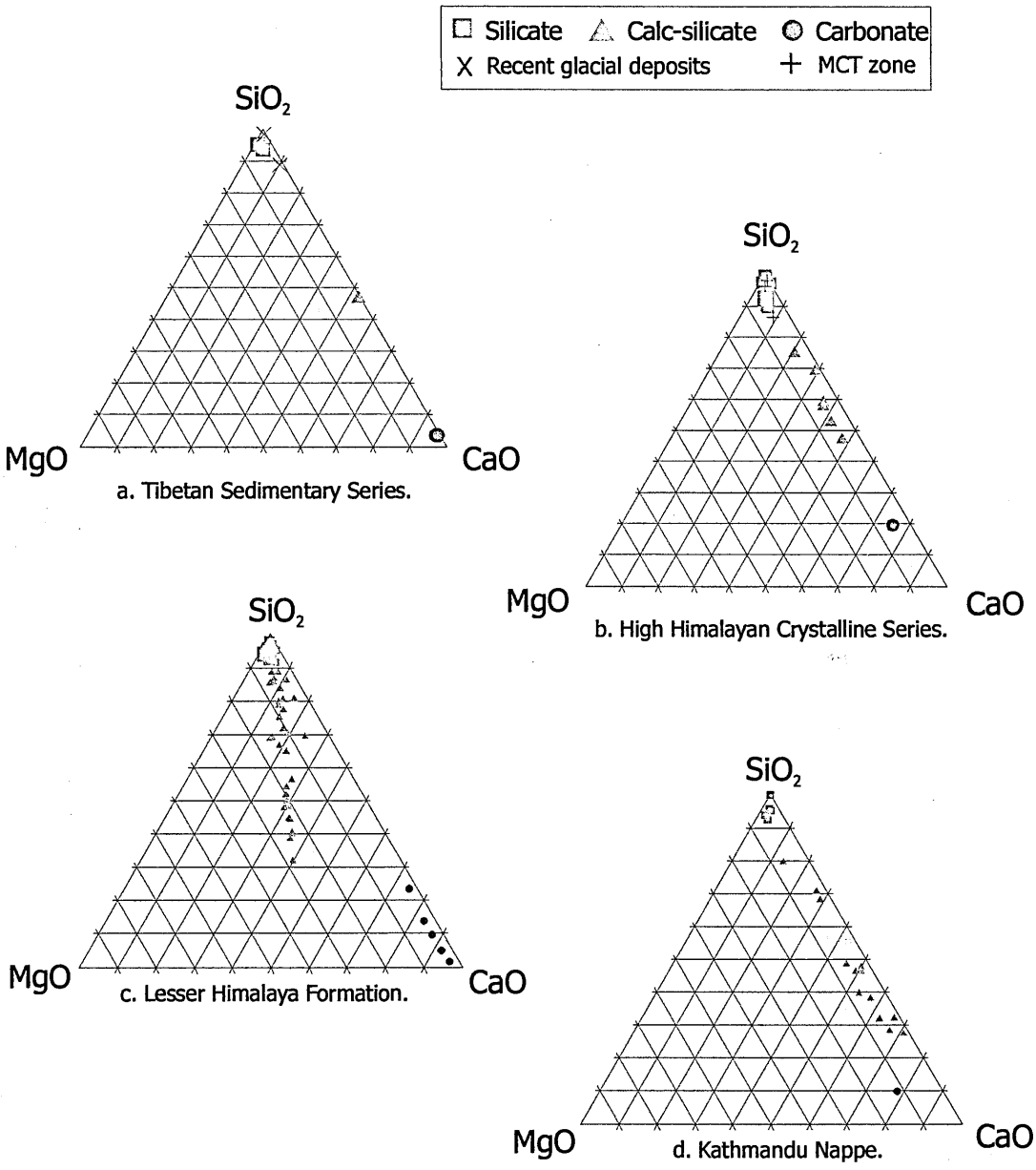

Fig. 7.2. Triangular plots showing the chemical composition of bedrock samples collected from the Bhote Kosi valley.

but are unusually radiogenic, with $^{87}Sr/^{86}Sr$ of 0.797-0.798 despite an $^{87}Rb/^{86}Sr$ of <1. BK16, the remaining carbonate sample, is from the Malekhu Limestone, although the massive limestone units described by Stöcklin and Bhattarai (1980) were not found outcropping in this study. BK16 appears to be a pure carbonate in thin section, XRF analysis revealing that quartz is also likely to be present (SiO_2 =

14%), possibly as a cement. The Rb and Sr concentrations of BK16 are approximately equal (~ 35 ppm), while the Sr-isotopic ratio is even more radiogenic than that of the stromatolitic samples (0.973).

Several marble samples from the Kathmandu Nappe (the Bhainsedobhan Marble) were collected from the small Everest Quarry, which lies beside a tributary of the Chak Khola (locality BK53 / BK105). Only one of these samples (BK53b) was of sufficient purity to be regarded as a carbonate rather than a calc-silicate (plotting separately on fig. 7.2), with modal analysis of the thin section revealing >90% calcite, forming subhedral medium-coarse crystals (0.2 mm). Small amounts of other minerals are present, including quartz, biotite (possibly phlogopite) and iron oxides, which are evenly dispersed amongst the calcite crystals, although mica banding is noted in calc-silicate samples from the same site. The amount of mica present in BK53b is small, as is reflected in the low Rb (11 ppm) and high Sr (217 ppm) of the rock. BK53b is moderately radiogenic, with an $^{87}Sr/^{86}Sr$ of 0.712 and $^{87}Rb/^{86}Sr$ of 0.144, very similar to T29c from the HHCS.

In fig. 7.3 mean chemical data for carbonates (but not calc-silicates) of the HHCS, LHF and Kathmandu Nappe are normalised to the mean TSS value in order to provide a graphic comparison of the different Himalayan units. In the case of the HHCS and Kathmandu Nappe only single samples are available, but these provide the closest approximation of the carbonate components of more abundant associated calc-silicates, being identical in appearance and composition with the exception of a lower abundance of silicate minerals. The carbonates of the HHCS, LHF and

(i).

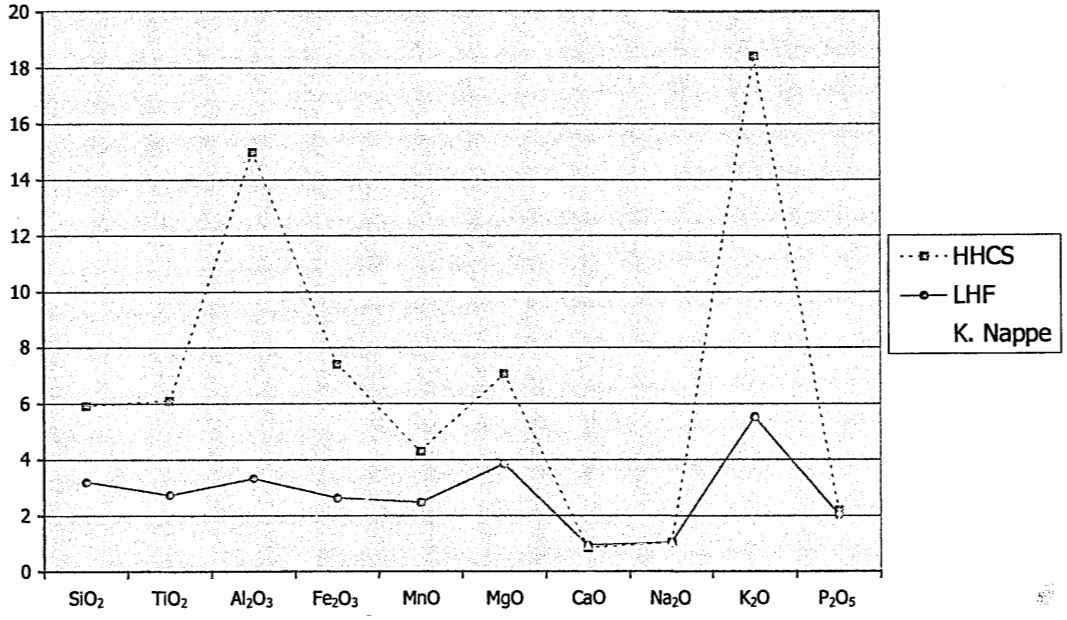

(ii).

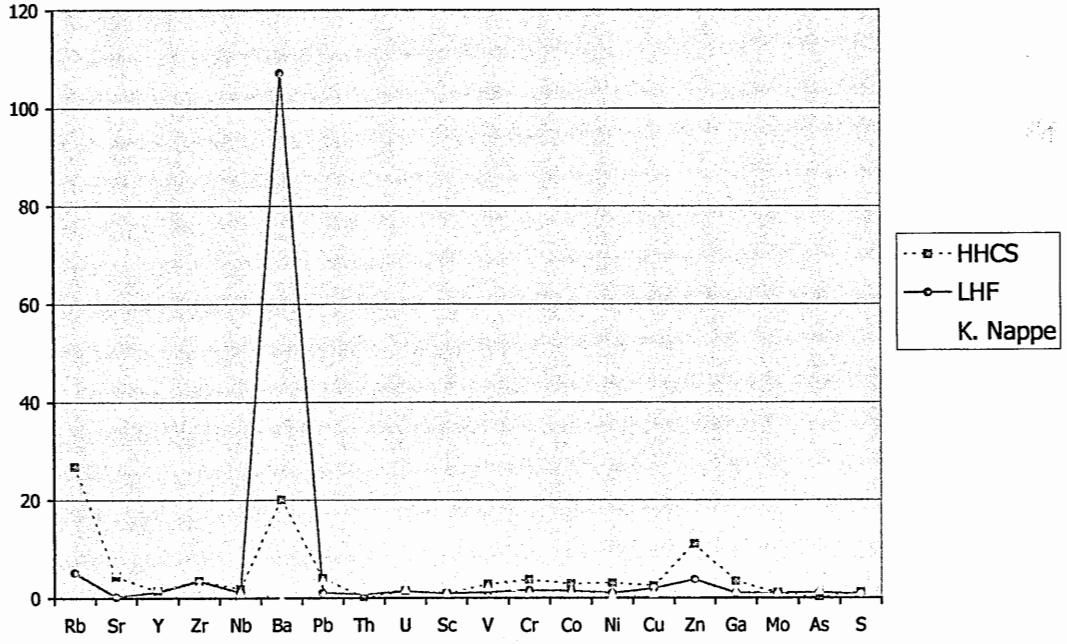

Fig. 7.3. Mean carbonate major (i) and trace (ii) element compositions for the HHCS, LHF and Kathmandu Nappe in the Bhote Kosi catchment normalised to mean Bhote Kosi TSS carbonate composition.

Kathmandu Nappe are enriched in all the major elements (relative to TSS carbonate) except calcium and sodium, reflecting the slight impurities in these units. The carbonate from the Kathmandu Nappe appears to be the purest, that from the HHCS the most impure, consistent with visual observations. T29c shows a tenfold enrichment in aluminium and potassium, whilst the LHF carbonates also contain appreciable potassium (> 5 times that of the TSS). All three units are enriched in the majority of trace elements, again as would be expected as a result of the slight silicate impurities in the carbonate material. The Lesser Himalaya is marked by major depletion in strontium coupled with extreme enrichment in barium (more than 100 greater than in the TSS), with less extreme enrichment in rubidium, zirconium and zinc. The HHCS sample is also marked by enrichment in Ba, Rb, Zr and Zn (in addition to other elements), although the Ba enrichment is not as great as that observed in the Lesser Himalaya, while considerable strontium enrichment is observed, in marked contrast to the carbonate of the LHF. The sample from the Kathmandu Nappe is enriched in Sr but not Rb, and contains no Ba at all.

7.2. Silicates.

Two samples with a silicate composition (clearly defined on the SiO_2-MgO-CaO plot with >90% SiO_2) were collected from the Tibetan Sedimentary Series (T19 and T23, see table C1). Both are mudstones largely composed of quartz fragments in a fine matrix of quartz and iron oxide. Occasional larger feldspar grains are additionally observed in sample T19. Strontium and rubidium chemistry is inconsistent. Sample T23 contains 160 ppm Rb and 94 ppm Sr with an $^{87}Sr/^{86}Sr$ of 0.752 and $^{87}Rb/^{86}Sr$ of

4.927. T19 was not analysed for Sr-isotopes but is likely to be less radiogenic, having a low Rb/Sr of 0.3 (Rb = 70 ppm, Sr = 243 ppm).

Silicate rocks (again clearly defined on fig. 7.2 with >90% SiO_2) collected from the HHCS comprised mostly gneisses and schists, all metamorphosed to biotite or garnet grade, with staurolite present in schist sample BK1 collected close to the MCT at Kodari, and sillimanite in a mica schist collected 9 km south of the STDS (sample T27b). Intrusive tourmaline granite and associated migmatites were also sampled. Rb concentrations in these samples range from 60 to 465 ppm, Sr from 21 to 209 ppm (within the range noted in fig. 1.12b), with no systematic variations noted between the schists, gneisses and granites. Rb/Sr (also $^{87}Rb/^{86}Sr$) is typically greater than 1, and as high as 8 in the staurolite-grade schist. The Sr-isotope chemistry of the HHCS is well established so isotopic analysis was only carried out on two samples. The staurolite schist has an $^{87}Sr/^{86}Sr$ of 0.805, fairly typical of the HHCS (fig. 1.12a). The mineralogy of sample T29g differed from that of other samples, comprising quartz, plagioclase and pyroxene with only trace mica, and was found to be unradiogenic ($^{87}Sr/^{86}Sr$ = 0.717). It is possible that this sample, closely associated with calc-silicates, is merely a siliceous part of a calc-silicate body, and is highly unlikely to typify silicate rocks in the HHCS of the Bhote Kosi.

Samples were also collected from the MCT zone at Tatopani. These comprise (table C2) two samples of augen gneiss (BK17 and BK111) in addition to a calcareous greywacke. Nd-isotope (ε_{Nd} = -16.1) analysis of the latter indicates that it may be part of the HHCS, while BK17 and BK111 are possibly Lesser Himalayan augen gneisses (see section 1.3.3.3). The fine-grained greywacke comprises evenly dispersed quartz

and calcite in a quartz - mica matrix, and shows chemistry similar to that of the HHCS schists, containing relatively little Rb (43 ppm) and Sr (83 ppm), and yielding a radiogenic Sr-isotope ratio (0.805). The augen gneisses are Rb-rich (~300-400 ppm), while remaining relatively low in strontium (~45 ppm). Isotopic analysis of BK17 reveals an $^{87}Sr/^{86}Sr$ of 1.12 and $^{87}Rb/^{86}Sr$ of 26.7. These values perhaps provide an indication of the potential input from the Lesser Himalayan crystallines (gneisses) that form a significant part of the catchment of the Sun Kosi Nadi tributary of the Bhote Kosi and also constitute a significant portion of the Lesser Himalaya in the catchments of the Arun, Tamur and Tama Kosi tributary of the Sun Kosi (see plate 6 and plate 7).

The composition of silicate samples (again defined as having >90% SiO_2 in fig. 7.2) obtained from the Lesser Himalaya differs between those from the Kuncha Group and those that form the silicate component of the Nawakot Group. From the Kuncha Group, two metasandstones (BK21 and BK25), the predominant lithology of this unit, and a phyllite (BK8) were collected. A modal analysis of the two metasandstones reveals an important difference. BK21 comprises >80% quartz with diffuse grains of muscovite and trace carbonate, while BK25 has a higher mica content (as much as 50%) and contains no carbonate. This contrasting mineralogy is reflected in the greater $^{87}Rb/^{86}Sr$ (6.3) and $^{87}Sr/^{86}Sr$ (0.850) of BK25 compared with BK21 (2.3 and 0.729 respectively). Sample BK8 (phyllite) comprises ~80% quartz in addition to both muscovite and biotite. This sample is very low in Sr (22 ppm) with an $^{87}Rb/^{86}Sr$ of 8.77 and $^{87}Sr/^{86}Sr$ of 1.16, reflecting the abundance of mica.

The silicate units of the Nawakot Group were collected from the Dandagaon Phyllites / Nourpul Formation (indistinguishable in the field), Benighat Slates and Malekhu Limestone / Robang Formation (again indistinguishable) and are typically phyllites or schists comprising principally biotite mica (typically >50%) and quartz. Meta-greywackes and impure metasandstones were also obtained, predominantly composed of quartz (~90%), biotite (green biotite in sample BK12a) and occasional carbonate. Strontium levels in all samples are low (generally <50 ppm), while Rb is variable, being higher in the phyllites and mica schists (>125 – 300 ppm), lower in the metasandstones and meta-greywackes. It should be noted that sample BK122MV (see table C3) is a mineral vein composed largely of quartz and thus the above description is not applicable. This sample is not included as part of the mean LHF composition discussed below. All of the Nawakot Group silicate samples analysed were highly radiogenic ($^{87}Sr/^{86}Sr$ = 0.80 – 1.16), consistent with other studies (see fig. 1.12a), and more radiogenic than those of the Kuncha Group, the predominant silicates of the Lesser Himalaya in terms of aerial extent.

Several samples, fine-grained two-mica and biotite-garnet schists, were obtained from the Kalitar Formation of the Kathmandu Nappe, which underlies the Bhainsedobhan Marble in the Everest Quarry. Thin section analysis reveals a mica content of 20-30%. Rb (123-207 ppm) is in excess of Sr (54-101 ppm) in all samples (mean $^{87}Rb/^{86}Sr$ = 7.301), which have Sr-isotope ratios of 0.77-0.79. A further sample, from the Chisapani Quartzite, was collected upstream of the Everest Quarry. This virtually pure quartzite (94% SiO_2) is characterised by both low Sr and Rb, and thus a moderate $^{87}Sr/^{86}Sr$ (0.75).

(i).

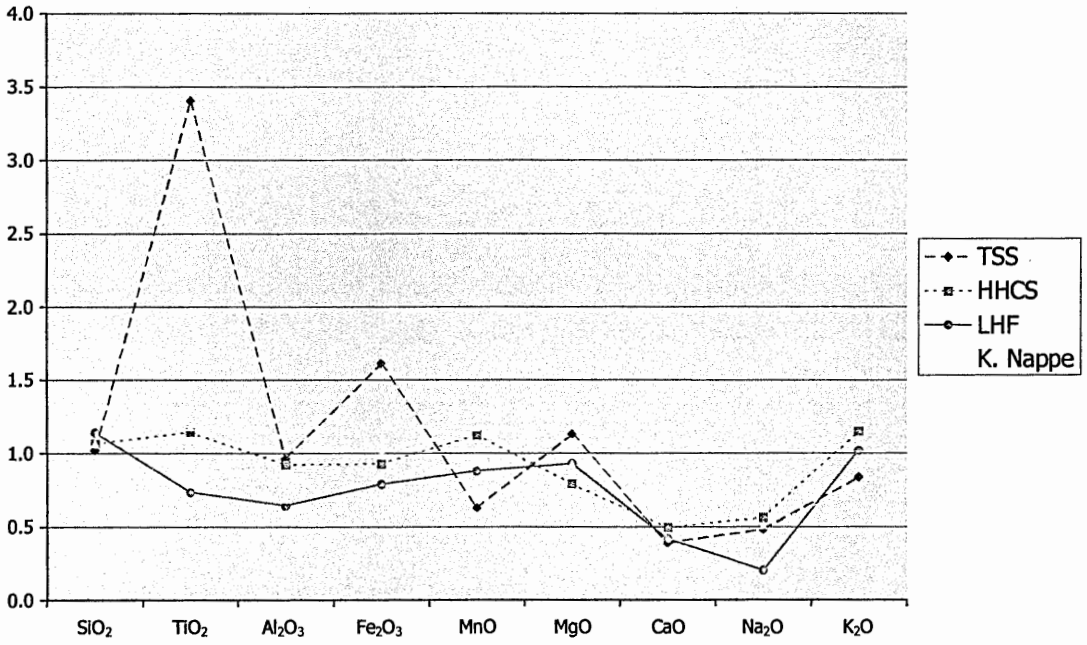

(ii).

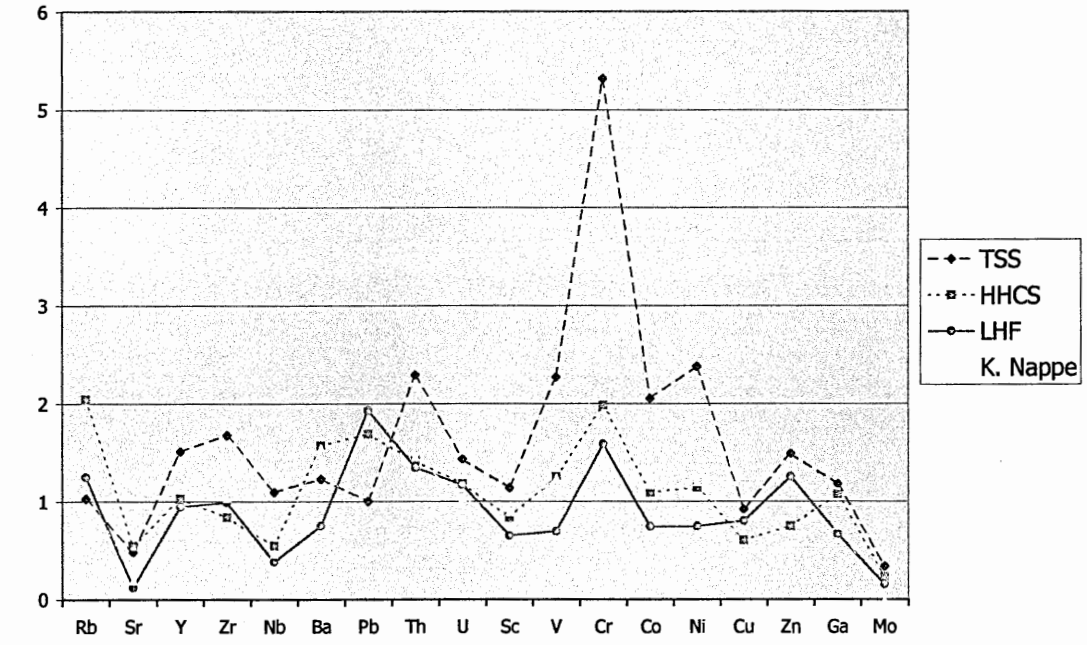

Fig. 7.4. Mean major (i) and trace (ii) element composition of Bhote Kosi silicates normalised to average upper continental crust.

Fig. 7.4 compares the average silicate composition of the samples collected form the TSS, HHCS, LHF and Kathmandu Nappe, normalised to the average composition of the upper continental crust (UCC) (Taylor and McLennan, 1985). A general pattern of depletion relative to UCC is observed for the major elements (fig. 7.4a), with the exception of SiO_2, and in the case of the High Himalayan Crystalline Series and the Lesser Himalaya, K_2O. This likely reflects the prevalence of quartz and mica in the samples, particularly in the LHF. The Tibetan Sedimentary Series mudstones are enriched in both titanium and iron relative to both UCC and the other lithological units of the Himalaya. Trace element patterns are similar in all four units (fig. 7.4b), with notable thorium and chromium peaks, and low levels of strontium, niobium, scandium, vanadium, copper and molybdenum. Strontium depletion relative to upper continental crust is particularly pronounced both in the Lesser Himalaya and the samples from the Kathmandu Nappe. Levels of rubidium are enriched in the HHCS relative to the other Himalayan geological units, which contain approximately the same amount as the upper continental crust. The Lesser Himalaya are depleted in most other trace elements in comparison with the other Himalayan units, notable exceptions being lead, copper and zinc. In contrast to carbonates of the LHF, silicates from the LHF contain less Ba than those from the TSS, HHCS and Kathmandu Nappe, and are depleted relative to the UCC.

7.3. Calc-Silicates.

The only calc-silicate sample (equidistant between the TSS silicates and carbonates on a SiO_2-MgO-CaO plot, see fig. 7.2) obtained from the Tibetan Sedimentary Series is a calcareous siltstone. Thin section observation reveals an extremely fine grained

rock in which fragmental quartz is the only identifiable mineral. XRF analysis (table C1) shows that calcitic material forms a substantial part of the matrix (CaO > 30%), while fine carbonate veins are also observed. The Rb concentration (~45 ppm) is approximately half the strontium content and the rock is relatively unradiogenic, with an $^{87}Sr/^{86}Sr$ of 0.715.

The calc-silicates of the High Himalayan Crystalline Series (which again fall clearly between silicates and carbonates in fig. 7.2) are distinctive in hand specimen, with coarse crystals (average grain size 0.3-3 mm) of calcite (~40-50%), plagioclase feldspar (~20%), pyroxene (~15-30%) and quartz (~10-20%). One sample also contains biotite (T29f). Titanite is an abundant accessory mineral, as reflected by the titanium peak on fig. 7.6a. The amount of rubidium present in these rocks is remarkably variable, ranging between 7 and 153 ppm. Strontium concentrations are almost as high (~700 ppm) as those of the associated purer carbonate sample (T29c), resulting in low $^{87}Rb/^{86}Sr$ (mean = 0.248), whilst the calc-silicates are slightly more radiogenic ($^{87}Sr/^{86}Sr$ = 0.711 - 0.715). Similiar strontium chemistry is observed in Formation II marbles by Galy *et al.* (1999) and English *et al.* (2000). Assuming that T29c is representative of the carbonate component of the calc-silicates, with its Sr-isotope ratio of 0.710, the $^{87}Sr/^{86}Sr$ of the silicate component is not likely to be extremely high.

As the focus of this study, the bulk of the bedrock dataset comprises calc-silicates of the Lesser Himalayan Formation. The amount of carbonate material in these samples is variable, forming a continuous series from samples that differ only slightly in composition from the pure silicates described above (but all <90% SiO_2 on fig. 7.2),

to rocks in which carbonate accounts for >70% of the bulk rock. In all cases the carbonate material is dolomite, distinct from the pure carbonates of the LHF (fig. 7.2), and indeed from the pure carbonates and calc-silicates collected from the TSS, HHCS and Kathmandu Nappe, which are all limestones. Carbonate is most abundant is samples from the Dhading Dolomite (>50 - >70%), such as BK15 and BK123, in which the only other major mineral observed is quartz. Mica (muscovite and biotite) is additionally present in samples BK5 and BK56 (1-8), forming 10-15% of the rock. The mica is both finely dispersed throughout these samples in addition to forming distinct bands. BK5 also displays quartz and carbonate banding. All samples from the Dhading Dolomite are fine grained (~0.02 - ~0.1 mm), with some coarser crystals of quartz and dolomite (up to 0.5 mm), often forming veins and lenses. The Sr content of these samples is consistently low (54 - 78 ppm), indicative of the dolomitisation of diagenetic limestone (Yoo *et al.*, 2000; Bickle *et al.*, 2001) while appreciable Rb is only present in those samples where mica occurs (27 – 118 ppm), with little in the remaining samples (6 - 7 ppm, $^{87}Rb/^{86}Sr < 0.5$). Isotope ratios show similar variability, being low in samples BK123 ($^{87}Sr/^{86}Sr = 0.712$) and BK 5 (0.721) in comparison with the other samples (0.745 - 0.794). Sr-isotope ratios between 0.708 and 0.716 are globally common in dolomites as a result of diagenesis and dolomitisation (Banner, 1995).

Even more radiogenic are the calc-silicates collected from the Dandagaon Phyllites and Nourpul Formation. As noted for the Dhading Dolomite, the carbonate proportion is variable, from <20% in thin section (BK12d) to ~60% (BK6 and BK14a). The remaining minerals are again quartz (10-30%) and mica (typically <15%, both muscovite and biotite are observed), while dark organic matter is often

additionally present. Typical grain size ranges between 0.01 and 0.05 mm, while sample BK11 is coarser (0.1 - 2 mm). Mica, quartz or dolomite banding is noted in several samples. Strontium concentrations are in the same range as observed in the carbonates and silicates of the Lesser Himalaya (28 - 40 ppm), with the exception of sample BK11, which contains 190 ppm of Sr (higher than previously recorded in other studies and making this sample ideal for laser ablation). The abundance of Rb is also variable, between 2 and >200 ppm. Samples depleted in Rb (<10 ppm, $^{87}Rb/^{86}Sr < 1$) are less radiogenic ($^{87}Sr/^{86}Sr = 0.73 - 0.76$) than the remainder (0.79-1.11).

The calc-silicates of the Benighat Slates comprise extremely fine-grained, graphite-rich calc-slates. These samples contain abundant Rb (>250 ppm), with Sr contents of less than 100 ppm. Isotopic analysis of sample BK4 yields an $^{87}Sr/^{86}Sr$ of 0.923. Intercalated within the slates are more carbonate rich units (the Jhiku Beds), two samples from which have lower Rb (<100 ppm), but maintain relatively high $^{87}Rb/^{86}Sr$ (>5). A further sample, BK54a, which forms part of a thicker, more massive carbonate unit, comprises only equigranular quartz and dolomite (~30% carbonate) together with accessory iron oxides, and is depleted in both Rb and Sr (<30 ppm). All three samples from the Jhiku Beds are radiogenic ($^{87}Sr/^{86}Sr >0.89$).

Samples BK113a-e and BK114a-f appear to belong to the Benighat Slates when plotted on the geological map of Stöcklin and Bhattarai (1980), but are lithologically different from the slates and intercalated carbonates described above. Sample BK113b is a strontium rich, moderately radiogenic calc-silicate described in more detail in section 6.6. BK114a-e are fine-grained (~0.05 mm), comprise largely quartz

with subordinate dolomite (~20%) biotite (~20%) and graphite, and have a largely uniform chemistry. Rb content varies between 79 and 139 ppm, Sr from 33 to 71 ppm, with $^{87}Rb/^{86}Sr$ between 6 and 8 and $^{87}Sr/^{86}Sr$ from 0.91 to 0.98.

A single calc-silicate sample (BK116) falls within the Malekhu Limestone when plotted on the map of Stöcklin and Bhattarai (1980), but is similar in appearance (in both outcrop, hand specimen and thin section) to samples BK113a-e and BK114a-e, although with muscovite present and only occasional biotite crystals. BK116 contains abundant Sr (139 ppm) and has a high $^{87}Sr/^{86}Sr$ of 0.835.

Calc-silicates collected from the Bhainsedobhan Marble of the Kathmandu Nappe are similar in appearance to the calc-silicates described above from the HHCS (although lacking the distinctive green pyroxene crystals). Sample BK104a comprises coarse (0.5 - 2 mm), well formed calcite crystals with much smaller (~0.05 mm) quartz crystals dispersed throughout. Clearly visible in hand specimen, discrete bands of mica are also present, forming no more than 5-10% of any specimen. Sample BK104a contains ~70% carbonate, although XRF data (table D4 and fig. 7.2) suggests that the calcite:quartz ratio of the Bhainsedobhan Marble is variable, from the almost pure carbonate described in section 7.1 (BK53b) to sample BK105a which contains >50% SiO_2. Strontium is least abundant in BK105a (80 ppm), and more prevalent in the calcite-rich samples (up to 350 ppm), although not reaching the high concentrations observed in the HHCS carbonates and calc-silicates. Rb varies between 15 and 65 ppm, although $^{87}Rb/^{86}Sr$ never exceeds 1, and samples are no more than moderately radiogenic ($^{87}Sr/^{86}Sr$ = 0.711 - 0.721). Sample BK53a exemplifies the subordinate intercalations of schist noted in the Bhainsedobhan

Marble by Stöcklin (1980) and can only marginally be classified as a calc-silicate. Thin section reveals a composition of approximately 50% quartz and 45% mica (a fairly even split of muscovite and biotite / phlogopite), with ~5% carbonate material. XRF analysis shows an Rb/Sr ratio greater than 1.

The average calc-silicate compositions of the TSS, HHCS, LHF and Kathmandu Nappe were normalised to both the average upper continental crustal composition (fig. 7.5) and that of the TSS carbonates (fig. 7.6). TSS data are based on the single sample described in section 7.3 and should therefore be treated with caution. Major element plots (fig. 7.5a and fig. 7.6a) reveal few surprises. When normalised to average UCC, all of the Himalayan calc-silicate lithologies show enrichment in Ca (reflecting the carbonate component) and are consequently depleted in the other elements. Enrichment in Mg is also observed in the LHF calc-silicates, reflecting the presence of dolomite rather than calcite. A converse pattern is noted when the samples are normalised to average TSS carbonate, with depletion in calcium and sodium, but enrichment in the other major elements relative to "pure" carbonate owing to the presence of the silicate component. A particularly high enrichment in potassium reflects the mica content of the calc-silicates of all the Himalayan units.

Calc-silicates are also generally depleted in trace elements relative to average upper continental crust and enriched (particularly in Rb, Zr, Ba, Cr and Zn) relative to average TSS carbonate. Concentrations of rubidium are highest in the High Himalayan Crystalline Series and Lesser Himalayan Formation, the most likely explanation for this being higher mica contents (observed in thin section). The

(i).

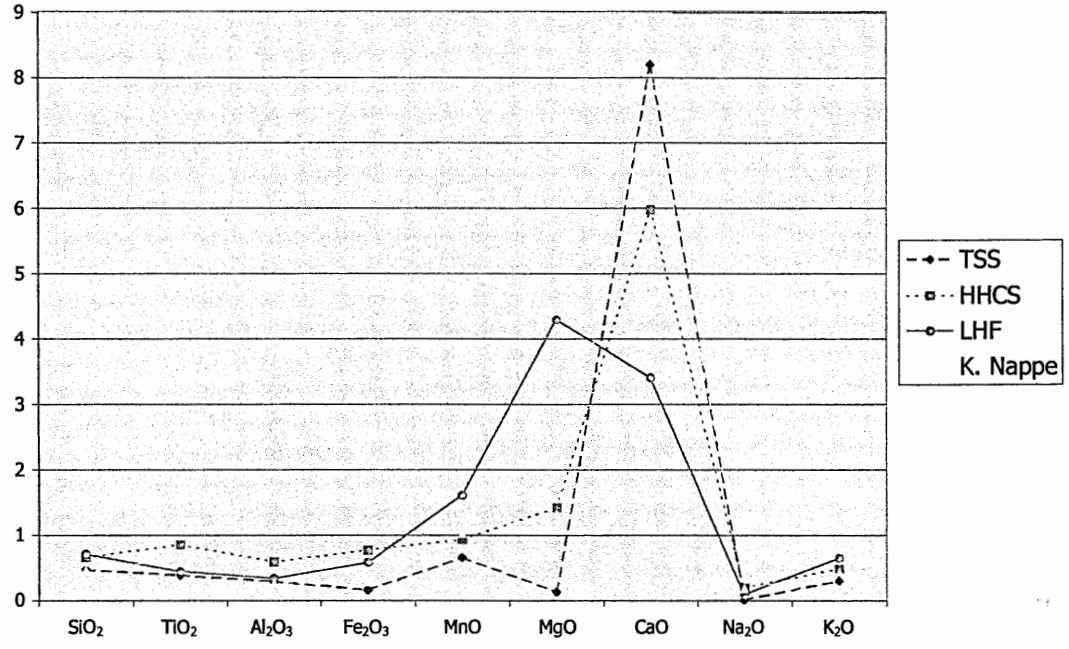

(ii).

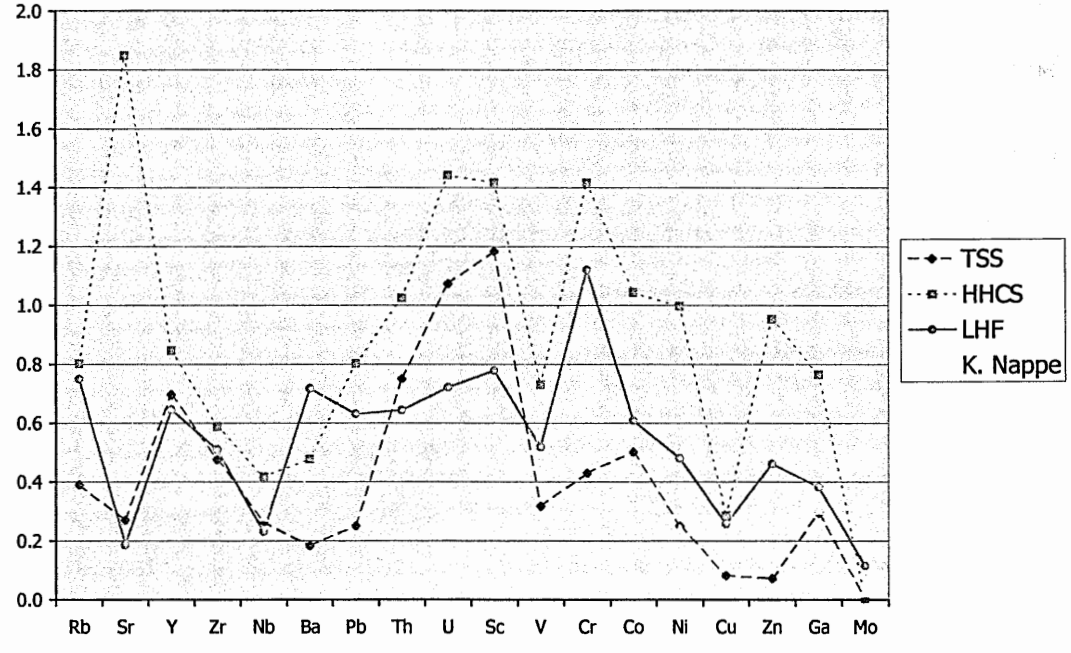

Fig. 7.5. Mean major (i) and trace (ii) elemental composition of Bhote Kosi calc-silicate bedrock normalised to average upper continental crust.

(i).

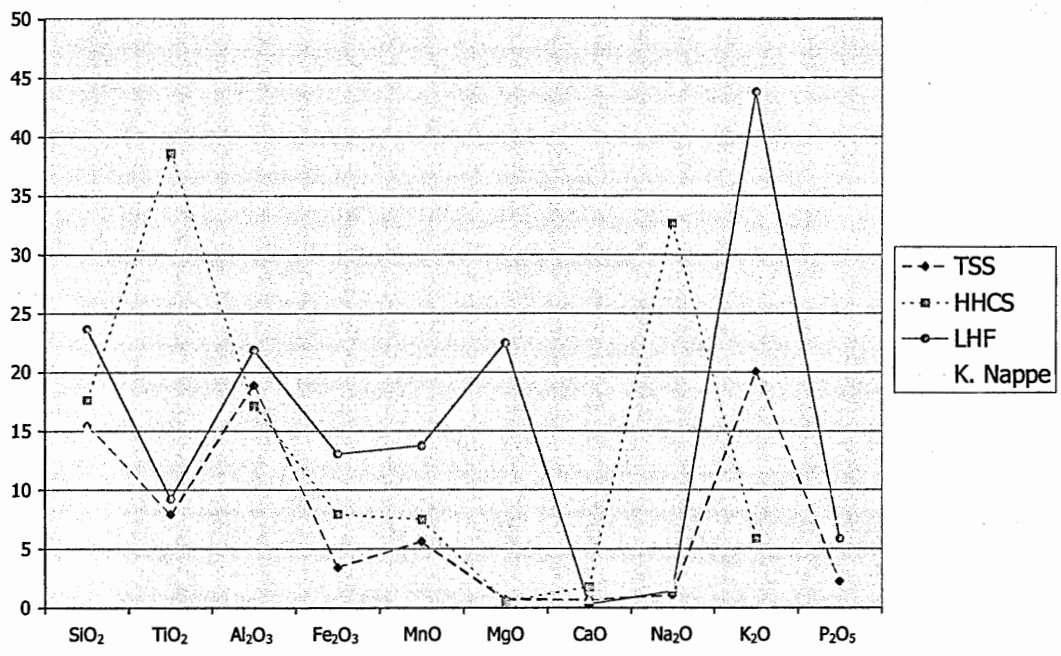

(ii).

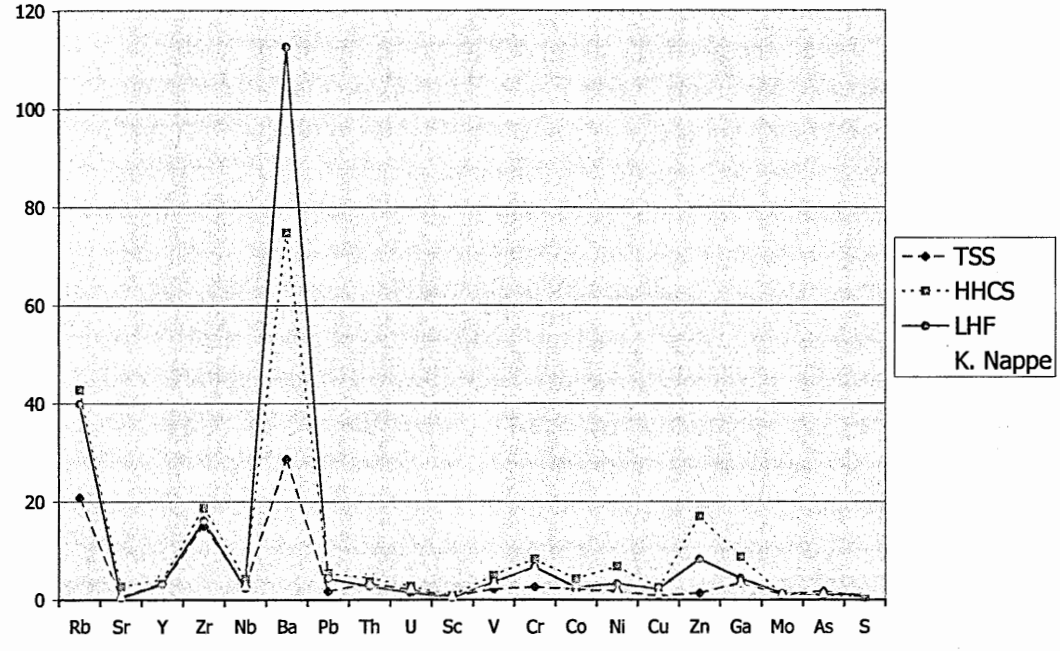

Fig. 7.6. Mean major (i) and trace (ii) elemental composition of Bhote Kosi calc-silicate bedrock normalised to mean Bhote Kosi TSS carbonate composition.

barium enrichment in the calc-silicates of the Lesser Himalaya is considerable, as previously noted in the limestones of the same formation, the Ba content of these rocks being over 100 times that of TSS carbonates, although considerable enrichment is also noted in the HHCS and Kathmandu Nappe calc-silicates. As previously observed in both silicates and carbonates, strontium concentrations are at their lowest in the Lesser Himalaya, while by contrast Sr is abundant in the HHCS calc-silicates, in excess even of the pure limestones of the TSS.

7.4. Interpretive Summary.

Fig. 7.7 and fig. 7.8 summarise the strontium chemistry of bedrock samples collected from the Bhote Kosi, revealing a largely familiar picture, previously documented for

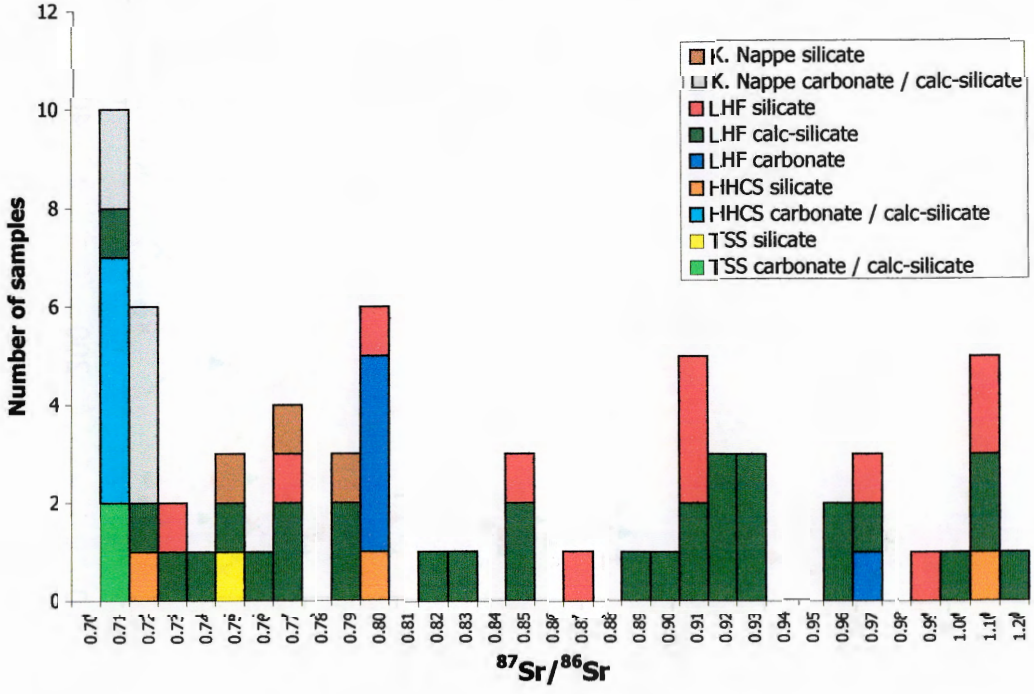

Fig. 7.7. Strontium chemistry of bedrock samples collected from the Bhote Kosi catchment.

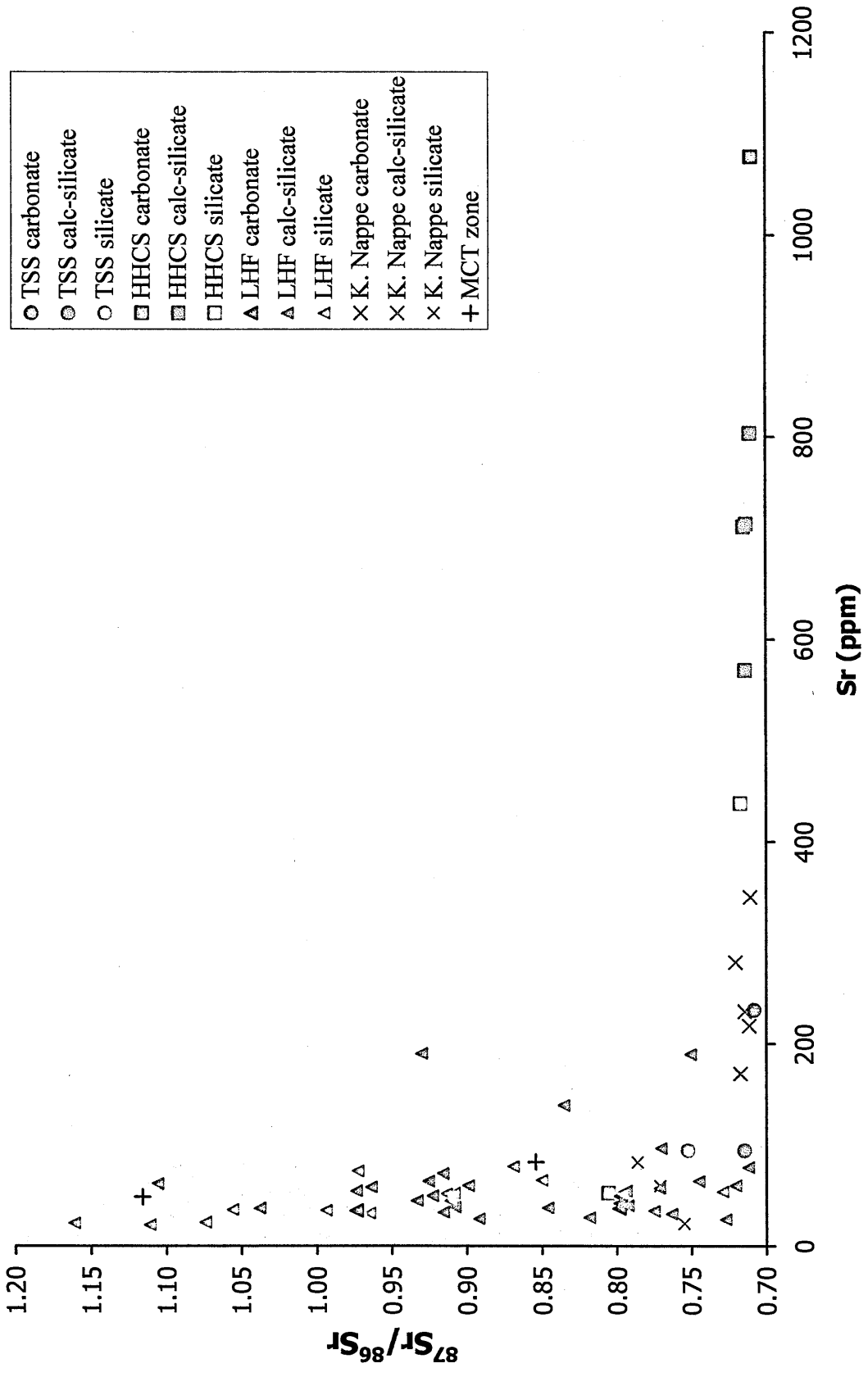

Fig. 7.8. Strontium chemistry of bedrock samples collected from the Bhote Kosi catchment.

other parts of the Himalaya (see fig. 1.12a and b). Carbonates of the TSS and HHCS (in addition to the Kathmandu Nappe) are charcterised by low $^{87}Sr/^{86}Sr$ and high strontium concentrations, while silicates of all units are radiogenic, with ratios increasing progressively from the TSS to the HHCS and LHF. Strontium concentrations are lower, particularly so in the Lesser Himalaya.

The few limestones that it was possible to collect from the Lesser Himalaya were also marked by low Sr concentrations and high Ca/Sr ratios (~8,500). The Bhote Kosi limestones are much more radiogenic than those previously described in other studies (fig. 1.12a). Whilst providing an indication of the chemistry and composition of carbonate material in the Lesser Himalayan calc-silicates, the scarcity of pure limestones in the Lesser Himalaya of the Bhote Kosi largely precludes them from having a major input on the dissolved $^{87}Sr/^{86}Sr$. Calc-silicates are the dominant lithology of the Nawakot Group, however, again typically displaying a low Sr concentration, but combined with highly variable Sr-isotope ratios (0.712 – 1.106). A comparison of moderately and highly radiogenic calc-silicates reveals a clear difference. Those samples with lower $^{87}Sr/^{86}Sr$ (all from the Dhading Dolomite) contain less mica (none in the case of the least radiogenic sample), and are characterised by low Al_2O_3 (<1%) and Rb (<10 ppm). Calc-silicates from the Himachal and Kumaun Himalaya, comprising only dolomite and quartz (and indeed calcite and quartz) were analysed by Singh *et al.* (1998) and found to be no more than moderately radiogenic ($^{87}Sr/^{86}Sr$ = 0.708 – 0.731) in most cases, while leachate analysis of a radiogenic ($^{87}Sr/^{86}Sr$ = 0.773) LHF calc-silicate by Bickle et al. (2001) has revealed carbonate material with low $^{87}Sr/^{86}Sr$ (0.7111). This raises the possibility that the rapid increase in dissolved $^{87}Sr/^{86}Sr$ in the Bhote Kosi as it crosses

the Nawakot Group is the result of radiogenic strontium inputs from the abundant micas in these calc-silicates, and that the carbonate component might be relatively unradiogenic.

There are some potential problems with such a suggestion. Mica is present in calc-silicates of the HHCS and yet these rocks do not show high Sr-isotope ratios. Indeed, it is not Rb enrichment that is the distinguishing feature of the LHF calc-silicates in fig. 7.5b and fig. 7.6b, but their depletion in strontium and enrichment in barium that is unique, features also noted in the few LHF limestones obtained. Mean barium content (239 ppm) is also high in a set of intercalated calc-silicate samples from the LHF of the Garhwal Himalaya (Bickle and Harris, pers. comm.), although as with the Bhote Kosi dataset, values are highly variable around this mean. Barium can substitute for strontium in limestones and dolomites, and thus Ba enrichment coupled with Sr depletion might be interpreted as a sign of hydrothermal alteration of the Lesser Himalaya. In the TSS, HHCS and samples from the Kathmandu Nappe increasing barium concentrations are observed moving from carbonate to calc-silicate to silicate (table 7.1), with the bulk of the barium in these units residing in silicate. In the Lesser Himalaya, however, average carbonate, calc-silicate and silicate compositions have similar Ba abundances. Table 7.1 also shows a clear pattern of Sr concentrations in the TSS, HHCS and Kathmandu Nappe, this time with increasing enrichment from silicate to calc-silicate to carbonate. Once again, in the Lesser Himalaya, concentrations are relatively uniform when comparing average carbonate, calc-silicate and silicate. This hints towards chemical exchange and equilibration occurring between the different units of the Lesser Himalaya, although

Table 7.1. Mean composition of the principal lithologies of the Bhote Kosi from bedrock samples collected for this study.

	Tibetan Sedimentary Series			High Him. Crystalline Series			Lesser Himalayan Form.			Kathmandu Nappe		
	Carbonate	Calc-silicate	Silicate	Carbonate	Calc-silicate	Silicate	Carbonate	Calc-silicate	Silicate	Carbonate	Calc-silicate	Silicate
wt. %												
SiO_2	1.97	30.39	67.19	11.64	42.90	70.10	6.29	46.61	75.26	5.69	30.03	69.98
TiO_2	0.02	0.19	1.70	0.15	0.42	0.57	0.07	0.22	0.37	0.08	0.31	0.59
Al_2O_3	0.23	4.34	14.58	3.44	8.88	13.98	0.76	5.03	9.75	0.96	3.81	10.42
Fe_2O_3	0.20	0.67	7.24	1.48	3.42	4.16	0.52	2.61	3.54	1.17	1.18	4.47
MnO	0.007	0.039	0.038	0.030	0.055	0.07	0.017	0.096	0.053	0.054	0.061	0.070
MgO	0.42	0.27	2.48	2.96	3.12	1.74	1.61	9.43	2.04	6.92	2.90	2.03
CaO	54.58	34.42	1.62	45.18	25.09	2.05	50.29	14.29	1.75	45.27	33.34	4.56
Na_2O	0.00	0.01	1.86	0.04	0.74	2.18	0.01	0.33	0.78	0.00	0.67	1.97
K_2O	0.05	1.00	2.83	0.92	1.63	3.90	0.28	2.19	3.46	0.31	1.44	2.58
P_2O_5	0.01	0.02	0.18	0.03	0.07	0.13	0.02	0.07	0.09	0.04	0.09	0.14
LOI	43.56	28.43	4.03	34.22	15.87	0.75	41.30	20.63	2.98	41.58	28.26	3.84
ppm												
Rb	2.10	43.50	115.10	56.10	89.55	228.65	10.76	83.76	139.63	10.80	38.68	129.78
Sr	249.20	94.20	168.50	1076.80	646.63	190.76	41.50	64.74	41.71	217.30	181.41	65.83
Y	4.55	15.30	33.15	5.90	18.58	22.58	5.12	14.17	20.81	10.10	22.38	27.97
Zr	6.00	90.00	318.00	21.00	111.42	159.15	20.64	96.64	186.92	46.40	317.39	196.60
Nb	2.50	6.60	27.30	4.50	10.42	13.62	2.40	5.74	9.54	2.30	6.98	11.52
Ba	3.50	100.00	674.00	70.00	261.27	860.72	374.98	394.10	410.55	12.20	229.98	847.22
Pb	3.00	5.00	20.00	12.00	16.00	33.72	2.88	12.58	38.56	10.00	26.10	8.60
Th	2.50	8.00	24.50	0.00	10.93	15.12	1.60	6.87	14.37	2.60	13.47	15.52
U	1.50	3.00	4.00	2.00	4.03	3.30	1.84	2.01	3.26	3.20	3.20	2.88
Sc	22.00	13.00	12.50	17.00	15.57	9.17	19.56	8.54	7.15	18.70	16.16	9.78
V	9.00	19.00	136.00	25.00	43.70	74.78	9.38	31.07	41.63	20.20	27.95	74.00
Cr	6.00	15.00	186.00	22.00	49.52	69.23	8.94	39.18	55.48	8.70	37.58	80.88
Co	2.50	5.00	20.50	7.00	10.42	10.89	3.56	6.07	7.42	3.80	3.47	11.62
Ni	3.00	5.00	47.50	9.00	19.90	22.76	2.70	9.59	14.92	2.00	4.83	23.85
Cu	3.00	2.00	23.00	7.00	7.10	15.04	5.82	6.38	20.00	4.80	3.33	17.33
Zn	4.00	5.00	105.50	44.00	67.57	52.75	14.80	32.71	88.99	14.40	90.32	29.22
Ga	1.50	5.00	20.00	5.00	12.97	18.23	1.46	6.48	11.35	1.80	5.15	12.73
Mo	0.00	0.00	0.50	0.00	0.00	0.35	0.00	0.17	0.22	0.00	0.03	0.00
As	5.00	8.00	3.50	0.00	3.97	3.04	5.26	5.12	5.19	7.80	5.90	3.25
S	208.00	70.00	543.00	228.00	70.00	100.73	161.40	186.57	208.50	836.00	360.83	103.33
$^{87}Rb/^{86}Sr$	0.0484	1.3369	4.9271	0.1508	0.2484	5.65	1.0744	4.7979	9.9496	0.1438	0.5049	7.3007
$^{87}Sr/^{86}Sr$	0.708193	0.714764	0.752396	0.710038	0.713285	0.76	0.841693	0.862016	0.941332	0.711621	0.716061	0.770617
$^{143}Nd/^{144}Nd$				0.511719	0.511612	0.51	0.511351	0.511348	0.511360	0.511617	0.511630	0.511551
ε_{Nd}				-17.927	-20.023	-17.87	-25.097	-25.170	-24.930	-19.922	-19.672	-21.201
Rb/Sr	0.008	0.462	0.683	0.052	0.138	1.20	0.259	1.294	3.347	0.050	0.213	1.971
Sr/(Ca+Mg)	5.54E-04	3.32E-04	5.98E-03	2.77E-03	2.88E-03	6.99E-03	9.83E-05	3.72E-04	1.57E-03	5.26E-04	6.24E-04	1.33E-03
Na/Sr	0.00	0.79	81.89	0.28	8.47	84.66	1.22	37.84	138.19	0.00	27.39	221.75
Ca/Sr	1565	2611	69	300	277	77	8660	1577	300	1489	1314	495
Ba/Sr	0.01	1.06	4.00	0.07	0.40	4.51	9.04	6.09	9.84	0.06	1.27	12.87

this exchange is strictly limited to Ba and Sr, the most mobile elements in hydrothermal fluids. Depletion of carbonate material in strontium by hydrothermal alteration might leave a greater proportion of ^{87}Sr sourced predominantly in micas. Alternatively, isotopic equilibration might have occurred between the silicate and

carbonate portions of these rocks. This is suggested by the presence of radiogenic mica-free pure carbonates in the Dandagaon Phyllites / Nourpul Group (and also two samples noted by Singh *et al.*, 1998, in the Himachal and Kumaun Himalaya), which are closely associated with radiogenic phyllites. Additionally, the extremely high $^{87}Sr/^{86}Sr$ of certain calc-silicates would require unrealistically high ratios in the silicate portion of the rock if it is assumed that the carbonate portion remains unradiogenic. Isotopic analysis of pure silicates, often closely associated with calc-silicates, silicate-dominated bedload (this study) and mica separates (Bickle *et al.*, 2001) indicates that such high $^{87}Sr/^{86}Sr$ (>1.5) is unlikely. The occurrence of relatively unradiogenic calc-silicates in such a scenario is explained by the lack of a source of radiogenic Sr with which carbonate might exchange, with an absence of mica in the samples themselves, together with a lack of closely associated silicates.

In the remainder of the chapter the evidence for radiogenic carbonate material within the Lesser Himalayan calc-silicates, and the evidence for isotopic exchange between carbonate and silicate, is examined in further detail.

7.5. $^{87}Sr/^{86}Sr$ vs $^{87}Rb/^{86}Sr$ in the Bedrock of the Bhote Kosi.

For those samples for which isotopic analysis was undertaken, $^{87}Rb/^{86}Sr$ ratios can be calculated. Table 7.1 shows a consistent increase in $^{87}Rb/^{86}Sr$ from carbonate to calc-silicate to silicate in the TSS, HHCS and LHF, with the highest average ratio found in silicates of the Lesser Himalaya. An isochron plot of $^{87}Rb/^{86}Sr$ against $^{87}Sr/^{86}Sr$ reveals whether the amount of ^{87}Rb present in a rock can account for the measured $^{87}Sr/^{86}Sr$ through radioactive decay since its formation (or the time elapsed since

resetting as the result of major metamorphism). A sample in which the calculated $^{87}Rb/^{86}Sr$ cannot account for the measured $^{87}Sr/^{86}Sr$ (with a plausible initial $^{87}Sr/^{86}Sr$) is referred to as "unsupported" and must have either lost ^{87}Rb or acquired ^{87}Sr in the time since formation or metamorphism in order to explain its current Sr-isotope ratio. When considering carbonates, the former is an unlikely scenario, as carbonate typically contains little rubidium, while metamorphic decarbonation reactions do not generate new Rb-bearing phases such as amphibole (Bickle *et al.*, 2001).

Fig. 7.10 shows $^{87}Sr/^{86}Sr$ plotted against $^{87}Rb/^{86}Sr$ for the samples collected from the Lesser Himalaya, while fig. 7.9 shows the same for samples obtained from the other units of the catchment. Reference isochrons are shown for 2500 Ma, 1800 Ma and 500 Ma. 2500 Ma is the oldest possible age of the Lesser Himalaya, while metamorphism of these rocks occurred at 1800 Ma, additionally the oldest age of the HHCS. The HHCS and possibly the LHF were subject to metamorphism at 500 Ma. In both figures, an initial $^{87}Sr/^{86}Sr$ of 0.709 is assumed, although marine $^{87}Sr/^{86}Sr$ was probably lower than this at 1800 Ma (~0.705 – 0.707, Veizer, 1989; Burns *et al.*, 1994), even lower at 2500 Ma. Average continental crust is also believed to have had $^{87}Sr/^{86}Sr$ of less than 0.709 at 1800 Ma (Rollinson, 1993).

On fig. 7.9 all rocks of the HHCS, with one exception, fall below the 1800 Ma isochron. Both the carbonate and calc-silicate samples were collected from the same site, and are likely to be of similar age and thus would be expected to define an isochron if strontium remains undisturbed by metamorphism. The carbonate sample falls on the 500 Ma isochron while the calc-silicate samples lie above, indicating that some exchange of strontium with intrusive granitic pegmatites might have occurred.

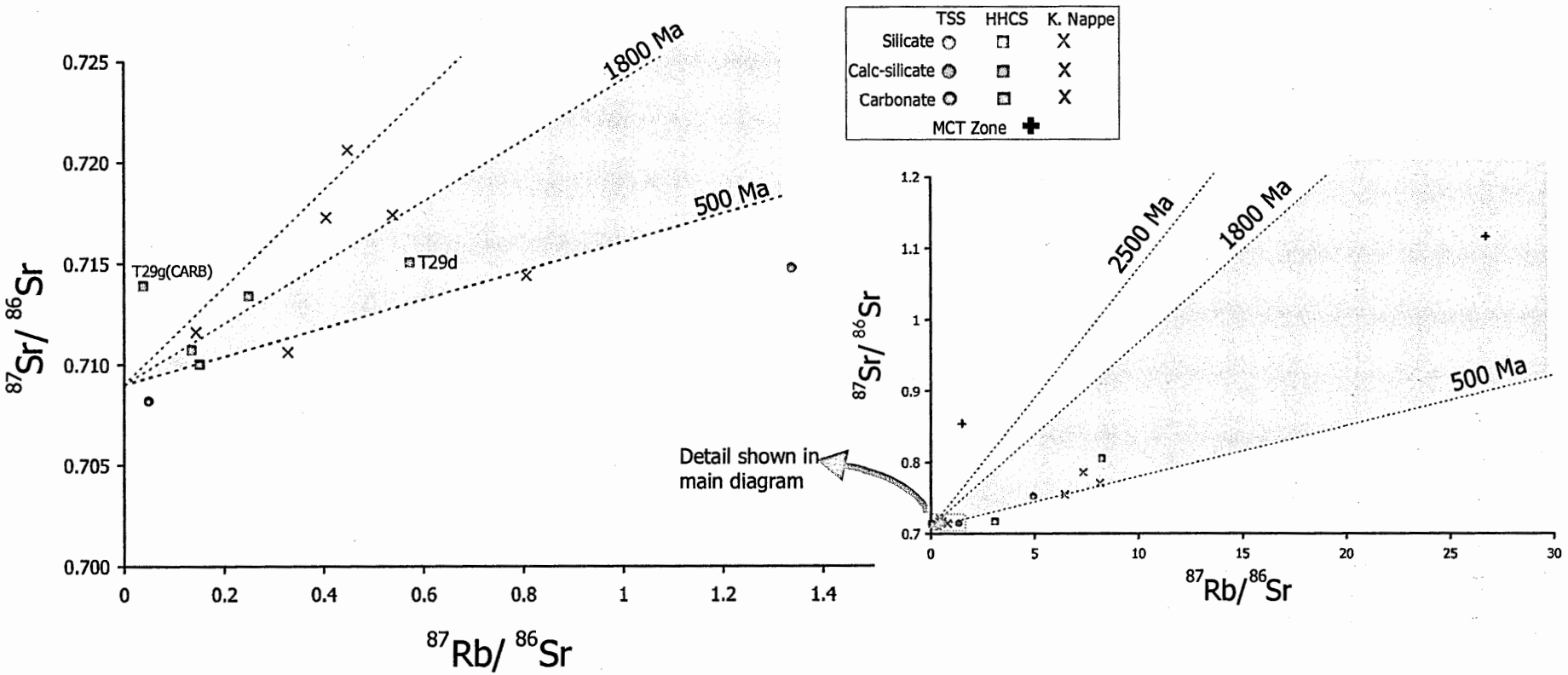

Fig. 7.9. $^{87}Sr/^{86}Sr$ vs $^{87}Rb/^{86}Sr$ in samples collected from the Tibetan Sedimentary Series, the High Himalayan Crystalline Series and the MCT Zone in the Bhote Kosi and from the Kathmandu Nappe in the Chak Khola catchment.

Substantial exchange would be needed in order to make an impact upon the strontium-rich calc-silicates. The occurrence of such exchange is clear, however, in the case of sample T29g(CARB) (the "CARB" differentiates the calc-silicate from adjoining silicate material in the same sample), which is clearly unsupported even at 1800 Ma. Moderately radiogenic unsupported calc-silicates in the HHCS of the Garhwal Himalaya are also reported by Bickle *et al.* (2001). Samples from the Kathmandu Nappe are all supported at 1800 Ma, although show a similar pattern to those of the HHCS, with one sample falling exactly on the 1800 Ma isochron, with others falling below the 500 Ma isochron. Once again these samples were collected from the same site and so would be expected to have a similar age. As would be expected, samples from the TSS fall below the 500 Ma isochron, reflecting their younger age.

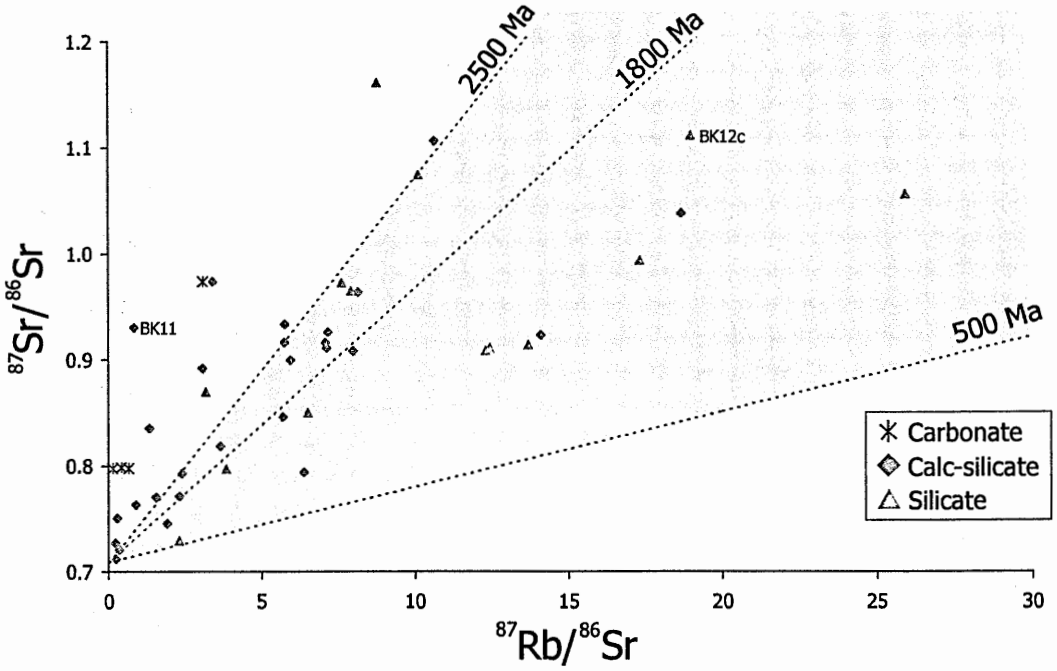

Fig. 7.10. $^{87}Sr/^{86}Sr$ vs $^{87}Rb/^{86}Sr$ in Lesser Himalayan samples collected from the Bhote Kosi.

In the Lesser Himalayan Formation (fig. 7.10), carbonate samples are clearly unsupported and therefore isotopic exchange with associated silicates is required to explain their current $^{87}Sr/^{86}Sr$ (see section 7.6). Assuming an age of 2500 Ma, the majority of calc-silicate samples are supported, although most are unsupported if an ge of 1800 Ma is invoked. A few samples remain supported even at 1800 Ma. There is no apparent pattern to explain these variations. Relatively unradiogenic ($^{87}Sr/^{86}Sr$ ~0.73) through to highly radiogenic (~1.1) samples are found to be unsupported at 2500 Ma, representing samples comprising mostly carbonate through to those where silicate mineralogy is dominant. Additionally, supported and unsupported calc-silicates are not confined to particular lithological units with calc-silicates of both types obtained from the Dhading Dolomite, Benighat Slates and Dandagaon Phyllites / Nourpul Formation. The above observations suggest that any isotopic exchange is on relatively local (metre) scale. Indeed, the samples do not form any sort of isochron on fig. 7.10 and thus the isotopic equilibration of all rocks during a major metamorphic event is precluded. Unexpectedly, unsupported silicate samples are also observed in fig. 7.10 These rocks, being highly radiogenic and with relatively high $^{87}Rb/^{86}Sr$, have possibly have lost ^{87}Rb rather than gained ^{87}Sr. Diffusion gradients would allow for Rb loss by silicates to calc-silicates or carbonates, while transfer of Rb in the other direction would not be expected and therefore is unlikely to explain the unsupported calc-silicate and carbonate samples. Fig. 7.10 provides evidence of strontium isotopic exchange between silicates and carbonates and calc-silicates and strongly suggests the presence of radiogenic carbonate material within the calc-silicates of the LHF. Supported samples might also contain radiogenic carbonate, however, as a result of exchange between carbonate and silicate minerals *within* the

sample. In section 7.7, we provide the first direct evidence of both types of isotopic exchange.

7.6. Lesser Himalayan Traverses.

Several traverses were collected from the Nawakot Group with the aim of obtaining sequences of closely associated silicates and calc-silicates or carbonates, in order to study possible isotopic exchange. Identifying such sequences in the field proved to be far from easy, principally because of the difficulty of identifying the calc-silicates in the field due to both the lack of calcitic material (i.e. that fizzes with dilute acid) and to the very fine crystal size of the LHF. Many of the traverses that were collected, despite appearing suitable in outcrop, with distinct superficial differences, yielded rocks of largely similar composition. These include traverse BK56 (calc-silicates of the Dhading Dolomite), BK117 (silicates of the Robang Formation) and BK124 (calc-silicates of the Nourpul Formation). Traverse BK114 comprises several calc-silicate samples (BK114 a-e) collected at varying distance from a pure silicate. All samples are radiogenic however, with no observed relationship between the distance from the silicate and $^{87}Sr/^{86}Sr$ (the least radiogenic sample is in fact that closest to the silicate).

Traverse BK127 (fig. 7.11 and fig. 7.12) comprises limestone (possibly stromatolitic) of the Dandagaon Phyllites / Nourpul Formation, overlain by and overlying mica schists. Samples were collected from either side of both the upper and lower boundaries between carbonate and silicate (fig. 7.12). The mica schists are extremely radiogenic ($^{87}Sr/^{86}Sr = 0.91 - 0.97$) and are characterised by high $^{87}Rb/^{86}Sr$ (8 – 12).

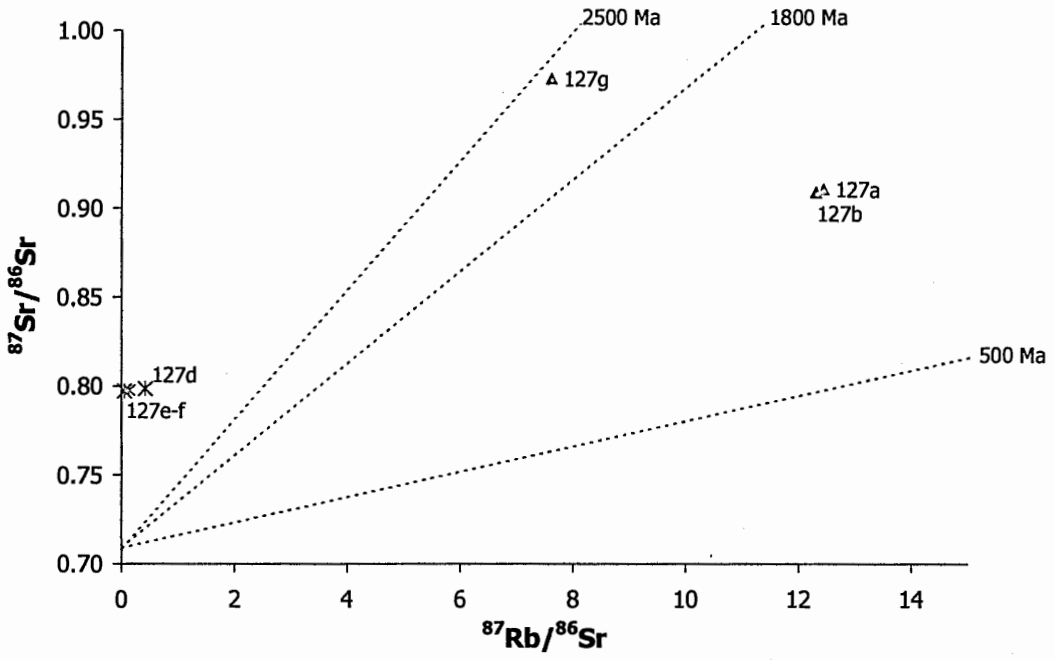

Fig. 7.11. $^{87}Sr/^{86}Sr$ vs $^{87}Rb/^{86}Sr$ in samples from the BK127 traverse in the Lesser Himalaya. Carbonates are represented by blue stars, silicates by red triangles.

The carbonates are also radiogenic (~0.797), although not to the same extent as the silicates, and contain negligible Rb ($^{87}Rb/^{86}Sr$ <1). A sample obtained from the middle of the carbonate horizon (BK127e) has virtually identical rubidium and strontium chemistry to those bordering the silicate, suggesting the occurrence of isotopic exchange on the scale of the carbonate unit (~1 metre), with no signs of a diffusion gradient. Fig. 7.11 shows that the carbonates are unsupported, while the Sr-isotope ratios of the silicates can be explained through natural isotope decay. If it is assumed that the carbonates of the traverse would have an $^{87}Sr/^{86}Sr$ of no more than 0.72 in the absence of Sr-exchange processes (fig. 7.11), it would be necessary for

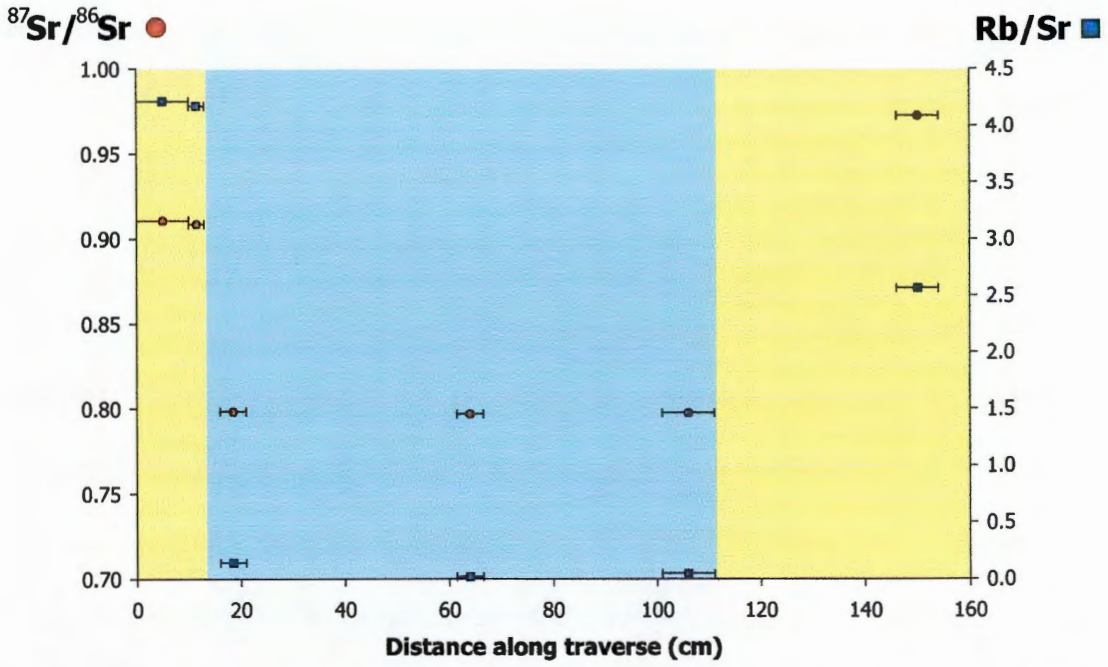

Fig. 7.12. Changes in $^{87}Sr/^{86}Sr$ and Rb/Sr ratios along a carbonate / silicate traverse in the Lesser Himalaya of the Bhote Kosi (samples BK127a-g).

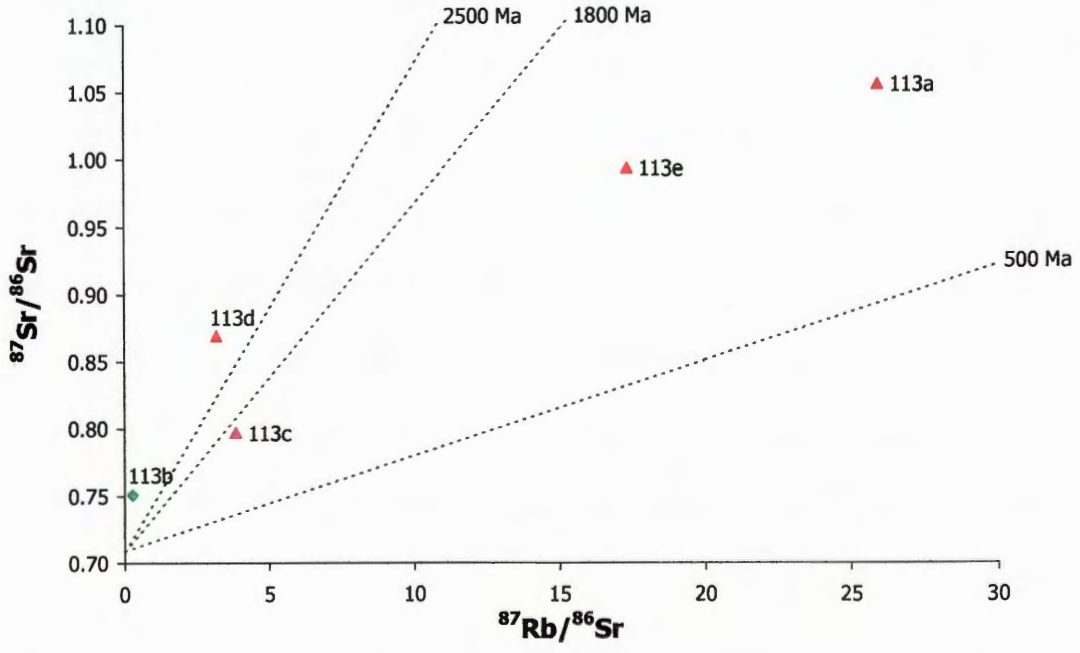

Fig. 7.13. $^{87}Sr/^{86}Sr$ vs $^{87}Rb/^{86}Sr$ in rocks of traverse BK113 collected in the Lesser Himalaya. The calc-silicate sample is shown as a green diamond, the surrounding silicate samples as red triangles.

approximately one-third of the strontium currently present in the carbonates to have originated from surrounding silicate to explain their current measured $^{87}Sr/^{86}Sr$.

Traverse BK113 was collected from the Benighat Slates. Sample BK113b is a calc-silicate, overlain by micaceous metasandstones (BK113c-d), with mica schist below (BK113a). Fig. 7.14 shows that the calc-silicate is moderately radiogenic ($^{87}Sr/^{86}Sr$ = 0.750), and is unsupported (fig. 7.13), the $^{87}Rb/^{86}Sr$ of 0.28 again suggesting that the maximum Sr-isotope ratio resulting from undisturbed radioactive Rb decay would be ~0.72. The overlying metasandstones are more radiogenic ($^{87}Sr/^{86}Sr$ = 0.80 - 0.87) with moderate $^{87}Rb/^{86}Sr$ (3 - 4), while the underlying mica schist is considerably more radiogenic still ($^{87}Sr/^{86}Sr$ = 1.06, $^{87}Rb/^{86}Sr$ = 26). To account for the $^{87}Sr/^{86}Sr$ in excess of 0.72 would require ~25% of the Sr in the calc-silicate to have originated from the overlying metasandstone (assuming an average Sr-isotope ratio of 0.75 in this unit), or for 10% to have exchanged from the more radiogenic mica schists below (assuming a maximum $^{87}Sr/^{86}Sr$ of 1.06). Fig. 7.13 also shows that one of the metasandstones (BK113d) is unsupported, in contrast to the samples of mica schist, which fall well below the 1800 Ma isochron. This indicates that isotopic exchange might additionally have taken place between the highly radiogenic mica schists and less radiogenic metasandstones. Fig. 7.13 indicates that sample BK113d would obtain an $^{87}Sr/^{86}Sr$ of ~0.8 through natural decay over a period of 1800 Ma. Therefore, ~30% of its bulk Sr would have resulted from the exchange of Sr with the mica schists (again, assuming a maximum $^{87}Sr/^{86}Sr$ of 1.06 in the schists) to obtain the measured $^{87}Sr/^{86}Sr$ of 0.869. Trace vein carbonate is observed in sample BK113d.

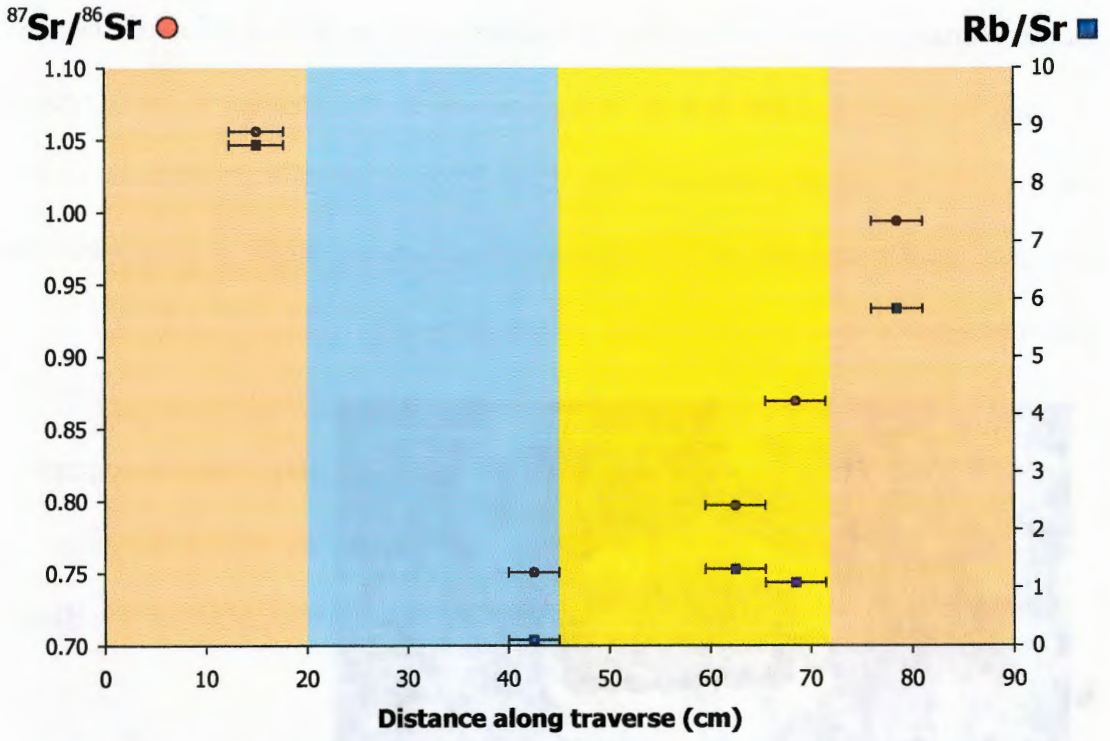

Fig. 7.14. Changes in $^{87}Sr/^{86}Sr$ and Rb/Sr ratios along a carbonate / silicate traverse in the Lesser Himalaya of the Bhote Kosi (samples BK113a-e).

7.7. Laser Ablation Analysis of Carbonate in Calc-Silicates.

The results presented above provide strong circumstantial evidence indicating that carbonate material within the Nawakot Group calc-silicates is highly radiogenic. The only direct evidence of radiogenic carbonate, however, is from the sparse limestone samples. Bickle *et al.* (2001) have found high $^{87}Sr/^{86}Sr$ ratios in leachates from LHF calc-silicates of the Deoban Formation in the Garhwal Himalaya (the stratigraphical equivalent of the Dhading Dolomite of the Bhote Kosi; Valdiya, 1986), but considerable doubt remains regarding the significance of these results owing to potential input from easily released grain boundary strontium from silicate minerals. To overcome this problem, individual carbonate crystals within LHF calc-silicates were analysed by laser ablation MC-ICP-MS. Unfortunately, the calc-silicates of the

Lesser Himalaya do not readily lend themselves to this technique, primarily because of their fine grain size and low Sr concentrations. It was possible to make several analyses of two samples from the LHF. In addition, a calc-silicate from the HHCS was analysed for comparison; with abundant strontium and large calcite crystals this provided a much more suitable sample for this technique.

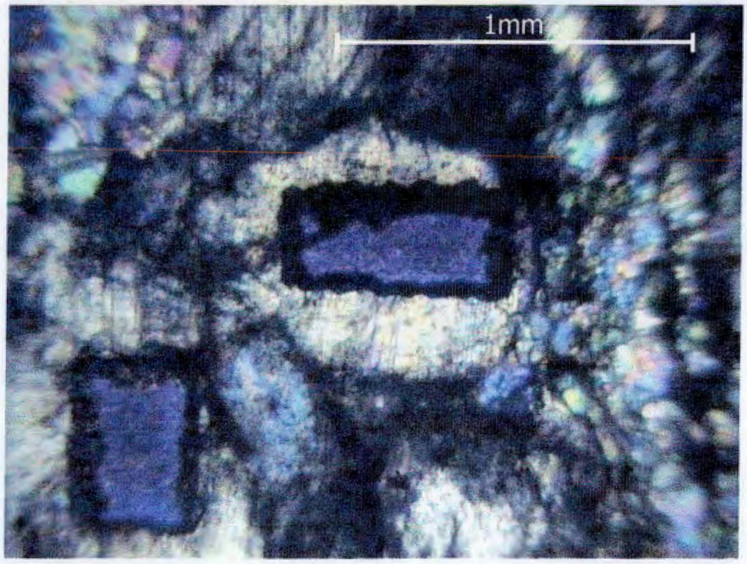

Fig. 7.15. Photograph of ablated dolomite crystal in sample BK11.

Sample BK11 was collected from the Dandagaon Phyllites / Nourpul Formation. In thin section the dominant mineral observed is dolomite (>60%), which occurs as coarse crystals up to 2 mm (excellent for laser analysis). The rest of the rock consists of finer crystals (0.05 - 0.1 mm) of quartz, green biotite and opaque iron minerals. Distinct quartz-rich bands are observed in which biotite is also more prevalent (~10% compared with <5% in carbonate-rich parts of the rock). XRF analysis reveals 190 ppm of strontium, much higher than the average for Lesser Himalayan calc-silicates in this study, and 54 ppm rubidium ($^{87}Rb/^{86}Sr$ of 0.8), more consistent with what would be expected from a "normal" carbonate. The coarse grain size enabled isotopic analysis of six individual dolomite crystals (fig. 7.15) yielding $^{87}Sr/^{86}Sr$ of 0.9305 - 0.9349. The bulk rock $^{87}Sr/^{86}Sr$ of 0.9302 is well within the error of all six analyses

(fig. 7.16). This is clear evidence that the carbonate material within BK11 is extremely radiogenic, and that isotopic homogenisation has occurred between the carbonate and silicate portions of the rock. The bulk rock Sr-isotope ratio for BK11 is unsupported (fig. 7.10) and thus the radiogenic strontium is likely to have originated from an external source. The laser ablation MC-ICP-MS allows an estimate (± 50%) of Rb/Sr to be made, which from the six analyses of BK11 lies between 8×10^{-4} and 8×10^{-5}, confirming that the carbonate material is unsupported in the extreme.

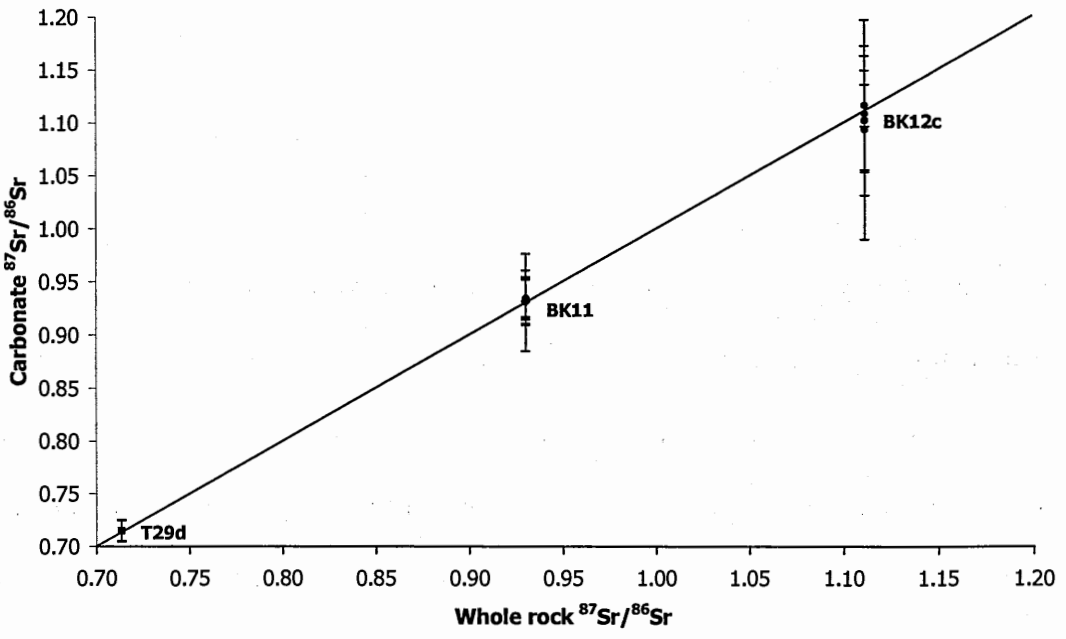

Fig. 7.16. Carbonate $^{87}Sr/^{86}Sr$ measured by laser ablation plotted against whole rock $^{87}Sr/^{86}Sr$. Error bars are shown for each of the ablation samples, and all samples fall close to the 1:1 reference line.

Sample BK12c is in fact classified in this study as a silicate, thin section analysis showing that carbonate material comprises only a few percent, occurring as discrete pockets within quartz (~40%) and muscovite (~50-55%). Both quartz and carbonate crystals reach up to 1 mm, allowing laser ablation of five dolomite crystals (fig. 7.17). BK12c has a chemical composition more typical of the Lesser Himalaya than BK11, containing very little strontium (20 ppm) and with a high $^{87}Rb/^{86}Sr$ (19.0). Laser ablation produced $^{87}Sr/^{86}Sr$ between 1.093 and 1.116 in the dolomite (fig. 7.16), well within error of the bulk rock $^{87}Sr/^{86}Sr$ ratio of 1.111. This once again demonstrates isotopic homogenisation between the carbonate and silicate components of the rock. The high Sr-isotopic ratio of BK12c is shown to be supported by its high $^{87}Rb/^{86}Sr$ content at <1800 Ma and thus in this case it is possible to explain the presence of radiogenic carbonate in this sample through isotopic exchange with silicate (mica) on the grain size scale. Estimates of carbonate Rb/Sr content range between 4×10^{-3} and 5×10^{-4} (± 50%), thus again revealing the carbonate material itself to be strongly unsupported.

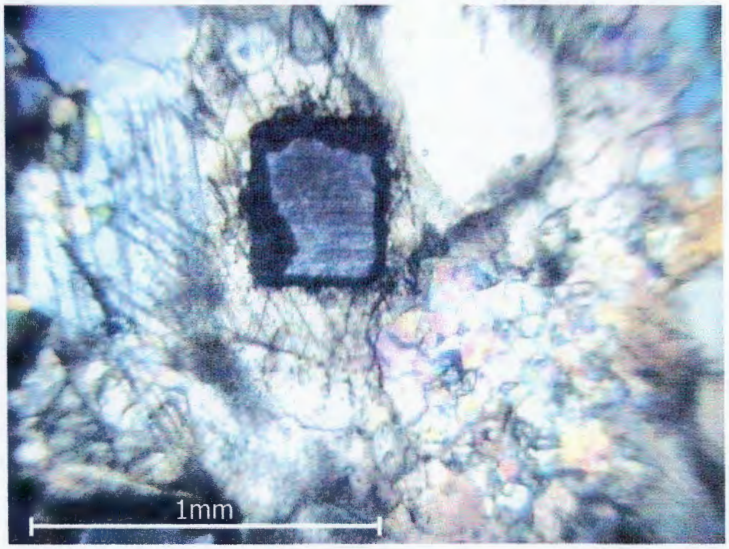

Fig. 7.17. Photograph of laser ablated dolomite crystal within sample BK12c. Closely associated mica can be seen below and to the right of the carbonate.

Sample T29d is a calc-silicate typical of those collected from the High Himalayan Crystalline Series, comprising coarse (0.3 - 2 mm), well-formed calcite crystals (~60-70% in thin section) and finer quartz (~15%), pyroxene (~15%) and occasional weathered feldspar. As in other associated samples, T29d is marked by high Sr (714 ppm) and low $^{87}Rb/^{86}Sr$ (0.25). Five calcite crystals were ablated (fig. 7.18a and b) giving a consistent $^{87}Sr/^{86}Sr$ of 0.715, slightly higher than the bulk rock ratio of 0.713, although the bulk rock ratio falls well within the error on the carbonate samples (fig. 7.16). Once again the sample appears to be reasonably homogenous isotopically. The ablation Rb/Sr estimate, which ranges between 4×10^{-3} and 5×10^{-4}, again shows that the carbonate material within this sample could not have obtained its current measured $^{87}Sr/^{86}Sr$ simply through decay of the rubidium present. crystals are clearly observed above.

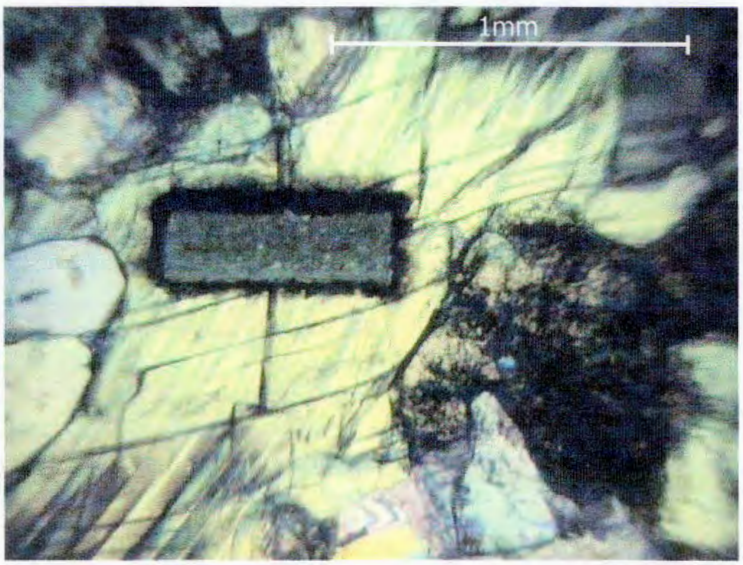

Fig. 7.18a. Photograph of laser ablated calcite crystal in sample T29d from the High Himalayan Crystalline Series.

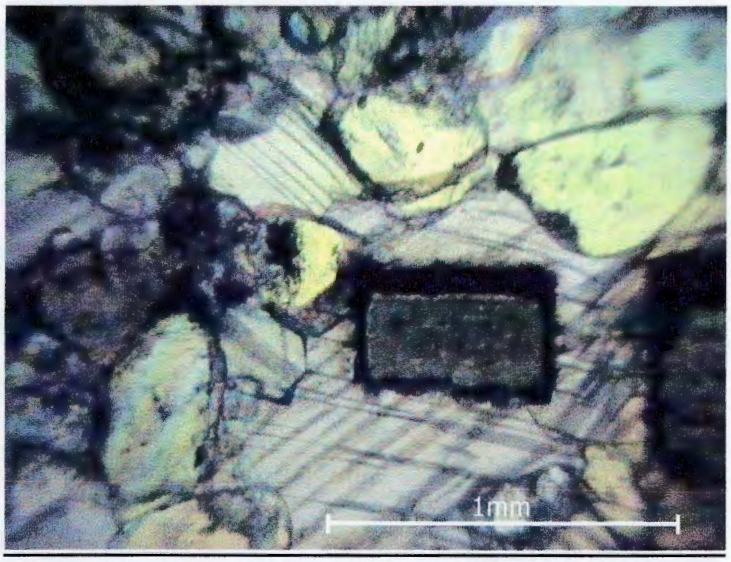

Fig. 7.18b. Laser ablated calcite crystal in sample T29d. Rounded quartz

7.8. The Source of High $^{87}Sr/^{86}Sr$ in Lesser Himalayan Carbonate.

In section 7.4, it was established that the carbonates and calc-silicates of the Lesser Himalaya are marked by high $^{87}Sr/^{86}Sr$ and low Sr concentrations, the latter possibly resulting, at least in part, from barium substitution. It was not clear, however, whether Sr depletion of carbonate had led to a prominent impact for radiogenic silicate (carbonate typically dominates weathering inputs into rivers owing to its higher strontium content in addition to its greater weatherability), or the carbonate itself had acquired high $^{87}Sr/^{86}Sr$ during alteration. The second half of this chapter suggests there is indeed evidence of a prominent role for isotopic exchange in the Lesser Himalaya. Laser ablation MC-ICP-MS analysis provides the first direct measurement of carbonate material in LHF calc-silicates. Results indicate that the carbonate has the same $^{87}Sr/^{86}Sr$ as whole rock, even though rubidium is almost entirely absent. The precise nature and extent of isotopic exchange remains unclear. Radiogenic carbonate within a supported sample, such as BK12c, could be the result

of exchange between crystals in the same sample, while in samples unsupported on a bulk scale, such as BK11 or the limestones of the BK127 traverse, exchange with neighbouring silicate, or perhaps even fluid from a more distant source, is required. The presence of unsupported silicate rocks (lacking even trace carbonate in thin section) (fig. 7.10) supports the latter suggestion, although the presence of supported, unradiogenic calc-silicates (e.g. BK123) indicates that any exchange process is not pervasive throughout the Nawakot Group. The results of laser ablation isotopic analysis reveal that carbonate and silicate within the same rock have almost identical Sr-isotopic ratios despite vastly differing Rb/Sr ratios. This strongly suggests that little time has elapsed since isotopic equilibration occurred i.e. that isotopic exchange occurred during the Himalayan Orogeny.

Chapter 8

The Impact of Bhote Kosi Strontium Fluxes on Marine $^{87}Sr/^{86}Sr$.

In chapter 5, the link between the weathering of carbonate material of the Lesser Himalaya and the strontium isotope ratio of Himalayan rivers is clearly demonstrated. The Lesser Himalayan Formation is not the dominant source of fluvial strontium, however, this typically being the limestones of the Tibetan Sedimentary Series, which despite having low $^{87}Sr/^{86}Sr$ in Himalayan terms (~0.72) are still considerably more radiogenic than seawater (~ 0.709). In this chapter the likely strontium fluxes arising from each geological unit of the Bhote Kosi are calculated, and subsequently the impact of each upon the $^{87}Sr/^{86}Sr$ ratio of seawater. This is crucially important if the findings from the Bhote Kosi are to be applied to the debate regarding the use of the dissolved $^{87}Sr/^{86}Sr$ of seawater as a silicate weathering proxy.

8.1. Strontium Fluxes in the Bhote Kosi.

Water flux data for the Bhote Kosi are limited to measurements made at Barabise during 1965 (HMG Nepal Department of Irrigation, Hydrology and Meteorology, as published in Alford, 1992). Barabise is positioned approximately midway between the MCT and

the confluence of the Bhote Kosi and the Indrawati (see plate 2) and thus these flux measurements reveal little about the relative fluxes which might be expected from the different geological units of the Bhote Kosi. An estimate of such fluxes can be calculated using average monthly rainfall data (Chalise *et al.*, 1996) for the Bhote Kosi (fig. 2.4 - 2.6), as shown in table 8.1. From these values, strontium fluxes can be calculated using the mean strontium concentrations in the dissolved load obtained for the rivers traversing the Tibetan Sedimentary Series, High Himalayan Crystalline Series and Lesser Himalayan Formation as given in section 5.6.8 (see table E1), which are corrected for atmospheric inputs as described in section 4.1.

Month	Geology	Area underlain (km^2)	Average precip. (mm)	Mean [Sr^{2+}] (µmol/l)	Water flux (m^3)	Strontium flux (mol/ month)
September	TSS	608	188.6	2.097	8.60E+07	1.80E+05
	HHCS	2098	399.2	0.219	6.28E+08	1.37E+05
	LHF	722	386.8	0.128	2.09E+08	2.68E+04
	Total				**9.24E+08**	**3.44E+05**
October	TSS	608	28.7	2.097	1.31E+07	2.74E+04
	HHCS	2098	94.2	0.219	1.48E+08	3.24E+04
	LHF	722	94.7	0.203	5.13E+07	1.04E+04
	Total				**2.13E+08**	**7.02E+04**
November	TSS	608	8.3	2.097	3.79E+06	7.96E+03
	HHCS	2098	17.2	0.219	2.70E+07	5.90E+03
	LHF	722	14.3	0.203	7.73E+06	1.57E+03
	Total				**3.85E+07**	**1.54E+04**
December	TSS	608	7.5	2.097	3.42E+06	7.18E+03
	HHCS	2098	17.5	0.219	2.75E+07	6.02E+03
	LHF	722	17.5	0.203	9.48E+06	1.92E+03
	Total				**4.04E+07**	**1.51E+04**

Table 8.1. Calculated monthly water and strontium fluxes from the major lithologies of the Bhote Kosi. Fluxes are adjusted for 25% evapotranspiration (Alford, 1992).

Table 8.1. shows that, as would be expected, strontium fluxes decline during the post-monsoon season, with a fivefold decrease in the overall Bhote Kosi flux between

September and October, a further fourfold decrease between October and November, remaining constant between November and December, by which time baseflow is reached. Table 8.1. suggests that the dominant sources of the Bhote Kosi strontium flux are the TSS (39-52%) and HHCS (38-46%), with a much smaller flux from the LHF (8-15%). The calculations in table 8.1 take no account of water originating as rainfall falling on the the TSS or HHCS, which subsequently passes over and weathers bedrock of downstream LHF units. Thus, the Sr flux estimates in table 8.1 provide an underestimate of the Sr flux from the Lesser Himalaya (and the HHCS to a lesser extent), but are still useful in ascertaining the *minimum* impact of the LHF on seawater.

To counter the problem outlined above the water flux of the Bhote Kosi at Dolalghat (the downstream sampling point in the Bhote Kosi) was calculated, again using the rainfall data of Chalise *et al.* (1996). The relative strontium fluxes from the TSS, HHCS and LHF can then be apportioned according to the results of the mass balance calculations carried out in section 5.6.8 (table E1). Estimates of the actual strontium flux from each unit were then calculated, as shown in table 8.2, from the strontium concentrations of the samples collected at Dolalghat (BK74 in September, BK35 in November). The main uncertainty in this approach is the assumption that these spot sample strontium concentrations are representative of the Bhote Kosi throughout the whole month in which they were taken. This uncertainty can be checked by comparing the calculated Sr fluxes for the whole of the Bhote Kosi in table 8.2 with those in table 8.1 (minimum fluxes). Table 8.2 gives an overall strontium flux for November which is within 10% of that in table 8.1, indicating that the strontium concentration measured in

sample BK35 is broadly representative for this month. In September, however, the calculation in table 8.2 produces a strontium flux only 50% of that calculated in table 8.1, indicating that sample BK74 is not representative of the September chemistry of the Bhote Kosi. This was expected as sample BK74 was collected following a major rainstorm, and thus the measured Sr concentration in this case is more likely to be representative of the monsoon months.

Month	Geology	Area undelain (km^2)	Average precip. (mm)	$[Sr^{2+}]$ (µmol/l)	Water flux (m^3)	Strontium flux (mol/ month)	% from mass balance
Septmber	All	3428	359.2	0.189	9.24E+08	1.75E+05	
	Atmos.					1.94E+04	11.1%
	TSS					6.67E+04	38.2%
	HHCS					3.11E+04	17.8%
	LHF					5.74E+04	32.9%
November	All	3428	15.7	0.336	4.04E+07	1.36E+04	
	Atmos.					8.56E+02	6.3%
	TSS					7.89E+03	58.1%
	HHCS					1.28E+03	9.4%
	LHF					3.56E+03	26.2%

Table 8.2. Water and strontium fluxes calculated for the Bhote Kosi at Dolalghat using strontium concentrations from samples BK74 and BK35 and the results of a strontium mixing plot (fig. 5.24 and fig. 5.25). Fluxes are adjusted for 25% evapotranspiration.

8.2. The Impact of the Bhote Kosi Strontium Flux on Marine $^{87}Sr/^{86}Sr$.

The impact of any river strontium flux on the $^{87}Sr/^{86}Sr$ of seawater can be calculated using the following equation;

Equation 8.1.

$$y = \left(\frac{J_{sw}\, r_{sw} + r_x\, J_x}{J_{sw} + J_x}\right) - r_{sw}$$

Where;

y = river impact on marine $^{87}Sr/^{86}Sr$.

J = Sr flux.

r = $^{87}Sr/^{86}Sr$.

$_x$ = river.

$_{sw}$ = seawater.

	J (mol/month x 10^{10})	$^{87}Sr/^{86}Sr$	Impact on marine $^{87}Sr/^{86}Sr$	
September				
TSS	1.804E-05	0.7203	4.80E-07	**20.2%**
HHCS	1.137E-05	0.7379	7.90E-07	**33.1%**
LHF	2.692E-06	0.8793	1.11E-06	**46.7%**
Total	3.211E-05		2.38E-06	
October				
TSS	2.744E-06		7.30E-08	**11.0%**
HHCS	3.237E-06	0.7379	2.25E-07	**33.8%**
LHF	9.641E-07	0.8656	3.66E-07	**55.2%**
Total	6.944E-06		6.64E-07	
November				
TSS	7.956E-07	0.7203	2.12E-08	**18.0%**
HHCS	5.904E-07	0.7379	4.10E-08	**34.9%**
LHF	1.453E-07	0.8656	5.52E-08	**47.0%**
Total	1.531E-06		1.17E-07	
December				
TSS	7.176E-07	0.7203	1.91E-08	**14.9%**
HHCS	6.015E-07	0.7379	4.18E-08	**32.5%**
LHF	1.781E-07	0.8656	6.77E-08	**52.6%**
Total	1.497E-06		1.29E-07	
Total Sr in seawater	0.4115 mol x 10^{10}	0.7093		

Table 8.3. Calculated impact on seawater $^{87}Sr/^{86}Sr$ of strontium fluxes from the different lithological units of the Bhote Kosi basin as calculated in table 7.1.

	J (mol/month x 10^{10})	$^{87}Sr/^{86}Sr$	Impact on marine $^{87}Sr/^{86}Sr$	
September				
Atmospheric	1.938E-06	0.7140	2.21E-08	**0.90%**
TSS	6.668E-06	0.7203	1.77E-07	**6.40%**
HHCS	3.107E-06	0.7379	2.16E-07	**7.70%**
LHF	5.743E-06	0.8793	2.37E-06	**85.10%**
Total	1.746E-05		2.79E-06	
November				
Atmospheric	8.558E-08	0.7140	9.77E-10	**0.70%**
TSS	7.893E-07	0.7203	2.10E-08	**12.60%**
HHCS	1.277E-07	0.7379	8.87E-09	**5.30%**
LHF	3.559E-07	0.8656	1.35E-07	**81.40%**
Total	1.358E-06		1.66E-07	
Total Sr in seawater	0.4115 mol x 10^{10}	0.7093		

Table 8.4. Calculated impact on seawater $^{87}Sr/^{86}Sr$ of strontium fluxes from the different lithological units of the Bhote Kosi basin as calculated in table 7.2.

Using equation 8.1, tables 8.3 and 8.4 shows the calculated impacts on seawater of the Bhote Kosi fluxes listed in table 8.1 and 8.2. If the results from the Bhote Kosi are taken as representative of the central Himalaya as a whole then they reveal a potential major role for the weathering of Lesser Himalayan carbonate in the impact of the Ganges-Brahmaputra on seawater $^{87}Sr/^{86}Sr$. Table 8.3 shows that a minimum 44-57% of the impact of the strontium of the Bhote Kosi on the marine Sr-isotope ratio is the result of the weathering of the Lesser Himalaya, while table 8.4 suggests that a more realistic figure exceeds 80%. This is far in excess of the proportion of the strontium flux in the Bhote Kosi accounted for by the Lesser Himalaya, the result of the high $^{87}Sr/^{86}Sr$ of LHF weathering inputs. According to the mass balance carried out in section 5.6.8, ~70% of the strontium from the LHF (when adjusted for atmospheric input as are the data in

tables 8.1-8.4) is accounted for by carbonate weathering, thus suggesting that 35-55% of the impact of the Bhote Kosi upon marine $^{87}Sr/^{86}Sr$ is the result of the weathering of Lesser Himalayan carbonate.

Despite the Tibetan Sedimentary Series being the dominant source of dissolved strontium in the Bhote Kosi, and the fact that ~75% of the water flux of the Bhote Kosi originates from the area occupied by the High Himalayan Crystalline Series (table 8.1), table 8.4 suggests that only ~20% of the impact of the Bhote Kosi strontium flux on marine $^{87}Sr/^{86}Sr$ is resultant from the Sr fluxes from these units. In the case of the TSS, this is accounted for by the relatively low $^{87}Sr/^{86}Sr$ of strontium weathered from these rocks (compared with the LHF), while in the case of the HHCS a lower $^{87}Sr/^{86}Sr$ (relative to the Lesser Himalaya) is coupled with the resistivity to weathering of the largely gneissic and granitic bedrock.

In table 8.4, the impact of the September flux from the HHCS dominates slightly (8%) over that from the TSS (6%), while in November it is the TSS input that is of greater importance (12% compared with 5% for the HHCS). This would appear to suggest that monsoonal precipitation increases the importance of the HHCS (and LHF) by increasing the contrast between the water flux from north of the Himalayan range (which is much less owing to the orographic rainshadow effect of the range) and that from south of the high mountains. This theory is supported to an extent by the rainfall and flux data of table 8.1, which shows that between September and December rainfall in the TSS is consistently approximately half that south of the MCT except in October when it drops

to approximately one-third. Water flux from the TSS is calculated to be consistently around ten times less than that from south of the MCT, twenty times less in October. It is certainly plausible that the storm after which sample BK74 was collected brought a surge of water from the southern flanks of the Himalaya, temporarily increasing the proportion of Bhote Kosi strontium from the HHCS and LHF.

Table 8.4 shows that, despite waters being more dilute, the increased strontium flux in September results in an almost twentyfold increase in the impact of Bhote Kosi on marine $^{87}Sr/^{86}Sr$. The crucial importance of the monsoon period on the impact of Himalayan rivers upon seawater is clearly demonstrated. The September sampling carried out for this project provides indications as to the changes in water chemistry that might be expected during the monsoon, particularly for samples such as BK74, which were collected subsequent to significant rainfall. Table 8.4 and table 5.3 suggest that the importance of the Lesser Himalaya, and of LHF carbonates in particular, is unabated at this time. Indeed, the data suggest that strontium input from the weathering of the LHF might become more prominent during the monsoon in terms of its impact on seawater. This could only be confirmed, however, through monsoon sampling.

8.3. Predicting Marine $^{87}Sr/^{86}Sr$ in the Absence of the Lesser Himalaya.

The $^{87}Sr/^{86}Sr$ of seawater can be calculated using the following equation;

Equation 8.2.

$$R_{sw} = \frac{((J_{hy}\, r_{hy}) + (J_{dia}\, r_{dia}) + (J_{GB}\, r_{GB}) + (J_{riv}\, r_{riv}))}{J_{sw}}$$

Where;

J = strontium flux.

r = $^{87}Sr/^{86}Sr$.

$_{sw}$ = seawater.

$_{hy}$ = hydrothermal input from mid-ocean ridges.

$_{dia}$ = diagenetic input from alteration of basalt.

$_{GB}$ = input from the Ganges-Brahmaputra.

$_{riv}$ = input from other rivers.

Using this equation it is possible to make an estimate of the expected $^{87}Sr/^{86}Sr$ of seawater in the absence of the uplift of the Lesser Himalaya. In doing this the values given in table 8.5 are used.

Flux	J (mol/yr x 10^{10})	$^{87}Sr/^{86}Sr$
Seawater	4.94	0.7093
Hydrothermal	1.33	0.7035
Diagenetic	0.34	0.7084
Ganges-Brahmaputra	0.07	0.7295
Global rivers (-G-B)	3.20	0.7114
Global rivers	3.27	0.7118

Table 8.5. Global strontium fluxes assumed in this study (sources: Palmer and Edmond, 1989; Hodell *et al.*, 1990; Galy *et al.*, 1999).

In order to calculate seawater $^{87}Sr/^{86}Sr$ in the absence of the Lesser Himalaya it is essential to know the current proportion of strontium in the Ganges-Brahmaputra derived from Himalayan and non-Himalayan sources. This can be done as follows;

Equation 8.3.

$$f = \frac{(r_{GB} - r_{non\text{-}Him})}{(r_{Him} - r_{non\text{-}Him})}$$

Where;

f= the present day proportion of strontium in the Ganges-Brahmaputra derived from the Himalaya.

r = $^{87}Sr/^{86}Sr$.

$_{Him}$ = Himalayan input into the Ganges-Brahmaputra.

$_{Non\text{-}Him}$ = Non-Himalayan input into the Ganges-Brahmaputra.

Assuming that $^{87}Sr/^{86}Sr$ from non-Himalayan sources is 0.715 (Krishnaswami *et al.*, 1992) and that Himalayan inputs have an overall $^{87}Sr/^{86}Sr$ of 0.75 (that of the Sapt Kosi), f is calculated to be 0.41. The $^{87}Sr/^{86}Sr$ of the Ganges-Brahmaputra in the absence of the Lesser Himalaya ($r_{GB\text{-}LHF}$) can now be calculated as follows;

Equation 8.4.

$$r_{GB\text{-}LHF} = r_{Him\text{-}LHF}\, f + r_{non\text{-}Him}\, 1 - f$$

Where $r_{Him\text{-}LHF}$ is the $^{87}Sr/^{86}Sr$ of the Himalayan strontium flux prior to the uplift of the Lesser Himalaya. It is estimated that this value lies between 0.72 (the $^{87}Sr/^{86}Sr$ of the TSS, inputs from which are likely to predominate over those from the HHCS) and 0.73 (slightly higher than the $^{87}Sr/^{86}Sr$ of the Bhote Kosi at the MCT). Assuming this range of values, equation 8.4 was used to predict that the $^{87}Sr/^{86}Sr$ of the Ganges-Brahmaputra prior to the exposure of the Lesser Himalaya would have been between 0.717 and 0.721. Modern marine $^{87}Sr/^{86}Sr$ in the absence of Lesser Himalayan input can now be calculated using equation 8.2, resulting in a range between 0.70914 and 0.71919. Thus, it is concluded that modern seawater would have an $^{87}Sr/^{86}Sr$ ratio that is 0.00011 – 0.00016 lower in the absence of the uplift of the Lesser Himalaya, inputs from which have been shown in previous chapter 5 to be dominated by input from carbonate. This is equal to the increase in the marine $^{87}Sr/^{86}Sr$ in the last 2.5 – 6 Ma. If the Lesser Himalaya were only extensively exposed in the last 5 Ma then potentially the uplift of the LHF could explain the entire increase in marine $^{87}Sr/^{86}Sr$ between 5 Ma and the present day. Assuming an older exhumation of the Lesser Himalaya (Robinson *et al.*,

2000; Chesley *et al.*, 2000; France-Lanord and Galy, 2001), weathering of this unit would still account for a substantial part of the increase in the marine strontium isotope record during this period, the exact proportion dependent upon the assumed time of Lesser Himalayan uplift.

Chapter 9

Conclusions

9.1. Summary of Thesis Findings.

The marked increase in dissolved $^{87}Sr/^{86}Sr$ noted in the Bhote Kosi downstream of the MCT is not exceptional, being a feature common to several Himalayan river studies (Derry and France-Lanord, 1996a; Galy *et al.*, 1999; English *et al.*, 2000; Bickle *et al.*, 2001), but the role of carbonate dissolution in this trend has remained uncertain. Principal components analyses and multiple regression, unbiased by user interpretation, reveal a strong, positive statistical link between the Lesser Himalaya, and in particular the calc-silicates of the Nawakot Group, and dissolved $^{87}Sr/^{86}Sr$. Sampling of tributaries draining only the Nawakot Group indicates that these rivers are consistently radiogenic ($^{87}Sr/^{86}Sr > 0.8$), and whilst highly variable, mass balance calculations suggest that on average ~70% of this dissolved strontium is a consequence of carbonate dissolution.

The unusually low strontium concentration of carbonate in the Lesser Himalaya is the principal reason for previous workers (e.g. Singh *et al.*, 1998; Galy *et al.* 1999) rejecting the possibility of a potentially prominent role for these units in determining dissolved Sr-isotope ratios in the Himalaya. This important consideration has been fully evaluated in

this work, however, by applying the Ca/Sr ratio obtained from tributaries of the Bhote Kosi draining only the Lesser Himalaya to the mass balance calculations (section 5.6.8). This cannot be done for mixed-lithology rivers when a uniform carbonate composition needs to be assumed (e.g. Galy *et al.*, 1999). Adopting this more realistic Sr/Ca ratio reduces the calculated dissolved strontium flux of the Bhote Kosi that has been derived from the LHF carbonates from >60% (Harris *et al.*, 1998) to ~30%. Using a combination of mass balance, strontium mixing calculations and flux estimates it is shown that despite this reduced calculated input, it is the Lesser Himalaya that has the predominant impact (>80%) upon marine $^{87}Sr/^{86}Sr$ when the water from the Bhote Kosi reaches the Bay of Bengal. The impact of the Bhote Kosi itself on seawater is of course negligible, but assuming that the Bhote Kosi is typical of the rest of the central Himalaya, the findings outlined above provide an important addition to the body of knowledge of the link between dissolved $^{87}Sr/^{86}Sr$ and silicate weathering in the Himalaya.

Singh *et al.* (1998) contest that the situation in the Bhote Kosi is, however, atypical of the Himalaya as a whole, the majority of carbonate samples collected by these authors from the LHF of the Kumaun and Himachal Himalaya being relatively unradiogenic ($^{87}Sr/^{86}Sr$ = 0.71-0.73). We show in section 7.3 that Lesser Himalayan calc-silicates with comparable $^{87}Sr/^{86}Sr$ are present in the Bhote Kosi, and it was these specimens that were most readily identified as carbonate-bearing in the field. Extensive sampling of the Bhote Kosi indicates that in fact mica-bearing calc-silicates are the dominant lithology of the Nawakot Group (as also indicated by the original mapping of Stöcklin, 1980 and Stöcklin and Bhattarai, 1980), with such rocks found to be highly radiogenic (see also

English *et al.*, 2000 and Bickle *et al*, 2001) yet not readily identified as carbonate-bearing in the field. Therefore, it appears that Singh *et al.* (1998) may have underestimated the typical Sr-isotopic input of Lesser Himalayan carbonate by selectively sampling the most "obvious" (i.e. the most pure) carbonates, largely ignoring calc-silicates (with the exception of two samples, both of which have high $^{87}Sr/^{86}Sr$). Bhote Kosi tributaries draining only the Lesser Himalaya (only the Nawakot Group in many cases) are consistently radiogenic ($^{87}Sr/^{86}Sr > 0.8$) regardless of the carbonate contribution to total Sr as revealed by mass balance. This would not be expected if a less radiogenic carbonate endmember was contributing to dissolved $^{87}Sr/^{86}Sr$ inputs in these rivers. The use of multiple regression equations, created using the data from this study, to predict $^{87}Sr/^{86}Sr$ in larger Himalayan rivers (with a direct impact on the Ganges-Brahmaputra, and therefore upon the marine strontium record) strongly indicates that findings for the Bhote Kosi are likely to be repeated if similarly detailed studies were carried out for other Himalayan rivers (except perhaps those with abundant hot springs).

Whilst the presence of radiogenic carbonate material within the Lesser Himalaya, both from pure lithologies and as components within calc-silicates, appears unequivocal, the cause of such high $^{87}Sr/^{86}Sr$ remains far from fully resolved. The work presented in chapter 7 indicates that in many cases there in no need to invoke anything more complex than the impurity of the carbonate material and the great age of the Lesser Himalayan Formation. In a number of samples, however, a comparison of $^{87}Rb/^{86}Sr$ and $^{87}Sr/^{86}Sr$ demonstrates the occurrence of isotopic exchange between silicate and carbonate. The presence of both relatively unradiogenic and highly radiogenic carbonate in the Nawakot

Group suggests that isotopic exchange is a localised occurrence, possibly between minerals on the hand specimen scale rather than between large units. Laser ablation ICPMS is shown in this work to be a viable technique for the analysis of carbonate crystals within Lesser Himalayan calc-silicates, and the initial results obtained by this method indicate recent (i.e. Himalayan) homogenisation of strontium isotopes.

The information presented throughout this thesis leads to the conclusion that, prior to the uplift of the Lesser Himalaya, the $^{87}Sr/^{86}Sr$ of the Himalayan fluvial input to seawater might indeed have been a proxy for silicate weathering. This is evidenced by examination of bedrock from the Tibetan Sedimentary Series and High Himalayan Crystalline Series (see sections 7.1 - 7.3) and by statistical analysis of catchments in which the Lesser Himalaya is not exposed (fig. 5.14). Subsequent to the uplift of the Lesser Himalayan Formation, Himalayan rivers were, and presently are, a poor proxy for silicate weathering owing largely to the rapid weathering of carbonate with high $^{87}Sr/^{86}Sr$. In addition, the weathering of the extremely radiogenic Lesser Himalaya (both silicate and carbonate) potentially allows major changes in the weathering of the High Himalayan Crystalline Series (and therefore overall silicate weathering) to go unrecognised in the fluvial strontium record. Therefore, while the Raymo-Ruddiman theory of global cooling in the Cenozoic linked to the Himalayan orogeny may indeed be tenable, the use of the marine $^{87}Sr/^{86}Sr$ record as evidence of, and indeed to quantify, this link is unwarranted, as is the use of marine $^{87}Sr/^{86}Sr$ as a proxy for the orogenic silicate weathering feedback in the GEOCARB II model (Berner, 1994).

9.2. Sources of Uncertainty and Shortfalls of Research.

One of the potential problems with the work presented in this thesis is that detailed analysis is largely confined to the sampling of a single river, the Bhote Kosi, with the Langtang Khola - Trisuli acting as a "control" study owing to the virtual absence of Nawakot Group calc-silicates. In chapter 5, the multiple regression equations formulated from the Bhote Kosi dataset are used to predict the $^{87}Sr/^{86}Sr$ in larger Himalayan rivers, and a good degree of success is achieved. These predictions are not perfect, however, and neither were they expected to be. Even though it is clear from this and other studies that geology is by far the predominant influence upon dissolved Sr-isotope ratios, other factors (e.g. climate, vegetative cover, land use), not accounted for in this study, affect the interaction between bedrock and the dissolved load of Himalayan rivers.

In addition to those created by sampling over a limited area, further uncertainties arise because of the limited time period over which sampling was undertaken. Sound reasoning lay behind the selection of the Himalayan dry season for sampling (see appendix G) but an examination of tables 8.3 and 8.4 reveals that the impact on seawater of the September strontium flux from the Bhote Kosi is an order of magnitude greater than that in November or December. The impact of the strontium flux at the peak of the monsoon (July and August) is likely to be greater still, yet still little is known about Himalayan river chemistry during this crucial period, largely due to the practical difficulties of undertaking fieldwork at this time. September sampling provides an indicator of changes that might be expected in the monsoon, and both statistical and

mass balance analyses firmly indicate that the prominent role of Lesser Himalayan carbonate is likely to be maintained as rainfall and water flux increases.

In addition to the above a number of other uncertainties are noted;

(i). Percentage geological coverages, defined from the geological maps in chapter 2, are an integral part of the statistical analyses presented in chapter 5. Whilst all known sources were consulted when drawing the geological maps, and they are accurate to the best of our present knowledge, considerable uncertainties remain, and in recent years important revisions have been made (e.g. Searle *et al.*, 1997, Searle, 1999) to the initial work of the Nepal Department of Mines and Geology, and may continue to be made.

(ii). The effectiveness and accuracy of strontium mixing diagrams, as used in chapter 5, depends upon being able to assign "typical" values for the Sr inputs of the different Himalayan lithologies. Whilst $^{87}Sr/^{86}Sr$ ratios are reasonably consistent in each case, considerable uncertainty is associated with assigning mean Sr^{2+} concentrations owing to the large range observed in sampled catchments. If chloride is assumed to be conservative, hydrological influences can be accounted for by normalising Sr^{2+} to Cl^-, although in the Himalaya, where hot springs and possible outcropping evaporites potentially provide significant sources of chloride, this technique is not applicable.

(iii). Flux calculations are made from rainfall data rather than true flux measurements. Whilst a blanket correction is made for evapotranspiration, considerable uncertainty is

introduced as this method assumes that all the water falling as rain finds its way into river courses in the same month, taking no account of possible water storage. The actual fluxes are, however, not crucial, as the actual impact of the Bhote Kosi on seawater is negligible. The flux calculations serve the purpose of demonstrating that the high $^{87}Sr/^{86}Sr$ of Lesser Himalayan inputs results in them having the major impact upon marine $^{87}Sr/^{86}Sr$ without any need for them to dominate the overall strontium flux.

(iv). Unlike a statistical approach, the mass balance used in chapter 5 requires certain assumptions to be made which have uncertainty attached. A large amount of data is available from this and previous studies to constrain the Ca/Sr of carbonate inputs and the Na/Sr of silicate inputs, but uncertainty remains, whilst evaporite inputs are assessed only from data from the Mustang Graben (Galy *et al.*, 1999) and thus remain poorly constrained on the Himalayan scale.

9.3. Potential for Future Research.

A number of the uncertainties described above could be addressed in future work, and whilst the proposed link between $^{87}Sr/^{86}Sr$ and silicate weathering appears increasingly to be ill founded, the importance of understanding the weathering processes of the Himalaya, and the likely effects of the orogeny on marine chemistry and global climate, remains undiminished. Strontium isotope studies might still have a significant role to play in this ongoing research, potentially in combined studies with other isotopic systems (such as lithium or uranium series), which might be useful in discriminating

inputs from Lesser Himalayan carbonate, which as this study shows, impedes the meaningful application of dissolved $^{87}Sr/^{86}Sr$ to studies of Himalayan silicate weathering. Such further work could also incorporate the following;

(i) The role of land usage upon Himalayan river chemistry remains poorly documented and a future study could incorporate digital land use, vegetation cover and climatic data into statistical analyses in the same way as was done for geological coverage in this work.

(ii) Monsoon sampling is essential in any future work. The only chemical data for sampling undertaken at the height of the monsoon (July and August) is for the large rivers of the Gangetic plain (Sarin *et al.*, 1989, Galy and France-Lanord 1999), the latter work indicating significant monsoonal chemical changes including variation in relative rates of silicate and carbonate weathering. As yet, however, there is a lack of detailed studies of Himalayan river chemistry during this period.

(iii). This work only accounts for strontium in surface waters and takes no account of groundwater composition. The work of Basu *et al.* (2001) demonstrates a significant role for groundwater strontium on the scale of the Ganges-Brahmaputra, and shows that surface water $^{87}Sr/^{86}Sr$ ratios reflect those of groundwaters, while groundwater strontium concentrations are much higher (ten times) than those of surface waters. These findings are based on work in the Ganges-Brahmaputra floodplain and as yet there are no groundwater data for Himalayan rivers, which would be extremely useful in further

interpreting the results of this work as well as those of previous and future surface water studies.

This study demonstrates that laser ablation isotopic analysis is an extremely useful tool for the in-situ analysis of carbonate material in calc-silicate rocks. The limited work carried out using this technique suggests that isotopic exchange in the Lesser Himalaya occurred during the Himalayan orogeny. A full study using LA-ICPMS could further establish the timing and extent of isotopic exchange in the different units of the Nawakot Group, sampling different parts of the Himalaya to determine whether the observations noted in the bedrock of the Bhote Kosi are a common feature.

References

Ahmad, T., Harris, N., Bickle M., Chapman, H., Bunbury, J. and Prince, C. (2000). "Isotopic constraints on the structural relationships between the Lesser Himalayan Series and the High Himalayan Series, Garhwal Hmalaya." Geological Society of America Bulletin **112**: 467-477.

Alford, D. (1992). "Hydrological Aspects of the Himalayan region." ICIMOD Occasional Paper **18**.

Amatya, K. M., Jnawali, B. M., Shrestha, P. L., Maske, N D. and Hoppe, P. (1994). Geological Map of Nepal. Nepal Department of Mines and Geology, Kathmandu (Nepal).

Arita, K., Ohta, Y., Akiba, Ch. and Maruo, Y. (1973). "Kathmandu Region." In Geology of the Nepal Himalayas (ed. Hashimoto, S., Ohta, Y. and Akiba, Ch.), pp.99-145. Saikon Publishing Company Limited, Sapporo (Japan).

Arita, K. (1983). "Origin of the inverted metamorphism of the Lower Himalayas central Nepal." Tectonophysics **95**: 43-60.

Arita, K., Sharma, T. and Fujii, Y. (1984a). "Geology and structure of the Jajarkot-Piuthan area central Nepal." Journal of the Nepal Geological Society **4**: 5-27.

Arita, K., Shiraishi, K. and Hayashi, D. (1984b). "Geology of western Nepal and a comparison with Kumaon India." Journal of the Faculty of Science, Hokkaido University **IV (21)**: 1-20.

Auden, J. B. (1935). "Traverses in the Himalaya." Records of the Geology Survey of India **69**: 123-167.

Ayres, M. W. (1997). Trace-Element Behaviour During High-Grade Metamorphism and Anatexis of the Himalayas. PhD thesis, The Open University (UK).

Banner, J. L. (1995). "Application of trace element and isotope geochemistry of strontium to studies of carbonate diagenesis." Sedimentology **42**: 805-824.

Bassoullet, J. P. and Mouterde, R. (1977). "Les formations sedimentaires Mesozoiques du domaine Tibetain de l'Himalaya du Nepal." Himalaya: Sciences de la Terre. Colloques Internationaux du Centre National de la Recherche Scientifique **268**: 53-60.

Basu, A. R., Jacobsen, S. B., Poreda, R. J., Dowling, C. B. and Aggarwal, P. K. (2001). "Large groundwater strontium flux to the oceans from the Bengal Basin and the marine strontium isotope record." Science **293**: 1470-1473.

Beck, R. A., Burbank, D. W., Sercombe, W. J., Riley, G. W., Barndt, J. K., Berry, J. R., Afzal., J., Khan, A. M., Jurgen, H., Metje, J., Cheema, A., Shafique, N. A., Lawrence, R. D. and Khan, M. A. (1995). "Stratigraphic evidence for an early collision between Northwest India and Asia." Nature **373**: 55-58.

Berner, R. A., Lassaga, A. C. and Garrels, R. M. (1983). "The carbonate-silicate geochemical cycle and its effect on atmospheric carbon dioxide over the past 100 million years." American Journal of Science **283 (7)**: 641-683.

Berner, R. A. (1991). "A model for atmospheric CO_2 over Phanerozoic time." American Journal of Science **291 (4)**: 339-376.

Berner, R. A. (1995). "Chemical weathering and its effect on atmospheric CO_2 and climate." In Chemical Weathering Rates of Silicate Minerals (ed. White, A. F. and Brantley, S. L.) **31:** 565-583. Mineralogical Society of America, Washington D. C. (USA).

Berner, R. A. and Berner, E. K. (1997). "Silicate weathering and climate." In Tectonic Uplift and Climate Change (ed. Ruddiman, W. F.) pp.354-365. Plenum Press, New York (USA).

Bhattacharya, A. K., Bhatnagar, G. S., Narayan Das, G. R., Gupta, J. N., Chabria, T. and Bhalla, N. S. (1982). "Rb-Sr dating and geological interpretation of sheared granite-gneisses of Brijanigad-Ingedinala, Bhilangana Valley, Tehri District, U.P." Himalayan Geology **12**: 212-224.

Bickle, M. J., Chapman, H. J., Wickham, S. M. and Peters, M. T. (1995). "Strontium and oxygen isotope profiles across marble-silicate contacts, Lizzies Basin, East Humbolt Range, Nevada: constraints on metamorphic fluid flow." Contributions to Mineralogy and Petrology **121**: 400-413.

Bickle, M., Chapman, H., Bunbury, J., Harris N. and Fairchild, I. (1997a). "Orogenic control of seawater Sr isotopic compositions: constraints from Himalayan rivers." Journal of Conference Abstracts, EUG IX, Strasbourg (France).

Bickle, M. J., Chapman, H. J., Ferry, J. M., Rumble III, D. and Falick, A. E. (1997b). "Fluid-flow and diffusion in the Waterville Limestone, south-central Maine: constraints from strontium, oxygen and carbon isotope profiles." Journal of Petrology **38**: 1489-1512.

Bickle, M. J., Harris, N. B. W., Bunbury, J. M., Chapman, H. J., Fairchild, I. J. and Ahmad, T. (2001). "Controls on the $^{87}Sr/^{86}Sr$ of carbonates in the Garhwal Himalaya, headwaters of the Ganges." Journal of Geology **109**: 737-753.

Bickle, M. J., Bunbury, J., Chapman, H. J., Harris, N. B. W., Fairchild, I. and Ahmad, T. (2002). "Fluxes of Sr into the headwaters of the Ganges." *in press*

Bilham, R., Larson, K., Feymuller, R. and Members, P. I. (1997). "GPS measurements of present-day coverage across the Nepal Himalaya." Nature **386**: 61-64.

Birchfield, G. E. and Wertman, J. (1983). "Topography, albedo-temperature feedback, and climate sensitivity." Science **219**: 284-285.

Blum, J. D. and Erel, Y. (1995). "A silicate weathering mechanism linking increases in marine $^{87}Sr/^{86}Sr$ with global glaciation." Nature **373**: 415-418.

Blum, J. D., Gazis, C. A., Jacobson, A. D. and Chamberlain, C. P. (1998). "Carbonate versus silicate weathering in the Raikhot watershed within the High Himalayan Crystalline Series." Geology **26**: 411-414.

Bordet, P. (1961). Recherches geologiques dans l'Himalaya du Nepal, region du Makalu. Centre National de la Recherche Scientifique , Paris (France).

Bordet, P., Colchen, M., Krummenacher, D., Le Fort, P., Mouterde, R. and Remy, M. (1971). Recherches Geologiques dans l'Himalaya du Nepal, region de la Thakkhola. Centre National de la Recherche Scientifique, Paris (France).

Bordet, P., Colchen, M. and Le Fort, P. (1972). "Some features of the geology of the Annapurna range, Nepal Himalaya." Himalayan Geology **2**: 537-563.

Bordet, P., Colchen, M and Le Fort, P. (1975). Recherches geologiques dans l'Himalaya du Nepal, region du Nyi-Shang pp.138. Centre National de la Recherche Scientifique, Paris (France).

Borghi, S. and Lombardo, B. (1995). "A mineralogical record of exhumation in the Tibetan Slab of eastern Chomolungma region (southern Tibet)." Journal of Conference Absracts,10th Himalaya-Karakorum-Tibet Workshop. Geologisches Institut des ETH, Mitteilungen (Germany)

Brantley, S. L., Chesley, J. T. and Stilling, L. L. (1998). "Isotopic release rates of strontium measured from weathering feldspars." Geochimica et Cosmochimica Acta **62**: 1493-1500.

Brass, G. W. (1976). "The variation in the marine $^{87}Sr/^{86}Sr$ ratio during Phanerozoic time: Interpretation using a flux model." Geochimica et Cosmochimica Acta **40**: 721-730.

Briais, A., Taponnier, P. and Pautot, G. (1989). "Constraints of Sea Beam data on crustal fabrics and seafloor spreading in the South China Sea." Earth and Planetary Science Letters **95 (3-4)**: 307-320.

Briais, A., Patriat, P. and Taponnier, P. (1993). "Updated interpretation of magnetic anomalies and seafloor spreading stages in the South China Sea; implications for the Tertiary tectonics of southeast Asia." Journal of Geophysical Research **B98 (4)**: 6299-6328.

Brunel, M. (1975). "La nappe du Mahabharat, Himalaya du Nepal Central." Comptes Rendus Hebdomadaires des Seances de l'Academie des Sciences, Serie D **280 (5)**: 551-554.

Brunel, M. (1983). "Etude Petro-Structurale des Chevauchements Ductiles en Himalaya (Nepal Oriental et Himalaya du Nord-Ouest)." PhD Thesis, Universite de Paris VII (France).

Brunel, M. and Kienast, J. -R. (1986). "Etude petro-structurale des chevauchements ductiles Himalayens sur la transversale de l'Everest-Makalu (Nepal Oriental)." Canadian Journal of Earth Sciences **23 (8)**: 1117-1137.

Burbank, D. W., Leland, J., Fielding, E., Anderson, R. S., Brozovic, N., Reid, M. R. and Duncan, C. (1996). "Bedrock incision, rock uplift and threshold hillslopes in the northwestern Himalayas." Nature **379**: 505-510.

Burchfiel, B. C., Chen, Z., Hodges, K. V., Liu, Y., Royden, L. H., Deng, C. and Xu, J. (1992). "The South Tibetan Detachment System, Himalayan orogen: Extension contemporaneous with and parallel to shortening in a collisional mountain belt." Geologoical Society of America Special Paper **269**.

Burg, J. P., Brunel, M., Gapais, D., Chen, G. M. and Liu, G. H. (1984). "Deformation of leucogranites of the crystalline Main Central Thrust sheet in southern Tibet (China)." Journal of Structural Geology **6**: 535-542.

Burke, W. H., Denison, R. E., Hetherington, E. A., Koepnick, R. B., Nelson, H. F. and Otto, J. B. (1982). "Variation of seawater $^{87}Sr/^{86}Sr$ throughout Phanerozoic time." Geology **10**: 516-519.

Burns, S. J., Haudenschild, U. and Matter, A. (1994). "The strontium isotopic composition of carbonates from the late Precambrian (approximately 560-540 Ma) Huqf Group of Oman." Chemical Geology **111 (1-4)**: 269-282.

Cameron, E. M., Hall, G. E. M., Veizerl, J. and Krouse, K. H. (1995). "Isotopic and elemental hydrogeochemistry of a major river system; Fraser River, British Colombia, Canada." Chemical Geology **122 (1-4)**: 149-169.

Carosi, R., Lombardo, B., Musumeci, G. and Pertusati, P. C. (1999). "Geology of the Higher Himalayan Crystallines in Himal (Eastern Nepal)." Journal of Asian Earth Sciences **17**: 785-803.

Chalise, S. R., Shrestha, M. L., Thapa, K. B., Shrestha, B. R. and Bajracharya, B. (1996). Climatic and Hydrological Atlas of Nepal. International Centre for Integrated Mountain Development (ICIMOD), Kathmandu (Nepal).

Chesley, J. T., Quade, J. and Ruiz, J. (2000). "The Os and Sr isotopic record of Himalayan paleorivers: Himalayan tectonics and influence on ocean chemistry." Earth and Planetary Science Letters **179**: 115-124.

Chou, L., Garrels, R. M. and Wollast, R. (1989). "Comparitive study of the kinetics and mechanisms of dissolution of carbonate minerals." Kinetic Geochemistry; Chemical Geology (ed. Schott, J. and Lasaga, A. C.) **78 (3-4)**: 269-282. Elsevier, Amsterdam.

Colchen, M., Le Fort, P. and Pêcher, A. (1980). Carte Geologique Annapurna-Manaslu-Ganesh, Himalaya du Nepal. Centre National de la Recherche Scientifique, Paris (France).

Collins, R. and Jenkins, A.. (1996). "The impact of agricultural land use on stream chemistry in the middle hills of the Himalayas, Nepal." Journal of Hydrology **185 (1-4)**: 71-86.

Colombo, F., Lombardo, B. and Pognante, U. (1995). "Lhotse and Makalu revisited: new data on the HT-LP metamorphism at the top of the Tibetan Slab." Journal of Conference Abstracts, 10th Himalaya-Karakorum-Tibet Workshop, Geologishes Institut des ETH, Mitteilungen (Germany).

Copeland, P., Parrish, R. R. and Harrison, T. M. (1988). "Identification of inherited radiogenic Pb in monazite and its implications for U-Pb systematics." Nature **333**: 760-763

Copeland, P., Harrison, T. M., Hodges, K. V., Maruejul, P., Le Fort, P. and Pêcher, A. (1991). "An early Pliocene thermal perturbation of the Main Central Thrust, central Nepal: Implications for Himalayan tectonics." Journal of Geophysical Research **96**: 8475-8500.

Copeland, P. (1997). "The growth of the Himalaya and the Tibetan Plateau." In Tectonic Uplift and Climate Change (ed. Ruddiman, W. F.) pp.20-40. Plenum Press, New York (USA).

DeCelles, P. G., Gehrels, G. E., Quade, J., Ojha, T. P., Kapp, P. A. and Upreti, B. N. (1998). "Neogene foreland basin deposits, erosional unroofing, and the kinematic history of the Himalayan fold-thrust belt, western Nepal." Geological Society of America Bulletin **110**: 2-21.

Deniel, C., Vidal, P., Fernandez, A., Le Fort, P. and Peucat, J. J. (1987). "Isotopic study of the Manaslu granite (Himalaya, Nepal); inference on the age and source of Himalayan leucogranites." Contributions to Mineralogy and Petrology **96 (1)**: 78-92.

DePaolo, D. J. and Ingram, B. L. (1985). "High-resolution sratigraphy with strontium isotopes." Science **227**: 938-941.

DePaolo, D. J. (1986). "Detailed record of the Neogene Sr isotopic evolution of seawater from DSDP site 590B". Geology **14 (2)**: 103-106.

Derry, L. A. and France-Lanord, C. (1996a). "Neogene Himalayan weathering history and river $^{87}Sr/^{86}Sr$: impact on the marine Sr record." Earth and Planetary Science Letters **142**: 59-74.

Derry, L. A. and France-Lanord, C. (1996b). "Neogene growth of the sedimentary organic carbon reservoir." Paleoceanography **11 (3)**: 267-275.

Derry, L. A. and France-Lanord, C. (1997). "Himalayan weathering and erosion fluxes." In Tectonic Uplift and Climate Change (ed. Ruddiman, W. F.) pp.290-312. Plenum Press, New York (USA).

Dewey, J. F., Shackelton, R. M., Chang, C. and Sun, Y. (1988). "The tectonic evolution of the Tibetan Plateau". The Geological Evolution of Tibet; report of the 1985 Royal Society – Academia Sinica geotraverse of the Qinghai-Xizang Plateau. Philosophical Transactions of the Royal Society of London. **A327**: 379-413.

Dhar, B. L., Jha, M. N. and Kukretee, S. P. (1988). "Mineralogy of soils under forests in the Lesser Himalaya." Journal of Indian Soil Science **36**: 151-157.

Douglas, G. B., Gray, C.M., Hart, B.T. and Beckett, R. (1995). "A strontium isotopic investigation of the origin of suspended particulate matter (SPM) in the Murray-Darling River System, Australia." Geochimica et Cosmochimica Acta **59**: 3799-3815.

Edmond, J. M. (1992). "Himalayan tectonics, weathering processes and the strontium isotope record in marine limestones." Science **258**: 1594-1597.

Edmond, J. M., Palmer, M. R., Measures, C. I., Grant, B. and Stallard, R. F. (1995). "The fluvial geochemistry and denudation rate of the Guyana Shield in Venezuela, Colombia and Brazil." Geochimica et Cosmochimica Acta **59**: 3301-3325.

Engebretson, D. C., Kelley, K. P., Cashman, H. J. and Richards, M. A. (1992). GSA Today **2 (5)**: 93-95.

English, N. B., Quade J., DeCelles, P. G. and Garizone, C. N. (2000). "Geologic control of Sr and major element chemistry in Himalayan rivers, Nepal." Geochimica et Cosmochimica Acta **64 (15)**: 2549-2566.

Evans, M. J., Derry, L. A., Anderson, S. P. and France-Lanord, C. (2001). "Hydrothermal source of radiogenic Sr to Himalayan rivers." Geology **29 (9)**: 803-806.

Fairchild, I. J., Bradby, L., Sharp, M. and Tison, J. -L. (1994). "Hydrochemistry of carbonate terrains in alpine glacial settings." Earth Surface Processes and Landforms **19**: 33-54.

Fairchild, I. J. and Kilawee, J. A. (1995). "Selective leaching in glacierized terrains and implications for retention of primary chemical signals in carbonate rocks." In Procedings of the 8th International Symposium on Water-Rock Interaction (ed. Kharaka, Y. K., Chadaev, O. V) pp. 79-82. A. A. Balkema, Rotterdam (Netherlands).

Farrell, J. W., Clemens, S. C. and Gromet, L. P. (1995). "Improved chronostratigraphic reference curve of late Neogene seawater $^{87}Sr/^{86}Sr$." Geology **23 (5)**: 403-406.

Ferrara, G., Lombardo, B. and Tonarini, S. (1983). "Rb/Sr geochronology of granites and gneisses from the Mount Everest region, Nepal Himalaya." Geologishe Rundschau **72**: 119-136.

Foster, G. L. (2000). The Pre-Neogene Thermal History of the Nanga Parbat Haramosh Massif and the North-west Himalaya. PhD Thesis, The Open University (UK).

France-Lanord, C. and Le Fort, P. (1988). "Crustal melting and granite genesis during the Himalayan collision orogenesis." Transactions of the Royal Society of Edinburgh **99**: 183-195.

France-Lanord, C., Derry, L. and Michard, A., (1993). "Evolution of the Himalaya since Miocene time: isotopic and sedimentological evidence from the Bengal Fan." Himalayan Tectonics. Geological Society of London Special Publications **74**. Geological Society of London, London (UK).

France-Lanord, C. and Derry, L. (1996). "The seawater Sr record and processes of erosion and weathering in the Himalaya." Journal of Conference Abstracts, V. M. Goldscmidt Conference, Heidelberg (Germany). Cambridge Publications (UK).

France-Lanord, C. and Derry, L. A. (1997). "Organic carbon burial forcing of the carbon cycle from Himalayan erosion." Nature **390**: 65-67.

France-Lanord, C. and Galy, A. (2001). "The history of Himalayan erosion: What did we learn from the study of the modern system?" Journal of Asian Earth Sciences **19 (3A)**: 37-38.

Fuchs, G. and Frank, W. (1970). "The geology of west Nepal between the rivers Kali Gandaki and Thulo Bheri." Jahrbuch der Geologischen Bundesanstalt. Sonderband **18:** 45-50.

Fuchs, G. (1977). "The geology of the Karnali and Dolpo regions west Nepal." Jahrbuch der Geologischen Bundesanstaldt Wien **120 (2)**; 165-217.

Gaillardet, J., Dupre, B. and Allègre, C. J. (1997). "Chemical and physical denudation in the Amazon river basin." Chemical Geology **142**: 141-173.

Gaillardet, J., Dupre, B., Louvat, P. and Allègre, C. J. (1999). "Global silicate weathering and CO_2 consumption rates deduced from the chemistry of large rivers." Chemical Geology **159**: 3-30.

Galy, A., France-Lanord, C., Hurtrez, J. E. and Lucazeau, F. (1996). "Mass transfer during Himalayan erosion during the Monsoon: Mineralogical and geochemical constraints." AGU 1996 Fall Meeting. Eos, Transactions of the American Geophysical Union **77 (46)**: 236.

Galy, A. and France-Lanord, C. (1999). "Weathering processes in the Ganges-Brahmaputra basin and the riverine alkalinity budget." Chemical Geology **159**: 31-60.

Galy, A., France-Lanord, C. and Derry, L. A. (1999). "The strontium isotope budget of Himalayan rivers in Nepal and Bangladesh." Geochimica et Cosmochimica Acta **63 (13/14)**: 1905-1925.

Gansser, A. (1964). Geology of the Himalayas. Wiley Interscience, New York (USA).

Gardner, R. and Walsh, N. (1996). "Chemical weathering of metamorphic rocks from low elevations in the southern Himalaya." Chemical Geology **127**: 161-176.

Guillot, S., Hodges, K. P., Le Fort, P. and Pêcher, A. (1994). "New constraints on the age of the Manaslu leucogranite: Evidence for episodic tectonic denudation in the central Himalaya." Geology **22**: 559-562.

Hagen, T., Dyhrenfurth, G. -O., Von Furer-Haimendorf, C. and Schneider, E. (1963). Mount Everest: Formation, Population and Exploraton of the Everest Region. Oxford University Press (UK).

Hagen, T. (1969). "Report on the geological survey of Nepal preliminary reconnaissance: Zurich." Memoires de la Societe Helvetique des Sciences Naturelles: **185**.

Hagen, T. (1980). Nepal. Oxford and IBH Publishing Company, New Delhi (India).

Handa, B. K. (1969). "Chemical composition of monsoon rains over Calcutta: Part I." Tellus **22**: 95-100.

Harris, N. (1995). "Significance of weathering Himalayan metasedimentary rocks and leucogranites for the Sr isotope evolution of seawater during the early Miocene." Geology **23**: 795-798.

Harris, N., Bickle, M., Chapman, H., Fairchild, I. and Bunbury, J. (1998). "The significance of Himalayan rivers for silicate weathering rates: evidence from the Bhote Kosi tributary." Chemical Geology **144**: 205-220.

Harris, N. (2000). "Has mountain building caused global cooling? The role of the Himalaya and the Tibetan Plateau in climate control." Science Spectra **23**: 24-32.

Harris, N. B. W. and Open University S339 course team (2001). Mountain Building. The Open University, Milton Keynes (UK).

Harrison, T. M., Wenji, C., Leloup, P. H., Ryerson, F. J. and Taponnier, P. (1992). "An early Miocene transition in deformation regime within the Reed River fault zone, Yunnan, and its significance for Indo-Asian tectonics." Journal of Geophysical Research B**97 (5)**: 7159-7182.

Harrison, T. M., Leloup, P. H., Ryerson, F. J., Taponnier, P., Lacassin, R. and Wenji, C. (1994). Tectonics of Asia. Cambridge University Press (UK).

Harrison, T. M., McKeegan, K. D. and Le Fort, P. (1995). "Detection of inherited monazite in the Manaslu leucogranite by $^{208}Pb/^{232}Th$ ion microprobe dating: crystallization age and tectonic implications." Earth and Planetary Science Letters **133 (3-4)**: 271-282.

Harrison, T. M., Ryerson, F. J., Le Fort, P., Yin, A., Lovera, O. M. and Catlos, E. J. (1997). "A late Miocene-Pliocene origin for the central Himalayan inverted metamorphism." Earth and Planetary Science Letters **146**: E1-E7.

Harrison, T. M., Grove, M., Lovera, O. M. and Catlos, E. J. (1998). "A model for the origin of Himalayan anatexis and inverted metamorphism." Journal of Geophysical Research **103**: 27,017-27,032.

Harrison, T. M., Grove, M., Lovera, O. M., Catlos, E. J. and D'Andrea, J. (1999). "The origin of Himalayan anatexis and inverted metamorphism: Models and constraints." Journal of Asian Earth Sciences **17 (5-6)**: 753-770.

Hashimoto, S., Ohta, Y. and Akiba, C. (1973). Geology of the Nepal Himalayas. Saikon Publishing Company Limited, Tokyo (Japan).

Hasnain, S. I. and Thayyen, R. J. (1996). "Sediment transport and solute variation in meltwaters of Dokriani glacier (Bamak), Garhwal Himalaya." Journal of the Geological Society of India **47 (6)**: 731-739.

Hayashi, D. Fujii, Y., Yoneshiro, T. and Kizaki, K. (1984). "Observations on the geology of the Karnali region west Nepal." Journal of the Nepal Geological Society **4**: 29-40.

Heim, A. and Gansser, A. (1939). "Central Himalaya: Geological observations of the Swiss expedition 1936." Memoires de la Societe Helvetique des Sciences Naturelles **73 (1)**: 1-245.

Helz, G. R. and Holland, H. D. (1965). "The solubility and geologic occurrence of strontianite." Geochimica et Cosmochimica Acta **29**: 1303-1315.

Herail, G., Mascle, G. and Delcaillau, B. (1986). "Les Siwaliks de l'Himalaya du Nepal: un example d'evolution geodynamique d'un prisme d'accretion intracontnental." In Evolution des Domaines Orogeniques d'Asie Meridionale (de la Turquie a L'Indonesie) (ed. Le Fort, P., Colchen, M. and Montenat, C.) **47:** 155-182. Nancy Science de la Terre, Nancy (France).

Hess, J., Bender, M. L. and Schilling, J. –G. (1986). "Evolution of the ratio of $^{87}Sr/^{86}Sr$ in seawater from Cretaceous to present." Science **231**: 979-984.

Hess, J., Bender, M. L. and Schilling, J. -G. (1991). "Assessing seawater/basalt exchange of strontium isotopes in hydrothermal processes on the flanks of mid-ocean ridges." Earth and Planetary Science Letters **103 (1-4)**: 133-142.

Heuberger, H., Masch, L., Preuss, E. and Schroker, A. (1984). "Quaternary landslides and rock fusion in Central Nepal and the Tyrolean Alps." Mountain Research and Development **4 (4)**: 345-362.

Hodell, D. A., Mead, G. A. and Mueller, P. A. (1990). "Variation in the strontium isotope composition of seawater (8 Ma to present): Implications for chemical weathering rates and dissolved fluxes to the oceans." Chemical Geology **80**: 291-307.

Hodges, K. V., Hubbard, M. S. and Silverberg, D. S. (1988). "Metamorphic constraints on the thermal evolution of the central Himalayan orogen." Tectonic Evolution of the Himalayas and Tibet. Philosophical Transactions of the Royal Society of London **A326**: 257-280.

Hodges, K. V., Parrish, R. R., Housh, T. B., Lux, D. R., Burchfiel, B. C., Royden, L. H., and Chen, Z. (1992). "Simultaneous Miocene extension and shortening in the Himalayan Orogen." Science **258**: 1466-1470.

Hodges, K. V., Burchfiel, B. C., Royden, L. H., Chen, Z., Lovera, O. M. and Liu, Y. (1993). "The metamorphic signature of contemporaneous extension and shortening in the central Hmalayan orogen: data from the Nyalam transect, southern Tibet." Journal of Metamorphic Geology **10**: 439-452.

Hodges, K. V., Parrish, R. R. and Searle, M. P. (1996). "Tectonic evolution of the central Anapurna Range, Nepalese Himalayas." Tectonics **15**: 1264-1291.

Hubbard, M. S. and Harrison, T. M. (1989). "$^{40}Ar/^{39}Ar$ age constraints on deformation and metamorphism in the Main Central Thrust zone and Tibetan Slab, Eastern Nepal Himalaya." Tectonics **8**: 865-880.

Inger, S. I. (1991). Metamorphism and Granite Genesis in the Langtang Region, North-Central Nepal. PhD Thesis. The Open University, Milton Keynes (UK).

Inger, S. and Harris, N. (1992). "Tectonothermal evolution of the High Himalayan Crystalline sequence, Langtang Valley, northern Nepal." Journal of Metamorphic Geology **10**: 439-452.

Inger, S. and Harris, N. (1993). "Geochemical constraints on leucogranite magmatism in the Langtang Valley, Nepal Himalaya." Journal of Petrology **34 (2)**: 345-368.

Jackson, M. and Bilham, R. (1994). "Constraints on Himalayan deformation inferred from vertical velocity fields in Nepal and Tibet." Journal of Geophysical Research **B99 (7)**: 13,897-13,912.

Jacobson, S. B., and Kaufman, A.J. (1999). "The Sr, C and O isotopic evolution of Neoproterozoic seawater." Chemical Geology **161**: 37-57.

Jacobson, A. D. and Blum, J. D. (2000). "Ca/Sr and $^{87}Sr/^{86}Sr$ geochemistry of disseminated calcite in Himalayan silicate rocks from Nanga Parbat: Influence on river-water chemistry." Geology **28**: 463-466.

Joshi, P. R. (1973). Report on the geology of the Bhimphedi-Chisasami area, with map. Nepal Department of Mines and Geology, Kathmandu (Nepal).

Kai, K. (1981). "Rb/Sr geochronology of the rocks of the Himalaya, Eastern Nepal. Part I. The metamorphic age of the Himalayan gneiss." Memoirs of the Faculty of Science, Kyoto University, Series of Geology and Mineralogy **47**: 135-148.

Kerrick, D. M., Caldeira, K. (1993). "Paleoatmospheric consequences of CO_2 released during early Cenozoic regional metamorphism in the Tethyan orogen." Chemical Geology **108 (1-4)**: 201-230.

Knowles, P. and Allardice, D. (1992). White Water Nepal. Rivers Publishing / Menasha Ridge Press, Leicester (UK) / Birmingham, Alabama (USA).

Koepnik, R. B., Burke, W. H., Denison W. E., Hetherington, E. A., Nelson, H. F., Otto, J. B. and Waite, L. E. (1985). "Construction of the seawater $^{87}Sr/^{86}Sr$ curve for the Cenozoic and Cretaceous; supporting data." Chemical Geology **58 (1-2)**: 55-81.

Kominz, M. A. (1984). "Oceanic ridge volumes and sea level change - an error analysis." American Association of Petrology and Geology Memoirs. **36**: 109-127.

Kortaba, M., Sokolowski, A., and Bogacz, W. (1981). "Hydrogeological investigations in the Kali Gandaki thermal springs area (Nepal Himalayas)." Bulletin of the Polish Academy of Sciences **29**: 283-291.

Krishnaswami, S., Trivedi, J. R., Sarin, M. M., Ramesh, R., and Sharma, K. K. (1992). "Strontium isotopes and rubidium in the Ganga-Brahmaputra river system: Weathering in the Himalaya, fluxes to the Bay of Bengal and contributions to the evolution of oceanic $^{87}Sr/^{86}Sr$." Earth and Planetary Science Letters **109**: 243-253.

Kumar, R. (1980). "Outline of the stratigraphy of Central Nepal." In Stratigraphy and Correlation of Lesser Himalayan Formations (ed. Valdiya, K. S. and Bhatta, S. S) pp.180-190. Hindustan Publishing Company, Delhi (India).

Kutzbach, J. E., Guetter, P. J., Ruddiman, W. F. and Prell, W. L. (1989). "Sensitivity of climate to late Cenozoic uplift in southern Asia and the American West; numerical experiments." Journal of Geophysical Research **D94 (15)**: 18,393-18,407.

Lasaga, A. C., Soler, J. M., Ganor, J., Burch, T. E. and Nagy, K. L. (1994). "Chemical weathering rate laws and global geochemical cycles." Geochimica et Cosmochimica Acta **58**: 2361-2386.

Le Fort, P. (1975a). "Himalaya: The collided range. Present knowledge of the continental arc." American Journal of Science **A275**: 1-44.

Le Fort, P. (1975b). "Les formations cristallophyliennes de la 'Dalle du Tibet' en Marsyandi." In Recherches Geologiques dans l'Himalaya du Nepal Region du Nyi-Shang (ed. Bordet, P.) pp.21-47. Paris Editions du Centre National de la Recherche Scientifique, Paris (France).

Le Fort, P. (1981). "Manaslu leucogranite: a collision signature of the Himalaya. A model for its genesis and emplacement." Journal of Geophysical Research **86**: 10,545-10,568.

Le Fort, P., Debon, F. and Sonet, J. (1983). "The lower Paleozoic 'Lesser Himalayan' granitic belt: emphasis on the Simchar pluton of central Nepal." In Granites of Himalaya, Karakorum and Hindu-Kush (ed. Shams, F. A.) pp.235-255. Institute of Geology, Punjab University, Lahore (Pakistan).

Leloup, P. H. and Kienast, J. -R. (1993). "High-temperature metamorphism in a major strike-slip shear zone; the Ailao Shan - Red River, People's Republic of China". Earth and Planetary Science Letters **118 (1-4)**: 213-234.

Lombardo, B., Pertusati, P. C. and Borghi, S. (1993). "Geology and tectonomagmatic evolution of the eastern Himalaya along Chomolungma-Makalu transect." In Himalayan Tectonics. Geological Society Special Publications **74** (ed. Treloar, P. J. and Searle, M. P.). Geological Society of London, London (UK).

MacFarlane, A., Hodges, K. V. and Lux, D. (1992). "A structural analysis of the Main Central Thrust zone Langtang National Park, Central Nepal Himalaya." Geological Society of America Bulletin **104**: 1389-1402.

Maruo, Y., Ohta, Y., Akiba, C. and Arita, K. (1973). "Chautara region." In Geology of the Nepal Himalayas (ed. Hashimoto, S., Ohta, Y. and Akiba, C.) pp.69-97. Saikon Publishing Company Limited, Sapporo (Japan).

Maruo, Y. and Kizaki, K. (1983). "Thermal structure in the nappes of the eastern Nepal Himalayas." In Granites of Himalaya, Karakorum and Hindu Kush (ed Shams, F. A.) pp.271-286. Institute of Geology, Punjab University, Lahore (Pakistan).

Massey, J. A. (1994). Metamorphism, Melting, and Fluids During Himalayan Orogenesis. PhD Thesis, The Open University, Milton Keynes (UK).

McCauley, S. E. and DePaolo, D. J. (1997). "The marine $^{87}Sr/^{86}Sr$ and $\delta^{18}O$ records." In Tectonic Uplift and Climate Change (ed. Ruddiman, W. F.) pp.428-467. Plenum Press, New York (USA).

Meybeck, M. (1987). "Global chemical weathering of surficial rocks estimated from river dissolved loads." American Journal of Science **287**(401-428).

Meybeck, M. and Ragu, A. (1997). "River discharges to the oceans: an assessment of suspended solids, major ions and nutrients." *Unpublished data.*

Miller, K. G., Fairbanks, R. G. and Mountain, G. S. (1987). "Tertiary oxygen isotope synthesis, sea level history and continental margin erosion." Paleoceanography **2 (1)**: 1-19.

Miller, C., Thoni, M., Grasemann, B., Klotzli, U., Guntli, P. and Dragantis, E. (2001). "The early Palaeozoic magmatic event in the Northwest Himalaya, India: source, tectonic setting and age of emplacement." Geological Magazine **138 (3)**: 237-251.

Molnar, P. (1984). "Structure and tectonics of the Himalaya; constraints and implications of geophysical data."Annual Review of Earth and Planetary Sciences **12**: 489-518.

Moore, W. S. (1997). "High fluxes of radium and barium from the north of the Ganges-Brahmaputra River during low river discharge suggest a large groundwater source." Earth and Planetrary Science Letters **150**: 141-150.

Mugnier, J. L., Letrumy, P., Mascle, G., Huyghe, P. and Chalaron, E. (1999). "The Siwaliks of Western Nepal II. Mechanics of the thrust wedge." Journal of Asian Earth Sciences **17 (5-6)**: 643-657.

Nagdir, B. B., Gandotra, V. M., Nanda, M. M., Pawde, M. B. and Sharma, P. N. (1968-1973). Nepal mission field reports. Geological Survey of India, Calcutta and Kathmandu (India / Nepal).

Négrel, P., Allègre, C.J., Dupre, B. and Lewin, E. (1993). "Erosion sources determined by inversion of major and trace element ratios in river water: the Congo Basin case." Earth and Planetary Science Letters **120**: 59-76.

Nepal Department of Mines and Geology (1984). Geological Map of Eastern Nepal. Nepal Department of Mines and Geology, Kathmandu (Nepal).

Nepal Department of Mines and Geology (1985). Geological Map of Central Nepal. Nepal Department of Mines and Geology, Kathmandu (Nepal).

Oliver, G. J. H., Johnson, M. R. W. and Fallick, A. E. (1995). "Age of metamorphism in the Lesser Himalaya and the Main Central Thrust Zone, Garhwal India: results of illite crystallinity, ^{40}Ar-^{39}Ar fusion and K-Ar studies." Geological Magazine **132**: 139-149.

Palmer, M. R., and Edmond, J. M. (1989). "The strontium isotope budget of the modern ocean." Earth and Planetary Science Letters **92**: 11-26.

Palmer, M. R. and Edmond, J. M. (1992). "Controls over the strontium isotope composition of river water." Geochimica et Cosmochimica Acta **56**: 2099-2111.

Pande, K., Sarin, M. M, Trivedi, J. R., Krishnaswami, S. and Sharma, K. K. (1994). "The Indus River system (India-Pakistan): major-ion chemistry, uranium and Sr isotopes." Chemical Geology **116**: 245-259.

Pandey, M. R., Tandukar, R. P., Avouac, J. P., Lave, J. and Massot, J. P. (1995). "Interseismic strain accumulation on the Himalayan crustal ramp (Nepal)." Geophysical Research Letters **22**: 751-754.

Parrish, R. R. and Hodges K. V. (1996). "Isotopic constraints on the age and provenance of the Lesser and Greater Himalayan sequences." Geological Society of America Bulletin **108 (7)**: 904-911.

Pêcher, A. (1975). "The Main Central Thrust of the Nepal Himalaya and the related metamorphism in the Modi-Khola cross-section (Annapurna Range)." Himalayan Geology **5**: 115-132.

Pêcher, A. and Le Fort, P. (1977). "Origin and significance of the Lesser Himalayan augen gneisses" Himalaya: Sciences de la Terre. Colloques Internationaux du Centre National de la Recherche Scientifique **268:** 319-329.

Pêcher, A. and Le Fort, P. (1986). "The metamorphism in Central Himalaya, its relations with the thrust tectonic." In Evolution des Domaines Orogeniques d'Asie Meridionale (de la Turquie a l'Indonesie) (ed. Le Fort, P., Colchen, M. and Montenat, C.) **47**: 285-309. Nancy (France).

Pêcher, A. (1989). "The metamorphism in Central Himalaya." Journal of Metamorphic Geology **7**: 31-41.

Peucker-Ehrenbrink, B. and Blum, J. D. (1998). "Re-Os isotope systematics and weathering of Precambrian crustal rocks: Implications for the marine Os isotope record." Geochimica et Cosmochimica Acta **62**: 3193-3203.

Pognante, U. and Benna, P. (1993). "Metamorphic zonation, migmatization, and leucogranites along the Everest transect of Eastern Nepal and Tibet: record of exhumation history." In Himalayan Tectonics. Geological Society Special Publications **74** (ed. Treloar, P. J. and Searle, M. P.) pp.323-340. Geological Society of London, London (UK).

Potts, P. J., Webb, P. C. and Watson, J. S. (1984). "Energy dispersive X-ray flourescence of silicate rocks for major and trace elements." X-ray Spectrometry **13**: 2-15.

Prince, C. I. (1999). The Timing of Prograde Metamorphism in the Garhwal Himalaya, India. PhD Thesis, The Open University, Milton Keynes (UK).

Quade, J., Roe, L., DeCelles, P. G. and Ojha, T. P. (1997). "The late Neogene $^{87}Sr/^{86}Sr$ record of lowland Himalayan rivers." Science **276**: 1828-1831.

Rai, S. M., Guillot, S., Le Fort, P. and Upreti, B. N. (1998). "Pressure-temperature evolution in the Kathmandu and Gosainkund regions, central Nepal." Journal of Asian Earth Sciences **16 (2-3)**: 283-298.

Raymo, M. E. and Ruddiman, W. F. (1988). "Influence of late Cenozoic mountain building on ocean geochemical cycles." Geology **16**: 649-653.

Raymo, M. E. (1991). "Geochemical evidence supporting T. C. Chmaberlain's theory of glaciation." Geology **19 (4)**: 344-347.

Raymo, M. E. and Ruddiman, W. F. (1992). "Tectonic forcing of late Cenozoic climate." Nature **359**: 117-122.

Raymo, M. E. (1994). "The Himalayas, organic carbon burial, and climate in the Miocene." Paleoceanography **9 (3)**: 399-404.

Reddy, S. M., Searle, M. P. and Massey, J. A. (1993). "Sructural evolution of the High Himalayan gneiss sequence, Langtang Valley, Nepal." In Himalayan Tectonics. Geological Society Special Publications **74** (ed. Treloar, P. J. and Searle, M. P.) pp.375-389. Geological Society of London, London (UK).

Reeve, A. S. and Perry, E. C. (1994). "Carbonate geochemistry and the concentrations of aqueous Mg^{2+}, Sr^{2+} and Ca^{2+}: Western north coast of the Yucatan, Mexico." Chemical Geology **112 (1-2)**: 105-117.

Richter, F. M. and DePaolo, D. J. (1987). "Numerical models for diagenesis and the Neogene Sr isotopic evolution of seawater from DSDP site 590B". Earth and Planetary Science Letters **83 (1-4)**: 27-38.

Richter, F. M. and DePaolo, D. J. (1988). "Diagenesis and Sr isotopic evolution of seawater using data from DSDP 590B and 575." Earth and Planetary Science Letters **90 (4)**: 382-394.

Richter, F. M., Rowley, D. B. and DePaolo, D. J. (1992). "Sr isotope evolution of seawater: the role of tectonics." Earth and Planetary Science Letters **109**: 11-23.

Robinson, D. M., DeCelles, P. G., Patchett, P. J. and Garzione, C. N. (2001). "The kinematic evolution of the Nepalese Himalaya interpreted from Nd isotopes." Earth and Planetary Science Letters **192 (4)**: 507-521.

Rolfo, F. *et al.* (2001). Unpublished cross section of the Bhote Kosi.

Rollinson, H. (1993). Using Geochemical Data: Evaluation, Presentation, Interpretaton. Longman, Harlow (UK).

Rowe, K. (2001). "Hydropower In Nepal". Unpublished website article.

Ruddiman, W. F., Raymo, M. E. and McIntyre, A. (1986). "Matuyama 41,00-year cycles; North Atlantic Ocean and Northern Hemisphere ice sheets." Earth and Planetary Science Letters **80 (1-2)**: 117-129.

Ruddiman, W. F., Prell, W. L. and Raymo, M. E. (1989). "Late Cenozoic uplift in southern Asia and the American West; rationale for general circulation modeling experiments." Journal of Geophysical Research **D94 (15)**: 18,379-18,391.

Ruddiman, W. F. and Kutzbach, J. E. (1989). "Forcing of late Cenozoic Northern Hemisphere climate by plateau uplift in southern Asia and the American West." Journal of Geophysical Research **94 (15)**: 18,409-18,427.

Sakai, H. (1983). "Geology of the Tansen Group of the Lesser Himalaya in Nepal." Memoirs of the Faculty of Science Kyushu University **Series D Geology (25)**: 27-74.

Sakai, H. (1985). "Geology of the Kali Gandaki Supergroup of the Lesser Himalayas in Nepal." Memoirs of the Faculty of Science Kyushu University **Series D Geology (25)**: 337-397.

Sarin, M. M., Krishnaswami, S., Dilli, K., Somayajula, B. L. K. and Moore, W. S. (1989). "Major ion chemistry of the Ganga-Brahmaputra river system: Weatheirng processes and fluxes to the Bay of Bengal." Geochimica et Cosmochimica Acta **53**: 997-1009.

Sarin, M. M., Krishnaswami, K. K., Somayajulu, B. L. K. and Moore, W. S. (1990). "Chemistry of uranium, thorium and radium isotopes in the Ganga-Brahmaputra river system: Weathering processes and fluxes to the Bay of Bengal." Geochimica et Cosmochimica Acta **54**: 1387-1396.

Sarin, M. M., Krishnaswami, S., Trivedi, J. R. and Sharma, K. K. (1992). "Major ion chemistry of the Ganga source waters: Weathering in the high altitude Himalaya." Procedings of the Indian Academy of Sciences: Earth and Planetary Science **101 (1)**: 89-98.

Schäerer, U. and Allègre, C. J. (1983). "The Palung granite (Himalaya): high resolution U-Pb systematics in zircon and monazite." Earth and Planetary Science Letters **63**: 423-432.

Schäerer, U. (1984). "The effect of initial ^{230}Th disequilibrium on young U-Pb ages: the Makalu case, Himalaya." Earth and Planetary Science Letters **67**: 191-204.

Schäerer, U., Xu, R. and Allègre, C. (1986). "U-(Th)-Pb systematics and ages of Himalayan leucogranites, south Tibet." Earth and Planetary Science Letters **77**: 35-48.

Schäerer, U., Taponier, P., Lacassin, L., Leloup, P. H., Zhond, D. and Zhi, S. (1990). "Intraplate tectonics in Asia; a precise age for large-scale Miocene movement along the Ailao Shan – Red River shear zone." Earth and Planetary Science Letters **97 (1-2)**: 65-77.

Schelling, D. and Arita, K. (1991). "Thrust tectonics, crustal shortening, and the structure of the far-eastern Nepal Himalaya." Tectonics **10 (5)**: 851-862.

Schelling, D. (1992). "The tectonostratigraphy and structure of the eastern Nepal Himalaya." Tectonics **11**: 925-943.

Searle, M. P., Parrish, R. R., Hodges, K. V., Hurford, A., Ayres, M. W. and Whitehouse, M. J. (1997). "Shisha Pangma leucogranite, south Tibetan Himalaya: Field relations, geochemistry, age, origin, and emplacement." The Journal of Geology **105**: 295-317.

Searle, M. P. (1999a). "Extensional and compressional faults in the Everest-Lhotse massif, Khumbu Himalaya, Nepal." Journal of the Geological Society of London **156**: 227-240.

Searle, M. P. (1999b). "Emplacement of Himalayan leucogranites by magma injection along giant sill complexes: examples from the Cho Oyu, Gyachung Kang and Everest leucogranites (Nepal Himalaya)." Journal of Asian Earth Sciences **17**: 773-783.

Seeber, L. and Armbruster, J. G. (1981). "Great detachment earthquakes along the Himalayan arc and long-term forecasting." In Earthqake Prediction - An International Review. Maurice Ewing Series **4**: 103-120. American Geophysical Union (USA).

Sequira, R. and Kelkar, D. (1978). "Geochemical implications of summer monsoonal rainwater composition over India." Journal of Applied Meteorology **17**: 1390-1396.

Sharma, T., Kansakar, D. R. and Kizaki, K. (1984). "Geology and tectonics of the region between Kali Gandaki and Bheri rivers in central west Nepal." Bulletin of the College of Science, University of the Ryukyus **38**: 57-102.

Shirey, S. B. and Walker, R. J. (1998). "Re-Os isotopes in cosmochemistry and high-temperature geochemistry." Annual Revue of Earth and Planetary Sciences **26**: 423-500.

Shrestha, S. B., Maskey, N. D., Sharma, T. and Bashyal, R. P. (1993). "Atlas of mineral resources of the ESCAP region." In Geology and Mineral Resources of Nepal Explanatory Brochure **9**. United Nations / ESCAP, New York (USA).

Singh, S. K., Trivedi, J. R., Pande, K., Ramesh, R. and Krishnaswami, S. (1998). "Chemical and strontium, oxygen and carbon isotopic compositions of carbonates from the Lesser Himalaya: Implications to the Sr isotope composition of the source waters of the Ganga, Ghaghara and the Indus Rivers." Geochimica et Cosmochimica Acta **62**: 743-755.

Srivastava, P. and Mitra, G. (1994). "Thrust geometries and deep structure of the outer and Lesser Himalaya, Kumaon and Garhwal (India): Implications for evolution of the Himalayan fold-and-thrust belt." Tectonics **13**: 89-109.

Stallard, R. F. and Edmond, J. M. (1983). "Geochemistry of the Amazon 2. The influence of geology and weathering environment on the dissolved load." Journal of Geophysical Research **88**: 9671-9688.

Stöcklin, J. (1980). "Geology of Nepal and its regional frame." Journal of the Geological Society London **137**: 1-34.

Stöcklin, J. and Bhattarai, K. D. (1980). Geology of the Kathmandu Area and Central Mahabharat Range, Nepal Himalaya. Nepal Department of Mines and Geology / United Nations Development Program (Nepal / USA).

Stordal, M. C. and Wasserburg, G.J. (1983). "Sm-Nd and Rb-Sr measurements on river water, suspended load and sediment from the Mississippi delta." EOS, Transactions of the American Geophysical Union **64 (52)**: 1064.

Subramanian, V., Sitasawad, R., Abbas, N. and Jha, P. K. (1987). "Environmental geology of the Ganga River Basin." Journal of the Geological Society of India **30:** 335-355.

Sundquist, E. T. (1991). "Steady- and non-steady-state carbonate-silicate controls on atmospheric CO_2". Quaternary Science Reviews **10 (2-3)**: 283-296.

Taponnier, P., Peltzer, G. and Armijo, R. (1986). "On the mechanics of the collision between India and Asia." Collision tectonics. Geological Society Special Publications **19**: 115 - 157.

Taponnier, P., Lacassin, R., Leloup, P. H., Schäerer, U., Zhong, D., Wu, H., Liu, X., Ji, S., Zhang, L. and Zhong, J. (1990). "The Ailao Shan / Red River metamorphic belt; Tertiary left-lateral shear between Indochina and South China." Nature **343**: 431-437.

Taylor, S. R. and McLennan, S. M. (1985). The Continental Crust: its Composition and Evolution. Blackwell Scientific Publications, Oxford (UK).

Taylor, A. S., Blum, J. D., Lasaga, A. C. and MacInnis, I. N. (2000). "Kinetics of dissolution and Sr release during biotite and phlogopite weathering." Geochimica et Cosmochimica Acta **64 (7)**: 1191-1208.

Tejwani, K. C. (1996). Unpublished data.

Tokuoka, T., Takayasu, K., Yoshida, M. and Hisatomi, K. (1986). "The Churia (Siwalik) group of the Arung Khola area, west central Nepal." Memoirs of the Faculty of Science of Shimane University **20**: 135-210.

Tonarini, S., Lombardo, B., Ferrara, G. and Marcassa, P. (1994). "Partial melting in the Namche Migmatite of Khumbu Himal (Nepal Himalaya)." Mineralogica Petrografica Acta **37**: 277-294.

Trivedi, J. R., Gopalan, K. and Valdiya, K. S. (1984). "Rb-Sr ages of granitic rocks within the Lesser Himalayan nappes, Kumaun, India." Journal of the Geological Society of India **25**: 641-654.

Trivedi, J. R. (1990). Geochronological studies of Himalayan granitoids. PhD Thesis. Gujarat University (India).

Upreti, B. N. (1996). "Stratigraphy of the western Nepal Lesser Himalaya: a synthesis." Journal of the Nepal Geological Society **13**: 11-28.

Upreti, B. N. (1999). "An overview of the stratigraphy and tectonics of the Nepal Himalaya." Journal of Asian Earth Sciences **17**: 577-606.

Upreti, B. N. and Le Fort, P. (1999). "Lesser Himalayan crystalline nappes of Nepal; problems of their origin." Special paper - Geological Society of America **328**: 225-238.

Upreti, B. N. and Rai, S. M. (2000). Geological Excursion Guide Along the Kodari (Nepal - China Border) - Kathmandu Road Section (Arniko Highway) pp.46-64. Tribhuvan University / Tri-Chandra Campus, Kathmandu / Ghantaghar (Nepal).

Valdiya, K. S. (1986). "Correlation of Lesser Himalayan formations of Nepal and Kumaun." Sciences de la Terre **47**: 361-383.

Valdiya, K. S. (1995). "Proterozoic sedimentation and Pan-African geodynamic development in the Himalaya." Precambrian Research **74**: 35-55.

Valdiya, K. S. (1998). Dynamic Himalaya. Universities Press (India) Ltd, Hyderabad (India).

Vance, D. and Harris, N. (1999). "Timing of prograde metamorphism in the Zanskar Himalaya." Geology **27**: 395-398.

Veizer, J. (1989). "Strontium isotopes in seawater through time." Annual Revue of Earth and Planetary Sciences **17**: 141-167.

Villa, I. M. (1990). "Geochronology and excess Ar geochemistry of the Lhotse Nup leucogranite, Nepal Himalaya." Journal of Volcanology and Geothermal Research **44**: 89-103.

Villa, I., Tonarini, S. and Lombardo, B. (1998). "Rb/Sr and Ar/Ar ages of muscovites from leucogranites of the Chomolungma-Cho Oyu region, southern Tibet." Procedings of the 13th Himalaya-Karakorum-Tibet Workshop, Peshawar (Pakistan).

Visona, D. and Lombardo, B. (2002). "Two-mica tourmaline leucogranites from the Everest-Makalu region (Nepal-Tibet). Himalayan leucogranite genesis by isobaric heating." Lithos **62 (3-4)**: 125-150.

Wadleigh, M. A., Veizer, J. and Brooks, C. (1985). "Strontium and its isotopes in Canadian rivers: Fluxes and global implications." Geochimica et Cosmochimica Acta **49**: 1727-1736.

Wager, L. R. (1965). "Injected granite sheets of the Rongbuk valley and the northern face of Mount Everest." India Mining Geology and Metallurgy Institute D. N. Wadia Commemorative Volume pp. 358-379.

Wake, C. P., Mayaewski, P. A. and Spencer, M. J. (1990). "A review of central Asian glaciochemical data." Annals of Glaciology **14**: 301-306.

Wake, C. P., Mayewski, P. A., Zichu, X., Ping, W. and Zhongqin, L. (1993). "Regional distribution of monsoon and desertdust signals recorded in Asian glaciers." Geophysical Research Letters **30**: 1411-1414.

Wang, Z. and Zhen, X. (1975). "Imbricate structure in the northern slope of Jolmo Lungma and discussion of the uplift of the Himalaya." In Scientific Exploration of Jolmo Lungma pp.199-221. Science Publishing House, Beijing (PR China).

Webster, J. G., Brown, K. L. and Vincent, W. F. (1994). "Regional distribution of monsoon and desert dust signals recorded in Asian glaciers." Geophysical Research Letters **30**: 171-186.

White, N. M., Pringle, M., Garzanti, E., Bickle, M., Najman, Y., Chapman, H. and Friend, P. (2002). "Constraints on the exhumation and erosion of the High Himalayan Slab, NW India, from foreland basin deposits." Earth and Planetary Science Letters **195**: 29-44.

Whittington, A., Foster, G., Harris, N, Vance, D. and Ayres, M. (1999). "Lithostratigraphic correlations in the western Himalaya - An isotopic approach." Geology **27 (7)**: 585-588.

Windley, B. F. (1983). "Metamorphism and tectonics of the Himalayas." Journal of the Geological Society of London **140**: 849-866.

Xianghui, L., Chengshan, W., Upreti, B. N., Rejean, H., Shun, L., Zhifei, L. and Rai, S. M. (2000). Field Guidebook for Himalaya Excursion. 15th Himalaya-Karakoram-Tibet Workshop, Chengdu (PR China).

Yang, C. K., Telmer, K. and Veizer, J. (1996). "Chemical dynamics of the 'St Lawrence' riverine system: δD_{H2O}, $\delta^{18}O_{H2O}$, $\delta^{13}C_{DIC}$, $\delta^{34}S_{sulfate}$ and dissolved $^{87}Sr/^{86}Sr$." Geochimica et Cosmochimica Acta **60**: 851-866.

Yin, C. H. and Kuo S. T. (1978). "Stratigraphy of the Mount Jolmo Lungma and its North slope." Scientia Sinica **21**: 629-644.

Yoo, C. M., Greg, J. M. and Shelton, K. L. (2000). "Dolomitization and dolomite neomorphism: Trenton and Black River Limestones (Middle Ordovician) Northern Indiana, USA." Journal of Sedimentary Research **70**: 265-274.

Zachos, J. C., Stott, L. D. and Lohmann, K. C. (1994). "Evolution of early Cenozoic marine temperatures." Paleoceanography **9 (2)**: 353-387.

Website References.

bihar.8m.com – Website of the Bihar province of India.

www.dams.org – Website of the World Commission on Dams (WCD).

www.doi.gov.np – Website of HMG Nepal Ministry of water Resources, Department of Irrigation.

www.ledco-nepal.com – Website of Lamjung Electricity Development Company Limited.

www.nepalnews.com.np – Current affairs website in Nepal.

www.panasia.org.sg – Website for Pan Asia Networking.

Topography Maps.

Discover Nepal 1:110,000 *Khumbu* map.

Nelles Schneider Nepal 1:50,000 series.

Survey Department HMG Nepal and Government of Finland *Finnmap* 1:50,000 and Nepal 1:25,000 series.

US Defense Mapping Agency Aerospace Center TPC 1:500,000 series.

Appendix A

Water Chemistry

List of tables.

Geology abbreviations:

TSS: Tibetan Sedimentary series. HHCS: High Himalaya Crystalline Series.

LHF: Lesser Himalayan Formation. LHC: Nawakot Group calc-silicates.

LHSM: Kuncha Group silicate metasediments.

LHSC: Lesser Himalayan crystalline gneisses.

NB. All dissolved species are quoted after correction for atmospheric inputs (see section 3.1). Samples in which the charge balance (difference between total major cations and total major anions in Eq/l) exceeds 20% were excluded from all analysis.

Table A1. Water samples collected from the Bhote Kosi mainstream.

	Locality	BKT1	BKT2	BKT3	BKT4	BKT5	BKT6	BKT7	BK43
	Date of collection	Sep-98	Sep-98	Sep-98	Sep-98	Sep-98	Sep-98	Sep-98	Dec-98
GPS	N	28° 28.450'	28° 26.180'	28° 22.500'	28° 18.250'	28° 13.330'	28° 06.030'	27° 58.190'	27° 58.157'
	E	86° 89.180'	86° 08.670'	86° 05.620'	86° 02.020'	85° 59.880'	86° 01.230'	85° 57.620'	85° 57.467'
	Dist. from source (km)	0.00	15.33	24.00	34.33	43.67	59.67	75.33	75.33
	Temperature (°C)	18.4	14.5	13.8	14.1	9.0	7.3	7.3	4.5
	pH	8.43	8.25	7.52	7.24	7.80	7.50	7.50	8.19
Cations	Na^+	130.58	361.56	58.09	180.50	92.03	58.31	64.16	133.60
(µmol/l)	Mg^{2+}	515.10	1112.59	158.04	269.44	171.68	87.47	55.79	84.15
	Si	122.00	89.53	46.50	98.32	72.79	50.93	79.00	110.99
	K^+	35.16	29.79	10.11	42.65	22.15	23.03	22.89	25.04
	Ca^{2+}	1554.18	1805.62	975.98	996.59	691.46	376.40	265.95	426.79
	Rb^+	0.021	0.008	0.007	0.052	0.024	0.027	0.035	0.037
	Sr^{2+}	3.559	5.419	2.097	1.513	1.097	0.548	0.419	0.591
Anions	HCO_3^-	2592.34	1930.87	1612.22	1783.31	1228.07	765.67	347.06	903.56
(µmol/l)	Cl^-	8.49	2.01	4.26	6.52	3.42	1.44	8.78	
	NO_3^-	6.60	14.74	4.38	10.59	0.00	-4.69	4.69	
	SO_4^{2-}	1298.08	2812.16	453.11	423.24	279.33	183.02	112.06	
	Charge balance (%)	82.6	82.2	91.8	102.9	101.2	88.3	116.9	N/A
	(corrected for atmos.)	82.7	82.2	92.4	104.1	102.8	89.4	125.0	N/A
	$^{87}Sr/^{86}Sr$	0.711511 ± 25	0.722001 ± 10	0.720252 ± 9	0.723829 ± 13	0.723636 ± 8	0.724670 ± 13	0.726746 ± 22	0.727614 ± 12
% Geology	TSS	100.00	100.00	100.00	68.52	57.71	38.14	34.25	34.25
	HHCS	0.00	0.00	0.00	31.48	42.29	61.86	65.75	65.75
LHF	LHC	0.00	0.00	0.00	0.00	0.00	0.00	0.00	0.00
	LHSM	0.00	0.00	0.00	0.00	0.00	0.00	0.00	0.00
	LHSC	0.00	0.00	0.00	0.00	0.00	0.00	0.00	0.00

Table A1. Water samples collected from the Bhote Kosi mainstream.

	Locality	BK76	BK78	BK80	BK42	BK81	BK44	BK58	BK40
	Date of collection	Oct-99	Oct-99	Oct-99	Dec-98	Oct-99	Dec-98	Sep-99	Dec-98
GPS	N	27° 58.157'	27° 56.886'	27° 56.484'	27° 55.575'	See note 1	27° 53.091'	27° 53.048'	27° 52.971'
	E	85° 57.467'	85° 57.124'	85° 56.846'	85° 56.047'		85° 54.745'	85° 54.769'	85° 54.179'
	Dist. from source (km)	75.33	78.33	78.67	81.00	81.00	85.33	85.33	86.50
	Temperature (°C)	10.0	11.1	11.7	9.2	13.9	8.5	16.7	9.0
	pH	8.15	8.04	8.11	7.83	7.90	8.07	7.95	7.94
Cations	Na^+	83.51	76.45	77.34	146.07	80.85	132.67	53.25	129.87
(µmol/l)	Mg^{2+}	56.17	51.01	52.14	83.86	51.55	123.64	70.10	136.35
	Si	111.18	95.56	97.63	117.13	17.46	118.47	94.62	108.92
	K^+	23.71	17.69	17.63	24.91	21.62	32.89	20.46	33.88
	Ca^{2+}	392.43	267.48	264.93	370.29	209.33	413.55	245.84	414.06
	Rb^+	0.029	0.026	0.027	0.038	0.031	0.045	0.025	0.044
	Sr^{2+}	0.593	0.385	0.385	0.515	0.449	0.538	0.337	0.486
Anions	HCO_3^-	578.98	485.26	492.17	770.56	432.21	934.56	539.35	946.56
(µmol/l)	Cl^-	9.15	10.12	7.55		5.14		4.86	
	NO_3^-	8.69	7.92	7.65		27.03		17.01	
	SO_4^{2-}	110.08	95.38	94.61		86.28		152.23	
	Charge balance (%)	117.2	101.2	100.7	N/A	94.7	N/A	81.0	N/A
	(corrected for atmos.)	122.9	105.3	104.7	N/A	98.0	N/A	81.5	N/A
	$^{87}Sr/^{86}Sr$	0.728989 ± 7	0.731310 ± 8	0.731555 ± 6	0.732179 ± 14		0.740133 ± 20	0.745678 ± 5	0.745004 ± 776
% Geology	TSS	34.25	31.70	31.70	30.49	30.49	29.93	29.93	28.98
	HHCS	65.75	68.30	68.30	69.30	69.30	68.33	68.33	67.80
LHF	LHC	0.00	0.00	0.00	0.21	0.21	1.67	1.67	2.97
	LHSM	0.00	0.00	0.00	0.00	0.00	0.00	0.00	0.00
	LHSC	0.00	0.00	0.00	0.00	0.00	0.07	0.07	0.25

1. Approx. 100m downstream of Bhote Kosi hydroelectricity project dam site.

Table A1. Water samples collected from the Bhote Kosi mainstream.

	Locality	BK60	BK85	BK86	BK34	BK89	BK62	BK63	BK31
	Date of collection	Sep-99	Oct-99	Oct-99	Nov-98	Oct-99	Sep-99	Sep-99	Nov-98
GPS	N	See note 2	27° 52.494'	27° 51.856'	27° 50.712'	27° 49.821'	27° 49.046'	27° 48.870'	27° 48.366'
	E		85° 52.949'	85° 52.645'	85° 52.825'	85° 52.112'	85° 52.865'	85° 53.016'	85° 53.383'
	Dist. from source (km)	86.50	88.00	89.67	91.17	93.50	94.83	96.33	97.83
	Temperature (°C)	17.3	15.1	15.3	12.4	14.7	17.1	17.4	12.7
	pH	7.96	8.49	8.50	7.96	8.43	8.16	8.27	8.12
Cations	Na^+	63.41	65.90	75.30	90.92	70.66	48.02	36.12	99.48
(µmol/l)	Mg^{2+}	119.15	103.50	153.13	133.96	163.41	154.81	125.65	179.02
	Si	81.44	93.53	114.77	101.63	113.90	92.40	86.67	121.02
	K^+	21.56	23.84	27.88	30.47	29.66	28.56	24.13	38.19
	Ca^{2+}	313.28	248.90	284.78	316.08	311.81	280.46	198.92	383.02
	Rb^+	0.027	0.034	0.035	0.045	0.042	0.038	0.032	0.051
	Sr^{2+}	0.258	0.317	0.346	0.366	0.346	0.257	0.189	0.415
Anions	HCO_3^-	600.94	491.81	724.78	950.56	962.49	734.57		996.56
(µmol/l)	Cl^-	2.19	2.23	7.56		5.86	12.22	0.23	5.64
	NO_3^-	8.07	5.31	4.89		5.85	7.54	5.54	20.41
	SO_4^{2-}	135.74	90.89	87.03		90.17	74.53	66.92	109.54
	Charge balance (%)	104.0	110.8	104.0	N/A	89.7	101.6	N/A	99.5
	(corrected for atmos.)	107.6	116.6	107.4	N/A	91.0	104.8	N/A	101.6
	$^{87}Sr/^{86}Sr$	0.752337 ± 7	0.753521 ± 8	0.755684 ± 7	0.754169 ± 10	0.757317 ± 5	0.763410 ± 9	0.764328 ± 8	0.755595 ± 10
% Geology	TSS	28.98	28.97	28.41	28.32	28.18	28.04	28.03	27.93
	HHCS	67.80	67.76	66.67	66.44	66.13	65.79	65.73	65.53
LHF	LHC	2.97	3.02	4.54	4.72	4.77	4.82	4.82	4.82
	LHSM	0.00	0.00	0.02	0.16	0.56	0.99	1.06	1.36
	LHSC	0.25	0.25	0.36	0.36	0.36	0.36	0.36	0.36

2. Approx. 100m downstream of the confluence of the Bhote Kosi and the Chaku Khola.

Table A1. Water samples collected from the Bhote Kosi mainstream.

	Locality	BK99	BK100	BK55	BK98	BK33	BK64	BK29	BK134
	Date of collection	Oct-99	Oct-99	Sep-99	Oct-99	Nov-98	Sep-99	Nov-98	Nov-99
GPS	N	27° 48.351'	27° 47.878'	See note 3	27° 46.792'	27° 46.212'	27° 45.875'	27° 44.022'	27° 44.049'
	E	85° 53.416'	85° 53.733'		85° 53.592'	85° 53.039'	85° 52.673'	85° 46.830'	85° 46.908'
	Dist. from source (km)	97.83	99.17	100.67	100.67	102.67	102.67	113.33	113.33
	Temperature (°C)	13.4	13.6	18.9	13.7	14.0	20.6	13.3	6.0
	pH	8.27	8.30	8.18	8.36	8.19	8.16	8.17	8.00
Cations	Na^+	39.27	63.82	53.16	46.04	82.93	51.34	98.59	81.25
(µmol/l)	Mg^{2+}	105.54	112.14	164.92	102.45	151.66	153.93	198.19	184.98
	Si	84.56	82.16	99.23	87.39	96.25	87.61	132.35	85.90
	K^+	19.95	19.52	29.55	17.74	31.33	31.80	40.14	33.75
	Ca^{2+}	106.71	212.86	309.98	178.48	325.75	232.10	444.86	340.26
	Rb^+	0.023	0.021	0.040	0.024	0.044	0.040	0.051	0.045
	Sr^{2+}	0.275	0.210	0.303	0.221	0.345	0.194	0.409	0.358
Anions	HCO_3^-	519.28	544.96	761.48	503.03	961.56	752.41	1043.56	909.85
(µmol/l)	Cl^-	0.59	16.90	0.00	7.31		5.95	6.24	2.58
	NO_3^-	8.59	8.85	6.10	7.16		7.04	17.24	7.91
	SO_4^{2-}	49.06	52.27	82.20	42.86		64.90	98.90	80.52
	Charge balance (%)	77.2	103.9	107.0	99.4	N/A	93.4	109.6	104.8
	(corrected for atmos.)	77.2	108.6	110.8	103.7	N/A	95.5	112.7	107.8
	$^{87}Sr/^{86}Sr$	0.769753 ± 8		0.759946 ± 6		0.759345 ± 18	0.771223 ± 15	0.759235 ± 11	0.763282 ± 5
% Geology	TSS	27.93	27.64	27.58	27.58	26.56	26.56	25.19	25.19
	HHCS	65.53	64.85	64.67	64.67	62.59	62.59	59.34	59.34
LHF	LHC	4.82	5.32	5.32	5.32	6.52	6.52	6.86	6.86
	LHSM	1.36	1.77	2.01	2.01	2.83	2.83	6.71	6.71
	LHSC	0.36	0.42	0.42	0.42	1.50	1.50	1.90	1.90

3. Bhote Kosi 15 m upstream of confluence of the Bhote Kosi and Sun kosi Nadi

Table A1. Water samples collected from the Bhote Kosi mainstream.

	Locality	BK28	BK133	BK45	BK46	BK35	BK74	BK38	BK70
	Date of collection	Nov-98	Nov-99	Dec-98	Dec-98	Nov-98	Sep-99	Nov-98	Sep-99
GPS	N	27° 43.428'	27° 43.018'	27° 42.825'	27° 40.022'	27° 38.452'	27° 38.452'	27° 37.787'	27 37.478
	E	85° 46.703'	85° 46.431'	85° 45.851'	85° 43.526'	85° 42.536'	85° 42.536'	85° 42.741'	85° 42.741'
	Dist. from source (km)	115.17	115.17	116.67	123.00	125.33	125.33	126.50	126.50
	Temperature (°C)	13.6	16.0	12.0	12.6	19.1	21.1	15.4	
	pH	8.03	7.99			8.08	8.12	7.66	
Cations	Na^+	98.73	79.56			88.12	42.47	87.37	65.06
(µmol/l)	Mg^{2+}	163.58	151.33			140.12	103.50	104.59	22.23
	Si	142.48	136.63			124.10	107.15	135.36	
	K^+	39.05	30.13			34.51	25.23	31.01	23.05
	Ca^{2+}	343.82	273.08			321.68	220.96	291.91	94.14
	Rb^+	0.000	0.037			0.044	0.033	0.037	
	Sr^{2+}	0.355	0.302			0.315	0.168	0.297	
Anions	HCO_3^-	850.56	733.83	884.56	872.56	832.56	651.39	814.56	
(µmol/l)	Cl^-	5.31	0.87				0.96		14.44
	NO_3^-	17.40	6.20				8.14		3.01
	SO_4^{2-}	91.95	73.91				47.35		12.01
	Charge balance (%)	105.8	104.2	N/A	N/A	N/A	92.5	110.8	N/A
	(corrected for atmos.)	109.0	107.9	N/A	N/A	N/A	94.9	111.9	N/A
	$^{87}Sr/^{86}Sr$	0.762498 ± 17	0.765723 ± 11			0.763802 ± 24	0.782241 ± 7	0.759129 ± 20	
% Geology	TSS	19.84	19.84	19.82	19.45	19.37	19.37	14.20	14.20
	HHC	61.72	61.72	61.70	60.55	60.26	60.26	65.67	65.67
	LHC	7.46	7.46	7.46	7.32	7.29	7.29	7.67	7.67
	LHSM	9.05	9.05	9.09	10.79	11.19	11.19	10.94	10.94
	LHSC	1.93	1.93	1.93	1.89	1.89	1.89	1.52	1.52

Table A1. Water samples collected from the Bhote Kosi mainstream.

	Locality	BK75	BK39
	Date of collection	Sep-99	Nov-98
GPS	N	27 37.478	27° 36.294'
	E	85° 42.741'	85° 43.395'
	Dist. from source (km)	126.50	130.50
	Temperature (°C)		15.6
	pH		7.86
Cations	Na^+	65.36	90.74
(µmol/l)	Mg^{2+}	21.56	106.73
	Si	128.32	143.28
	K^+	22.32	29.47
	Ca^{2+}	85.59	277.40
	Rb^+	0.019	0.036
	Sr^{2+}	0.152	0.295
Anions	HCO_3^-		701.56
(µmol/l)	Cl^-	35.58	
	NO_3^-	18.39	
	SO_4^{2-}	19.63	
	Charge balance (%)	N/A	N/A
	(corrected for atmos.)	N/A	N/A
	$^{87}Sr/^{86}Sr$	0.746209 ± 9	0.758585 ± 26
% Geology	TSS	14.20	14.19
	HHC	65.67	65.63
	LHC	7.67	7.70
	LHSM	10.94	10.96
	LHSC	1.52	1.52

Table A2. Water samples collected from tributaries of the Bhote Kosi.

	Locality	BK77	BK79	BK126	BK82	BK83	BK93	BK92	BK41
	River	Lipin Khola	Jun Khola	Unnamed	Khukundal K	Junrimba K	Chaku Khola	Chaku Khola	Chaku Khola
	Date of collection	Oct-99	Oct-99	Oct-99	Oct-99	Oct-99	Oct-99	Oct-99	Dec-98
GPS	N	27° 57.400'	27° 56.528'	27° 56.466'	27° 56.466'	27° 54.400'	27° 55.055'	27° 52.174'	27° 53.012'
	E	85° 56.466'	85° 56.875'	85° 56.180'	85° 56.005'	85° 55.062'	85° 56.270'	85° 56.490'	85° 54.849'
	Dist. from source (km)	77.0	78.7	80.0	81.7	83.7	86.0	86.0	86.0
	Temperature (°C)	11.2	13.9	15.8	18.3	17.0	15.9	15.0	12.2
	pH	7.73	8.09	7.76	9.01	8.54	8.34	8.58	8.02
Cations	Na^+	82.98	56.76	47.35	33.42	50.20	37.99	22.96	46.86
(µmol/l)	Mg^{2+}	4.51	39.05	46.43	714.87	194.88	84.70	216.07	287.82
	Si	105.29		127.52	13.56	135.32	108.27	96.72	
	K^+	12.05	24.91	25.48	90.47	41.83	29.19	35.55	59.32
	Ca^{2+}	20.21	75.92	150.82	833.13	264.98	125.29	326.52	372.66
	Rb^+	0.040		0.031	0.119	0.048	0.028	0.046	
	Sr^{2+}	0.099		0.100	0.791	0.168	0.034	0.164	
Anions	HCO_3^-	180.98	236.23	438.12	2409.59	815.46	411.88	957.13	1069.56
(µmol/l)	Cl^-	0.00	0.78	12.47	1.77	16.75	2.00	5.07	
	NO_3^-	13.09	24.78	2.27	16.04	4.55	3.15	5.11	
	SO_4^{2-}	13.09	29.67	101.78	251.61	66.10	39.66	68.23	
	Charge balance (%)	70.2	91.7	72.1	108.6	101.5	94.1	101.1	N/A
	(corrected for atmos.)	65.6	97.0	71.2	109.9	104.4	98.1	103.6	N/A
	$^{87}Sr/^{86}Sr$	0.778051 ± 13	0.751206 ± 12	0.801717 ± 998	0.859310 ± 28	0.851927 ± 13	1.252681 ± 41	0.852184 ± 10	0.849519 ± 10
% Geology	TSS	0.00	0.00	0.00	0.00	0.00	0.00	0.00	0.00
	HHCS	100.00	97.97	86.48	0.00	44.90	0.00	86.00	56.81
LHF	LHC	0.00	2.03	13.52	100.00	47.45	100.00	11.50	36.78
	LHSM	0.00	0.00	0.00	0.00	0.00	0.00	0.00	0.00
	LHSC	0.00	0.00	0.00	0.00	7.65	0.00	2.50	6.40

Table A2. Water samples collected from tributaries of the Bhote Kosi.

	Locality	BK57	BK91	BK94	BK59	BK84	BK90	BK87	BK88
	River	Chaku Khola	Chaku Khola	Unnamed	Unnamed	Kahule Khola	Ghatte Khola	Phanphunge K	Malati Khola
	Date of collection	Sep-99	Oct-99	Oct-99	Sep-99	Oct-99	Oct-99	Oct-99	Oct-99
GPS	N	27° 53.005'	27° 52.904'	27° 52.995'	27° 52.822'	27° 52.387'	27° 51.260'	27° 50.479'	27° 49.780'
	E	85° 54.858'	85° 54.970'	85° 54.425'	85° 54.376'	85° 52.897'	85° 52.435'	85° 52.886'	85° 51.987'
	Dist. from source (km)	86.0	86.0		87.3	88.0	90.5	92.2	93.5
	Temperature (°C)	18.4	16.4	18.7	22.3	19.0	20.0	16.5	20.0
	pH	8.23	8.65	9.09	8.61	8.91	9.05	8.90	9.03
Cations	Na^+	10.57	32.31	23.34	26.28	37.72	25.20	6.68	26.12
(µmol/l)	Mg^{2+}	136.60	217.87	580.98	780.70	422.80	638.88	396.70	447.80
	Si	70.87	96.36	106.46	125.41	111.54	103.62	91.93	105.47
	K^+	23.73	42.10	88.46	80.89	51.54	75.62	25.87	45.56
	Ca^{2+}	312.27	330.34	766.28	743.37	605.19	866.29	420.20	590.17
	Rb^+	0.033	0.051	0.111	0.083	0.091	0.121	0.054	0.057
	Sr^{2+}	0.150	0.156	0.267	0.274	0.218	0.167	0.124	0.151
Anions	HCO_3^-	914.76	952.88	2768.93	2748.00	1863.82	2837.79	1598.30	1967.65
(µmol/l)	Cl^-	0.00	8.39	2.50	0.03	8.45	33.50	0.00	32.12
	NO_3^-	3.65	3.70	3.92	5.08	10.73	18.65	9.64	7.20
	SO_4^{2-}	55.82	69.18	199.53	95.87	84.90	1.82	22.86	6.97
	Charge balance (%)	89.4	103.3	88.0	106.0	103.0	106.3	99.2	104.7
	(corrected for atmos.)	90.5	106.1	88.4	107.1	104.5	107.5	100.8	106.3
	$^{87}Sr/^{86}Sr$	0.852775 ± 12	0.858328 ± 9	0.844200 ± 10	0.849515 ± 7	0.832314 ± 10	0.833300 ± 17	0.803231 ± 13	0.861569 ± 9
% Geology	TSS	0.00	0.00	0.00	0.00	0.00	0.00	0.00	0.00
	HHCS	56.81	56.81	0.00	0.00	14.95	0.00	0.00	0.00
LHF	LHC	36.78	36.78	100.00	100.00	76.95	65.00	33.33	16.98
	LHSM	0.00	0.00	0.00	0.00	0.00	35.00	66.67	83.02
	LHSC	6.40	6.40	0.00	0.00	8.10	0.00	0.00	0.00

Table A2. Water samples collected from tributaries of the Bhote Kosi.

	Locality	BK61	BK68	BK96	BK95	BK129	BK130	BK131	BK128
	River	Bimegodhan K	Khagdal K	Khagdal K	Damar Khola	Sun Kosi Nadi	Hadi Khola	Kahre Khola	Sun Kosi Nadi
	Date of collection	Sep-99	Sep-99	Oct-99	Oct-99	Nov-99	Nov-99	Nov-99	Nov-99
GPS	N	27° 48.803'	27° 48.130'	27° 48.206'	27° 48.071'	27° 46.929'	27° 46.952'	27° 47.063'	27° 46.948'
	E	85° 52.869'	85° 53.598'	85° 53.658'	85° 54.339'	85° 57.596'	85° 57.579'	85° 57.059'	85° 56.685'
Dist. from source (km)		94.8	97.8	97.8	98.0	100.7	100.7	100.7	100.7
Temperature (°C)		21.0		19.4	19.8	16.7	16.5	18.8	16.5
pH		8.38		8.44	8.38	7.95	8.06	7.38	7.93
Cations	Na^+	53.92	23.19	23.86	49.88	24.80	29.28	52.10	30.30
(µmol/l)	Mg^{2+}	76.47	189.30	204.70	51.38	224.62	320.42	64.73	240.00
	Si	93.75	85.21	87.61	126.28	23.77	47.07	153.66	21.87
	K^+	24.23	40.82	44.63	42.28	32.39	52.54	28.53	42.49
	Ca^{2+}	309.47	258.82	269.26	127.96	326.31	461.71	66.89	327.93
	Rb^+	0.025	0.047	0.050	0.029	0.043	0.050	0.035	0.044
	Sr^{2+}	0.038	0.085	0.093	0.071	0.219	0.260	0.058	0.207
Anions	HCO_3^-	1009.84		1092.86	412.23	900.04	1138.15	261.39	947.73
(µmol/l)	Cl^-	4.41	7.18	6.21	26.65	0.00	0.08	0.00	0.00
	NO_3^-	21.03	8.04	13.24	20.40	0.00	1.93	7.11	0.93
	SO_4^{2-}	1.98	13.65	18.97	24.10	50.38	114.65	5.67	79.86
Charge balance (%)		81.3	N/A	87.3	86.6	112.0	116.8	110.0	106.3
(corrected for atmos.)		81.8	N/A	88.4	88.8	115.8	120.2	122.9	109.0
$^{87}Sr/^{86}Sr$		0.917047 ± 17	0.863322 ± 10	0.873754 ± 14	0.894672 ± 11			0.964589 ± 16	
% Geology	TSS	0.00	0.00	0.00	0.00	0.00	0.00	0.00	0.00
	HHCS	0.00	0.00	0.00	0.00	0.00	20.75	0.00	9.87
LHF	LHC	0.00	81.29	81.29	0.00	27.04	11.01	79.37	32.74
	LHSM	100.00	9.03	9.03	100.00	60.71	1.26	0.00	18.54
	LHSC	0.00	9.68	9.68	0.00	12.24	66.98	20.63	38.86

Table A2. Water samples collected from tributaries of the Bhote Kosi.

	Locality	BK32	BK67	BK69	BK97	BK30	BK132	BK101	BK103
	River	Sun Kosi Nadi	Sun Kosi Nadi	Dabi Khola	Dabi Khola	Balephi Khola	Balephi Khola	Ev. Quarry	Ev. Quarry
Date of collection		Nov-98	Sep-99	Sep-99	Oct-99	Nov-98	Nov-99	Oct-99	Oct-99
GPS	N	27° 46.711'	27° 46.711'	27° 45.950'	See note 1	27° 44.679'	27° 44.085'	27° 40.811'	27° 41.072'
	E	85° 53.726'	85° 53.726'	85° 52.482'		85° 46.763'	85° 46.982'	85° 36.921'	85° 36.724'
Dist. from source (km)		100.7	100.7	103.8	103.8	114.2	114.2	125.5	125.5
Temperature (°C)		15.4			18.7	15.1	16.4	23.1	22.8
pH		8.04			8.29	7.87	7.69	7.83	7.87
Cations	Na^+	48.33	24.89	36.08	33.81	88.92	71.53	341.99	326.60
(µmol/l)	Mg^{2+}	241.71	185.90	131.27	92.46	93.93	86.25	98.50	42.19
	Si	117.02	85.87	133.29	84.41	146.51	147.42	551.24	419.79
	K^+	47.81	29.53	49.51	25.40	41.63	26.40	35.87	28.43
	Ca^{2+}	341.79	228.03	262.64	176.75	218.28	182.22	731.41	275.87
	Rb^+	0.057	0.045	0.035	0.029	0.042	0.032	0.018	0.012
	Sr^{2+}	0.157	0.097	0.117	0.092	0.236	0.198	0.492	0.412
Anions	HCO_3^-	1080.56			466.63	544.56	640.76	1935.41	980.68
(µmol/l)	Cl^-	0.56	0.00	8.58	0.00	11.13	0.00	10.54	52.20
	NO_3^-	6.36	2.45	2.79	9.86	4.77	8.16	4.60	15.61
	SO_4^{2-}	88.14	39.12	20.61	5.16	84.69	60.67	3.64	0.36
Charge balance (%)		98.0	N/A	N/A	114.1	99.8	81.8	102.5	92.7
(corrected for atmos.)		99.9	N/A	N/A	122.8	103.4	82.4	104.1	94.5
	$^{87}Sr/^{86}Sr$	0.869126 ± 47		0.887311 ± 12	0.856156 ± 16	0.770923 ± 21	0.775931 ± 10	0.733068 ± 19	0.737687 ± 7
% Geology	TSS	0.00	0.00	0.00	0.00	0.00	0.00	0.00	0.00
	HHCS	8.07	8.07	0.00	0.00	72.84	72.84	100.00	100.00
LHF	LHC	40.34	40.34	36.59	36.59	10.03	10.03	0.00	0.00
	LHSM	19.80	19.80	37.80	37.80	15.00	15.00	0.00	0.00
	LHSC	31.78	31.78	25.61	25.61	2.13	2.13	0.00	0.00

1. Dabi Khola 50 m upstream of confluence with the Bhote Kosi.

Table A2. Water samples collected from tributaries of the Bhote Kosi.

	Locality	BK53	BK102	BK107	BK106	BK108	BK109	BK37	BK65
	River	Ev. Quarry	Ev. Quarry	Ev. Quarry	Chak Khola	Chak Khola	Chak Khola	Chak Khola	Chak Khola
	Date of collection	Sep-99	Oct-99	Oct-99	Oct-99	Oct-99	Oct-99	Nov-98	Sep-99
GPS	N	27° 40.823'	27° 40.871'	27° 40.777'	27° 40.789'	27° 40.494'	27° 39.798'	27° 38.761'	27° 38.703'
	E	85° 37.030'	85° 37.117'	85° 37.629'	85° 37.652'	85° 37.823'	85° 39.209'	85° 42.092'	85° 42.127'
	Dist. from source (km)	125.5	125.5	125.5	125.5	125.5	125.5	125.5	125.5
	Temperature (°C)	28.7	24.3	23.4	23.6	24.8	25.0	17.8	29.9
	pH	8.58	7.99	8.10	7.61	7.94	8.02	8.12	8.32
Cations	Na^+	389.60	377.49	337.95	263.33	269.81	258.23	282.98	16.87
(µmol/l)	Mg^{2+}	107.10	68.46	72.24	59.23	61.08	92.96	225.59	188.00
	Si	356.54	460.46	448.11	346.91	358.31	332.90	283.08	324.94
	K^+	40.01	40.82	34.27	25.80	27.15	26.60	33.91	32.50
	Ca^{2+}	680.77	456.82	473.11	206.75	249.41	324.23	460.38	393.20
	Rb^+	0.023	0.022	0.017	0.014	0.014	0.015	0.028	0.026
	Sr^{2+}	0.708	0.475	0.470	0.308	0.318	0.396	0.525	0.505
Anions	HCO_3^-	1737.10	1195.56	1392.67	687.62	754.03	889.85	1760.56	972.10
(µmol/l)	Cl^-	9.25	42.86	38.29	51.95	59.94	47.91	0.00	34.82
	NO_3^-	4.37	15.82	15.34	31.46	30.79	31.81	0.00	24.67
	SO_4^{2-}	13.33	4.28	4.93	8.25	7.32	26.22	0.00	71.81
	Charge balance (%)	110.6	113.0	98.7	100.7	103.2	106.2	96.2	100.7
	(corrected for atmos.)	112.8	116.3	100.5	104.3	106.8	109.5	95.9	103.1
	$^{87}Sr/^{86}Sr$	0.733728 ± 15	0.736347 ± 7	0.737437 ± 6	0.740294 ± 9	0.739725 ± 13	0.745792 ± 7	0.765353 ± 24	0.757309 ± 9
% Geology	TSS	0.00	0.00	0.00	0.00	0.00	0.00	0.00	0.00
	HHCS	100.00	100.00	100.00	84.27	88.41	78.95	65.55	65.55
LHF	LHC	0.00	0.00	0.00	15.73	11.59	21.05	34.45	34.45
	LHSM	0.00	0.00	0.00	0.00	0.00	0.00	0.00	0.00
	LHSC	0.00	0.00	0.00	0.00	0.00	0.00	0.00	0.00

Table A2. Water samples collected from tributaries of the Bhote Kosi.

	Locality	BK71	BK52	BK50	BK49	BK48	BK36	BK66	BK72
	River	Chak Khola	Indrawati	Indrawati	Malemchi K	Indrawati	Indrawati	Indrawati	Indrawati
	Date of collection	Sep-99	Sep-99	Sep-99	Sep-99	Sep-99	Nov-98	Sep-99	Sep-99
GPS	N	27° 38.703'	27° 52.988'	27° 49.998'	27° 49.940'	27° 49.709'	27° 38.425'	27° 38.544'	27° 38.544'
	E	85° 42.127'	85° 36.795'	85° 34.656'	85° 34.454'	85° 34.668'	85° 42.403'	85° 42.388'	85° 42.388'
	Dist. from source (km)	125.5	125.5	125.5	125.5	125.5	125.5	125.5	125.5
	Temperature (°C)	24.7	22.1	20.7	22.1	23.1	19.1	23.3	21.8
	pH	7.80	7.18	7.92	8.07	8.52	8.05	7.60	7.57
Cations	Na^+	204.01	14.28	61.77	25.68	73.97	112.21	60.48	73.25
(µmol/l)	Mg^{2+}	61.66	0.68	9.97	2.17	7.97	42.74	14.27	22.73
	Si	142.00	129.04	147.81	164.34	170.87		125.74	69.41
	K^+	27.26	3.77	16.14	7.27	18.12	28.61	19.51	23.05
	Ca^{2+}	161.63	89.87	116.82	77.52	94.86	170.92	90.86	76.95
	Rb^+	0.015	0.006	0.018	0.013	0.019		0.019	0.021
	Sr^{2+}	0.186	0.133	0.161	0.167	0.192		0.158	0.153
Anions	HCO_3^-	588.88		237.99	328.33	271.68	437.56		259.31
(µmol/l)	Cl^-	32.46	2.62	0.00	0.00	3.76		8.45	6.76
	NO_3^-	43.70	2.48	1.43	7.29	3.67		5.56	13.68
	SO_4^{2-}	28.07	10.56	9.35	8.69	8.47		12.45	11.93
	Charge balance (%)	91.6	N/A	112.8	60.4	93.9	N/A	N/A	91.7
	(corrected for atmos.)	94.0	N/A	128.4	54.5	100.6	N/A	N/A	97.4
	$^{87}Sr/^{86}Sr$	0.748609 ± 47	0.736972 ± 12	0.736354 ± 6	0.735835 ± 8	0.735118 ± 16	0.742419 ± 22	0.743226 ± 22	0.744445 ± 26
% Geology	TSS	0.00	0.00	0.00	0.00	0.00	0.00	0.00	0.00
	HHCS	65.55	100.00	100.00	100.00	100.00	83.66	83.66	83.66
LHF	LHC	34.45	0.00	0.00	0.00	0.00	5.65	5.65	5.65
	LHSM	0.00	0.00	0.00	0.00	0.00	10.14	10.14	10.14
	LHSC	0.00	0.00	0.00	0.00	0.00	0.55	0.55	0.55

Table A2. Water samples collected from tributaries of the Bhote Kosi.

	Locality	**BK73**	**BK47**
	River	Indra. / Chak K.	Jhiku Khola
	Date of collection	Sep-99	Sep-99
GPS	**N**	See note 2	27° 38.543'
	E		85° 37.033'
	Dist. from source (km)	125.5	N/A
	Temperature (°C)	22.0	26.4
	pH	7.60	8.34
Cations	**Na^+**	85.68	444.17
(µmol/l)	**Mg^{2+}**	27.77	47.57
	Si	138.92	324.87
	K^+	25.80	30.92
	Ca^{2+}	97.15	198.87
	Rb^+	0.027	0.016
	Sr^{2+}	0.176	0.486
Anions	**HCO_3^-**	253.12	
(µmol/l)	**Cl^-**	1.96	71.95
	NO_3^-	7.74	2.35
	SO_4^{2-}	10.75	15.07
	Charge balance (%)	112.4	N/A
	(corrected for atmos.)	127.1	N/A
	$^{87}Sr/^{86}Sr$	0.74459 ± 16	0.734363 ± 8
% Geology	**TSS**	0.00	0.00
	HHCS	82.41	100.00
LHF	**LHC**	7.64	0.00
	LHSM	9.44	0.00
	LHSC	0.51	0.00

2. Indrawati / Chak Khola mixed just upstream of confluence with the Bhote Kosi.

Table A3. Water samples collected from the Langtang Khola - Trisuli mainstream.

	Locality	L14	L15	L31	L12	L30	L16	L17	L19
Date of collection		Oct-98	Oct-98	Sep-99	Oct-98	Sep-99	Oct-98	Oct-98	Oct-98
GPS	N	28° 14.312'	28° 12.911'	28° 12.040'	28° 12.570'	28° 12.739'	28° 12.634'	28° 11.971'	28° 09.223'
	E	85° 41.888'	85° 40.506'	85° 38.305'	85° 33.549'	85° 32.801'	85° 32.772'	85° 27.442'	85° 23.959'
Dist. from source (km) (Langtang Khola)		Source	4.25	7.25	16.00	17.00	18.00	25.50	34.00
Dist. from source (km) (Trisuli)		N/A	N/A	N/A	N/A	N/A	N/A	N/A	N/A
Temperature (°C)		3.2	4.5	5.4	6.7	6.6	3.3	8.5	12.0
pH		7.38	7.51	7.57	7.25	7.79	7.49	7.33	7.18
Cations (µmol/l)	Na^+	76.77	43.89	46.42	71.44	34.84	51.08	63.14	64.34
	Mg^{2+}	99.76	57.64	34.64	44.54	17.80	28.62	26.08	27.25
	Si	89.86	34.89	40.91	62.55	45.71	53.69	61.61	73.70
	K^+	52.61	24.39	24.07	26.00	11.22	20.18	21.31	20.65
	Ca^{2+}	352.73	244.32	235.16	283.00	153.16	207.16	201.31	174.10
	Rb^+	0.075	0.018	0.020	0.023	0.012	0.018	0.022	0.026
	Sr^{2+}	0.735	0.405	0.309	0.366	0.191	0.271	0.267	0.258
Anions (µmol/l)	HCO_3^-	551.56	410.56	374.34	400.56	306.72	310.56	319.56	279.56
	Cl^-	24.96	1.59	1.90	3.43	0.84	1.38	3.52	4.69
	NO_3^-	37.34	2.31	0.95	19.97	1.79	9.19	11.94	3.08
	SO_4^{2-}	171.64	161.05	99.98	135.66	74.29	101.26	98.15	95.59
Charge balance (%)		104.7	89.3	100.9	103.7	83.2	98.8	97.1	97.0
(corrected for atmos.)		108.1	91.3	105.7	108.2	84.7	103.7	101.5	101.9
$^{87}Sr/^{86}Sr$		0.738446 ± 12	0.738030 ± 20	0.737159 ± 7	0.736814 ± 30	0.738712 ± 7	0.738050 ± 19	0.738618 ± 15	0.739760 ± 21
% Geology	TSS	0.00	0.00	0.00	0.00	0.00	0.00	0.00	0.00
	HHCS	100.00	100.00	100.00	100.00	100.00	100.00	100.00	100.00
LHF	LHC	0.00	0.00	0.00	0.00	0.00	0.00	0.00	0.00
	LHSM	0.00	0.00	0.00	0.00	0.00	0.00	0.00	0.00
	LHSC	0.00	0.00	0.00	0.00	0.00	0.00	0.00	0.00

Table A3. Water samples collected from the Langtang Khola - Trisuli mainstream.

	Locality	L32	L8	L6	L28	L3	L25	L21
		Sep-99	Oct-98	Oct-98	Sep-99	Oct-98	Sep-99	Dec-98
GPS	N	28° 09.327'	28° 09.289'	28° 09.834'	28° 09.828'	28° 09.441'	28° 09.473'	27° 55.660'
	E	85° 23.862'	85° 23.885'	85° 20.652'	85° 20.614'	85° 19.952'	85° 19.928'	85° 08.946'
Dist. from source (km) (Langtang Khola)		34.00	35.00	40.50	40.50	44.00	44.00	76.50
Dist. from source (km) (Trisuli)		N/A	N/A	120.60	120.60	127.50	127.50	190.50
Temperature (°C)		9.9	9.1	14.3	12.4	13.7	15.3	14.8
pH		7.37	7.38	8.14	7.55	7.27	7.77	7.82
Cations (µmol/l)	Na^+	41.80	71.09	82.04	47.84	97.93	57.24	161.20
	Mg^{2+}	16.29	21.65	23.91	16.86	87.97	75.72	103.54
	Si	60.87	74.17	92.08	79.98	96.40	71.12	143.78
	K^+	15.75	22.80	27.10	20.91	28.72	20.71	36.75
	Ca^{2+}	132.15	154.23	172.27	115.37	315.83	312.27	358.84
	Rb^+	0.016	0.019	0.023	0.019	0.032	0.027	0.044
	Sr^{2+}	0.194	0.229	0.245	0.187	0.599	0.572	0.661
Anions (µmol/l)	HCO_3^-	297.80	270.56	320.56	115.82	624.56	341.93	766.56
	Cl^-	0.00	7.65	11.13	1.15	19.16	4.89	33.96
	NO_3^-	2.05	17.74	1.35	2.28	23.27	2.49	17.79
	SO_4^{2-}	54.07	86.40	90.50	51.83	143.29	126.79	139.24
Charge balance (%)		85.2	91.5	93.7	124.4	95.7	131.1	99.9
(corrected for atmos.)		86.9	95.1	97.6	149.5	98.0	141.6	102.4
$^{87}Sr/^{86}Sr$		0.740242 ± 33	0.740315 ± 27	0.740622 ± 34	0.741981 ± 8	0.725689 ± 21	0.723374 ± 6	0.734071 ± 15
% Geology	TSS	0.00	0.00	0.00	0.00	37.28	37.28	32.44
	HHCS	100.00	100.00	100.00	100.00	60.96	60.96	55.14
LHF	LHC	0.00	0.00	0.00	0.00	0.85	0.85	1.70
	LHSM	0.00	0.00	0.00	0.00	0.92	0.92	10.41
	LHSC	0.00	0.00	0.00	0.00	0.00	0.00	0.30

Table A4. Water samples collected from tributaries of the Langtang Khola - Trisuli.

	Locality	L11	L29	L10	L18	L20	L27	L5	L26
	River	Unnamed	Unnamed	Unnamed	Tanmarche Khola	Chopche Khola	Unnamed	Upper Trisuli (Bhote Kosi)	
	Date of collection	Oct-98	Sep-99	Oct-98	Oct-98	Oct-98	Sep-99	Oct-98	Sep-99
GPS	N	28° 12.603'	28° 12.996'	28° 12.980'	28° 09.329'	28° 08.425'	28° 10.344'	28° 09.952'	28° 09.921'
	E	85° 33.438'	85° 30.061'	85° 30.009'	85° 23.849'	85° 21.672'	85° 20.757'	85° 20.573'	85° 20.545'
	Dist. from source (km) (Langtang Khola)	16.05	20.00	21.00	34.25	37.50	N/A	41.50	41.50
	Dist. from source (km) (Trisuli)	N/A	N/A	N/A	N/A	N/A	120.00	120.50	120.50
	Temperature (°C)	5.9	N/A	7.6	12.2	11.6	17.8	14.4	23.1
	pH	7.29	7.90	7.35	7.28	6.88	7.68	7.52	7.68
Cations	Na^+	44.42	20.41	62.39	59.86	59.86	79.16	225.40	55.74
(µmol/l)	Mg^{2+}	24.11	12.02	13.38	7.57	18.97	114.32	107.52	84.36
	Si	56.09	31.57	34.61	145.93	178.46	293.64	95.92	77.04
	K^+	23.47	17.32	35.29	11.77	26.06	75.60	28.64	24.75
	Ca^{2+}	160.84	217.47	241.77	6.95	31.18	64.83	393.96	344.59
	Rb^+	0.021	0.023	0.034	0.010	0.023	0.023	0.038	0.030
	Sr^{2+}	0.216	0.139	0.150	0.078	0.081	0.219	0.675	0.637
Anions	HCO_3^-	237.56	340.57	248.56	52.56	70.56	123.26	709.56	513.22
(µmol/l)	Cl^-	3.79	0.00	25.32	6.59	0.00	20.97	17.75	4.87
	NO_3^-	22.48	0.30	54.94	2.14	1.74	22.53	12.16	2.87
	SO_4^{2-}	78.02	107.03	120.69	24.46	70.87	46.69	158.99	126.11
	Charge balance (%)	98.3	87.5	101.6	84.0	84.0	159.7	114.7	115.5
	(corrected for atmos.)	104.3	89.5	106.6	91.4	87.0	197.2	118.9	121.4
	$^{87}Sr/^{86}Sr$	0.744062 ± 15	0.738403 ± 9	0.735295 ± 15	0.755287 ± 28	0.764832 ± 24	0.748973 ± 7	0.725421 ± 15	0.722426 ± 5
% Geology	TSS	0.00	0.00	0.00	0.00	0.00	0.00	43.59	43.59
	HHCS	100.00	100.00	100.00	100.00	100.00	100.00	54.36	54.36
LHF	LHC	0.00	0.00	0.00	0.00	0.00	0.00	0.97	0.97
	LHSM	0.00	0.00	0.00	0.00	0.00	0.00	1.07	1.07
	LHSC	0.00	0.00	0.00	0.00	0.00	0.00	0.00	0.00

Table A4. Water samples collected from tributaries of the Langtang Khola - Trisuli.

		Locality	L24	L23	L22
		River	Unnamed	Unnamed	Unnamed
		Date of collection	Sep-99	Sep-99	
	GPS	N	28° 07.864'	28° 05.188'	27° 55.842'
		E	85° 18.934'	85° 16.295'	85° 09.372'
		Dist. from source (km) (Langtang Khola)	46.50	52.00	75.50
		Dist. from source (km) (Trisuli)	130.50	141.50	188.50
		Temperature (°C)	17.2	15.0	15.0
		pH	8.30	7.42	7.50
Cations		Na^+	41.72	43.89	146.33
(µmol/l)		Mg^{2+}	154.77	2.50	34.35
		Si	75.08	123.96	222.04
		K^+	58.33	14.57	13.08
		Ca^{2+}	229.81	0.00	37.90
		Rb^+	0.038	0.011	0.014
		Sr^{2+}	0.118	0.101	0.180
Anions		HCO_3^-	519.57	0.00	229.56
(µmol/l)		Cl^-	0.00	0.00	26.78
		NO_3^-	8.86	0.00	18.07
		SO_4^{2-}	46.99	0.00	2.19
		Charge balance (%)	130.0	N/A	99.5
		(corrected for atmos.)	139.7	N/A	109.0
		$^{87}Sr/^{86}Sr$	0.873083 ± 13	0.831713 ± 11	
% Geology		TSS	0.00	0.00	0.00
		HHCS	80.00	0.00	0.00
LHF		LHC	20.00	0.00	0.00
		LHSM	0.00	100.00	100.00
		LHSC	0.00	0.00	0.00

Table A5. Water samples collected from the Khumbu region (Dudh Kosi system).

	Locality	Ev1	Ev2	Ev3	Ev4	Ev5	Ev6	Ev7	Ev8
	River	Dudh Kosi	Dudh Kosi	Dudh Kosi	Imju Drangka	Imju Drangka	Imju Drangka	Imju Drangka	Bhote Kosi
	Date of collection	Sep-99	Sep-99	Sep-99	Oct-99	Oct-99	Oct-99	Oct-99	Oct-99
GPS	N	27° 44.635'	27° 46.463'	27° 49.978'	27° 52.223'	27° 53.635'	27° 53.456'	27° 51.002'	27° 49.089'
	E	85° 42.701'	86° 43.308'	86° 44.739'	86° 48.814'	86° 49.150'	86° 49.831'	86° 46.810'	86° 40.752'
Temperature (°C)		10.8	9.5	8.7	6.8	6.8	7.2	8.9	9.6
pH		7.72	8.03	7.71	7.72	7.32	7.88	7.78	7.80
Cations	Na^+	42.25	33.46	56.54	48.10	38.74	53.78	50.41	48.05
(µmol/l)	Mg^{2+}	8.41	7.44	9.94	9.47	12.29	7.03	8.58	9.39
	Si	63.53	58.78	42.76	49.48	51.26	47.09	62.92	
	K^+	14.24	11.63	22.19	17.29	18.66	21.12	17.76	11.15
	Ca^{2+}	113.97	124.40	118.96	137.00	166.55	116.74	117.86	100.93
	Rb^+	0.019	0.017	0.017	0.021	0.022	0.021	0.022	
	Sr^{2+}	0.091	0.093	0.079	0.126	0.187	0.083	0.101	
Anions	HCO_3^-	142.57	162.77	179.22	153.54	172.31	126.23	117.68	115.86
(µmol/l)	Cl^-	1.23	0.00	31.51	0.00	0.00	22.39	9.63	22.89
	NO_3^-	0.00	2.63	0.34	1.07	0.19	0.60	0.00	0.00
	SO_4^{2-}	52.27	53.20	63.16	67.16	86.95	48.34	58.49	49.50
Charge balance (%)		107.2	102.8	93.9	110.6	109.4	113.6	114.0	104.4
(corrected for atmos.)		121.3	113.6	99.7	124.0	119.8	131.1	131.4	117.7
$^{87}Sr/^{86}Sr$		0.746624 ± 11	0.746024 ± 13	0.745121 ± 26	0.747503 ± 16	0.743317 ± 9	0.755584 ± 13	0.749287 ± 13	
% Geology	TSS	3.81	4.05	7.06	7.61	5.52	10.50	6.08	0.06
	HHCS	79.25	77.98	67.77	64.63	50.50	77.60	26.43	89.46
	Leucogranite	16.93	17.98	25.17	27.76	43.98	11.90	67.49	10.47

Table A5. Water samples collected from the Khumbu region (Dudh Kosi system).

	Locality	**Ev9**	**Ev10**
	River	Bhote Kosi	Imju Drangka
	Date of collection	Oct-99	Oct-99
GPS	**N**	27° 47.474'	27° 47.486'
	E	86° 43.235'	86° 43.287'
	Temperature (°C)	8.5	8.1
	pH	7.78	7.91
Cations	**Na^+**	55.91	47.97
(µmol/l)	**Mg^{2+}**	9.49	4.44
	Si	80.64	86.41
	K^+	14.00	18.45
	Ca^{2+}	101.29	79.84
	Rb^+	0.019	0.037
	Sr^{2+}	0.073	0.112
Anions	**HCO_3^-**	117.91	134.17
(µmol/l)	**Cl^-**	9.62	1.32
	NO_3^-	1.51	1.57
	SO_4^{2-}	45.91	58.65
	Charge balance (%)	112.9	87.5
	(corrected for atmos.)	132.0	92.4
	$^{87}Sr/^{86}Sr$	0.751119 ± 12	0.743694 ± 12
% Geology	**TSS**	0.05	6.70
	HHCS	90.71	69.44
	Leucogranite	9.23	23.86

Table A6. Water samples collected from large Himalayan rivers.

	Locality	SK1	SK2	SK3	AN1	TN1
	River	Sapt Kosi	Sapt Kosi	Sun Kosi	Arun	Tamur
Date of collection		Nov-99	Nov-99	Nov-99	Nov-99	Nov-99
GPS	N	26° 52.947'	26° 51.788'	26° 55.069'	26° 55.101'	26° 54.695'
	E	87° 10.025'	87° 09.144'	87° 09.265'	87° 09.322'	87° 09.744'
Temperature (°C)		16.9	16.9	17.6	15.2	16.8
	pH	7.87	7.85	7.93	7.75	7.74
Cations	Na^+	130.32	132.99	117.36	168.42	119.80
(µmol/l)	Mg^{2+}	108.99	102.71	131.69	81.81	74.48
	Si	179.81	165.24	178.10	150.29	171.33
	K^+	35.73	35.51	42.10	33.99	28.45
	Ca^{2+}	298.02	308.96	345.61	336.44	212.38
	Rb^+	0.038	0.039	0.049	0.033	0.025
	Sr^{2+}	0.427	0.444	0.372	0.671	0.233
Anions	HCO_3^-	760.73	807.58	902.68	807.58	501.59
(µmol/l)	Cl^-	8.87	12.56	9.34	20.86	10.25
	NO_3^-	1.17	5.33	1.77	5.58	4.65
	SO_4^{2-}		103.70	86.47	127.11	94.53
Charge balance (%)		N/A	94.1	100.0	93.7	98.7
(corrected for atmos.)		N/A	96.0	102.5	95.5	102.3
	$^{87}Sr/^{86}Sr$	0.756521 ± 5	0.753414 ± 13	0.777701 ± 9	0.728828 ± 6	0.793565 ± 12
% Geology	TSS	33.49	33.49	3.10	57.33*	0.00
	HHCS	48.29	48.29	62.27	36.53	67.89
LHF	LHC	1.44	1.44	4.22	0.01	0.72
	LHSM	10.70	10.70	20.72	3.24	19.82
	LHSC	6.04	6.04	9.69	2.89	11.54
	Siwaliks	0.02	0.02	0.00	0.00	0.00

* TSS exposure in the Arun River incorporates considerable Quaternary sediment (17.25% of total catchment) and a small amount of Cenozoic leucogranite (1.49% of total catcment area).

Table A7. Hot spring samples collected from then Bhote Kosi and Langtang Khola / Trisuli catchments.
NB. H4 is a cold spring.

		Locality	H2	H5	H1	H3	H4
		River	Bhote Kosi (Tatopani)	Bhote Kosi (Tatopani)	Trisuli (Syabrubensi)	Trisuli (Syabrubensi)	Langtang Khola (Langshisha Karka)
		Date of collection	Dec-98	Oct-99	Oct-98	Sep-99	Sep-99
	GPS	N	27° 57.073'	27° 57.073'	28° 09.785'	28° 09.785'	28° 09.754'
		E	85° 56.721'	85° 56.721'	85° 20.289'	85° 20.289'	85° 20.327'
		Temperature (°C)		42.4		31.6	8.7
		pH	6.73	7.10	6.38	8.55	7.24
	Cations	Na^+	6238.02	4725.10	637.56	695.68	270.55
	(µmol/l)	Mg^{2+}	711.19	744.76	2187.69	2336.64	71.29
		Si	699.37	695.74	694.28	644.90	226.66
		K^+	718.17	621.39	533.22	541.83	28.38
		Ca^{2+}	1309.81	1141.39	2206.23	1150.30	337.71
		Rb^+	2.376	1.929	0.231	0.214	0.011
		Sr^{2+}	3.192	3.477	1.375	1.537	0.420
	Anions	HCO_3^-					
	(µmol/l)	Cl^-	1026.46	992.31	287.44	327.35	36.18
		NO_3^-	0.22	2.98	0.00	31.62	16.38
		SO_4^{2-}	1160.88	973.87	1764.88	1812.91	85.24
		$^{87}Sr/^{86}Sr$	0.792735 ± 9	0.792640 ± 6	0.870312 ± 9	0.863443 ± 8	0.741690 ± 14

Appendix B

Bedload Chemical Data

List of tables.

Table B1. Chemistry of bedload samples collected from the Bhote Kosi.

	Mainstream					
Sample Label	**BKT4**	**BK78**	**BK42**	**BK44**	**BK44(A)**	**BK44(B)**
(Fraction)					0.5-2.0mm	0.25-0.5mm
Year of collection	1998	1999	1998	1998	1998	1998
GPS N	28° 18.250'	27° 56.886'	27° 55.575'	27° 53.091'	27° 53.091'	27° 53.091'
E	86° 02.020'	85° 57.124'	85° 56.047'	85° 54.745'	85° 54.745'	85° 54.745'
Distance Downstream (km)	34.33	78.33	81.00	85.33	85.33	85.33
wt. %						
SiO_2	65.87	75.03	74.17		70.33	69.27
TiO_2	0.271	0.467	0.425		0.513	0.591
Al_2O_3	10.69	11.51	11.72		11.78	14.28
Fe_2O_3	2.12	3.92	6.21		3.97	4.73
MnO	0.037	0.131	0.238		0.073	0.079
MgO	0.73	0.97	1.29		2.81	2.39
CaO	8.83	2.02	1.68		2.60	1.45
Na_2O	1.89	1.94	1.57		1.66	1.36
K_2O	3.35	2.62	2.28		3.08	3.79
P_2O_5	0.096	0.222	0.124		0.158	0.079
LOI	6.92	1.26	1.05		3.42	2.56
ppm						
Rb	171.6	143.0	123.9	167.9	167.9	205.4
Sr	214.1	109.0	81.6	88.8	88.8	66.8
Y	16.4	72.3	57.3	32.6	32.6	24.8
Zr	121	532	204	244	244	167
Nb	6.7	11.6	10.7	12.1	12.1	15.0
Ba	391	410	365	505	505	636
Pb	36	26	21	23	23	26
Th	12	47	15	18	18	11
U	3	9	7	4	4	3
Sc	5	8	11	8	8	11
V	28	45	44	54	54	78
Cr	45	35	47	43	43	57
Co	6	5	9	8	8	10
Ni	11	15	14	15	15	21
Cu	6	10	10	15	15	23
Zn	55	45	46	58	58	68
Ga	13	13	12	16	16	19
Mo	0	0	0	0	0	0
As	9	8	22	8	8	6
S	80	173	225	260	260	318
$^{87}Sr/^{86}Sr$	0.725359 ±13		0.767369 ±14			
$^{143}Nd/^{144}Nd$	0.511682 ±6		0.511726 ±5			
ε_{Nd}	-18.6456		-17.7873			

Table B1 (continued).

Sample Label	BK44(C)	BK44(D)	BK57	BK40	BK85	BK86
(Fraction)	0.063-0.25mm	<0.063mm				
Year of collection	1998	1998	1999	1998	1999	1999
GPS N	27° 53.091'	27° 53.091'	See note 1	27° 52.971'	27° 52.494'	27° 51.856'
E	85° 54.745'	85° 54.745'		85° 54.179'	85° 52.949'	85° 52.645'
Distance Downstream (km)	85.33	85.33	86.00	86.50	88.00	89.67
wt. %						
SiO_2	71.65	68.72	75.62	77.52	70.35	71.44
TiO_2	0.471	0.529	0.305	0.310	0.416	0.364
Al_2O_3	10.79	11.90	9.53	9.47	10.26	8.92
Fe_2O_3	3.83	3.59	2.81	2.67	4.44	3.14
MnO	0.073	0.072	0.036	0.059	0.111	0.072
MgO	2.78	2.79	2.32	1.89	2.90	3.09
CaO	2.67	3.42	2.04	2.15	3.55	4.09
Na_2O	1.67	1.94	0.87	1.59	1.55	1.51
K_2O	2.79	2.98	3.33	2.52	2.42	2.08
P_2O_5	0.154	0.263	0.146	0.112	0.143	0.133
LOI	3.32	4.11	3.48	2.67	4.50	5.43
ppm						
Rb	153.8	143.6	215.0	133.0	124.0	105.0
Sr	88.5	108.4	32.0	75.2	74.0	68.0
Y	21.5	64.4	24.1	21.4	35.6	25.0
Zr	141	615	155	145	204	179
Nb	10.6	13.2	10.0	7.8	9.7	8.4
Ba	472	531	232	400	460	377
Pb	21	29	15	22	21	18
Th	11	43	17	13	16	15
U	4	10	5	4	4	4
Sc	8	8	4	4	9	7
V	53	44	25	38	50	43
Cr	48	38	35	35	39	33
Co	8	7	3	5	5	4
Ni	15	17	9	11	17	14
Cu	14	39	9	8	15	16
Zn	54	59	42	34	41	32
Ga	13	13	11	11	11	10
Mo	0	1	0	1	0	0
As	6	13	8	4	14	8
S	246	273	145	160	374	264
$^{87}Sr/^{86}Sr$				0.804260 ±8		
$^{143}Nd/^{144}Nd$				0.511652 ±8		
ε_{Nd}				-19.2308		

Note 1. Chaku Khola upstream of confluence with Bhote Kosi.

Table B1 (continued).

Sample Label (Fraction)	BK34	BK31	BK55	BK128	BK33	BK33(A) 0.5-2.0mm
Year of collection	1998	1998	1999	1999	1998	1998
GPS N	27° 50.712'	27° 48.366'	27° 49.709'	27° 46.948'	27° 46.212'	27° 46.212'
E	85° 52.825'	85° 53.383'	85° 34.668'	85° 56.685'	85° 53.039'	85° 53.039'
Distance Downstream (km)	91.17	97.83	100.67	100.67	102.67	102.67
wt. %						
SiO_2	75.23	71.64	68.77	77.62		75.23
TiO_2	0.309	0.361	0.424	0.231		0.274
Al_2O_3	8.94	9.97	8.95	9.62		7.42
Fe_2O_3	3.96	4.94	6.85	2.31		2.48
MnO	0.121	0.160	0.238	0.047		0.065
MgO	2.12	2.47	3.04	1.96		2.58
CaO	2.76	3.10	4.24	1.58		3.67
Na_2O	1.38	1.34	1.15	1.68		1.36
K_2O	2.20	2.40	2.00	2.94		1.92
P_2O_5	0.124	0.122	0.135	0.121		0.123
LOI	3.37	3.76	4.97	2.72		4.80
ppm						
Rb	114.5	130.0	107.0	161.0	99.0	99.0
Sr	64.1	71.0	64.0	40.0	63.3	63.3
Y	33.7	40.3	60.9	20.2	22.1	22.1
Zr	136	164	216	137	163	163
Nb	8.6	8.9	8.9	7.6	6.3	6.3
Ba	358	410	454	271	298	298
Pb	20	19	23	19	18	18
Th	11	14	18	13	9	9
U	2	5	7	5	4	4
Sc	6	8	10	3	5	5
V	35	45	49	33	29	29
Cr	40	48	123	46	30	30
Co	5	9	6	4	5	5
Ni	9	13	14	11	8	8
Cu	11	11	19	7	8	8
Zn	36	41	42	26	29	29
Ga	10	11	9	10	8	8
Mo	1	0	0	0	0	0
As	9	6	26	4	5	5
S	256	289	583	92	175	175
$^{87}Sr/^{86}Sr$	0.828492 ±13	0.813039 ±9			0.831914 ±33	
$^{143}Nd/^{144}Nd$	0.511557 ±6	0.511577 ±5			0.511607 ±5	
ε_{Nd}	-21.0840	-20.6939			-20.1087	

Table B1 (continued).

Sample Label	BK33(B)	BK33(C)	BK33(D)	BK29	BK28	BK35
(Fraction)	0.25-0.5mm	0.063-0.25mm	<0.063mm			
Year of collection	1998	1998	1998	1998	1998	1998
GPS N	27° 46.212'	27° 46.212'	27° 46.212'	27° 44.022'	27° 43.428'	27° 38.452'
E	85° 53.039'	85° 53.039'	85° 53.039'	85° 46.836'	85° 46.703'	85° 42.536'
Distance Downstream (km)	102.67	102.67	102.67	113.33	115.17	125.33
wt. %						
SiO_2	76.37	79.77	73.01	71.21	73.96	75.95
TiO_2	0.312	0.244	0.339	0.377	0.469	0.420
Al_2O_3	10.17	8.47	6.68	9.25	12.70	10.47
Fe_2O_3	3.32	2.23	2.62	3.14	3.35	3.33
MnO	0.092	0.041	0.071	0.053	0.056	0.056
MgO	1.60	1.53	3.29	3.35	1.10	1.86
CaO	1.55	1.74	5.00	3.66	1.40	2.45
Na_2O	1.32	1.43	1.37	1.25	2.11	1.87
K_2O	2.79	2.30	1.66	2.63	3.30	2.19
P_2O_5	0.074	0.068	0.184	0.126	0.118	0.131
LOI	2.25	2.30	6.36	5.33	0.92	2.20
ppm						
Rb	145.5	119.6	84.9	140.7	157.7	108.6
Sr	56.3	61.8	66.6	56.6	122.9	115.3
Y	28.1	14.6	42.9	22.0	25.7	22.6
Zr	116	94	484	197	176	129
Nb	8.9	6.4	8.5	9.5	11.7	8.9
Ba	394	313	292	436	501	364
Pb	28	19	19	14	24	17
Th	9	8	28	15	13	11
U	3	2	8	4	2	3
Sc	7	4	2	7	9	6
V	44	28	24	47	47	45
Cr	32	32	38	36	41	40
Co	6	4	6	7	8	7
Ni	12	8	9	13	15	14
Cu	13	10	14	10	9	11
Zn	43	33	30	44	42	38
Ga	13	10	7	11	15	12
Mo	0	0	1	0	0	0
As	5	2	6	5	0	1
S	156	155	202	164	83	144
$^{87}Sr/^{86}Sr$				0.757452 ±7		0.765239 ±9
$^{143}Nd/^{144}Nd$					0.511757 ±7	0.511626 ±6
ε_{Nd}					-17.1826	-19.7380

Table B1 (continued).

Sample Label (Fraction)	BK74	BK38	BK39	BK39(A)	BK39(B)	BK39(C)
Year of collection	1999	1998	1998	1998	1998	1998
				0.5-2.0mm	0.25-0.5mm	<0.25mm
GPS N	See note 2	27° 37.787'	27° 36.294'	27° 36.294'	27° 36.294'	27° 36.294'
E		85° 42.741'	85° 43.395'	85° 43.395'	85° 43.395'	85° 43.395'
Distance Downstream (km)	125.33	126.50	130.50	130.50	130.50	130.50
wt. %						
SiO_2	74.84	78.89		80.86	77.25	81.75
TiO_2	0.467	0.518		0.320	0.473	0.268
Al_2O_3	8.71	9.41		9.51	11.29	8.74
Fe_2O_3	3.47	4.56		2.19	3.10	1.89
MnO	0.051	0.149		0.026	0.032	0.026
MgO	2.21	1.09		1.09	1.41	1.00
CaO	3.13	1.52		1.37	1.05	1.62
Na_2O	1.48	1.30		1.91	1.71	1.96
K_2O	2.05	1.91		2.33	3.09	1.94
P_2O_5	0.189	0.160		0.048	0.047	0.060
LOI	3.32	1.24		1.24	1.44	1.42
ppm						
Rb	98.0	88.2	111.8	111.8	155.1	91.9
Sr	83.0	99.0	109.2	109.2	99.8	116.1
Y	41.5	56.9	11.3	11.3	13.0	16.5
Zr	292	336	125	125	145	160
Nb	10.2	11.6	7.6	7.6	11.4	6.7
Ba	320	385	401	401	511	342
Pb	17	16	19	19	20	20
Th	20	24	7	7	8	10
U	5	5	2	2	3	3
Sc	8	8	4	4	5	2
V	44	36	31	31	51	21
Cr	42	47	36	36	42	29
Co	5	7	7	7	9	6
Ni	19	12	12	12	16	9
Cu	16	9	6	6	10	9
Zn	33	30	30	30	44	26
Ga	10	11	11	11	14	8
Mo	0	0	0	0	1	0
As	6	3	3	3	2	2
S	897	107	60	60	55	56
$^{87}Sr/^{86}Sr$			0.768184 ±7			
$^{143}Nd/^{144}Nd$			0.511646 ±5			
ε_{Nd}			-19.3479			

Note 2. Bhote Kosi above confluence with Indrawati / Chak Khola.

Table B1 (continued).

	Tributaries					
Sample Label (Fraction)	**BK126**	**BK82**	**BK83**	**BK41**	**BK90**	**BK61**
Year of collection	1999	1999	1999	1998	1999	1999
GPS N	27° 55.961'	27° 55.266'	27° 54.400'	27° 53.012'	27° 51.286'	See note 3
E	85° 56.180'	85° 56.005'	85° 55.062'	85° 54.849'	85° 52.435'	
Distance Downstream (km)	80.00	81.67	83.67	86.00	90.50	94.83
wt. %						
SiO_2	75.48	65.72		79.58	68.09	77.12
TiO_2	0.412	0.385		0.218	0.238	0.478
Al_2O_3	10.78	8.81		9.12	4.94	10.07
Fe_2O_3	3.39	4.03		2.06	2.18	4.47
MnO	0.060	0.052		0.027	0.076	0.058
MgO	1.83	5.38		1.56	6.71	1.65
CaO	2.59	4.71		1.35	6.39	0.90
Na_2O	1.74	0.59		1.19	0.17	0.79
K_2O	2.08	2.53		3.48	1.64	3.02
P_2O_5	0.138	0.114		0.110	0.076	0.100
LOI	2.04	8.16		2.30	10.49	1.72
ppm						
Rb	102.0	124.0	22.0	199.8	54.0	122.0
Sr	71.0	49.0	74.0	30.4	22.0	31.0
Y	24.8	19.4	26.1	17.5	11.1	22.3
Zr	157	126	71	93	141	155
Nb	10.1	8.8	7.5	8.8	4.3	8.7
Ba	356	472	435	271	342	475
Pb	15	14	10	20	8	14
Th	11	12	10	14	9	15
U	2	4	2	5	2	3
Sc	9	10	9	4	6	9
V	48	79	24	18	29	66
Cr	34	46	42	30	30	56
Co	5	5	5	5	5	8
Ni	16	21	9	7	11	22
Cu	13	12	17	9	6	22
Zn	40	53	29	37	19	34
Ga	12	10	2	10	6	11
Mo	0	1	0	0	0	0
As	7	7	26	2	5	6
S	187	549	586	99	45	36
$^{87}Sr/^{86}Sr$				1.390854 ±9		
$^{143}Nd/^{144}Nd$				0.511419 ±5		
ε_{Nd}				-23.7760		

Note 3. Binegodhan Khola.

Table B1 (continued).

Sample Label	BK32	BK30	BK30(A)	BK30(B)	BK30(C)	BK30(D)
(Fraction)			1.0-2.0mm	0.5-1.0mm	0.25-0.5mm	0.063-0.25mm
Year of collection	1998	1998	1998	1998	1998	1998
GPS N	27° 46.711'	27° 44.079'	27° 44.079'	27° 44.079'	27° 44.079'	27° 44.079'
E	85° 53.726'	85° 46.763'	85° 46.763'	85° 46.763'	85° 46.763'	85° 46.763'
Distance Downstream (km)	100.67	114.17	114.17	114.17	114.17	114.17
wt. %						
SiO_2	76.52	67.14	67.14	56.73	61.45	64.36
TiO_2	0.266	0.646	0.646	0.620	0.521	0.630
Al_2O_3	9.26	13.03	13.03	17.39	15.56	13.52
Fe_2O_3	3.09	10.63	10.63	15.38	14.38	13.84
MnO	0.080	0.343	0.343	0.681	0.536	0.465
MgO	2.15	1.88	1.88	2.41	2.21	1.93
CaO	1.63	2.17	2.17	2.49	1.93	2.05
Na_2O	1.36	1.42	1.42	0.82	1.06	1.26
K_2O	2.59	1.86	1.86	2.54	2.03	1.50
P_2O_5	0.125	0.161	0.161	0.110	0.084	0.115
LOI	2.85	0.83	0.83	0.25	0.26	0.35
ppm						
Rb	148.7	95.1	95.1	119.3	102.1	79.3
Sr	38.8	95.4	95.4	58.2	68.8	82.1
Y	26.3	113.8	113.8	182.8	175.1	141.7
Zr	88	252	252	212	214	209
Nb	7.3	15.8	15.8	15.3	14.7	15.8
Ba	283	338	338	459	351	278
Pb	18	20	20	19	17	16
Th	15	22	22	19	17	18
U	4	6	6	6	5	7
Sc	5	24	24	41	40	33
V	39	64	64	81	68	62
Cr	33	70	70	95	75	82
Co	6	15	15	18	19	13
Ni	10	18	18	20	18	17
Cu	8	19	19	31	26	29
Zn	37	51	51	63	62	57
Ga	11	14	14	18	15	13
Mo	0	0	0	0	0	0
As	2	6	6	0	4	7
S	94	466	466	565	540	486
$^{87}Sr/^{86}Sr$	1.112521 ±9	0.762327 ±10	0.786348 ±8	0.766390 ±9	0.761682 ±9	0.760671 ±9
$^{143}Nd/^{144}Nd$	0.511348 ±7	0.511689 ±5				0.511704 ±6
ε_{Nd}	-25.1609	-18.5121				-18.2165

Table B1 (continued).

Sample Label (Fraction)	BK30(E) <0.063mm	BK36	BK37	BK65	BK66	BK66RPT
Year of collection	1998	1998	1998	1999	1999	1999
GPS N	27° 44.079'	27° 38.425'	27° 38.761'	See note 4	See note 5	See note 5
E	85° 46.763'	85° 42.403'	85° 42.092'			
Distance Downstream (km)	114.17	125.50	125.50	125.50	125.50	125.50
wt. %						
SiO_2	71.34	76.62	79.34	77.98	72.83	72.82
TiO_2	0.722	0.583	0.386	0.547	0.700	0.687
Al_2O_3	11.32	11.54	9.28	10.20	12.43	12.27
Fe_2O_3	6.16	3.75	2.86	3.63	4.59	4.56
MnO	0.138	0.054	0.031	0.052	0.062	0.063
MgO	1.67	1.14	1.30	1.24	1.82	1.81
CaO	2.62	1.03	1.22	1.26	1.21	1.22
Na_2O	1.87	1.57	0.95	1.22	1.55	1.53
K_2O	2.06	2.94		2.76	3.10	3.03
P_2O_5	0.262	0.113	0.064	0.083	0.170	0.164
LOI	1.48	1.68	2.82	1.99	2.29	2.29
ppm						
Rb	104.2	136.4	139.1	142.0	160.0	160.0
Sr	126.3	123.3	52.0	74.0	101.0	101.0
Y	90.1	34.7	20.7	28.3	57.2	57.2
Zr	522	388	159	234	806	806
Nb	16.1	12.7	9.4	12.0	13.9	13.9
Ba	362	601	454	517	580	580
Pb	26	19	19	19	19	19
Th	51	23	10	18	43	43
U	15	5	3	2	7	7
Sc	13	8	6	9	10	10
V	54	58	40	50	80	80
Cr	62	48	40	46	68	68
Co	14	8	8	7	9	9
Ni	21	18	14	19	26	26
Cu	34	12	10	11	15	15
Zn	52	47	40	40	50	50
Ga	13	13	10	13	15	15
Mo	1	1	0	0	0	0
As	16	3	5	5	5	5
S	447	55	128	185	123	123
$^{87}Sr/^{86}Sr$		0.746311 ±14	0.787314 ±12			
$^{143}Nd/^{144}Nd$		0.511656 ±5	0.511628 ±5			
ε_{Nd}		-19.1528	-19.6990			

Note 4. Chak Khola upstream of confluence with Indrawati.
Note 5. Indrawati opposite the confluence with the Chak Khola.

Table B1 (continued).

Sample Label (Fraction)	**BK47**
Year of collection	1999
GPS N	27° 38.543'
E	85° 37.033'
Distance Downstream (km)	Jhiku Khola
wt. %	
SiO_2	75.64
TiO_2	0.694
Al_2O_3	11.41
Fe_2O_3	3.99
MnO	0.062
MgO	1.33
CaO	0.95
Na_2O	1.37
K_2O	3.37
P_2O_5	0.092
LOI	1.93
ppm	
Rb	163.0
Sr	83.0
Y	33.7
Zr	421
Nb	15.6
Ba	739
Pb	21
Th	21
U	3
Sc	8
V	62
Cr	88
Co	7
Ni	23
Cu	10
Zn	44
Ga	15
Mo	0
As	1
S	30
$^{87}Sr/^{86}Sr$	
$^{143}Nd/^{144}Nd$	
ε_{Nd}	

Table B2. Chemistry of bedload samples collected from the Langtang Khola - Trisuli.

	Mainstream					
Sample Label (Fraction)	**L14**	**L31**	**L12**	**L16**	**L28**	**L21**
Year of collection	1998	1999	1998	1998	1999	1998
GPS N	28° 14.312'	28° 12.040'	28° 12.570'	28° 12.142'	28° 09.828'	27° 55.660'
E	85° 41.888'	85° 38.305'	85° 33.549'	85° 38.780'	85° 20.014'	85° 08.946'
Distance Downstream (km)	Source	7.25	16.00	18.00	40.50	76.50
wt. %						
SiO_2	78.66	74.33	73.79	73.87	67.99	78.22
TiO_2	0.179	0.425	0.319	0.355	0.652	0.406
Al_2O_3	11.76	12.58	13.31	13.22	16.85	10.08
Fe_2O_3	1.22	2.57	2.01	2.18	4.07	3.02
MnO	0.020	0.035	0.031	0.033	0.056	0.051
MgO	0.41	0.68	0.69	0.77	1.18	1.10
CaO	1.20	2.50	2.08	1.98	1.00	1.44
Na_2O	2.63	2.90	3.00	2.90	2.12	1.52
K_2O	3.21	3.11	3.53	3.58	3.99	2.32
P_2O_5	0.102	0.262	0.145	0.155	0.117	0.152
LOI	1.03	0.56	0.67	0.63	2.08	1.45
ppm						
Rb	147.3	146.0	170.3	179.5	182.0	117.4
Sr	152.7	200.0	194.7	185.9	143.0	93.0
Y	12.4	81.9	24.8	28.4	42.6	30.4
Zr	151	904	195	240	490	357
Nb	4.6	11.9	7.9	9.8	16.5	9.4
Ba	374	464	472	450	1020	377
Pb	31	30	35	36	22	18
Th	8	61	13	17	28	20
U	5	18	5	6	5	5
Sc	2	6	3	6	13	4
V	16	31	22	22	82	37
Cr	31	45	27	26	63	50
Co	3	5	5	5	7	8
Ni	5	14	8	9	18	12
Cu	4	20	7	7	9	9
Zn	23	26	31	35	65	37
Ga	13	13	15	15	21	12
Mo	0	1	0	1	0	0
As	3	16	7	9	1	3
S	29	286	88	94	60	64
$^{87}Sr/^{86}Sr$						
$^{143}Nd/^{144}Nd$						
ε_{Nd}						

Table B2 (continued).

Sample Label (Fraction)	**L21-RPT**
Year of collection	1998
GPS N	27° 55.660'
E	85° 08.946'
Distance Downstream (km)	76.50
wt. %	
SiO_2	79.17
TiO_2	0.415
Al_2O_3	10.05
Fe_2O_3	3.04
MnO	0.047
MgO	1.11
CaO	1.44
Na_2O	1.52
K_2O	2.34
P_2O_5	0.150
LOI	1.46
ppm	
Rb	117.0
Sr	93.0
Y	31.0
Zr	358
Nb	9.5
Ba	403
Pb	20
Th	18
U	6
Sc	8
V	37
Cr	45
Co	5
Ni	14
Cu	9
Zn	35
Ga	12
Mo	0
As	6
S	55
$^{87}Sr/^{86}Sr$	
$^{143}Nd/^{144}Nd$	
ε_{Nd}	

Table B2 (continued).

	Tributaries					
Sample Label	**L5**	**L5(A)**	**L5(B)**	**L5(C)**	**L5(D)**	**L5(E)**
(Fraction)		1.0-2.0mm	0.5-1.0mm	0.25-0.5mm	0.063-0.25mm	<0.063mm
Year of collection	1998	1998	1998	1998	1998	1998
GPS N	28° 09.952'	28° 09.952'	28° 09.952'	28° 09.952'	28° 09.952'	28° 09.952'
E	85° 20.573'	85° 20.573'	85° 20.573'	85° 20.573'	85° 20.573'	85° 20.573'
Distance Downstream (km)	41.50	41.50	41.50	41.50	41.50	41.50
wt. %						
SiO_2	71.78	71.65	69.38	71.53	73.37	68.72
TiO_2	0.396	0.392	0.297	0.272	0.303	0.781
Al_2O_3	11.09	11.27	11.66	11.27	10.71	10.78
Fe_2O_3	3.67	3.59	2.34	2.75	3.37	6.70
MnO	0.103	0.102	0.046	0.062	0.096	0.248
MgO	0.97	0.95	0.91	0.86	0.89	1.27
CaO	4.59	4.61	5.70	4.68	3.90	4.91
Na_2O	2.09	2.16	2.20	2.10	2.20	1.98
K_2O	2.64	2.67	3.16	2.83	2.44	1.92
P_2O_5	0.149	0.146	0.089	0.077	0.106	0.347
LOI	2.83	2.74	4.29	3.25	2.72	1.97
ppm						
Rb	126.0	121.7	139.5	130.6	114.8	95.6
Sr	164.0	157.6	185.8	162.8	147.8	153.3
Y	63.2	65.3	20.0	25.6	33.5	194.3
Zr	361	359	117	107	113	901
Nb	9.9	10.4	7.7	7.2	7.4	24.4
Ba	398	384	457	408	358	330
Pb	27	26	28	24	25	28
Th	41	36	10	9	12	145
U	10	10	4	2	2	42
Sc	8	7	6	8	7	18
V	34	36	33	34	30	57
Cr	30	38	28	40	44	56
Co	5	7	4	6	7	15
Ni	11	11	10	7	10	19
Cu	11	8	10	12	12	28
Zn	36	35	35	34	34	56
Ga	12	13	13	12	12	12
Mo	0	0	0	0	0	0
As	9	10	4	4	5	65
S	162	169	112	114	122	489
$^{87}Sr/^{86}Sr$						
$^{143}Nd/^{144}Nd$						
ε_{Nd}						

Table B2 (continued).

Sample Label (Fraction)	**L10**
Year of collection	1998
GPS N	28° 12.980'
E	85° 30.009'
Distance Downstream (km)	21.00
wt. %	
SiO_2	70.96
TiO_2	0.544
Al_2O_3	13.32
Fe_2O_3	4.34
MnO	0.106
MgO	1.41
CaO	1.89
Na_2O	2.60
K_2O	3.61
P_2O_5	0.205
LOI	0.58
ppm	
Rb	199.7
Sr	96.4
Y	42.8
Zr	317
Nb	14.2
Ba	487
Pb	20
Th	27
U	10
Sc	11
V	51
Cr	59
Co	11
Ni	18
Cu	11
Zn	34
Ga	17
Mo	1
As	0
S	93
$^{87}Sr/^{86}Sr$	
$^{143}Nd/^{144}Nd$	
εNd	

Appendix C

Bedrock Chemical Data

List of tables.

List of abbreviations used in table C1 – table C4:

Rock type:	**S:** Silicate.	**C-S:** Calc-silicate.	**C:** Carbonate.
	Sst: Sandstone.	Phy: Phyllite.	Sch: Schist.
	Lst: Limestone.	Dol: Dolomite.	Sil: Silicate.
	Mbl: Marble.	Gla: Glacial.	Gn: Gneiss.
	SiSt: Siltstone.	Mst: Mudstone.	Sh: Shale.
	Calc: Calcareous.	sill: Sillimanite.	dol: Dolomitic.
	bt: Biotite.	mic: Micaceous	gra: Graphytic.
	gt: Garnet.	imp: Impure.	Qz: Quartz.

Minerals present:	C: Calcite.	Q: Quartz.	M: Muscovite.
	B: Biotite.	Py: Pyroxene.	Pl: Plagioclase.
	Gt: Garnet.	Sill: Sillimanite.	St: Staurolite.
	Gr: Graphite.	D: Dolomite.	Ch: Chlorite.

Units of the Lesser Himalayan Formation:

rb: Robang Formation.	ml: Malekhu Limestone.
bg: Benighat Slates.	jk: Jhiku Beds.
dh: Dhading Dolomite.	np: Nourpul Formation.
da: Dandagaon Phyllites.	kn: Kuncha Group.

Units of the Kahtmandu Nappe:

cp: Chisapani Quartzite.

bd: Bhainsedobhan Marble.

ra: Raduwar Formation.

Table C1. Chemical composition of rocks of the Tibetan Sedimentary Series from the Bhote kosi.

Sample Label	T17	T18	T24e	T19
Unit	TSS	TSS	TSS	TSS
Lithology	Lst	Lst	Calc-SiSt	Mst
Major Minerals	C	C	Q,C	
C / C-S / S	C	C	C-S	S
GPS N	28° 30.080'	28° 28.570'	28° 22.310'	28° 28.270'
E	86° 06.590'	86° 09.470'	86° 05.450'	86° 89.410'
wt. %				
SiO_2	2.02	1.92	30.39	73.66
TiO_2	0.030	0.018	0.190	2.576
Al_2O_3	0.40	0.06	4.34	11.70
Fe_2O_3	0.22	0.18	0.67	6.48
MnO	0.008	0.006	0.039	0.029
MgO	0.52	0.32	0.27	2.48
CaO	54.42	54.74	34.42	2.58
Na_2O	0.00	0.00	0.01	1.76
K_2O	0.08	0.02	1.00	2.58
P_2O_5	0.014	0.010	0.022	0.204
LOI	43.44	43.68	28.43	3.83
ppm				
Rb	3.9	0.3	43.5	70.3
Sr	233.1	265.3	94.2	242.7
Y	5.4	3.7	15.3	30.7
Zr	8	4	90	452
Nb	2.9	2.1	6.6	34.1
Ba	7	0	100	566
Pb	2	4	5	13
Th	4	1	8	11
U	3	0	3	4
Sc	21	23	13	7
V	14	4	19	141
Cr	8	4	15	193
Co	3	2	5	18
Ni	3	3	5	37
Cu	2	4	2	8
Zn	5	3	5	79
Ga	2	1	5	16
Mo	0	0	0	0
As	5	5	8	2
S	268	148	70	1021
$^{87}Rb/^{86}Sr$	0.0484		1.3369	
$^{87}Sr/^{86}Sr$	0.708192 ±7		0.714764 ±27	
$^{143}Nd/^{144}Nd$				
ε_{Nd}				

Table C1 (continued).

Sample Label	T23	T15	T16
Unit	TSS	Recent	Recent
Lithology	Sh	Gla	Gla
Major Minerals	Q,M,C		
C / C-S / S	S	S	S
GPS N	28° 24.129'	28° 31.020'	28° 30.250'
E	86° 06.830'	86° 09.280'	86° 08.160'
wt. %			
SiO_2	60.72	65.53	69.31
TiO_2	0.826	0.487	0.351
Al_2O_3	17.45	11.64	10.01
Fe_2O_3	8.00	2.14	11.51
MnO	0.046	0.035	0.342
MgO	2.48	0.72	0.45
CaO	0.65	7.50	0.68
Na_2O	1.96	1.87	1.54
K_2O	3.08	3.25	3.16
P_2O_5	0.149	0.148	0.129
LOI	4.23	6.62	2.88
ppm			
Rb	159.9	194.3	199.3
Sr	94.3	149.1	84.3
Y	35.6	30.0	31.8
Zr	184	298	128
Nb	20.5	12.6	8.8
Ba	782	452	425
Pb	27	34	38
Th	38	14	11
U	4	2	7
Sc	18	9	14
V	131	41	59
Cr	179	791	524
Co	23	9	49
Ni	58	20	77
Cu	38	8	9
Zn	132	64	150
Ga	24	16	14
Mo	1	1	1
As	5	6	7
S	65	72	112
$^{87}Rb/^{86}Sr$	4.9271		6.8577
$^{87}Sr/^{86}Sr$	0.752396 ±19		0.734472 ±10
$^{143}Nd/^{144}Nd$			0.511700 ±4
ε_{Nd}			-18.2945

Table C2. Chemical composition of rocks of the High Himalayan Crystalline Series from the Bhote Kosi.

Sample Label	T29c	T29b	T29d	T29e	T29f
Unit	HHCS	HHCS	HHCS	HHCS	HHCS
Lithology	impure Mbl	Calc-Sil	Calc-Sil	Calc-Sil	Calc-Sil
Major Minerals	C,Q,B,Py,Pl	C,Q,Py,Pl	C,Q,Py	C,Q,B,Py	Q,Py,B,Pl
C / C-S / S	C	C-S	C-S	C-S	C-S
GPS N	28° 11.494'	28° 11.494'	28° 11.494'	28° 11.494'	28° 11.494'
E	85° 59.088'	85° 59.088'	85° 59.088'	85° 59.088'	85° 59.088'
wt. %					
SiO_2	11.64	40.08	36.72	30.13	51.28
TiO_2	0.146	0.528	0.442	0.374	0.040
Al_2O_3	3.44	9.93	11.38	10.05	0.89
Fe_2O_3	1.48	4.07	4.22	3.57	0.67
MnO	0.030	0.072	0.052	0.044	0.011
MgO	2.96	3.57	3.84	3.33	1.17
CaO	45.18	25.99	29.36	30.63	21.98
Na_2O	0.04	0.96	0.46	0.20	0.02
K_2O	0.92	2.71	1.12	2.70	0.26
P_2O_5	0.026	0.080	0.078	0.049	0.008
LOI	34.22	11.57	13.33	18.35	37.19
ppm					
Rb	56.1	140.5	61.4	152.7	37.4
Sr	1076.8	710.9	713.6	817.9	803.5
Y	5.9	21.4	15.3	15.0	4.6
Zr	21	154	77	61	17
Nb	4.5	11.9	10.1	8.8	3.6
Ba	70	380	382	214	38
Pb	12	21	9	13	11
Th	0	13	10	8	1
U	2	5	5	4	0
Sc	17	11	20	16	19
V	25	40	57	47	17
Cr	22	52	57	52	12
Co	7	12	10	10	7
Ni	9	22	25	19	10
Cu	7	6	8	15	4
Zn	44	30	63	63	61
Ga	5	13	16	14	5
Mo	0	0	0	0	0
As	0	0	2	6	6
S	228	53	48	176	56
$^{87}Rb/^{86}Sr$	0.1508	0.5722	0.2491		0.1347
$^{87}Sr/^{86}Sr$	0.710038 ±9	0.715073 ±8	0.713412 ±8		0.710736 ±8
$^{143}Nd/^{144}Nd$	0.511719 ±5	0.511648 ±5	0.511512 ±3		
ε_{Nd}	-17.9269	-19.3089	-21.9596		

Table C2 (continued).

Sample Label	T29g-Carb	BK51b	T24b	T24g	T26b
Unit	HHCS	HHCS	HHCS	HHCS	HHCS
Lithology	Calc-Sil	Calc-Sil	bt Sch	Migmatite	sill-gt Gn
Major Minerals			Q,Pl,B,Ch	Q,M,Pl	
C / C-S / S	C-S	C-S	S	S	S
GPS N	28° 11.494'	27° 54.476'	28° 22.310'	28° 22.310'	28° 20.170'
E	85° 59.088'	85° 38.034'	86° 05.450'	86° 05.450'	86° 03.030'
wt. %					
SiO_2	43.64	55.56	64.55	73.19	60.91
TiO_2	0.534	0.622	0.862	0.138	0.848
Al_2O_3	10.00	11.00	15.88	14.61	17.59
Fe_2O_3	3.82	4.17	5.13	0.81	6.32
MnO	0.072	0.081	0.061	0.009	0.080
MgO	3.32	3.50	2.09	0.35	2.54
CaO	27.12	15.48	2.95	0.69	3.43
Na_2O	0.96	1.83	2.96	1.99	2.61
K_2O	0.16	2.83	3.50	6.78	4.41
P_2O_5	0.096	0.135	0.184	0.226	0.141
LOI	10.71	4.08	0.86	0.84	0.74
ppm					
Rb	7.4	137.9	260.2	425.4	310.9
Sr	569.2	264.7	269.1	96.2	266.7
Y	26.2	29.0	29.1	9.0	24.4
Zr	168	192	304	51	177
Nb	14.9	13.2	17.8	8.0	19.1
Ba	15	539	1166	400	1020
Pb	26	16	35	47	22
Th	16	18	24	4	18
U	8	2	2	3	2
Sc	16	11	13	2	15
V	42	59	91	11	97
Cr	49	75	85	16	105
Co	10	14	14	2	15
Ni	18	25	29	4	35
Cu	4	6	14	2	8
Zn	109	79	83	30	93
Ga	14	16	22	24	23
Mo	0	0	0	0	0
As	6	4	3	8	0
S	52	35	53	26	37
$^{87}Rb/^{86}Sr$	0.0376				
$^{87}Sr/^{86}Sr$	0.713917 ±7				
$^{143}Nd/^{144}Nd$	0.511674 ±10				
ε_{Nd}	-18.8017				

Table C2 (continued).

Sample Label	T27b	T29g-Sil	T31a	T40a	BK1	BK48
Unit	HHCS	HHCS	HHCS	HHCS	HHCS	HHCS
Lithology	sill Gn	Pegmatite	gt-bt Sch	Gn	gt-bt Sch	gt-mic Sch
Major Minerals	Q,B,Pl,Gt,Sill	Q,M,Py,Pl	Q,B,Pl,Gt	Q,B,Pl	Q,B,Gt,St,Pl	
C / C-S / S	S	S	S	S	S	S
GPS N	28° 18.140'	28° 11.494'	28° 09.990'	28° 09.508'	Kodari	27° 49.709'
E	86° 02.010'	85° 59.088'	85° 59.090'	85° 59.577'		85° 34.668'
wt. %						
SiO_2	59.29	72.86	59.64	85.01	62.77	61.40
TiO_2	0.941	0.047	0.861	0.272	0.743	0.886
Al_2O_3	19.32	14.33	18.11	7.62	16.92	15.34
Fe_2O_3	6.91	0.09	7.18	1.85	5.92	8.38
MnO	0.049	0.004	0.065	0.053	0.189	0.194
MgO	2.92	0.05	2.95	0.53	3.24	2.55
CaO	2.37	2.13	3.49	0.59	4.13	2.06
Na_2O	3.19	0.79	3.50	2.20	1.15	2.87
K_2O	3.59	9.00	2.91	1.64	3.21	3.90
P_2O_5	0.121	0.048	0.132	0.048	0.177	0.141
LOI	0.88	0.56	0.55	0.64	1.38	1.00
ppm						
Rb	265.6	465.2	214.9	60.7	147.0	208.9
Sr	197.1	437.8	301.5	93.8	52.2	304.4
Y	27.8	2.2	29.0	12.7	36.4	35.5
Zr	180	8	157	106	174	184
Nb	20.9	4.4	19.7	6.3	18.1	19.3
Ba	320	631	604	376	601	3600
Pb	16	66	10	15	20	125
Th	21	2	19	6	27	26
U	5	2	4	2	6	7
Sc	17	1	14	2	15	16
V	109	3	105	23	237	96
Cr	119	10	117	32	103	105
Co	19	0	21	3	19	18
Ni	48	3	46	7	31	29
Cu	57	5	12	2	34	28
Zn	78	5	23	18	56	178
Ga	28	16	24	8	21	19
Mo	0	0	0	0	4	0
As	1	1	11	4	0	3
S	213	26	43	31	514	124
$^{87}Rb/^{86}Sr$		3.0770			8.2250	
$^{87}Sr/^{86}Sr$		0.717247 ±6			0.805334 ±101	
$^{143}Nd/^{144}Nd$		0.511722 ±15				
ε_{Nd}		-17.8654				

Table C2 (continued).

Sample Label	BK51a	BK110	BK2	BK17	BK111
Unit	HHCS	HHCS	MCT zone	MCT zone	MCT zone
Lithology	mic Sch	Gn	Greywacke	augen Gn	augen Gn
Major Minerals			Q,C?,B,Gr	Q,B,M,Pl	
C / C-S / S	S	S	C-S	S	S
GPS N	27° 54.476'	27° 57.101'	27° 57.149'	27° 56.122'	Tatopani
E	85° 38.034'	85° 57.287'	85° 56.473'	85° 57.866'	
wt. %					
SiO_2	82.66	88.77	71.46	66.62	76.53
TiO_2	0.476	0.212	0.146	0.775	0.278
Al_2O_3	7.91	6.12	2.74	14.30	11.84
Fe_2O_3	2.39	0.82	2.89	5.92	2.30
MnO	0.026	0.011	0.072	0.060	0.025
MgO	1.75	0.14	3.85	1.40	0.34
CaO	0.50	0.24	7.56	1.26	1.10
Na_2O	1.33	1.36	0.27	2.10	2.35
K_2O	1.61	2.36	0.98	6.77	4.91
P_2O_5	0.206	0.036	0.042	0.266	0.114
LOI	0.49	0.36	10.97	0.51	0.45
ppm					
Rb	84.1	72.3	42.6	428.7	291.7
Sr	21.3	58.3	83.1	48.3	41.3
Y	29.3	13.0	15.5	48.9	51.0
Zr	272	138	319	179	137
Nb	10.9	5.3	4.3	26.4	15.9
Ba	131	619	137	615	317
Pb	3	12	39	29	31
Th	13	6	6	31	37
U	2	1	2	8	9
Sc	5	1	1	11	4
V	42	10	15	40	15
Cr	38	32	28	44	21
Co	6	2	4	14	5
Ni	16	2	7	14	2
Cu	1	3	4	4	2
Zn	6	11	40	73	32
Ga	9	6	4	21	17
Mo	0	0	1	0	0
As	2	1	5	0	3
S	20	21	112	71	29
$^{87}Rb/^{86}Sr$			1.5043	26.7034	
$^{87}Sr/^{86}Sr$			0.854190 ±8	1.116142 ±11	
$^{143}Nd/^{144}Nd$			0.511814 ±6		
ε_{Nd}			-16.0707		

Table C3. Chemical composition of rocks of the Lesser Himalayan Formation from the Bhote Kosi.

Sample Label	BK13a	BK16	BK4	BK5	BK6
Unit	LH	LH	LH	LH	LH
Lithology	Lst	Lst	dol-bt Phy	dol-bt Sch	dol Sch
Major Minerals	C	C	Q,D,B,M	D,Q,M	D,Q,B,M
C / C-S / S	C	C	C-S	C-S	C-S
Subdivision	da / np	ml	bg	dh	np
GPS N	27° 52.573'	27° 55.832'	27° 54.843'	27° 53.509'	27° 52.767'
E	85° 53.745'	85° 56.156'	85° 56.007'	85° 54.902'	85° 54.222'
wt. %					
SiO_2	8.20	14.00	59.93	52.50	30.03
TiO_2	0.064	0.112	0.656	0.126	0.191
Al_2O_3	0.70	2.14	13.31	3.30	3.62
Fe_2O_3	0.32	1.82	5.76	1.35	1.91
MnO	0.018	0.034	0.159	0.068	0.044
MgO	1.90	1.22	3.46	11.54	14.20
CaO	49.46	44.26	4.26	12.09	18.81
Na_2O	0.00	0.02	0.34	0.34	0.08
K_2O	0.24	0.82	6.78	0.76	1.73
P_2O_5	0.026	0.030	0.153	0.046	0.046
LOI	41.31	36.75	4.95	18.60	29.24
ppm					
Rb	9.4	36.0	234.7	45.4	72.8
Sr	41.9	34.6	49.2	57.1	37.5
Y	5.7	7.3	28.0	7.1	10.2
Zr	21	43	215	29	50
Nb	2.0	4.1	17.1	3.7	4.3
Ba	414	228	1313	91	276
Pb	0	11	11	10	17
Th	1	4	23	3	7
U	4	2	4	2	3
Sc	19	20	12	6	7
V	11	18	72	12	25
Cr	7	20	83	19	30
Co	3	4	13	5	8
Ni	3	8	21	8	12
Cu	6	6	3	2	2
Zn	8	46	19	27	23
Ga	0	4	18	5	6
Mo	0	0	0	0	0
As	5	9	12	1	2
S	208	147	39	37	42
$^{87}Rb/^{86}Sr$	0.6547	3.0883	14.0916	2.3146	5.6924
$^{87}Sr/^{86}Sr$	0.797428 ±12	0.973459 ±13	0.923174 ±11	0.771214 ±6	0.846107 ±11
$^{143}Nd/^{144}Nd$	0.511450 ±6		0.511253 ±6	0.511442 ±5	
ε_{Nd}	-23.1712		-27.0141	-23.3273	

Table C3 (continued).

Sample Label	BK11	BK12b	BK12d	BK14a	BK14b	BK15
Unit	LH	LH	LH	LH	LH	LH
Lithology	dol-bt Sch	Cinter	dol-bt Sch	dol Sch	dol Sch	dol Sil
Major Minerals	D,Q,B		Q,M,D	D,Q,B,	D,Q,M,B,Gr	D,Q
C / C-S / S	C-S	C-S	C-S	C-S	C-S	C-S
Subdivision	da / np	da / np	da / np	da / np	da / np	dh
GPS N	27° 52.514'	27° 52.514'	27° 52.514'	27° 52.511'	27° 52.511'	1 km N
E	85° 53.441'	85° 53.441'	85° 53.441'	85° 54.285'	85° 54.285'	Chaku
wt. %						
SiO_2	48.07	63.88	60.26	54.80	48.06	24.70
TiO_2	0.231	0.114	0.417	0.578	0.326	0.030
Al_2O_3	4.12	2.87	13.15	13.95	7.13	0.44
Fe_2O_3	5.45	0.92	4.20	5.56	2.92	0.44
MnO	0.676	0.035	0.125	0.063	0.187	0.040
MgO	4.47	2.72	4.01	1.77	7.44	16.70
CaO	17.16	12.77	5.35	7.22	11.86	23.20
Na_2O	1.11	0.01	0.55	0.94	1.50	0.00
K_2O	1.49	1.00	5.44	7.38	3.67	0.22
P_2O_5	0.028	0.033	0.157	0.139	0.085	0.018
LOI	17.69	26.65	6.26	7.15	17.46	35.84
ppm						
Rb	53.9	90.1	216.6	230.6	103.3	7.2
Sr	190.2	27.5	61.2	36.9	38.2	59.6
Y	47.8	10.6	25.1	25.0	19.1	2.3
Zr	52	82	156	169	165	6
Nb	5.7	6.8	12.9	14.1	9.8	1.3
Ba	79	271	493	444	240	24
Pb	16	5	13	25	15	9
Th	4	8	14	18	10	1
U	1	1	3	4	3	1
Sc	22	16	10	16	8	5
V	47	39	59	90	34	8
Cr	45	30	43	77	48	7
Co	6	5	6	9	7	3
Ni	9	11	13	34	15	0
Cu	3	13	3	4	2	1
Zn	7	14	16	13	20	61
Ga	5	9	16	20	8	1
Mo	0	0	0	0	0	0
As	4	3	1	4	4	4
S	57	51	35	51	30	38
$^{87}Rb/^{86}Sr$	0.8377		10.6379	18.6636	7.9766	0.3499
$^{87}Sr/^{86}Sr$	0.930227 ±11		1.106057 ±11	1.038053 ±15	0.907966 ±9	0.720756 ±7
$^{143}Nd/^{144}Nd$						
ε_{Nd}						

Table C3 (continued).

Sample Label	BK26	BK27	BK54a	BK115	BK116	BK119
Unit	LH	LH	LH	LH	LH	LH
Lithology	dol Sil	dol Slate	dol Sil	dol Sch	dol Sch	dol-mic Sch
Major Minerals	Q,D,Gr	Q,B,M,D,Gr	Q,D,Pl			Q,D,B,Gr
C / C-S / S	C-S	C-S	C-S	C-S	C-S	C-S
Subdivision	bg / kn	bg (jk)	bg	bg	ml	bg (jk)
GPS N	27° 38.987'	27° 37.733'	27° 39.751'	27° 55.577'	27° 55.538'	27° 55.254'
E	85° 42.484'	85° 42.657'	85° 39.270'	85° 56.216'	85° 56.308'	85° 55.878'
wt. %						
SiO_2	45.61	52.32	75.16	55.93	35.90	54.34
TiO_2	0.157	0.385	0.173	0.542	0.216	0.200
Al_2O_3	3.93	9.17	3.14	17.87	4.67	6.13
Fe_2O_3	1.90	5.00	2.10	7.40	4.36	3.13
MnO	0.039	0.060	0.052	0.099	0.072	0.374
MgO	9.66	5.69	3.11	4.98	10.42	7.42
CaO	15.30	8.62	6.72	4.86	17.55	10.82
Na_2O	0.48	0.52	1.00	0.84	0.62	0.19
K_2O	1.12	3.20	0.57	4.69	1.21	3.61
P_2O_5	0.098	0.087	0.038	0.127	0.126	0.082
LOI	23.20	14.37	9.31	2.25	26.01	15.78
ppm						
Rb	51.2	154.6	27.7	275.4	63.1	119.4
Sr	96.3	63.8	26.5	92.2	138.7	59.2
Y	13.1	25.8	16.1	25.7	18.9	15.6
Zr	56	164	189	139	83	82
Nb	4.7	10.6	4.8	11.3	4.5	4.8
Ba	171	341	63	358	104	561
Pb	6	15	3	35	14	13
Th	3	14	7	18	5	7
U	4	4	2	4	2	3
Sc	7	8	5	17	9	6
V	44	55	14	109	48	28
Cr	20	54	36	93	42	33
Co	5	10	4	15	7	9
Ni	16	19	4	22	14	11
Cu	9	11	6	6	2	3
Zn	36	69	7	126	65	40
Ga	5	11	3	22	6	8
Mo	2	0	0	0	1	0
As	4	7	7	0	4	6
S	63	64	239	429	469	27
$^{87}Rb/^{86}Sr$	1.5476	7.1600	3.0785		1.3326	5.9444
$^{87}Sr/^{86}Sr$	0.770206 ±7	0.925815 ±9	0.891838 ±12		0.835441 ±7	0.899438 ±8
$^{143}Nd/^{144}Nd$	0.511350 ±8				0.511351 ±2	0.511314 ±3
ε_{Nd}	-25.1269				-25.0983	-25.8352

Table C3 (continued).

Sample Label	BK122REG	BK123	BK8	BK12a	BK12c
Unit	LH	LH	LH	LH	LH
Lithology	dol-mic Sch	Dol	Phy	Greywacke	Sch
Major Minerals	D,Q	D,Q	Q,M	Q,B,Pl,D	Q,M,B
C / C-S / S	C-S	C-S	S	S	S
Subdivision	dh	dh	kn	da / np	da / np
GPS N	27° 53.505'	27° 53.345'	27° 47.884'	27° 52.514'	27° 52.514'
E	85° 54.882'	85° 54.825'	85° 53.741'	85° 53.441'	85° 53.441'
wt. %					
SiO_2	53.16	33.19	77.89	78.56	75.85
TiO_2	0.134	0.026	0.355	0.155	0.193
Al_2O_3	3.33	0.27	10.73	6.43	8.67
Fe_2O_3	1.47	0.54	1.97	1.86	2.72
MnO	0.072	0.040	0.020	0.071	0.084
MgO	12.28	14.53	3.91	1.79	2.01
CaO	12.15	20.70	0.13	3.09	2.78
Na_2O	0.20	0.00	0.35	1.14	0.06
K_2O	1.01	0.13	2.01	3.67	3.59
P_2O_5	0.066	0.016	0.077	0.055	0.062
LOI	18.41	31.25	2.61	3.37	4.05
ppm					
Rb	62.0	6.4	64.7	77.3	128.7
Sr	54.0	77.6	22.3	22.9	20.4
Y	8.9	1.0	19.4	10.5	14.5
Zr	30	6	160	97	136
Nb	2.2	0.8	9.5	5.8	8.6
Ba	87	163	298	203	365
Pb	10	6	8	21	5
Th	3	1	14	5	13
U	1	0	3	2	3
Sc	6	7	6	1	3
V	15	9	29	19	31
Cr	21	18	28	23	29
Co	4	2	4	2	5
Ni	6	0	15	3	6
Cu	5	0	1	2	233
Zn	27	26	26	4	9
Ga	5	1	14	5	11
Mo	0	0	0	0	0
As	4	3	1	0	1
S	65	32	21	27	36
$^{87}Rb/^{86}Sr$	3.4080	0.2387	8.7659	10.1156	18.9720
$^{87}Sr/^{86}Sr$	0.973464 ±20	0.711916 ±17	1.161299 ±12	1.074226 ±12	1.111380 ±11
$^{143}Nd/^{144}Nd$	0.511200 ±3	0.511200 ±10			
ε_{Nd}	-28.0526	-28.0510			

Table C3 (continued).

Sample Label	BK13b	BK21	BK25	BK112	BK120	BK121
Unit	LH	LH	LH	LH	LH	LH
Lithology	bt Sch	meta-Sst	meta-Sst	gra Phy	Sch	mic Sch
Major Minerals	Q,M,B	Q,M,Ch	Q,Gr			
C / C-S / S	S	S	S	S	S	S
Subdivision	da / np	kn	kn	rb	bg	bg
GPS N	27° 52.573'	27° 42.420'	27° 38.987'	27° 56.502'	27° 55.082'	27° 54.983'
E	85° 53.745'	85° 45.690'	85° 42.450'	85° 56.808'	85° 55.860'	85° 55.744'
wt. %						
SiO_2	65.87	68.22	84.79	63.24	75.53	62.16
TiO_2	0.670	0.553	0.231	0.610	0.319	0.613
Al_2O_3	16.17	15.57	4.00	18.14	9.71	15.72
Fe_2O_3	5.99	5.38	1.36	5.06	2.65	5.12
MnO	0.039	0.057	0.027	0.033	0.090	0.086
MgO	2.45	2.15	0.68	2.44	1.37	3.29
CaO	0.72	0.46	3.74	0.55	1.65	2.32
Na_2O	1.18	0.84	0.34	0.65	0.30	0.30
K_2O	4.92	3.39	1.09	5.23	6.21	6.89
P_2O_5	0.128	0.139	0.044	0.242	0.126	0.157
LOI	1.81	2.72	3.94	3.75	2.08	3.80
ppm						
Rb	237.5	143.9	42.5	251.8	170.2	292.1
Sr	51.2	64.9	53.4	28.8	38.4	31.8
Y	32.4	27.3	12.1	30.4	21.0	23.8
Zr	190	188	95	161	339	171
Nb	15.3	14.8	4.6	12.5	9.4	15.2
Ba	561	633	231	518	458	986
Pb	16	19	10	10	10	6
Th	24	24	6	19	16	21
U	5	6	2	4	5	4
Sc	17	9	3	15	3	12
V	94	62	20	105	25	75
Cr	102	73	33	94	50	72
Co	13	12	4	7	4	15
Ni	32	31	6	5	9	28
Cu	19	16	4	10	2	4
Zn	49	56	19	106	7	67
Ga	18	20	6	21	9	18
Mo	0	0	0	4	0	0
As	2	0	1	1	3	7
S	45	21	54	1534	29	32
$^{87}Rb/^{86}Sr$	13.6903	6.5041	2.3074			
$^{87}Sr/^{86}Sr$	0.913729 ±13	0.850169 ±10	0.729204 ±8			
$^{143}Nd/^{144}Nd$	0.511425 ±5	0.511232 ±6				
ε_{Nd}	-23.6589	-27.4268				

Table C3 (continued).

Sample Label	BK122MV	BK125	BK126	BK56(1)	BK56(2)
Unit	LH	LH	LH	LH	LH
Lithology	Qz vein	Sch	Sch	impure Dol	impure Dol
Major Minerals				Q,D,B?,Gr	
C / C-S / S	S	S	S	C-S	C-S
Subdivision	dh	da / np	bg / ml	dh	dh
GPS N	27° 53.505'	27° 52.522'	27° 55.961'	Chaku	Chaku
E	85° 54.882'	85° 53.703'	85° 56.180'		
wt. %					
SiO_2	89.58	66.63	66.58	33.82	33.31
TiO_2	0.023	0.677	0.634	0.142	0.172
Al_2O_3	1.64	15.48	15.53	2.73	2.93
Fe_2O_3	0.45	5.69	5.69	1.24	1.19
MnO	0.015	0.050	0.043	0.062	0.052
MgO	2.15	2.37	2.47	14.02	13.89
CaO	2.93	1.54	0.79	19.89	19.66
Na_2O	0.36	2.86	1.67	0.01	0.01
K_2O	0.14	3.61	4.59	1.65	1.83
P_2O_5	0.041	0.146	0.132	0.064	0.060
LOI	3.79	1.00	1.52	29.97	29.90
ppm					
Rb	8.1	160.8	179.8	42.0	46.6
Sr	34.3	68.9	45.2	63.9	65.1
Y	1.8	38.5	30.6	4.7	4.5
Zr	8	209	189	25	28
Nb	0.6	14.5	14.4	2.5	2.7
Ba	12	324	525	1163	1298
Pb	14	22	14	10	8
Th	0	24	23	3	4
U	-1	5	3	2	1
Sc	1	14	14	8	6
V	2	74	84	20	22
Cr	21	112	98	28	24
Co	3	15	16	7	5
Ni	0	28	30	4	4
Cu	18	24	24	11	12
Zn	6	41	39	20	19
Ga	1	19	18	4	4
Mo	0	0	0	0	0
As	1	4	0	10	11
S	180	37	33	37	44
$^{87}Rb/^{86}Sr$	0.6877			1.9086	
$^{87}Sr/^{86}Sr$	0.774839 ±9			0.745316 ±8	
$^{143}Nd/^{144}Nd$				0.511276 ±8	
ε_{Nd}				-26.5729	

Table C3 (continued).

Sample Label	BK56(3)	BK56(4)	BK56(5)	BK56(6)	BK56(7)	BK56(8)
Unit	LH	LH	LH	LH	LH	LH
Lithology	impure Dol	impure Dol	impure Dol	impure Dol	impure Dol	impure Dol
Major Minerals				Q,D,M		Q,D,M
C / C-S / S	C-S	C-S	C-S	C-S	C-S	C-S
Subdivision	dh	dh	dh	dh	dh	dh
GPS N	Chaku	Chaku	Chaku	Chaku	Chaku	Chaku
E						
wt. %						
SiO_2	31.70	28.19	25.53		44.75	33.52
TiO_2	0.174	0.190	0.092		0.306	0.168
Al_2O_3	2.92	3.76	1.83		7.34	4.05
Fe_2O_3	1.13	1.22	1.21		1.34	1.19
MnO	0.056	0.060	0.068		0.045	0.060
MgO	14.19	14.62	15.54		9.85	13.01
CaO	20.17	20.57	22.40		13.00	18.33
Na_2O	0.03	0.04	0.00		0.10	0.02
K_2O	1.75	2.16	1.10		4.02	2.08
P_2O_5	0.074	0.068	0.064		0.097	0.066
LOI	30.30	31.25	33.84		19.83	27.94
ppm						
Rb	44.5	60.7	29.2	26.6	118.2	65.2
Sr	67.3	69.2	67.5	63.1	54.1	64.3
Y	6.5	6.1	6.7	7.3	10.0	7.0
Zr	44	41	33	51	81	34
Nb	3.9	4.0	2.5	2.4	7.3	4.1
Ba	916	1173	325	256	1171	436
Pb	7	5	6	4	21	4
Th	3	6	3	5	7	5
U	0	1	2	1	1	1
Sc	10	9	9	8	10	8
V	23	26	17	14	38	28
Cr	37	20	24	34	40	33
Co	3	5	4	2	8	3
Ni	4	5	4	2	9	4
Cu	6	7	5	6	29	11
Zn	15	13	13	11	13	16
Ga	4	5	2	2	9	6
Mo	0	0	0	0	0	0
As	8	7	4	6	18	6
S	28	33	28	22	48	24
$^{87}Rb/^{86}Sr$					6.3741	
$^{87}Sr/^{86}Sr$					0.793698 ±9	
$^{143}Nd/^{144}Nd$						
ε_{Nd}						

Table C3 (continued).

Sample Label	BK113a	BK113b	BK113c	BK113d	BK113e
Unit	LH	LH	LH	LH	LH
Lithology	mic Sch	dol Sil	mic meta-Sst	mic meta-Sst	mic Sch
Major Minerals				Q,D	
C / C-S / S	S	C-S	S	S	S
Subdivision	bg??	bg??	bg??	bg??	bg??
GPS N	27° 56.695'	27° 56.695'	27° 56.695'	27° 56.695'	27° 56.695'
E	85° 55.858'	85° 55.858'	85° 55.858'	85° 55.858'	85° 55.858'
wt. %					
SiO_2	62.19	52.79	83.00	76.75	73.10
TiO_2	0.586	0.092	0.157	0.195	0.465
Al_2O_3	14.00	1.53	3.69	5.03	10.84
Fe_2O_3	6.55	3.64	1.38	2.11	3.43
MnO	0.041	0.090	0.027	0.041	0.021
MgO	3.95	7.90	1.35	2.25	2.05
CaO	0.74	14.61	3.00	4.75	0.54
Na_2O	0.92	0.31	0.35	0.63	1.03
K_2O	5.52	0.59	2.73	2.46	4.89
P_2O_5	0.145	0.036	0.033	0.064	0.114
LOI	3.16	21.28	4.40	6.42	2.44
ppm					
Rb	307.7	18.2	68.3	84.7	202.7
Sr	35.5	189.3	51.8	78.2	34.8
Y	32.6	14.5	11.5	16.5	26.8
Zr	308	114	148	217	264
Nb	16.4	2.9	3.9	5.3	12.0
Ba	559	104	457	439	677
Pb	13	24	8	39	47
Th	20	4	5	7	18
U	6	2	2	2	4
Sc	12	6	1	3	8
V	77	11	6	13	47
Cr	73	36	34	54	51
Co	6	3	3	5	8
Ni	14	7	6	7	20
Cu	11	1	6	13	36
Zn	60	36	12	51	61
Ga	20	3	2	4	14
Mo	0	0	0	0	1
As	0	4	5	10	7
S	1190	141	53	633	620
$^{87}Rb/^{86}Sr$	25.9299	0.2793	3.8479	3.1830	17.3225
$^{87}Sr/^{86}Sr$	1.056067 ±11	0.750543 ±5	0.796900 ±8	0.869163 ±8	0.993743 ±17
$^{143}Nd/^{144}Nd$			0.511428 ±3	0.511519 ±3	
ε_{Nd}			-23.5941	-21.8212	

Table C3 (continued).

Sample Label	BK114a	BK114b	BK114c	BK114d	BK114e	BK114f
Unit	LH	LH	LH	LH	LH	LH
Lithology	dol Phy	dol Phy	dol Phy	dol Phy	dol Phy	Phy
Major Minerals				Q,B,D	Q,B,M,D	
C / C-S / S	C-S	C-S	C-S	C-S	C-S	S
Subdivision	bg??	bg??	bg??	bg??	bg??	bg??
GPS N	27° 55.710'	27° 55.710'	27° 55.710'	27° 55.710'	27° 55.710'	27° 55.710'
E	85° 56.767'	85° 56.767'	85° 56.767'	85° 56.767'	85° 56.767'	85° 56.767'
wt. %						
SiO_2	68.35	65.59	63.87	59.18	59.81	87.67
TiO_2	0.192	0.451	0.184	0.402	0.175	0.127
Al_2O_3	3.68	8.86	3.81	8.78	4.22	3.01
Fe_2O_3	3.16	2.99	3.48	3.87	4.00	2.00
MnO	0.050	0.033	0.058	0.051	0.062	0.079
MgO	4.57	4.80	5.21	6.02	6.34	0.61
CaO	8.84	6.30	10.45	9.11	11.49	1.91
Na_2O	0.02	1.17	0.01	0.82	0.02	0.21
K_2O	1.85	3.32	1.99	3.41	2.33	1.59
P_2O_5	0.039	0.101	0.042	0.102	0.046	0.042
LOI	9.55	6.37	10.86	8.94	11.48	3.16
ppm						
Rb	79.1	138.8	86.6	159.0	107.7	85.2
Sr	33.0	71.3	44.5	57.9	44.6	31.9
Y	20.1	21.2	18.8	23.4	19.2	13.3
Zr	209	233	130	166	138	201
Nb	6.0	11.3	5.6	10.6	5.5	4.5
Ba	157	486	170	447	182	265
Pb	10	27	9	22	11	80
Th	5	15	6	12	6	8
U	1	4	2	4	1	3
Sc	5	7	8	10	7	3
V	17	47	17	42	18	9
Cr	44	60	39	88	49	31
Co	8	8	8	11	8	4
Ni	11	16	11	20	8	9
Cu	10	6	11	11	16	6
Zn	52	67	64	102	64	294
Ga	4	9	5	9	6	5
Mo	1	1	0	0	0	0
As	7	4	1	7	2	16
S	540	446	913	661	1618	94
$^{87}Rb/^{86}Sr$	7.0758	5.7466	5.7543	8.1435	7.1251	7.9212
$^{87}Sr/^{86}Sr$	0.915892 ±9	0.915998 ±10	0.933365 ±8	0.963675 ±11	0.911023 ±9	0.964799 ±17
$^{143}Nd/^{144}Nd$			0.511593 ±5			
ε_{Nd}			-20.3892			

Table C3 (continued).

Sample Label	BK117a	BK117b	BK117c	BK117d	BK124a
Unit	LH	LH	LH	LH	LH
Lithology	Sil	Sil	Sil	Sil	dol Sil
Major Minerals					
C / C-S / S	S	S	S	S	C-S
Subdivision	ml / rb??	ml / rb??	ml / rb??	ml / rb??	np
GPS N	27° 56.090'	27° 56.090'	27° 56.090'	27° 56.090'	27° 52.751'
E	85° 55.572'	85° 55.572'	85° 55.572'	85° 55.572'	85° 54.257'
wt. %					
SiO_2	86.86	85.12	88.34	84.75	19.66
TiO_2	0.119	0.151	0.179	0.149	0.094
Al_2O_3	2.46	3.72	4.04	3.67	1.99
Fe_2O_3	2.24	2.76	1.81	2.69	1.41
MnO	0.090	0.093	0.057	0.090	0.088
MgO	1.08	1.21	0.71	1.17	17.54
CaO	2.81	2.27	0.97	2.30	24.61
Na_2O	0.10	0.16	0.21	0.17	0.00
K_2O	1.31	2.04	2.07	2.01	0.85
P_2O_5	0.026	0.043	0.039	0.043	0.052
LOI	3.62	3.04	2.18	3.31	36.98
ppm					
Rb	49.3	51.3	69.2	83.1	32.7
Sr	25.4	31.1	26.4	33.3	39.8
Y	10.3	11.7	11.8	13.8	6.7
Zr	196	262	218	199	30
Nb	3.7	3.8	5.0	4.9	2.8
Ba	172	215	301	265	191
Pb	66	180	197	82	2
Th	6	7	6	7	3
U	2	2	2	2	3
Sc	2	3	1	1	9
V	9	10	9	9	11
Cr	40	24	34	26	18
Co	3	3	3	5	4
Ni	6	8	7	10	3
Cu	5	4	5	6	1
Zn	252	267	299	290	4
Ga	4	4	3	3	3
Mo	0	0	0	0	0
As	13	8	14	25	2
S	52	69	55	86	21
$^{87}Rb/^{86}Sr$					2.3967
$^{87}Sr/^{86}Sr$					0.792566 ±18
$^{143}Nd/^{144}Nd$					
ε_{Nd}					

Table C3 (continued).

Sample Label	BK124b	BK124c	BK124d	BK127a	BK127b(1)
Unit	LH	LH	LH	LH	LH
Lithology	dol Sil	dol Sil	dol Sil	bt Sch	bt Sch
Major Minerals	D,Q,M	D,Q	D,Q		
C / C-S / S	C-S	C-S	C-S	S	S
Subdivision	np	np	np	da / np	da / np
GPS N	27° 52.751'	27° 52.751'	27° 52.751'	27° 52.573'	27° 52.573'
E	85° 54.257'	85° 54.257'	85° 54.257'	85° 53.745'	85° 53.745'
wt. %					
SiO_2	37.66	26.25	28.24	66.56	66.58
TiO_2	0.118	0.042	0.082	0.617	0.638
Al_2O_3	2.19	0.57	1.62	15.58	16.04
Fe_2O_3	0.78	1.08	1.04	6.07	6.12
MnO	0.076	0.108	0.064	0.041	0.035
MgO	13.31	16.32	14.66	2.45	2.55
CaO	18.94	23.53	21.17	0.52	0.64
Na_2O	0.01	0.00	0.00	1.12	1.31
K_2O	1.36	0.27	1.02	4.53	4.85
P_2O_5	0.038	0.020	0.058	0.116	0.116
LOI	28.50	35.09	34.50	2.13	1.86
ppm					
Rb	34.6	9.6	2.0	188.8	214.1
Sr	27.7	31.6	26.0	44.8	51.6
Y	6.2	3.3	1.1	31.0	30.9
Zr	69	12	5	186	182
Nb	2.9	1.5	1.1	15.0	15.3
Ba	314	45	2	468	477
Pb	3	8	2	31	16
Th	4	1	2	23	22
U	1	1	1	5	4
Sc	7	7	3	16	17
V	14	9	6	80	82
Cr	63	26	18	98	97
Co	2	2	3	17	14
Ni	1	2	1	30	31
Cu	2	8	0	18	13
Zn	4	4	3	46	44
Ga	3	1	0	20	20
Mo	0	0	0	0	0
As	3	5	6	2	2
S	22	26	20	47	30
$^{87}Rb/^{86}Sr$	3.6528	0.8837	0.2230	12.4341	
$^{87}Sr/^{86}Sr$	0.818218 ±20	0.763306 ±20	0.726984 ±23	0.910598 ±14	
$^{143}Nd/^{144}Nd$	0.511203 ±10	0.511358 ±5	0.511167 ±10		
ε_{Nd}	-28.0001	-24.9735	-28.6983		

Table C3 (continued).

Sample Label	BK127b(2)	BK127c	BK127d	BK127e	BK127f	BK127g
Unit	LH	LH	LH	LH	LH	LH
Lithology	bt Sch	Lst	Lst	Lst	Lst	bt Sch
Major Minerals						
C / C-S / S	S	C	C	C	C	S
Subdivision	da / np	da / np	da / np	da / np	da / np	da / np
GPS N	27° 52.573'	27° 52.573'	27° 52.573'	27° 52.573'	27° 52.573'	27° 52.573'
E	85° 53.745'	85° 53.745'	85° 53.745'	85° 53.745'	85° 53.745'	85° 53.745'
wt. %						
SiO_2	66.58	0.83		5.64	2.76	70.54
TiO_2	0.638	0.044		0.060	0.046	0.358
Al_2O_3	16.04	0.16		0.58	0.23	14.12
Fe_2O_3	6.12	0.11		0.25	0.12	3.88
MnO	0.035	0.014		0.012	0.008	0.032
MgO	2.55	1.45		1.72	1.77	2.51
CaO	0.64	53.60		50.82	53.30	0.84
Na_2O	1.31	0.01		0.00	0.00	2.38
K_2O	4.85	0.07		0.19	0.06	3.68
P_2O_5	0.116	0.020		0.026	0.018	0.086
LOI	1.86	43.41		41.66	43.38	1.28
ppm						
Rb	216.5		5.3	0.8	2.3	189.3
Sr	51.9		37.1	45.1	48.8	73.8
Y	31.1		7.1	3.4	2.1	27.0
Zr	181		23	9	7	165
Nb	15.6		2.6	1.4	1.9	14.0
Ba	478		381	414	439	444
Pb	15		2	1	0	12
Th	23		0	2	1	28
U	3		0	2	2	6
Sc	19		21	17	20	7
V	86		5	4	9	29
Cr	102		9	5	3	34
Co	16		3	3	5	11
Ni	29		1	1	1	16
Cu	14		7	7	4	2
Zn	47		9	6	5	30
Ga	20		1	1	1	14
Mo	0		0	0	0	0
As	0		1	6	6	4
S	30		147	158	147	26
$^{87}Rb/^{86}Sr$	12.3053		0.4170	0.0518	0.1376	7.6130
$^{87}Sr/^{86}Sr$	0.908475 ±12		0.798339 ±30	0.796956 ±10	0.797548 ±27	0.972538 ±22
$^{143}Nd/^{144}Nd$	0.511341 ±1		0.511257 ±3		0.511347 ±30	0.511195 ±4
ε_{Nd}	-25.3005		-26.9391		-25.1796	-28.1485

Table C4. Chemical composition of rocks of the Kathmandu Nappe.

Sample Label	BK53b	BK53a	BK53c	BK53d	BK53(1)
Unit	Kath	Kath	Kath	Kath	Kath
Lithology	Mbl	Calc-Sch	bt Sch	gt Sch	imp Mbl
Major Minerals	C,Q	C,B,M,Q	Q,B,C		
C / C-S / S	C	C-S	S	S	C-S
Subdivision	bd	bd	ra	ra	bd
GPS N	27° 40.823'	27° 40.823'	27° 40.823'	27° 40.823'	27° 40.823'
E	85° 37.030'	85° 37.030'	85° 37.030'	85° 37.030'	85° 37.030'
wt. %					
SiO_2	5.69	59.44	68.65	68.09	24.74
TiO_2	0.076	0.557	0.903	0.710	0.272
Al_2O_3	0.96	8.82	15.10	13.26	2.88
Fe_2O_3	1.17	1.95	4.79	5.72	0.83
MnO	0.054	0.034	0.071	0.102	0.056
MgO	6.92	5.25	1.60	3.32	3.10
CaO	45.27	10.18	1.82	2.29	37.34
Na_2O	0.00	1.28	3.82	2.80	0.63
K_2O	0.31	3.31	3.25	2.41	1.10
P_2O_5	0.042	0.182	0.175	0.162	0.078
LOI	41.58	8.59	1.03	0.85	31.85
ppm					
Rb	10.8	99.8	203.6	123.0	31.6
Sr	217.3	81.8	101.2	54.1	170.0
Y	10.1	25.8	48.4	31.9	25.7
Zr	46	315	305	201	305
Nb	2.3	12.7	20.2	12.6	6.8
Ba	12	275	549	422	150
Pb	10	12	14	9	22
Th	3	16	32	17	13
U	3	2	4	5	4
Sc	19	9	13	12	14
V	20	45	80	104	29
Cr	9	52	80	113	35
Co	4	4	15	15	3
Ni	2	6	25	35	5
Cu	5	4	2	19	2
Zn	14	33	30	50	6
Ga	2	13	17	17	5
Mo	0	0	0	0	0
As	8	6	2	6	5
S	836	101	24	36	114
$^{87}Rb/^{86}Sr$	0.1438				0.5383
$^{87}Sr/^{86}Sr$	0.711621 ± 10				0.7174043 ±5
$^{143}Nd/^{144}Nd$	0.511617 ±4				
ε_{Nd}	-19.9216				

Table C4 (continued).

Sample Label	BK53(2)	BK53(3)	BK53(4)	BK53(5)	BK53(6)
Unit	Kath	Kath	Kath	Kath	Kath
Lithology	imp Mbl	imp Mbl	imp Mbl	imp Mbl	imp Mbl
Major Minerals					
C / C-S / S	C-S	C-S	C-S	C-S	C-S
Subdivision	bd	bd	bd	bd	bd
GPS N	27° 40.823'	27° 40.823'	27° 40.823'	27° 40.823'	27° 40.823'
E	85° 37.030'	85° 37.030'	85° 37.030'	85° 37.030'	85° 37.030'
wt. %					
SiO_2	25.61	32.78	30.73	19.82	17.93
TiO_2	0.400	0.336	0.302	0.284	0.206
Al_2O_3	3.48	3.84	4.00	2.56	2.09
Fe_2O_3	1.09	0.96	0.69	0.95	0.91
MnO	0.058	0.050	0.050	0.062	0.062
MgO	4.47	4.12	2.20	3.48	3.10
CaO	34.67	31.02	33.79	39.13	42.66
Na_2O	0.61	0.73	0.98	0.45	0.43
K_2O	1.28	1.44	1.35	0.90	0.72
P_2O_5	0.112	0.098	0.092	0.084	0.068
LOI	30.82	27.63	31.85	33.66	35.69
ppm					
Rb	35.9	30.3	23.8	20.7	16.8
Sr	153.1	149.6	170.3	165.9	170.2
Y	26.8	22.4	23.5	27.4	28.2
Zr	684	431	353	415	243
Nb	9.4	7.6	5.3	7.0	4.9
Ba	111	157	118	84	78
Pb	15	13	15	14	16
Th	22	12	14	16	11
U	5	2	5	2	4
Sc	16	14	18	19	23
V	31	24	23	21	21
Cr	28	36	20	24	17
Co	5	4	3	2	2
Ni	4	5	4	4	2
Cu	1	2	3	2	3
Zn	8	6	5	5	4
Ga	5	5	3	3	3
Mo	1	0	0	0	0
As	7	6	5	7	4
S	257	196	181	358	373
$^{87}Rb/^{86}Sr$			0.4047		
$^{87}Sr/^{86}Sr$			0.717271 ±6		
$^{143}Nd/^{144}Nd$			0.511588 ±3		
ε_{Nd}			-20.4809		

Table C4 (continued).

Sample Label	BK104a	BK104b	BK104c	BK104d	BK105a
Unit	Kath	Kath	Kath	Kath	Kath
Lithology	imp Mbl	Quartzite	imp Mbl	imp Mbl	imp Mbl
Major Minerals	Q,C,B				
C / C-S / S	C-S	S	C-S	C-S	C-S
Subdivision	bd	cp	bd	bd	bd
GPS N	27° 40.934'	27° 40.934'	27° 40.934'	27° 40.934'	27° 40.801'
E	85° 36.730'	85° 36.730'	85° 36.730'	85° 36.730'	85° 37.039'
wt. %					
SiO_2	30.46	94.14	19.49	16.94	52.09
TiO_2	0.328	0.226	0.256	0.168	0.177
Al_2O_3	5.37	3.32	3.28	2.69	2.26
Fe_2O_3	1.93	1.13	1.10	0.96	1.29
MnO	0.076	0.017	0.114	0.062	0.042
MgO	1.60	0.13	0.99	1.07	2.35
CaO	32.17	0.05	40.60	44.27	22.06
Na_2O	1.01	0.11	0.48	0.55	0.11
K_2O	2.16	1.53	1.46	1.21	0.92
P_2O_5	0.102	0.047	0.074	0.056	0.041
LOI	25.39	0.51	31.85	34.66	19.49
ppm					
Rb	64.5	48.1	43.3	39.0	29.6
Sr	231.6	21.7	280.1	344.6	80.0
Y	18.0	10.8	15.2	9.6	14.4
Zr	125	154	165	77	122
Nb	7.5	4.4	5.6	3.7	3.4
Ba	205	1850	131	202	1058
Pb	13	3	22	143	8
Th	11	8	10	8	7
U	4	0	4	3	2
Sc	17	0	20	21	10
V	32	15	29	30	22
Cr	36	31	27	47	70
Co	5	1	5	2	3
Ni	11	3	4	5	2
Cu	4	2	8	7	2
Zn	8	2	609	387	5
Ga	7	2	4	5	4
Mo	0	0	0	0	0
As	8	2	17	0	2
S	741	73	886	646	289
$^{87}Rb/^{86}Sr$	0.8062	6.4423	0.4478	0.3275	
$^{87}Sr/^{86}Sr$	0.714394 ±6	0.754737 ±15	0.720615 ±8	0.710621 ±4	
$^{143}Nd/^{144}Nd$			0.511671 ±7		
ε_{Nd}			-18.8632		

Table C4 (continued).

Sample Label	**BK105b**	**BK105c**	**BK105d**	**BK105e**
Unit	**Kath**	**Kath**	**Kath**	**Kath**
Lithology	imp Mbl	imp Mbl	Sch	Sch
Major Minerals				
C / C-S / S	**C-S**	**S**	**S**	**S**
Subdivision	**bd**	**bd**	**ra**	**ra**
GPS N	27° 40.801'	27° 40.801'	27° 40.801'	27° 40.801'
E	85° 37.039'	85° 37.039'	85° 37.039'	85° 37.039'
wt. %				
SiO_2	30.28	54.71	70.20	64.12
TiO_2	0.478	0.192	0.673	0.831
Al_2O_3	4.43	2.31	12.56	15.99
Fe_2O_3	1.54	1.37	6.83	7.00
MnO	0.066	0.046	0.082	0.104
MgO	3.08	2.17	1.76	3.22
CaO	32.21	20.61	1.47	1.10
Na_2O	0.78	0.10	3.12	1.86
K_2O	1.43	0.96	3.11	4.21
P_2O_5	0.126	0.056	0.185	0.186
LOI	27.69	18.25	0.77	1.62
ppm				
Rb	28.9	31.8	207.4	164.8
Sr	179.7	76.5	82.5	59.0
Y	31.6	15.3	29.7	31.7
Zr	573	137	178	205
Nb	9.9	3.3	16.0	12.6
Ba	191	1115	470	678
Pb	21	8	9	9
Th	23	6	15	15
U	3	2	2	5
Sc	14	8	9	17
V	30	22	71	151
Cr	59	47	80	135
Co	5	3	15	21
Ni	6	3	25	51
Cu	3	3	76	3
Zn	8	4	28	62
Ga	6	2	17	21
Mo	0	0	0	0
As	3	3	5	3
S	188	408	55	24
$^{87}Rb/^{86}Sr$			7.3288	8.1311
$^{87}Sr/^{86}Sr$			0.786054 ±7	0.771059 ±10
$^{143}Nd/^{144}Nd$			0.511551 ±2	
ε_{Nd}			-21.2009	

Table C5. Chemical composition of rocks from the Langtang Khola - Trisuli.

Sample Label	**L1b**	**L2**
Unit	**LH**	**LH**
Lithology	Phyllite	Phyllite
C / C-S / S	**S**	**S**
Subdivision	**Both Kuncha Group**	
GPS N	28° 07.294'	28° 09.359'
E	85° 18.512'	85° 19.529'
wt. %		
SiO_2	76.72	76.14
TiO_2	0.4	0.4
Al_2O_3	12.14	12.30
Fe_2O_3	3.22	3.66
MnO	0.0	0.0
MgO	0.99	1.14
CaO	0.39	0.22
Na_2O	1.41	0.55
K_2O	2.97	3.43
P_2O_5	0.1	0.1
LOI	1.33	1.60
ppm		
Rb	146.7	176.5
Sr	63.0	43.6
Y	20.8	23.5
Zr	181	197
Nb	10.2	11.9
Ba	531	514
Pb	21	19
Th	15	21
U	3	5
Sc	6	9
V	38	37
Cr	39	43
Co	7	10
Ni	17	17
Cu	6	7
Zn	46	57
Ga	15	15
Mo	0	1
As	1	1
S	31	26
$^{87}Rb/^{86}Sr$		
$^{87}Sr/^{86}Sr$		
$^{143}Nd/^{144}Nd$		
ε_{Nd}		

Appendix D

Results of Principal Components Analyses

List of tables.

Geology abbreviations:

TSS: Tibetan Sedimentary series.

HHCS: High Himalayan Crystalline Series.

LHC: Nawakot Group calc-silicates.

LHS: Kuncha Group silicate metasediments and Lesser Himalayan crystalline gneisses.

LHtotal: Lesser Himalayan Formation (LHC + LHS).

Tables D1 – D9 show r values for principal components analyses carried out using the computer programme XLSTAT™. Statistically significant r values are shown in all tables in bold type. The confidence level (p) is 0.05 i.e. there is a 95% certainty that the observed statistical relationship is not due to chance and the null hypothesis can be rejected. This is based on a two-tailed test i.e. one in which the difference from the null hypothesis may be positive or negative.

Table D1. Principal components analysis of Bhote Kosi data.

	$^{87}Sr/^{86}Sr$	Sr^{2+}	Temp.	pH	Na^+	Mg^{2+}	Si	K^+	Ca^{2+}	Rb^+	HCO_3^-	Cl^-	NO_3^-	SO_4^{2-}	%TSS	%HHCS	%LHC	%LHS	%LHtotal
$^{87}Sr/^{86}Sr$	*	**-0.298**	0.040	**0.338**	**-0.389**	0.098	-0.225	**0.286**	-0.201	**0.313**	0.006	-0.172	-0.113	-0.185	**-0.400**	**-0.555**	**0.685**	**0.379**	**0.756**
Sr^{2+}	**-0.298**	*	-0.149	-0.074	**0.364**	**0.569**	-0.064	-0.052	**0.850**	-0.194	**0.397**	-0.081	-0.022	**0.959**	**0.794**	-0.249	-0.210	-0.216	**-0.293**
Temp.	0.040	-0.149	*	0.176	**0.377**	-0.040	**0.608**	0.152	-0.073	-0.067	0.135	**0.512**	**0.445**	-0.184	**-0.503**	0.178	0.164	0.069	0.167
pH	**0.338**	-0.074	0.176	*	**-0.282**	**0.539**	-0.162	**0.583**	0.222	**0.628**	**0.520**	-0.045	-0.088	0.006	**-0.270**	**-0.393**	**0.469**	**0.275**	**0.527**
Na^+	**-0.389**	**0.364**	**0.377**	**-0.282**	*	-0.046	**0.790**	-0.110	**0.286**	**-0.436**	0.126	**0.555**	**0.360**	**0.268**	0.071	**0.450**	**-0.356**	**-0.287**	**-0.448**
Mg^{2+}	0.098	**0.569**	-0.040	**0.539**	-0.046	*	-0.257	**0.661**	**0.784**	**0.579**	**0.802**	-0.147	-0.040	**0.643**	**0.271**	**-0.608**	**0.453**	0.034	**0.367**
Si	-0.225	-0.064	**0.608**	-0.162	**0.790**	-0.257	*	-0.041	-0.028	**-0.344**	0.060	**0.682**	**0.339**	-0.170	**-0.329**	**0.529**	-0.190	-0.186	**-0.259**
K^+	**0.286**	-0.052	0.152	**0.583**	-0.110	**0.661**	-0.041	*	**0.358**	**0.813**	**0.732**	0.022	0.031	-0.007	**-0.280**	**-0.438**	**0.684**	0.081	**0.573**
Ca^{2+}	-0.201	**0.850**	-0.073	0.222	**0.286**	**0.784**	-0.028	**0.358**	*	0.215	**0.805**	-0.062	-0.071	**0.782**	**0.637**	**-0.418**	0.051	-0.129	-0.040
Rb^+	**0.313**	-0.194	-0.067	**0.628**	**-0.436**	**0.579**	**-0.344**	**0.813**	0.215	*	**0.599**	-0.185	-0.122	-0.128	-0.224	**-0.499**	**0.679**	0.118	**0.591**
HCO_3^-	0.006	**0.397**	0.135	**0.520**	0.126	**0.802**	0.060	**0.732**	**0.805**	**0.599**	*	0.041	-0.034	**0.338**	0.176	**-0.481**	**0.398**	0.019	**0.315**
Cl^-	-0.172	-0.081	**0.512**	-0.045	**0.555**	-0.147	**0.682**	0.022	-0.062	-0.185	0.041	*	**0.679**	-0.159	**-0.273**	**0.295**	-0.106	-0.009	-0.086
NO_3^-	-0.113	-0.022	**0.445**	-0.088	**0.360**	-0.040	**0.339**	0.031	-0.071	-0.122	-0.034	**0.679**	*	-0.028	-0.205	0.077	0.004	0.100	0.064
SO_4^{2-}	-0.185	**0.959**	-0.184	0.006	**0.268**	**0.643**	-0.170	-0.007	**0.782**	-0.128	**0.338**	-0.159	-0.028	*	**0.706**	**-0.307**	-0.121	-0.149	-0.184
%TSS	**-0.400**	**0.794**	**-0.503**	**-0.270**	0.071	**0.271**	**-0.329**	**-0.280**	**0.637**	-0.224	0.176	**-0.273**	-0.205	**0.706**	*	-0.190	**-0.402**	**-0.281**	**-0.480**
%HHCS	**-0.555**	-0.249	0.178	**-0.393**	**0.450**	**-0.608**	**0.529**	**-0.438**	**-0.418**	**-0.499**	**-0.481**	**0.295**	0.077	**-0.307**	-0.190	*	**-0.593**	**-0.518**	**-0.770**
%LHC	**0.685**	-0.210	0.164	**0.469**	**-0.356**	**0.453**	-0.190	**0.684**	0.051	**0.679**	**0.398**	-0.106	0.004	-0.121	**-0.402**	**-0.593**	*	0.042	**0.791**
%LHS	**0.379**	-0.216	0.069	**0.275**	**-0.287**	0.034	-0.186	0.081	-0.129	0.118	0.019	-0.009	0.100	-0.149	**-0.281**	**-0.518**	0.042	*	**0.645**
%LHtotal	**0.756**	**-0.293**	0.167	**0.527**	**-0.448**	**0.367**	**-0.259**	**0.573**	-0.040	**0.591**	**0.315**	-0.086	0.064	-0.184	**-0.480**	**-0.770**	**0.791**	**0.645**	*

Table D2. Principal components analysis of Bhote Kosi data mainstream data.

	$^{87}Sr/^{86}Sr$	Sr^{2+}	Temp.	pH	Na^{+}	Mg^{2+}	Si	K^{+}	Ca^{2+}	Rb^{+}	HCO_3^{-}	%TSS	%HHCS	%LHC	%LHS	%LHtotal
$^{87}Sr/^{86}Sr$	*	**-0.582**	**0.506**	0.326	**-0.431**	-0.283	**0.405**	**0.345**	**-0.616**	**0.377**	**-0.469**	**-0.730**	**0.536**	**0.929**	**0.684**	**0.813**
Sr^{2+}	**-0.582**	*	0.057	0.044	**0.787**	**0.917**	-0.181	0.029	**0.974**	**-0.487**	**0.822**	**0.892**	**-0.897**	**-0.444**	-0.277	**-0.357**
Temp.	**0.506**	0.057	*	0.305	-0.174	0.173	0.211	0.143	0.044	-0.062	0.110	-0.011	-0.151	**0.483**	**0.371**	**0.432**
pH	0.326	0.044	0.305	*	0.011	0.204	0.344	0.122	-0.031	0.019	-0.020	-0.134	0.119	0.246	-0.012	0.092
Na^{+}	**-0.431**	**0.787**	-0.174	0.011	*	**0.839**	0.117	0.303	**0.754**	-0.173	**0.589**	**0.542**	**-0.533**	-0.323	-0.183	-0.247
Mg^{2+}	-0.283	**0.917**	0.173	0.204	**0.839**	*	-0.029	0.260	**0.863**	-0.336	**0.716**	**0.679**	**-0.734**	-0.164	-0.109	-0.136
Si	**0.405**	-0.181	0.211	0.344	0.117	-0.029	*	**0.597**	-0.164	0.264	-0.040	**-0.431**	0.283	**0.529**	**0.555**	**0.568**
K^{+}	**0.345**	0.029	0.143	0.122	0.303	0.260	**0.597**	*	0.121	**0.476**	0.323	-0.158	0.015	**0.492**	**0.377**	**0.440**
Ca^{2+}	**-0.616**	**0.974**	0.044	-0.031	**0.754**	**0.863**	-0.164	0.121	*	**-0.412**	**0.914**	**0.927**	**-0.935**	**-0.453**	-0.281	**-0.363**
Rb^{+}	**0.377**	**-0.487**	-0.062	0.019	-0.173	-0.336	0.264	**0.476**	**-0.412**	*	-0.211	**-0.489**	**0.488**	0.329	0.110	0.204
HCO_3^{-}	**-0.469**	**0.822**	0.110	-0.020	**0.589**	**0.716**	-0.040	0.323	**0.914**	-0.211	*	**0.840**	**-0.891**	-0.263	-0.168	-0.213
%TSS	**-0.730**	**0.892**	-0.011	-0.134	**0.542**	**0.679**	**-0.431**	-0.158	**0.927**	**-0.489**	**0.840**	*	**-0.948**	**-0.621**	**-0.468**	**-0.550**
%HHCS	**0.536**	**-0.897**	-0.151	0.119	**-0.533**	**-0.734**	0.283	0.015	**-0.935**	**0.488**	**-0.891**	**-0.948**	*	**0.363**	0.171	0.257
%LHC	**0.929**	**-0.444**	**0.483**	0.246	-0.323	-0.164	**0.529**	**0.492**	**-0.453**	0.329	-0.263	**-0.621**	**0.363**	*	**0.830**	**0.935**
%LHS	**0.684**	-0.277	**0.371**	-0.012	-0.183	-0.109	**0.555**	**0.377**	-0.281	0.110	-0.168	**-0.468**	0.171	**0.830**	*	**0.974**
%LHtotal	**0.813**	**-0.357**	**0.432**	0.092	-0.247	-0.136	**0.568**	**0.440**	**-0.363**	0.204	-0.213	**-0.550**	0.257	**0.935**	**0.974**	*

Table D3. Principal components analysis for Bhote Kosi catchments draining the Lesser Himalayan Formation.

	$^{87}Sr/^{86}Sr$	Sr^{2+}	Temp.	pH	Na^{+}	Mg^{2+}	Si	K^{+}	Ca^{2+}	Rb^{+}	HCO_3^{-}	Cl^{-}	NO_3^{-}	SO_4^{2-}	%LHC	%LHS	%LHtotal
$^{87}Sr/^{86}Sr$	*	-0.304	-0.352	-0.406	0.359	-0.477	0.183	-0.360	-0.513	-0.455	-0.521	-0.171	-0.286	-0.164	0.233	-0.209	0.177
Sr^{2+}	-0.304	*	0.029	0.470	-0.201	**0.705**	**-0.729**	**0.746**	**0.676**	**0.717**	**0.589**	-0.137	0.077	**0.859**	0.455	-0.453	-0.033
Temp.	-0.352	0.029	*	0.177	0.033	0.287	0.113	0.281	0.310	0.144	0.345	0.348	0.378	-0.128	-0.098	0.124	0.235
pH	-0.406	0.470	0.177	*	**-0.672**	**0.717**	-0.511	**0.574**	**0.800**	**0.684**	**0.789**	0.376	0.128	0.397	0.103	-0.106	-0.037
Na^{+}	0.359	-0.201	0.033	**-0.672**	*	**-0.583**	0.298	-0.301	-0.503	-0.437	**-0.576**	-0.047	0.258	-0.131	-0.274	0.245	-0.216
Mg^{2+}	-0.477	**0.705**	0.287	**0.717**	**-0.583**	*	-0.344	**0.869**	**0.957**	**0.895**	**0.962**	0.115	-0.121	**0.605**	0.484	-0.480	-0.026
Si	0.183	**-0.729**	0.113	-0.511	0.298	-0.344	*	-0.320	-0.394	-0.370	-0.298	0.126	-0.321	-0.520	-0.134	0.115	-0.147
K^{+}	-0.360	**0.746**	0.281	**0.574**	-0.301	**0.869**	-0.320	*	**0.862**	**0.905**	**0.850**	0.128	-0.033	**0.766**	**0.565**	**-0.558**	-0.003
Ca^{2+}	-0.513	**0.676**	0.310	**0.800**	-0.503	**0.957**	-0.394	**0.862**	*	**0.933**	**0.984**	0.233	0.027	**0.584**	0.371	-0.377	-0.095
Rb^{+}	-0.455	**0.717**	0.144	**0.684**	-0.437	**0.895**	-0.370	**0.905**	**0.933**	*	**0.903**	0.163	0.004	**0.673**	**0.543**	**-0.558**	-0.181
HCO_3^{-}	-0.521	**0.589**	0.345	**0.789**	**-0.576**	**0.962**	-0.298	**0.850**	**0.984**	**0.903**	*	0.210	-0.042	**0.538**	0.386	-0.385	-0.040
Cl^{-}	-0.171	-0.137	0.348	0.376	-0.047	0.115	0.126	0.128	0.233	0.163	0.210	*	0.435	-0.341	-0.409	0.414	0.089
NO_3^{-}	-0.286	0.077	0.378	0.128	0.258	-0.121	-0.321	-0.033	0.027	0.004	-0.042	0.435	*	-0.186	-0.499	0.506	0.112
SO_4^{2-}	-0.164	**0.859**	-0.128	0.397	-0.131	**0.605**	-0.520	**0.766**	**0.584**	**0.673**	**0.538**	-0.341	-0.186	*	**0.572**	**-0.580**	-0.132
%LHC	0.233	0.455	-0.098	0.103	-0.274	0.484	-0.134	**0.565**	0.371	**0.543**	0.386	-0.409	-0.499	**0.572**	*	**-0.993**	-0.052
%LHS	-0.209	-0.453	0.124	-0.106	0.245	-0.480	0.115	**-0.558**	-0.377	**-0.558**	-0.385	0.414	0.506	**-0.580**	**-0.993**	*	0.167
%LHtotal	0.177	-0.033	0.235	-0.037	-0.216	-0.026	-0.147	-0.003	-0.095	-0.181	-0.040	0.089	0.112	-0.132	-0.052	0.167	*

Table D4. Principal components analysis for Bhote Kosi catchments in which the Lesser Himalayan Formation is absent.

	$^{87}Sr/^{86}Sr$	Sr^{2+}	Temp.	pH	Na^{+}	Mg^{2+}	Si	K^{+}	Ca^{2+}	Rb^{+}	HCO_3^{-}	Cl^{-}	NO_3^{-}	SO_4^{2-}	%TSS	%HHCS
$^{87}Sr/^{86}Sr$	*	**-0.702**	**0.501**	0.171	0.354	**-0.576**	**0.635**	0.046	**-0.726**	-0.127	**-0.520**	**0.520**	0.257	**-0.601**	**-0.930**	**0.930**
Sr^{2+}	**-0.702**	*	-0.072	0.138	0.198	**0.968**	-0.293	0.164	**0.942**	-0.302	**0.668**	-0.236	0.255	**0.972**	**0.811**	**-0.811**
Temp.	**0.501**	-0.072	*	0.414	**0.672**	-0.060	**0.774**	**0.470**	0.021	-0.458	0.306	**0.509**	0.405	-0.100	**-0.484**	**0.484**
pH	0.171	0.138	0.414	*	0.267	0.164	0.207	0.097	0.070	-0.338	0.075	0.018	0.075	0.163	-0.205	0.205
Na^{+}	0.354	0.198	**0.672**	0.267	*	0.294	**0.802**	**0.762**	0.314	-0.304	**0.531**	**0.597**	**0.635**	0.197	-0.284	0.284
Mg^{2+}	**-0.576**	**0.968**	-0.060	0.164	0.294	*	-0.230	0.238	**0.893**	-0.254	**0.599**	-0.217	0.307	**0.990**	**0.695**	**-0.695**
Si	**0.635**	-0.293	**0.774**	0.207	**0.802**	-0.230	*	**0.588**	-0.136	-0.301	0.255	**0.720**	0.459	-0.306	**-0.659**	**0.659**
K^{+}	0.046	0.164	**0.470**	0.097	**0.762**	0.238	**0.588**	*	0.376	0.253	**0.627**	0.403	0.465	0.122	-0.131	0.131
Ca^{2+}	**-0.726**	**0.942**	0.021	0.070	0.314	**0.893**	-0.136	0.376	*	-0.198	**0.864**	-0.196	0.231	**0.863**	**0.782**	**-0.782**
Rb^{+}	-0.127	-0.302	-0.458	-0.338	-0.304	-0.254	-0.301	0.253	-0.198	*	-0.175	-0.256	-0.219	-0.305	-0.003	0.003
HCO_3^{-}	**-0.520**	**0.668**	0.306	0.075	**0.531**	**0.599**	0.255	**0.627**	**0.864**	-0.175	*	0.062	0.247	**0.529**	**0.495**	**-0.495**
Cl^{-}	**0.520**	-0.236	**0.509**	0.018	**0.597**	-0.217	**0.720**	0.403	-0.196	-0.256	0.062	*	**0.752**	-0.246	-0.447	0.447
NO_3^{-}	0.257	0.255	0.405	0.075	**0.635**	0.307	0.459	0.465	0.231	-0.219	0.247	**0.752**	*	0.283	-0.049	0.049
SO_4^{2-}	**-0.601**	**0.972**	-0.100	0.163	0.197	**0.990**	-0.306	0.122	**0.863**	-0.305	**0.529**	-0.246	0.283	*	**0.727**	**-0.727**
%TSS	**-0.930**	**0.811**	**-0.484**	-0.205	-0.284	**0.695**	**-0.659**	-0.131	**0.782**	-0.003	**0.495**	-0.447	-0.049	**0.727**	*	**-1.000**
%HHCS	**0.930**	**-0.811**	**0.484**	0.205	0.284	**-0.695**	**0.659**	0.131	**-0.782**	0.003	**-0.495**	0.447	0.049	**-0.727**	**-1.000**	*

Table D5. Principal components analysis of Bhote Kosi samples collected in September.

	$^{87}Sr/^{86}Sr$	Sr^{2+}	Temp.	pH	Na^{+}	Mg^{2+}	Si	K^{+}	Ca^{2+}	Rb^{+}	HCO_3^{-}	Cl^{-}	NO_3^{-}	SO_4^{2-}	%TSS	%HHCS	%LHC	%LHS	%LHtotal
$^{87}Sr/^{86}Sr$	*	-0.391	0.281	**0.437**	-0.362	0.014	-0.077	0.304	-0.260	0.411	0.062	-0.133	0.156	-0.299	**-0.490**	-0.278	**0.491**	**0.724**	**0.899**
Sr^{2+}	-0.391	*	-0.271	0.054	**0.574**	**0.772**	-0.100	0.041	**0.937**	-0.338	**0.615**	-0.071	-0.024	**0.966**	**0.834**	**-0.603**	-0.211	-0.184	-0.296
Temp.	0.281	-0.271	*	**0.578**	0.125	-0.092	**0.742**	0.266	-0.242	0.013	-0.011	**0.433**	**0.428**	-0.261	**-0.594**	0.299	0.347	0.127	0.361
pH	**0.437**	0.054	**0.578**	*	0.112	0.338	**0.482**	0.390	0.133	0.141	0.344	0.026	0.009	0.105	-0.253	-0.088	0.350	0.178	0.400
Na^{+}	-0.362	**0.574**	0.125	0.112	*	0.409	0.381	0.139	**0.548**	-0.317	0.370	0.121	0.185	**0.560**	0.280	-0.047	-0.226	-0.143	-0.278
Mg^{2+}	0.014	**0.772**	-0.092	0.338	0.409	*	-0.061	**0.564**	**0.818**	0.206	**0.761**	-0.127	-0.001	**0.823**	**0.511**	**-0.678**	0.356	-0.147	0.173
Si	-0.077	-0.100	**0.742**	**0.482**	0.381	-0.061	*	0.255	-0.035	-0.059	0.111	**0.517**	0.210	-0.150	-0.395	0.373	0.149	-0.107	0.040
K^{+}	0.304	0.041	0.266	0.390	0.139	**0.564**	0.255	*	0.289	**0.806**	**0.671**	0.026	0.009	0.052	-0.117	-0.333	**0.751**	-0.091	**0.520**
Ca^{2+}	-0.260	**0.937**	-0.242	0.133	**0.548**	**0.818**	-0.035	0.289	*	-0.093	**0.840**	-0.090	-0.091	**0.862**	**0.819**	**-0.726**	-0.033	-0.156	-0.137
Rb^{+}	0.411	-0.338	0.013	0.141	-0.317	0.206	-0.059	**0.806**	-0.093	*	0.313	-0.186	-0.209	-0.307	-0.246	-0.155	**0.649**	-0.051	**0.469**
HCO_3^{-}	0.062	**0.615**	-0.011	0.344	0.370	**0.761**	0.111	**0.671**	**0.840**	0.313	*	-0.061	-0.104	**0.516**	**0.523**	**-0.749**	0.372	-0.071	0.240
Cl^{-}	-0.133	-0.071	**0.433**	0.026	0.121	-0.127	**0.517**	0.026	-0.090	-0.186	-0.061	*	**0.759**	-0.109	-0.177	0.120	0.182	-0.098	0.072
NO_3^{-}	0.156	-0.024	**0.428**	0.009	0.185	-0.001	0.210	0.009	-0.091	-0.209	-0.104	**0.759**	*	0.031	-0.202	-0.074	0.196	0.241	0.324
SO_4^{2-}	-0.299	**0.966**	-0.261	0.105	**0.560**	**0.823**	-0.150	0.052	**0.862**	-0.307	**0.516**	-0.109	0.031	*	**0.734**	**-0.557**	-0.168	-0.140	-0.231
%TSS	**-0.490**	**0.834**	**-0.594**	-0.253	0.280	**0.511**	-0.395	-0.117	**0.819**	-0.246	**0.523**	-0.177	-0.202	**0.734**	*	**-0.632**	-0.370	-0.240	**-0.459**
%HHCS	-0.278	**-0.603**	0.299	-0.088	-0.047	**-0.678**	0.373	-0.333	**-0.726**	-0.155	**-0.749**	0.120	-0.074	**-0.557**	**-0.632**	*	-0.232	-0.304	-0.398
%LHC	**0.491**	-0.211	0.347	0.350	-0.226	0.356	0.149	**0.751**	-0.033	**0.649**	0.372	0.182	0.196	-0.168	-0.370	-0.232	*	-0.105	**0.704**
%LHS	**0.724**	-0.184	0.127	0.178	-0.143	-0.147	-0.107	-0.091	-0.156	-0.051	-0.071	-0.098	0.241	-0.140	-0.240	-0.304	-0.105	*	**0.632**
%LHtotal	**0.899**	-0.296	0.361	0.400	-0.278	0.173	0.040	**0.520**	-0.137	**0.469**	0.240	0.072	0.324	-0.231	**-0.459**	-0.398	**0.704**	**0.632**	*

Table D6. Principal components analysis of Bhote Kosi samples collected in the dry season.

	$^{87}Sr/^{86}Sr$	Sr^{2+}	Temp.	pH	Na^{+}	Mg^{2+}	Si	K^{+}	Ca^{2+}	Rb^{+}	HCO_3^{-}	%TSS	%HHCS	%LHC	%LHS	%LHtotal
$^{87}Sr/^{86}Sr$	*	**-0.611**	0.141	0.291	**-0.442**	0.213	-0.289	0.253	-0.161	0.229	-0.008	**-0.467**	**-0.682**	**0.721**	**0.298**	**0.725**
Sr^{2+}	**-0.611**	*	-0.267	-0.180	**0.484**	-0.026	0.236	0.027	**0.409**	-0.042	0.169	**0.471**	**0.535**	**-0.352**	**-0.573**	**-0.605**
Temp.	0.141	-0.267	*	0.076	**0.433**	0.112	**0.634**	0.235	0.106	-0.065	0.278	**-0.794**	-0.032	0.256	0.176	**0.299**
pH	0.291	-0.180	0.076	*	**-0.497**	**0.798**	**-0.413**	**0.638**	**0.563**	**0.715**	**0.635**	-0.231	**-0.564**	**0.489**	0.294	**0.546**
Na^{+}	**-0.442**	**0.484**	**0.433**	**-0.497**	*	**-0.423**	**0.936**	-0.249	0.063	**-0.542**	0.011	-0.144	**0.703**	**-0.404**	**-0.382**	**-0.533**
Mg^{2+}	0.213	-0.026	0.112	**0.798**	**-0.423**	*	**-0.359**	**0.868**	**0.775**	**0.903**	**0.861**	**-0.318**	**-0.597**	**0.629**	0.209	**0.603**
Si	-0.289	0.236	**0.634**	**-0.413**	**0.936**	**-0.359**	*	-0.177	0.074	**-0.507**	0.078	**-0.374**	**0.580**	-0.279	-0.237	**-0.352**
K^{+}	0.253	0.027	0.235	**0.638**	-0.249	**0.868**	-0.177	*	**0.742**	**0.835**	**0.810**	**-0.402**	**-0.515**	**0.649**	0.117	**0.564**
Ca^{2+}	-0.161	**0.409**	0.106	**0.563**	0.063	**0.775**	0.074	**0.742**	*	**0.680**	**0.935**	-0.140	-0.149	0.277	-0.069	0.171
Rb^{+}	0.229	-0.042	-0.065	**0.715**	**-0.542**	**0.903**	**-0.507**	**0.835**	**0.680**	*	**0.726**	-0.148	**-0.607**	**0.628**	0.125	**0.553**
HCO_3^{-}	-0.008	0.169	0.278	**0.635**	0.011	**0.861**	0.078	**0.810**	**0.935**	**0.726**	*	**-0.374**	**-0.302**	**0.446**	0.065	**0.378**
%TSS	**-0.467**	**0.471**	**-0.794**	-0.231	-0.144	**-0.318**	**-0.374**	**-0.402**	-0.140	-0.148	**-0.374**	*	**0.347**	**-0.549**	**-0.360**	**-0.630**
%HHCS	**-0.682**	**0.535**	-0.032	**-0.564**	**0.703**	**-0.597**	**0.580**	**-0.515**	-0.149	**-0.607**	**-0.302**	**0.347**	*	**-0.753**	**-0.634**	**-0.947**
%LHC	**0.721**	**-0.352**	0.256	**0.489**	**-0.404**	**0.629**	-0.279	**0.649**	0.277	**0.628**	**0.446**	**-0.549**	**-0.753**	*	0.083	**0.812**
%LHS	**0.298**	**-0.573**	0.176	0.294	**-0.382**	0.209	-0.237	0.117	-0.069	0.125	0.065	**-0.360**	**-0.634**	0.083	*	**0.649**
%LHtotal	**0.725**	**-0.605**	**0.299**	**0.546**	**-0.533**	**0.603**	**-0.352**	**0.564**	0.171	**0.553**	**0.378**	**-0.630**	**-0.947**	**0.812**	**0.649**	*

Table D7. Principal components analysis of samples from the Langtang Khola - Trisuli.

	$^{87}Sr/^{86}Sr$	Sr^{2+}	Temp.	pH	Na^{+}	Mg^{2+}	Si	K^{+}	Ca^{2+}	Rb^{+}	HCO_3^{-}	Cl^{-}	NO_3^{-}	SO_4^{2-}	%TSS	%HHCS	%LHC	%LHS	%LHtotal
$^{87}Sr/^{86}Sr$	*	-0.738	-0.324	-0.461	-0.412	-0.663	0.408	-0.270	-0.864	-0.346	-0.808	-0.407	-0.282	-0.670	-0.699	0.678	-0.586	-0.215	-0.289
Sr^{2+}	-0.738	*	0.327	0.301	0.616	0.983	0.101	0.643	0.919	0.746	0.939	0.609	0.268	0.839	0.763	-0.770	0.739	0.449	0.515
Temp.	-0.324	0.327	*	0.241	0.413	0.363	0.489	-0.045	0.210	0.043	0.320	0.232	-0.201	0.014	0.736	-0.731	0.669	0.342	0.411
pH	-0.461	0.301	0.241	*	0.205	0.243	-0.192	0.046	0.353	0.052	0.421	0.248	-0.157	0.177	0.256	-0.285	0.336	0.343	0.352
Na^{+}	-0.412	0.616	0.413	0.205	*	0.694	0.402	0.391	0.590	0.460	0.700	0.644	0.181	0.494	0.685	-0.710	0.725	0.538	0.589
Mg^{2+}	-0.663	0.983	0.363	0.243	0.694	*	0.225	0.637	0.882	0.731	0.932	0.637	0.253	0.826	0.805	-0.817	0.794	0.504	0.572
Si	0.408	0.101	0.489	-0.192	0.402	0.225	*	0.148	-0.177	0.194	0.030	0.287	-0.139	-0.155	0.301	-0.336	0.400	0.409	0.421
K^{+}	-0.270	0.643	-0.045	0.046	0.391	0.637	0.148	*	0.642	0.936	0.542	0.759	0.677	0.737	0.244	-0.270	0.316	0.313	0.324
Ca^{2+}	-0.864	0.919	0.210	0.353	0.590	0.882	-0.177	0.642	*	0.683	0.931	0.616	0.423	0.905	0.691	-0.697	0.666	0.400	0.461
Rb^{+}	-0.346	0.746	0.043	0.052	0.460	0.731	0.194	0.936	0.683	*	0.622	0.761	0.596	0.707	0.351	-0.371	0.397	0.329	0.351
HCO_3^{-}	-0.808	0.939	0.320	0.421	0.700	0.932	0.030	0.542	0.931	0.622	*	0.650	0.266	0.807	0.787	-0.809	0.811	0.567	0.629
Cl^{-}	-0.407	0.609	0.232	0.248	0.644	0.637	0.287	0.759	0.616	0.761	0.650	*	0.691	0.561	0.496	-0.545	0.633	0.616	0.638
NO_3^{-}	-0.282	0.268	-0.201	-0.157	0.181	0.253	-0.139	0.677	0.423	0.596	0.266	0.691	*	0.457	0.105	-0.108	0.114	0.081	0.090
SO_4^{2-}	-0.670	0.839	0.014	0.177	0.494	0.826	-0.155	0.737	0.905	0.707	0.807	0.561	0.457	*	0.505	-0.505	0.474	0.264	0.310
%TSS	-0.699	0.763	0.736	0.256	0.685	0.805	0.301	0.244	0.691	0.351	0.787	0.496	0.105	0.505	*	-0.993	0.911	0.466	0.561
%HHCS	0.678	-0.770	-0.731	-0.285	-0.710	-0.817	-0.336	-0.270	-0.697	-0.371	-0.809	-0.545	-0.108	-0.505	-0.993	*	-0.955	-0.570	-0.657
%LHC	-0.586	0.739	0.669	0.336	0.725	0.794	0.400	0.316	0.666	0.397	0.811	0.633	0.114	0.474	0.911	-0.955	*	0.788	0.852
%LHS	-0.215	0.449	0.342	0.343	0.538	0.504	0.409	0.313	0.400	0.329	0.567	0.616	0.081	0.264	0.466	-0.570	0.788	*	0.994
%LHtotal	-0.289	0.515	0.411	0.352	0.589	0.572	0.421	0.324	0.461	0.351	0.629	0.638	0.090	0.310	0.561	-0.657	0.852	0.994	*

Table D8. Principal components analysis of samples from the Khumbu region.

	$^{87}Sr/^{86}Sr$	Sr^{2+}	Temp.	pH	Na^{+}	Mg^{2+}	Si	K^{+}	Ca^{2+}	Rb^{+}	HCO_3^{-}	Cl^{-}	NO_3^{-}	SO_4^{2-}	%TSS	%HHCS	%Granite
$^{87}Sr/^{86}Sr$	*	-0.532	-0.122	0.342	0.505	-0.152	-0.105	0.085	-0.186	-0.299	-0.661	0.407	-0.066	-0.634	0.185	0.219	-0.257
Sr^{2+}	-0.532	*	-0.546	**-0.737**	-0.501	0.457	-0.172	0.129	**0.697**	0.259	0.414	-0.522	-0.209	**0.917**	0.144	-0.478	0.473
Temp.	-0.122	-0.546	*	0.374	-0.211	-0.236	0.278	-0.532	-0.394	-0.244	-0.098	-0.054	0.022	-0.516	-0.492	0.203	-0.132
pH	0.342	**-0.737**	0.374	*	0.068	**-0.823**	0.319	-0.310	**-0.711**	0.130	-0.389	0.087	0.638	**-0.807**	0.040	0.372	-0.392
Na^{+}	0.505	-0.501	-0.211	0.068	*	-0.049	0.028	0.579	-0.426	0.024	-0.405	**0.733**	-0.307	-0.336	0.175	0.067	-0.098
Mg^{2+}	-0.152	0.457	-0.236	**-0.823**	-0.049	*	-0.516	0.084	**0.814**	-0.622	0.459	0.062	-0.439	0.603	-0.228	-0.248	0.293
Si	-0.105	-0.172	0.278	0.319	0.028	-0.516	*	-0.451	**-0.706**	0.597	-0.590	-0.431	0.378	-0.379	-0.566	0.213	-0.131
K^{+}	0.085	0.129	-0.532	-0.310	0.579	0.084	-0.451	*	0.082	0.213	0.164	**0.679**	-0.554	0.334	**0.748**	-0.330	0.223
Ca^{2+}	-0.186	**0.697**	-0.394	**-0.711**	-0.426	**0.814**	**-0.706**	0.082	*	-0.486	0.580	-0.156	-0.308	**0.744**	0.137	-0.368	0.361
Rb^{+}	-0.299	0.259	-0.244	0.130	0.024	-0.622	0.597	0.213	-0.486	*	-0.271	-0.308	0.129	0.112	0.239	-0.149	0.117
HCO_3^{-}	-0.661	0.414	-0.098	-0.389	-0.405	0.459	-0.590	0.164	0.580	-0.271	*	0.050	0.014	0.638	0.139	-0.011	-0.011
Cl^{-}	0.407	-0.522	-0.054	0.087	**0.733**	0.062	-0.431	**0.679**	-0.156	-0.308	0.050	*	-0.316	-0.241	0.368	0.061	-0.122
NO_3^{-}	-0.066	-0.209	0.022	0.638	-0.307	-0.439	0.378	-0.554	-0.308	0.129	0.014	-0.316	*	-0.331	-0.289	0.504	-0.477
SO_4^{2-}	-0.634	**0.917**	-0.516	**-0.807**	-0.336	0.603	-0.379	0.334	**0.744**	0.112	0.638	-0.241	-0.331	*	0.210	-0.547	0.534
%TSS	0.185	0.144	-0.492	0.040	0.175	-0.228	-0.566	**0.748**	0.137	0.239	0.139	0.368	-0.289	0.210	*	-0.312	0.164
%HHCS	0.219	-0.478	0.203	0.372	0.067	-0.248	0.213	-0.330	-0.368	-0.149	-0.011	0.061	0.504	-0.547	-0.312	*	**-0.988**
%Granite	-0.257	0.473	-0.132	-0.392	-0.098	0.293	-0.131	0.223	0.361	0.117	-0.011	-0.122	-0.477	0.534	0.164	**-0.988**	*

Table D9. Principal components analysis for the full data set from this study.

	$^{87}Sr/^{86}Sr$	Sr^{2+}	Temp.	pH	Na^{+}	Mg^{2+}	Si	K^{+}	Ca^{2+}	Rb^{+}	HCO_3^{-}	Cl^{-}	NO_3^{-}	SO_4^{2-}	%TSS	%HHCS	%LHC	%LHS	%LHtotal
$^{87}Sr/^{86}Sr$	*	**-0.243**	**0.210**	**0.415**	**-0.302**	0.202	-0.085	**0.331**	-0.077	**0.336**	0.153	-0.133	-0.072	-0.154	**-0.319**	**-0.567**	**0.714**	**0.422**	**0.778**
Sr^{2+}	**-0.243**	*	0.019	0.029	**0.393**	**0.579**	0.002	0.047	**0.839**	-0.109	**0.427**	-0.027	0.049	**0.950**	**0.765**	**-0.306**	-0.136	-0.162	-0.196
Temp.	**0.210**	0.019	*	**0.479**	**0.405**	**0.242**	**0.636**	**0.318**	0.202	0.119	**0.431**	**0.389**	0.201	-0.069	-0.096	**-0.313**	**0.329**	**0.226**	**0.377**
pH	**0.415**	0.029	**0.479**	*	-0.084	**0.594**	0.086	**0.552**	**0.362**	**0.552**	**0.628**	0.037	-0.083	0.048	-0.067	**-0.555**	**0.539**	**0.340**	**0.600**
Na^{+}	**-0.302**	**0.393**	**0.405**	-0.084	*	0.050	**0.775**	0.023	**0.344**	**-0.296**	**0.230**	**0.551**	**0.282**	**0.275**	0.171	0.184	**-0.250**	-0.190	**-0.297**
Mg^{2+}	0.202	**0.579**	**0.242**	**0.594**	0.050	*	-0.070	**0.686**	**0.813**	**0.598**	**0.834**	-0.070	0.033	**0.621**	**0.306**	**-0.672**	**0.532**	0.129	**0.472**
Si	-0.085	0.002	**0.636**	0.086	**0.775**	-0.070	*	0.110	0.100	-0.184	**0.235**	**0.604**	**0.218**	-0.127	-0.186	0.181	-0.040	-0.051	-0.059
K^{+}	**0.331**	0.047	**0.318**	**0.552**	0.023	**0.686**	0.110	*	**0.455**	**0.854**	**0.753**	0.136	0.198	0.038	-0.123	**-0.522**	**0.676**	0.173	**0.605**
Ca^{2+}	-0.077	**0.839**	0.202	**0.362**	**0.344**	**0.813**	0.100	**0.455**	*	**0.298**	**0.832**	0.015	0.056	**0.751**	**0.624**	**-0.529**	0.177	-0.020	0.120
Rb^{+}	**0.336**	-0.109	0.119	**0.552**	**-0.296**	**0.598**	-0.184	**0.854**	**0.298**	*	**0.612**	-0.062	0.055	-0.089	-0.118	**-0.523**	**0.664**	0.185	**0.603**
HCO_3^{-}	0.153	**0.427**	**0.431**	**0.628**	**0.230**	**0.834**	**0.235**	**0.753**	**0.832**	**0.612**	*	0.107	0.066	**0.332**	**0.262**	**-0.631**	**0.500**	0.152	**0.461**
Cl^{-}	-0.133	-0.027	**0.389**	0.037	**0.551**	-0.070	**0.604**	0.136	0.015	-0.062	0.107	*	**0.570**	-0.125	-0.125	0.114	-0.061	0.024	-0.031
NO_3^{-}	-0.072	0.049	0.201	-0.083	**0.282**	0.033	**0.218**	0.198	0.056	0.055	0.066	**0.570**	*	0.017	-0.084	-0.008	0.035	0.067	0.065
SO_4^{2-}	-0.154	**0.950**	-0.069	0.048	**0.275**	**0.621**	-0.127	0.038	**0.751**	-0.089	**0.332**	-0.125	0.017	*	**0.651**	**-0.296**	-0.081	-0.122	-0.131
%TSS	**-0.319**	**0.765**	-0.096	-0.067	0.171	**0.306**	-0.186	-0.123	**0.624**	-0.118	**0.262**	-0.125	-0.084	**0.651**	*	**-0.333**	**-0.280**	-0.197	**-0.323**
%HHCS	**-0.567**	**-0.306**	**-0.313**	**-0.555**	0.184	**-0.672**	0.181	**-0.522**	**-0.529**	**-0.523**	**-0.631**	0.114	-0.008	**-0.296**	**-0.333**	*	**-0.629**	**-0.541**	**-0.785**
%LHC	**0.714**	-0.136	**0.329**	**0.539**	**-0.250**	**0.532**	-0.040	**0.676**	0.177	**0.664**	**0.500**	-0.061	0.035	-0.081	**-0.280**	**-0.629**	*	0.119	**0.815**
%LHS	**0.422**	-0.162	**0.226**	**0.340**	-0.190	0.129	-0.051	0.173	-0.020	0.185	0.152	0.024	0.067	-0.122	-0.197	**-0.541**	0.119	*	**0.672**
%LHtotal	**0.778**	-0.196	**0.377**	**0.600**	**-0.297**	**0.472**	-0.059	**0.605**	0.120	**0.603**	**0.461**	-0.031	0.065	-0.131	**-0.323**	**-0.785**	**0.815**	**0.672**	*

Appendix E

Mass Balance Calculations

List of tables.

Table E1. Mass balance calculation of contributions from atmospheric, evaporite, silicate and carbonate sources to total dissolved strontium in monolithologic rivers of the Bhote Kosi basin. These results were further used to define the endpoints shown in fig. 4.24 and fig. 4.25 and in the calculations for the Bhote Kosi illustrated in table 4.3 and fig. 4.27.

					Sr contributions (micromol/litre)						
	Na^+	Ca^{2+}	Sr^{2+}	Cl^-	Evap	Sil	Sil*	Carb	Atm	Evap	Evap*
TSS											
BKT3	58.09	975.98	2.097	4.26	0.007	0.077		0.643	**0.99**	**0.89**	
HHCS											
L6	82.04	172.27	0.245	11.13	0.017	0.101		0.105	7.89	7.05	
BK48	73.97	94.86	0.192	3.76	0.006	0.100		0.054	9.87	3.26	
Mean									**8.88**	**5.15**	
St Dev									1.40	2.68	
LHF (dry season)											
BK82	33.42	833.13	0.791	1.77	0.001	0.045	0.026	0.207	2.59	0.39	0.42
BK93	37.99	125.29	0.034	2.00	0.001	0.051	0.030	0.030	~~37.95~~	~~0.86~~	~~1.17~~
BK94	23.34	766.28	0.267	2.50	0.001	0.030	0.017	0.191	7.30	0.60	0.63
BK90	25.20	866.29	0.167	33.50	0.019	0.000	0.000	0.217	11.18	7.20	7.20
BK87	6.68	420.20	0.124	0.00	0.000	0.010	0.006	0.105	14.45	0.00	0.00
BK88	26.12	590.17	0.151	32.12	0.018	0.000	0.000	0.148	12.21	9.69	9.69
BK96	23.86	269.26	0.093	6.21	0.004	0.025	0.015	0.066	18.35	3.05	3.42
BK95	49.88	127.96	0.071	26.65	0.015	0.033	0.019	0.031	22.77	14.84	17.98
BK131	52.10	66.89	0.058	0.00	0.000	0.074	0.043	0.014	26.65	0.00	0.00
BK97	33.81	176.75	0.092	0.00	0.000	0.048	0.028	0.042	18.67	0.00	0.00
BK129	24.80	326.31	0.219	0.00	0.000	0.035	0.021	0.080	18.67	0.00	0.00
Mean									**15.28**	**3.58**	**3.93**
St Dev									7.22	5.25	6.02
LHF (September)											
BK59	26.28	743.37	0.274	0.03	0.000	0.037	0.022	0.185	7.12	0.01	0.01
BK61	53.92	309.47	0.038	4.41	0.003	0.071	0.041	0.075	~~35.69~~	~~1.09~~	~~1.36~~
BK68	23.19	258.82	0.085	7.18	0.004	0.023	0.013	0.064	19.88	3.61	4.04
BK69	36.08	262.64	0.117	8.58	0.005	0.039	0.023	0.064	15.20	3.83	4.52
Mean									**14.07**	**2.49**	**2.85**
St Dev									6.46	2.15	2.48
LHF (all)									**15.00**	**3.32**	**3.69**
St Dev									6.81	4.65	5.33

* Denotes calculations in which a Na/Sr ratio of 1200 is used for the silicate contribution (see section 4.6.3).

** Assuming that all Sr unaccounted by mass balance is derived from carbonate (see section 4.6.5).

Sr contributions (%)					Total Sr (micromol/litre)		% of	% of	$^{87}Sr/^{86}Sr$	$1/[Sr^{2+}]$
Sil	Sil*	Carb	Carb*	Carb**	Predicted	Predicted*	measured	measured*		
10.47		**87.64**		**95.59**	0.748		35.67		**0.720252**	**0.477**
41.69		43.37			0.245		99.88		0.740622	4.080
56.51		30.35			0.181		94.41		0.735118	5.217
49.10		**36.86**							**0.737870**	**4.648**
10.48		9.20							0.004	0.804
17.41	10.97	79.61	86.02		0.274	0.255	34.63	32.25	0.859310	1.264
~~38.87~~	~~30.68~~	~~22.32~~	~~30.20~~		0.103	0.082	300.26	237.86	~~1.252681~~	~~29.129~~
12.45	7.69	79.66	84.38		0.243	0.230	90.99	86.34	0.844200	3.749
0.00	0.00	81.62	81.62		0.257	0.257	154.18	154.18	0.833300	5.996
7.14	4.32	78.40	81.23		0.135	0.131	108.83	105.63	0.803231	8.046
0.00	0.00	78.10	78.10		0.187	0.187	123.92	123.92	0.861569	6.620
21.62	14.18	56.98	64.05		0.116	0.106	124.31	113.08	0.873754	10.699
32.35	22.86	30.05	36.40		0.100	0.086	140.73	121.32	0.894672	14.038
61.66	55.35	11.70	18.00		0.110	0.079	189.48	135.84	0.964589	17.298
43.26	32.42	38.07	48.91		0.112	0.092	122.18	100.19	0.856156	10.929
24.89	16.64	56.44	64.69		0.137	0.122	62.47	55.73		4.568
22.08	**16.44**	**59.06**	**64.34**						**0.865642**	**8.321**
19.55	17.03	25.01	23.12						0.045	5.040
15.68	9.84	77.19	83.03		0.243	0.227	88.74	83.04	*0.849515*	*3.651*
~~30.70~~	~~22.36~~	~~32.51~~	~~40.58~~		0.169	0.140	447.04	369.15	0.917047	26.431
20.17	13.14	56.34	62.94		0.112	0.102	132.21	120.95	0.863322	11.817
30.71	21.10	50.26	59.19		0.129	0.113	110.49	96.52	0.887311	8.534
22.19	**14.69**	**61.26**	**68.39**						**0.879299**	**12.608**
7.72	5.79	14.12	12.82						0.029617	9.807
22.10	**16.04**	**59.57**	**65.27**						**0.865911**	**8.553**
17.23	14.96	22.43	20.77						0.040	6.563

	Na^+	Ca^{2+}	Sr^{2+}	Cl^-	Sr contributions (micromol/litre) Evap	Sil	Sil*	Carb	Atm	Evap	Evap*
TSS											
BKT3	58	976	2.10	4	0.007	0.077		0.643	0.99	0.89	
NAG34	563	1367	5.58	458	0.704	0.151		0.897	0.38	40.04	
Mean									**0.68**	**20.46**	
St Dev									0.44	27.68	
HHCS											
L6	82	172	0.25	11	0.017	0.101		0.105	7.89	7.05	
Ev9	56	101	0.07	10	0.015	0.066		0.061	~~22.27~~	~~8.08~~	
BK48	74	95	0.19	4	0.006	0.100		0.054	9.87	3.26	
KN95	175	67	0.23	11	0.017	0.234		0.023	9.13	5.61	
KN102	230	159	0.28	23	0.035	0.296		0.078	7.50	7.99	
Mo84			0.16								
Mean									**8.60**	**5.98**	
St Dev									1.10	2.06	
LHF											
BK82	33	833	0.79	2	0.001	0.045	0.026	0.207	2.59	0.39	0.42
BK93	38	125	0.03	2	0.001	0.051	0.030	0.030	~~37.95~~	~~0.86~~	~~1.17~~
BK94	23	766	0.27	2	0.001	0.030	0.017	0.191	7.30	0.60	0.63
BK90	25	866	0.17	34	0.019	0.000	0.000	0.217	11.18	7.20	7.20
BK87	7	420	0.12	0	0.000	0.010	0.006	0.105	14.45	0.00	0.00
BK88	26	590	0.15	32	0.018	0.000	0.000	0.148	12.21	9.69	9.69
BK96	24	269	0.09	6	0.004	0.025	0.015	0.066	18.35	3.05	3.42
BK95	50	128	0.07	27	0.015	0.033	0.019	0.031	22.77	14.84	17.98
BK131	52	67	0.06	0	0.000	0.074	0.043	0.014	26.65	0.00	0.00
BK97	34	177	0.09	0	0.000	0.048	0.028	0.042	18.67	0.00	0.00
MO107	267	248	0.50	19	0.011	0.354	0.207	0.050	4.20	2.51	3.89
MO110			0.64								
MO125	203	138	0.20	21	0.012	0.260	0.152	0.025	10.50	3.61	5.68
MO100	245	140	0.30	17	0.010	0.326	0.190	0.024	7.00	2.52	4.05
NAG3	87	578	0.54	68	0.039	0.027	0.016	0.144	3.89	17.82	18.84
94-12			0.20								
NH7			0.30								
Lisni Khola	74	252		19							
Unnamed K	75	156	0.10	17	0.010	0.083	0.048	0.036	21.88	5.90	8.06
Talkoti Ghat	41	92		21							
Dungri Khola	47	546	0.17	19	0.011	0.040	0.023	0.135	12.35	5.12	5.62
Bailu Ghat	90	359	0.39	28	0.016	0.089	0.052	0.087	5.38	7.92	9.81
Dil Ghat	24	696	0.17	26	0.015	0.000	0.000	0.174	12.21	6.90	6.90
Jidear Khola	70	781	0.84	21	0.012	0.070	0.041	0.193	2.51	4.26	4.76
Taru Ghat	71	292	0.18								
Jiuli Ghat	42	773	0.27	32	0.018	0.014	0.008	0.193	7.87	7.48	7.68
Kalanga G	52	714	0.24	32	0.018	0.029	0.017	0.178	8.94	7.42	7.84
Nayagari G	38	928	0.16	38	0.022	0.000	0.000	0.232	13.38	7.41	7.41
Dhung Ghat	67	906	0.28	38	0.022	0.041	0.024	0.225	7.45	6.97	7.42
Mean									**11.44**	**5.53**	**6.24**
St Dev									6.76	4.63	5.05

Sr contributions (%)					Total Sr (micromol/litre)		% of	% of		
Sil	Sil*	Carb	Carb*	Carb**	Predicted	Predicted*	measured	measured*	$^{87}Sr/^{86}Sr$	$1/[Sr^{2+}]$
10.47		87.64		95.59	0.748		35.67		0.720252	0.477
8.56		51.03		84.44	1.773		31.78		0.716811	0.179
9.52		**69.33**		**90.01**					**0.718531**	**0.328**
1.35		25.89		7.89					0.002	0.211
41.69		43.37			0.245		99.88		0.740622	4.080
~~36.13~~		~~33.52~~			0.163		222.79		0.751119	13.644
56.51		30.35			0.181		94.41		0.735118	5.217
77.70		7.56			0.295		128.26		0.739971	4.348
66.80		17.71			0.430		153.75		0.742865	3.571
									0.751755	6.250
60.67		**24.75**							**0.743575**	**6.185**
15.33		15.53							0.007	3.774
17.41	10.97	79.61	86.02		0.274	0.255	34.63	32.25	0.859310	1.264
~~38.87~~	~~30.68~~	~~22.32~~	~~30.20~~		0.103	0.082	300.26	237.86	~~1.252681~~	~~29.129~~
12.45	7.69	79.66	84.38		0.243	0.230	90.99	86.34	0.844200	3.749
0.00	0.00	81.62	81.62		0.257	0.257	154.18	154.18	0.833300	5.996
7.14	4.32	78.40	81.23		0.135	0.131	108.83	105.63	0.803231	8.046
0.00	0.00	78.10	78.10		0.187	0.187	123.92	123.92	0.861569	6.620
21.62	14.18	56.98	64.05		0.116	0.106	124.31	113.08	0.873754	10.699
32.35	22.86	30.05	36.40		0.100	0.086	140.73	121.32	0.894672	14.038
61.66	55.35	11.70	18.00		0.110	0.079	189.48	135.84	0.964589	17.298
43.26	32.42	38.07	48.91		0.112	0.092	122.18	100.19	0.856156	10.929
81.84	74.12	11.46	17.79		0.436	0.288	87.15	57.62	0.806902	2.000
									0.777690	1.563
78.24	71.80	7.64	12.02		0.318	0.210	159.20	105.03	0.793888	5.000
84.37	79.13	6.11	9.83		0.380	0.244	126.68	81.44	0.803140	3.333
12.45	7.68	65.84	69.60		0.231	0.219	42.69	40.60	0.759260	1.852
									0.785173	5.000
									0.789914	3.333
									0.789141	
50.31	40.11	21.92	29.96		0.150	0.115	155.91	119.95	0.973603	10.417
									0.953543	
18.85	12.08	63.68	69.95		0.207	0.190	121.74	111.94	0.984027	5.882
43.82	31.68	42.87	53.13		0.212	0.175	54.42	44.95	1.040463	2.564
0.00	0.00	80.89	80.89		0.210	0.210	122.07	122.07	0.810372	5.814
24.83	16.21	68.40	76.52		0.296	0.267	35.43	31.93	0.735234	1.198
									0.978062	5.682
5.84	3.50	78.82	80.95		0.246	0.240	92.26	90.03	0.789636	3.745
11.60	7.14	72.05	76.08		0.245	0.233	104.41	99.34	0.811170	4.255
0.00	0.00	79.21	79.21		0.275	0.275	174.98	174.98	0.794235	6.369
13.30	8.26	72.27	76.88		0.309	0.292	109.64	103.52	0.753807	3.546
28.24	**22.70**	**54.79**	**59.61**						**0.847144**	**5.777**
27.61	25.65	27.90	26.53						0.081	4.036

Table E2 (previous page).

Mass balance calculation of contributions from atmospheric, evaporite, silicate and carbonate sources to total dissolved strontium in monolithologic rivers sampled in this work and by Galy *et al.* (1999) and English *et al.* (2000). These results were further used to define the endpoints shown in fig. 4.26 and in the calculations for rivers other than the Bhote Kosi illustrated in table 4.3 and fig. 4.27.

* Denotes calculations in which a Na/Sr ratio of 1200 is used for the silicate contribution (see section 4.6.3).

** Assuming that all Sr unaccounted by mass balance is derived from carbonate (see section 4.6.5).

Table E3 (following page).

Mass balance calculation of contributions from atmospheric, evaporite, silicate and carbonate sources to total dissolved strontium in monolithologic rivers sampled in this work but not used for subsequent calculations in section 4.6.8. of chapter 4.

Sample	Na^+	Ca^{2+}	Sr^{2+}	Cl^-	Sr contribution (µmol/l) Evap	Sil	Carb	Sr contribution (%) Atm	Evap	Sil	Carb	Carb**	Predicted Sr (µmol/l)	% of measured	$^{87}Sr/^{86}Sr$	$1/[Sr^{2+}]$
TSS																
BKT2	361.56	1805.62	5.419	2.01	0.003	0.514	1.156	0.39	0.18	30.59	68.84	90.26	1.694	31.25	0.722031	0.185
HHCS																
L14	76.77	352.73	0.735	24.96	0.038	0.074	0.228	2.78	10.96	21.12	65.14		0.362	49.23	0.738478	1.361
L15	43.89	244.32	0.405	1.59	0.002	0.060	0.157	4.93	1.06	26.10	67.91		0.241	59.59	0.738062	2.472
L31	46.42	235.16	0.309	1.90	0.003	0.064	0.151	6.36	1.26	27.40	64.98		0.238	77.07	0.737213	3.234
L12	71.44	283.00	0.366	3.43	0.005	0.097	0.180	5.43	1.77	32.58	60.22		0.303	82.86	0.736847	2.734
L30	34.84	153.16	0.191	0.84	0.001	0.049	0.098	9.89	0.79	29.69	59.64		0.168	88.03	0.738803	5.226
L16	51.08	207.16	0.271	1.38	0.002	0.071	0.131	7.18	0.96	32.21	59.65		0.226	83.12	0.738084	3.684
L17	63.14	201.31	0.267	3.52	0.005	0.085	0.126	7.30	2.31	36.41	53.97		0.238	89.24	0.738651	3.752
L19	64.34	174.10	0.258	4.69	0.007	0.085	0.108	7.52	3.33	39.29	49.85		0.222	85.82	0.739793	3.874
L32	41.80	132.15	0.194	0.00	0.000	0.060	0.083	9.75	0.00	37.89	52.36		0.163	83.97	0.740298	5.144
L8	71.09	154.23	0.229	7.65	0.012	0.091	0.094	8.41	5.48	42.19	43.93		0.218	95.21	0.740349	4.372
L6	82.04	172.27	0.245	11.13	0.017	0.101	0.105	7.89	7.05	41.69	43.37		0.245	99.88	0.740655	4.080
L11	44.42	160.84	0.216	3.79	0.006	0.058	0.102	8.86	3.21	31.93	56.01		0.187	86.38	0.744096	4.627
L29	20.41	217.47	0.139	0.00	0.000	0.029	0.142	13.16	0.00	14.77	72.07		0.192	138.82	0.738461	7.215
L10	62.39	241.77	0.150	25.32	0.039	0.053	0.156	12.26	13.77	18.73	55.25		0.269	179.01	0.735315	6.651
L18	59.86	6.95	0.078	6.59	0.010	0.076	0.000	21.30	9.25	69.46	0.00		0.107	138.19	0.755327	12.886
L20	59.86	31.18	0.081	0.00	0.000	0.086	0.013	20.66	0.00	69.00	10.33		0.119	147.99	0.764872	12.403
Ev9	55.91	101.29	0.073	9.62	0.015	0.066	0.061	22.27	8.08	36.13	33.52		0.163	222.79	0.751185	13.644
BK103	326.60	275.87	0.412	52.20	0.080	0.392	0.147	4.85	12.33	60.20	22.62		0.641	155.43	0.737761	2.426
BK53	389.60	680.77	0.708	9.25	0.014	0.543	0.403	2.88	1.44	54.93	40.75		0.982	138.74	0.733821	1.413
BK102	377.49	456.82	0.475	42.86	0.066	0.478	0.260	4.23	7.85	56.95	30.96		0.825	173.65	0.736420	2.105
BK107	337.95	473.11	0.470	38.29	0.059	0.428	0.275	4.27	7.40	53.75	34.58		0.783	166.60	0.737510	2.126
BK106	263.33	206.75	0.308	51.95	0.080	0.302	0.110	6.39	15.22	57.51	20.88		0.513	166.55	0.740369	3.249
BK52	14.28	89.87	0.133	2.62	0.004	0.017	0.058	13.64	4.41	18.20	63.76		0.100	75.21	0.736972	7.518
BK50	61.77	116.82	0.161	0.00	0.000	0.088	0.070	11.53	0.00	49.44	39.02		0.179	111.06	0.737052	6.209
BK47	444.17	198.87	0.486	71.95	0.111	0.532	0.083	4.14	14.63	70.27	10.96		0.746	153.44	0.734363	2.056

Sample	X_{Ca}	Na^+/Sr^{2+}	
BK48	48.66	385.90	Catchments draining only the
BK50	57.07	383.50	HHCS
BK52	82.75	107.35	
Ev9	56.06	762.86	
L8	57.17	310.82	
L10	68.52	414.94	
L11	63.61	205.53	
L12	66.59	195.34	
L15	65.99	108.48	
L16	67.47	188.18	
L17	64.55	236.91	
L18	**8.07**	**771.40**	
L19	60.80	249.24	
L20	**22.92**	**742.44**	
L29	81.38	147.23	
L30	70.57	182.08	
L31	69.10	150.09	
L32	64.15	215.01	
BK61	66.68	1425.05	Catchments draining only the
BK95	47.13	700.22	LHF silicate metasediments
L22	**16.36**	**811.19**	

Table E4. X_{Ca} (Ca^{2+} as a % of total cations) and Na^+/Sr^{2+} of catchments draining only the High Himalayan Crystalline Series and the silicate metasediments of the Lesser Himalayan Formation. Carbonate-free chemistry is approached in those catchments where X_{Ca} is less than 30% (Galy *et al.*, 1999), which are shown in bold.

Sample	CaO (wt. %)	Sr (ppm)	Ca/Sr		
BK13a	49.5	41.9	8436		Pure limestones
BK16	44.3	34.6	9142		
BK127e	50.8	45.1	8053	Mean	
BK127f	53.3	48.8	7806	**8360**	
BK15	23.2	59.6	2782		Most pure dolomites
BK56(4)	20.6	69.2	2124		
BK56(5)	22.4	67.5	2372		
BK124a	24.6	39.8	4419		
Bk124c	23.5	31.6	5322	Mean	
Bk124d	21.2	26.0	5819	**3806**	

Table E5. Ca/Sr ratios of limestones and the purest dolomites collected from the Lesser Himalaya of the Bhote Kosi catchment.

Appendix F

Results of Laser Ablation

Sample	Unit	*Whole rock* $^{87}Sr/^{86}Sr$	*Rb/Sr*	Normalised $^{87}Sr/^{86}Sr$	Propagated error	Norm. Rb/Sr (+/- 50%)
BK11-1	**LHF**	*0.930212*	*0.2834*	0.934799	± 0.0256	0.000084
BK11-2				0.933161	± 0.0188	0.000859
BK11-3				0.930531	± 0.0458	0.000148
BK11-4				0.931195	± 0.0208	0.000134
BK11-5				0.934365	± 0.0198	0.000188
BK11-6				0.934896	± 0.0183	0.000303
BK12c-1	**LHF**	*1.111401*	*6.3088*	1.101952	± 0.0704	0.007542
BK12c-2				1.093425	± 0.1037	0.003992
BK12c-3				1.102495	± 0.0467	0.000944
BK12c-4				1.116392	± 0.0197	0.000460
BK12c-5				1.108480	± 0.0548	0.001159
T29d-1	**HHCS**	*0.713452*	*0.1867*	0.714938	± 0.0102	0.005779
T29d-2				0.714905	± 0.0103	0.000280
T29d-3				0.715017	± 0.0095	0.000383
T29d-4				0.715108	± 0.0097	0.000905
T29d-5				0.715091	± 0.0102	0.005961

Table F1. Results of laser ablation multi collector inductively coupled plasma mass spectrometry carried out on carbonate from calc-salicate rocks of the Bhote Kosi catchment.

Appendix G

Standard and Sample Repeat Data.

List of tables.

Table G1a. Ion chromatograph data for anion standards (1998).

	Measured values (ppm)			Difference from expected (%)		
Standard	**Cl^-**	**NO_3^-**	**SO_4^{2-}**	**Cl^-**	**NO_3^-**	**SO_4^{2-}**
1	1.898	1.002	1.994	5.111	0.184	0.308
1	1.977	0.972	2.035	1.136	2.772	1.740
1	2.089	1.003	2.040	4.450	0.300	2.000
2	4.833	2.537	5.061	3.349	1.466	1.212
2	4.860	2.535	5.007	2.809	1.402	0.138
2	4.881	2.508	4.992	2.380	0.320	0.160
3	9.998	4.892	10.007	0.020	2.160	0.070
3	10.065	5.029	10.199	0.653	0.579	1.988
3	10.002	4.982	10.087	0.020	0.360	0.870
4	15.010	7.533	15.154	0.069	0.445	1.027
4	14.923	7.483	15.295	0.515	0.233	1.968
4	14.909	7.610	14.960	0.607	1.467	0.267
5	20.190	10.013	20.947	0.947	0.134	4.737
5	19.995	9.875	20.445	0.027	1.249	2.226
5	19.974	9.900	20.015	0.130	1.000	0.075
			Mean	**1.482**	**0.938**	**1.252**

Standard	**Cl^-**	**NO_3^-**	**SO_4^{2-}**	**Mean**
1	1.988	0.992	2.023	
2	4.858	2.527	5.020	
3	10.022	4.968	10.098	
4	14.947	7.542	15.136	
5	20.053	9.930	20.469	

Standard	**Cl^-**	**NO_3^-**	**SO_4^{2-}**	**SD**
1	0.096	0.017	0.025	
2	0.024	0.016	0.036	
3	0.038	0.070	0.096	
4	0.055	0.064	0.168	
5	0.119	0.074	0.467	

Standard	**Cl^-**	**NO_3^-**	**SO_4^{2-}**	**%SD**
1	4.832	1.755	1.250	
2	0.500	0.637	0.719	
3	0.377	1.401	0.954	
4	0.368	0.851	1.112	
5	0.593	0.742	2.280	

Table G1b. Ion chromatograph data for anion standards (1999).

	Measured values (ppm)			Difference from expected (%)		
Standard	**Cl^-**	**NO_3^-**	**SO_4^{2-}**	**Cl^-**	**NO_3^-**	**SO_4^{2-}**
1	1.989	0.963	2.002	0.550	3.700	0.100
1	1.956	1.008	2.011	2.200	0.800	0.550
1	1.912	0.976	2.005	4.400	2.400	0.250
2	4.778	2.424	4.890	4.440	3.040	2.200
2	5.063	2.411	4.921	1.260	3.560	1.580
2	4.788	2.393	4.770	4.240	4.280	4.600
3	9.899	4.973	9.881	1.010	0.540	1.190
3	9.707	4.968	9.885	2.930	0.640	1.150
3	9.265	4.913	9.615	7.350	1.740	3.850
4	15.188	7.791	15.595	1.253	3.880	3.967
4	15.177	7.498	15.143	1.180	0.027	0.953
4	15.166	7.506	15.003	1.107	0.080	0.020
5	21.033	10.310	20.518	5.165	3.100	2.590
5	20.867	10.063	20.169	4.335	0.630	0.845
5	19.974	9.910	20.348	0.130	0.900	1.740
			Mean	**2.770**	**1.954**	**1.706**

Standard	**Cl^-**	**NO_3^-**	**SO_4^{2-}**	**Mean**
1	1.952	0.982	2.006	
2	4.876	2.409	4.860	
3	9.624	4.951	9.794	
4	15.177	7.598	15.247	
5	20.625	10.094	20.345	

Standard	**Cl^-**	**NO_3^-**	**SO_4^{2-}**	**SD**
1	0.039	0.023	0.005	
2	0.162	0.016	0.080	
3	0.325	0.033	0.155	
4	0.011	0.167	0.309	
5	0.570	0.202	0.175	

Standard	**Cl^-**	**NO_3^-**	**SO_4^{2-}**	**%SD**
1	1.979	2.358	0.228	
2	3.317	0.646	1.641	
3	3.378	0.672	1.580	
4	0.072	2.197	2.029	
5	2.762	1.999	0.858	

Table G2. Standard and sample repeats run by ICP-MS (units are ppm except Sr and Rb which are in ppb).

Sample	Na	Mg	Si	K	Ca	Rb	Sr
AN1	4.189	2.360	4.393	1.511	15.500	2.807	61.38
AN1	4.063	2.263	4.184	1.455	15.650	2.757	59.32
AN1	4.138	2.333	4.406	1.495	15.830	2.779	60.28
AN1	4.128	2.102	4.048	1.394	14.190	2.798	59.31
AN1	4.127	2.131	4.096	1.379	14.050	2.739	58.47
AN1	4.191	2.336	4.370	1.533	15.910	2.817	62.12
AN1	4.159	2.319	4.274	1.510	15.940	2.807	61.62
AN1	4.253	2.379	4.415	1.511	16.040	2.826	61.44
AN1	4.031	2.181	4.251	1.440	14.520	2.817	60.60
AN1	4.104	2.180	4.227	1.424	14.490	2.810	59.47
AN1	4.064	2.213	4.380	1.480	14.910	2.838	60.18
AN1	4.203	2.374	4.408	1.479	15.120	2.783	60.20
AN1	4.096	2.097	4.068	1.394	14.130	2.760	58.56
AN1	4.120	2.125	4.107	1.396	14.300	2.748	59.40
Mean	**4.133**	**2.242**	**4.259**	**1.457**	**15.041**	**2.792**	**60.168**
SD	**0.061**	**0.107**	**0.139**	**0.053**	**0.757**	**0.031**	**1.150**
%SD	**1.485**	**4.769**	**3.260**	**3.611**	**5.033**	**1.114**	**1.912**
SK2	3.281	2.701	4.700	1.501	13.400	3.312	39.70
SK2	3.348	2.674	4.633	1.494	13.230	3.277	39.78
SK2	3.256	2.511	4.358	1.430	12.830	3.218	38.87
SK2	3.270	2.604	4.515	1.458	13.050	3.248	39.19
SK2	3.228	2.560	4.510	1.463	13.140	3.233	39.47
SK2	3.245	2.517	4.386	1.443	12.810	3.216	38.79
Mean	**3.271**	**2.595**	**4.517**	**1.465**	**13.077**	**3.251**	**39.30**
SD	**0.042**	**0.080**	**0.134**	**0.028**	**0.230**	**0.038**	**0.419**
%SD	**1.281**	**3.080**	**2.961**	**1.906**	**1.760**	**1.155**	**1.065**
TN1	3.019	2.003	4.965	1.227	9.149	2.145	21.88
TN1	2.961	1.926	4.734	1.200	9.445	2.133	21.65
TN1	2.949	1.910	4.643	1.206	9.748	2.153	21.94
TN1	2.987	1.966	4.676	1.191	9.493	2.132	21.61
TN1	3.023	1.972	4.747	1.213	9.265	2.132	22.21
TN1	3.043	1.999	4.784	1.206	9.747	2.113	21.88
TN1	3.018	1.967	4.685	1.176	9.618	2.111	21.54
Mean	**3.000**	**1.963**	**4.748**	**1.203**	**9.495**	**2.131**	**21.82**
SD	**0.035**	**0.035**	**0.107**	**0.016**	**0.230**	**0.015**	**0.233**
%SD	**1.167**	**1.762**	**2.255**	**1.347**	**2.424**	**0.719**	**1.067**

Table G2 (cont.)

Sample	Na	Mg	Si	K	Ca	Rb	Sr
NIST1630(10X)	2.929	0.554	0.391	0.091	0.778	12.92	0.211
NIST1630(10X)	2.910	0.565	0.397	0.091	0.816	13.07	0.206
NIST1630(10X)	3.041	0.627	0.483	0.092	0.589	13.29	0.191
NIST1630(10X)	2.851	0.542	0.369	0.095	0.821	13.22	0.212
NIST1630(10X)	2.923	0.562	0.391	0.093	0.809	13.00	0.211
NIST1630(10X)	2.909	0.562	0.413	0.101	0.798	13.36	0.218
NIST1630(10X)	3.048	0.614	0.477	0.081	0.552	12.92	0.181
NIST1630(10X)	3.085	0.620	0.486	0.087	0.586	13.66	0.182
NIST1630(10X)	3.014	0.618	0.475	0.088	0.563	13.16	0.189
NIST1630(10X)	2.971	0.573	0.400	0.093	0.817	13.17	0.214
NIST1630(10X)	2.620	0.530	0.377	0.075	0.644	11.39	0.183
NIST1630(10X)	2.953	0.604	0.475	0.096	0.602	13.27	0.205
Mean	**2.938**	**0.581**	**0.428**	**0.090**	**0.698**	**13.036**	**0.20**
SD	**0.121**	**0.034**	**0.047**	**0.007**	**0.116**	**0.558**	**0.014**
%SD	**4.131**	**5.816**	**10.914**	**7.689**	**16.598**	**4.277**	**6.957**
SLRS-4	2.129	1.517	1.898	0.605	5.595	1.476	26.94
SLRS-4	2.092	1.356	1.740	0.554	5.305	1.430	25.97
SLRS-4	2.107	1.475	1.793	0.582	5.762	1.458	26.82
SLRS-4	2.153	1.523	1.889	0.613	5.785	1.475	27.00
SLRS-4	2.148	1.508	1.832	0.603	5.875	1.466	27.24
SLRS-4	2.090	1.320	1.666	0.538	5.211	1.433	25.72
SLRS-4	2.071	1.420	1.825	0.567	5.370	1.441	25.81
SLRS-4	2.089	1.392	1.745	0.552	5.308	1.444	25.78
SLRS-4	2.145	1.369	1.767	0.557	5.322	1.438	25.95
SLRS-4	2.117	1.473	1.854	0.601	5.822	1.436	27.02
Mean	**2.114**	**1.431**	**1.795**	**0.574**	**5.504**	**1.451**	**26.36**
SD	**0.031**	**0.077**	**0.075**	**0.027**	**0.252**	**0.018**	**0.623**
%SD	**1.443**	**5.365**	**4.163**	**4.711**	**4.571**	**1.232**	**2.362**

Table G2 (cont.)

Sample	Na	Mg	Si	K	Ca	Rb	Sr
L32	1.221	0.570	1.704	0.696	6.163	1.313	18.37
L32	1.236	0.564	1.675	0.704	6.184	1.328	18.42
L32	1.219	0.574	1.677	0.703	6.395	1.343	18.35
L32	1.224	0.563	1.689	0.729	6.298	1.370	18.80
L32	1.238	0.577	1.710	0.734	6.451	1.390	18.68
L32	1.261	0.588	1.725	0.715	6.515	1.419	18.51
L32	1.294	0.605	1.759	0.730	6.391	1.418	18.39
L32	1.279	0.587	1.715	0.711	6.358	1.525	18.29
L32	1.239	0.581	1.709	0.704	6.301	1.468	18.02
L32	1.229	0.574	1.724	0.689	6.115	1.458	17.75
L32	1.234	0.559	1.636	0.679	6.129	1.474	17.95
L32	1.238	0.557	1.612	0.683	6.181	1.449	17.74
L32	1.244	0.559	1.647	0.683	6.100	1.460	17.92
L32	1.240	0.548	1.620	0.669	6.006	1.443	17.72
Mean	**1.243**	**0.572**	**1.686**	**0.702**	**6.256**	**1.418**	**18.21**
SD	**0.022**	**0.015**	**0.044**	**0.020**	**0.152**	**0.062**	**0.356**
%SD	**1.735**	**2.646**	**2.582**	**2.888**	**2.425**	**4.367**	**1.955**

Table G3. Accuracy of ICP-MS standard analyses.

NIST 1640	**Na**	**Mg**	**Si**	**K**	**Ca**	**Sr**	**Rb**
Published	29.350	5.819	4.730	0.994	7.045	124.200	2.000
Published (diluted)	3.424	0.679	0.552	0.116	0.822	14.490	0.233
	2.929	0.554	0.391	0.091	0.778	12.92	0.211
	2.910	0.565	0.397	0.091	0.816	13.07	0.206
	3.041	0.627	0.483	0.092	0.589	13.29	0.191
	2.851	0.542	0.369	0.095	0.821	13.22	0.212
	2.923	0.562	0.391	0.093	0.809	13.00	0.211
	2.909	0.562	0.413	0.101	0.798	13.36	0.218
	3.048	0.614	0.477	0.081	0.552	12.92	0.181
	3.085	0.620	0.486	0.087	0.586	13.66	0.182
	3.014	0.618	0.475	0.088	0.563	13.16	0.189
	2.971	0.573	0.400	0.093	0.817	13.17	0.214
	2.620	0.530	0.377	0.075	0.644	11.39	0.183
	2.953	0.604	0.475	0.096	0.602	13.27	0.205
Mean difference from certified value (%)	**14.205**	**14.460**	**22.480**	**22.185**	**15.092**	**10.037**	**14.145**

SLRS-4	**Na**	**Mg**	**Si**	**K**	**Ca**	**Sr**	**Rb**
Published	2.40	1.60		0.68	6.20	26.30	
	2.172	1.548	1.937	0.617	5.709	27.490	1.506
	2.135	1.384	1.776	0.565	5.413	26.500	1.459
	2.150	1.505	1.830	0.594	5.880	27.367	1.488
	2.197	1.554	1.928	0.625	5.903	27.551	1.505
	2.192	1.539	1.869	0.615	5.995	27.796	1.496
	2.133	1.347	1.700	0.549	5.317	26.245	1.462
	2.113	1.449	1.862	0.578	5.480	26.337	1.470
	2.132	1.420	1.781	0.563	5.416	26.306	1.473
	2.189	1.397	1.803	0.568	5.431	26.480	1.467
	2.160	1.503	1.892	0.614	5.941	27.571	1.465
Mean difference from certified value (%)	**10.115**	**8.463**		**13.414**	**8.896**	**2.568**	

Table G3 (cont.)

Multi element standard	**Na**	**Mg**	**Si**	**K**	**Ca**	**Sr**	**Rb**	
Dulution 1	0.508	0.508		0.509	0.509	4.999		Calculated
	0.501	0.518		0.519	0.485	4.989		
	0.499	0.498		0.514	0.499	5.028		
	0.485	0.506		0.515	N/A	4.940		
Dilution 2	0.999	0.999		1.000	1.001	9.827		Calculated
	0.993	1.014		1.011	0.999	9.878		
	1.009	1.009		0.996	0.961	9.823		
	0.991	1.018		1.012	0.962	10.020		
Dilution 3	1.967	1.967		1.968	1.971	19.341		Calculated
	1.959	1.980		1.961	1.954	19.180		
	1.990	1.990		1.976	1.901	19.610		
	1.933	1.942		1.958	1.930	19.220		
Dilution 4	4.928	4.929		4.932	4.939	48.468		Calculated
	4.978	4.869		4.882	4.930	48.710		
	4.926	4.959		4.887	4.898	47.860		
	4.972	4.836		4.916	5.030	48.290		
Dilution 5	9.767	9.768		9.774	9.788	96.051		Calculated
	9.749	9.817		9.794	9.893	96.020		
	9.767	9.771		9.790	9.948	96.360		
	9.758	9.841		9.778	10.230	96.190		
Mean difference from calculated value (%)	**1.041**	**1.125**		**0.709**	**2.249**	**0.664**		

High concentration calcium standard	**Na**	**Mg**	**Si**	**K**	**Ca**	**Sr**	**Rb**	
					52.197			Calculated
					52.180			
					52.180			
					52.120			
Mean difference from calculated value (%)					**0.071**			

Table G3 (cont.)

Rb standard	Na	Mg	Si	K	Ca	Sr	Rb	
Dulution 1							0.261	Calculated
							0.248	
							0.258	
							0.264	
Dilution 2							0.508	Calculated
							0.506	
							0.505	
							0.509	
Dilution 3							0.996	Calculated
							1.011	
							0.993	
							0.983	
Dilution 4							2.010	Calculated
							2.045	
							2.051	
							2.009	
Dilution 5							5.025	Calculated
							4.874	
							4.881	
							4.804	
Mean difference from calculated value (%)							**1.709**	

Table G4a. Repeat XRF (major element) analyses.

wt. %	Expected	WS-E	WS-E	WS-E	WS-E	WS-E	WS-E	WS-E	WS-E	WS-E	WS-E	WS-E	WS-E	WS-E
SiO_2	**51.1**	51.13	51.34	51.23	51.13	51.26	51.28	51.11	51.20	51.15	51.19	51.31	51.26	51.02
TiO_2	**2.4**	2.428	2.442	2.425	2.447	2.459	2.442	2.445	2.452	2.453	2.440	2.403	2.418	2.458
Al_2O_3	**13.78**	13.77	13.89	13.9	13.94	13.88	13.88	13.67	13.74	13.91	13.86	13.8	13.77	13.70
Fe_2O_3	**13.15**	13.23	13.2	13.26	13.23	13.34	13.32	13.37	13.36	13.32	13.32	13.19	13.2	13.26
MnO	**0.171**	0.171	0.169	0.171	0.171	0.169	0.171	0.174	0.171	0.173	0.169	0.169	0.167	0.173
MgO	**5.55**	5.59	5.6	5.57	5.59	5.63	5.61	5.62	5.61	5.62	5.59	5.66	5.63	5.64
CaO	**8.95**	9.07	9.07	9.11	9.07	9.16	9.16	9.18	9.17	9.18	9.13	8.97	8.97	9.08
Na_2O	**2.47**	2.45	2.45	2.43	2.44	2.49	2.48	2.47	2.47	2.47	2.52	2.44	2.41	2.50
K2O	**1**	1	1.01	1	1.01	1.01	1.01	1.01	1.01	1.00	1.00	0.98	0.98	1.00
P_2O_5	**0.3**	0.304	0.309	0.31	0.307	0.303	0.304	0.313	0.311	0.304	0.305	0.3	0.297	0.306
LOI	**0.85**	0.85	0.85	0.85	0.85	0.84	0.84	0.84	0.84	0.84	0.84	0.86	0.86	0.85

										Reproducibility			Accuracy	
wt. %	WS-E	WS-E	WS-E	WS-E	WS-E	WS-E	WS-E	WS-E	WS-E	Mean	SD	%SD	Mean diff. from exp.	%
SiO_2	51.13	51.15	50.95	51.181	51.131	51.16	51.3	51.2	51.13	**51.18**	**0.093**	**0.18**	**0.10**	**0.20**
TiO_2	2.446	2.443	2.438	2.385	2.407	2.407	2.414	2.398	2.42	**2.43**	**0.021**	**0.87**	**0.032**	**1.33**
Al_2O_3	13.80	13.97	13.96	13.799	13.785	13.68	13.73	13.95	13.96	**13.83**	**0.097**	**0.70**	**0.09**	**0.65**
Fe_2O_3	13.21	13.19	13.19	13.035	13.122	13.2	13.19	13.22	13.18	**13.23**	**0.080**	**0.60**	**0.10**	**0.73**
MnO	0.171	0.171	0.168	0.166	0.169	0.169	0.17	0.168	0.171	**0.170**	**0.002**	**1.15**	**0.002**	**0.93**
MgO	5.62	5.61	5.57	5.594	5.581	5.6	5.59	5.6	5.59	**5.60**	**0.022**	**0.40**	**0.05**	**0.99**
CaO	9.06	9.07	9	9.078	9.105	9.01	9.01	9.03	9.01	**9.08**	**0.066**	**0.73**	**0.13**	**1.41**
Na_2O	2.48	2.47	2.44	2.459	2.432	2.43	2.43	2.42	2.44	**2.46**	**0.028**	**1.15**	**0.03**	**1.05**
K2O	1.00	1	0.99	1.004	1.015	1	0.99	1	1.01	**1.00**	**0.010**	**0.95**	**0.01**	**0.70**
P_2O_5	0.300	0.302	0.31	0.309	0.308	0.306	0.306	0.304	0.301	**0.305**	**0.004**	**1.32**	**0.006**	**1.89**
LOI	0.85	0.85	0.85	0.85	0.85	0.85	0.85	0.85	0.85	**0.85**	**0.006**	**0.69**	**0.00**	**0.32**

Table G4a (cont.)

wt. %	Expected	OUG94	OUG94	OUG94	OUG94	OUG94	OUG94	OUG94	OUG94	OUG94	OUG94	OUG94	OUG94	OUG94
SiO_2	**69.95**	69.91	69.89	69.68	69.69	69.78	69.70	69.92	69.76	69.80	69.68	69.82	69.7	69.65
TiO_2	**0.314**	0.318	0.317	0.319	0.321	0.317	0.316	0.319	0.318	0.317	0.319	0.314	0.314	0.322
Al_2O_3	**14.66**	14.53	14.64	14.72	14.74	14.59	14.61	14.42	14.48	14.65	14.62	14.47	14.48	14.42
Fe_2O_3	**3.050**	3	3	3.01	3.02	3.03	3.04	3.04	3.04	3.04	3.04	3.04	3.03	3.01
MnO	**0.075**	0.076	0.075	0.076	0.075	0.074	0.078	0.076	0.076	0.076	0.075	0.077	0.076	0.076
MgO	**1.04**	1.03	1.04	1.01	1.03	1.02	1.02	1.04	1.04	1.04	1.02	1.03	1.04	1.04
CaO	**1.34**	1.38	1.36	1.36	1.37	1.37	1.37	1.37	1.36	1.39	1.37	1.33	1.35	1.36
Na_2O	**4.6**	4.64	4.68	4.65	4.66	4.68	4.67	4.67	4.72	4.66	4.66	4.56	4.6	4.69
K2O	**2.96**	2.98	2.97	2.98	2.99	2.99	3.00	2.99	3.02	2.99	3.02	2.96	2.96	2.95
P_2O_5	**0.165**	0.169	0.161	0.165	0.166	0.163	0.167	0.173	0.170	0.172	0.167	0.169	0.166	0.172
LOI	**1.97**	1.97	1.97	1.97	1.97	2.04	2.04	2.04	2.04	2.04	2.04	1.97	1.97	1.97

										Reproducibility			Accuracy	
wt. %	OUG94	OUG94	OUG94	OUG94	OUG94	OUG94	OUG94	OUG94	OUG94	Mean	SD	%SD	Mean diff. from exp.	%
SiO_2	69.79	69.83	69.69	70.26	70.27	69.75	69.85	69.67	69.57	**69.80**	**0.175**	**0.25**	**0.20**	**0.29**
TiO_2	0.320	0.319	0.318	0.310	0.311	0.311	0.308	0.317	0.320	**0.317**	**0.004**	**1.18**	**0.00**	**1.29**
Al_2O_3	14.52	14.70	14.73	14.61	14.66	14.42	14.44	14.69	14.63	**14.58**	**0.109**	**0.75**	**0.11**	**0.72**
Fe_2O_3	3.01	3.02	3.00	2.97	2.96	3.02	3.00	3.00	3.00	**3.01**	**0.023**	**0.77**	**0.035**	**1.16**
MnO	0.077	0.077	0.078	0.074	0.074	0.077	0.076	0.075	0.076	**0.076**	**0.001**	**1.52**	**0.001182**	**1.58**
MgO	1.04	1.04	1.03	1.06	1.07	1.05	1.04	1.03	1.03	**1.04**	**0.014**	**1.38**	**0.01**	**1.01**
CaO	1.36	1.35	1.37	1.36	1.37	1.36	1.36	1.35	1.34	**1.36**	**0.012**	**0.92**	**0.02**	**1.68**
Na_2O	4.67	4.68	4.64	4.73	4.67	4.64	4.64	4.60	4.64	**4.66**	**0.037**	**0.79**	**0.06**	**1.30**
K2O	2.96	2.98	2.95	2.99	2.97	2.98	2.95	2.98	2.97	**2.98**	**0.020**	**0.66**	**0.02**	**0.72**
P_2O_5	0.166	0.168	0.170	0.164	0.165	0.167	0.165	0.166	0.166	**0.167**	**0.003**	**1.80**	**0.003**	**1.68**
LOI	1.97	1.97	1.97	1.97	1.97	1.97	1.97	1.97	1.97	**1.99**	**0.032**	**1.60**	**0.02**	**0.97**

Table G4a (cont.)

wt. %	BK66	BK66	Mean	SD	%SD
SiO_2	72.83	72.82	**72.83**	**0.007**	**0.01**
TiO_2	0.7	0.687	**0.694**	**0.009**	**1.33**
Al_2O_3	12.43	12.27	**12.35**	**0.113**	**0.92**
Fe_2O_3	4.59	4.56	**4.58**	**0.021**	**0.46**
MnO	0.062	0.063	**0.063**	**0.001**	**1.13**
MgO	1.82	1.81	**1.82**	**0.007**	**0.39**
CaO	1.21	1.22	**1.22**	**0.007**	**0.58**
Na_2O	1.55	1.53	**1.54**	**0.014**	**0.92**
K2O	3.1	3.03	**3.07**	**0.049**	**1.61**
P_2O_5	0.17	0.164	**0.167**	**0.004**	**2.54**
LOI	2.29	2.29	**2.29**	**0.000**	**0.00**

wt. %	SK1	SK1	Mean	SD	%SD
SiO_2	76.53	75.86	**76.20**	**0.474**	**0.62**
TiO_2	0.44	0.422	**0.431**	**0.013**	**2.95**
Al_2O_3	10.99	10.91	**10.95**	**0.057**	**0.52**
Fe_2O_3	4.02	3.95	**3.99**	**0.049**	**1.24**
MnO	0.084	0.079	**0.082**	**0.004**	**4.34**
MgO	1.33	1.29	**1.31**	**0.028**	**2.16**
CaO	1.82	1.77	**1.80**	**0.035**	**1.97**
Na_2O	1.65	1.61	**1.63**	**0.028**	**1.74**
K2O	2.5	2.49	**2.50**	**0.007**	**0.28**
P_2O_5	0.127	0.125	**0.126**	**0.001**	**1.12**
LOI	1.32	1.32	**1.32**	**0.000**	**0.00**

Table G4b. Repeat XRF (trace element) analyses.

Sample: BHVO-1

ppm	Expected												
Rb	**11**	9.9	9.3	9.6	10	10	9	9.9	10.0	9.8	9.4	9.4	9.3
Sr	**403**	402	407	406	406	406	407	405	403	403	407	403	404
Y	**27.6**	28.2	28.5	29.2	28.8	29	30.5	28.1	29	28.7	26.9	28.6	28.9
Zr	**179**	175	177	176	176	180	180	177	176	174	177	175	178
Nb	**19.0**	19.3	18.7	18.9	18.9	19.2	19.2	18.6	19.5	19.4	19.2	18.8	19.5
Ba	**139**	152	150	143	137	146	151	146	145	150	151	151	148
Pb	**2.6**	2	2	3	4	5	1	2	2	0	1	4	2
Th	**1.08**	2	0	2	3	2	2	3	2	2	2	2	3
U	**0.42**	1	0	1	1	2	0	1	0	0	0	2	1
Sc	**31.8**	35	33	33	33	35	35	35	34	36	33	31	33
V	**317**	318	310	320	314	326	327	324	315	320	318	322	307
Cr	**289**	287	286	289	288	292	293	292	291	294	289	292	289
Co	**45**	51	51	50	49	38	40	49	51	53	49	50	48
Ni	**121**	118	121	118	121	125	125	119	120	118	122	118	123
Cu	**136**	139	144	141	142	137	140	140	136	138	137	138	141
Zn	**105**	108	108	111	111	110	110	111	107	109	109	111	112
Ga	**21**	22	22	23	21	21	21	22	22	22	23	21	20
Mo	**1.02**	0	0	0	0	0	0	0	0	0	0	0	0
As	**0.40**	0	0	0	2	0	4	5	0	1	0	0	0
S	**102**	170	176	170	171	172	172	167	166	165	166	165	162

Sample: QLO-1

ppm	Expected												
Rb	**74**	73.7	74.5	74.5	74.5	75	75	73.6	73.3	73.9	74.4	73.5	74.2
Sr	**336**	334	335	337	337	333	336	337	336	337	337	333	334
Y	**24.0**	25.6	24.7	25.4	25.9	25.1	25.4	25.6	25	25.4	25.6	25.8	25.7
Zr	**185**	189	189	189	190	192	191	189	189	190	190	189	191
Nb	**10.3**	11	10.4	10.5	10.8	10.2	10.2	10.8	11	10.9	11.1	11.2	10.6
Ba	**1370**	1392	1384	1370	1349	1378	1380	1375	1374	1381	1375	1383	1415
Pb	**20.4**	17	19	19	20	19	18	18	16	19	19	18	18
Th	**4.5**	4	4	6	5	4	5	5	6	4	5	3	4
U	**1.94**	3	3	2	1	2	4	3	2	2	0	1	1
Sc	**8.9**	10	10	10	7	8	6	10	10	9	8	10	7
V	**54**	55	51	46	55	52	48	51	51	45	48	47	49
Cr	**3.2**	4	4	6	6	5	5	5	6	7	4	6	5
Co	**7.2**	15	15	16	15	12	11	13	14	15	18	13	14
Ni	**5.8**	1	5	3	4	7	5	5	3	6	4	5	5
Cu	**29**	28	29	30	29	27	28	29	29	28	30	28	29
Zn	**61**	61	61	61	62	60	62	61	63	62	62	63	64
Ga	**17**	16	17	16	17	16	17	17	16	17	16	17	16
Mo	**2.6**	1	1	2	1	1	1	1	2	2	2	3	2
As	**3.5**	3	4	5	4	4	6	8	1	4	2	2	3
S	**30**	100	99	100	94	92	88	94	90	93	96	88	89

								Reproducibility			Accuracy	
								Mean	SD	%SD	Mean diff. from exp.	%
9.2	10.3	9.7	10.8	10.5	9.3	10.1	9.4	**9.7**	**0.47**	**4.82**	**1.26**	**11.41**
402	402	405	406	405	403	402	407	**404**	**1.97**	**0.49**	**1.97**	**0.49**
28.1	28.9	28.4	28.8	28.2	28.2	28.5	28.5	**29**	**0.67**	**2.34**	**1.07**	**3.88**
177	177	178	179	177	176	177	177	**177**	**1.54**	**0.87**	**2.24**	**1.25**
18.3	19.3	19.2	19.3	20.0	19.5	19.6	20.2	**19.2**	**0.45**	**2.35**	**0.41**	**2.16**
137	147	148	157	152	147	156	147	**148**	**5.21**	**3.52**	**8.69**	**6.25**
7	6	5	1	3	2	3	3	**3**	**1.83**	**64.23**	**1.43**	**54.81**
1	1	1	2	0	0	1	2	**2**	**0.94**	**56.76**	**0.91**	**83.89**
0	0	2	3	1	2	0	2	**1**	**0.99**	**106.50**	**0.88**	**209.76**
32	36	31	33	31	32	29	33	**33**	**1.82**	**5.50**	**1.42**	**4.45**
311	322	319	315	330	316	317	323	**319**	**5.84**	**1.83**	**4.78**	**1.51**
289	290	291	290	290	289	287	292	**290**	**2.13**	**0.74**	**1.84**	**0.64**
49	51	47	48	49	49	51	47	**48**	**3.59**	**7.42**	**4.66**	**10.36**
118	117	120	121	119	118	116	120	**120**	**2.49**	**2.08**	**2.27**	**1.87**
137	139	139	142	138	142	136	141	**139**	**2.23**	**1.60**	**3.43**	**2.52**
111	112	112	112	114	111	114	112	**111**	**1.80**	**1.62**	**5.78**	**5.50**
21	22	22	21	21	22	20	22	**22**	**0.81**	**3.76**	**0.73**	**3.45**
0	0	1	0	0	0	0	1	**0**	**0.31**	**307.79**	**0.92**	**90.20**
0	0	4	0	0	4	5	2	**1**	**1.86**	**137.22**	**1.37**	**341.25**
165	157	162	155	157	159	161	153	**165**	**6.28**	**3.82**	**62.55**	**61.32**

								Reproducibility			Accuracy	
								Mean	SD	%SD	Mean diff. from exp.	%
73.7	74.1	73.8	74.2	75.3	74	74.1	75.5	**74.2**	**0.60**	**0.81**	**0.49**	**0.66**
334	335	334	336	334.9	337.2	334	336	**335**	**1.39**	**0.41**	**1.22**	**0.36**
25.3	25.5	26.2	25.1	24.3	25.4	25.6	25	**25**	**0.43**	**1.69**	**1.38**	**5.75**
189	189	191	192	191	191	191	189	**190**	**1.14**	**0.60**	**4.41**	**2.38**
11.3	11.3	11.5	10.6	10.7	11.0	11.4	11.4	**10.9**	**0.40**	**3.63**	**0.62**	**5.97**
1378	1353	1366	1373	1376	1374	1378	1393	**1377**	**13.72**	**1.00**	**10.70**	**0.78**
21	20	18	17	17	19	17	17	**18**	**1.18**	**6.46**	**2.19**	**10.74**
6	5	6	6	6	5	6	6	**5**	**0.93**	**18.65**	**0.91**	**20.22**
1	2	4	3	2	2	3	2	**2**	**1.02**	**47.66**	**0.77**	**39.69**
10	7	10	9	7	8	7	8	**8**	**1.33**	**15.69**	**1.08**	**12.13**
48	44	50	50	52	45	48	52	**49**	**3.00**	**6.10**	**4.83**	**8.94**
5	7	6	6	6	7	5	7	**6**	**0.96**	**17.19**	**2.36**	**73.59**
12	14	11	12	10	13	13	12	**13**	**1.86**	**13.91**	**6.17**	**85.69**
3	4	4	6	3	4	4	5	**4**	**1.32**	**30.65**	**1.65**	**28.45**
28	28	28	31	29	26	29	29	**29**	**1.08**	**3.77**	**0.82**	**2.83**
64	65	65	65	64	64	63	65	**63**	**1.60**	**2.55**	**2.02**	**3.31**
18	17	16	17	17	17	17	16	**17**	**0.55**	**3.29**	**0.49**	**2.85**
3	3	3	2	2	2	3	2	**2**	**0.72**	**36.82**	**0.84**	**32.12**
3	4	4	2	5	2	5	5	**4**	**1.55**	**40.67**	**1.26**	**35.86**
89	88	88	84	94	88	93	90	**92**	**4.45**	**4.85**	**61.85**	**206.17**

Table G4b (cont.)

Sample: DNC-1

ppm	Expected												
Rb	**4.5**	4.2	4.4	3.9	3.5	4	4	4.7	3.7	4.3	3.8	4.6	3.7
Sr	**145**	147	148	148	148	148	149	147	147	147	149	148	147
Y	**18.0**	19.8	18.8	19.9	19.6	20.2	19.5	18.8	18.9	19.7	19.2	19.9	19.7
Zr	**41**	41	39	41	40	41	41	40	41	40	40	41	41
Nb	**3.0**	2.2	3.3	2.3	2.1	2.4	2.1	2.5	2.3	2.6	2.5	2.8	3
Ba	**114**	114	108	108	104	107	107	108	110	115	112	113	103
Pb	**6.3**	8	7	6	7	7	7	7	6	5	8	5	7
Th	**0.20**	0	2	0	-1	0	0	1	1	2	0	0	0
U	**0.10**	0	2	1	0	0	1	-1	1	1	1	1	1
Sc	**31.0**	28	31	30	32	26	33	33	33	27	33	30	32
V	**148**	144	150	149	146	148	143	145	148	148	147	148	147
Cr	**285**	273	274	271	272	277	270	274	276	272	274	273	274
Co	**54.7**	68	63	63	63	51	51	66	66	65	65	63	65
Ni	**247**	248	249	247	248	257	258	248	248	249	247	252	249
Cu	**96**	98	98	98	98	95	95	93	95	94	94	96	97
Zn	**66**	69	71	69	69	70	68	68	68	69	69	71	70
Ga	**15**	12	15	15	15	15	15	13	14	14	14	14	15
Mo	**0.7**	0	0	0	0	0	0	0	0	0	0	0	0
As	**0.2**	5	0	1	1	0	5	0	2	0	0	2	0
S	**392**	434	425	425	423	433	426	423	423	426	442	432	434

Sample: W-2

ppm	Expected												
Rb	**20**	20.6	20.8	21.5	19.6	20	21	20.8	19.9	19.9	19.9	21.4	20.2
Sr	**194**	199	200	201	200	199	198	200	199	201	200	200	199
Y	**24.0**	21.9	22.9	22.8	23.1	22.6	21.8	22.7	23.7	22.4	22.2	23.2	23.2
Zr	**94**	93	93	95	94	95	95	92	95	93	93	93	95
Nb	**7.9**	8	7.1	7.9	8	8.4	8	7.8	7.9	8.2	7	8	8.3
Ba	**182**	185	166	177	177	181	176	177	177	182	177	177	177
Pb	**9.3**	7	7	6	8	6	6	6	7	7	5	7	8
Th	**2.2**	1	3	4	1	4	1	3	3	1	1	4	2
U	**0.53**	0	1	2	0	1	2	1	3	0	0	0	0
Sc	**35**	36	35	37	32	37	39	38	33	38	39	39	39
V	**262**	263	259	263	266	269	268	255	265	267	262	268	263
Cr	**93**	95	97	96	96	98	95	96	96	93	99	95	96
Co	**44**	52	50	49	48	39	38	49	46	50	53	50	52
Ni	**70**	67	70	67	67	74	72	68	66	68	67	68	70
Cu	**103**	107	106	107	105	104	104	101	105	103	103	103	106
Zn	**77**	78	81	82	81	78	80	81	79	81	80	81	83
Ga	**20**	18	18	19	19	17	19	19	19	18	17	17	18
Mo	**0.6**	0	0	0	0	0	0	0	0	0	0	0	0
As	**1.24**	2	3	0	0	0	0	0	2	0	0	5	0
S	**79**	216	210	213	214	216	212	206	206	206	207	202	205

								Reproducibility			Accuracy	
								Mean	SD	%SD	Mean diff. from exp.	%
4.3	5	4.2	4.6	4.5	4	4.1	4	**4**	**0.38**	**9.12**	**0.42**	**9.22**
148	148	148	148	147.5	148.1	146	147	**148**	**0.68**	**0.46**	**2.79**	**1.92**
18.8	18.5	18.0	19.6	18.1	19.8	19.1	19.5	**19.3**	**0.62**	**3.22**	**1.27**	**7.06**
40	40	42	40	40	41	39	41	**40**	**0.78**	**1.94**	**0.69**	**1.68**
2.7	2.9	2.4	2.9	1.6	3.1	3.2	3.1	**2.6**	**0.44**	**16.93**	**0.47**	**15.67**
108	110	111	118	109	103	108	114	**110**	**3.97**	**3.62**	**4.97**	**4.36**
5	8	5	8	5	6	4	6	**6**	**1.18**	**18.93**	**1.03**	**16.35**
0	1	1	0	2	1	0	0	**0**	**0.70**	**146.16**	**0.53**	**265.00**
0	0	0	0	0	1	0	0	**0**	**0.65**	**157.85**	**0.52**	**520.00**
34	29	30	28	28	30	32	31	**31**	**2.28**	**7.48**	**1.61**	**5.19**
147	145	144	149	149	151	152	144	**147**	**2.43**	**1.65**	**1.97**	**1.33**
273	273	276	273	271	275	274	274	**273**	**1.79**	**0.66**	**11.64**	**4.08**
65	64	68	64	63	63	66	63	**63**	**4.48**	**7.08**	**9.30**	**17.00**
252	247	251	252	250	250	249	249	**250**	**3.03**	**1.21**	**3.02**	**1.22**
93	98	98	98	97	97	96	97	**96**	**1.83**	**1.91**	**1.59**	**1.66**
72	73	71	69	70	72	70	70	**70**	**1.47**	**2.10**	**3.82**	**5.78**
13	14	14	16	14	14	17	14	**14**	**1.03**	**7.18**	**0.99**	**6.57**
0	0	0	0	0	0	0	0	**0**	**0.00**		**0.70**	**100.00**
1	0	2	0	1	0	0	1	**1**	**1.56**	**143.48**	**1.08**	**537.50**
432	429	425	409	411	429	424	428	**427**	**7.49**	**1.76**	**34.65**	**8.84**

								Reproducibility			Accuracy	
								Mean	SD	%SD	Mean diff. from exp.	%
21.5	20.6	20.5	20.9	20.3	21.5	20.7	20.9	**20.6**	**0.59**	**2.85**	**0.70**	**3.48**
198	197	199	200	200.4	199	199	200	**199**	**0.92**	**0.46**	**5.45**	**2.81**
23.4	24.1	23.6	23.5	23.4	23.1	23.1	23.4	**23**	**0.60**	**2.61**	**1.01**	**4.19**
92	92	95	94	95	96	95	94	**94**	**1.20**	**1.28**	**1.02**	**1.08**
7.8	7.1	8.0	7.8	9.2	8.7	8.1	8.3	**8.0**	**0.52**	**6.47**	**0.36**	**4.56**
182	176	169	180	179	175	177	180	**177**	**4.20**	**2.37**	**4.95**	**2.72**
8	10	7	7	8	9	5	8	**7**	**1.26**	**17.88**	**2.31**	**24.78**
4	2	4	3	3	2	3	4	**3**	**1.21**	**45.64**	**1.10**	**50.00**
3	1	3	1	2	1	2	0	**1**	**1.08**	**98.53**	**0.94**	**178.11**
37	37	35	35	38	36	36	37	**37**	**1.95**	**5.33**	**2.13**	**6.09**
266	263	264	256	263	262	262	271	**264**	**4.07**	**1.54**	**3.40**	**1.30**
98	95	98	97	99	97	97	97	**97**	**1.41**	**1.46**	**3.54**	**3.81**
48	49	49	50	49	46	48	49	**48**	**3.69**	**7.68**	**4.64**	**10.53**
69	68	68	70	70	69	68	69	**69**	**1.88**	**2.73**	**1.85**	**2.64**
104	104	107	105	107	105	103	105	**105**	**1.60**	**1.53**	**1.89**	**1.83**
82	81	83	84	84	84	84	83	**81**	**1.93**	**2.37**	**4.47**	**5.80**
18	19	20	20	19	19	18	18	**18**	**0.86**	**4.65**	**1.61**	**8.03**
0	0	0	0	0	0	0	0	**0**	**0.00**		**0.60**	**100.00**
2	0	1	3	1	3	4	1	**1**	**1.54**	**114.16**	**1.27**	**102.26**
206	202	198	202	193	197	203	200	**206**	**6.38**	**3.10**	**126.70**	**160.38**

Table G4b (cont.)

Sample: BK127b

ppm		**Rpt.**	Mean	SD	%SD
Rb	214	217	**215**	**1.70**	**0.79**
Sr	52	52	**52**	**0.21**	**0.41**
Y	30.9	31.1	**31.0**	**0.14**	**0.46**
Zr	182	181	**182**	**0.92**	**0.51**
Nb	15.3	15.6	**15.5**	**0.21**	**1.37**
Ba	477	478	**477**	**1.34**	**0.28**
Pb	16	15	**15**	**0.85**	**5.55**
Th	22	23	**23**	**0.85**	**3.74**
U	4	3	**3**	**0.57**	**18.25**
Sc	17	19	**18**	**1.34**	**7.66**
V	82	86	**84**	**3.11**	**3.70**
Cr	97	102	**100**	**3.96**	**3.98**
Co	14	16	**15**	**0.92**	**6.11**
Ni	31	29	**30**	**1.34**	**4.43**
Cu	13	14	**13**	**0.49**	**3.76**
Zn	44	47	**46**	**2.19**	**4.79**
Ga	20	20	**20**	**0.00**	**0.00**
Mo	0	0	**0**	**0.00**	
As	2	0	**1**	**1.56**	**141**
S	30	30	**30**	**0.00**	**0.00**

Table G5a. Reproducibility of the NBS 987 Sr standard.

Location	Technique	Date(s)	Mean $^{87}Sr/^{86}Sr$	2 SD	n
Cambridge	TIMS	28 Jun - 6 Jul 1999	0.710260	1.50E-05	7
Cambridge	TIMS	1 - 10 Feb 2000	0.710265	2.18E-05	5
Cambridge	TIMS	15 - 22 Mar 2000	0.710256	1.74E-05	4
OU	TIMS	5 - 12 Oct 2000	0.710219	3.44E-05	8
OU	ICP-MS	27 - 28 June 2001	0.710167	3.23E-05	10
OU	ICP-MS	17 July 2001	0.710180	5.43E-05	6
OU	ICP-MS	20 July 2001	0.710257	4.35E-05	3
OU	ICP-MS	24 July 2001	0.710236	5.57E-05	6
OU	ICP-MS	25 July 2001	0.710304	2.71E-05	6
OU	ICP-MS	28 - 29 Nov 2001	0.710298	4.12E-05	6
OU	ICP-MS	11 - 12 Jan 2001	0.710294	4.04E-05	20
OU	ICP-MS	13 - 14 Jan 2001	0.710279	2.66E-05	7
OU	ICP-MS	30 - 31 Jan 2001	0.710287	5.87E-05	12

Table G5b. Reproducibility of the Johnson and Mathey Nd standard.

Location	Technique	Date(s)	Mean $^{87}Sr/^{86}Sr$	2 SD	n
OU	TIMS	18 Oct - 3 Nov	0.511760	2.49E-05	13
OU	ICP-MS	7 Aug 01	0.511820	5.69E-06	6
OU	ICP-MS	8 Aug 01	0.511826	4.40E-06	6
OU	ICP-MS	15 Aug 01	0.511799	9.35E-06	6
OU	ICP-MS	16 Aug 01	0.511799	9.35E-06	5

Table G6. Repeats of water, rock and bedload samples analysed for $^{87}Sr/^{8}$ using TIMS at Cambridge and TIMS and MC-ICP-MS at the OU.

Sample	$^{87}Sr/^{86}Sr$	
T29f	0.710773 +/- 8	Samples run by TIMS
	0.710698 +/- 18	at Cambridge and MC-ICP-MS
H5	0.792644 +/- 6	at the OU
	0.792636 +/- 25	
BK63	0.759288 +/- 7	
	0.759298 +/- 8	
BK78	0.730376 +/- 80	
	0.730451 +/- 8	
BK86	0.753263 +/- 56	
	0.753333 +/- 7	
BK89	0.754780 +/- 5	
	0.754895 +/- 33	
AN1	0.728397 +/- 6	
	0.728359 +/- 43	
T29b	0.715069 +/- 8	Samples run by TIMS
	0.715077 +/- 5	at Cambridge
L10	0.732697 +/- 24	
	0.732672 +/- 15	
BK29	0.757036 +/- 20	
	0.757018 +/- 11	
BK41	0.849525 +/- 10	
	0.849513 +/- 17	
BKT4	0.725348 +/- 13	
	0.725370 +/- 19	
HBVO-1	0.703486 +/- 9	Samples run by TIMS
	0.703435 +/- 7	at the OU and Cambridge
HBVO-1	0.703486 +/- 9	
	0.703488 +/-7	
BK15	0.720788 +/- 7	Sample run by TIMS
	0.720723 +/- 28	at the OU
T29d	0.713444 +/-11	Samples run by MC-ICP-MS
	0.713379 +/- 8	at the OU
BK5	0.771209 +/- 16	
	0.771219 +/- 5	
BK26	0.770224 +/- 7	
	0.770187 +/- 6	
BK122REG	0.973423 +/- 20	
	0.973505 +/- 10	
BK123	0.711923 +/- 17	
	0.711909 +/- 24	

Table G7. Repeats of rock and bedload samples analysed for $^{143}Nd/^{144}Nd$ by TIMS and MC-ICP-MS at the OU.

Sample	**$^{143}Nd/^{144}Nd$**	
BK30	0.511686 +/- 5	TIMS
	0.511691 +/- 6	
BK21	0.511230 +/- 6	
	0.511233 +/- 6	
BK104c	0.511655 +/- 7	MC-ICP-MS
	0.511687 +/- 10	
BK127b	0.511330 +/- 2	
	0.511351 +/- 5	
BK127d	0.511244 +/- 9	
	0.511270 +/- 3	
BK127g	0.511196 +/- 4	
	0.511193 +/- 5	
BHVO-1	0.512843 +/- 3	
	0.512820 +/- 6	

Table G8a. Standard data for laser MC-ICP-MS analyses (day 1).

Standard		$^{87}Sr/^{86}Sr$	exp. corr.	Rb/Sr
100ppbNBS987 + 10ppb Y		0.710249	0.0011	1.936E-05
100ppbNBS987 + 10ppb Y		0.710284	0.0017	2.084E-05
100ppbNBS987 + 10ppb Y		0.710230	0.0014	1.374E-05
100ppbNBS987 + 10ppb Y		0.710275	0.0016	1.516E-05
100ppbNBS987 + 10ppb Y		0.710280	0.0015	5.527E-05
100ppbNBS987 + 10ppb Y		0.710275	0.0016	5.240E-05
100ppbNBS987 + 10ppb Y		0.710231	0.0015	5.241E-05
100ppbNBS987 + 10ppb Y		0.710239	0.0017	1.868E-05
	Mean	**0.7102578**		
	SD	**2.308E-05**		
	%SD	**0.003249**		
	Norm. factor	**1.000025**		
100ppbNBS987 + 10ppb Rb+Y		0.710323	0.0019	0.1438
100ppbNBS987 + 10ppb Rb+Y		0.710293	0.0021	0.1438
100ppbNBS987 + 10ppb Rb+Y		0.710264	0.0017	0.1439
100ppbNBS987 + 10ppb Rb+Y		0.710339	0.0021	0.1412
	Mean	**0.7103047**		**0.1438**
	SD	**3.287E-05**		**0.001298**
	%SD	**0.004627**		**0.902682**
	Norm. factor	**1.000091**		**1.4384**
Modern Coral		0.709586	0.0156	
Modern Coral		0.709436	0.0085	
Modern Coral		0.709285	0.0133	
Modern Coral		0.709383	0.0108	
	Mean	**0.709423**		
	SD	**1.253E-04**		
	%SD	**0.017669**		

Table G8b. Standard data for laser MC-ICP-MS analyses (day 2).

Standard		$^{87}Sr/^{86}Sr$	exp. corr.	Rb/Sr
100ppbNBS987 + 10ppb Y		0.710343	0.0019	3.480E-05
100ppbNBS987 + 10ppb Y		0.710309	0.0020	3.500E-05
100ppbNBS987 + 10ppb Y		0.710340	0.0022	5.280E-05
100ppbNBS987 + 10ppb Y		0.710353	0.0017	4.010E-05
	Mean	**0.710336**		
	SD	**1.892E-05**		
	%SD	**0.002663**		
	Norm. factor	**1.000136**		
100ppbNBS987 + 10ppb Rb+Y		0.710334	0.0025	0.1424
100ppbNBS987 + 10ppb Rb+Y		0.710378	0.0021	0.1427
100ppbNBS987 + 10ppb Rb+Y		0.710426	0.0019	0.1429
100ppbNBS987 + 10ppb Rb+Y		0.710407	0.0020	0.1428
100ppbNBS987 + 10ppb Rb+Y		0.710434	0.0018	0.1428
100ppbNBS987 + 10ppb Rb+Y		0.710302	0.0027	0.1421
	Mean	**0.710380**		**0.1426**
	SD	**5.284E-05**		**0.000291**
	%SD	**0.007439**		**0.203977**
	Norm. factor	**1.000197**		**1.4262**
Modern Coral		0.709479	0.0082	
Modern Coral		0.709446	0.0087	
Modern Coral		0.709515	0.0077	
Modern Coral		0.709347	0.0080	
Modern Coral		0.709446	0.0116	
	Mean	**0.709446**		
	SD	**6.245E-05**		
	%SD	**0.008803**		

Appendix H

Principal Components Analysis; Residual Plots and Data Exclusions.

List of figures.

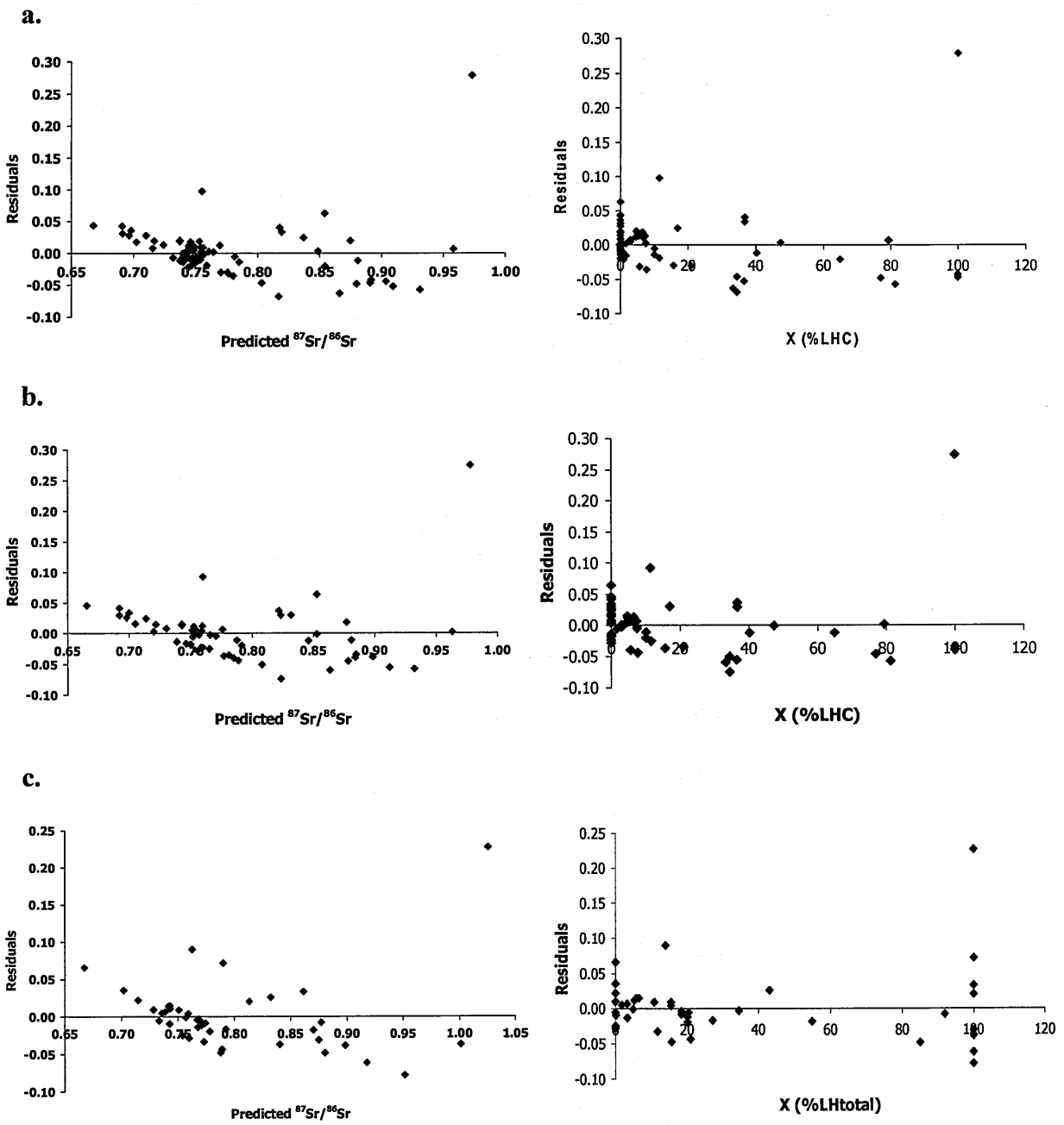

Fig. H1. Plots of residuals versus predicted $^{87}Sr/^{86}Sr$ and the most significant X predictor. a. Full dataset (equation 5.1). b. Bhote Kosi data (equation 5.2). c. Bhote Kosi dry season data (equation 5.3).

a.

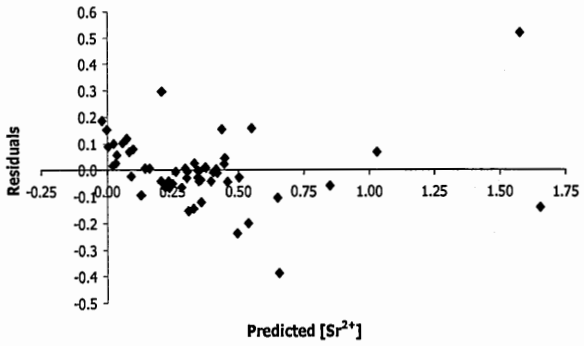
Residuals
Predicted [Sr2+]

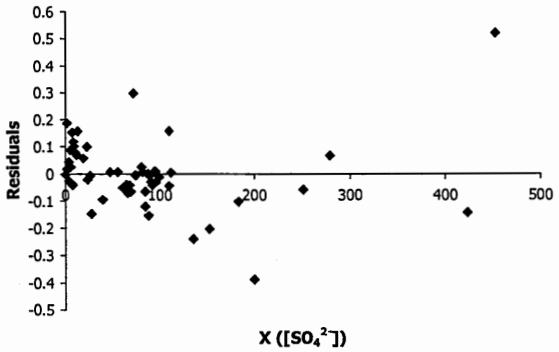
Residuals
X ([SO4 2-])

b.

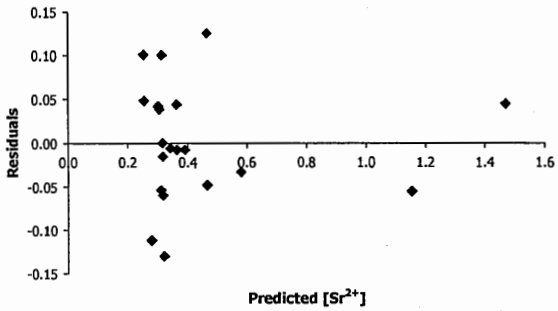
Residuals
Predicted [Sr2+]

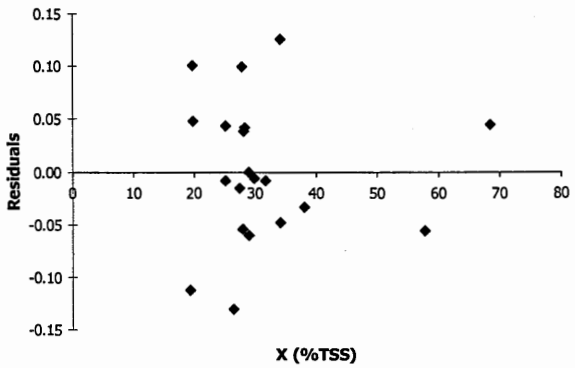
Residuals
X (%TSS)

c.

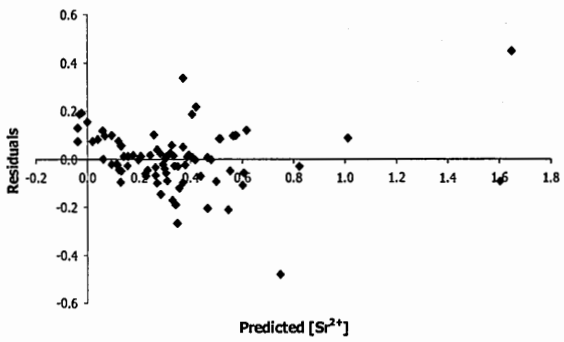
Residuals
Predicted [Sr2+]

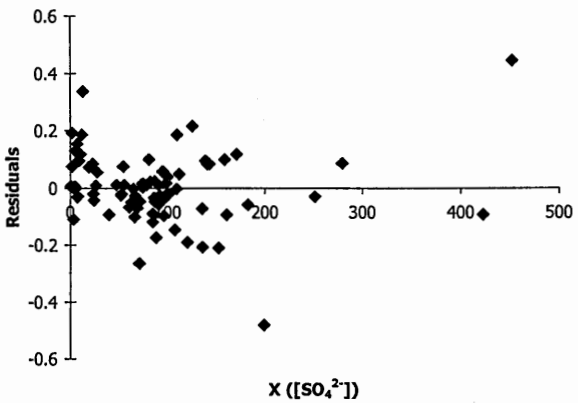
Residuals
X ([SO4 2-])

d.

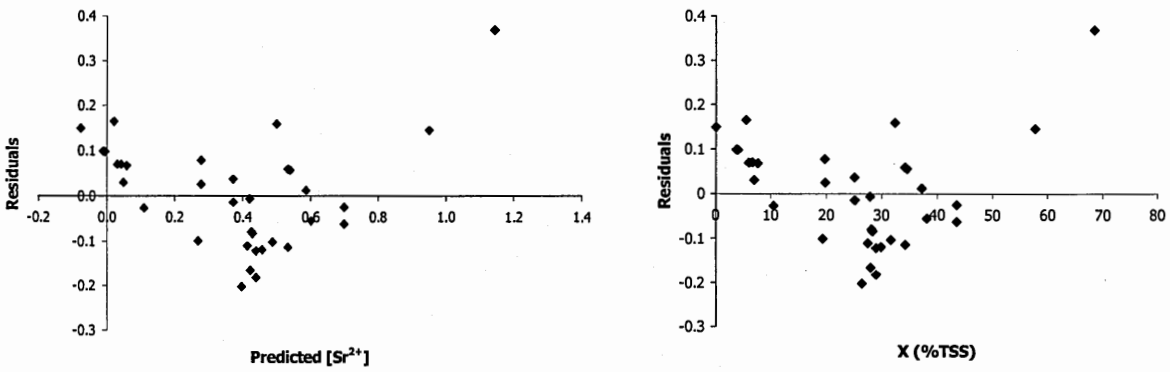

e.

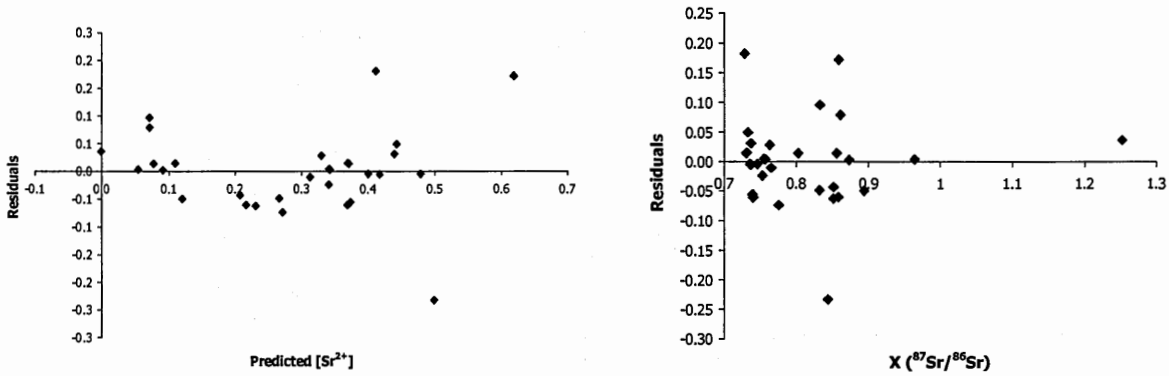

Fig. H2. Plots of residuals versus predicted dissolved strontium concentration and the most significant X predictor. a. Full data set (equation 5.4). b. Full data set (geological coverage variables only) (equation 5.5). c. Bhote Kosi data (equation 5.6). d. Bhote Kosi data (geological coverage variables only) (equation 5.7). e. Bhote Kosi dry season data (equation 5.8).

In the case of regression equations 5.4 and 5.6, in which sulphate concentrations are the predominant predictor of strontium concentration in the full and Bhote Kosi datasets, it was found that better correlations were achieved (fig. G3) by excluding samples BKT1 and BKT2, which have extremely high concentrations of sulphate. In the case of regression equations 5.5 and 5.7, in which the amount of Tibetan Sedimentary Series bedrock present in catchments is the principal predictor of strontium concentration, correlations were considerably improved (fig. G4) by including only mixed lithology catchments and excluding those which drain only the TSS or do not drain the TSS at all.

a.

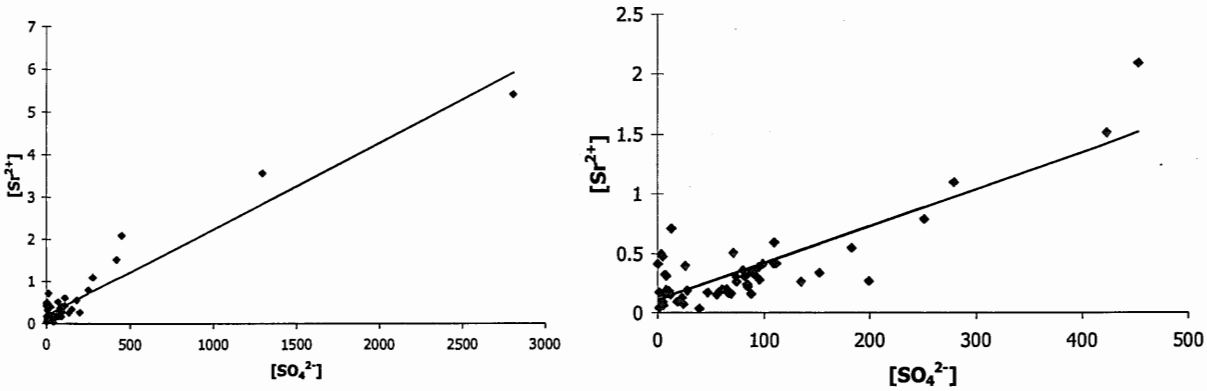

b.

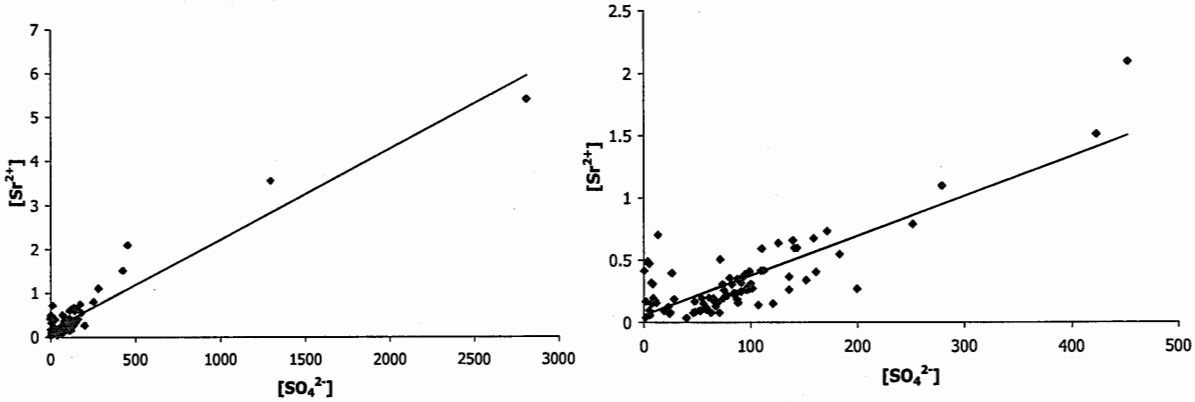

Fig. H3. $[Sr^{2+}]$ versus $[SO_4^{2-}]$ for the full dataset (a) and Bhote Kosi data only (b) showing the improved correlations (right) when samples BKT1 and BKT2, which have extremely high sulphate concentrations, are excluded.

a.

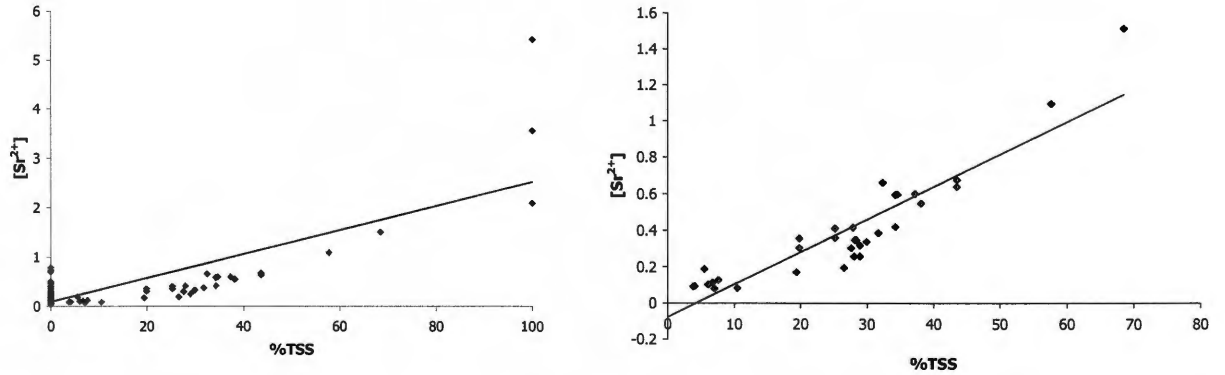

b.

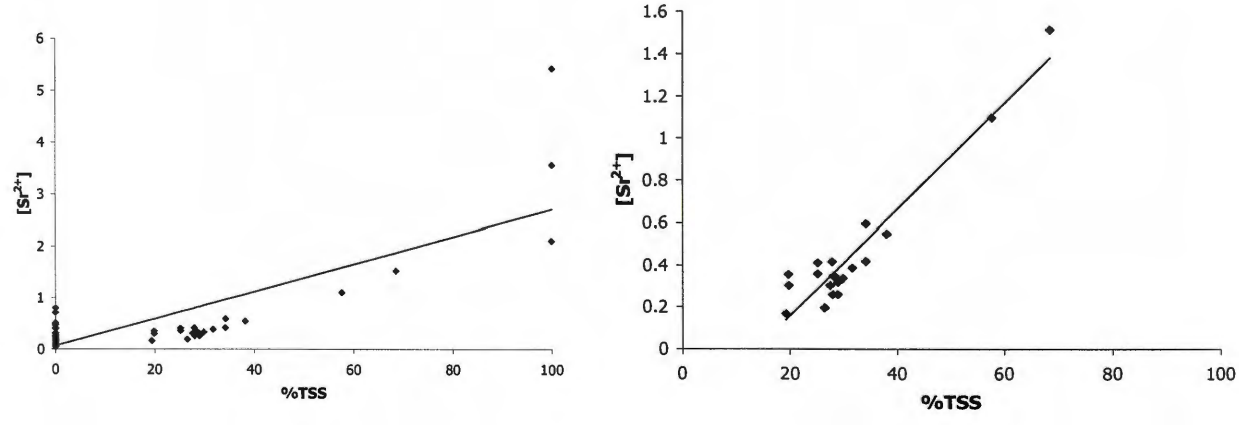

Fig. H4. $[Sr^{2+}]$ versus %TSS for the full dataset (a) and Bhote Kosi data only (b) showing the improved regression correlation achieved (right) when catchments draining 0% and 100% TSS bedrock are removed.

Appendix I

Conference Abstracts

Parts of this thesis have been presented at international conferences during the course of this study, as listed below:

Oliver, L., Harris, N., Dise, N. and Bickle, M. (2000). *The effect of Lesser Himalayan calc-silicates on the $^{87}Sr/^{86}Sr$ of the Bhote Kosi River of Nepal – Implications for Himalayan weathering, the marine $^{87}Sr/^{86}Sr$ record and global climate.* Earth Science Frontiers **vol. 7:** p.396-397. 15th Himalaya-Karakoram-Tibet Workshop, Chengdu.

Oliver, L. S., Harris, N., Dise, N., and Bickle, M. (2000). *The effect of Lesser Himalayan calc-silicates on the $^{87}Sr/^{86}Sr$ of the Bhote Kosi River of Nepal – Implications for Himalayan weathering, the marine $^{87}Sr/^{86}Sr$ record and global climate.* Journal of Conference Abstracts **vol. 5:** p.757. Goldscmidt 2000, Oxford.

Oliver, L., Harris, N. B. W., Dise, N., Bickle, M. and Thornton, G. (2001). *Testing the validity of dissolved $^{87}Sr/^{86}Sr$ as a proxy for silicate weathering in the Himalaya.* Journal of Asian Earth Sciences **vol. 19,** no. 3A: p.49. 16th Himalaya-Karakorum-Tibet Workshop, Graz.

Oliver, L., Harris, N., Dise, N. Bickle, M. and Thornton, G. (2001). *Testing the validity of dissolved $^{87}Sr/^{86}Sr$ as a proxy for silicate weathering in the Himalaya.* Journal of Conference Abstracts **vol. 6**: p.109. EUG XI, Strasbourg.